UNIVERSIDADE TÉCNICA DE LISBOA

INSTITUTO SUPERIOR TÉCNICO

Black Hole Solutions
and
Pair Creation of Black Holes
in
Three, Four and Higher Dimensional Spacetimes

Óscar João Campos Dias

Dissertação para obtenção do Grau de Doutor em Física

(PhD Thesis)

December 2003

Jury:

Luis Bento	Examinator
Stanley Deser	Examinator
Jorge Dias de Deus	President of the Jury
Alfredo Barbosa Henriques	Examinator
José Pizarro de Sande e Lemos	Supervisor
Jorge Romão	Examinator

Black Hole Solutions
and
Pair Creation of Black Holes
in
Three, Four and Higher Dimensional Spacetimes

Óscar João Campos Dias

Dissertação para obtenção do Grau de Doutor em Física

(PhD Thesis)

December 2003

Black Hole Solutions
and
Pair Creation of Black Holes
in
Three, Four and Higher Dimensional
Spacetimes

Óscar João Campos Dias

February 1, 2008

Resumo

Buracos negros são importantes em astrofísica, uma vez que resultam do colapso gravitacional de uma estrela massiva ou aglomerados de estrelas, e em física porque revelam propriedades da física fundamental, como propriedades termodinámicas e quânticas da gravitação.

Para melhor se entender a física dos buracos negros são necessárias soluções exactas que descrevem um ou vários buracos negros. Nesta tese estudamos soluções exactas em três, quatro e dimensões mais altas. O estudo em três dimensões justifica-se pela simplificação do problema, enquanto que a discussão em dimensões superiores a quatro se justifica porque diversas teorias indicam que existem dimensões extra no universo. Nesta tese, em qualquer das dimensões acima indicadas, estudamos soluções exactas com um só buraco negro e soluções exactas que representam um par de buracos negros acelerados. Estas últimas soluções são então usadas para estudar em detalhe o processo quântico de criação de pares de buracos negros num campo externo. Também determinamos a radiação gravitacional emitida durante este processo de criação.

PALAVRAS-CHAVE:
Soluções exactas de buracos negros; Pares de buracos negros acelerados, Métrica-C; Criação quântica de pares de buracos negros; Radiação gravitacional; Espaços-tempo em D dimensões; Espaços de fundo com constante cosmológica.

Abstract

Black holes, first found as solutions of Einstein's General Relativity, are important in astrophysics, since they result from the gravitational collapse of a massive star or a cluster of stars, and in physics since they reveal properties of the fundamental physics, such as thermodynamic and quantum properties of gravitation.

In order to better understand the black hole physics we need exact solutions that describe one or more black holes. In this thesis we study exact solutions in three, four and higher dimensional spacetimes. The study in 3-dimensions is important due to the simplification of the problem, while the discussion in higher dimensions is essential due to the fact that many theories indicate that extra dimensions exist in our universe. In this thesis, in any of the dimensions mentioned above, we study exact solutions with a single black hole and exact solutions that describe a pair of uniformly accelerated black holes, with the acceleration source being well identified. This later solutions are then used to study in detail the quantum process of black hole pair creation in an external field. We also compute the gravitational radiation released during this pair creation process.

KEY-WORDS:
Exact black hole solutions; Pair of accelerated black holes, C-metric; Pair creation of black holes; Gravitational radiation; D-dimensional spacetimes; Cosmological constant backgrounds.

Acknowledgements

Contents

Preface

The research included in this thesis has been carried out at Centro Multidisciplinar de Astrofísica (CENTRA) in the Physics Department of Instituto Superior Técnico. I declare that this thesis is not substantially the same as any that I have submitted for a degree or diploma or other qualification at any other University and that no part of it has already been or is being concurrently submitted for any such degree or diploma or any other qualification.

Chapter 2 was done in collaboration with Professor José Lemos and Dr. Carlos Herdeiro. Chapters 3-9 are the outcome of collaborations with Professor José Lemos. Chapter 10 was done in collaboration with Professor José Lemos, Vitor Cardoso and Nuno Santos. Chapters 11 and 12 were done in collaboration with Professor José Lemos and Vitor Cardoso. All these chapters have been submitted with minor modifications for publication.

A list of the works published included in this thesis are listed below.

- O. J. C. Dias, J. P. S. Lemos, *Rotating magnetic solution in three dimensional Einstein gravity*, JHEP **0201**: 006 (2002); [hep-th/0201058] (Chapter 2).

- V. Cardoso, S. Yoshida, O. J. C. Dias, J. P. S. Lemos, *Late-time tails of wave propagation in higher dimensional spacetimes*, Phys. Rev. D **68**, 061503 (2003) [Rapid Communications]; [hep-th/0307122] (mentioned in Chapter 2).

- O. J. C. Dias, J. P. S. Lemos, *Static and rotating electrically charged black holes in three-dimensional Brans-Dicke gravity theories*, Phys. Rev. D **64**, 064001 (2001); [hep-th/0105183] (Chapter 3).

- O. J. C. Dias, J. P. S. Lemos, *Magnetic point sources in three dimensional Brans-Dicke gravity theories*, Phys. Rev. D **66**, 024034 (2002); [hep-th/0206085] (Chapter 3).

- O. J. C. Dias, J. P. S. Lemos, *Magnetic strings in anti-de Sitter general relativity*, Class. Quantum Grav. **19**, 2265 (2002); [hep-th/0110202] (mentioned in Chapter 4).

- O. J. C. Dias, J. P. S. Lemos, *Pair of accelerated black holes in a anti-de Sitter background: the AdS C-metric*, Phys. Rev. D **67**, 064001 (2003); [hep-th/0210065] (Chapter 6).

- O. J. C. Dias, J. P. S. Lemos, *Pair of accelerated black holes in a de Sitter background: the dS C-metric*, Phys. Rev. D **67**, 084018 (2003); [hep-th/0301046] (Chapter 6).

- O. J. C. Dias, J. P. S. Lemos, *The extremal limits of the C-metric: Nariai, Bertotti-Robinson and anti-Nariai C-metrics*, Phys. Rev. D**68** (2003) 104010; [hep-th/0306194] (Chapter 7).

- O. J. C. Dias, J. P. S. Lemos, *False vacuum decay: Effective one-loop action for pair creation of domain walls*, J. Math. Phys. **42**, 3292 (2001); [hep-ph/0103193] (Chapter 8).

- O. J. C. Dias, *Pair creation of particles and black holes in external fields*, [gr-qc/0106081] (Chapter 8).

- O. J. C. Dias, J. P. S. Lemos, *Pair creation of de Sitter black holes on a cosmic string background*, Phys. Rev. D**69** (2004) 084006; [hep-ph/0310068] (Chapter 9).

- O. J. C. Dias, *Pair creation of anti-de Sitter black holes on a cosmic string background*, Phys. Rev. D**70** (2004) 024007 (Chapter 9).

- V. Cardoso, O. J. C. Dias, J. P. S. Lemos, *Nariai, Bertotti-Robinson and anti-Nariai solutions in higher dimensions*, Phys. Rev. D**70** (2004) 024002 (Chapter 10).

- N. L. Santos, O. J. C. Dias, J. P. S. Lemos, *Global embedding Minkowskian spacetime procedure in higher dimensional black holes: Matching between Hawking temperature and Unruh temperature*, Phys. Rev. D, in press (2004) (mentioned in Chapter 10).

- O. J. C. Dias, J. P. S. Lemos, *Pair creation of higher dimensional black holes on a de Sitter background*, Phys. Rev. D, submitted (2004); [hep-th/0410279] (Chapter 11).

- V. Cardoso, O. J. C. Dias, J. P. S. Lemos, *Gravitational radiation in D-dimensional spacetimes*, Phys. Rev. D **67**, 064026 (2003); [hep-th/0212168] (Chapter 12).

Chapter 1

Overview

Contents

1.1 Overview on black holes

Black holes have begun to be entities of theoretical interest when they have been found as exact solutions of the Einstein equations with peculiar features. Although the actual universal name "black hole" has been introduced only in 1968 by Wheeler[a], the first black hole solution has been found by Schwarzschild in 1916, just a few months after the publication of General Relativity by Einstein. As proved by Birkhoff in 1923, the Schwarzschild solution describes the external gravitational field generated by a static spherical mass. It was much later found that one is in the presence of a black hole when the mass M is inside a critical radius, $r_+ = \frac{2GM}{c^2} \sim 3\frac{M}{M_\odot}$ km (where G is Newton's constant and c is the light velocity), known as the event horizon of the black hole. This horizon acts like an one-way membrane: particles and radiation can cross it from outside, but they cannot escape from its interior. An observer that is at rest at infinity sees an infalling observer taking an infinite amount of time to approach the horizon but, according to the infalling observer, his crossing through the horizon is done in a finite amount of time and, once he has done this fatal step, he is unavoidably pushed into the central curvature singularity at $r = 0$ where he suffers an infinite tidal force. These properties of the Schwarzschild black hole are best synthesized in its Carter-Penrose diagram, Fig. 1.1. These kind of causal diagrams have been progressively developed by works of

---

[a]In this overview section when we refer to a work we will only specify the author and the year of publication. Being reference works they can easily be found in the books. For this purpose we suggest, e.g., the book of Frolov and Novikov [1].

Eddington, Finkelstein, Kruskal, Carter and Penrose, and we will make a first contact with them here since they will be very useful along this thesis.
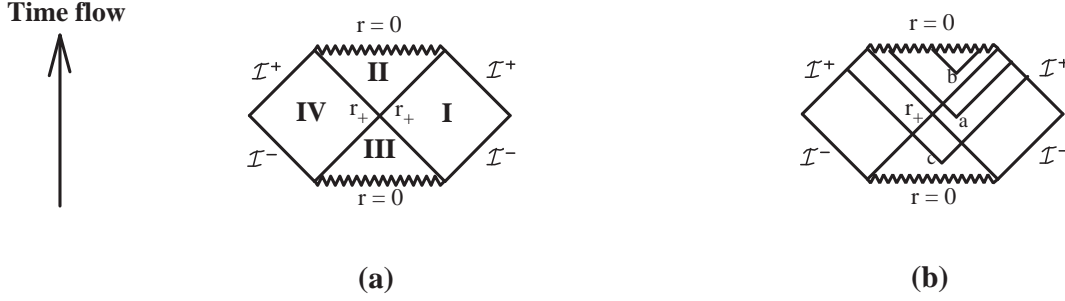
Figure 1.1: Carter-Penrose diagram of the Schwarzschild black hole. Time flows into the top of the diagram, and light rays move necessarily along 45° lines. The zigzag line represents the $r = 0$ curvature singularity, $\mathcal{I}$ represents the infinity $r = \infty$ (whose points have been brought to a finite position by an appropriate coordinate transformation), and the two mutually perpendicular lines, r_+, represent the black hole event horizon. (a) Region II represents the black hole interior, region III is the white hole interior, and regions I and IV represent the exterior space, $r_+ < r < +\infty$. (b) The paths that a light ray can follow determine the properties of the region from where they are emitted. We observe that in fact these diagrams represent a dynamic wormhole solution.

In the Carter-Penrose diagrams, a null particle (e.g., a light ray) moves necessarily towards the top along 45° lines, while timelike particles can move into the top of the diagrams only along a curve whose tangent vector must do an angle less than 45° with the vertical line. The curvature singularity, $r = 0$, of the Schwarzschild black hole is represented by a zigzag line in Fig. 1.1. Region IV is equivalent to region I, and both represent the region outside the black hole horizon, $r_+ < r < +\infty$. A null ray that is sent from a point a in these regions can move towards $r = 0$, after crossing r_+, but it is also free to move into the future infinity $\mathcal{I}^+$ [see Fig. 1.1.(b)]. Note that regions I and IV are casually disconnected: no null or timelike particle can start in region I and reach region IV. Region II is interpreted as the interior of the black hole horizon, since a null ray emitted from a point in its interior [e.g., point b in Fig. 1.1.(b)] necessarily hits the future curvature singularity, and cannot cross the horizon towards region I or IV (the discussion also applies to timelike particles). Region III is interpreted as the interior of the white hole, since any particle, e.g. the light ray that is emitted from point c in Fig. 1.1.(b), is necessarily expelled out from region III, i.e., it necessarily crosses the horizon towards region I or IV. We remark that regions III and IV were not present in the original solution of Schwarzschild. They appear after the realization that this original solution could be extended.

The inclusion of an electric charge Q also yields an exact static spherical solution which is known as the Reissner-Nordström black hole (1918) when $Q^2 \leq GM^2$. Finally, an angular momentum J can be added to the system yielding a stationary, axisymmetric solution which when $Q = 0$ is known as the Kerr solution (1963), and when $Q \neq 0$ is called Kerr-Newman solution (1965). These solutions describe a black hole when the condition $\frac{J^2 c^2}{G^2 M^2} + \frac{Q^2}{G} \leq M^2$ is satisfied. When the equality holds in the above relations we have the extreme black hole solutions which have zero temperature. When the above constraints are violated we have a naked singularity, a visible singularity not surrounded by a horizon. The uniqueness theorems (whose proofs have been given by Israel, Robinson and Carter, among others in 1968 and in the following decade) state that the only static or stationary solutions of the Einstein-Maxwell equations that are asymptotically flat and have regular horizons are the above solutions characterized only by the parameters M, Q and J. All the other parameters that specified the initial state before the formation of the black hole are radiated away during the creation process. This simple description of a black hole is well summarized by the well-known metaphoric statement of Wheeler: "a black hole has no hair". The construction of a formalism to compute these hairs M, Q and J has been carried by Arnowitt, Deser and Misner (1963), by Regge

and Teiltelboim (1974), and by Brown and York (1993), among others. In the seventies, Price, Wald, Chandrasekhar and Detweiler have also proven that the above black holes are stable with respect to small perturbations [2].

The theory of black holes has been strongly connected to the theory of gravitational collapse after the work of Oppenheimer and Snyder (1939) and Penrose's theorem (1965): a realistic, slightly non-spherical complete collapse leads unavoidably to the formation of a black hole and a singularity (for a detailed description of the theory of gravitational collapse see the work of Harrison, Thorne, Wakano and Wheeler [3]). Oppenheimer and Volkoff (1939) have shown that when a neutron star (first predicted by Zwicky in 1934) forms, after the explosion of the massive progenitor star, its mass must be smaller than $M_{OV} \sim 3M_\odot$ (in fact Oppenheimer and Volkoff first found the value $0.7M_\odot$, but a more accurate account on the nuclear processes yields the value $3M_\odot$). This is the maximum mass that the pressure of neutron degenerate matter can support against further gravitational collapse. The existence of a maximum mass for degenerate matter had been realized previously by Chandrasekhar (1935), in the case of electron degenerate matter. He has shown that white dwarfs must have a mass smaller than $M_C \sim 1.4M_\odot$. Thus, black holes formed thought the gravitational collapse of stellar matter have necessarily a mass $M > 3M_\odot$. In the context of gravitational collapse towards a black hole, two important conjectures have been formulated, the cosmic censorship and the hoop conjectures. The cosmic censorship conjecture (Penrose, 1969) forbids the existence of naked singularities, while the hoop conjecture (Thorne, 1972) states that black holes form when and only when a mass M gets compacted into a region whose circumference in every direction is less than its Schwarzschild circumference $\frac{4\pi GM}{c^2}$. During the last decade, a great effort has been initiated in order to detect the energetic astrophysical processes predicted to be powered by black holes. Mainly, the astrophysics are looking into the X-ray emitting sources that can be found in the accretion of matter into a binary stellar system and into an active galactic nuclei. These efforts have by now already provided a set of serious black hole candidates in a binary system with masses that belong to the range $5M_\odot - 20M_\odot$ (where $M_\odot$ is the solar mass), and in an active galactic nuclei with masses that belong to the supermassive range $10^6 M_\odot - 10^{10} M_\odot$.

Black holes have entered in the domain of physics during the 1970s when it has been shown that they are thermodynamic objects. Indeed Bardeen, Carter and Hawking (1973), supported by previous work of Christodoulou (1970) and Penrose (1971), have shown that black holes obey the so called four laws of black hole mechanics. The first one is known as the zero law and states that the surface gravity is constant along the horizon of the black hole, even when this is not spherically symmetric as occurs with the Kerr solution. The surface gravity, k_h, can be interpreted as the force that must be exerted on a rope at infinite to hold a unit mass at rest near the horizon of the black hole. The first law (an energy conservation law) states that when one throws an infinitesimal amount of matter into a stationary black hole described by M, J and Q, it will evolve into a new stationary black hole in such a way that the change in the hairs of the system satisfies

$$c^2 dM = \frac{k_h c^2}{8\pi G} d\mathcal{A} + \Omega_h dJ + \Phi_h dQ, \qquad (1.1)$$

where $\mathcal{A}$ is the surface area of the horizon, Ω_h is the angular velocity at the horizon, and Φ_h is the electric potential at the horizon. The second law states that the area of the black hole horizon cannot decrease during any physical process, $d\mathcal{A} \geq 0$ (this classical law was later replaced by the generalized second law which states that the sum of the black hole entropy plus the exterior matter entropy can never decrease). Finally, the third law states that it is impossible to reduce the surface gravity to zero by a finite number of processes. The surface gravity of the Kerr-Newman black hole is given by

$$k_h = \frac{4\pi c^2}{\mathcal{A}} \sqrt{\frac{G^2 M^2}{c^4} - \frac{J^2}{M^2 c^2} - \frac{GQ^2}{c^4}}, \qquad (1.2)$$

and thus $k_h = 0$ implies $\frac{J^2 c^2}{G^2 M^2} + \frac{Q^2}{G} = M^2$, which as we saw above is the condition for an extreme black hole. If the state $k_h < 0$ could be reached we would have a naked singularity. Hence, the cosmic censorship conjecture stated by Penrose plays the role of the third law.

These laws are purely classical and resemble the usual four laws of thermodynamics, if one admits that $\mathcal{A}$ is proportional to the entropy, as suggested by Bekenstein (1973,1974), and that k_h is proportional to the black hole temperature. At first, this resemblance was only an analogy since if the black hole had a temperature it would have to radiate, in a clear contradiction with the known classical fact that nothing could escape from the black hole horizon. However, in a revolutionary work, Hawking (1975), using a semiclassical treatment in which the gravitational field of the black hole is treated classically but the matter is treated quantum mechanically, has shown that the black holes do indeed radiate a spectrum characteristic of a blackbody with a Hawking temperature given by

$$T_h = \frac{\hbar k_h}{2\pi k_B}, \tag{1.3}$$

where $\hbar = h/(2\pi)$ is the Planck constant, k_B is the Boltzmann constant, and the associated Bekenstein-Hawking entropy is

$$S_h = \frac{\mathcal{A}_h}{4} \frac{k_B c^3}{\hbar G}. \tag{1.4}$$

Actually, the spectrum is not a perfect blackbody one due to the so called greybody factor: the emission rate of particles is proportional to the cross-section for a particle to be absorbed by the black hole and this cross-section is not constant, which leads to deviations from the pure blackbody emission spectrum. For a Schwarzschild back hole we have $T_h = \frac{\hbar c^3}{8\pi G k_B} \frac{1}{M} \sim 10^{-7} \frac{M_\odot}{M}$ K and $S_h = \frac{4\pi G k_B}{\hbar c} M^2 \sim 10^{53} \left(\frac{M}{M_\odot}\right)^2$ Js^{-1}. At this point some remarks are justified. First note that the four fundamental constants of nature, c, G, k_B and $\hbar$ (that are the fingerprints of relativity, gravitation, statistical mechanics and quantum mechanics) are, for the first time, unified in a single formula. Second, in standard statistical mechanics, the entropy of a system originates in the counting of quantum states which are macroscopically indistinguishable. Now, the Bekenstein-Hawking entropy of a black hole has not yet been fully explained as a consequence of such state counting. Third, note that the Hawking temperature of the Schwarzschild back hole is inversely proportional to the mass. Thus its heat capacity is negative and the black hole is quantum mechanically unstable since as it loses mass, its temperature grows and the particle emission rate grows (the black hole evaporates). The rate of mass loss per unit time can be estimated using the Stefan-Boltzmann law, $-\frac{dE}{dt} \sim \sigma \mathcal{A}_h T_h^4$ with $E = Mc^2$ and $\sigma = \pi^2 k_B^4/(60\hbar^3 c^2)$,

$$-\frac{dM}{dt} \sim \frac{\hbar c^6}{G^2} \frac{1}{M^2} \sim 10^{-44} \left(\frac{M_\odot}{M}\right)^2 \text{ kg s}^{-1}, \tag{1.5}$$

to which corresponds an evaporation lifetime given by

$$\tau \sim \frac{G^2}{\hbar c^4} M^3 \sim 10^{71} \left(\frac{M}{M_\odot}\right)^3 \text{ s}. \tag{1.6}$$

Third, note that although the Hawking evaporation would constitute a definite proof of the black hole nature of a compact object, it will be very difficult to be ever observed by astronomical means. Indeed, an astrophysical black hole with a mass $M \sim M_\odot$ has a Hawking temperature of only $T_h \sim 10^{-7}$ K to which corresponds a total dissipating power of $|d(Mc^2)/dt| \sim 10^{-27}$ W.

If one has some hope in observing the Hawking evaporation one must then look for possible physical processes that lead to the formation of mini-black holes with Planck sizes ($\ell_{Pl} \sim 1.616 \times 10^{-33}$ cm, $m_{Pl} \sim 2.177 \times 10^{-5}$ g). For example, a black hole with $M = 10^3 m_{Pl}$ would have a temperature $T_h \sim 10^{28}$ K and a total dissipating power of $\sim 10^{43}$ W, and thus the Hawking evaporating process would be extremely energetic and passible of being observed. A process that might lead to the formation of such Planckian black holes has been proposed by Zel'dovich and Novikov (1967), and by Hawking (1971). These black holes are called primordial since they can have been produced only

in the very early universe when very large local deviations from homogeneity were possible. Let t be the time elapsed since the Big Bang and R the size of a fluctuation in the metric, i.e., of an inhomogeneity in the metric that describes the universe. Then, when ct is of the order of R, the gravitational forces can locally stop the cosmic expansion of an agglomerate of matter and reverse it into complete collapse if the self gravitational potential energy of the matter exceeds the internal energy: $\frac{GM^2}{R} \geq pR^3$, where p is the pressure. Now, during the radiation era the relation between the pressure and the density is $p \sim \rho c^2$ and, according to the Einstein-de Sitter model of the early universe, the density and the time are related by $G\rho \sim t^{-2}$. From these relations one finds that the mass of the primordial black hole is related to the cosmic time by $M \sim \frac{c^3}{G}t \sim 10^{35}\, t$. Thus, at the Planck time, $t \sim 10^{-43}$s, mini-black holes may form with the Planck mass $M \sim 10^{-8}$kg, at time $t \sim 10^{-4}$s, black holes with $M_\odot \sim 10^{30}$kg may be produced, and at the time of nucleosynthesis, $t \sim 100$s, supermassive black holes with $10^7 M_\odot$ may be created. Now, some primordial mini-black holes should by now be in the last stage of the Hawking evaporation process, and thus we should be detecting the highly energetic γ-ray bursts released during this exploding process. These events have not been observed, which indicates that the average density of the primordial black holes is low or zero. On the other side the hypothesis that the active galactic nuclei are fed by the accretion of matter into central supermassive black holes with masses $10^6 M_\odot - 10^{10} M_\odot$, as suggested by Lynden-Bell (1969), may favor the rapid formation of supermassive black holes in the early universe.

Another process that allows the formation of mini-black holes is the gravitational analogue of the Schwinger (1951) quantum process of pair creation of particles in an external electric field. Recall that this Schwinger process is based on the fact that virtual, short-lived, particles are constantly being created and rapidly annihilated in the physical vacuum, so that it is stable. However, in the presence of an external electric field, some of these particle-antiparticle pairs may receive enough energy to materialize and become real. This leads to the quantum creation of the pair that is then accelerated away also by the external Lorentz force. At the heuristic level one can estimate the probability of this pair creation process as follows. Let $\mathcal{E}$ be the external field strength, and e and m the charge and mass of the particle, respectively. A pair separated by a distance ℓ can be created if ℓ is of the order of the Compton length of the particle, $\lambda = \frac{\hbar}{mc}$, and if the work done by the field along this distance, $W = e\mathcal{E}\ell$, is at least equal to the energy needed to materialize the pair, $E_0 = 2mc^2$. An estimate for the probability of pair creation is then given by the Boltzmann factor $\Gamma \sim \exp{-\frac{E_0}{W}} \sim \exp{-\frac{2m^2c^3}{e\mathcal{E}\hbar}}$. Unfortunately, in order to observe this effect one must have a huge external critical field, $\mathcal{E}_{\mathrm{cr}} \sim 10^{18}\,\mathrm{V\,m^{-1}}$. So, at $t = 0$ (say), a pair is materialized at $x = \pm\frac{\ell}{2} \sim \frac{mc^2}{e\mathcal{E}}$. Now, one can go further and analyze the subsequent evolution of the pair. It is accelerated apart by the Lorentz force describing the uniformly accelerated hyperbolic motion (the Rindler motion), $x^2 - c^2t^2 = (\ell/2)^2$. Differentiating this relation one obtains the velocity and thus, the energy of the particle, $E = \frac{2mc^2}{\sqrt{1-v^2/c^2}} = 2xe\mathcal{E}$. Hence, after the creation, the work done by the field along the distance between the pair, $2x$, is used to accelerate the pair. The complete process is schematically represented in Fig. 1.2.

This Schwinger process also holds for other particles and background fields. One example is the pair creation of solitons and domain walls that accompany the decay of a false vacuum. We will discuss this process in chapter 8. The gravitational analogue of the Schwinger process, that leads to the pair creation of black holes in an external field, has proposed by Gibbons (1986). In order to turn a pair of virtual black holes into a real one, we also need a background field that provides the energy needed to materialize the pair, and that furnishes the force necessary to accelerate away the black holes once they are created. This background field can be: (i) an external electromagnetic field with its Lorentz force, (ii) the positive cosmological constant Λ, or inflation, (iii) a cosmic string with its tension, (iv) a combination of the above fields, or (v) a domain wall with its gravitational repulsive energy. We will make an overview of these processes in section 1.3.3, and we will analyze some of these processes in great detail in chapter 9. To study these processes we must have exact solutions of the Einstein equations that describe the pair of uniformly accelerated black holes in the external field, after they are created. Fortunately, these solutions exist and we will make a historical

presentation of them in section 1.3.2, and we will discuss them in detail in chapter 6. Finally, an important process that accompanies the production of the black hole pair is the emission of electromagnetic and gravitational radiation. An estimate for the amount of gravitational radiation released during the pair creation period will be given in section 1.3.4 and explicitly computed in chapter 12.
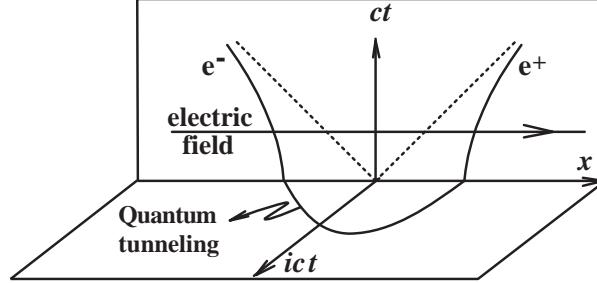
Figure 1.2: During the imaginary time it a quantum tunnelling process occurs, with the energy for the materialization being provided by the external electric field. This leads to the creation (at $t = 0$) of a particle-antiparticle pair $(e^- e^+)$ at $x = \pm \frac{\ell}{2}$. This pair is then separated apart by the external Lorentz force, describing the hyperbolic uniform accelerated motion, $x^2 - c^2 t^2 = (\ell/2)^2$. The semi-circle trajectory that represents the tunnelling process is obtained by euclideanizing the time $(t \to it)$ in the hyperbolic equation of motion, yielding $x^2 + c^2 t^2 = (\ell/2)^2$.

Nowadays, it is important to study black holes not only in an asymptotically flat spacetime, but also in spacetimes with a negative cosmological constant ($\Lambda < 0$), i.e., asymptotically anti-de Sitter (AdS) spacetimes, and in spacetimes with a positive cosmological constant ($\Lambda > 0$), i.e., asymptotically de Sitter (dS) spacetimes. One of the motivations to study AdS solutions, as we shall see in section 1.2, comes from the fact that the only black holes that 3-dimensional gravity can provide live in an AdS background. Another motivation is related to supergravities in 11 dimensions, that provide a dynamic mechanism that spontaneously compactifies 7 of the 11 dimensions and yields a vacuum state with topology $AdS_4 \times S^7$, with an energy density given by $\Lambda = -3g^2/(4\pi G)$, where g is the coupling constant of the theory. Thus, its vacuum is described by an AdS spacetime. If such theory is correct, it means that AdS should be considered as a symmetric phase of the theory that must have been broken to yield our actual background. String theory provides a further motivation to analyze AdS backgrounds, through the AdS/CFT correspondence conjecture of Maldacena [4]. This duality conjecture states a correspondence between supergravity on an AdS space and a conformal field theory (CFT) on the boundary of that space. The connection bridge between the string theory on AdS and the gauge theory is supported by the large N limit of t'Hooft, where N is the number of charged colors of the theory. This relationship has been motivated by the studies on higher dimensional black holes (p-branes), and by their full string theory description as D-branes of Polchinski. In addition, AdS spacetimes have other interesting features: (i) it is one of the rare backgrounds yielding a consistent interaction with massless higher spins, (ii) it allows a consistent string theory in any dimension, not only at the critical ones, and (iii) it permits a clear definition of mass, charge and angular momentum (a property that is shared with the asymptotically flat case).

The properties of the dS solutions also deserve a detailed investigation. The main motivation to study them comes from recent astronomical observations that seem to indicate that our universe is filled by a $\Lambda > 0$ background. The dS background plays also a crucial role in the inflationary era undergone by the early universe, and supergravities theories in a dS space have also been connected to a conformal field theory (CFT) in the boundary of the space, through the dS/CFT duality conjecture of Strominger.

Both the de Sitter and anti-de Sitter spacetimes allow the existence of spherically symmetric black hole solutions that are the direct counterparts of the asymptotically flat Schwarzschild, Reissner-

Nordström, Kerr and Kerr-Newman black holes, and in chapter 5 we will make a brief comparison between these black holes in the $\Lambda < 0$, $\Lambda = 0$ and $\Lambda > 0$ backgrounds. In this aspect, the AdS spacetime has a richer structure than the other two. Indeed, the 4-dimensional AdS background also allows black holes with a non-spherical topology. This has been an unexpected result since a topological theorem of Hawking [5] states that if the spacetime is asymptotically flat and globally hyperbolic, and the dominant energy condition holds, then the topology of the black holes must be spherical. At the time of its formulation, this theorem was supported by the spherical topology of the know black holes. The reason why in the AdS background one can have black holes with non-spherical horizons is obviously due to the presence of a negative Λ. So, besides the spherical solutions, the AdS case allows two other families of solutions, namely, solutions with cylindrical, toroidal, or planar topology [6]-[10], and solutions with hyperbolic topology [11] (these are usually called topological).

The first non-spherical AdS black hole, that we will discuss in chapter 5, has been found by Lemos [6]. These solutions have a planar symmetry, i.e., they include black holes with cylindrical, toroidal, and planar horizons, and can be formed through gravitational collapse as shown by Lemos [12]. The interest on these spacetimes, and in AdS in general, relies also in the fact that they can be used to test the cosmic censorship and hoop conjectures. Indeed, as shown in [12], (i) spherical collapse with $\Lambda < 0$ may lead to massless naked singularities (in contradiction with the cosmic censorship conjecture), (ii) cylindrical, toroidal or planar collapse with $\Lambda < 0$ does not produce naked singularities (in accordance with the cosmic censorship conjecture), and (iii) cylindrical, toroidal or planar collapse with $\Lambda < 0$ leads to the formation of the black holes with cylindrical, toroidal, and planar horizons found in [6], which gives a clear counter-example to the hoop conjecture. Static and rotating electric charged black holes that are the electric counterparts of the black holes found in [13] have been obtained by Lemos and Zanchin [7], and magnetic solutions with cylindrical or toroidal topology have been constructed by Dias, and Lemos [8] (see chapter 5).

1.2   Black holes in 3-dimensional spacetimes

1.2.1   Exact solutions

Einstein gravity in a 3-dimensional background has some unusual features that clearly differentiate it from the 4-dimensional Einstein gravity (see Gott and Alpert [14], Giddings, Abbot and Kuchař [15], Deser, Jackiw and t' Hooft [16], and Barrow, Burd and Lancaster [17]). Any vacuum solution with $\Lambda = 0$ is flat, and any vacuum solution with non-vanishing cosmological constant has constant curvature. This follows from the fact that the Weyl tensor in 3 dimensions is identically zero. The 3-dimensional spacetime has no local degrees of freedom, and thus its dynamics is substantially different from the one of the 4-dimensional case. In particular, there are no gravitational waves, and no gravitons. Moreover, there is no Newtonian limit, that is, there is no gravitational force between masses. Note, however, that the absence of gravitational dynamics in general relativity by no way means that 3-dimensional spacetimes are trivial and out of interest. Indeed, as we shall discuss, one can study solutions generated by point sources, one can construct a time machine, and one can build a topological black hole solution. Furthermore, quantization of the gravitational field has been attempted with some successes in a 3-dimensional background.

• *Spacetimes generated by point sources in 3-dimensions*

The issue of spacetimes generated by point sources (no event horizon) in 3-dimensional Einstein theory has been object of many studies (for reviews see [19, 20, 18]). These sources can be viewed as normal sections of straight cosmic strings. In 1963, Staruszkiewicz [21] has begun the analysis of 3-dimensional Einstein gravity without cosmological constant ($\Lambda = 0$) coupled to a static massive point source. The corresponding space has a conical geometry, i.e., it is everywhere flat except at the location of the point source. The space can be obtained from the Minkoswki space by suppressing a wedge and identifying its edges. The wedge has an opening angle which turns to be proportional to the source mass. Deser, Jackiw and t' Hooft [16] have generalized the analysis of [21] in order

to find the spacetime solutions generated by an arbitrary number of static massive point sources. These static multi-source solutions are possible because of the absence of gravitational interaction in 3-dimensional general relativity. Once more the geometry is conical with a wedge angle suppressed at each source proportional to its mass. They have also constructed the solution corresponding to a massless spinning point source in 3-dimensional Einstein gravity with $\Lambda = 0$. The extension to include massive spinning sources has been achieved by Clément [22]. Their results indicate that (besides the conical geometry already present in the spinless case) the spacetime can be seen as characterized by a helical structure since a complete loop around the source ends with a shift in time proportional to the angular momentum. In the context of Einstein-Maxwell theory but still with $\Lambda = 0$, Deser and Mazur [23] and Gott, Simon and Alpert [24] have found the solutions produced by electric charged point sources. These spacetimes once more have a conical geometry with a helical structure. Due to the slow fall off of the electric field in 3-dimensions, the system has infinite total energy. That is, asymptotically the electric field goes as $\frac{1}{r}$ (while in 4-dimensions it falls as $\frac{1}{r^2}$), the energy density behaves as $\frac{1}{r^2}$ (while in 4-dimensions it goes as $\frac{1}{r^4}$), and therefore the spatial integral of the electric field diverges not only at the origin but also at infinity. Static charged multi-source solutions are not possible because, due the absence of gravitational interaction, the electric repulsion cannot be balanced by a gravitational attraction. Barrow, Burd and Lancaster [17] found the horizonless spacetime generated by a magnetic charged point source in a $\Lambda = 0$ background. Melvin [25] also describes the exterior solution of electric and magnetic stars in the above theory. 3-dimensional static spacetimes generated by open or closed one-dimensional string sources with or without tension (in a $\Lambda = 0$ background) have been constructed by Deser and Jackiw [26]. The extension to the rotating string source has been done by Grignani and Lee [27] and by Clément [28]. Other exact solutions in 3-dimensional Einstein gravity theory produced by extended and stationary sources have been found by Menotti and Seminara [29].

The spacetimes generated by point sources in 3-dimensional Einstein gravity with non-vanishing cosmological constant ($\Lambda \neq 0$) have been obtained by Deser and Jackiw [30] and by Brown and Henneaux [31]. In the de Sitter case ($\Lambda > 0$) there is no one-particle solution. The simplest solution describes a pair of antipodal particles on a sphere with a wedge removed between poles and with points on its great circle boundaries identified. In the anti-de Sitter case ($\Lambda < 0$), the simplest solution describes a hyperboloid with a wedge removed proportional to the source mass located at the vertex of the wedge.

- *Time machines in 3-dimensional spacetimes*

In a clear example of the richness of 3-dimensional Einstein gravity, Gott [32], in 1991, has shown that it is possible to construct a time machine (see also Cutler [33]), i.e., a solution that allows the existence of closed timelike curves (regions that violate causality and that allow an observer to travel backwards in time). All that is needed is two particles in a flat background passing through each other with a velocity greater than a certain critical value, that is related with the deficit angle (discussed above) associated with the particles. However, Deser, Jackiw and t' Hooft [16], and Carrol, Fahri and Guth [34] soon proved that Gott's construction was tachyonic, i.e., the mass system that leads to the appearance of closed timelike curves corresponds to an effective mass travelling faster than light. Moreover, Carrol, Fahri, Guth and Olum [35], and Menotti and Seminara [36] have shown that the total momentum of Gott universe is spacelike. Holst [37] has constructed the AdS analogue of Gott universe, and concluded that it still is tachyonic. Moreover, for closed universes, t'Hooft [38] has shown that if one starts with a spacetime without closed timelike curves and tries to insert them through Gott's construction, then the universe will always collapse before they have an opportunity to appear. Thus, the analysis of 3-dimensional Einstein gravity has been important to show that nature prevents the creation of time machines.

- *Black holes in 3-dimensional Einstein gravity*

In what concerns black hole solutions in 3-dimensional Einstein gravity, quite surprisingly (since the 3-dimensional spacetime is quite poor at the dynamical level), Bañados, Teitelboim and Zanelli [39] have found a black hole solution (the BTZ black hole), with mass and angular momentum, that is asymptotically AdS. The existence of this black hole gets even more remarkable when one realizes that the BTZ metric has constant curvature and thus there can be no curvature singularity at the origin. As discussed in detail by Bañados, Henneaux, Teitelboim, and Zanelli [40], the BTZ black hole can be expressed as a topological quotient of AdS_3 by a group of isometries. This is, the BTZ black hole can be obtained through identifications along an isometry of the AdS_3 spacetime, and in order to avoid closed timelike curves, the origin must be a topological singularity (a boundary of the spacetime). Qualitatively, the reason why the black hole exists only in an AdS background can be understood as follows. The radius of an event horizon (r_+) in a D-dimensional spacetime is expected to be proportional to $G_D M$, where G_D is the D-dimensional Newton's constant. Now, in mass units G_D has dimension M^{2-D}. Thus, $G_D M$ (and r_+) is dimensionless in $D = 3$, and there is no length scale in $D = 3$. The cosmological constant provides this length scale for the horizon, but only when $\Lambda < 0$ (AdS case). One may argue that this is due to the fact that the AdS background is attractive, i.e., an analysis of the geodesic equations indicates that particles in this background are subjected to a potential well that attracts them (and so it is possible to concentrate matter into a small region), while the dS background is repulsive (in practice, if we try to construct a dS black hole through identifications along an isometry of the dS_3 spacetime, we verify that the possible horizon is inside the region that contains closed timelike curves). In many ways, the BTZ black hole has properties similar to the ones of the 4-dimensional black holes. For example, it has an event horizon and, in the rotating case, it has an inner horizon and the angular momentum has a maximum bound. It can also be formed through the collapse of matter as shown by Mann and Ross [41]. Matschull [42], Holst and Matschull [43], and Birmingham and Sen [44] have shown that the BTZ black hole can be created when two point particles with sufficient energy collide in the AdS background. We must however be careful with some clear differences that exist between the BTZ black hole and the 4-dimensional black holes, specially in what concerns thermodynamic properties (see Carlip and Teitelboim [45]). Indeed, the temperature of the BTZ black hole goes as $T_{\mathrm{BTZ}} \sim \sqrt{M}$ and tends to zero when M decreases. The BTZ black hole then has positive heat capacity, and complete evaporation of it takes an infinite amount of time. Stellar equilibrium in 3-dimensions has been discussed by Cruz and Zanelli [46], and by Lubo, Rooman and Spindel [47].

The extension to include a radial electric field in the BTZ black hole has been done by Clément [48] and Martínez, Teitelboim and Zanelli [49] (this solution reduces to those of [23, 24] when $\Lambda = 0$). Again, due to the slow fall off of the electric field in 3-dimensions, the system has infinite total energy. The presence of the electric energy-momentum tensor implies that the spacetime has no longer constant curvature, and the electric BTZ black hole cannot be expressed as a topological quotient of AdS_3 by a group of isometries. The rotating charged black hole is generated from the static charged solution (already found in [39]) through the application of a rotation Lorentz boost. A BTZ solution with an azimuthal electric field was found by Cataldo [50]. This solution is horizonless, and reduces to empty AdS_3 spacetime when the charge vanishes. Pure magnetic solutions with $\Lambda < 0$, that reduce to the neutral BTZ black hole solution when the magnetic source vanishes, also exist. Notice that, in oppose to what occurs in 4-dimensions where the the Maxwell tensor and its dual are 2-forms, in 3-dimensions the Maxwell tensor is still a 2-form, but its dual is a 1-form (in practice, the Maxwell tensor has only three independent components: two for the electric vector field, and one for the scalar magnetic field). As a consequence, the magnetic solutions are radically different from the electric solutions in 3-dimensions. The static magnetic solution has been found by Clément [48], Hirschmann and Welch [51] and Cataldo and Salgado [52]. This spacetime generated by a static magnetic point source is horizonless and has a conical singularity at the origin. The extension to include rotation and a new interpretation for the source of magnetic field has been made by Dias and Lemos [53]. Other black hole solutions of 3-dimensional Einstein-Maxwell theory have also been found by Kamata and Koikawa [54, 55], Cataldo and Salgado [56] and Chan [57], assuming self dual or anti-self dual conditions between the electromagnetic fields. In chapter

2 we will analyze in detail the BTZ family of solutions, with a special focus on the topological construction leading to the rotating massive BTZ black hole, and on the magnetic BTZ solution.

- *Other 3-dimensional gravities and their black holes*

In order to turn the 3-dimensional dynamics more similar with the realistic 4-dimensional one, we can manage a way by which we introduce local degrees of freedom. This is done by coupling an extra field to the Einstein general relativity. One way to do this, as proposed by Deser, Jackiw and Templeton [58] in 1982, is to add a Chern-Simmons term yielding an alternative theory to Einstein gravity called topological massive gravity. The new term appears as a counterterm in the renormalization of quantum field theory in a 3-dimensional gravitational background [59]. The attractive interaction between masses is Yukawa-like, and is mediated by a massive scalar graviton. This theory is perturbatively renormalizable [60]. Spacetimes generated by point sources in this theory have been obtained by Carlip [61], by Gerbert [62], and by Deser and Steif [63]. Clément [64], Fernando and Mansouri [65] and Dereli and Obukhov [66] have analyzed self-dual solutions for the Einstein-Maxwell-Chern-Simons theory in 3-dimensions.

Another generalization can be obtained by coupling a scalar field to Einstein gravity, yielding a so called dilaton gravity. The most general form of this kind of gravity was proposed by Wagoner [67] in 1970. The scalar field provides a local dynamical degree of freedom to the theory, and models of this kind (i.e., under certain choices of the parameters) appear naturally in string theory. Some choices of the parameters of the theory yield dilaton gravities that have black hole solutions. One of these theories, that we will study in this thesis, is an Einstein-dilaton gravity of the Brans-Dicke type in a $\Lambda < 0$ background, first discussed by Lemos [6]. This theory is specified by a Brans-Dicke parameter, ω, and contains seven different cases. Each ω can be viewed as yielding a different dilaton gravity theory, with some of these being related with other known special theories. For instance, for $\omega = -1$ one gets the simplest low-energy string action [68], and for $\omega = 0$ one gets a theory related (through dimensional reduction) to 4-dimensional general relativity with one Killing vector [6, 7, 8]. This is, the $\omega = 0$ black holes are the direct counterparts of the 4-dimensional AdS black holes with toroidal or cylindrical topology first discussed by Lemos, in the same way that a point source in 3-dimensions is the direct cousin of a cosmic string in 4-dimensions. For $\omega = \pm\infty$ the theory reduces to the pure 3-dimensional general relativity. This is, the $\omega = \pm\infty$ black holes are the BTZ ones. Moreover, the case $\omega > -1$ yields gravities whose black holes have a structure and properties similar to the BTZ black hole, but with a feature that might be useful: the $\omega > -1$ black holes have dynamical degrees of freedom, which implies for example that the origin has a curvature singularity and that gravitational waves can propagate in the spacetime. The neutral black holes of this Brans-Dicke theory were found and analyzed by Sá, Kleber and Lemos [69, 70]. The pure electric charged black holes have been analysed by Dias and Lemos [71], and the pure magnetic solutions have been discussed by Dias and Lemos [72]. We will analyze in detail these black holes in chapter 3. Other examples of dilaton black holes include the electric black hole solutions of Chan and Mann [73], the self dual solutions of Fernando [74], the magnetic solutions of Kiem and Park [75], Park and Kim [76] and Koikawa, Maki and Nakamula [77], and the solutions found by Chen [78]. For a detailed discussion on classical and quantum aspects of 3-dimensional gravity we refer the reader to Carlip's book [79], Jackiw's book [19], Brown's book [20], and to the reviews [80].

1.2.2   Pair creation of black holes in 3-dimensions

In chapters 9 and 11 we will analyze in detail the pair creation process of 4-dimensional black holes and of higher dimensional black holes, respectively. The process of quantum pair creation of black holes in an external field in a 3-dimensional background has not been analyzed yet, as far as we know. In chapter 4, we will try to understand the difficulties associated with this issue, and we will also propose a possible background in which the pair creation process in 3-dimensions might be analyzed.

1.3 Black holes in 4-dimensional spacetimes

1.3.1 Exact single black hole solutions

In a 4-dimensional asymptotically flat background there four well-known solutions that represent a single black hole, namely the Schwarzschild black hole ($M \neq 0$, $Q = 0$, $J = 0$), the Reissner-Nordström black hole ($M \neq 0$, $Q \neq 0$, $J = 0$), the Kerr black hole ($M \neq 0$, $Q = 0$, $J \neq 0$) and the Kerr-Newman black hole ($M \neq 0$, $Q \neq 0$, $J \neq 0$). In an asymptotically AdS or dS background the above solutions are also present, and in the AdS case there are also black hole solutions with non-spherical topology (see the end of section 1.1). In this thesis we will deal essentially with the static solutions. For a review on some of the properties of these black holes see, e.g., chapter 5 of this thesis.

1.3.2 Pair of accelerated black holes: the C-metric and the Ernst solution

In 4-dimensional spacetime the Einstein equation (in vacuum or in the presence of matter fields) allow a wide variety of solutions and, in particular, of black hole solutions, as displayed in [81]. The main difficulty is then the appropriate physical interpretation of these solutions, with many of them being left apparently without known physical interest. One of the best examples of this statement is the C-metric solution, found by Levi-Civita [82] and by Weyl [83] in 1918-1919, that has been interpreted only fifty years after its discovery by Kinnersley and Walker [84], although some works during this gap period have dealt with it. From this solution one can construct another exact solution known as Ernst solution [85]. The C-metric and the Ernst solution describe two uniformly accelerated black holes in opposite directions, and the acceleration source is perfectly identified. We can better understand these solutions going back to the pair of oppositely charged particles (without a horizon) that are created in the Schwinger process, and then describe an uniformly accelerated hyperbolic motion approaching asymptotically the velocity of light. This accelerated 2-particle system is represented in Fig. 1.3, which is simply an extension to negative values of t of the $ct - x$ plane of Fig. 1.2. During the negative time the two particles approach each other until they come at rest at $t = 0$, and then they reverse their motion driving away from each other. In Fig. 1.4.(a), one represents schematically the C-metric. To construct it, each particle of Fig. 1.2 has been replaced by a black hole with its horizons (h_- and $h+$) that describes a hyperbolic motion due to the string tension, T. When the black holes are charged, their acceleration can also be furnished by an external electromagnetic field, and this solution is exactly described by the Ernst solution. The schematic figure representing this last solution is sketched in Fig. 1.4.(b).

It is important to note that the C-metric and the Ernst solution are one of the few exact solutions that contain already a radiative term. This means, being accelerated, the black holes necessarily release radiation and the information concerning the radiative properties are already included in the metrics that describe these solutions. Moreover, as we shall discuss in subsection 1.3.3 these solutions also describe appropriately the quantum process of black hole pair creation in an external field and the consequent motion of the created pair.
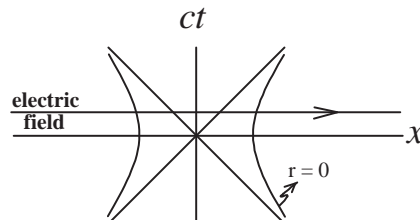
Figure 1.3: Two oppositely charged particles without a horizon describe an uniformly accelerated hyperbolic motion, approaching asymptotically the velocity of light. This figure is simply an extension to negative values of t of the $ct - x$ plane of Fig. 1.2.

C-metric

Ernst solution

(a)

(b)
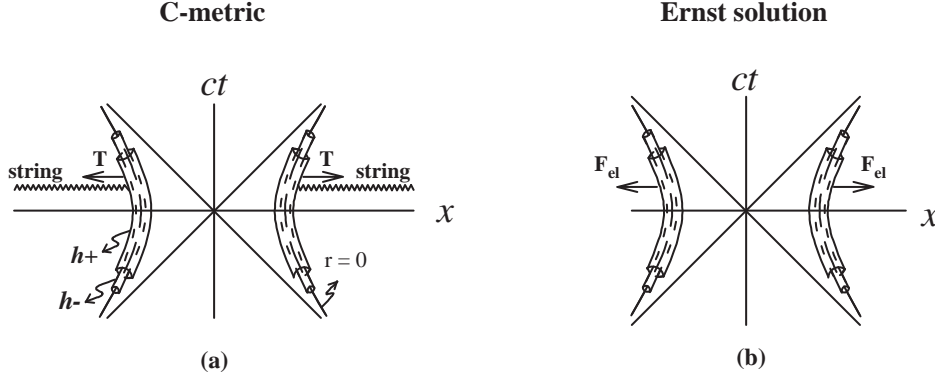
Figure 1.4: (a) Schematic figure representing the C-metric, i.e., two black holes with their horizons (h_- and $h+$) that describe a hyperbolic motion due to the strings tension, T. The string is represented by the zigzag line. Instead of the strings, we could alternatively have a single strut in between the black holes with its outward tension providing the acceleration. (b) When the black holes are charged, their acceleration can also be furnished by the electromagnetic force F_{el}, and this solution is exactly described by the Ernst solution.

The extension of the Levi-Civita$-$Weyl solution [82, 83] to the $\Lambda \neq 0$ case has been done by Plebański and Demiański [86] in 1976. In this thesis (see chapter 6), we analyze in detail the properties, and physical interpretation of the C-metric in an AdS background [87], and in a dS background [88]. We have thus extended for the cosmological constant case the physical interpretation of the flat case [84]. In particular we have concluded that while the flat C-metric and dS C-metric describe a pair of accelerated black holes with any acceleration, the AdS C-metric only describes a pair of accelerated black holes if their acceleration satisfies $A > \sqrt{|\Lambda|/3}$. We can interpret this as due to the fact that the AdS background is attractive, i.e., an analysis of the geodesic equations indicates that particles in this background are subjected to a potential well that attracts them. Therefore, if we want to have a pair of black holes accelerating apart, we will have to furnish a sufficient force that overcomes this cosmological constant background attraction. We then expect that a pair of accelerated black holes is possible only if acceleration A is higher than a critical value. Our analysis in [87, 88] is essentially based on the geometric description of the solution in the cosmological constant 4-hyperboloid embedded in a 5-dimensional Minkowski spacetime, and on the study of the causal structure of the solution (Carter-Penrose diagrams). The information provided by the geometric description of the C-metric on the 4-hyperboloid is displayed in Fig. 1.5. More precisely, in Fig. 1.5.(a), the dS spacetime is represented by the 4-hyperboloid $-(z^0)^2 + (z^1)^2 + (z^2)^2 + (z^3)^2 + (z^4)^2 = \ell^2$ ($\ell = \sqrt{3/\Lambda}$) embedded in a 5-dimensional Minkowski spacetime. The directions z^2 and z^3 are suppressed, z_0 is a time coordinate, and z^1 and z^2 are space coordinates. In the pure dS spacetime (acceleration $A = 0$), its origin describes the two hyperbolic trajectories that result from the intersection of the hyperboloid surface with the $z^4 = 0$ plane. Basically, this indicates that the dS solution already represents two black holes being accelerated by the cosmological constant. In the dS C-metric case ($A \neq 0$), its origin describes the two hyperbolic lines lying on the dS hyperboloid that result from the intersection of the hyperboloid surface with the z^4=constant$< \ell$ plane. This indicates that the solution represents two black holes being accelerated by the cosmological constant and, in addition, by the string tension that provides the extra acceleration A. In Fig. 1.5.(b), the AdS spacetime ($A = 0$) is represented by the 4-hyperboloid $-(z^0)^2 + (z^1)^2 + (z^2)^2 + (z^3)^2 - (z^4)^2 = -\ell^2$ ($\ell = \sqrt{3/|\Lambda|}$) embedded in a 5-dimensional Minkowski spacetime, but this time with two timelike coordinates, z^0 and z^4. If $A < 1/\ell$, see Fig. 1.5.(b.i), the origin of the AdS C-metric moves in the hyperboloid along the circle with z^1=constant< 0. When $A = 0$ this circle is at the plane $z^1 = 0$ and has a radius ℓ. In both cases this indicates that we have a single black hole. If $A > 1/\ell$, see Fig. 1.5.(b.ii), the origin of the AdS C-metric moves along the two hyperbolic lines, that result from the intersection of the hyperboloid surface with the z^4=constant$> \ell$ plane. These hyperbolic lines indicate that in this

case the solution represents two black holes being accelerated.
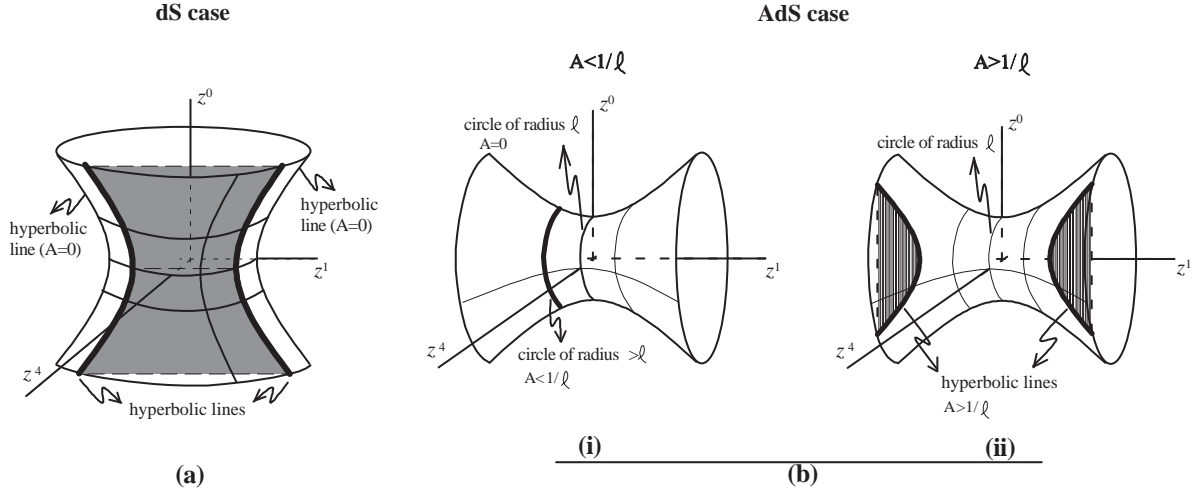
Figure 1.5: (a) The dS spacetime can be represented as a 4-hyperboloid, $-(z^0)^2 + (z^1)^2 + (z^2)^2 + (z^3)^2 + (z^4)^2 = \ell^2$ ($\ell = \sqrt{3/\Lambda}$), embedded in a 5-dimensional Minkowski spacetime with one timelike coordinate, z^0. The origin of the dS C-metric describes the two hyperbolic trajectories. This indicates that the solution represents two black holes being accelerated apart. (b) The AdS spacetime can also be represented as a 4-hyperboloid, $-(z^0)^2 + (z^1)^2 + (z^2)^2 + (z^3)^2 - (z^4)^2 = -\ell^2$ ($\ell = \sqrt{3/|\Lambda|}$), embedded in a 5-dimensional Minkowski spacetime, but this time with two timelike coordinates, z^0 and z^4. (i) If $A < 1/\ell$ the origin of the AdS C-metric moves in the hyperboloid along a circle. This indicates that we have a single black hole. (ii) If $A > 1/\ell$ the origin of the AdS C-metric moves along the two hyperbolic lines. These hyperbolic lines indicate that the solution represents two black holes being accelerated apart.

An example of the information provided by the Carter-Penrose diagrams of the C-metric, that leads to the physical interpretation given to the C-metric, is schematically displayed in Fig. 1.6. More precisely, in Fig. 1.6.(a), we show again two particles describing an uniformly accelerated hyperbolic motion. In Fig. 1.6.(b), the dashed lines represent the two particles, and each one of these is now replaced by a black hole represented here by its Carter-Penrose diagram, which was sketched before in Fig. 1.1. Finally, in Fig. 1.6.(c), the result of this operation is shown. It yields the Carter-Penrose diagram of the C-metric, where one identifies two accelerated black holes approaching asymptotically the velocity of light, i.e., two black holes separated by an acceleration horizon, r_A.
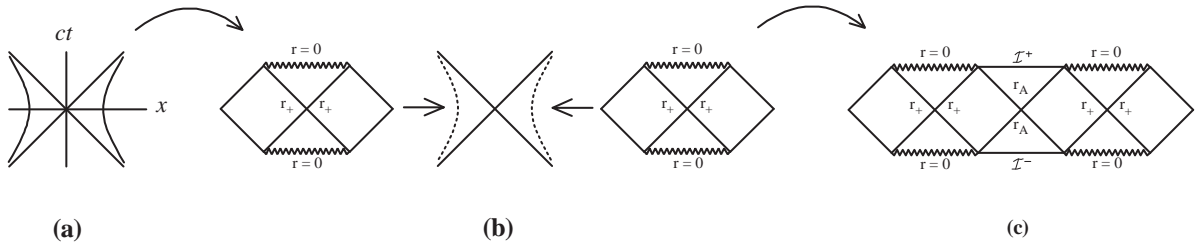
Figure 1.6: Schematic operation leading to the Carter-Penrose diagram of the C-metric, where one identifies two accelerated black holes approaching asymptotically the velocity of light, i.e., two black holes separated by an acceleration horizon, r_A.

At this point, a remark is relevant. Israel and Khan [90] have found a $\Lambda = 0$ solution that represents two (or more) collinear Schwarzschild black holes interacting with each other in such a way that allows dynamical equilibrium. In this solution, the two black holes are connected by a

strut that exerts an outward pressure which cancels the inward gravitational attraction, and so the distance between the two black holes remains fixed, and they are held in equilibrium (see also Bach and Weyl [91], Aryal, Ford and Vilenkin [92], and Costa and Perry [93]). Now, the flat C-metric solution reduces to a single non-accelerated black hole free of struts or strings when the acceleration parameter A vanishes. Thus, when we take the limit $A = 0$, the flat C-metric does not reduce to the static solution of Israel and Khan. The reason for this behavior can be found in the causal diagrams of the two solutions (see Fig. 1.7).
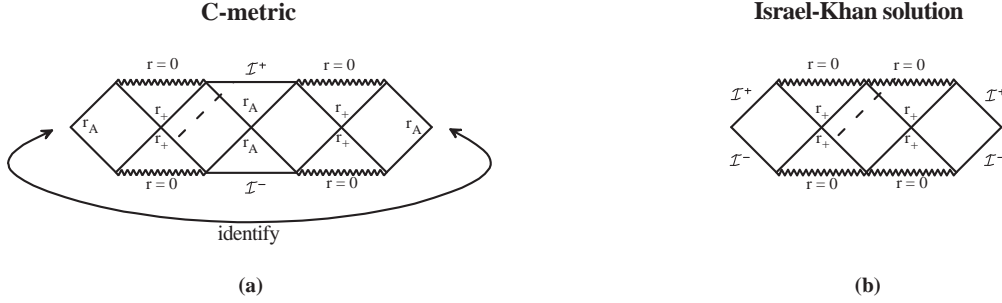
Figure 1.7: Carter-Penrose diagram of the C-metric and of the Israel-Khan solution along the direction that connects the two black holes. The dashed line represents a null ray that is sent from the vicinity of the event horizon of one of the black holes towards the other black hole. (a) In the case of the C-metric this ray can never reach the other black. Thus, there is no gravitational interaction between the black holes. (b) In the Israel-Khan solution the null ray can reach the second black hole, and so they attract each other gravitationally. In this solution, the two black holes are connected by a strut that exerts an outward pressure which cancels the inward gravitational attraction, and so the distance between the two black holes remains fixed.

In particular, the black holes described by the C-metric do not interact gravitationally. Their acceleration is provided only by the tension of the strings or of the strut, without opposition from gravitational attraction. A similar discussion applies in an external background field. Indeed, Tomimatsu [94] has found a solution, that is the charged counterpart of the neutral Israel-Khan solution [90], in which two Reissner-Nordtröm black holes are held in equilibrium. In this case the gravitational attraction between the black holes is cancelled by the electric repulsion, and this occurs only when the black holes are extreme, $M_i = Q_i$. Tomimatsu has generalized for the black hole case, the relativistic treatment used by Bonnor [95] and Ohta and Kimura [96] to study the equilibrium system of two charged particles. The Ernst solution does not reduce to [94] when $A = 0$, once again because there is no gravitational force between the two Reissner-Nordtröm black holes.

Now, an exact solution that exists in a dS background is the Nariai solution, which can be connected with the near-extreme Schwarzschild-dS solution by taking an appropriate extremal limit introduced by Ginsparg and Perry [97]. Following the procedure of [97], we have further generated new solutions [89] that are the C-metric counterparts of the already known Nariai, Bertotti-Robinson and anti-Nariai solutions. These solutions are conformal to the direct topological product of two 2-dimensional manifolds of constant curvature. We also give a physical interpretation to these solutions, e.g., in the Nariai C-metric (with topology $dS_2 \times \tilde{S}^2$) to each point in the deformed 2-sphere $\tilde{S}^2$ corresponds a dS_2 spacetime, except for one point which corresponds a dS_2 spacetime with an infinite straight strut or string. It is unstable and decays into a slightly non-extreme black hole pair accelerated by a strut or by strings.

In what follows we give a historical overview on the C-metric, Ernst solution and Nariai, Bertotti-Robinson and anti-Nariai solutions. But first we give a brief description of the properties of strings, struts and domain walls.

• *Strings, struts and domain walls*

We have already made reference (and we will do it again) to gravitational objects other than black holes, namely strings/struts and domain walls. Here we briefly comment on their main properties. We work at the level of the Newtonian limit, but the full general relativity analysis yields the same result.

Consider a static distribution of matter with an energy-momentum tensor given by $T^\mu_\nu = \text{diag}(\rho, p_1, p_2, p_3)$, where $\rho = T^0_0$ is the mass density of the system and $p_i = T_i$ are the pressures along the three directions. The Newtonian limit of Einstein equations for this distribution is given by $\nabla^2 \Phi = 4\pi G(\rho - T^i_i)$, where Φ is the gravitational potential. For non-relativistic matter, $p_i \ll \rho$, and we recover the classical Poisson equation, $\nabla^2 \Phi = 4\pi G\rho$. For a straight string along the z-axis one has $p_3 = -\rho$ and $p_1 = 0$ and $p_2 = 0$, and thus one gets $\nabla^2 \Phi = 0$. So, a straight string produces no gravitational potential in its vicinity, and suffers a tension along the z-axis that points inward. A general relativity analysis carried by Vilenkin [98], and by Ipser and Sikivie [99] shows that the geometry around the straight string is conical, i.e., it can be obtained from the Minkoswki space by suppressing a wedge (with a deficit angle proportional to the line mass density, $\delta = 8\pi G\rho$) and identifying its edges. So its line element is equal to the Minkowski one but the angle in the plane normal to the string varies in the range $0 \le \phi < 2\pi - \delta$ [see Fig. 1.8.(a)]. A straight strut has similar properties, the only difference being the fact that its line mass density is negative and its tension along the z-axis points outward. Thus, instead of a deficit angle ($\delta < 0$), it produces an excess angle ($\delta > 0$) [see Fig. 1.8.(b)].

In what concerns a domain wall, its properties are much different from those of an usual massive wall. Indeed, a domain wall lying in the yz-plane has a wall tension in the y and z directions that is equal to the surface mass density of the domain wall, $p_1 = 0$ and $p_2 = p_3 = \rho$. Its Newtonian limit is $\nabla^2 \Phi = -4\pi G\rho$ and thus it produces a repulsive gravitational field. The general relativity analysis [98, 99] confirms these properties.
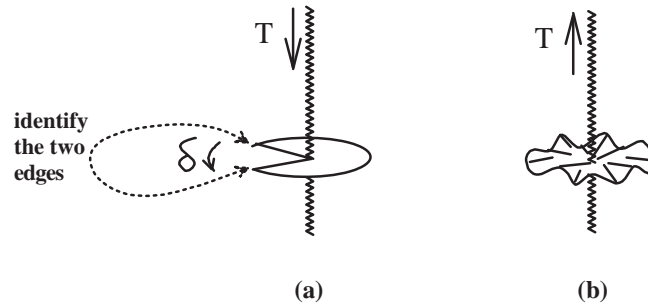
Figure 1.8: (a) Schematic representation of a string (positive mass density, $\rho > 0$) with its tension that points inward, $T = -\rho$, and its deficit angle $\delta > 0$. The two edges are identified, so a complete loop around a plane normal to it yields $\Delta\phi = 2\pi - \delta < 2\pi$. (b) Schematic representation of a strut (negative mass density, $\rho < 0$) with its tension that points outwards, $T = -\rho$, and its excess angle $\delta < 0$. A complete loop around a plane normal to it yields $\Delta\phi = 2\pi - \delta > 2\pi$.

• *Historical overview on the C-metric and on the Ernst solution*

The original C-metric has been found Levi-Civita [82] and by Weyl [83] in 1918-1919. During the following decades, many authors have rediscovered it and studied its mathematical properties (see [81] for references). In 1963 Ehlers and Kundt [100] have classified degenerated static vacuum fields and put this Levi-Civita solution into the C slot of the table they constructed. From then onwards this solution has been called C-metric. This spacetime is stationary, axially symmetric, Petrov type D, and is an exact solution which includes a radiative term. Although the C-metric had been studied from a mathematical point of view along the years, its physical interpretation remained unknown until 1970 when Kinnersley and Walker [84], in a pathbreaking work, have shown that the solution describes two uniformly accelerated black holes in opposite directions. Indeed, they noticed

that the original solution was geodesically incomplete, and by defining new suitable coordinates they have analytically extended it and studied its causal structure. The solution has a conical singularity in one of its angular poles that was interpreted by them as due to the presence of a strut in between pushing the black holes away, or as two strings from infinity pulling in each one of the black holes. The strut or the strings lie along the symmetry axis and cause the acceleration of the black hole pair. This work also included for the first time the charged version of the C-metric. In an important development, Ernst in 1976 [85], through the employment of an appropriate transformation, has removed all the conical singularities of the charged C-metric by appending an external electromagnetic field (the magnetic solution is written in [85], while the explicit electric solution can be found in Brown [101]). Asymptotically, the Ernst solution reduces to the Melvin universe [102]. In the Ernst solution the acceleration of the pair of oppositely charged black holes is provided by the Lorentz force associated to the external field. The geometrical properties of the C-metric were further investigated by Farhoosh and Zimmerman [103], and the asymptotic properties of the C-metric were analyzed by Ashtekar and Dray [104] who have shown that null infinity admits a conformal completion, has a spherical section, and moreover that the causal diagrams drawn in [84] were not quite accurate. The issue of physical interpretation of the C-metric has been recovered by Bonnor [105], but now following a different approach. He transformed the C-metric into the Weyl form in which the solution represents a finite line source (that corresponds to the horizon of the black hole), a semi-infinite line mass (corresponding to a horizon associated with uniform accelerated motion) and a strut keeping the line sources apart. By applying a further transformation that enlarges this solution, Bonnor confirmed the physical interpretation given in [84]. Bonnor's procedure has been simplified by Cornish and Uttley and extended to include the massive charged solution [106]. More recently, Yongcheng [107], starting from the metric of two superposed Schwarzschild black holes, has derived the C-metric under appropriate conditions. The black hole uniqueness theorem for the C-metric has been proven by Wells [108] and the geodesic structure of the C-metric has been studied by Pravda and Pravdova [109]. The limit when the acceleration goes to infinity has been analyzed by Podolský and Griffiths [110] who have shown that in this limit the solution is analogous to the one which describes a spherical impulsive gravitational wave generated by a snapping string. We note that the C-metric is an important and explicit example of a general class of asymptotically flat radiative spacetimes with boost-rotation symmetry and with hypersurface orthogonal axial and boost Killing vectors. The geometric properties of this general class of spacetimes have been investigated by Bičák and Schmidt [111] and the radiative features were analyzed by Bičák [112] (see the recent review of Pravda and Pravdova [113] on this class of spacetimes and the role of the C-metric).

Relevant generalizations to the C-metric were made by Plebański and Demiański in 1976 [86] and by Dowker, Gauntlett, Kastor and Traschen in 1994 [114]. Plebański and Demiański, in addition to the mass (m) and electromagnetic charge (q), have included into the solution a NUT parameter, a rotation and a cosmological constant term (Λ), and Dowker et al have further included a dilaton field non-minimally coupled. Thus, the most general C-metric has eight parameters, so far, namely, acceleration, mass, electric and magnetic charges, NUT parameter, rotation, cosmological constant and dilaton field. The C-metric with mass and electromagnetic charges alone have been extensively studied as shown above, and from now on we will refer to it as the flat C-metric (i.e., C-metric with $\Lambda = 0$). The C-metric with a NUT parameter has not been studied, as far as we know. The flat spinning C-metric has been studied by Farhoosh and Zimmerman [115], Letelier and Oliveira [116] and by Bičák and Pravda [117]. In particular, in [117] the flat spinning C-metric has been transformed into the Weyl form and interpreted as two uniformly accelerated spinning black holes connected by a strut. This solution constitutes an example of a spacetime with an axial and boost Killing vectors which are not hypersurface orthogonal. Dowker et al generalized the flat C-metric and flat Ernst solution to include a dilaton field and applied these solutions for the first time in the context of quantum pair creation of black holes, that once created accelerate apart. Dowker and Thambyahpillai [118] have found a C-metric family that describes multi-black holes being accelerated apart, and Hong and Teo [272] have rewritten the C-metric in a new form that,

among other advantages, facilitates the computations that deal with the C-metric.

Our contribution in this field is related with the physical interpretation of the cosmological constant C-metric introduced by Plebański and Demiański [86]. The de Sitter (dS) case ($\Lambda > 0$) has been analyzed by Podolský and Griffiths [120], and discussed in detail by Dias and Lemos [88]. The anti-de Sitter (AdS) case ($\Lambda < 0$) has been studied, in special instances, by Emparan, Horowitz and Myers [121] and by Podolský [122], and in its most general case by Dias and Lemos [87]. In general the C-metric (either flat, dS or AdS) describes a pair of accelerated black holes. Indeed, in the flat and dS backgrounds this is always the case. However, in an AdS background the situation is not so simple and depends on the relation between the acceleration A of the black holes and the cosmological length $\ell = \sqrt{3/|\Lambda|}$. One can divide the AdS study into three cases, namely, $A < 1/\ell$, $A = 1/\ell$ and $A > 1/\ell$. The $A < 1/\ell$ case was the one analyzed by Podolský [122], and the $A = 1/\ell$ case has been investigated by Emparan, Horowitz and Myers [121], which has acquired an important role since the authors have shown that, in the context of a lower dimensional Randall-Sundrum model, it describes the final state of gravitational collapse on the brane-world. The geodesic structure of this solution has been studied by Chamblin [123]. Both cases, $A < 1/\ell$ and $A = 1/\ell$, represent one single accelerated black hole. The $A > 1/\ell$ AdS C-metric describes a pair of accelerated black holes in an AdS background. The analysis performed in [87, 88] was supported on a thorough analysis of the causal structure of the solution, together with the description of the solution in the 4-hyperboloid that describe the AdS and dS solutions, and with the study of the physics of the strut or string. When the acceleration is zero the C-metric in any cosmological constant background reduces to a single non-accelerated black hole with the usual properties.

We remark that in a cosmological constant background we cannot remove the conical singularities through the application of the Harrison transformation [124] used by Ernst in the flat case. Indeed, the Harrison transformation applied by Ernst does not leave invariant the cosmological term in the action. Therefore, applying the Harrison transformation to the cosmological constant C-metric solutions does not yield a new solution of the Einstein-Maxwell theory in a cosmological constant background.

● *The extremal limits of the C-metric:*
Nariai, Bertotti-Robinson and anti-Nariai C-metrics

There are other very interesting solutions of general relativity with generic cosmological constant, that are neither pure (like the AdS, Minkowski and dS) nor contain a black hole (like the Schwarzschild, Reissner-Nordström, Kerr, and Kerr-Newman), and somehow can be considered intermediate type solutions. These are the Nariai, Bertotti-Robinson, and anti-Nariai solutions. The Nariai solution [125, 126] solves exactly the Einstein equations with $\Lambda > 0$, without or with a Maxwell field, and has been discovered by Nariai in 1951 [125]. It is the direct topological product of $dS_2 \times S^2$, i.e., of a (1+1)-dimensional dS spacetime with a round 2-sphere of fixed radius. The Bertotti-Robinson solution [127] is an exact solution of the Einstein-Maxwell equations with any Λ, and was found independently by Bertotti and Robinson in 1959. It is the direct topological product of $AdS_2 \times S^2$, i.e., of a (1+1)-dimensional AdS spacetime with a round 2-sphere of fixed radius. The anti-Nariai solution, i.e., the AdS counterpart of the Nariai solution, also exists [128] and is an exact solution of the Einstein equations with $\Lambda < 0$, without or with a Maxwell field. It is the direct topological product of $AdS_2 \times H_2$, with H_2 being a 2-hyperboloid.

Three decades after Nariai's paper, Ginsparg and Perry [97] connected the Nariai solution with the Schwarzschild-dS solution. They showed that the Nariai solution can be generated from a near-extreme dS black hole, through an appropriate limiting procedure in which the black hole horizon approaches the cosmological horizon. A similar extremal limit generates the Bertotti-Robinson solution and the anti-Nariai solution from an appropriate near extreme black hole (see, e.g. [128]). One of the aims of Ginsparg and Perry was to study the quantum stability of the Nariai and the Schwarzschild-dS solutions [97]. It was shown that the Nariai solution is in general unstable and, once created, decays through a quantum tunnelling process into a slightly non-extreme black hole pair (for a complete review and references on this subject see, e.g., Bousso [129], and later

discussions on chapter 7 of this thesis). The same kind of process happens for the Bertotti-Robinson and anti-Nariai solutions.

As we just saw, there is yet another class of related metrics, the C-metric class, which represent not one, but two black holes, being accelerate apart from each other. These black holes can also inhabit a dS, flat or AdS background. It is therefore of great interest to apply the Ginsparg-Perry procedure to these metrics in order to find a new set of exact solutions with a clear physical and geometrical interpretation. This has been done by Dias and Lemos [89] (and will be recovered in chapter 7), where we addressed the issue of the extremal limits of the C-metric with a generic Λ following [97], in order to generate the C-metric counterparts ($A \neq 0$) of the Nariai, Bertotti-Robinson and anti-Nariai solutions ($A = 0$), among others.

1.3.3 Quantum pair creation of black holes in external fields

In nature there are few known processes that allow the production of black holes. The most well known and better studied is the gravitational collapse of a massive star or cluster of stars. Due to the fermionic degeneracy pressure these black holes cannot have a mass below the Oppenheimer-Volkoff limiting mass. Another one, as we already mentioned in subsection 1.1, is the quantum Schwinger-like process [130] of black hole pair creation in an external field. These black holes can have Plank dimensions and thus their evolution is ruled by quantum effects. Moreover, gravitational pair creation involves topology changing processes, and allows a study of the statistical properties of black holes, namely: it favors the conjecture that the number of internal microstates of a black hole is given by the exponential of one-quarter of the area of the event horizon, and it gives useful clues to the discussion of the black hole information paradox.

In this thesis we study in detail the quantum process in which a cosmic string breaks in an AdS background and in a dS background, and a pair of black holes is created at the ends of the string [131, 132]. The energy to materialize and accelerate the black holes comes from the strings tension, and we have explicitly computed the pair creation rates. In Fig. 1.9, we show a schematic description of the process. We start, as indicated in Fig. 1.9.(a), with a straight string that is going to be broken. When the string breaks, as sketched in Fig. 1.9.(b), two black holes are created at the ends of the string, and the strings tension T immediately accelerate apart the black hole pair. The black holes described by the C-metric have non-spherical horizons, due to the presence of a conical singularity in at least one of their poles that signals the presence of the string.

(a)   (b)
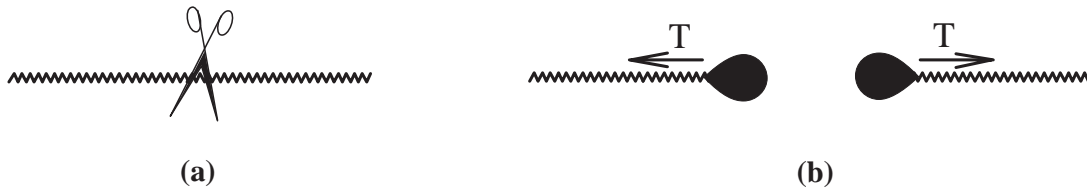
Figure 1.9: Schematic description of the black hole pair creation when a straight string breaks.

In the dS case the cosmological constant background acceleration makes a positive contribution to the process, while in the AdS case the cosmological constant background acceleration contributes negatively. In particular, in the AdS case, pair creation of black holes is possible only when the acceleration provided by the string tension is higher than $\sqrt{|\Lambda|/3}$. We have thus extended for the cosmological constant case a pair creation process that in the flat case had been discussed in [133]-[136]. We remark that in principle our explicit values for the pair creation rates [131, 132] also apply to the process of pair creation in an external electromagnetic field, with the acceleration being provided in this case by the Lorentz force instead of being furnished by the string tension. There is no Ernst solution in a cosmological constant background, and thus we cannot discuss analytically the process. However, physically we could in principle consider an external electromagnetic field that supplies the same energy and acceleration as our strings and, from the results of the $\Lambda = 0$ case

(where the pair creation rates in the string and electromagnetic cases agree), we expect that the results found in [131, 132] do not depend on whether the energy is being provided by an external electromagnetic field or by strings.

As an example of our results and to understand the physical interpretation that is associated with the process, we give the pair creation rates Γ of nonextreme black holes with $m = q$ when a string breaks in the dS, flat and AdS backgrounds, respectively:

$$\Gamma_{\text{dS}}^{\text{C-metric}} \propto \exp\left[\frac{3\pi}{64\Lambda}\frac{1}{mA}\left(1 - \sqrt{\frac{1-4mA}{1+4mA}}\right)\left(1 + \sqrt{1-(4mA)^2} - \frac{4m}{\sqrt{3}}\sqrt{\Lambda+3A^2}\right) - \frac{3\pi}{\Lambda}\frac{\sqrt{1-4mA}}{\sqrt{1+4mA}}\right],$$

where the acceleration, $A > 0$, and the mass parameter m of the black holes must satisfy $mA \leq \frac{\sqrt{3}}{4}\frac{1}{\sqrt{\Lambda+3A^2}}$,

$$\Gamma_{\text{flat}}^{\text{C-metric}} \propto \exp\left[-\frac{\pi}{4A^2}\frac{-1+4mA+\sqrt{1-(4mA)^2}}{\sqrt{1-(4mA)^2}}\right],$$

where the acceleration, $A > 0$, and the mass parameter m of the black holes must satisfy $0 < mA \leq \frac{1}{4}$,

$$\Gamma_{\text{AdS}}^{\text{C-metric}} \propto \exp\left[-\frac{4\pi m^2}{\omega_+(\omega_+^2-1)}\left(-\frac{\omega_+-\omega_-}{(\omega_++\alpha)(\omega_-+\alpha)} + \frac{1}{\omega_+-\alpha} + \frac{1}{1+\sqrt{1-\frac{8|\Lambda|m^2}{3}\frac{3\omega_-^2-1}{\omega_-^2(1-\omega_-^2)^2}}}\frac{1-3\omega_-^2}{\omega_-(1-\omega_-^2)}\right)\right],$$

where the acceleration A and the mass m of the black holes must satisfy the conditions $A > \sqrt{\frac{|\Lambda|}{3}}$ and $0 < mA \leq \frac{1}{4}$, and we have $\omega_\pm = \sqrt{1 \pm 4mA}$ and $\alpha = \sqrt{1 - \frac{4m}{\sqrt{3}}\sqrt{3A^2-|\Lambda|}}$. In the three cases, $\Lambda < 0$, $\Lambda = 0$ and $\Lambda > 0$, we conclude that for a fixed Λ and A as the mass and charge of the black holes increase, the probability they have to be pair created decreases monotonically. This is the expected result since the materialization of a higher mass implies the need of a higher energy. We can also discuss the behavior of the pair creation rate as a function of the acceleration A provided by the strings, for a fixed Λ and m. This evolution is schematically represented in Fig. 9.9, in the three cosmological constant backgrounds. In general, for any Λ background, the pair creation rate increases monotonically with A. The physical interpretation of this result is clear: the acceleration A of the black hole pair is provided by the string. When the energy of the string is higher (i.e., when its mass density or the acceleration that it provides is higher), the probability that it breaks and produces a black hole pair with a given mass is also higher. This behavior is better understood if we make a analogy with a thermodynamical system, with the mass density of the string being the analogue of the temperature T. Indeed, from the Boltzmann factor, $e^{-E_0/(k_B T)}$ (where k_B is the Boltzmann constant), one knows that a higher background temperature T turns the nucleation of a particle with energy E_0 more probable. Similarly, a background string with a higher mass density turns the creation of a black hole pair with mass $2m$ more probable. In a flat background [see Fig. 1.10.(a)], the pair creation rate is zero when $A = 0$ [133]. In this case, the flat C-metric reduces to a single black hole, and since we are studying the probability of pair creation, the corresponding rate is naturally zero. This does not mean that a single black hole cannot be materialized from the quantum vacuum, it only means that this latter process is not described by the C-metric. The creation probability of a single black hole in a hot bath has been considered in [138]. In a dS background [see Fig. 1.10.(b)], the pair creation rate is not zero when $A = 0$ [131]. This means that even in the absence of the string, the positive cosmological constant is enough to provide the energy to materialize the black hole pair [169]. If in addition one has an extra energy provided by the string, the process becomes more favorable [131]. In the AdS case [see Fig. 1.10.(c)], the negative cosmological constant makes a negative contribution to the process, and black hole pair creation is possible only when the acceleration provided by the strings overcomes the AdS background attraction. The branch $0 < A \leq \sqrt{|\Lambda|/3}$ represents the creation probability of

a single black hole when the acceleration provided by the broken string is not enough to overcome the AdS attraction, and was not studied in this thesis.

Strictly speaking, the domain of validity of the pair creation rates displayed above is $mA \ll 1$, for which the radius of the black hole, $r_+ \sim m$, is much smaller than the typical distance between the black holes at the creation moment, $\ell \sim 1/A$ (this value follows from the Rindler motion $x^2 - t^2 = 1/A^2$ that describes the uniformly accelerated motion of the black holes). So, for $mA \sim 1$ one has $r_+ \sim \ell$ and the black holes start interacting with each other.
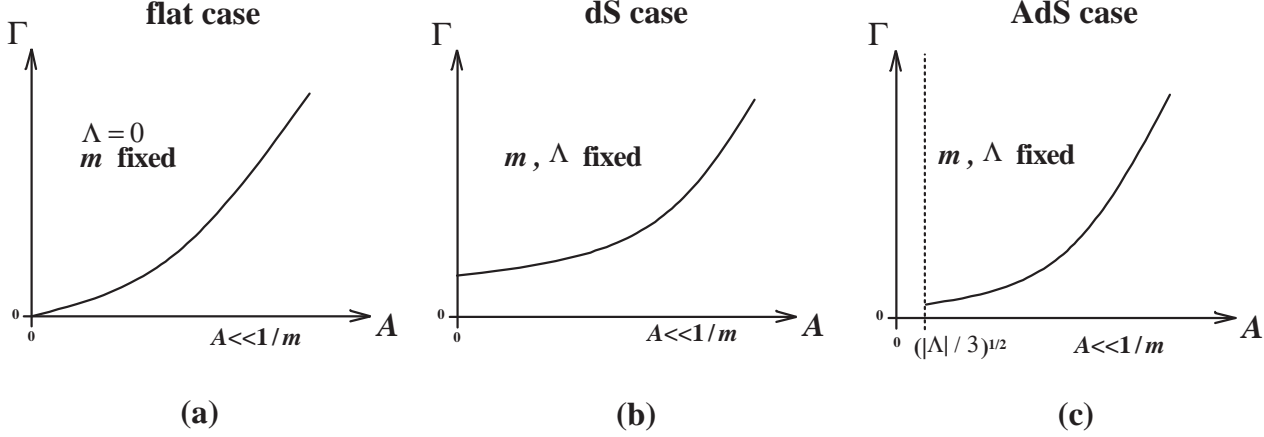
Figure 1.10: General behavior of the black hole pair creation rate Γ as a function of the acceleration A provided by the strings, when a cosmic string breaks: (a) in a flat background ($\Lambda = 0$) [133], (b) in a dS background ($\Lambda > 0$) [131], and (c) in an AdS background ($\Lambda < 0$) [132].

● *Historical overview on quantum pair creation of particles in external fields*

The evaluation of the black hole pair creation rate has been done at the semiclassical level using the instanton method (this method is also called saddle point approximation). An instanton is an Euclidean solution that interpolates between the initial and final states of a classicaly forbidden transitation, and is a saddle point for the Euclidean Feynmann path integral that describes the pair creation rate. This instanton method has been introduced by Langer in his work about decay of metastable termodynamical states [139], and in the absence of gravity, it has been applied to several different studies. For example, Coleman and Callan [140, 141], Coleman and Luccia [142], and Voloshin [143] have computed the bubble production rate that accompanies the cosmological phase transitions in a (3+1) dimensional scalar theory. Stone [144], Kiselev and Selivanov [145, 146, 147], and Voloshin [148, 149] have discussed the soliton pair production that accompanies the decay of false vacuum in a (1+1)-dimensional scalar theory, and in Dias, Lemos [150] the study of this process has been recovered, in the spirit of an effective one-loop action approach, and extended to include domain wall pair creation (see Miller, Cardenas, Garcia-Perez, More, Beckwith, and McCarten [151] for experimental evidence of this process). Affleck and Manton [152], in the Yang-Mills-Higgs theory, have studied monopole pair production in a weak external magnetic field, and Affleck, Alvarez and Manton [153], have studied e^+e^- boson pair production in a weak external electric field.

● *Historical overview on quantum pair creation of black holes in external fields*

The instanton method has been also introduced also as a framework of quantum gravity, with successful results in the analysis of gravitational thermodynamic issues and black hole pair production processes, among others (see [154]). The regular instantons that describe the process we are interested in - the pair creation of black holes in an external field - can be obtained by analytically continuing (i) a solution found by Ernst [85], (ii) the de Sitter black hole solutions, (iii) the C-metric [84], (iv) a combination of the above solutions, or (v) the domain wall solution [98, 99]. To each one of these five families of instantons corresponds a different way by which energy can be furnished in order to materialize the pair of black holes and then to accelerate them apart. In case (i) the

energy is provided by the electromagnetic Lorentz force, in case (ii) the strings tension furnishes this energy, in case (iii) the energy is provided by the rapid cosmological expansion associated to the positive cosmological constant Λ, in case (iv) the energy is provided by a combination of the above fields, and finally in case (v) the energy is given by the repulsive gravitational field of the domain wall.

It was believed that the only black hole pairs that could be nucleated were those whose Euclidean sector was free of conical singularities (instantons). This regularity condition restricted the mass and charge of the black holes that could be produced, and physically it meant that the only black holes that could be pair produced were those that are in thermodynamic equilibrium. However, Wu [155], and Bousso and Hawking [156] have shown that Euclidean solutions with conical singularities (sub-maximal instantons) may also be used as saddle points for the pair creation process, as long as the spacelike boundary of the manifold is chosen in order to contain the conical singularity and the metric is specified there. In this way, pair creation of black holes whose horizons are not in thermodynamic equilibrium is also allowed.

We will now describe the studies that have been done on pair creation of black holes in an external field.

(i) The suggestion that the pair creation of black holes could occur in quantized Einstein-Maxwell theory has been given by Gibbons [157] in 1986, who has proposed that extremal black holes could be produced in a background magnetic field and that the appropriate instanton describing the process could be obtained by euclideanizing the extremal Ernst solution. This idea has been recovered by Giddings and Garfinkle [158] who confirmed the expectation of [157] and, in addition, they have constructed an Ernst instanton that describes pair creation of non-extremal black holes. The explicit calculation of the rate for this last process has lead Garfinkle, Giddings and Strominger [159] to conclude that the pair creation rate of non-extremal black holes is enhanced relative to the pair creation of monopoles and extremal black holes by a factor $e^{S_{\rm bh}}$, where $S_{\rm bh} = \mathcal{A}_{\rm bh}/4$ is the Hawking-Bekenstein entropy of the black hole and $\mathcal{A}_{\rm bh}$ is the area of the black hole event horizon. This issue of black hole pair creation in a background magnetic field and the above relation between the pair creation rate and the entropy has been further investigated by Dowker, Gaunlett, Kastor and Traschen [114], by Dowker, Gaunlett, Giddings and Horowitz [160], and by Ross [161], but now in the context of the low energy limit of string theory and in the context of five-dimensional Kaluza-Klein theory. To achieve their aim they have worked with an effective dilaton theory which, for particular values of the dilaton parameter, reduces to the above theories, and they have explicitly constructed the dilaton Ernst instantons that describe the process. The one-loop contribution to the magnetic black hole pair creation problem has been given by Yi [162]. Brown [101, 163] has analyzed the pair creation of charged black holes in an electric external field. Hawking, Horowitz and Ross [164] (see also Hawking and Horowitz [165]) have related the action that governs the rate of pair creation of extremal black holes with the area of the acceleration horizon. In the non-extremal case, the action has an additional contribution from the area of the black hole horizon. From these relations emerges an explanation for the fact, mentioned above, that the pair creation rate of non-extremal black holes is enhanced relative to the pair creation of extremal black holes by precisely the factor $e^{\mathcal{A}_{\rm bh}/4}$. For a detailed discussion concerning the reason why this factor involves only $\mathcal{A}_{\rm bh}$ and not two times this value see also Emparan [166]. It has to do with the fact that the internal microstates of two members of the black hole pair are correlated.

(ii) The pair creation process of de Sitter (dS) black holes has been also investigated. Notice that the dS black hole solution can be interpreted as a pair of dS black holes that are being accelerated apart by the positive cosmological constant. The cosmological horizon can be seen as an acceleration horizon that impedes the causal contact between the two black holes, and this analogy is perfectly identified for example when we compare the Carter-Penrose diagrams of the C-metric and of the dS black holes. The study on pair creation of black holes in a dS background has begun in 1989 by Mellor and Moss [167], who have identified the gravitational instantons that describe the process (see also Romans [168] for a detailed construction of these instantons). The explicit evaluation of the pair creation rates of neutral and charged black holes accelerated by a cosmological constant

has been done by Mann and Ross [169]. This process has also been discussed in the context of the inflationary era undergone by the universe by Bousso and Hawking [170]. Garattini [171], and Volkov and Wipf [172] have computed the one-loop factor for this pair creation process, something that at the gravity quantum level is not an easy task. Booth and Mann [173] have analyzed the cosmological pair production of charged and rotating black holes. Pair creation of dilaton black holes in a dS background has also been discussed by Bousso [174].

(iii) In 1995, Hawking and Ross [133] and Eardley, Horowitz, Kastor and Traschen [134] have discussed a process in which a cosmic string breaks and a pair of black holes is produced at the ends of the string. The string tension then pulls the black holes away, and the C-metric provides the appropriate instantons to describe their creation. In order to ensure that this process is physically consistent Achúcarro, Gregory and Kuijken [135], and Gregory and Hindmarsh [136] have shown that a conical singularity can be replaced by a Nielson-Olesen vortex. This vortex can then pierce a black hole [135], or end at it [136]. Moreover, it has been suggested that even topologically stable strings can end at a black hole [133]-[137].

(iv) We can also consider a pair creation process, analyzed by Emparan [175], involving cosmic string breaking in a background magnetic field. In this case the Lorentz force is in excess or in deficit relative to the net force necessary to furnish the right acceleration to the black holes, and this discrepancy is eliminated by the string tension. The instantons describing this process are a combination of the Ernst and C-metric intantons. Another processes that involve black hole pair creation in a combination of background fields are the ones, already discussed above, in which a cosmic string breaks in a dS background [131], and in an AdS background [132].

(v) The gravitational repulsive energy of a domain wall provides another mechanism for black hole pair creation. This process has been analyzed by Caldwell, Chamblin and Gibbons [176], and by Bousso and Chamblin [177] in a flat background, while in an anti-de Sitter background the pair creation of topological black holes (with hyperbolic topology) has been analyzed in by Mann [178].

Other studies concerning the process of pair creation in a generalized background is done in [179, 180].

• *Pair creation of magnetic vs electric black holes*

During a while it has been noticed that the pair creation of electric black holes was apparently enhanced relative to the pair creation of magnetic black holes. This was a consequence of the fact that the Maxwell action has opposite signs in the two cases. Now, this discrepancy between the two pair creation rates was not consistent with the idea that electric and magnetic black holes should have identical quantum properties. This issue has been properly and definitively clarified by Hawking and Ross [181] and by Brown [163], who have shown that the magnetic and electric solutions differ not only in their actions, but also in the nature of the boundaries conditions that can be imposed on them. More precisely, one can impose the magnetic charge as a boundary condition at infinity but, in the electric case, one instead imposes the chemical potential as a boundary condition. As a consequence they proposed that the electric action should contain an extra Maxwell boundary term. This term cancels the opposite signs of the Maxwell action, and the pair creation rate of magnetic and electric black holes is equal.

• *Pair creation of black holes and the information loss problem*

The process of black hole pair creation gives also useful clues to the discussion of the black hole information loss problem [182]. Due to the thermal Hawking radiation the black holes evaporate. This process implies that one of the following three scenarios occurs (see [183] for nice reviews): (i) the information previously swallowed to the black hole is destroyed, (ii) this information is recovered to the exterior through the Hawking radiation, or (iii) the endpoint of the evaporation is a Plank scale remnant which stores the information. There are serious difficulties associated to each one of this scenarios. Scenario (i) implies non-unitarity and violation of energy conservation, scenario (ii) implies violation of locality and causality, and the main problem with scenario (iii) is that a huge energy is needed in order to store all the information that has been swallowed by the black hole,

and a Planck scale remnant has very little energy. Pair creation of black holes has been used to test these scenarios. Indeed, it has been argued [183] that if one demands preservation of unitarity and of locality then a careful analysis of the one-loop contribution to the pair creation process indicates that the Hawking process would leave behind a catastrophic infinite number of remnants. So the remnant hypothesis seems to be discarded, although some escape solutions can be launched [183]. On the other side, Hawking, Horowitz and Ross [164] have called attention to the fact that the same instantons that describe pair creation can, when reversed in time, describe their pair annihilation, as long as the black holes have appropriate initial conditions such that they come to rest at the right critical separation (this annihilation process was also discussed by Emparan [166]). One can then construct [164] an argument that favors the information loss scenario: black holes previously produced as a particle-antiparticle pair can accrete information and annihilate, with their energy being given off as electromagnetic and gravitational radiation. Therefore, the information loss scenario seems to occur at least in this annihilation process.

1.3.4 Energy released during black hole pair creation in an external field

If one tries to predict the spectrum of radiation coming from pair creation, one expects of course a spectrum characteristic of accelerated masses, but one also expects a previous signal indicating pair creation. In other words, the process of pair creation itself, which involves the sudden creation of particles that suffer a violent acceleration that takes them to some final velocity in a very short time, must imply emission of radiation. The sudden creation of pairs can be viewed for our purposes as an instantaneous creation of particles, i.e., the time reverse process of instantaneous collisions. Now, the gravitational energy released in this last process can be estimated using a technique developed by Weinberg [184], known as the hard collision formalism. We argue that this formalism also applies to instantaneous creation of particles (see [185]). The total energy, i.e., the energy spectrum integrated over all frequencies diverges, so one needs a physical cutoff frequency that can be estimated by the uncertainty principle, $\omega_c \sim \frac{E}{\hbar}$. We then find that the total gravitational energy released during the 4-dimensional black hole pair creation process is given by [185] (see chapter 12)

$$\Delta E = \frac{4Gc}{\pi} \frac{\gamma^3 M^3}{\hbar} \, , \tag{1.7}$$

where M is the mass of each one of the created black holes and $\gamma = (1 - v^2/c^2)^{-1/2}$ is the Lorentz factor. This value can lead, under appropriate numbers of M and γ to huge quantities, and is a very good candidate to emission of gravitational radiation. For example, for black holes with 30 times the Planck mass and with 10% of the velocity of light, the gravitational energy released is $\Delta E \sim 10^{13}$ J, which is about 100 times the rest energy of the pair.

This process is quite similar to another pure quantum-mechanical process, the beta decay. The electromagnetic radiation emitted during beta decay has been computed classically by Chang and Falkoff [186] and is also presented in Jackson [187]. The classical calculation is similar in all aspects to the the instantaneous collision formalism, assuming the sudden acceleration to energies E of a charge initially at rest, and requires also a cutoff in the frequency, which has been assumed to be given by the uncertainty principle $\omega_c \sim \frac{E}{\hbar}$. Assuming this cutoff one finds that the agreement between the classical calculation and the quantum calculation [186] is extremely good (specially in the low frequency regime), and more important, it was verified experimentally. Hence, we have a good degree of confidence to believe that our estimate (1.7) for the black pair creation process is also good.

After the pair creation and after the emission of radiation according to (1.7), the created pair of black holes accelerates away and, consequently, they continue to release gravitational and electromagnetic energy. In a $\Lambda = 0$ background, the gravitational radiative properties of the accelerated black holes described by the C-metric have been analyzed by Bičák [112], and Pravda and Pravdova [113]. In a dS background, the gravitational radiation emitted by uniformly accelerated sources without horizons has been analyzed by Bičák and Krtouš [188], and the radiative properties of

accelerated black holes have been studied by Krtouš and Podolský [189]. In an AdS background the energy released by a pair of accelerated black holes has been discussed in detail by Podolský, Ortaggio and Krtouš [190].

1.4 Black holes in higher dimensional spacetimes

1.4.1 Exact black hole solutions

By suggesting the existence of an extra dimension, besides the usual (3+1)-dimensions that our daily experiments realize, Kaluza and Klein in the 1920s unified for the first time gravity and electromagnetism. Indeed, they realized that 5-dimensional vacuum general relativity (i.e., satisfying $^5G_{AB} = 0$ with A and B taking the values $0, 1, 2, 3, 4$, and G_{AB} being the usual Einstein tensor), contained 4-dimensional general relativity in the presence of an electromagnetic field (i.e., satisfying $^4G_{\alpha\beta} = \frac{8\pi G}{c^4} \, ^4T^{\text{Max}}_{\alpha\beta}$ with α and β taking the values $0, 1, 2, 3$, and $T^{\text{Max}}_{\alpha\beta}$ being the usual Maxwell tensor) together with Maxwell's laws of electromagnetism and an equation for a scalar field. The dominant view is then that the extra dimension is not observed on experimentally accessible energy scales because it is compactified. The Kaluza-Klein mechanism has unified also matter and geometry since the photon that is present in the 4-dimensional spacetime is a manifestation of empty 5-dimensional spacetime. The key point to the Kaluza-Klein unification is the realization that to a 4-dimensional gauge symmetry [e.g., the $U(1)$ gauge invariance of Maxwell theory] corresponds a geometric symmetry (an invariance with respect to coordinate transformations) in the extra dimension. Thus, the main achievement of Kaluza-Klein proposal has been the demonstration that different uncorrelated phenomena that occur in 4-dimensional spacetime can be manifestations of the same 5-dimensional theory. From then onwards the theories of strong and weak nuclear interactions have been developed, and several attempts to unify the 4-dimensional theories in a single $D > 5$ higher-dimensional theory have been tried with some successes (for a nice review see Overduin and Wesson [191]). Among others, two theories emerged, during the decade of 80, that embodied the Kaluza-Klein compactification idea: supergravity and superstring theory. Supergravity theories have the new ingredient of supersymmetry, which states that each boson has a fermion cousin and vice-versa. Mathematical consistency requires $D \leq 11$, and in these theories the case $D = 11$ plays a very special role due, among others reasons, to its uniqueness and to its dynamical mechanism that spontaneously compactifies 7 of the 11 dimensions. However, supergravity theories also suffer from serious problems, one of them being the fact that they are non-renormalizable theories. The interest on supergravity theories shifted to superstring theories, with the former being the low energy limit of the later. Superstring theories are supersymmetric generalizations of string theories, in which the notion that particles are point-like is abandoned and replaced by the assumption that fundamental objects are excitations of strings. Thus, the study of physics in higher dimensional spacetimes is of great importance nowadays.

Now, black holes play their role in this D-dimensional context. We give two detailed examples. First, the idea that elementary particles might behave as black holes and vice-versa is a very attractive one. In principle one might expect such a scenario when the Compton length, $\lambda = \frac{\hbar}{Mc}$, associated to a given mass is smaller than the corresponding Schwarzschild radius, $r_+ = \frac{2GM}{c^2}$, i.e., when the mass of the object is smaller than the Planck mass, $M_4 = \sqrt{\hbar c/G}$. Since this is a discussion at the quantum gravity level, superstring theories provide appropriate tools to analyze the problem. In particular, some superstring states have been connected to extreme D-dimensional black holes. This is an encouraging result since if one wants to identify stable elementary particles with black holes, these later must be extreme. As a second example, in which we are particularly interested on, we point out to the recent investigations, by Arkani-Hamed, Dimopoulos Dvali and Antoniadis [193], that propose the existence of extra large dimensions in our Universe in order to solve the hierarchy problem, i.e., the huge difference between the electroweak scale, $M_{\text{EW}} \sim 1\,\text{TeV}$, and the 4-dimensional Planck scale, $M_4 = \sqrt{\hbar c/G} \sim 10^{16}\,\text{TeV}$. The new main proposal of the so called

TeV-scale gravity (for reviews see, e.g., [192]) is that the fundamental Planck scale, M_{Pl}, has the same size of the electroweak scale, $M_{Pl} \sim M_{EW} \ll M_4$, but the 4-dimensional gravity is weak (i.e., the observed apparent Planck scale M_4 is large) due to dilution of gravity in large or warped extra dimensions. At this point the most accepted approach introduces a link to a brane-world scenario. According to this scenario, matter and fields of Standard Model inhabit our 4-dimensional world, the brane, whereas the gravitational degrees of freedom would propagate throughout all dimensions, including the extra ones. By now, experimental measurements involving submillimiter distances, and studies on astrophysical and cosmological implications of large extra dimensions, among others (see, e.g., references on [192]), require the existence of at least three extra dimensions ($D > 6$) in order that $M_{Pl} \sim M_{EW}$. More precisely, the actual experimental bounds on the Planck fundamental mass indicate that $M_{Pl} \gtrsim 1.1\,\text{TeV} - 0.8\,\text{TeV}$ for $D = 7$ to $D = 10$.

One of the most spectacular consequences of this scenario would be the production of black holes at the Large Hadron Collider (LHC) at CERN, and the consequent experimental data relative to black hole decay. This possibility has been pointed out by Argyres, Dimopoulos and March-Russsel [194], by Banks and Fischler [195], and by Emparan, Horowitz and Myers [196], and has been quantified by Giddings and Thomas [197], and by Dimopoulos and Landsberg [198]. Now, the LHC is designed to operate at an center of mass energy of 14 TeV, so if $M_{Pl} \sim 1\,\text{TeV}$ we will indeed be able to produce mini-black holes at LHC through the collisions of partons (quarks and gluons). One can estimate the creation rate as follows. Due to the fact that our description is only known at the semiclassical level, one first sets that the black hole mass is above the Planck mass, $M \sim 5\,\text{TeV} - 10\,\text{TeV}$ (say). Then, in the TeV-scale gravity/brane-world scenario one must work with two approximations. First, one requires that the black holes are heavy compared with M_{Pl} in order to ensure that the gravitational field of the brane can be neglected. The second approximation is to deal with black holes that are small compared with the size of the extra dimensions. In the context of these approximations the appropriate D-dimensional black holes are described by the Tangherlini-Myers-Perry solution [202, 203]. To proceed, one needs to know the parton density in a proton (which is known with some accuracy), and the cross section σ of black hole production in a parton-parton collision. This cross section can be estimated from pure geometric arguments following the Thorne's hoop conjecture: a black hole is created when the impact parameter, b, of the colliding partons is less than the Schwarzschild radius, r_+, associated with the energy involved in the process. Hence $\sigma \sim \pi r_+^2 \sim E^{\frac{2}{D-3}}$. This estimate has been further investigated by D'Eath, and Payne [199], by Yoshino and Nambu [200], and by Eardley and Giddings [201] who generalized a construction by Penrose to find trapped surfaces on the union of two shock waves, describing boosted Schwarzschild black holes. Their final conclusion is that the above geometrical estimate for sigma is sufficiently accurate. Putting everything together, the final result [197, 198] indicates that if the TeV-scale gravity scenario is correct, then LHC will produce black holes with masses larger than 5 TeV at the rate of about 1 per second. One would really be in the presence of a black hole factory. Moreover, these black holes will decay leaving definite signatures.

Since black holes in D-dimensions are important one should ask which are the exact solutions that one can find. The natural higher dimensional generalization (which contains the $D = 4$ solution as a special case) of the Schwarzschild black hole and of the Reissner-Nordström black hole has been obtained by Tangherlini [202] (for a AdS, flat and dS background). Myers and Perry [203] have found the higher dimensional counterparts of the the Kerr and Kerr-Newman black holes. The global structure of the non-rotating solutions is similar to their 4-dimensional counterparts. In particular, the black hole exists when $Q^2 \leq G_D M^2$, where G_D is the D-dimensional Newton's constant. In what concerns the rotating solutions, the properties of the higher dimensional black holes are also similar to the ones of the 4-dimensional case, with two important exceptions: for odd D there are black hole solutions with negative mass, and for $D \geq 6$ the angular momentum is not bounded, i.e., it can have an arbitrary large value. However, recently Emparan and Myers (2003) have shown that there is a dynamical decay mechanism that turns these black holes unstable at large enough rotation. Tangherlini [202] has also found the higher dimensional Schwarzschild and

Reissner-Nordström black holes in an asymptotically AdS and dS spacetime. In chapter 10, we discuss in detail the extreme cases of the higher dimensional dS black holes, i.e., we will give the explicit range of the mass and charge for which one has an extreme black hole [211]. Moreover, we will find the higher dimensional Nariai and Bertotti-Robinson solutions [211]. Besides the above black holes, the higher dimensional spacetimes admit a richer variety of black hole solutions. As examples, we mention the D-dimensional black holes of Boulware, Deser [204], of Callan, Myers and Perry (1988), Gibbons and Maeda (1988), of Cvetic and Youm [205], and of Cvetic and Larsen [206] that are solutions of the string action. Supersymmetric rotating black holes were found by Gibbons and Herdeiro [207], and by Herdeiro [208]. With non-spherical horizons, one has the 5-dimensional rotating black ring solution of Emparan and Reall [209] (which has a horizon with topology $S^2 \times S^1$), and the black p-branes whose horizons have topology $S^{D-2} \times \mathbb{R}^p$.

1.4.2 Quantum pair creation of higher dimensional black holes

We have already commented on the collision process at LHC that might lead to the formation of higher dimensional black holes. Another process that can create black holes in a D-dimensional spacetime is the Schwinger-like pair creation process in an external field. As we saw in section 1.3, in order to study analytically this process one needs an exact solution that describes a pair of accelerated black holes in the external field. In a 4-dimensional background, the C-metric, the Ernst solution and the dS black hole solution, among others, provided such an exact solution. In spite of some efforts, the higher dimensional generalization of the C-metric and of the Ernst solution have not been found yet. However, the D-dimensional dS black hole solution exists [202], and it describes a pair of accelerated black holes. Its properties are discussed in detail in [210, 211] (see chapter 10). We can then analyze analytically the pair creation process of higher dimensional dS black holes, which are accelerated apart by the cosmological constant expansion [212] (see chapter 11).

1.4.3 Gravitational radiation in higher dimensional spacetimes. Energy released during black hole production

Gravitational radiation is an essential feature related to black hole physics. In 4-dimensional spacetimes there has been a detailed analysis of the properties of gravitational radiation, due to the possibility of detecting it from astrophysical sources.

In the context of black holes in D-dimensional spacetimes it is important to extend the 4-dimensional results to higher dimensional spacetimes. This has done in [185] (see also chapter 12 of this thesis). More concretely, by solving the retarded gravitational potentials in even D-dimensions, we were able to generalize many of the results about gravitational waves (in a flat background) to higher dimensions: we extended the quadrupole formula to higher dimensions, we extended Weinberg's "zero time collision" formalism to higher dimensions, and we have considered radiation processes in the vicinities of higher dimensional Tangherlini black holes [202].

The analysis of gravitational radiation in higher dimensional spacetimes is also important in the context of the TeV-scale gravity and its prediction concerning the production of black holes at the LHC. After the being produced, the black hole will decay, i.e., it will shed its extra initial hair until it settles into a Kerr or Schwarzschild black hole. Afterwards quantum processes take place. In this thesis we are interested on the first phase that accompanies the black hole production. One of the experimental signatures of this phase will be a missing energy, perhaps a large fraction of the center of mass energy [220]. This will happen because when the partons collide to form a black hole, some of the initial energy will be converted to gravitational waves, and due to the small amplitudes involved, there is no gravitational wave detector capable of detecting them, so they will appear as missing energy. Thus, the collider will in fact serve indirectly as a gravitational wave detector. This calls for the calculation of the energy given away as gravitational waves when two high energy particles collide to form a black hole, which lives in all the dimensions. In a 4-dimensional background this calculation has been done by D'Eath and Payne [199]. In a higher dimensional background, the calculation has been carried following distinct approaches by Yoshino and Nambu [200] (following

a formalism developed by [201]), by Cardoso, Dias and Lemos [185] (see chapter 12 of this thesis), and by Berti, Cavaglià and Gualtieri [221]. We find that the energy spectrum, i.e., the energy per unit of frequency and per unit of solid angle is [185]

$$\frac{d^2E}{d\omega d\Omega} = \frac{2\mathcal{G}}{(2\pi)^{D-2}} \frac{D-3}{D-2} \frac{\gamma_1^2 m_1^2 v_1^2 (v_1+v_2)^2 \sin\theta^4}{(1-v_1\cos\theta)^2(1+v_2\cos\theta)^2} \times \omega^{D-4}, \tag{1.8}$$

where m_i, v_i, and $\gamma_i = (1-v_i^2)^{-1/2}$ (with $i = 1, 2$) are, respectively, the mass, the velocity, and the Lorentz factor of the two colliding particles, and θ is the angle that the line defined by the colliding particles makes with the direction of the radiation. The formalism used in [185] assumes a hard collision, i.e., a collision lasting zero seconds [184].

1.5   Organization of the thesis

This thesis is divided in three parts. Briefly, part I deals with black holes and pair creation in 3 dimensions. Part II deals with the same subject but in 4-dimensional spacetimes, and part III is devoted to the same issue but in higher dimensional black holes.

The plan of the thesis is then as follows:

• *Part I. Black holes and pair creation in 3 dimensions*

Chapter 2. The BTZ family of black holes. In this chapter, we review the main properties of 3-dimensional Einstein gravity, we show the explicit topological construction that leads to the BTZ black hole, we briefly mention the electric charged BTZ black hole, and we discuss in detail the magnetic BTZ solution.

Chapter 3. Three dimensional dilaton black holes of the Brans-Dicke type. In this chapter, we analyze in detail the neutral, electric and magnetic solutions of a 3-dimensional Einstein-dilaton gravity of the Brans-Dicke type.

Chapter 4. Pair creation of black holes in three dimensions. The process of quantum pair creation of black holes in an external field in a 3-dimensional background has not been analyzed yet. In this chapter, we will try to understand the difficulties associated with this issue, and we will also propose a possible background in which the pair creation process in 3-dimensions might be analyzed.

• *Part II. Black holes and pair creation in 4 dimensions*

Chapter 5. Black holes in a generalized Λ background. In this chapter, we give an overview of all the static 4-dimensional black holes that are solutions of the Einstein equations in an AdS, flat, and dS background. Special attention is dedicated to an AdS magnetic solution with cylindrical/toroidal symmetry. This chapter introduces also a description of some tools that will be used in later chapters.

Chapter 6. Pair of accelerated black holes: the C-metric in a generalized Λ background. In this chapter, we make a detailed discussion on the properties and physical interpretation of the AdS C-metric, flat C-metric (and Ernst solution), and dS C-metric.

Chapter 7. The extremal limits of the C-metric: Nariai, Bertotti-Robinson and anti-Nariai C-metrics. In this chapter, we apply the Ginsparg-Perry procedure [97] to the C-metrics in order to find a new set of exact solutions with a clear physical and geometrical interpretation. In particular, we generate the C-metric counterparts of the Nariai, Bertotti-Robinson and anti-Nariai solutions, among others.

Chapter 8. False vacuum decay: effective one-loop action for pair creation of domain walls. This chapter can be seen as an introductory toy model for the black hole pair creation analysis. We propose an effective one-loop action to describe the domain wall pair creation process that accompanies the false vacuum decay of a scalar field (in the absence of gravity). We compute the pair creation rate, including the one-loop contribution, using the instanton method that is also used to compute pair creation rates of black holes.

Chapter 9. Pair creation of black holes on a cosmic string background. In this chapter, we discuss in detail the creation of a black hole pair when a cosmic string breaks, in an AdS, flat and dS

background. The instantons that describe the process are constructed from the AdS, flat and dS C-metrics. We explicitly compute the pair creation rates.

- *Part III. Black holes and pair creation in higher dimensions*

Chapter 10. Black holes in higher dimensional spacetimes. In this chapter, we discuss the higher dimensional Tangherlini black holes in an AdS, flat, and dS background. In particular, we find the explicit range of the mass and charge for which one has an extreme black hole. Moreover, we will find the higher dimensional Nariai and Bertotti-Robinson solutions.

Chapter 11. Pair creation of black holes in higher dimensional spacetimes. In this chapter, we discuss in detail the creation of a higher dimensional Tangherlini black hole pair in a dS background. The instantons that describe the process are constructed from the dS Tangherlini solution. We explicitly compute the pair creation rates.

Chapter 12. Gravitational radiation in D-dimensional spacetimes and energy released during black hole pair creation. In this chapter, we construct the formalism to study linearized gravitational waves in flat D-dimensional spacetimes. This extension of the 4-dimensional formalism is non-trivial, due to the behavior of the D-dimensional Green's function. We find the D-dimensional quadrupole formula, and we apply it to two cases: a particle in circular motion in a generic background, and a particle falling into a D-dimensional Schwarzschild black hole. We also consider the hard collision between two particles, i.e., the collision takes zero seconds, and introduce a cutoff frequency necessary to have meaningful results. We then use it to compute the gravitational energy released during the possible black hole formation at the LHC, and to estimate the gravitational radiation emitted during the process of black hole pair creation in an external field.

Part I

Black holes and pair creation in 3 dimensions

Chapter 2

The BTZ black hole

Contents

In section 2.1, we will review some of the unusual properties of 3-dimensional Einstein gravity.

Bañados, Teitelboim and Zanelli [39] have found a black hole solution (the BTZ black hole), with mass and angular momentum, that is asymptotically AdS. As discussed in detail by Bañados, Henneaux, Teitelboim, and Zanelli [40] (see also Steif [227]), the BTZ black hole can be expressed as a topological quotient of AdS_3 by a group of isometries. In section 2.2, we will show in detail the topological construction that leads to the rotating neutral BTZ black hole.

The extension to include a radial electric field in the BTZ black hole has been done by Clément [48] and Martínez, Teitelboim and Zanelli [49] (this solution reduces to those of [23, 24] when $\Lambda = 0$). A BTZ solution with an azimuthal electric field was found by Cataldo [50]. In section 2.3, we will discuss briefly these electric BTZ solutions.

Pure magnetic solutions with $\Lambda < 0$, that reduce to the neutral BTZ black hole solution when the magnetic source vanishes, also exist. The static magnetic solution has been found by Clément [48], Hirschmann and Welch [51] and Cataldo and Salgado [52]. The extension to include rotation and a new interpretation for the source of magnetic field has been made by Dias and Lemos [53]. In section 2.4, we will discuss in detail these solutions.

Other black hole solutions of 3-dimensional Einstein-Maxwell theory have also been found by Kamata and Koikawa [54, 55], Cataldo and Salgado [56] and Chan [57], assuming self dual or anti-self dual conditions between the electromagnetic fields.

2.1 Properties of three dimensional general relativity

The Einstein equations $G_{\mu\nu} + \Lambda g_{\mu\nu} = 8\pi G T_{\mu\nu}$ can also be written, in 3-dimensions, as

$$R_{\mu\nu} = 2\Lambda g_{\mu\nu} + 8\pi G \left(T_{\mu\nu} - g_{\mu\nu}T\right) . \tag{2.1}$$

The choice of the energy-momentum tensor $T_{\mu\nu}$ completely determines the Ricci tensor $R_{\mu\nu}$, but in general it does not determine the Riemann tensor $R_{\mu\nu\alpha\sigma}$. However, and this is the fundamental difference between 3-dimensional and 4-dimensional gravities, in 3-dimensions the Weyl tensor (the traceless part of $R_{\mu\nu\alpha\sigma}$) vanishes, and so the Riemann tensor depends linearly on the Ricci tensor,

$$R_{\mu\nu\alpha\sigma} = g_{\mu\alpha}R_{\nu\sigma} + g_{\nu\sigma}R_{\mu\alpha} - g_{\nu\alpha}R_{\mu\sigma} - g_{\mu\sigma}R_{\nu\alpha} - \frac{1}{2}\left(g_{\mu\alpha}g_{\nu\sigma} - g_{\mu\sigma}g_{\nu\alpha}\right)R . \tag{2.2}$$

Inserting (2.1) in this last relation one indeed concludes that $R_{\mu\nu\alpha\sigma}$ is completely determined by $T_{\mu\nu}$ and by the cosmological constant Λ. In particular, regions of spacetime with $T_{\mu\nu} = 0$ are regions of constant curvature, with $R_{\mu\nu\alpha\sigma} = \Lambda (g_{\mu\alpha}g_{\nu\sigma} - g_{\mu\sigma}g_{\nu\alpha})$, and $R = 6\Lambda$.

General relativity in a 3-dimensional spacetime has no Newtonian limit in the sense that there is no gravitational force between static point sources. In order to see this limit we start, has in 4-dimensions, from a slightly perturbed Minkowski background (for simplicity, but without loss of generality, we deal this issue only with the case $\Lambda = 0$). To be more general let us work on a D-dimensional spacetime described by a metric $g_{\mu\nu}$ that approaches asymptotically the D-dimensional Minkowski metric $\eta_{\mu\nu} = \text{diag}(-1, +1, \cdots, +1)$, and write

$$g_{\mu\nu} = \eta_{\mu\nu} + h_{\mu\nu} \qquad \mu, \nu = 0, 1, \cdots, D-1 , \tag{2.3}$$

where $h_{\mu\nu}$ is small, so that it represents small corrections to the flat background. Then in later chapter 12.1.1 we show that the first order Einstein field equations yield

$$\Box h_{\mu\nu} = -16\pi G_D \left(T_{\mu\nu} - \frac{1}{D-2} \eta_{\mu\nu} T \right) , \tag{2.4}$$

where $\Box = \eta^{\mu\nu}\partial_\mu\partial_\nu$ is the D-dimensional Laplacian, $T_{\mu\nu}$ is the energy-momentum tensor, and G_D is the D-dimensional Newton's constant. Now, in the Newtonian limit we set as usual $T_{00} \sim \rho$ (where ρ is the mass density) and we neglect the other components of $T_{\mu\nu}$. In these conditions, (2.4) yields

$$\Box h_{00} = -16\pi G_D \frac{D-3}{D-2}\rho . \tag{2.5}$$

In order to recover the Poisson equation, $\Box\Phi = 4\pi G_D\rho$, where Φ is the gravitational potential, we set $h_{00} = -4\frac{D-3}{D-2}\Phi$. To proceed, we apply the geodesic equation, $\frac{d^2 x^\alpha}{d\tau^2} + \Gamma^\alpha_{\mu\nu}\frac{dx^\mu}{d\tau}\frac{dx^\nu}{d\tau} = 0$, to (2.3) yielding $\partial_t^2 x^i - \frac{1}{2}\partial_i h_{00} = 0$. Inserting (2.4) one finally has

$$\frac{d^2 x^i}{dt^2} + \frac{2(D-3)}{D-2}\frac{d\Phi}{dx^i} = 0 . \tag{2.6}$$

For $D = 4$ we get the usual Newtonian equation of motion, while for $D = 3$ we confirm that the acceleration is zero, that is static point sources feel no gravitational force. The above discussion can be extended to the $\Lambda \neq 0$ case, withe the Poisson equation replaced by the Liouville equation, $\Box\Phi + 2\Lambda e^\Phi = -16\pi G_D\rho$

Another unusual property of 3-dimensional gravity is the absence of gravitational waves. In chapter 12.1.2 we shall count the number of polarization states of a gravitational wave in D dimensions. We shall see that this number is given by $D(D+1)/2 - D - D = D(D-3)/2$. From this computation we conclude that gravitational waves are indeed present only when $D > 3$.

Propagation of massless fields (other than the gravitational ones, obviously) in a 3-dimensional spacetime has also a property radically different from the propagation in a 4-dimensional background. Indeed, in 3-dimensions, a pulse of electromagnetic or scalar waves travels not only along the light cone but also spreads out behind it, and slowly dies off in tails (this happens even in the absence of any kind of black hole or matter and is due only to the intrinsic dimension of the spacetime). That is, in 4-dimensions if one lights a lighter for five seconds and then turn it off, any observer at rest relative to the candle will see the light for exactly five seconds and then suddenly fade out completely. However, in a 3-dimensional spacetime, after the light source is turned off one will still see its shinning light, slowly fading away but never completely (see Soodak and Tiersten [228], and Cardoso, Yoshida, Dias and Lemos [229]). This is due to the fact that in 4-dimensions the retarded Green's function is

$$G^{\text{ret}}(t, \mathbf{x}) = \frac{1}{4\pi}\frac{\delta(t-r)}{r} , \tag{2.7}$$

where $\delta(t-r)$ is the delta function, while in 3-dimensions it is given by

$$G^{\text{ret}}(t, \mathbf{x}) = \frac{\Theta(t)}{2\pi}\frac{1}{\sqrt{t^2 - r^2}} , \tag{2.8}$$

where $\Theta(t)$ is the step Heaviside function defined as

$$\Theta(t) = \begin{cases} 1 & \text{if } t > 0 \\ 0 & \text{if } t < 0 \,. \end{cases} \tag{2.9}$$

Thus, while the 4-dimensional retarded Green's function is supported only on the light cone, the 3-dimensional one this support extends also to the interior of the light cone. So in 3-dimensions light propagates at the usual velocity of light, c, but also with velocities smaller c and this justifies the slow, and never complete fading away.

The gravitational field of a spinning point source (in a $\Lambda = 0$ background) is given by [16, 21, 22]

$$ds^2 = -(dt - 4GJd\phi)^2 + dr^2 + (1 - 4GM)^2 r^2 d\phi^2 \,, \tag{2.10}$$

where M and J are, respectively, the mass and the angular momentum of the point source, and the identification of coordinates, $(t, \phi) \sim (t, \phi + 2\pi)$, holds. This line element can be brought into the flat metric through the coordinate transformation $\tilde{t} = t + 4GJ\phi$, $\tilde{\phi} = (1 - 4GM)\phi$, yielding $ds^2 = -d\tilde{t}^2 + dr^2 + r^2 d\tilde{\phi}^2$. However, due to the coordinate transformation, the usual identification of coordinates no longer holds and has been replaced by the new one, $(\tilde{t}, \tilde{\phi}) \sim (\tilde{t} + 8\pi GJ, \tilde{\phi} + 2\pi[1 - 4GM])$. As a consequence, the spacetime (2.10) has a conic and an helical structure. Indeed, with the new coordinate identifications, one starts with the Minkowski spacetime, one cuts out a wedge with an opening angle $\delta = 8\pi GM$, and one identifies the opposite edges to form a cone with an extra time translation $8\pi GJ$. This spacetime also has the property that it admits closed timelike curves. This occurs when $g_{\phi\phi} < 0$, i.e., in a region in the vicinity of the point source with radius $r < \frac{4GJ}{1-4GM}$. Hence, the spacetime (2.10) represents a physical solution for distances greater than the above critical radius. For a spinless point source this problem does not occur. Static multi-source solutions also exist [16, 22] due to the absence of gravitational interaction in 3-dimensions. Once more the geometry has a conic and helical structure, with a wedge angle suppressed at each source proportional to its mass.

In a $\Lambda \neq 0$, the spacetimes generated by point sources in 3-dimensional Einstein gravity have also been found [30] and by Brown and Henneaux [31]. In the de Sitter case ($\Lambda > 0$) there is no one-particle solution. The simplest solution describes a pair of antipodal particles on a sphere with a wedge removed between poles and with points on its great circle boundaries identified [30]. In the anti-de Sitter case ($\Lambda < 0$), the simplest solution describes a hyperboloid with a wedge removed proportional to the source mass located at the vertex of the wedge [31].

2.2 The neutral BTZ black hole

2.2.1 Identifications in AdS_3

We will now consider [230] what kind of 'topological spacetimes' can be obtained by considering identifications in AdS_3. First, recall that AdS_3 is normally defined by its embedding in $\mathbb{M}^{2,2}$, parameterised by coordinates $x^i = (u, v, x, y)$ and with flat metric

$$ds^2 = -du^2 - dv^2 + dx^2 + dy^2 \,. \tag{2.11}$$

The AdS_3 'curve' is the hyperboloid

$$-u^2 - v^2 + x^2 + y^2 = -\ell^2 \,, \tag{2.12}$$

where $\ell = \sqrt{3/|\Lambda|}$ is the cosmological length. The isometry group of $\mathbb{M}^{2,2}$ is $ISO(2,2)$, and the Killing vector fields might be taken to be the timelike and spacelike rotations

$$J_{01} = v\partial_u - u\partial_v \,, \qquad J_{23} = y\partial_x - x\partial_y \,, \tag{2.13}$$

the four linearly independent boosts

$$J_{02} = u\partial_x + x\partial_u \,, \quad J_{03} = u\partial_y + y\partial_u \,, \quad J_{12} = v\partial_x + x\partial_v \,, \quad J_{13} = v\partial_y + y\partial_v \,, \tag{2.14}$$

and the four translations

$$P_u = \partial_u \ , \quad P_v = \partial_v \ , \quad P_x = \partial_x \ , \quad P_y = \partial_y \ . \tag{2.15}$$

Of these isometries, the translations do not leave the AdS_3 curve invariant. The isometry group of AdS_3 is only the $SO(2,2)$ generated by the two rotations and the four boosts.

Let ξ be one of the isometries of AdS_3. We wish to identify points along the orbits of ξ. Such identifications define a discrete subgroup of the isometry group, $G \subset SO(2,2)$, and the quotient

$$\mathcal{M}^{iden} \equiv \frac{AdS_3 \cong SL(2,\mathbb{R})}{G} \ , \tag{2.16}$$

defines a new spacetime $\mathcal{M}^{iden}$. The universal covering space of this spacetime, $\widetilde{\mathcal{M}^{iden}}$ is the universal covering space of AdS_3.

In practice, the identification is implemented by defining an angular coordinate ϕ, such that

$$\xi = \partial_\phi \ . \tag{2.17}$$

This angular direction will, of course, be an isometry of $\mathcal{M}^{iden}$. In order for the identification not to create closed timelike curves, one might also require that ξ should be spacelike. Thus one defines a 'radial' coordinate, r, such that

$$r^2 = \xi \cdot \xi \ . \tag{2.18}$$

The 'origin' $r = 0$ is when ξ becomes null. It will be faced as some kind of spacetime boundary, which may or may not be a conical singularity depending on the the action of ξ having fixed points or being free.

2.2.2 The construction leading to the BTZ black hole

Take

$$\xi = \frac{r_+}{\ell} J_{02} - \frac{r_-}{\ell} J_{13} = \frac{r_+}{\ell} \left(u\partial_x + x\partial_u \right) - \frac{r_-}{\ell} \left(v\partial_y + y\partial_v \right) \ , \tag{2.19}$$

where $r_\pm$ are constants, $r_+ > r_-$. That is we will be identifying points along a double boost: a boost in the (u, x)-plane and a boost in the (v, y)-plane. For $r_\pm \neq 0$ the action of this vector field has a fixed point only at $u = v = x = y = 0$, which does not belong to the hyperboloid. Hence this isometry acts freely on the hyperboloid. For $r_- = 0$, the points $u = x = 0$ are fixed points of the isometry action. Hence the one dimensional hyperboloid

$$-v^2 + y^2 = -\ell^2 \ , \tag{2.20}$$

is a surface of fixed points. So we expect a conical singularity for $r_- = 0$ but not for $r_\pm \neq 0$.

From (2.17) the angular coordinate in $\mathcal{M}^{iden}$ is

$$\partial_\phi = \frac{r_+}{\ell} \left(u\partial_x + x\partial_u \right) - \frac{r_-}{\ell} \left(v\partial_y + y\partial_v \right) \ . \tag{2.21}$$

Hence

$$
\begin{cases}
\dfrac{\partial x}{\partial \phi} = u\dfrac{r_+}{\ell} \\[2mm]
\dfrac{\partial u}{\partial \phi} = x\dfrac{r_+}{\ell}
\end{cases}
\Rightarrow
\begin{cases}
\dfrac{\partial^2 x}{\partial \phi^2} = \left(\dfrac{r_+}{\ell}\right)^2 x \\[2mm]
\dfrac{\partial^2 u}{\partial \phi^2} = \left(\dfrac{r_+}{\ell}\right)^2 u
\end{cases}
\text{and}
\begin{cases}
\dfrac{\partial y}{\partial \phi} = -v\dfrac{r_-}{\ell} \\[2mm]
\dfrac{\partial v}{\partial \phi} = -y\dfrac{r_-}{\ell}
\end{cases}
\Rightarrow
\begin{cases}
\dfrac{\partial^2 y}{\partial \phi^2} = \left(\dfrac{r_-}{\ell}\right)^2 y \\[2mm]
\dfrac{\partial^2 v}{\partial \phi^2} = \left(\dfrac{r_-}{\ell}\right)^2 v
\end{cases} . \tag{2.22}
$$

Taking the parameters on the hyperboloid to be (t, r, ϕ) the last equations imply that

$$
u, x = \alpha(t,r)
\begin{cases}
\sinh\left(\dfrac{r_+}{\ell}\phi + \beta(r,t)\right) \\[2mm]
\cosh\left(\dfrac{r_+}{\ell}\phi + \beta(r,t)\right)
\end{cases}
\ , \quad
v, y = \gamma(t,r)
\begin{cases}
\sinh\left(-\dfrac{r_-}{\ell}\phi + \delta(r,t)\right) \\[2mm]
\cosh\left(-\dfrac{r_-}{\ell}\phi + \delta(r,t)\right)
\end{cases}
\ , \tag{2.23}
$$

where, for each of the variables (u, v, x, y) either the 'cosh' or the 'sinh' solution could be taken. Thus, using simply (2.17) for our choice of Killing vector field (2.19) we have constrained the form of the embedding functions to be (2.23).

Next, we use the second requirement, namely the definition of the radial coordinate (2.18). This yields the condition

$$r^2 = \left(\frac{r_+}{\ell}\right)^2 (u^2 - x^2) + \left(\frac{r_-}{\ell}\right)^2 (v^2 - y^2) . \tag{2.24}$$

It seems therefore natural that if we take the solution cosh (sinh) for u, then we should take the solution sinh (cosh) for x. The same applies to the pair (v, y). Thus, for the first pair we have the two possible solutions

Possibility 1 for (u, x) ,
$$\begin{cases} u = \alpha(r, t) \sinh\left(\frac{r_+}{\ell}\phi + \beta(r, t)\right) \\ x = \alpha(r, t) \cosh\left(\frac{r_+}{\ell}\phi + \beta(r, t)\right) \end{cases} \Rightarrow \quad u^2 - x^2 = -\alpha(r, t)^2 , \tag{2.25}$$

Possibility 2 for (u, x) ,
$$\begin{cases} u = \alpha(r, t) \cosh\left(\frac{r_+}{\ell}\phi + \beta(r, t)\right) \\ x = \alpha(r, t) \sinh\left(\frac{r_+}{\ell}\phi + \beta(r, t)\right) \end{cases} \Rightarrow \quad u^2 - x^2 = \alpha(r, t)^2 . \tag{2.26}$$

Similarly, for the second pair we have the two possibilities

Possibility 1 for (v, y) ,
$$\begin{cases} v = \gamma(r, t) \sinh\left(-\frac{r_-}{\ell}\phi + \delta(r, t)\right) \\ y = \gamma(r, t) \cosh\left(-\frac{r_-}{\ell}\phi + \delta(r, t)\right) \end{cases} \Rightarrow \quad v^2 - y^2 = -\gamma(r, t)^2 , \tag{2.27}$$

Possibility 2 for (v, y) ,
$$\begin{cases} v = \gamma(r, t) \cosh\left(-\frac{r_-}{\ell}\phi + \delta(r, t)\right) \\ y = \gamma(r, t) \sinh\left(-\frac{r_-}{\ell}\phi + \delta(r, t)\right) \end{cases} \Rightarrow \quad v^2 - y^2 = \gamma(r, t)^2 . \tag{2.28}$$

Denote by $i \otimes j$ choosing possibility i for (u, x) and possibility j for (v, y). We will insert this several possibilities in (2.24). Since the left hand side of (2.24) only depends on r it is clear that the simplest solutions for the functions $\alpha(r, t)$ and $\gamma(r, t)$ will be functions of r only. Thus we take $\alpha(r)$ and $\gamma(r)$ from now on.

- $1 \otimes 1$ yields for (2.24),
$$\ell^2 r^2 = -(r_+)^2 \alpha(r)^2 - (r_-)^2 \gamma(r)^2 . \tag{2.29}$$

  Since the functions $\alpha(r, t)$ and $\gamma(r, t)$ are supposed to be real functions this condition is impossible to solve.

- $1 \otimes 2$ yields for (2.24),
$$\ell^2 r^2 = -(r_+)^2 \alpha(r)^2 + (r_-)^2 \gamma(r)^2 . \tag{2.30}$$

  The solution is
$$\alpha(r) = \sqrt{\frac{r_-^2 - r^2}{r_+^2 - r_-^2}}\, \ell , \quad \gamma(r) = \sqrt{\frac{r_+^2 - r^2}{r_+^2 - r_-^2}}\, \ell , \tag{2.31}$$

  which is only valid for $r < r_- < r_+$, which we call *region III*.

- $2 \otimes 1$ yields for (2.24),
$$\ell^2 r^2 = (r_+)^2 \alpha(r)^2 - (r_-)^2 \gamma(r)^2 . \tag{2.32}$$

  The solution is
$$\alpha(r) = \sqrt{\frac{r^2 - r_-^2}{r_+^2 - r_-^2}}\, \ell , \quad \gamma(r) = \sqrt{\frac{r^2 - r_+^2}{r_+^2 - r_-^2}}\, \ell , \tag{2.33}$$

  which is only valid for $r_- < r_+ < r$, which we call *region I*.

- $2 \otimes 2$ yields for (2.24),

$$\ell^2 r^2 = (r_+)^2 \alpha(r)^2 + (r_-)^2 \gamma(r)^2 . \tag{2.34}$$

The solution is

$$\alpha(r) = \sqrt{\frac{r^2 - r_-^2}{r_+^2 - r_-^2}}\, \ell , \qquad \gamma(r) = \sqrt{\frac{r_+^2 - r^2}{r_+^2 - r_-^2}}\, \ell , \tag{2.35}$$

which is only valid for $r_- < r < r_+$, which we call *region II*.

Thus, the embedding functions of the BTZ black hole are, in Region I

$$
\left\{
\begin{aligned}
u &= \alpha(r) = \sqrt{\frac{r^2 - r_-^2}{r_+^2 - r_-^2}}\, \ell \cosh\left(\frac{r_+}{\ell}\phi + \beta(r,t)\right) \\
x &= \alpha(r) = \sqrt{\frac{r^2 - r_-^2}{r_+^2 - r_-^2}}\, \ell \sinh\left(\frac{r_+}{\ell}\phi + \beta(r,t)\right)
\end{aligned}
\right.
\qquad
\left\{
\begin{aligned}
v &= \gamma(r) = \sqrt{\frac{r^2 - r_+^2}{r_+^2 - r_-^2}}\, \ell \sinh\left(-\frac{r_-}{\ell}\phi + \delta(r,t)\right) \\
y &= \gamma(r) = \sqrt{\frac{r^2 - r_+^2}{r_+^2 - r_-^2}}\, \ell \cosh\left(-\frac{r_-}{\ell}\phi + \delta(r,t)\right)
\end{aligned}
\right.
\tag{2.36}
$$

in region II

$$
\left\{
\begin{aligned}
u &= \alpha(r) = \sqrt{\frac{r^2 - r_-^2}{r_+^2 - r_-^2}}\, \ell \cosh\left(\frac{r_+}{\ell}\phi + \beta(r,t)\right) \\
x &= \alpha(r) = \sqrt{\frac{r^2 - r_-^2}{r_+^2 - r_-^2}}\, \ell \sinh\left(\frac{r_+}{\ell}\phi + \beta(r,t)\right)
\end{aligned}
\right.
\qquad
\left\{
\begin{aligned}
v &= \gamma(r) = \sqrt{\frac{r_+^2 - r^2}{r_+^2 - r_-^2}}\, \ell \cosh\left(-\frac{r_-}{\ell}\phi + \delta(r,t)\right) \\
y &= \gamma(r) = \sqrt{\frac{r_+^2 - r^2}{r_+^2 - r_-^2}}\, \ell \sinh\left(-\frac{r_-}{\ell}\phi + \delta(r,t)\right)
\end{aligned}
\right.
\tag{2.37}
$$

and in region III

$$
\left\{
\begin{aligned}
u &= \alpha(r) = \sqrt{\frac{r_-^2 - r^2}{r_+^2 - r_-^2}}\, \ell \sinh\left(\frac{r_+}{\ell}\phi + \beta(r,t)\right) \\
x &= \alpha(r) = \sqrt{\frac{r_-^2 - r^2}{r_+^2 - r_-^2}}\, \ell \cosh\left(\frac{r_+}{\ell}\phi + \beta(r,t)\right)
\end{aligned}
\right.
\qquad
\left\{
\begin{aligned}
v &= \gamma(r) = \sqrt{\frac{r_+^2 - r^2}{r_+^2 - r_-^2}}\, \ell \cosh\left(-\frac{r_-}{\ell}\phi + \delta(r,t)\right) \\
y &= \gamma(r) = \sqrt{\frac{r_+^2 - r^2}{r_+^2 - r_-^2}}\, \ell \sinh\left(-\frac{r_-}{\ell}\phi + \delta(r,t)\right)
\end{aligned}
\right.
\tag{2.38}
$$

Choosing, for instance, the parameterization in region I, we can now compute the metric induced on the hypersurface (2.12) by (2.11). Since our parameterization already obeys all the constraints, still with $\beta(r,t)$ and $\gamma(r,t)$ unspecified, we take

$$\beta(r,t) = \beta t , \quad \delta(r,t) = \delta t , \tag{2.39}$$

with β, δ constants. The induced metric becomes

$$
ds^2 = \frac{r^2 \ell^2 dr^2}{(r^2 - r_+^2)(r^2 - r_-^2)} + r^2 d\phi^2 + \left[r^2(\beta r_+ + \delta r_-) - r_+ r_-(\beta r_- + \delta r_+)\right]\frac{2\ell d\phi dt}{r_+^2 - r_-^2} \\
+ \frac{\ell^2 dt^2}{r_+^2 - r_-^2}\left[r^2(\beta^2 - \delta^2) + r_+^2 \delta^2 - r_-^2 \beta^2\right]
\tag{2.40}
$$

Taking $\beta = -\chi r_-$ and $\delta = \chi r_+$, for constant χ, the cross terms becomes r independent. Since β and δ should have dimension $(length)^{-1}$, take $\chi = 1/\ell^2$. Then, the metric becomes

$$ds^2 = -\frac{(r^2 - r_+^2)(r^2 - r_-^2)}{r^2 \ell^2}dt^2 + \frac{r^2 \ell^2 dr^2}{(r^2 - r_+^2)(r^2 - r_-^2)} + r^2\left(d\phi - \frac{r_+ r_-}{\ell r^2}dt\right)^2 , \tag{2.41}$$

which is the standard BTZ metric. Alternatively, writing

$$m = \frac{r_+^2 + r_-^2}{\ell^2} , \qquad J = \frac{2 r_+ r_-}{\ell} , \tag{2.42}$$

the metric becomes

$$ds^2 = -\left(-m + \frac{r^2}{\ell^2} + \frac{J^2}{4r^2}\right) dt^2 - \frac{dr^2}{\left(-m + \frac{r^2}{\ell^2} + \frac{J^2}{4r^2}\right)} + r^2 \left(d\phi - \frac{J}{2r^2}\right)^2 . \tag{2.43}$$

m and J are interpreted as mass and angular momentum of the black hole, respectively.

2.3 The electric BTZ solutions

2.3.1 The BTZ black hole with a radial electric field

2.3.1.a Static black hole with a radial electric field

The gravitational field of the static electric BTZ black hole is [49]

$$ds^2 = -f^2 dt^2 + f^{-2} dr^2 + r^2 d\phi^2 , \qquad \text{with} \quad f^2 = r^2 - m - \frac{q^2}{4} \ln r^2 , \tag{2.44}$$

where m, and q are the mass and electric charge of the black hole, and the electromagnetic vector potential 1-form is

$$A = -q \ln r \, dt . \tag{2.45}$$

The function f^2 goes to $+\infty$ when $r \to 0$ and when $r \to +\infty$. It has a minimum at $r_{\min} = |q|/2$, and the value of f^2 at this minimum is $f^2_{\min} = -m + (q/2)^2 \left[1 - \ln(q/2)^2\right]$. When $f^2_{\min}$ is negative, f^2 has two roots and the corresponding charged black hole has two horizons. When these two roots coincide one has an extreme charged black hole and, finally, when f^2 is positive one has a naked singularity. The parameters m and q that represent these three regions are represented in Fig. 2.1, withdrawn from [49].
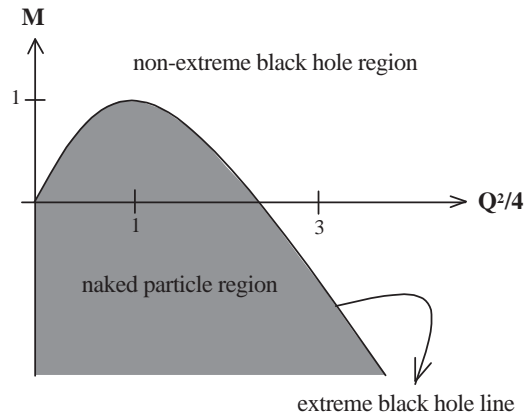
Figure 2.1: Values of the mass and of the charge of the static electric BTZ solution for which one has a non-extreme black hole, an extreme black hole, and a naked particle. The line represents the function $m = (q/2)^2 \left[1 - \ln(q/2)^2\right]$.

When $0 < m < 1$, for small values of the charge there is a black hole solution. Then, for a fixed mass in this interval, when the charge increases slightly there is a finite range of q where we find no black hole solution and, surprisingly, when this charge grows above a critical value we have again a black hole solution, no matter how big the charge is. This is in clear contrast with the usual charged solutions in (3+1)-dimensional spacetimes, for which the black hole solutions exist only when the charge is below a certain critical value. Moreover, and also in oppose to what happens in (3+1)-dimensions, there exist black holes with negative mass as long as the charge is big enough.

2.3.1.b   Rotating black hole with a radial electric field

The angular momentum is added to the solution (2.44) and (2.45) through the application of a Lorentz rotation boost in the t-φ plane [49, 232], $t \mapsto \frac{t - \varpi\varphi}{\sqrt{1 - \varpi^2}}$ and $\varphi \mapsto \frac{\varphi - \varpi t}{\sqrt{1 - \varpi^2}}$, where $\varpi^2 \leq 1$ is the rotation velocity parameter, and $\sqrt{1 - \varpi^2}$ is the usual Lorentz boost factor. The gravitational field of the rotating electric BTZ black hole is then [49]

$$ds^2 = -N^2 F^2 dt^2 + F^{-2} dR^2 + R^2 (d\varphi + N^\varphi dt)^2 \,, \tag{2.46}$$

where

$$R^2 = \frac{r^2 - \varpi^2 f^2}{1 - \varpi^2} \,, \quad F^2 = \left(\frac{dR}{dr}\right)^2 f^2 \,, \quad N = \frac{r}{R} \frac{dr}{dR} \,, \quad \text{and} \quad N^\varphi = \frac{\varpi(f^2 - r^2)}{R^2(1 - \varpi^2)} \,, \tag{2.47}$$

and f^2 is defined in (2.44). Under the above Lorentz boost the potential (2.45) transforms into

$$A = -\frac{q \ln r}{\sqrt{1 - \varpi^2}} (dt - \varpi d\varphi) \,. \tag{2.48}$$

The rotating electric BTZ black hole can have a maximum of two horizons which are the direct counterparts of the two horizons of the static electric BTZ solution. The ADM mass, angular momentum, and electric charge of the solution are given [49], respectively, by $M = \left[m(1 + \varpi^2) - \varpi^2 q^2/2\right]/(1 - \varpi^2)$, $J = 2\varpi(m - q^2/4)$, and $Q = q/\sqrt{1 - \varpi^2}$.

2.3.2   The BTZ solution with an azimuthal electric field

To conclude this brief overview on the electric counterparts of the BTZ solution, we mention that Cataldo [50] has found a horizonless BTZ solution with an azimuthal electric field, whose gravitational field is given by

$$ds^2 = -r^2 dt^2 + g^{-2} dr^2 + r^2 d\phi^2 \,, \quad \text{with} \quad g^2 = \frac{r^2}{\ell^2} + \frac{q^2}{r^2} \,, \tag{2.49}$$

where q is the electric charge of the solution, and with electromagnetic vector potential 1-form given by

$$A = -\frac{q}{r^2} \phi \, dt \,, \tag{2.50}$$

to which corresponds the above mentioned azimuthal electric field. When we set $q = 0$ (2.49) yields the empty AdS_3 spacetime.

2.4   The magnetic BTZ solution

In this section, we discuss in detail the static [48, 51, 52] and rotating [53] magnetic solution, that reduces to the BTZ solution when the magnetic field source vanishes. In particular, the conserved quantities (mass, angular momentum and electric charge), as well as their upper bounds, are defined, and we give a physical interpretation for the magnetic field source.

   The plan of this section is the following. In Section 2.4.1 we study the static magnetic solution found in [48, 51, 52] and its properties. Section 2.4.2 is devoted to the rotating magnetic solution. The angular momentum is added in section 2.4.2.a through a rotational Lorentz boost. In section 2.4.2.b we calculate the mass, angular momentum, and electric charge of both the static and rotating solutions and in section 2.4.2.c we set relations between the conserved charges. The rotating magnetic solution is written as a function of its hairs in section 2.4.2.d and we show that it reduces to the rotating BTZ solution when the magnetic source vanishes. In section 2.4.3 we give a physical interpretation for the origin of the magnetic field source.

2.4.1   Static solution. Analysis of its general structure

2.4.1.a   Static solution

Einstein gravity with a negative cosmological constant and a source of magnetic field (or Einstein–Maxwell–anti de Sitter gravity) in three dimensions can be characterized by the action

$$S = \frac{1}{16\pi G} \int d^3 x \sqrt{-g} \big[R - 2\Lambda - F^{\mu\nu} F_{\mu\nu} \big] \tag{2.51}$$

where g is the determinant of the metric $g_{\mu\nu}$, R the Ricci scalar, $F_{\mu\nu}$ the electromagnetic tensor given in terms of the vector potential A_μ by $F_{\mu\nu} = \partial_\mu A_\nu - \partial_\nu A_\mu$, and Λ is the cosmological constant. In this subsection we study the static point source solution of action (2.51) found by Hirschmann and Welch [51] and by Cataldo and Salgado [52]. The point source generates a gravitational field and a magnetic field. Written in the gauge presented in [51], the static solution is given by the following metric and vector potential 1-form

$$
\begin{aligned}
ds^2 &= -(r^2/\ell^2 - m)dt^2 + [r^2 + \chi_{\mathrm{m}}^2 \ln | \, r^2/\ell^2 - m \, |]d\varphi^2 \\
&\quad + r^2(r^2/\ell^2 - m)^{-1}[r^2 + \chi_{\mathrm{m}}^2 \ln | \, r^2/\ell^2 - m \, |]^{-1}dr^2 \, ,
\end{aligned}
\tag{2.52}
$$

$$A = \frac{1}{2}\chi_{\mathrm{m}} \ln | \, r^2/\ell^2 - m \, | d\varphi \, , \tag{2.53}$$

where t, r and φ are the time, the radial and the angular coordinates, respectively, χ_{m} is an integration constant which measures the intensity of the magnetic field source and $\ell \equiv -\frac{1}{\sqrt{\Lambda}}$ is the cosmological length. This spacetime reduces to the three dimensional BTZ black hole solution of Bañados, Teitelboim and Zanelli [39, 40] when the magnetic source vanishes. The parameter m is the mass of this uncharged solution.

The g_{rr} function is negative for $r < r_+$ and positive for $r > r_+$, where r_+ is such that

$$r_+^2 + \chi_{\mathrm{m}}^2 \ln | \, r_+^2/\ell^2 - m \, | = 0 \, , \tag{2.54}$$

and the condition $r_+^2 > m\ell^2$ is obeyed. One might then be tempted to say that the solution has an horizon at $r = r_+$ and consequently that one is in the presence of a magnetically charged black hole. However, this is not the case. In fact, one first notices that the metric components g_{rr} and $g_{\varphi\varphi}$ are related by $g_{\varphi\varphi} = [g_{rr}(r^2 - m\ell^2)/(\ell^2 r^2)]^{-1}$. Then, when g_{rr} becomes negative (which occurs for $r < r_+$) so does $g_{\varphi\varphi}$ and this leads to an apparent change of signature from $+2$ to -2. This strongly indicates [231] that an incorrect extension is being used and that one should choose a different continuation to describe the region $r < r_+$. By introducing a new radial coordinate, $\rho^2 = r^2 - r_+^2$, one obtains a spacetime that is both null and timelike geodesically complete for $r \geq r_+$ [51],

$$
\begin{aligned}
ds^2 &= -\frac{1}{\ell^2}(\rho^2 + r_+^2 - m\ell^2)dt^2 + \left[\rho^2 + \chi_{\mathrm{m}}^2 \ln\left(1 + \frac{\rho^2}{r_+^2 - m\ell^2} \right) \right] d\varphi^2 \\
&\quad + \ell^2\rho^2(\rho^2 + r_+^2 - m\ell^2)^{-1} \left[\rho^2 + \chi_{\mathrm{m}}^2 \ln\left(1 + \frac{\rho^2}{r_+^2 - m\ell^2} \right) \right]^{-1} d\rho^2 \, ,
\end{aligned}
\tag{2.55}
$$

where $0 \leq \rho < \infty$. This static spacetime has no curvature singularity, but it presents a conical geometry and, in particular, it has a conical singularity at $\rho = 0$ which can be removed if one identifies φ with the period $T_\varphi = 2\pi\nu$ where [51]

$$\nu = \frac{\exp(\beta/2)}{[1 + \chi_{\mathrm{m}}^2 \exp(\beta)/\ell^2]} \, , \tag{2.56}$$

and $\beta = r_+^2/\chi_{\mathrm{m}}^2$. Near the origin, metric (2.55) describes a spacetime which is locally flat but has a conical singularity at $\rho = 0$ with an angle deficit $\delta\varphi = 2\pi(1 - \nu)$.

2.4.1.b   Geodesic structure

We want to study the geodesic motion and, in particular, to confirm that the spacetime described by (2.55) is both null and timelike geodesically complete, i.e., that every null or timelike geodesic starting from an arbitrary point either can be extended to infinite values of the affine parameter along the geodesic or ends on a singularity. The equations governing the geodesics can be derived from the Lagrangian

$$\mathcal{L} = \frac{1}{2} g_{\mu\nu} \frac{dx^\mu}{d\tau} \frac{dx^\nu}{d\tau} = -\frac{\delta}{2} \,, \tag{2.57}$$

where τ is an affine parameter along the geodesic which, for a timelike geodesic, can be identified with the proper time of the particle along the geodesic. For a null geodesic one has $\delta = 0$ and for a timelike geodesic $\delta = +1$. From the Euler-Lagrange equations one gets that the generalized momenta associated with the time coordinate and angular coordinate are constants: $p_t = E$ and $p_\varphi = L$. The constant E is related to the timelike Killing vector $(\partial/\partial t)^\mu$ which reflects the time translation invariance of the metric, while the constant L is associated to the spacelike Killing vector $(\partial/\partial\varphi)^\mu$ which reflects the invariance of the metric under rotation. Note that since the spacetime is not asymptotically flat, the constants E and L cannot be interpreted as the energy and angular momentum at infinity.

From the metric we can derive the radial geodesic,

$$\dot{\rho}^2 = -\frac{1}{g_{\rho\rho}} \frac{E^2 g_{\varphi\varphi} + L^2 g_{tt}}{g_{tt} g_{\varphi\varphi}} - \frac{\delta}{g_{\rho\rho}} \,. \tag{2.58}$$

Using the two useful relations $g_{tt} g_{\varphi\varphi} = -\rho^2/g_{\rho\rho}$ and $g_{\varphi\varphi} = [g_{\rho\rho}(\rho^2 + r_+^2 - m\ell^2)/(\ell^2 \rho^2)]^{-1}$, we can write (2.58) as

$$\rho^2 \dot{\rho}^2 = \left[\frac{\ell^2 E^2}{\rho^2 + r_+^2 - m\ell^2} - \delta \right] \frac{\rho^2}{g_{\rho\rho}} + L^2 g_{tt} \,. \tag{2.59}$$

(i) Null geodesics $(\delta = 0)$ − Noticing that $1/g_{\rho\rho}$ is always positive for $\rho > 0$ and zero for $\rho = 0$, and that g_{tt} is always negative we conclude the following about the null geodesic motion. The first term in (2.59) is positive (except at $\rho = 0$ where it vanishes), while the second term is always negative. We can then conclude that spiraling $(L \neq 0)$ null particles coming in from an arbitrary point are scattered at the turning point $\rho_{\rm tp} > 0$ and spiral back to infinity. If the angular momentum L of the null particle is zero it hits the origin (where there is a conical singularity) with vanishing velocity.
(ii) Timelike geodesics $(\delta = +1)$ − Timelike geodesic motion is possible only if the energy of the particle satisfies $E > (r_+^2 - ml^2)^{1/2}/\ell$. In this case, spiraling timelike particles are bounded between two turning points that satisfy $\rho_{\rm tp}^{\rm a} > 0$ and $\rho_{\rm tp}^{\rm b} < \sqrt{\ell^2(E^2 + m) - r_+^2}$, with $\rho_{\rm tp}^{\rm b} \geq \rho_{\rm tp}^{\rm a}$. When the timelike particle has no angular momentum $(L = 0)$ there is a turning point located at $\rho_{\rm tp}^{\rm b} = \sqrt{\ell^2(E^2 + m) - r_+^2}$ and it hits the conical singularity at the origin $\rho = 0$. Hence, we confirm that the spacetime described by (2.55) is both timelike and null geodesically complete.

2.4.2   Rotating magnetic solution

2.4.2.a   Addition of angular momentum

Now, we want to endow the spacetime solution (2.55) with a global rotation, i.e., we want to add angular momentum to the spacetime. In order to do so we perform the following rotation boost in the t-φ plane (see e.g. [49, 71, 232])

$$\begin{aligned} t &\mapsto \gamma t - \ell \omega \varphi \,, \\ \varphi &\mapsto \gamma \varphi - \frac{\omega}{\ell} t \,, \end{aligned} \tag{2.60}$$

where γ and ω are constant parameters. Substituting (2.60) into (2.55) and (2.53) we obtain the stationary spacetime generated by a magnetic source

$$
\begin{aligned}
ds^2 &= -\frac{1}{\ell^2}\left[(\gamma^2 - \omega^2)\rho^2 + \gamma^2(r_+^2 - m\ell^2) - \omega^2\chi_{\mathrm{m}}^2 \ln\left(1 + \frac{\rho^2}{r_+^2 - m\ell^2}\right)\right]dt^2 \\
&\quad -\frac{\gamma\omega}{\ell}\left[-(r_+^2 - m\ell^2) + \chi_{\mathrm{m}}^2 \ln\left(1 + \frac{\rho^2}{r_+^2 - m\ell^2}\right)\right]2dtd\varphi \\
&\quad +\ell^2\rho^2(\rho^2 + r_+^2 - m\ell^2)^{-1}\left[\rho^2 + \chi_{\mathrm{m}}^2 \ln\left(1 + \frac{\rho^2}{r_+^2 - m\ell^2}\right)\right]^{-1}d\rho^2 \\
&\quad +\left[(\gamma^2 - \omega^2)\rho^2 - \omega^2(r_+^2 - m\ell^2) + \gamma^2\chi_{\mathrm{m}}^2 \ln\left(1 + \frac{\rho^2}{r_+^2 - m\ell^2}\right)\right]d\varphi^2 , \quad (2.61) \\
A &= -\frac{\omega}{\ell}A(\rho)dt + \gamma A(\rho)d\varphi , \quad (2.62)
\end{aligned}
$$

with $A(\rho) = \chi_{\mathrm{m}} \ln\left[(\rho^2 + r_+^2)/\ell^2 - m\right]/2$. We set $\gamma^2 - \omega^2 = 1$ because in this way when the angular momentum vanishes ($\omega = 0$) we have $\gamma = 1$ and so we recover the static solution.

Solution (2.61) represents a magnetically charged stationary spacetime and also solves the three dimensional Einstein-Maxwell-AdS gravity action (2.51). Transformations (2.60) generate a new metric because they are not permitted global coordinate transformations [233]. Transformations (2.60) can be done locally, but not globally. Therefore, the metrics (2.55) and (2.61) can be locally mapped into each other but not globally, and as such they are distinct.

Chen [78] has applied T-duality to [51] in order to write a rotating metric. However, the properties of the spacetime were not studied.

2.4.2.b Mass, angular momentum and electric charge of the solutions

Both the static and rotating solutions are asymptotically anti-de Sitter. This fact allows us to calculate the mass, angular momentum and the electric charge of the static and rotating solutions. To obtain these quantities we apply the formalism of Regge and Teitelboim [234] (see also [49, 71]). We first write (2.61) in the canonical form involving the lapse function $N^0(\rho)$ and the shift function $N^\varphi(\rho)$

$$
ds^2 = -(N^0)^2 dt^2 + \frac{d\rho^2}{f^2} + H^2(d\varphi + N^\varphi dt)^2 , \quad (2.63)
$$

where $f^{-2} = g_{\rho\rho}$, $H^2 = g_{\varphi\varphi}$, $H^2 N^\varphi = g_{t\varphi}$ and $(N^0)^2 - H^2(N^\varphi)^2 = g_{tt}$. Then, the action can be written in the Hamiltonian form as a function of the energy constraint $\mathcal{H}$, momentum constraint $\mathcal{H}_\varphi$ and Gauss constraint G

$$
\begin{aligned}
S &= -\int dt d^2x[N^0\mathcal{H} + N^\varphi\mathcal{H}_\varphi + A_t G] + \mathcal{B} \\
&= -\Delta t \int d\rho N\nu\left[\frac{2\pi^2}{H^3} + 2f(fH_{,\rho})_{,\rho} + \frac{H}{\ell^2} + \frac{2H}{f}(E^2 + B^2)\right] \\
&\quad +\Delta t \int d\rho N^\varphi\nu\left[(2\pi)_{,\rho} + \frac{4H}{f}E^\rho B\right] + \Delta t \int d\rho A_t \nu\left[-\frac{4H}{f}\partial_\rho E^\rho\right] + \mathcal{B} ,
\end{aligned}
$$

$$(2.64)$$

where $N = \frac{N^0}{f}$, $\pi \equiv \pi_\varphi{}^\rho = -\frac{fH^3(N^\varphi)_{,\rho}}{2N^0}$ (with $\pi^{\rho\varphi}$ being the momentum conjugate to $g_{\rho\varphi}$), E^ρ and B are the electric and magnetic fields and $\mathcal{B}$ is a boundary term. The factor ν comes from the fact that, due to the angle deficit, the integration over φ is between 0 and $2\pi\nu$. Upon varying the action

with respect to $f(\rho)$, $H(\rho)$, $\pi(\rho)$ and $E^\rho(\rho)$ one picks up additional surface terms. Indeed,

$$
\begin{aligned}
\delta S &= -\Delta t N\nu \left[H_{,\rho}\delta f^2 - (f^2)_{,\rho}\delta H + 2f^2\delta(H_{,\rho}) \right] \\
&\quad + \Delta t N^\varphi [2\nu\delta\pi] + \Delta t A_t \left[-\nu\frac{4H}{f}\delta E^\rho \right] + \delta\mathcal{B} \\
&\quad + \text{(terms vanishing when the equations of motion hold)}. \tag{2.65}
\end{aligned}
$$

In order that the Hamilton's equations are satisfied, the boundary term $\mathcal{B}$ has to be adjusted so that it cancels the above additional surface terms. More specifically one has

$$
\delta\mathcal{B} = -\Delta t N \delta M + \Delta t N^\varphi \delta J + \Delta t A_t \delta Q_{\rm e} \,, \tag{2.66}
$$

where one identifies M as the mass, J as the angular momentum and $Q_{\rm e}$ as the electric charge since they are the terms conjugate to the asymptotic values of N, N^φ and A_t, respectively.

To determine the mass, the angular momentum and the electric charge of the solutions one must take the spacetime that we have obtained and subtract the background reference spacetime contribution, i.e., we choose the energy zero point in such a way that the mass, angular momentum and charge vanish when the matter is not present.

Now, note that (2.61) has an asymptotic metric given by

$$
-\frac{\gamma^2 - \omega^2}{\ell^2}\rho^2 dt^2 + \frac{\ell^2}{\rho^2}d\rho^2 + (\gamma^2 - \omega^2)\rho^2 d\varphi^2 \,, \tag{2.67}
$$

where $\gamma^2 - \omega^2 = 1$ so, it is asymptotically an anti-de Sitter spacetime. The anti-de Sitter spacetime is also the background reference spacetime, since the metric (2.61) reduces to (2.67) if the matter is not present ($m = 0$ and $\chi_{\rm m} = 0$).

Taking the subtraction of the background reference spacetime into account we have that the mass, angular momentum and electric charge are given by

$$
\begin{aligned}
M &= \nu\left[-H_{,\rho}(f^2 - f_{\rm ref}^2) + (f^2)_{,\rho}(H - H_{\rm ref}) - 2f^2(H_{,\rho} - H_{,\rho}^{\rm ref}) \right] \,, \\
J &= -2\nu(\pi - \pi_{\rm ref}) \,, \\
Q_{\rm e} &= \frac{4H}{f}\nu(E^\rho - E_{\rm ref}^\rho) \,. \tag{2.68}
\end{aligned}
$$

After taking the asymptotic limit, $\rho \to +\infty$, we finally have that the mass and angular momentum are

$$
\begin{aligned}
M &= \nu\left[(\gamma^2 + \omega^2)(m - r_+^2/\ell^2) - 2\chi_{\rm m}^2/\ell^2 \right] + \mathrm{Div_M}(\chi_{\rm m}, \rho) \,, \tag{2.69} \\
J &= 2\nu\gamma\omega(m\ell^2 - r_+^2 - \chi_{\rm m}^2)/\ell + \mathrm{Div_J}(\chi_{\rm m}, \rho) \,, \tag{2.70}
\end{aligned}
$$

where $\mathrm{Div_M}(\chi_{\rm m}, \rho)$ and $\mathrm{Div_J}(\chi_{\rm m}, \rho)$ are logarithmic terms proportional to the magnetic source $\chi_{\rm m}$ that diverge as $\rho \to +\infty$ (see also [57]). The presence of these kind of divergences in the mass and angular momentum is a usual feature present in charged solutions. They can be found for example in the electrically charged point source solution [23], in the electrically charged BTZ black hole [49] and in the electrically charged black holes of three dimensional Brans-Dicke gravity [71]. Following [49, 71, 23] the divergences on the mass can be treated as follows. One considers a boundary of large radius ρ_0 involving the system. Then, one sums and subtracts $\mathrm{Div_M}(\chi_{\rm m}, \rho_0)$ to (2.69) so that the mass (2.69) is now written as

$$
M = M(\rho_0) + \left[\mathrm{Div_M}(\chi_{\rm m}, \rho) - \mathrm{Div_M}(\chi_{\rm m}, \rho_0) \right] \,, \tag{2.71}
$$

where $M(\rho_0) = M_0 + \mathrm{Div_M}(\chi_{\rm m}, \rho_0)$, i.e.,

$$
M_0 = M(\rho_0) - \mathrm{Div_M}(\chi_{\rm m}, \rho_0) \,. \tag{2.72}
$$

The term between brackets in (2.71) vanishes when $\rho \to \rho_0$. Then $M(\rho_0)$ is the energy within the radius ρ_0. The difference between $M(\rho_0)$ and M_0 is $-\text{Div}_\text{M}(\chi_\text{m}, \rho_0)$ which is interpreted as the electromagnetic energy outside ρ_0 apart from an infinite constant which is absorbed in $M(\rho_0)$. The sum (2.72) is then independent of ρ_0, finite and equal to the total mass. In practice the treatment of the mass divergence amounts to forgetting about ρ_0 and take as zero the asymptotic limit: $\lim \text{Div}_\text{M}(\chi_\text{m}, \rho) = 0$.

To handle the angular momentum divergence, one first notices that the asymptotic limit of the angular momentum per unit mass (J/M) is either zero or one, so the angular momentum diverges at a rate slower or equal to the rate of the mass divergence. The divergence on the angular momentum can then be treated in a similar way as the mass divergence. So, one can again consider a boundary of large radius ρ_0 involving the system. Following the procedure applied for the mass divergence one concludes that the divergent term $-\text{Div}_\text{J}(\chi_\text{m}, \rho_0)$ can be interpreted as the electromagnetic angular momentum outside ρ_0 up to an infinite constant that is absorbed in $J(\rho_0)$.

Hence, in practice the treatment of both the mass and angular divergences amounts to forgetting about ρ_0 and take as zero the asymptotic limits: $\lim \text{Div}_\text{M}(\chi_\text{m}, \rho) = 0$ and $\lim \text{Div}_\text{J}(\chi_\text{m}, \rho) = 0$ in (2.69) and (2.70).

Now, we calculate the electric charge of the solutions. To determine the electric field we must consider the projections of the Maxwell field on spatial hypersurfaces. The normal to such hypersurfaces is $n^\nu = (1/N^0, 0, -N^\varphi/N^0)$ and the electric field is given by $E^\mu = g^{\mu\sigma} F_{\sigma\nu} n^\nu$. Then, from (2.68), the electric charge is

$$Q_\text{e} = -\frac{4Hf}{N^0} \nu(\partial_\rho A_t - N^\varphi \partial_\rho A_\varphi) = 2\nu \frac{\omega}{\ell} \chi_\text{m} \,. \tag{2.73}$$

Note that the electric charge is proportional to $\omega \chi_\text{m}$. Since in three dimensions the magnetic field is a scalar (rather than a vector) one cannot use Gauss's law to define a conserved magnetic charge. In the next section we will propose a physical interpretation for the origin of the magnetic field source and discuss the result obtained in (2.73).

The mass, angular momentum and electric charge of the static solutions can be obtained by putting $\gamma = 1$ and $\omega = 0$ on the above expressions [see (2.60)].

2.4.2.c Relations between the conserved charges

Now, we want to cast the metric (2.61) in terms of M, J, Q_e and χ_m. We can use (2.69) and (2.70) to solve a quadratic equation for γ^2 and ω^2. It gives two distinct sets of solutions

$$\gamma^2 = \frac{M\ell^2 + 2\chi_\text{m}^2}{2(m\ell^2 - r_+^2)} \frac{(2-\Omega)}{\nu} \,, \qquad \omega^2 = \frac{M\ell^2 + 2\chi_\text{m}^2}{2(m\ell^2 - r_+^2)} \frac{\Omega}{\nu} \,, \tag{2.74}$$

$$\gamma^2 = \frac{M\ell^2 + 2\chi_\text{m}^2}{2(m\ell^2 - r_+^2)} \frac{\Omega}{\nu} \,, \qquad \omega^2 = \frac{M\ell^2 + 2\chi_\text{m}^2}{2(m\ell^2 - r_+^2)} \frac{(2-\Omega)}{\nu} \,, \tag{2.75}$$

where we have defined a rotating parameter Ω, which ranges between $0 \le \Omega < 1$, as

$$\Omega \equiv 1 - \sqrt{1 - \frac{(m\ell^2 - r_+^2)^2}{(M\ell^2 + 2\chi_\text{m}^2)^2} \frac{\ell^2 J^2}{(m\ell^2 - r_+^2 - \chi_\text{m}^2)^2}} \,. \tag{2.76}$$

When we take $J = 0$ (which implies $\Omega = 0$), (2.74) gives $\gamma \ne 0$ and $\omega = 0$ while (2.75) gives the nonphysical solution $\gamma = 0$ and $\omega \ne 0$ which does not reduce to the static original metric. Therefore we will study the solutions found from (2.74). The condition that Ω remains real imposes a restriction on the allowed values of the angular momentum

$$\ell^2 J^2 \le \frac{(m\ell^2 - r_+^2 - \chi_\text{m}^2)^2}{(m\ell^2 - r_+^2)^2} (M\ell^2 + 2\chi_\text{m}^2)^2 \,. \tag{2.77}$$

The condition $\gamma^2 - \omega^2 = 1$ allows us to write $r_+^2 - m\ell^2$ as a function of M, Ω and $\chi_{\rm m}$,

$$r_+^2 - m\ell^2 = (M\ell^2 + 2\chi_{\rm m}^2)(\Omega - 1)/\nu \,. \tag{2.78}$$

This relation allows us to achieve interesting conclusions about the values that the parameters M, $\chi_{\rm m}$ and J can have. Indeed, if we replace (2.78) into (2.74) we get

$$\gamma^2 = \frac{(2 - \Omega)}{2(1 - \Omega)} \,, \qquad \omega^2 = \frac{\Omega}{2(1 - \Omega)} \,. \tag{2.79}$$

Since Ω ranges between $0 \le \Omega < 1$, we have $\gamma^2 > 0$ and $\omega^2 > 0$. Besides, one has that $r_+^2 > m\ell^2$ and $\nu > 0$ so from (2.71) we conclude that both the static and rotating solutions have negative mass. Therefore, from now one, whenever we refer to the mass of the solution we will set

$$M = -|M| \,, \tag{2.80}$$

unless otherwise stated.

Looking again to (2.78) we can also conclude that one must have

$$\chi_{\rm m}^2 < \frac{|M|\ell^2}{2} \,, \tag{2.81}$$

i.e., there is an upper bound for the intensity of the magnetic field strength.

From (2.70) we also see that the angular momentum is always negative indicating that the angular momentum and the angular velocity, ω, have opposite directions. This is the expected result since J is the inertial momentum times the angular velocity and the inertial momentum is proportional to the mass which is negative. Introducing (2.78) into (2.77) we find an upper bound for the angular momentum

$$|J| \le |M|\ell^2 - 2\chi_{\rm m}^2 + \nu\chi_{\rm m}^2/(1 - \Omega) \,. \tag{2.82}$$

Note that from (2.76) we can get the precise value of J as a function of M, Ω and $\chi_{\rm m}$.

Finally, we remark that the auxiliary equations (2.54), (2.56) and (2.79) allow us to define the auxiliary parameters r_+, ν and m as a function of the hairs M, Ω and $\chi_{\rm m}$.

2.4.2.d   The rotating magnetic solution

We are now in position to write the stationary spacetime (2.61) generated by a source of magnetic field in three dimensional Einstein-Maxwell-anti de Sitter gravity as a function of its hairs,

$$
\begin{aligned}
ds^2 \;=\; & -\frac{1}{\ell^2}\left[\rho^2 + \frac{1}{2\nu}(|M|\ell^2 - 2\chi_{\rm m}^2)(2 - \Omega) - \frac{Q_{\rm e}^2}{4\nu}\ln\left(1 + \frac{\nu\rho^2}{(|M|\ell^2 - 2\chi_{\rm m}^2)(1 - \Omega)}\right)\right]dt^2 \\
& +\frac{J}{\nu}\frac{(|M|\ell^2 - 2\chi_{\rm m}^2)(\Omega - 1) + \nu\chi_{\rm m}^2\ln\left(1 + \frac{\nu\rho^2}{(|M|\ell^2 - 2\chi_{\rm m}^2)(1 - \Omega)}\right)}{(|M|\ell^2 - 2\chi_{\rm m}^2)(1 - \Omega) + \nu\chi_{\rm m}^2}dtd\varphi \\
& +\frac{\ell^2\rho^2\left[\rho^2 + \chi_{\rm m}^2\ln\left(1 + \frac{\nu\rho^2}{(|M|\ell^2 - 2\chi_{\rm m}^2)(1 - \Omega)}\right)\right]^{-1}}{\rho^2 + (|M|\ell^2 - 2\chi_{\rm m}^2)(1 - \Omega)/\nu}d\rho^2 \\
& +\left[\rho^2 - (|M|\ell^2 - 2\chi_{\rm m}^2)\frac{\Omega}{2\nu} + \frac{2 - \Omega}{1 - \Omega}\frac{\chi_{\rm m}^2}{2}\ln\left(1 + \frac{\nu\rho^2}{(|M|\ell^2 - 2\chi_{\rm m}^2)(1 - \Omega)}\right)\right]d\varphi^2 \,, \quad (2.83)
\end{aligned}
$$

as well as the vector potential 1-form (2.62)

$$A = \frac{2}{\sqrt{1 - \Omega}}\left[-\frac{\sqrt{\Omega}}{\ell}A(\rho)dt + \sqrt{2 - \Omega}A(\rho)d\varphi\right] \,, \tag{2.84}$$

with $A(\rho) = (\chi_{\rm m}/2)\ln\left[\rho^2/\ell^2 + (|M| - 2\chi_{\rm m}^2/\ell^2)(1 - \Omega)/\nu\right]$.

If we set $\Omega = 0$ (and thus $J = 0$ and $Q_{\rm e} = 0$) we recover the static solution (2.55) [see (2.60)]. Finally if we set $\chi_{\rm m} = 0$ (and so $\nu = 1$) one gets

$$ds^2 = -\frac{1}{\ell^2}\left[\rho^2 - M\ell^2\frac{2-\Omega}{2}\right]dt^2 - Jdtd\varphi + \frac{\ell^2}{\rho^2 - M\ell^2(1-\Omega)}d\rho^2 + \left[\rho^2 + M\ell^2\frac{\Omega}{2}\right]d\varphi^2 , \tag{2.85}$$

where we have dropped the absolute value of M since now the mass can be positive. This is the rotating uncharged BTZ solution written, however, in an unusual gauge. To write it in the usual gauge we apply to (2.85) the radial coordinate transformation

$$\rho^2 = R^2 - M\ell^2\frac{\Omega}{2} \quad \Rightarrow \quad d\rho^2 = \frac{R^2}{R^2 - M\ell^2\Omega/2}dR^2 \tag{2.86}$$

and use the relation $J^2 = \Omega(2-\Omega)M\ell^2$ [see (2.76)] to obtain

$$ds^2 = -\left(\frac{R^2}{\ell^2} - M\right)dt^2 - Jdtd\varphi + \left(\frac{R^2}{\ell^2} - M + \frac{J^2}{4R^2}\right)^{-1}dR^2 + R^2d\varphi^2 . \tag{2.87}$$

So, as expected, (2.83) reduces to the rotating uncharged BTZ solution [39, 40] when the magnetic field source vanishes.

2.4.2.e Geodesic structure

The geodesic structure of the rotating spacetime is similar to the static spacetime (see section II.2), although there are now direct (corotating with $L > 0$) and retrograde (counter-rotating with $L < 0$) orbits. The most important result that spacetime is geodesically complete still holds for the stationary spacetime.

2.4.3 Physical interpretation of the magnetic source

When we look back to the electric charge given in (2.73), we see that it is zero when $\omega = 0$, i.e., when the angular momentum J of the spacetime vanishes. This is expected since in the static solution we have imposed that the electric field is zero (F_{12} is the only non-null component of the Maxwell tensor).

Still missing is a physical interpretation for the origin of the magnetic field source. The magnetic field source is not a Nielson-Oleson vortex solution since we are working with the Maxwell theory and not with an Abelian-Higgs model. We might then think that the magnetic field is produced by a Dirac point-like monopole. However, this is not also the case since a Dirac monopole with strength $g_{\rm m}$ appears when one breaks the Bianchi identity [235], yielding $\partial_\mu(\sqrt{-g}\tilde{F}^\mu) = g_{\rm m}\delta^2(\vec{x})$ (where $\tilde{F}^\mu = \epsilon^{\mu\nu\gamma}F_{\nu\gamma}/2$ is the dual of the Maxwell field strength), whereas in this work we have that $\partial_\mu(\sqrt{-g}\tilde{F}^\mu) = 0$. Indeed, we are clearly dealing with the Maxwell theory which satisfies Maxwell equations and the Bianchi identity

$$\frac{1}{\sqrt{-g}}\partial_\nu(\sqrt{-g}F^{\mu\nu}) = \frac{\pi}{2}\frac{1}{\sqrt{-g}}j^\mu , \tag{2.88}$$

$$\partial_\mu(\sqrt{-g}\tilde{F}^\mu) = 0 , \tag{2.89}$$

respectively. In (2.88) we have made use of the fact that the general relativistic current density is $1/\sqrt{-g}$ times the special relativistic current density $j^\mu = \sum q\delta^2(\vec{x} - \vec{x}_0)\dot{x}^\mu$.

We then propose that the magnetic field source can be interpreted as composed by a system of two symmetric and superposed electric charges (each with strength q). One of the electric charges is at rest with positive charge (say), and the other is spinning with an angular velocity $\dot{\varphi}_0$ and negative electric charge. Clearly, this system produces no electric field since the total electric charge is zero and the magnetic field is produced by the angular electric current. To confirm our interpretation,

we go back to (2.88). In our solution, the only non-vanishing component of the Maxwell field is $F^{\varphi\rho}$ which implies that only j^φ is not zero. According to our interpretation one has $j^\varphi = q\delta^2(\vec{x} - \vec{x}_0)\dot\varphi$, which one inserts in (2.88). Finally, integrating over ρ and φ we have

$$\chi_{\mathrm{m}} \propto q\dot\varphi_0 . \tag{2.90}$$

So, the magnetic source strength, χ_{m}, can be interpreted as an electric charge q times its spinning velocity.

Looking again to the electric charge given in (2.73), one sees that after applying the rotation boost in the t-φ plane to endow the initial static spacetime with angular momentum, there appears a net electric charge. This result was already expected since now, besides the scalar magnetic field ($F_{\rho\varphi} \neq 0$), there is also an electric field ($F_{t\rho} \neq 0$) [see (2.84)]. A physical interpretation for the appearance of the net electric charge is now needed. To do so, we return to the static spacetime. In this static spacetime there is a static positive charge and a spinning negative charge of equal strength at the center. The net charge is then zero. Therefore, an observer at rest (S) sees a density of positive charges at rest which is equal to the density of negative charges that are spinning. Now, we perform a local rotational boost $t' = \gamma t - \ell\omega\varphi$ and $\varphi' = \gamma\varphi - \frac{\omega}{\ell}t$ to an observer (S') in the static spacetime, so that S' is moving relatively to S. This means that S' sees a different charge density since a density is a charge over an area and this area suffers a Lorentz contraction in the direction of the boost. Hence, the two sets of charge distributions that had symmetric charge densities in the frame S will not have charge densities with equal magnitude in the frame S'. Consequently, the charge densities will not cancel each other in the frame S' and a net electric charge appears. This was done locally. When we turn into the global rotational Lorentz boost of (2.60) this interpretation still holds. The local analysis above is similar to the one that occurs when one has a copper wire with an electric current and we apply a translation Lorentz boost to the wire: first, there is only a magnetic field but, after the Lorentz boost, one also has an electric field. The difference is that in the present situation the Lorentz boost is a rotational one and not a translational one.

2.5 Summary and discussion

The BTZ black hole [39], with non-vanishing mass and angular momentum, is asymptotically AdS. This solution has constant curvature and thus there can be no curvature singularity at the origin. As discussed in detail in [40], the BTZ black hole can be expressed as a topological quotient of AdS_3 by a group of isometries. This is, the BTZ black hole can be obtained through identifications along an isometry of the AdS_3 spacetime, and in order to avoid closed timelike curves, the origin must be a topological singularity (a boundary of the spacetime). We have reviewed in detail this construction. Qualitatively, the reason why the black hole exists only in an AdS background can be understood as follows. The radius of an event horizon (r_+) in a D-dimensional spacetime is expected to be proportional to $G_D M$, where G_D is the D-dimensional Newton's constant. Now, in mass units G_D has dimension M^{2-D}. Thus, $G_D M$ (and r_+) is dimensionless in $D = 3$, and there is no length scale in $D = 3$. The cosmological constant provides this length scale for the horizon, but only when $\Lambda < 0$ (AdS case). One may argue that this is due to the fact that the AdS background is attractive, i.e., an analysis of the geodesic equations indicates that particles in this background are subjected to a potential well that attracts them (and so it is possible to concentrate matter into a small region), while the dS background is repulsive (in practice, if we try to construct a dS black hole through identifications along an isometry of the dS_3 spacetime, we verify that the possible horizon is inside the region that contains closed timelike curves).

The extension to include a radial electric field in the BTZ black hole has been done in [48, 49] (this solution reduces to those of [23, 24] when $\Lambda = 0$). Due to the slow fall off of the electric field in 3-dimensions, the system has infinite total energy. The presence of the electric energy-momentum tensor implies that the spacetime has no longer constant curvature, and the electric BTZ black hole cannot be expressed as a topological quotient of AdS_3 by a group of isometries. The rotating

charged black hole is generated from the static charged solution (already found in [39]) through the application of a rotation Lorentz boost. A BTZ solution with an azimuthal electric field was found in [50]. This solution is horizonless, and reduces to empty AdS_3 spacetime when the charge vanishes.

Pure magnetic solutions with $\Lambda < 0$, that reduce to the neutral BTZ black hole solution when the magnetic source vanishes, also exist and were reviewed in section 2.4. Notice that, in oppose to what occurs in 4-dimensions where the the Maxwell tensor and its dual are 2-forms, in 3-dimensions the Maxwell tensor is still a 2-form, but its dual is a 1-form (in practice, the Maxwell tensor has only three independent components: two for the electric vector field, and one for the scalar magnetic field). As a consequence, the magnetic solutions are radically different from the electric solutions in 3-dimensions. The static magnetic solution has been found in [48, 51, 52]. This spacetime generated by a static magnetic point source is horizonless and has a conical singularity at the origin. The extension to include rotation and a new interpretation for the source of magnetic field has been made in [53]. In [51], the static magnetic source has been interpreted as a kind of magnetic monopole reminiscent of a Nielson-Oleson vortex solution. In [53], we prefer to interpret the static magnetic field source as being composed by a system of two symmetric and superposed electric charges. One of the electric charges is at rest and the other is spinning. This system produces no electric field since the total electric charge is zero and the scalar magnetic field is produced by the angular electric current. When we apply a rotational Lorentz boost to add angular momentum to the spacetime, there appears an electric charge and an electric field.

Chapter 3

Three dimensional dilaton black holes of the Brans-Dicke type

Contents

In order to turn the 3-dimensional gravity dynamics more similar with the realistic 4-dimensional one, we can manage a way by which we introduce local degrees of freedom. One way to do this, is by coupling a scalar field to Einstein gravity, yielding a so called dilaton gravity. The most general form of this kind of gravity was proposed by Wagoner [67] in 1970. The scalar field provides a local dynamical degree of freedom to the theory, and models of this kind (i.e., under certain choices of the parameters) appear naturally in string theory. Some choices of the parameters of the theory yield dilaton gravities that have black hole solutions. One of these theories, which we will study in this chapter, is an Einstein-dilaton gravity of the Brans-Dicke type in a $\Lambda < 0$ background, first discussed by Lemos [6]. This theory is specified by a Brans-Dicke parameter, ω, and contains seven different cases. Each ω can be viewed as yielding a different dilaton gravity theory, with some of these being related with other known special theories. For instance, for $\omega = -1$ one gets the simplest low-energy string action [68], and for $\omega = 0$ one gets a theory related (through dimensional reduction) to 4-dimensional general relativity with one Killing vector [6, 7, 8]. This is, the $\omega = 0$ black holes are the direct counterparts of the 4-dimensional AdS black holes with toroidal or cylindrical topology first discussed by Lemos, in the same way that a point source in 3-dimensions is the direct cousin of a cosmic string in 4-dimensions. For $\omega = \pm\infty$ the theory reduces to the pure 3-dimensional general relativity. This is, the $\omega = \pm\infty$ black holes are the BTZ ones. Moreover, the case $\omega > -1$ yields gravities whose black holes have a structure and properties similar to the BTZ black hole, but with a feature that might be useful: the $\omega > -1$ black holes have dynamical degrees of freedom, which implies for example that the origin has a curvature singularity and that gravitational waves can propagate in the spacetime. The neutral black holes of this Brans-Dicke theory were found and analyzed by Sá, Kleber and Lemos [6, 69, 70]. The pure electric charged black holes have been analysed by Dias and Lemos [71], and the pure magnetic solutions have been discussed by Dias and Lemos [72]. We will analyze in detail these black holes in this chapter.

The plan of this chapter is as follows. In section 3.2 we briefly present the neutral black holes of the Brans-Dicke theory [6, 69, 70]. Then, in section 3.2, we discuss in detail the electric charged black holes (static and rotating) of the theory [71] and, in section 3.3, we do the same with the magnetic solutions [72]. Finally, in section 3.4, concluding remarks are given.

3.1   Neutral Brans-Dicke dilaton black holes

We work with an action of the Brans-Dicke type in three-dimensions written in the string frame as

$$S = \frac{1}{2\pi} \int d^3x \sqrt{-g}\, e^{-2\phi} \left[R - 4\omega(\partial\phi)^2 + \Lambda \right], \tag{3.1}$$

where g is the determinant of the 3-dimensional (3D) metric, R is the curvature scalar, ϕ is a scalar field called dilaton, $\Lambda < 0$ is the cosmological constant, ω is the three-dimensional Brans-Dicke parameter.

From the field equations of (3.1), one finds the following solutions (with many of them being black holes),

$$
\begin{aligned}
ds^2 &= -\left[(\alpha r)^2 - \frac{(\omega+1)}{2(\omega+2)} \frac{M(2-\Omega)}{(\alpha r)^{\frac{1}{\omega+1}}} \right] dt^2 - \frac{\omega+1}{2\omega+3} J \frac{1}{(\alpha r)^{\frac{1}{\omega+1}}} 2dtd\varphi \\
&\quad + \left[(\alpha r)^2 - \frac{M[2(\omega+1)-(2\omega+3)\Omega]}{2(\omega+2)(\alpha r)^{\frac{1}{\omega+1}}} \right]^{-1} dr^2 + \frac{1}{\alpha^2}\left[(\alpha r)^2 + \frac{M\Omega}{2(\alpha r)^{\frac{1}{\omega+1}}} \right] d\varphi^2, \\
&\qquad\qquad\qquad\qquad\qquad\qquad\qquad \text{for} \quad \omega \neq -2, -\frac{3}{2}, -1\,, \tag{3.2}
\end{aligned}
$$

$$
ds^2 = -\left(r^2 - \frac{J^2}{M} r \right) dt^2 - J\, r\, 2dtd\varphi + \left[r^2 - M\left(\frac{J^2}{M^2} - 1 \right) r \right]^{-1} dr^2 + \left(r^2 + Mr \right) d\varphi^2,
$$
$$
\text{for} \quad \omega = -2, \tag{3.3}
$$

$$
ds^2 = r^2 \Lambda \ln(br)\, dt^2 - \frac{dr^2}{r^2 \Lambda \ln(br)} + r^2 d\varphi^2, \qquad \text{for} \quad \omega = -\frac{3}{2}, \tag{3.4}
$$

where, for $\omega \neq -2, -\frac{3}{2}, -1$, α is defined as $\alpha = \sqrt{\left| \frac{(\omega+1)^2\Lambda}{(\omega+2)(2\omega+3)} \right|}$. M and J are, respectively, the ADM mass and angular momentum of the solutions, and we have defined the rotating parameter $\Omega \equiv 1 - \sqrt{1 - \frac{4(\omega+1)(\omega+2)}{(2\omega+3)^2} \frac{J^2\alpha^2}{M^2}}$ in such a way that $J = 0$ implies $\Omega = 0$. The condition that Ω remains real imposes, for $-2 > \omega > -1$, a maximum bound for the angular momentum: $|\alpha J| \leq \frac{|2\omega+3|M}{2\sqrt{(\omega+1)(\omega+2)}}$. For $-\frac{3}{2}$, one has $M = -\Lambda \ln b$ and $J = 0$, necessarily. For $\omega < -\frac{3}{2}$ and $\omega > -1$, the solutions have a curvature singularity located at $r = 0$, and for $-\frac{3}{2} < \omega < -1$ the curvature singularity is at $r = +\infty$. For $\omega = -\frac{3}{2}$, both $r = 0$ and $r = +\infty$ are singular. For $\omega = \pm\infty$ there is no curvature singularity. Many of this theories (i.e., for different ω) have black hole solutions. A detailed analysis of the character of the solutions can be found in [69, 70]. Here we do not go further in their study, since in next section we will study in detail these solutions when a charge Q is added to the system.

3.2   Electric Brans-Dicke dilaton black holes

In this section we find and study in detail the static and rotating electrically charged solutions of a Einstein-Maxwell-Dilaton action of the Brans-Dicke type. So, these are the electric counterparts of the solutions discussed in the last section [69, 70].

The electrically charged theory that we are going to study is specified by the extra electromagnetic field $F^{\mu\nu}$. It contains eight different cases. For $\omega = 0$ one gets a theory related (through dimensional reduction) to electrically charged four dimensional General Relativity with one Killing vector [7] and for $\omega = \pm\infty$ one obtains electrically charged three dimensional General Relativity [48, 49].

Since magnetically charged solutions in (2+1) dimensions have totally different properties from the electrically charged ones, we leave their study for section 3.3.

The plan of this section is the following. In Section 3.2.1 we set up the action and the field equations. The static general solution of the field equations are found in section 3.2.2 and we

write the scalar $R_{\mu\nu}R^{\mu\nu}$ which, in 3-dimensions, signals the presence of singularities. The angular momentum is added in section 3.2.3. In section 3.2.4 we use an extension of the formalism of Regge and Teitelboim to derive the mass, angular momentum, electric charge and dilaton charge of the black holes. In section 3.2.5 we study the properties of the different cases that appear naturally from the solutions. We work out in detail the causal structure and the geodesic motion of null and timelike particles for typical values of ω that belong to the different ranges. The Hawking temperature is computed in section 3.2.6.

3.2.1 Field equations of Brans-Dicke–Maxwell theory

We are going to work with an action of the Maxwell-Brans-Dicke type in three-dimensions written in the string frame as

$$S = \frac{1}{2\pi} \int d^3x \sqrt{-g}\, e^{-2\phi} \big[R - 4\omega(\partial\phi)^2 + \Lambda - F^{\mu\nu}F_{\mu\nu} \big], \tag{3.5}$$

where g is the determinant of the 3D metric, R is the curvature scalar, ϕ is a scalar field called dilaton, Λ is the cosmological constant, ω is the three-dimensional Brans-Dicke parameter and $F_{\mu\nu} = \partial_\mu A_\nu - \partial_\nu A_\mu$ is the Maxwell tensor, with A_μ being the vector potential. Varying this action with respect to $g^{\mu\nu}$, $F^{\mu\nu}$ and ϕ one gets the Einstein, Maxwell and ditaton equations, respectively

$$\tfrac{1}{2}G_{\mu\nu} - 2(\omega+1)\nabla_\mu\phi\nabla_\nu\phi + \nabla_\mu\nabla_\nu\phi - g_{\mu\nu}\nabla_\gamma\nabla^\gamma\phi + (\omega+2)g_{\mu\nu}\nabla_\gamma\phi\nabla^\gamma\phi - \tfrac{1}{4}g_{\mu\nu}\Lambda = \tfrac{\pi}{2}T_{\mu\nu}, \tag{3.6}$$

$$\nabla_\nu(e^{-2\phi}F^{\mu\nu}) = 0\,, \tag{3.7}$$

$$R - 4\omega\nabla_\gamma\nabla^\gamma\phi + 4\omega\nabla_\gamma\phi\nabla^\gamma\phi + \Lambda = -F^{\gamma\sigma}F_{\gamma\sigma}, \tag{3.8}$$

where $G_{\mu\nu} = R_{\mu\nu} - \tfrac{1}{2}g_{\mu\nu}R$ is the Einstein tensor, ∇ represents the covariant derivative and $T_{\mu\nu} = \tfrac{2}{\pi}(g^{\gamma\sigma}F_{\mu\gamma}F_{\nu\sigma} - \tfrac{1}{4}g_{\mu\nu}F_{\gamma\sigma}F^{\gamma\sigma})$ is the Maxwell energy-momentum tensor.

We want to consider now a spacetime which is both static and rotationally symmetric, implying the existence of a timelike Killing vector $\partial/\partial t$ and a spacelike Killing vector $\partial/\partial\varphi$. The most general static metric with a Killing vector $\partial/\partial\varphi$ with closed orbits in three dimensions can be written as $ds^2 = -e^{2\nu(r)}dt^2 + e^{2\mu(r)}dr^2 + r^2 d\varphi^2$, with $0 \leq \varphi \leq 2\pi$. Each different ω has a very rich and non-trivial structure of solutions which could be considered on its own. As in [69, 70] we work in the Schwarzschild gauge, $\mu(r) = -\nu(r)$, and compare different black hole solutions in different theories. For this ansatz the metric is written as

$$ds^2 = -e^{2\nu(r)}dt^2 + e^{-2\nu(r)}dr^2 + r^2 d\varphi^2. \tag{3.9}$$

We also assume that the only non-vanishing components of the vector potential are $A_t(r)$ and $A_\varphi(r)$, i.e. ,

$$A = A_t dt + A_\varphi d\varphi\,. \tag{3.10}$$

This implies that the non-vanishing components of the symmetric Maxwell tensor are F_{tr} and $F_{r\varphi}$.

Inserting the metric (3.9) into equation (3.6) one obtains the following set of equations

$$\phi_{,rr} + \phi_{,r}\nu_{,r} + \frac{\phi_{,r}}{r} - (\omega+2)(\phi_{,r})^2 - \frac{\nu_{,r}}{2r} + \frac{1}{4}\Lambda e^{-2\nu} = \frac{\pi}{2}e^{-4\nu}T_{tt}\,, \tag{3.11}$$

$$-\phi_{,r}\nu_{,r} - \frac{\phi_{,r}}{r} - \omega(\phi_{,r})^2 + \frac{\nu_{,r}}{2r} - \frac{1}{4}\Lambda e^{-2\nu} = \frac{\pi}{2}T_{rr}\,, \tag{3.12}$$

$$\phi_{,rr} + 2\phi_{,r}\nu_{,r} - (\omega+2)(\phi_{,r})^2 - \frac{\nu_{,rr}}{2} - (\nu_{,r})^2 + \frac{1}{4}\Lambda e^{-2\nu} = -\frac{\pi}{2}\frac{e^{-2\nu}}{r^2}T_{\varphi\varphi}\,, \tag{3.13}$$

$$0 = \frac{\pi}{2}T_{t\varphi} = e^{-2\nu}F_{tr}F_{\varphi r}\,, \tag{3.14}$$

where $_{,r}$ denotes a derivative with respect to r. In addition, inserting the metric (3.9) into equations (3.7) and (3.8) yields

$$\partial_r\big[e^{-2\phi}r(F^{tr} + F^{\varphi r})\big] = 0\,, \tag{3.15}$$

$$\omega\phi_{,rr} + 2\omega\phi_{,r}\nu_{,r} + \omega\frac{\phi_{,r}}{r} - \omega(\phi_{,r})^2 + \frac{\nu_{,r}}{r} + \frac{\nu_{,rr}}{2} + (\nu_{,r})^2 - \frac{1}{4}\Lambda e^{-2\nu} = \frac{1}{4}e^{-2\nu}F^{\gamma\sigma}F_{\gamma\sigma}\,. \tag{3.16}$$

3.2.2 The general static solution

From the above equations valid for a static and rotationally symmetric spacetime one sees that equation (3.14) implies that the electric and magnetic fields cannot be simultaneously non-zero, i.e., there is no static dyonic solution. In this work we will consider the electrically charged case alone ($A_\varphi = 0$, $A_t \neq 0$).

So, assuming vanishing magnetic field, one has from Maxwell equation (3.15) that

$$F_{tr} = -\frac{\chi}{4r}e^{2\phi},\tag{3.17}$$

where χ is an integration constant which, as we shall see in (3.45), is the electric charge. One then has that

$$F^{\gamma\sigma}F_{\gamma\sigma} = \frac{\chi^2}{8r^2}e^{4\phi},\quad T_{tt} = \frac{\chi^2}{16\pi r^2}e^{2\nu}e^{4\phi},$$

$$T_{rr} = -\frac{\chi^2}{16\pi r^2}e^{-2\nu}e^{4\phi}\ ,\quad T_{\varphi\varphi} = \frac{\chi^2}{16\pi}e^{4\phi}.\tag{3.18}$$

To proceed we shall first consider the case $\omega \neq -1$. Adding equations (3.11) and (3.12) one obtains $\phi_{,rr} = 2(\omega + 1)(\phi_{,r})^2$, yielding for the dilaton field the following solution

$$\phi = -\frac{1}{2(\omega + 1)}\ln[2(\omega + 1)r + a_1] + a_2\ ,\qquad w \neq -1\tag{3.19}$$

where a_1 and a_2 are constants of integration. One can, without loss of generality, choose $a_1 = 0$. Then, equation (3.19) can be written as

$$e^{-2\phi} = a(\alpha r)^{\frac{1}{\omega+1}},\qquad w \neq -1\ ,\tag{3.20}$$

where α is an appropriate constant that is proportional to the cosmological constant [see equation (3.25)]. The dimensionless constant a can be viewed as a normalization to the action (3.5). Since it has no influence in our calculations, apart a possible redefinition of the mass, we set $a = 1$. The vector potential $A = A_\mu(r)dx^\mu = A_t(r)dt$ with $A_t(r) = \int F_{tr}dr$ is then

$$A = \frac{1}{4}\chi(\omega + 1)(\alpha r)^{\frac{1}{\omega+1}}dt\ ,\qquad w \neq -1\ .\tag{3.21}$$

Inserting the solutions (3.17)-(3.20) in equations (3.11)-(3.16), we obtain for the metric

$$ds^2 = -\left[(\alpha r)^2 - \frac{b}{(\alpha r)^{\frac{1}{\omega+1}}} + \frac{k\chi^2}{(\alpha r)^{\frac{2}{\omega+1}}}\right]dt^2 + \frac{dr^2}{(\alpha r)^2 - \frac{b}{(\alpha r)^{\frac{1}{\omega+1}}} + \frac{k\chi^2}{(\alpha r)^{\frac{2}{\omega+1}}}} + r^2 d\varphi^2,$$

$$\text{for}\quad \omega \neq -2, -\frac{3}{2}, -1,\tag{3.22}$$

$$ds^2 = -\left[(1 + \frac{\chi^2}{4}\ln r)r^2 - br\right]dt^2 + \frac{dr^2}{(1 + \frac{\chi^2}{4}\ln r)r^2 - br} + r^2 d\varphi^2,$$

$$\text{for}\quad \omega = -2,\tag{3.23}$$

$$ds^2 = -r^2[-\Lambda\ln(br) + \chi^2 r^2]dt^2 + \frac{dr^2}{r^2[-\Lambda\ln(br) + \chi^2 r^2]} + r^2 d\varphi^2,$$

$$\text{for}\quad \omega = -\frac{3}{2},\tag{3.24}$$

where b is a constant of integration related with the mass of the solutions, as will be shown, and $k = \frac{(\omega+1)^2}{8(\omega+2)}$. For $\omega \neq -2, -\frac{3}{2}, -1$ α is defined as (we call your attention to a typo in [71] in this definition)

$$\alpha = \sqrt{\left|\frac{(\omega + 1)^2\Lambda}{(\omega + 2)(2\omega + 3)}\right|}.\tag{3.25}$$

For $\omega = -2, -\frac{3}{2}$ we set $\alpha = 1$. For $\omega = -2$ equations (3.11) and (3.12) imply $\Lambda = \chi^2/8$ so, in contrast with the uncharged case [69, 70], the cosmological constant is not null.

Now, we consider the case $\omega = -1$. From equations (3.11)-(3.16) it follows that $\nu = C_1$, $\phi = C_2$, where C_1 and C_2 are constants of integration, and that the cosmological constant and electric charge are both null, $\Lambda = \chi = 0$. So, for $\omega = -1$ the metric gives simply the three-dimensional Minkowski spacetime and the dilaton is constant, as occurred in the uncharged case [69, 70].

In (2+1) dimensions, the presence of a curvature singularity is revealed by the scalar $R_{\mu\nu}R^{\mu\nu}$

$$
\begin{aligned}
R_{\mu\nu}R^{\mu\nu} &= 12\alpha^4 + \frac{4\omega}{(\omega+1)^2}\frac{b\alpha^4}{(\alpha r)^{\frac{2\omega+3}{\omega+1}}} + \frac{(2\omega^2+4\omega+3)}{2(\omega+1)^4}\frac{b^2\alpha^4}{(\alpha r)^{\frac{2(2\omega+3)}{\omega+1}}} \\
&\quad - \frac{(\omega-1)}{(\omega+1)^2}\frac{k\chi^2\alpha^4}{(\alpha r)^{\frac{2(\omega+2)}{\omega+1}}} - \frac{(\omega^2+2\omega+2)}{(\omega+1)^4}\frac{k\chi^2 b\alpha^4}{(\alpha r)^{\frac{4\omega+7}{\omega+1}}} \\
&\quad - \frac{(\omega^2+2\omega+3)}{(\omega+1)^4}\frac{k^2\chi^4\alpha^4}{(\alpha r)^{\frac{4(\omega+2)}{\omega+1}}} , \\
&\qquad\qquad\qquad\qquad\qquad\qquad \text{for} \quad \omega \neq -2, -\frac{3}{2}, -1 , \qquad (3.26)
\end{aligned}
$$

$$
R_{\mu\nu}R^{\mu\nu} = 8 + \frac{32}{r} + \frac{6}{r^2} + \chi^2\left[6\ln r + \frac{4\ln r}{r} + \frac{3}{r} + 5\right] + \chi^4\left[\frac{3}{4}\ln^2 r + \frac{5}{4}\ln r + 9\right] ,
$$
$$
\text{for} \quad \omega = -2 , \qquad (3.27)
$$

$$
R_{\mu\nu}R^{\mu\nu} = \Lambda^2[12\ln^2(br) + 20\ln(br) + 9] + \Lambda\chi^2 r^2\left[5\ln(br) + \frac{9}{2}\right] + \frac{9}{16}\chi^4 r^4
$$
$$
\text{for} \quad \omega = -\frac{3}{2} . \qquad (3.28)
$$

An inspection of these scalars in (3.26)-(3.28) reveals that for $\omega < -2$ and $\omega > -1$ the curvature singularity is located at $r = 0$ and for $-\frac{3}{2} < \omega < -1$ the curvature singularity is at $r = +\infty$. For $-2 \leq \omega \leq -\frac{3}{2}$ both $r = 0$ and $r = +\infty$ are singular. For $\omega = \pm\infty$ spacetime has no curvature singularities. Note that in the uncharged case [69, 70], for $-2 \leq \omega < -\frac{3}{2}$ the curvature singularity is located only at $r = 0$.

3.2.3 The general rotating solution

In order to add angular momentum to the spacetime we perform the following coordinate transformations (see e.g. [70]-[232])

$$
\begin{aligned}
t &\mapsto \gamma t - \frac{\theta}{\alpha^2}\varphi , \\
\varphi &\mapsto \gamma\varphi - \theta t , \qquad (3.29)
\end{aligned}
$$

where γ and θ are constant parameters. Substituting (3.29) into (3.22)-(3.24) we obtain

$$
\begin{aligned}
ds^2 &= -\left[\left(\gamma^2 - \frac{\theta^2}{\alpha^2}\right)(\alpha r)^2 - \frac{\gamma^2 b}{(\alpha r)^{\frac{1}{\omega+1}}} + \frac{\gamma^2 k\chi^2}{(\alpha r)^{\frac{2}{\omega+1}}}\right]dt^2 \\
&\quad - \frac{\gamma\theta}{\alpha^2}\left[\frac{b}{(\alpha r)^{\frac{1}{\omega+1}}} - \frac{k\chi^2}{(\alpha r)^{\frac{2}{\omega+1}}}\right]2dtd\varphi + \frac{dr^2}{(\alpha r)^2 - \frac{b}{(\alpha r)^{\frac{1}{\omega+1}}} + \frac{k\chi^2}{(\alpha r)^{\frac{2}{\omega+1}}}} \\
&\quad + \left[\left(\gamma^2 - \frac{\theta^2}{\alpha^2}\right)r^2 + \frac{\theta^2}{\alpha^4}\frac{b}{(\alpha r)^{\frac{1}{\omega+1}}} - \frac{\theta^2}{\alpha^4}\frac{k\chi^2}{(\alpha r)^{\frac{2}{\omega+1}}}\right]d\varphi^2,
\end{aligned}
$$

$$
\text{for} \quad \omega \neq -2, -\frac{3}{2}, -1, \tag{3.30}
$$

$$
\begin{aligned}
ds^2 &= -\left[\left((\gamma^2 - \theta^2) + \frac{\gamma^2\chi^2}{4}\ln r\right)r^2 - \gamma^2 br\right]dt^2 + \gamma\theta\left[\frac{\chi^2}{4}r^2\ln r - br\right]2dtd\varphi \\
&\quad + \frac{dr^2}{(1 + \frac{\chi^2}{4}\ln r)r^2 - br} + \left[\left((\gamma^2 - \theta^2) - \frac{\theta^2\chi^2}{4}\ln r\right)r^2 + \theta^2 br\right]d\varphi^2,
\end{aligned}
$$

$$
\text{for} \quad \omega = -2, \tag{3.31}
$$

$$
\begin{aligned}
ds^2 &= -r^2[-\gamma^2\Lambda\ln(br) - \theta^2 + \gamma^2\chi^2 r^2]dt^2 - \gamma\theta r^2[\Lambda\ln(br) + 1 - \chi^2 r^2]2dtd\varphi \\
&\quad + \frac{dr^2}{r^2[-\Lambda\ln(br) + \chi^2 r^2]} + r^2[\theta^2\Lambda\ln(br) + \gamma^2 - \theta^2\chi^2 r^2]d\varphi^2,
\end{aligned}
$$

$$
\text{for} \quad \omega = -\frac{3}{2}. \tag{3.32}
$$

Introducing transformations (3.29) into (3.21) we obtain that the vector potential $A = A_\mu(r)dx^\mu$ is now given by

$$
A = \gamma A(r)dt - \frac{\theta}{\alpha^2}A(r)d\varphi, \qquad w \neq -1, \tag{3.33}
$$

where $A(r) = \frac{1}{4}\chi(\omega + 1)(\alpha r)^{\frac{1}{\omega+1}}$. Solutions (3.30)-(3.33) represent electrically charged stationary spacetimes and also solve (3.5). Analyzing the Einstein-Rosen bridge of the static solution one concludes that spacetime is not simply connected which implies that the first Betti number of the manifold is one, i.e., closed curves encircling the horizon cannot be shrunk to a point. So, transformations (3.29) generate a new metric because they are not permitted global coordinate transformations [233]. Transformations (3.29) can be done locally, but not globally. Therefore metrics (3.22)-(3.24) and (3.30)-(3.32) can be locally mapped into each other but not globally, and such they are distinct.

3.2.4 Mass, angular momentum and electric charge of the solutions

In this section we will calculate the mass, angular momentum, electric charge and dilaton charge of the static and rotating electrically charged black hole solutions. To obtain these quantities we apply the formalism of Regge and Teitelboim [234] (see also [49, 69, 70, 6]).

We first write the metrics (3.30)-(3.32) in the canonical form involving the lapse function $N^0(r)$ and the shift function $N^\varphi(r)$

$$
ds^2 = -(N^0)^2 dt^2 + \frac{dr^2}{f^2} + H^2(d\varphi + N^\varphi dt)^2, \tag{3.34}
$$

where $f^{-2} = g_{rr}$, $H^2 = g_{\varphi\varphi}$, $H^2 N^\varphi = g_{t\varphi}$ and $(N^0)^2 - H^2(N^\varphi)^2 = g_{tt}$. Then, the action can be written in the hamiltonian form as a function of the energy constraint $\mathcal{H}$, momentum constraint $\mathcal{H}_\varphi$

and Gauss constraint G

$$
\begin{aligned}
S &= -\int dt d^2x [N^0\mathcal{H} + N^\varphi\mathcal{H}_\varphi + A_t G] + \mathcal{B}\\
&= -\Delta t \int dr N \left[\frac{2\pi^2}{H^3}e^{-2\phi} - 4f^2(H\phi_{,r}e^{-2\phi})_{,r} - 2H\phi_{,r}(f^2)_{,r}e^{-2\phi}\right.\\
&\quad \left. +2f(fH_{,r})_{,r}e^{-2\phi} + 4\omega Hf^2(\phi_{,r})^2 e^{-2\phi} - \Lambda H e^{-2\phi} + \frac{2H}{f}e^{-2\phi}(E^2+B^2)\right]\\
&\quad +\Delta t \int dr N^\varphi \left[\left(2\pi e^{-2\phi}\right)_{,r} + \frac{4H}{f}e^{-2\phi}E^r B\right]\\
&\quad +\Delta t \int dr A_t \left[-\frac{4H}{f}e^{-2\phi}\partial_r E^r\right] + \mathcal{B}\,,
\end{aligned}
\tag{3.35}
$$

where $N = \frac{N^0}{f}$, $\pi \equiv \pi_\varphi{}^r = -\frac{fH^3(N^\varphi)_{,r}}{2N^0}$ (with $\pi^{r\varphi}$ being the momentum conjugate to $g_{r\varphi}$), E^r and B are the electric and magnetic fields and $\mathcal{B}$ is a boundary term. Upon varying the action with respect to $f(r)$, $H(r)$, $\pi(r)$, $\phi(r)$ and $E^r(r)$ one picks up additional surface terms. Indeed,

$$
\begin{aligned}
\delta S &= -\Delta t N \left[(H_{,r} - 2H\phi_{,r})e^{-2\phi}\delta f^2 - (f^2)_{,r}e^{-2\phi}\delta H - 4f^2 H e^{-2\phi}\delta(\phi_{,r})\right.\\
&\quad \left. +2H\left[(f^2)_{,r} + 4(\omega+1)f^2\phi_{,r}\right]e^{-2\phi}\delta\phi + 2f^2 e^{-2\phi}\delta(H_{,r})\right]\\
&\quad +\Delta t N^\varphi \left[2e^{-2\phi}\delta\pi - 4\pi e^{-2\phi}\delta\phi\right] + \Delta t A_t\left[-\frac{4H}{f}e^{-2\phi}\delta E^r\right] + \delta\mathcal{B}\\
&\quad +(\text{terms vanishing when the equations of motion hold}).
\end{aligned}
\tag{3.36}
$$

In order that the Hamilton's equations are satisfied, the boundary term $\mathcal{B}$ has to be adjusted so that it cancels the above additional surface terms. More specifically one has

$$
\delta\mathcal{B} = -\Delta t N \delta M + \Delta t N^\varphi \delta J + \Delta t A_t \delta Q\,,
\tag{3.37}
$$

where one identifies M as the mass, J as the angular momentum and Q as the electric charge since they are the terms conjugate to the asymptotic values of N, N^φ and A_t, respectively.

To determine the M, J and Q of the black hole one must take the black hole spacetime and subtract the background reference spacetime contribution, i.e., we choose the energy zero point in such a way that the mass, angular momentum and charge vanish when the black hole is not present.

Now, note that for $\omega < -2$, $\omega > -3/2$ and $\omega \neq -1$, spacetime (3.30) has an asymptotic metric given by

$$
-\left(\gamma^2 - \frac{\theta^2}{\alpha^2}\right)\alpha^2 r^2 dt^2 + \frac{dr^2}{\alpha^2 r^2} + \left(\gamma^2 - \frac{\theta^2}{\alpha^2}\right)r^2 d\varphi^2\,,
\tag{3.38}
$$

i.e., it is asymptotically an anti-de Sitter spacetime. In order to have the usual form of the anti-de Sitter metric we choose $\gamma^2 - \theta^2/\alpha^2 = 1$. For the cases $-2 \leq \omega \leq -3/2$ we shall also choose $\gamma^2 - \theta^2/\alpha^2 = 1$, as has been done for the uncharged case [69, 70]. For $\omega \neq -3/2, -1$ the anti-de Sitter spacetime is also the background reference spacetime, since the metrics (3.30) and (3.31) reduce to (3.38) if the black hole is not present ($b = 0$ and $\varepsilon = 0$). For $\omega = -3/2$ the above described procedure of choosing the energy zero point does not apply since for any value of b and ε one still has a black hole solution. Thus, for $\omega = -3/2$ the energy zero point is chosen arbitrarily to correspond to the black hole solution with $b = 1$ and $\varepsilon = 0$.

Taking the subtraction of the background reference spacetime into account and noting that $\phi - \phi_{\text{ref}} = 0$ and that $\phi_{,r} - \phi_{,r}^{\text{ref}} = 0$ we have that the mass, angular momentum and electric charge are given by

$$
\begin{aligned}
M &= (2H\phi_{,r} - H_{,r})e^{-2\phi}(f^2 - f_{\text{ref}}^2) + (f^2)_{,r}e^{-2\phi}(H - H_{\text{ref}}) - 2f^2 e^{-2\phi}(H_{,r} - H_{,r}^{\text{ref}})\,,\\
J &= -2e^{-2\phi}(\pi - \pi_{\text{ref}})\,,\\
Q &= \frac{4H}{f}e^{-2\phi}(E^r - E_{\text{ref}}^r)\,.
\end{aligned}
\tag{3.39}
$$

Then, for $\omega > -3/2$ and $\omega \neq -1$, we finally have that the mass and angular momentum are (after taking the appropriate asymptotic limit: $r \to +\infty$ for $\omega > -1$ and $r \to 0$ for $-3/2 < \omega < -1$, see the Penrose diagrams on section 6.3 to understand the reason for these limits)

$$
M = b\left[\frac{\omega + 2}{\omega + 1}\gamma^2 + \frac{\theta^2}{\alpha^2}\right] = M_{\text{Q}=0}\,,
$$

$$
J = \frac{\gamma\theta}{\alpha^2}b\frac{2\omega + 3}{\omega + 1} = J_{\text{Q}=0}\,, \qquad \text{for} \quad \omega > -3/2,\ \omega \neq -1\,, \tag{3.40}
$$

where $M_{\text{Q}=0}$ and $J_{\text{Q}=0}$ are the mass and angular momentum of the uncharged black hole. For $\omega < -3/2$, the mass and angular momentum are (after taking the appropriate asymptotic limit, $r \to +\infty$)

$$
M = b\left[\frac{\omega + 2}{\omega + 1}\gamma^2 + \frac{\theta^2}{\alpha^2}\right] + \text{Div}_{\text{M}}(\chi, r) = M_{\text{Q}=0} + \text{Div}_{\text{M}}(\chi, r)\,, \tag{3.41}
$$

$$
J = \frac{\gamma\theta}{\alpha^2}b\frac{2\omega + 3}{\omega + 1} + \text{Div}_{\text{J}}(\chi, r) = J_{\text{Q}=0} + \text{Div}_{\text{J}}(\chi, r)\,,
$$

$$
\text{for} \quad \omega < -3/2\,, \tag{3.42}
$$

where $\text{Div}_{\text{M}}(\chi, r)$ and $\text{Div}_{\text{J}}(\chi, r)$ are terms proportional to the charge χ that diverge at the asymptotic limit. The presence of these kind of divergences in the mass and angular momentum is a usual feature present in charged solutions. They can be found for example in the electrically charged point source solution [23], in the electric counterpart of the BTZ black hole [49], in the pure electric black holes of 3D Brans-Dicke action [71] and in the magnetic counterpart of the BTZ solution [53]. Following [23, 49], the divergences on the mass can be treated as follows. One considers a boundary of large radius r_0 involving the black hole. Then, one sums and subtracts $\text{Div}_{\text{M}}(\chi, r_0)$ to (3.41) so that the mass (3.41) is now written as

$$
M = M(r_0) + \left[\text{Div}_{\text{M}}(\chi, r) - \text{Div}_{\text{M}}(\chi, r_0)\right]\,, \tag{3.43}
$$

where $M(r_0) = M_{\text{Q}=0} + \text{Div}_{\text{M}}(\chi, r_0)$, i.e.,

$$
M_{\text{Q}=0} = M(r_0) - \text{Div}_{\text{M}}(\chi, r_0)\,. \tag{3.44}
$$

The term between brackets in (3.43) vanishes when $r \to r_0$. Then $M(r_0)$ is the energy within the radius r_0. The difference between $M(r_0)$ and $M_{\text{Q}=0}$ is $-\text{Div}_{\text{M}}(\chi, r_0)$ which is interpreted as the electromagnetic energy outside r_0 apart from an infinite constant which is absorbed in $M(r_0)$. The sum (3.44) is then independent of r_0, finite and equal to the total mass.

To handle the angular momentum divergence, one first notice that the asymptotic limit of the angular momentum per unit mass (J/M) is either zero or one, so the angular momentum diverges at a rate slower or equal to the rate of the mass divergence. The divergence on the angular momentum can then be treated in a similar way as the mass divergence. So, the divergent term $-\text{Div}_{\text{J}}(\chi, r_0)$ can be interpreted as the electromagnetic angular momentum outside r_0 up to an infinite constant that is absorbed in $J(r_0)$.

In practice the treatment of the mass and angular divergences amounts to forgetting about r_0 and take as zero the asymptotic limits: $\lim \text{Div}_{\text{M}}(\chi, r) = 0$ and $\lim \text{Div}_{\text{J}}(\chi, r) = 0$. So, for $\omega < -3/2$ the mass and angular momentum are also given by (3.40).

Interesting enough, as has been noticed in [49], is the fact that in four spacetime dimensions there occurs a similar situation. For example, the g_{tt} component of Reissner-Nordström solution can be written as $1 - \frac{2M(r_0)}{r} + Q^2(\frac{1}{r} - \frac{1}{r_0})$. The total mass $M = M(r_0) + \frac{Q^2}{2r_0}$ is independent of r_0 and $\frac{Q^2}{2r_0}$ is the electrostatic energy outside a sphere of radius r_0. In this case, since $\frac{Q^2}{2r_0}$ vanishes when $r_0 \to \infty$, one does not need to include an infinite constant in $M(r_0)$. Thus, in this general Brans-Dicke theory in 3D we conclude that both situations can occur depending on the value of ω. The $\omega > -3/2$, $\omega \neq -1$ case is analogous to the the Reissner-Nordström black hole in the sense that

it is not necessary to include an infinite constant in $M(r_0)$, while the case $\omega < -3/2$ is similar to the electrically charged BTZ black hole [49] since an infinite constant must be included in $M(r_0)$.

For $\omega = -3/2$ the mass and angular momentum are ill defined since the boundaries $r \to \infty$ and $r \to 0$ have logarithmic singularities in the mass term even in the absence of the electric charge.

Now, we calculate the electric charge of the black holes. To determine the electric field we must consider the projections of the Maxwell field on spatial hypersurfaces. The normal to such hypersurfaces is $n^\nu = (1/N^0, 0, -N^\varphi/N^0)$ so the electric field is $E^\mu = g^{\mu\sigma} F_{\sigma\nu} n^\nu$. Then, from (3.39), the electric charge is

$$Q = -\frac{4Hf}{N^0} e^{-2\phi} (\partial_r A_t - N^\varphi \partial_r A_\varphi) = \gamma\chi , \qquad \omega \neq -1 . \qquad (3.45)$$

The mass, angular momentum and electric charge of the static black holes can be obtained by putting $\gamma = 1$ and $\theta = 0$ on the above expressions [see (3.29)].

Now, we want to cast the metric in terms of M, J and Q. For $\omega \neq -2, -3/2, -1$, we can use (3.40) to solve a quadratic equation for γ^2 and θ^2/α^2. It gives two distinct sets of solutions

$$\gamma^2 = \frac{\omega+1}{2(\omega+2)} \frac{M(2-\Omega)}{b} , \qquad \frac{\theta^2}{\alpha^2} = \frac{M\Omega}{2b} , \qquad (3.46)$$

$$\gamma^2 = \frac{\omega+1}{2(\omega+2)} \frac{M\Omega}{b} , \qquad \frac{\theta^2}{\alpha^2} = \frac{M(2-\Omega)}{2b} , \qquad (3.47)$$

where we have defined a rotating parameter Ω as

$$\Omega \equiv 1 - \sqrt{1 - \frac{4(\omega+1)(\omega+2)}{(2\omega+3)^2} \frac{J^2\alpha^2}{M^2}} , \qquad \text{for} \quad \omega \neq -2, -3/2, -1 . \qquad (3.48)$$

When we take $J = 0$ (which implies $\Omega = 0$), (3.46) gives $\gamma \neq 0$ and $\theta = 0$ while (3.47) gives the nonphysical solution $\gamma = 0$ and $\theta \neq 0$ which does not reduce to the static original metric. Therefore we will study the solutions found from (3.46). For $\omega = -2$ we have $\gamma^2 = J^2/Mb$ and $\theta^2 = M/b$.

The condition that Ω remains real imposes for $-2 > \omega > -1$ a restriction on the allowed values of the angular momentum: $|\alpha J| \leq \frac{|2\omega+3|M}{2\sqrt{(\omega+1)(\omega+2)}}$. For $-2 > \omega > -1$ we have $0 \leq \Omega \leq 1$. In the range $-2 < \omega < -3/2$ and $-3/2 < \omega < -1$ we have $\Omega < 0$. The condition $\gamma^2 - \theta^2/\alpha^2 = 1$ fixes the value of b and from (3.45) we can write $k\chi^2$ as a function of b, M, Ω, Q. Thus,

$$b = \frac{M}{2(\omega+2)} \left[2(\omega+1) - (2\omega+3)\Omega \right] , \qquad (3.49)$$

$$k\chi^2 = \frac{b}{4}(\omega+1)\frac{Q^2}{M(2-\Omega)} , \qquad \text{for} \quad \omega \neq -2, -3/2, -1 , \qquad (3.50)$$

and

$$b = \frac{J^2 - M^2}{M} , \qquad \chi^2 = \frac{Q^2 Mb}{J^2} , \qquad \text{for} \quad \omega = -2 . \qquad (3.51)$$

The metrics (3.30) and (3.31) may now be cast in the form

$$
\begin{aligned}
ds^2 &= -\left[(\alpha r)^2 - \frac{(\omega+1)}{2(\omega+2)}\frac{M(2-\Omega)}{(\alpha r)^{\frac{1}{\omega+1}}} + \frac{(\omega+1)^2}{8(\omega+2)}\frac{Q^2}{(\alpha r)^{\frac{2}{\omega+1}}}\right]dt^2 \\
&\quad -\frac{\omega+1}{2\omega+3}J\left[(\alpha r)^{-\frac{1}{\omega+1}} - \frac{(\omega+1)Q^2}{4M(2-\Omega)}(\alpha r)^{-\frac{2}{\omega+1}}\right]2dtd\varphi \\
&\quad +\left[(\alpha r)^2 - \frac{M[2(\omega+1)-(2\omega+3)\Omega]}{2(\omega+2)(\alpha r)^{\frac{1}{\omega+1}}}\right.\\
&\quad \left.+\frac{(\omega+1)Q^2[2(\omega+1)-(2\omega+3)\Omega]}{8(\omega+2)(2-\Omega)(\alpha r)^{\frac{2}{\omega+1}}}\right]^{-1}dr^2 \\
&\quad +\frac{1}{\alpha^2}\left[(\alpha r)^2 + \frac{M\Omega}{2(\alpha r)^{\frac{1}{\omega+1}}} - \frac{(\omega+1)\,\Omega\,Q^2}{8(2-\Omega)(\alpha r)^{\frac{2}{\omega+1}}}\right]d\varphi^2,
\end{aligned}
$$

$$\text{for}\quad \omega \neq -2, -\frac{3}{2}, -1\,, \tag{3.52}$$

$$
\begin{aligned}
ds^2 &= -\left[\left(1+\frac{Q^2}{4}\ln r\right)r^2 - \frac{J^2}{M}r\right]dt^2 + J\left[\frac{Q^2M}{4J^2}r^2\ln r - r\right]2dtd\varphi \\
&\quad +\left[\left(1+\frac{Q^2}{4}\left(1-\frac{M^2}{J^2}\right)\ln r\right)r^2 - M\left(\frac{J^2}{M^2}-1\right)r\right]^{-1}dr^2 \\
&\quad +\left[\left(1-\frac{Q^2M^2}{4J^2}\ln r\right)r^2 + Mr\right]d\varphi^2, \qquad\qquad \text{for}\quad \omega = -2. \tag{3.53}
\end{aligned}
$$

Analyzing the function $\Delta = g_{rr}^{-1}$ in (3.30), (3.31), and (3.49)-(3.51) we can set the conditions imposed on the mass and angular momentum of the solutions obtained for the different values of $\omega \neq -3/2, -1$, in order that the black holes might exist. These conditions are summarized on Table 1.

We can mention the principal differences between the charged and uncharged theory. The charged theory has black holes which are not present in the uncharged theory for the following range of parameters: (i) $-\infty < \omega < -2$, $M < 0$; (ii) $\omega = -2$, $M > 0$, $|J| < M$; (iii) $-3/2 < \omega < -1$, $M < 0$, $|\alpha J| > M$; (iv) $-1 < \omega < +\infty$, $M > 0$, $M < |\alpha J| < (2\omega+3)M/2\sqrt{(\omega+1)(\omega+2)}$ and (v) $-1 < \omega < +\infty$, $M < 0$, $|\alpha J| < |M|$.

Range of ω	Black holes with $M > 0$	Black holes with $M < 0$
$-\infty < \omega < -2$	$|\alpha J| \leq \frac{|2\omega+3|M}{2\sqrt{(\omega+1)(\omega+2)}}$	$|\alpha J| \leq \frac{|(2\omega+3)M|}{2\sqrt{(\omega+1)(\omega+2)}}$
$\omega = -2$	might exist for any J	$|J| < |M|$
$-2 < \omega < -\frac{3}{2}$	do not exist for any J	might exist for any J
$-\frac{3}{2} < \omega < -1$	$|\alpha J| > M$	might exist for any J
$-1 < \omega < +\infty$	$|\alpha J| \leq \frac{(2\omega+3)M}{2\sqrt{(\omega+1)(\omega+2)}}$	$|\alpha J| \leq \frac{(2\omega+3)|M|}{2\sqrt{(\omega+1)(\omega+2)}}$

Table 1. Values of the angular momentum for which black holes with positive and negative masses might exist.

3.2.5 Causal and geodesic structure of the charged black holes

3.2.5.a Analysis of the causal structure

In order to study the causal structure we follow the procedure of Boyer and Lindquist [238] and Carter [239] and write the metrics (3.30)-(3.32) in the form [see (3.29)]

$$ds^2 = -\Delta\left(\gamma dt - \frac{\theta}{\alpha^2}d\varphi\right)^2 + \frac{dr^2}{\Delta} + r^2\left(\gamma d\varphi - \theta dt\right)^2 , \tag{3.54}$$

where

$$\Delta = (\alpha r)^2 - b(\alpha r)^{-\frac{1}{\omega+1}} + k\chi^2(\alpha r)^{-\frac{2}{\omega+1}} , \qquad \text{for} \quad \omega \neq -2, -3/2, -1, \tag{3.55}$$

$$\Delta = (1 + \frac{\chi^2}{4}\ln r)r^2 - br , \qquad \text{for} \quad \omega = -2, \tag{3.56}$$

$$\Delta = r^2[-\Lambda\ln(br) + \chi^2 r^2] , \qquad \text{for} \quad \omega = -\frac{3}{2} , \tag{3.57}$$

and in (3.55) b and $k\chi^2$ are given by (3.49) and (3.50).

Bellow we describe the general procedure to draw the Penrose diagrams. Following Boyer and Lindquist [238], we choose a new angular coordinate which straightens out the spiraling null geodesics that pile up around the event horizon. A good choice is

$$\bar\varphi = \gamma\varphi - \theta t . \tag{3.58}$$

Then (3.54) can be written as

$$ds^2 = -\Delta\left(\frac{1}{\gamma}dt - \frac{\theta}{\alpha^2\gamma}d\bar\varphi\right)^2 + \frac{dr^2}{\Delta} + r^2 d\bar\varphi^2 . \tag{3.59}$$

Now the null radial geodesics are straight lines at 45°. The advanced and retarded null coordinates are defined by

$$u = \gamma t - r_* , \qquad v = \gamma t + r_* , \tag{3.60}$$

where $r_* = \int \Delta^{-1}dr$ is the tortoise coordinate. In general, the integral defining the tortoise coordinate cannot be solved explicitly for the solutions (3.55)-(3.57). Moreover, the maximal analytical extension depends critically on the values of ω. There are seven cases which have to be treated separately: $\omega < -2$, $\omega = -2$, $-2 < \omega < -3/2$, $\omega = -3/2$, $-3/2 < \omega < -1$, $\omega > -1$ and $\omega = \pm\infty$. As we shall see, on some of the cases the Δ function has only one zero and so the black hole has one event horizon, for other cases Δ has two zeros and consequently two horizons are present. If Δ has one zero, $r = r_+$, we proceed as follows. In the region where $\Delta < 0$ we introduce the Kruskal coordinates $U = +e^{-ku}$ and $V = +e^{+kv}$ and so $UV = +e^{k(v-u)}$. In the region where $\Delta > 0$ we define the Kruskal coordinates as $U = -e^{-ku}$ and $V = +e^{+kv}$ in order that $UV = -e^{k(v-u)}$. The signal of the product UV is chosen so that the factor Δ/UV, that appears in the metric coefficient g_{UV}, is negative. The constant k is introduced in order that the limit of Δ/UV as $r \to r_+$ stays finite.

If Δ has two zeros, $r = r_-$ and $r = r_+$ (with $r_- < r_+$), one has to introduce a Kruskal coordinate patch around each of the zeros of Δ. The first patch constructed around r_- is valid for $0 < r < r_+$. For this patch, in the region where $\Delta < 0$ we introduce the Kruskal coordinates $U = +e^{+k_-u}$ and $V = +e^{-k_-v}$ and so $UV = +e^{k_-(u-v)}$. In the region where $\Delta > 0$ we define the Kruskal coordinates as $U = -e^{+k_-u}$ and $V = +e^{-k_-v}$ in order that $UV = -e^{k_-(u-v)}$. The metric defined by this Kruskal coordinates is regular in the patch $0 < r < r_+$ and, in particular, is regular at r_-. However, it is singular at r_+. To have a metric non singular at r_+ one has to define new Kruskal coordinates for the second patch which is constructed around r_+ and is valid for $r_- < r < \infty$. For this patch, in the region where $\Delta < 0$ we introduce the Kruskal coordinates $U = +e^{-k_+u}$ and $V = +e^{+k_+v}$ and so $UV = +e^{k_+(v-u)}$. In the region where $\Delta > 0$ we define the Kruskal coordinates as $U = -e^{-k_+u}$

and $V = +e^{+k_+ v}$ in order that $UV = -e^{k_+(v-u)}$. k_- and k_+ are constants obeying the same condition defined above for k and the sign of UV is also chosen in order to have metric coefficient $g_{UV} \propto \Delta/UV$ negative. Now, these two different patches have to be joined together. Finally, to construct the Penrose diagram one has to define the Penrose coordinates by the usual arctangent functions of U and V: $\mathcal{U} = \arctan U$ and $\mathcal{V} = \arctan V$.

The horizon is mapped into two mutual perpendicular straight null lines at 45°. In general, to find what kind of curve describes the lines $r = 0$ or $r = \infty$ one has to take the limit of UV as $r \to 0$, in the case of $r = 0$, and the limit of UV as $r \to \infty$, in the case of $r = \infty$. If this limit is ∞ the corresponding line is mapped into a curved null line. If the limit is -1 the corresponding line is mapped into a curved timelike line and finally, when the limit is $+1$ the line is mapped into a curved spacelike line. The asymptotic lines are drawn as straight lines although in the coordinates $\mathcal{U}$ and $\mathcal{V}$ they should be curved outwards, bulged. It is always possible to change coordinates so that the asymptotic lines are indeed straight lines.

The lines of infinite redshift, $r = r_{\mathrm{rs}}$, are given by the vanishing of the g_{tt} metric component. There are closed timelike curves, r_{CTC}, whenever $g_{\varphi\varphi} < 0$.

The Penrose diagram for the static charged black hole is similar to the one drawn for the corresponding rotating charged black hole. The only difference is that the infinite redshift lines coincide with the horizons and there are no closed timelike surfaces. This similarity is due to the fact that the rotating black hole is obtained from the static one by applying the coordinate transformations (3.29).

In practice, to find the curve that describes the asymptotic limits $r = 0$ and $r = \infty$, we can use a trick. We study the behavior of Δ at the asymptotic limits, i.e. we find which term of Δ dominates as $r \to 0$ and $r \to \infty$. Then, in the asymptotic region, we take $\Delta \sim \Delta_0$ in the vicinity of $r = 0$ and $\Delta \sim \Delta_\infty$ in the vicinity of $r = \infty$. The above procedure of finding the Kruskal coordinates is then applied to the asymptotic regions, e.g. in the vicinity of $r = \infty$ we can take $r_* \sim r_*^\infty = \int (\Delta_\infty)^{-1} dr$ and find the character of the $r = \infty$ curve from the limit of UV as $r \to \infty$.

3.2.5.b   Analysis of the geodesic structure

Let us now consider the geodesic motion. The equations governing the geodesics can be derived from the Lagrangian

$$\mathcal{L} = \frac{1}{2} g_{\mu\nu} \frac{dx^\mu}{d\tau} \frac{dx^\nu}{d\tau} = -\frac{\delta}{2} , \tag{3.61}$$

where τ is an affine parameter along the geodesic which, for a timelike geodesic, can be identified with the proper time of the particle along the geodesic. For a null geodesic one has $\delta = 0$ and for a timelike geodesic $\delta = +1$. From the Euler-Lagrange equations one gets that the generalized momentums associated with the time coordinate and angular coordinate are constants: $p_t = E$ and $p_\varphi = L$. The constant E is related to the timelike Killing vector $(\partial/\partial t)^\mu$ which reflects the time translation invariance of the metric, while the constant L is associated to the spacelike Killing vector $(\partial/\partial\varphi)^\mu$ which reflects the invariance of the metric under rotation. Note that since the spacetime is not asymptotically flat, the constants E and L cannot be interpreted as the local energy and angular momentum at infinity.

From the geodesics equations we can derive two equations which will be specially useful since they describe the behavior of geodesic motion along the radial coordinate. For $\omega < -2$ and $\omega > -1$ these are

$$r^2 \dot{r}^2 = -\left[r^2 \delta + \frac{(\omega + 2)c_0^2}{2(\omega + 1) - (2\omega + 3)\Omega} \right] \Delta + \frac{2(\omega + 1)c_1^2}{2(\omega + 1) - (2\omega + 3)\Omega} r^2 \tag{3.62}$$

$$r^2 \dot{r}^2 = (E^2 - \alpha^2 L^2) r^2 + \frac{M c_0^2}{2(\alpha r)^{\frac{1}{\omega+1}}} - \frac{\sqrt{2}(\omega + 1)}{16\sqrt{2 - \Omega}} \frac{c_0^2 Q^2}{(\alpha r)^{\frac{2}{\omega+1}}} - r^2 \delta \Delta . \tag{3.63}$$

For $-2 < \omega < -3/2$ and $-3/2 < \omega < -1$ the two useful equations are

$$r^2 \dot{r}^2 = -\left[r^2\delta - \frac{(\omega+2)c_0^2}{2(\omega+1) - (2\omega+3)\Omega}\right]\Delta + \frac{2(\omega+1)c_1^2}{2(\omega+1) - (2\omega+3)\Omega}r^2 \tag{3.64}$$

$$r^2 \dot{r}^2 = (E^2 - \alpha^2 L^2)r^2 - \frac{Mc_0^2}{2(\alpha r)^{\frac{1}{\omega+1}}} + \frac{\sqrt{2}(\omega+1)}{16\sqrt{2-\Omega}}\frac{c_0^2 Q^2}{(\alpha r)^{\frac{2}{\omega+1}}} - r^2\delta\Delta \ . \tag{3.65}$$

In the above equations Δ is the inverse of the metric component g_{rr} and we have introduced the definitions

$$c_0^2 = \left[\frac{\sqrt{|\Omega|}}{\alpha}E \mp \sqrt{\left|\frac{\omega+1}{\omega+2}\right|}\sqrt{2-\Omega}\,L\right]^2 , \quad \text{and} \tag{3.66}$$

$$c_1^2 = \left[\sqrt{\frac{2-\Omega}{2}}E - \sqrt{\left|\frac{\omega+2}{2(\omega+1)}\right|}\sqrt{|\Omega|}\,\alpha L\right]^2 , \tag{3.67}$$

where in (3.66) the minus sign is valid for $\omega < -2$ and $\omega > -1$ and the plus sign is applied when $-2 < \omega < -3/2$ or $-3/2 < \omega < -1$. There are turning points, $r_{\rm tp}$, whenever $\dot{r} = 0$. If this is the case, equations (3.62) and (3.64) will allow us to make considerations about the position of the turning point relatively to the position of the horizon. For this purpose it will be important to note that for $\omega < -2$ and $\omega > -1$ one has $0 \leq \Omega \leq 1$, and for $-2 < \omega < -3/2$ or $-3/2 < \omega < -1$ we have that $\Omega < 0$. As a first and general example of the interest of equations (3.62) and (3.64) note that the turning points coincide with the horizons when the energy and the angular momentum are such that $c_1 = 0$. From equations (3.63), (3.65) and after some graphic computation we can reach interesting conclusions.

3.2.5.c   Penrose diagrams and geodesics for each range of ω

We are now in position to draw the Penrose diagrams and study the geodesic motion. Besides the cases $\omega = -2$ and $\omega = -3/2$, for each different range of ω ($\omega < -2$, $-2 < \omega < -3/2$, $-3/2 < \omega < -1$, $\omega > -1$ and $\omega = \pm\infty$) we will consider a particular value of ω. These will be precisely the ones that have been analyzed in the uncharged study of action (3.5) [69, 70].

We will study the solutions with positive mass, $M > 0$, and describe briefly the Penrose diagrams of the solutions with negative mass.

A. Brans-Dicke theories with $\omega < -2$

For this range of ω there is the possibility of having black holes with positive mass whenever $|\alpha J| \leq \frac{|2\omega+3|M}{2\sqrt{(\omega+1)(\omega+2)}}$. We are going to analyze the typical case $\omega = -3$. The Δ function, (3.55), is

$$\Delta = (\alpha r)^2 - b\sqrt{\alpha r} + c(\alpha r) , \tag{3.68}$$

where from (3.49) and (3.50) one has that $b > 0$ and $c \equiv k\chi^2 < 0$ (if $M > 0$). For $|\alpha J| \leq \frac{3M}{2\sqrt{2}}$, Δ has always one and only one zero given by

$$r_+ = \frac{1}{3\alpha}\left[-2c + \frac{c^2}{s} + s\right] , \quad \text{where} \quad s = \left[\frac{1}{2}\left(27b^2 + 2c^3 + 3\sqrt{3}b\sqrt{27b^2 + 4c^3}\right)\right]^{\frac{1}{3}} , \tag{3.69}$$

$\Delta > 0$ for $r > r_+$ and $\Delta < 0$ for $r < r_+$. The curvature singularity at $r = 0$ is a spacelike line in the Penrose diagram while $r = +\infty$ is a timelike line. The Penrose diagram is drawn in figure 1. There is no extreme black hole for this case.

When we consider the solutions with negative mass we conclude that, for $|\alpha J| \leq \frac{3|M|}{2\sqrt{2}}$, one has black holes with two horizons, with one (extreme case) or a spacetime without black holes. For the

Figure 3.1: Penrose diagram for the $\omega = -3$, $M > 0$, $|\alpha J| \leq 3M/2\sqrt{2}$ black hole.
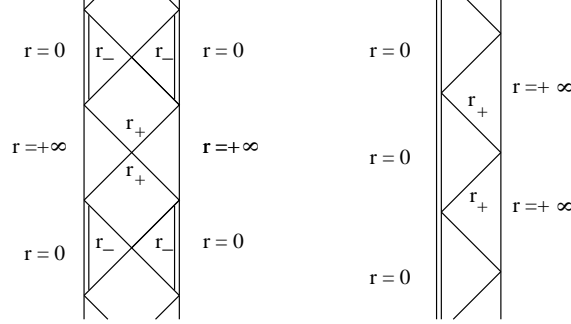
Figure 3.2: (a) Penrose diagram for the $\omega = -3$, $M < 0$, $|\alpha J| \leq 3|M|/2\sqrt{2}$ black hole with two horizons. (b) Penrose diagram for the $\omega = -3$, $M < 0$, $|\alpha J| \leq 3|M|/2\sqrt{2}$ extreme black hole.

black hole with two horizons the Penrose diagram is shown in figure 2.(a) of and the extreme black hole has a Penrose diagram which is drawn in figure 2.(b).

Let us now consider the geodesic motion. Analyzing (3.62) and noting that $0 \leq \Omega \leq 1$ we see that for the null and timelike geodesics the coefficient of Δ is always negative so, for $0 < r < r_+$, the first term of (3.62) is positive. Since the second term is positive or null we conclude that whenever there are turning points, they are $r_{\text{tp}}^1 = 0$ and $r_{\text{tp}}^2 \geq r_+$. From (3.63) we conclude the following about the geodesic motion. (i) If $E^2 - \alpha^2 L^2 \geq 0$ null particles produced at $r = 0$ escape to $r = +\infty$ and null particles coming in from infinity are scattered at $r_{\text{tp}}^1 = 0$ and spiral back to infinity. (ii) Null geodesics with $E^2 - \alpha^2 L^2 < 0$ are bounded between the singularity $r_{\text{tp}}^1 = 0$ and a maximum $(r_{\text{tp}}^2 \geq r_+)$ radial distance. The turning point r_{tp}^2 is exactly at the horizon r_+ if and only if the energy and the angular momentum are such that $c_1 = 0$. (iii) Null geodesics with energy and angular momentum such that $c_0 = 0$ can reach and "stay" at the curvature singularity $r = 0$. (iv) All the timelike geodesics present the same features as the null geodesics with $E^2 - \alpha^2 L^2 < 0$. So, any timelike geodesic is bounded within the region $r_{\text{tp}}^1 \leq r \leq r_{\text{tp}}^2$ (with $r_{\text{tp}}^1 = 0$ and $r_{\text{tp}}^2 \geq r_+$), and no timelike particle can either escape to infinity or reach and "stay" at $r = 0$. (v) Neither null or timelike geodesics have stable or unstable circular orbits.

B. Brans-Dicke theory with $\omega = -2$

For $\omega = -2$, Δ is given by (3.56) and, in the case $M > 0$, Δ has one zero given by

$$r_+ = b\left[4\chi^2 \text{ProdLog}\left(\frac{be^{\frac{1}{4\chi^2}}}{4\chi^2}\right)\right]^{-1}, \tag{3.70}$$

with $\text{ProdLog}(x) = z$ being such that $x = ze^z$. The scalar $R_{\mu\nu}R^{\mu\nu}$ (3.27) diverge at $r = 0$ and $r = +\infty$. For $|J| > |M|$, Δ is positive for $r > r_+$ and negative for $r < r_+$. At $r = +\infty$ the curvature singularity is timelike while $r = 0$ is a null curvature singularity. The Penrose diagram is represented in figure 3.(a). For $|J| < |M|$, unlike the uncharged case, the theory also has a black hole with a horizon located at r_+ given by (3.70). Δ is negative for $r > r_+$ and positive for $r < r_+$. The $r = +\infty$ curvature singularity is spacelike and $r = 0$ is a null curvature singularity. The Penrose diagram is drawn in figure 3.(b). For $|J| = |M|$ one has $b = \chi = 0$. Then, $r = 0$ is a naked null singularity and the boundary $r = \infty$ changes character and has no singularity, being a timelike line in the Penrose diagram drawn in figure 3.(c).
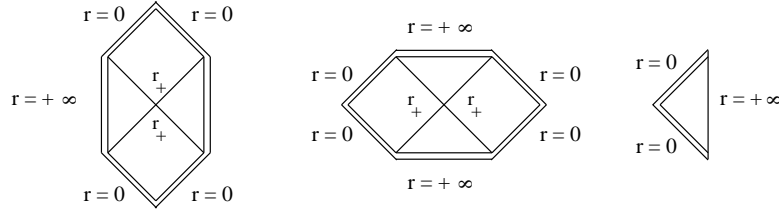
Figure 3.3: (a) Penrose diagram for the black hole of: i) $\omega = -2$, $M > 0$, $|J| > M$; ii) $\omega = -9/5$, $M < 0$. (b) Penrose diagram for the $\omega = -2$, $M > 0$, $|J| < M$ naked singularity. (c) Penrose diagram for the $\omega = -2$, $M > 0$, $|J| = M$ naked singularity.

Now, we study the geodesic motion for $M > 0$. The behavior of geodesic motion along the radial coordinate can be obtained from the following two equations

$$r^2 \dot{r}^2 = -\left[r^2 \delta + c_0^2\right]\Delta + c_1^2 r^2 \tag{3.71}$$

$$r^2 \dot{r}^2 = (E^2 - L^2)r^2 - \frac{\chi^2 c_0^2}{4}r^2 \ln r + \frac{J^2 - M^2}{M}c_0^2 r - r^2 \delta \Delta , \tag{3.72}$$

where

$$c_0^2 = \left[\left(\frac{J^2}{M^2} - 1\right)^{-1/2} E - \left(1 - \frac{M^2}{J^2}\right)^{-1/2} L\right]^2 , \tag{3.73}$$

$$c_1^2 = \left[\left(1 - \frac{M^2}{J^2}\right)^{-1/2} E - \left(\frac{J^2}{M^2} - 1\right)^{-1/2} L\right]^2 . \tag{3.74}$$

We first consider the case $|J| > M$. From equation (3.71) we conclude that whenever there are turning points, they are given by $r_{\rm tp}^1 = 0$ and $r_{\rm tp}^2 \geq r_+$. The turning point $r_{\rm tp}^2$ is exactly at the horizon r_+ if and only if the energy and the angular momentum are such that $c_1 = 0$, i.e, $E = ML/J$. From the graphic computation of (3.72) we conclude that: (i) the only particles that can escape to $r = +\infty$ or $r = 0$ are null particles that satisfy $c_0 = 0$ which implies $E = JL/M$; (ii) all other null geodesics and all timelike geodesics are bounded between $r_{\rm tp}^1 = 0$ and a maximum $(r_{\rm tp}^2 \geq r_+)$ radial distance.

For $|J| < M$ one has that: (i) timelike and null spiraling particles with $E \neq JL/M$ start at $r_{\rm tp} \geq r_+$ and reach infinity radial distances or timelike and null geodesics start at $r = +\infty$ and spiral toward $r_{\rm tp}$ and then return back to infinity; (ii) null particles can escape to $r = +\infty$ or $r = 0$ if $c_0 = 0$, i.e., $E = JL/M$; (iii) timelike geodesics with $E = JL/M$ can be bounded between $r_{\rm tp}^1 = 0$ and a maximum $(r_{\rm tp}^2 \geq r_+)$ radial distance, or start at $r_{\rm tp}^3 \geq r_+$ and reach infinity radial distances.

C. Brans-Dicke theories with $-2 < \omega < -3/2$

In this range of ω, spacetime has no black holes since from (3.49) and (3.50) one has $b < 0$ and $k\chi^2 > 0$ so the Δ function (3.55) is always positive. The curvature singularity $r = 0$ is a naked null singularity and the curvature singularity $r = +\infty$ is a naked timelike singularity. The Penrose diagram is drawn in figure 4.

When we consider the solutions with negative mass we conclude that one might have black holes with one horizon. If this is the case, the Penrose diagram is exactly equal to the one shown in figure 3.(a) (which represents the typical case $\omega = -9/5$).

Although there are no black holes with positive mass, it is interesting to study the geodesics that we might expect for this spacetime. From graphic computation of (3.65) we conclude the following for null and timelike geodesics. (i) For $E^2 - \alpha^2 L^2 \leq 0$ there is no possible motion. (ii) This situation also occurs for small positive values of $E^2 - \alpha^2 L^2$. (iii) However, when we increase the positive value of $E^2 - \alpha^2 L^2$ there is a critical value for which a stable circular orbit is allowed. (iii) And for positive values of $E^2 - \alpha^2 L^2$ above the critical value, null and timelike geodesics are bounded between a minimum $(r_{\rm tp}^1)$ and a maximum $(r_{\rm tp}^2)$ radial distance. (iv) Null particles with energy and
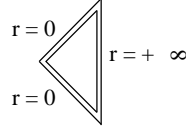
Figure 3.4: Penrose diagram for the spacetime of: i) $\omega = -2$, $M > 0$, $|J| = M$; ii) $-2 < \omega < -3/2$, $M > 0$; iii) $\omega = -3/2$ (large Λ/χ^2); iv) $\omega = -4/3$, $M < 0$, $|\alpha J| = M$ (the only difference is that $r = 0$ is a topological singularity rather than a curvature singularity).
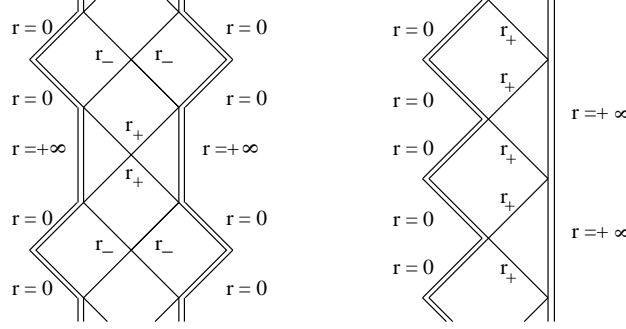
Figure 3.5: (a) Penrose diagram for the black hole with two horizons of: i) the $\omega = -3/2$, (small Λ/χ^2); ii) $\omega = -4/3$, $M < 0$, $|\alpha J| < |M|$ (the only difference is that $r = 0$ is a topological singularity rather than a curvature singularity). (b) Penrose diagram for the extreme black hole of: i) $\omega = -3/2$; ii) $\omega = -4/3$, $M < 0$, $|\alpha J| < |M|$ (the only difference is that $r = 0$ is a topological singularity rather than a curvature singularity).

angular momentum satisfying $c_0 = 0$ that are produced at $r = 0$ escape to $r = +\infty$ and null particles coming in from infinity are scattered at $r_{\text{tp}} = 0$ and spiral back to infinity. (vi) Timelike particles with energy and angular momentum satisfying $c_0 = 0$ are bounded within the region $0 \leq r \leq r_{\text{tp}}$, with r_{tp} finite.

D. Brans-Dicke theory with $\omega = -3/2$

In this case, Δ is given by (3.57). Depending on the value of $\frac{\Lambda}{\chi^2}$ one has black holes with two horizons (small $\frac{\Lambda}{\chi^2}$), with one (extreme case) or a spacetime without black holes (large $\frac{\Lambda}{\chi^2}$).

For the black hole with two horizons, we have $\Delta > 0$ in $r < r_-$ and $r > r_+$. For the patch $r_- < r < \infty$, the curvature singularity $r = \infty$ is mapped into two symmetrical timelike lines and the horizon $r = r_+$ is mapped into two mutual perpendicular straight lines at 45°. For the patch $0 < r < r_+$, the curvature singularity $r = 0$ is mapped into a pair of two null lines and the horizon $r = r_-$ is mapped into two mutual perpendicular straight lines at 45°. One has to join these two different patches and then repeat them over in the vertical. The resulting Penrose diagram is shown in figure 5.(a). For the extreme black hole the two curvature singularities $r = 0$ and $r = \infty$ are still null and timelike lines (respectively), but the event and inner horizon join together in a single horizon r_+. The Penrose diagram is like the one drawn in figure 5.(b). The spacetime with no black hole present has a Penrose diagram like the one represented in figure 4. Now, we study the geodesic motion. The behavior of geodesic motion along the radial coordinate can be obtained from the following two equations

$$r^2 \dot{r}^2 = -\left[r^2 \delta + c_0^2\right]\Delta + c_0^2 r^2 \tag{3.75}$$
$$\dot{r}^2 = c_0^2\left[\Lambda \ln(br) - \chi^2 r^2 + 1\right] - \delta \Delta , \tag{3.76}$$

where $c_0 = (\theta E - \gamma L)$. From equation (3.75) we conclude that whenever there are turning points, they are given by $r_{\text{tp}}^1 \leq r_-$ and $r_{\text{tp}}^2 \geq r_+$. The turning points coincide with the horizons if and only if the energy and the angular momentum are such that $c_0 = 0$. From the graphic computation of (3.76) we conclude that: (i) Whenever $c_0 = 0$ null particles describe stable circular orbits wherever
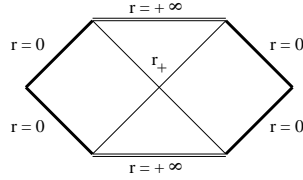
Figure 3.6: Penrose diagram for the black hole of: i) $\omega = -4/3$, $M > 0$, $|\alpha J| > M$; ii) $\omega = -4/3$, $M < 0$, $|\alpha J| > |M|$.

they are located; (ii) Null geodesics with $c_0 \neq 0$ and all timelike geodesics describe a bound orbit between r_{tp}^1 and r_{tp}^2.

For the extreme black hole the two horizons coincide so all null geodesics and all timelike geodesics describe a stable circular orbit.

E. Brans-Dicke theories with $-3/2 < \omega < -1$

For this range of ω there is the possibility of having black holes with positive mass whenever $|\alpha J| > M$ (Table 1). We are going to analyze the typical case $\omega = -4/3$. The Δ function, (3.55), is

$$\Delta = (\alpha r)^2 - b(\alpha r)^3 + c(\alpha r)^6 \,, \tag{3.77}$$

where from (3.49) and (3.50) one has that $b > 0$ and $c \equiv k\chi^2 < 0$ if $M > 0$ and $|\alpha J| > M$. Δ is negative for $r > r_+$ and positive for $r < r_+$, where r_+ is the only zero of Δ given by

$$r_+ = \frac{1}{2\alpha}\left(\frac{b}{c}\right)^{1/3}\left[\sqrt{s} - \sqrt{\frac{2}{\sqrt{s}} - s}\right], \quad \text{where}$$

$$s = \left[\frac{1}{2} + \frac{1}{2}\sqrt{1 - \frac{4^4 c}{3^3 b^4}}\right]^{\frac{1}{3}} + \left[\frac{1}{2} - \frac{1}{2}\sqrt{1 - \frac{4^4 c}{3^3 b^4}}\right]^{\frac{1}{3}}. \tag{3.78}$$

The physical curvature singularity is located inside the horizon at $r = +\infty$ and is a spacelike line in the Penrose diagram. At $r = 0$ there is a null topological singularity. The Penrose diagram is sketched in figure 6.

When we consider the solutions with negative mass we conclude that, for $|\alpha J| > |M|$, one has black holes with a Penrose diagram equal to the one drawn in figure 6. For $|\alpha J| < |M|$ one has black holes with two horizons, with one (extreme case) or a spacetime without black holes. For the black hole with two hor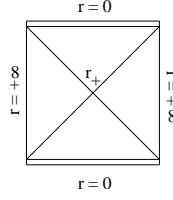izons the Penrose diagram is similar to the one shown in figure 5.(a) and the extreme black hole has a Penrose diagram which is similar to the one drawn in figure 5.(b). For $|\alpha J| = |M|$ the Penrose diagram is similar to figure 4. The only difference is the fact that $r = 0$ is now a topological singularity rather than a curvature singularity.

Let us now consider the geodesic motion for positive mass. Analyzing (3.64) and noting that from (3.48) the condition $|\alpha J| > M$ implies $\Omega < -2$ we conclude that, for null geodesics, whenever there are turning points, they are $r_{tp}^1 = 0$ and $r_{tp}^2 \geq r_+$. From (3.65) we conclude the following about the null geodesic motion. (i) For $E^2 - \alpha^2 L^2 \leq 0$ there is no possible motion. (ii) Null geodesics with $E^2 - \alpha^2 L^2 > 0$ are bounded between the singularity $r_{tp}^1 = 0$ and a maximum ($r_{tp}^2 \geq r_+$) radial distance. The turning point r_{tp}^2 is exactly at the horizon r_+ if and only if the energy and the angular momentum are such that $c_1 = 0$.

The timelike geodesic motion is radically different. (i) For $E^2 - \alpha^2 L^2 \leq 0$ we have timelike spiraling particles that start at r_{tp} and reach infinity radial distances or timelike geodesics that start at $r = +\infty$ and spiral toward r_{tp} and then return back to infinity. (ii) For small positive values of $E^2 - \alpha^2 L^2$, timelike particles that are produced at $r = 0$ escape to $r = +\infty$ and timelike particles coming in from infinity are scattered at $r_{tp} = 0$ and spiral back to infinity. (iii) When we increase the positive value of $E^2 - \alpha^2 L^2$ there is a critical value for which an unstable circular orbit is allowed. (iv) And for positive values of $E^2 - \alpha^2 L^2$ above the critical value, timelike particles are

allowed to be bounded between $r_{\text{tp}}^1 = 0$ and a maximum (r_{tp}^2) radial distance or to start at $r_{\text{tp}}^3 > r_{\text{tp}}^2$ and escape to infinity.

F. Brans-Dicke theories with $\omega > -1$

The range $\omega > -1$ is not discussed here since the properties of the typical case $\omega = 0$ have been presented in [7], where the three-dimensional gravity theory of $\omega = 0$ was obtained through dimensional reduction from four-dimensional General Relativity with one Killing vector field.

G. Brans-Dicke theory with $\omega = \pm\infty$

The case $\omega = \pm\infty$ is also not discussed here since this case reduces to the electrically charged BTZ black hole which has been studied in detail in [49, 242].

3.2.6   Hawking temperature of the charged black holes

To compute the Hawking temperature of the rotating black holes, one starts by writing the metric in the canonical form (3.34). To proceed it is necessary to first perform the coordinate transformation to coordinates t, $\tilde{\varphi}$ which corotate with the black hole. In other words, the angular coordinate φ must be changed to $\tilde{\varphi}$ defined by $\tilde{\varphi} = \varphi - \Omega_H t$, where $\Omega_H = -\frac{g_{t\varphi}}{g_{\varphi\varphi}}\big|_{r=r_+} = -N^\varphi(r_+)$ is the angular velocity of the black hole. With this transformation the metric (3.34) becomes

$$ds^2 = -(N^0)^2 dt^2 + \frac{dr^2}{f^2} + H^2\left[d\tilde{\varphi} + \left(N^\varphi(r) - N^\varphi(r_+)\right)dt\right]^2 , \tag{3.79}$$

Then, one applies the Wick rotation $t \to -i\tau$ in order to obtain the euclidean counterpart of (3.79). Now, one studies the behavior of the euclidean metric in the vicinity of the event horizon, r_+. In this vicinity, one can write $N^\varphi(r) - N^\varphi(r_+) \sim 0$ and take the expansion $\Delta(r) \sim \frac{d\Delta(r_+)}{dr}(r - r_+) + \cdots$. One proceeds applying the variable change $\frac{1}{\Delta(r)}dr^2 = d\rho^2$ so that one has $\rho = 2[\sqrt{\frac{r-r_+}{d\Delta(r_+)/dr}}$ and $\Delta(\rho) \sim [d\Delta(r_+)/dr]^2\rho^2/4$. With this procedure the euclidean metric in the vicinity of the event horizon can be cast in the form $ds^2 \sim (2\pi/\beta_H)^2\rho^2 d\tau^2 + d\rho^2 + H^2 d\tilde{\varphi}^2$. Applying a final variable change, $\bar{\tau} = (2\pi/\beta_H)\tau$, the metric becomes $ds^2 \sim \rho^2 d\bar{\tau}^2 + d\rho^2 + H^2 d\tilde{\varphi}^2$. To avoid the canonical singularity at the event horizon one must demand that the period of $\bar{\tau}$ is 2π which implies $0 \le \tau \le \beta_H$. Finally, the Hawking temperature is defined as $T_H = (\beta_H)^{-1}$.

Applying the above procedure, one finds for the Hawking temperature of the rotating black holes the following expressions

$$T_H = \frac{1}{4\pi}\sqrt{\frac{r_+^2\left[2\alpha r_+ + \frac{b}{\omega+1}(\alpha r_+)^{-\frac{\omega+2}{\omega+1}} - \frac{2k\chi^2}{\omega+1}(\alpha r_+)^{-\frac{\omega+3}{\omega+1}}\right]^2}{r_+^2 - \frac{\theta^2}{\alpha^4}\left[-b(\alpha r_+)^{-\frac{1}{\omega+1}} + k\chi^2(\alpha r_+)^{-\frac{2}{\omega+1}}\right]}} ,$$
$$\text{for}\quad \omega \ne -2, -\frac{3}{2}, -1 , \tag{3.80}$$

$$T_H = \frac{1}{4\pi}\sqrt{\frac{r_+^2\left[\frac{r_+}{2}\left(4 + \frac{\chi^2}{2} + \chi^2\ln r_+\right) - b\right]^2}{\left[1 - \frac{1}{4}\theta^2\chi^2\ln r_+\right]r_+^2 + \theta^2 b r_+}} , \quad \text{for}\quad \omega = -2 , \tag{3.81}$$

$$T_H = \frac{1}{4\pi}\sqrt{\frac{r_+^2\left[2\Lambda r_+\ln(br_+) + \Lambda br_+ - \frac{\chi^2 r_+^3}{4}\right]^2}{\Lambda\theta^2 r_+^2\ln(br_+) + \gamma^2 r_+^2 - \frac{\theta^2\chi^2 r_+^4}{16}}} ,$$
$$\text{for}\quad \omega = -3/2 , \tag{3.82}$$

where in (3.80), b, $k\chi^2$ and θ^2 are given by (3.49), (3.50) and (3.46), respectively.

The Hawking temperature of the static charged black holes can be obtained from (3.80)-(3.82) by taking $\gamma = 1$ and $\theta = 0$ [see (3.29)] (see also [6] for the $\omega = 0$ uncharged black hole).

3.3 Magnetic Brans-Dicke dilaton solutions

The issue of spacetimes generated by point sources in three dimensional (3D) Einstein theory has been object of many studies, as we reviewed in section 1.2.

The aim of this section is to find and study in detail the static and rotating magnetic charged solutions generated by a magnetic point source in the Einstein-Maxwell-Dilaton action of the Brans-Dicke that we are studying in this chapter. Here, we impose that the only non-vanishing component of the vector potential is $A_\varphi(r)$. For the $\omega = \pm\infty$ case, our solution reduces to the spacetime generated by a magnetic point source in 3D Einstein-Maxwell theory with $\Lambda < 0$, studied in [48], [51]-[53]. The $\omega = 0$ case is equivalent to 4D general relativity with one Killing vector analysed by Dias and Lemos [8].

The plan of this section is the following. In Section 3.3.1 we set up the action and the field equations. The static general solutions of the field equations are found in section 3.3.2 and we analyse in detail the general structure of the solutions. The angular momentum is added in section 3.3.3 and we calculate the mass, angular momentum, and electric charge of the solutions. In section 3.3.4 we give a physical interpretation for the origin of the magnetic field source.

3.3.1 Field equations of Brans-Dicke−Maxwell theory

We are going to work with an action of the Brans-Dicke−Maxwell type in 3D written in the string frame as

$$S = \frac{1}{2\pi} \int d^3x \sqrt{-g}\, e^{-2\phi} \big[R - 4\omega(\partial\phi)^2 + \Lambda + F^{\mu\nu}F_{\mu\nu} \big], \tag{3.83}$$

where g is the determinant of the 3D metric, R is the curvature scalar, $F_{\mu\nu} = \partial_\nu A_\mu - \partial_\mu A_\nu$ is the Maxwell tensor, with A_μ being the vector potential, ϕ is a scalar field called dilaton, ω is the 3D Brans-Dicke parameter and Λ is the cosmological constant. Varying this action with respect to $g^{\mu\nu}$, A_μ and ϕ one gets the Einstein, Maxwell and dilaton equations, respectively

$$\tfrac{1}{2}G_{\mu\nu} - 2(\omega+1)\nabla_\mu\phi\nabla_\nu\phi + \nabla_\mu\nabla_\nu\phi - g_{\mu\nu}\nabla_\gamma\nabla^\gamma\phi + (\omega+2)g_{\mu\nu}\nabla_\gamma\phi\nabla^\gamma\phi - \tfrac{1}{4}g_{\mu\nu}\Lambda = \tfrac{\pi}{2}T_{\mu\nu}, \tag{3.84}$$

$$\nabla_\nu(e^{-2\phi}F^{\mu\nu}) = 0\,, \tag{3.85}$$

$$R - 4\omega\nabla_\gamma\nabla^\gamma\phi + 4\omega\nabla_\gamma\phi\nabla^\gamma\phi + \Lambda = -F^{\gamma\sigma}F_{\gamma\sigma}, \tag{3.86}$$

where $G_{\mu\nu} = R_{\mu\nu} - \tfrac{1}{2}g_{\mu\nu}R$ is the Einstein tensor, ∇ represents the covariant derivative and $T_{\mu\nu} = \tfrac{2}{\pi}(g^{\gamma\sigma}F_{\mu\gamma}F_{\nu\sigma} - \tfrac{1}{4}g_{\mu\nu}F_{\gamma\sigma}F^{\gamma\sigma})$ is the Maxwell energy-momentum tensor.

3.3.2 General static solution. Analysis of its structure

3.3.2.a Field equations

We want to consider now a spacetime which is both static and rotationally symmetric, implying the existence of a timelike Killing vector $\partial/\partial t$ and a spacelike Killing vector $\partial/\partial\varphi$. We will start working with the following ansatz for the metric

$$ds^2 = -\alpha^2 r^2 dt^2 + e^{-2\mu(r)}dr^2 + \frac{e^{2\mu(r)}}{\alpha^2}d\varphi^2\,, \tag{3.87}$$

where the parameter α^2 is, as we shall see, an appropriate constant proportional to the cosmological constant Λ. It is introduced in order to have metric components with dimensionless units and

an asymptotically anti-de Sitter spacetime. The motivation for this choice for the metric gauge $[g_{tt} \propto -r^2$ and $(g_{rr})^{-1} \propto g_{\varphi\varphi}]$ instead of the usual "Schwarzschild" gauge $[(g_{rr})^{-1} = -g_{tt}$ and $g_{\varphi\varphi} = r^2]$ comes from the fact that we are looking for magnetic solutions. Indeed, let us first remember that the Schwarzschild gauge is usually an appropriate choice when we are interested on electric solutions. Now, we focus on the well known fact that the electric field is associated with the time component, A_t, of the vector potential while the magnetic field is associated with the angular component A_φ. From the above facts, one can expect that a magnetic solution can be written in a metric gauge in which the components g_{tt} and $g_{\varphi\varphi}$ interchange their roles relatively to those present in the "Schwarzschild" gauge used to describe electric solutions. This choice will reveal to be a good one to find solutions since the dilaton and graviton will decouple from each other on the fields equations (3.84) and (3.86). However, as we will see, for some values of the Brans-Dicke parameter ω it is not the good coordinate system to interpret the solutions.

We now assume that the only non-vanishing components of the vector potential are $A_t(r)$ and $A_\varphi(r)$, i.e.,

$$A = A_t dt + A_\varphi d\varphi . \tag{3.88}$$

This implies that the non-vanishing components of the anti-symmetric Maxwell tensor are F_{tr} and $F_{r\varphi}$. Use of metric (3.87) and equation (3.84) yields the following set of equations

$$\phi_{,rr} + 2\phi_{,r}\mu_{,r} - (\omega + 2)(\phi_{,r})^2 - \frac{\mu_{,rr}}{2} - (\mu_{,r})^2 + \frac{1}{4}\Lambda e^{-2\mu} = \frac{\pi}{2\alpha^2}\frac{e^{-2\mu}}{r^2}T_{tt} , \tag{3.89}$$

$$-\phi_{,r}\mu_{,r} - \frac{\phi_{,r}}{r} - \omega(\phi_{,r})^2 + \frac{\mu_{,r}}{2r} - \frac{1}{4}\Lambda e^{-2\mu} = \frac{\pi}{2}T_{rr} , \tag{3.90}$$

$$\phi_{,rr} + \phi_{,r}\mu_{,r} + \frac{\phi_{,r}}{r} - (\omega + 2)(\phi_{,r})^2 - \frac{\mu_{,r}}{2r} + \frac{1}{4}\Lambda e^{-2\mu} = -\frac{\pi}{2}\alpha^2 e^{-4\mu}T_{\varphi\varphi} , \tag{3.91}$$

$$0 = \frac{\pi}{2}T_{t\varphi} = e^{2\mu}F_{tr}F_{\varphi r} , \tag{3.92}$$

where $_{,r}$ denotes a derivative with respect to r. In addition, replacing the metric (3.87) into equations (3.85) and (3.86) yields

$$\partial_r\left[e^{-2\phi}r(F^{tr} + F^{\varphi r})\right] = 0 , \tag{3.93}$$

$$\omega\phi_{,rr} + 2\omega\phi_{,r}\mu_{,r} + \omega\frac{\phi_{,r}}{r} - \omega(\phi_{,r})^2 + \frac{\mu_{,r}}{r} + \frac{\mu_{,rr}}{2} + (\mu_{,r})^2 - \frac{1}{4}\Lambda e^{-2\mu} = \frac{1}{4}e^{-2\mu}F^{\gamma\sigma}F_{\gamma\sigma} . \tag{3.94}$$

3.3.2.b The general static solution. Causal structure

Equations (3.89)-(3.94) are valid for a static and rotationally symmetric spacetime. One sees that equation (3.92) implies that the electric and magnetic fields cannot be simultaneously non-zero, i.e., there is no static dyonic solution. In this work we will consider the magnetically charged case alone $(A_t = 0, A_\varphi \neq 0)$. For purely electrically charged solutions of the theory see [71]. So, assuming vanishing electric field, one has from Maxwell equation (3.93) that

$$F_{\varphi r} = \frac{\chi_{\mathrm{m}}}{4\alpha^2 r}e^{2\phi}, \tag{3.95}$$

where χ_{m} is an integration constant which measures the intensity of the magnetic field source. To proceed we shall first consider the case $\omega \neq -1$. Adding equations (3.90) and (3.91) yields $\phi_{,rr} = 2(\omega + 1)(\phi_{,r})^2$, and so the dilaton field is given by

$$e^{-2\phi} = (\alpha r)^{\frac{1}{\omega+1}}, \qquad \omega \neq -1 , \tag{3.96}$$

where α is a generic constant which will be appropriately defined below in equation (3.101). The 1-form vector potential $A = A_\mu(r)dx^\mu$ is then

$$A = -\frac{1}{4\alpha^2}\chi_{\mathrm{m}}(\omega + 1)(\alpha r)^{-\frac{1}{\omega+1}}d\varphi , \qquad \omega \neq -1 . \tag{3.97}$$

Replacing solutions (3.95)-(3.97) into equations (3.89)-(3.94) allows us to find the $e^{2\mu(r)}$ function for $\omega \neq \{-2, -3/2, -1\}$; $\omega = -2$ and $\omega = -3/2$, respectively

$$e^{2\mu(r)} = (\alpha r)^2 + \frac{b}{(\alpha r)^{\frac{1}{\omega+1}}} - \frac{k\chi_{\mathrm{m}}^2}{(\alpha r)^{\frac{2}{\omega+1}}}, \qquad (3.98)$$

$$e^{2\mu(r)} = \left(1 - \frac{\chi_{\mathrm{m}}^2}{4}\ln r\right)r^2 - br, \qquad (3.99)$$

$$e^{2\mu(r)} = r^2[-\Lambda\ln(br) - \chi_{\mathrm{m}}^2 r^2], \qquad (3.100)$$

where b is a constant of integration related with the mass of the solutions, as will be shown, and $k = \frac{(\omega+1)^2}{8\alpha^2(\omega+2)}$. For $\omega \neq -2, -3/2, -1$ α is defined as (we call your attention to a typo in [72] in this definition)

$$\alpha = \sqrt{\left|\frac{(\omega+1)^2\Lambda}{(\omega+2)(2\omega+3)}\right|}. \qquad (3.101)$$

For $\omega = -2, -3/2$ we set $\alpha = 1$. For $\omega = -2$ equations (3.89) and (3.90) imply $\Lambda = -\chi_{\mathrm{m}}^2/8$.

Now, we consider the case $\omega = -1$. From equations (3.89)-(3.94) it follows that $\mu = C_1$, $\phi = C_2$, where C_1 and C_2 are constants of integration, and that the cosmological constant and magnetic source are both zero, $\Lambda = 0 = \chi_{\mathrm{m}}$. So, for $\omega = -1$ the metric gives simply the 3D Minkowski spacetime and the dilaton is constant, as occurred in the uncharged case [69, 70].

Now, we must analyze carefully the radial dependence of the $e^{2\mu(r)}$ function defined in equations (3.98)-(3.100) which, recall, is related to the metric components through the relations $g_{rr} = e^{-2\mu}$ and $g_{\varphi\varphi} = e^{2\mu}/\alpha^2$. The shape of the $e^{2\mu(r)}$ function depends on the values of the Brans-Dicke parameter ω and on the values of the parameter b (where b is related to the mass of the solution as we shall see in section 3.3.3.b). Nevertheless, we can group the values of ω and b into a small number of cases for which the $e^{2\mu(r)}$ function has the same behavior. The general shape of the $e^{2\mu(r)}$ function for these cases is drawn in the Appendix. Generally, the $e^{2\mu(r)}$ function can take positive or negative values depending on the value of the coordinate r. However, when $e^{2\mu(r)}$ is negative, the metric components $g_{rr} = e^{-2\mu}$ and $g_{\varphi\varphi} = e^{2\mu}/\alpha^2$ become simultaneously negative and this leads to an apparent change of signature from $+1$ to -3. This strongly indicates that we are using an incorrect extension and that we should choose a different continuation to describe the region where the change of signature occurs [51, 231]. Moreover, analysing the null and timelike geodesic motion we conclude that null and timelike particles can never pass through the zero of $e^{2\mu(r)}$, r_+ (say), from the region where g_{rr} is positive into the region where g_{rr} is negative. This suggests that one can introduce a new coordinate system in order to obtain a spacetime which is geodesically complete for the region where both g_{rr} and $g_{\varphi\varphi}$ are positive [51, 231]. That is our next step. Then, in section 3.3.2.c, we will check the completeness of the spacetimes. The Brans-Dicke theories can be classified into seven different cases that we display and study below.

(i) Brans-Dicke theories with $-1 < \omega < +\infty$

The shape of the $e^{2\mu(r)}$ function is drawn in Fig. 1(a). We see that for $0 < r < r_+$ (where r_+ is the zero of $e^{2\mu(r)}$) g_{rr} and $g_{\varphi\varphi}$ become simultaneously negative and this leads to an apparent change of signature. One can however introduce a new radial coordinate ρ so that the spacetime is geodesically complete for the region where both g_{rr} and $g_{\varphi\varphi}$ are positive,

$$\rho^2 = r^2 - r_+^2. \qquad (3.102)$$

With this coordinate transformation, the spacetime generated by the static magnetic point source is finally given by

$$ds^2 = -\alpha^2 r^2(\rho)dt^2 + \frac{\rho^2}{r^2(\rho)}\frac{1}{f(\rho)}d\rho^2 + \frac{f(\rho)}{\alpha^2}d\varphi^2, \qquad (3.103)$$

where $0 \leq \rho < \infty$, and function $f(\rho)$, which is always positive except at $\rho = 0$ where it is zero, is given by

$$f(\rho) = \alpha^2 r^2(\rho) + \frac{b}{[\alpha^2 r^2(\rho)]^{\frac{1}{2(\omega+1)}}} - \frac{k\chi_m^2}{[\alpha^2 r^2(\rho)]^{\frac{1}{\omega+1}}} . \tag{3.104}$$

Along this section 3.3.2.b, in cases **(i)** and **(iii)** we will use the definition $r^2(\rho) \equiv \rho^2 + r_+^2$ in order to shorten the formulas. This spacetime has no horizons and so there are no magnetic black hole solutions, only magnetic point sources. In three dimensions, the presence of a curvature singularity is revealed by the scalar $R_{\mu\nu}R^{\mu\nu}$

$$\begin{aligned}
R_{\mu\nu}R^{\mu\nu} = &-\frac{4\omega}{(\omega+1)^2}\frac{b\alpha^4}{[\alpha^2 r^2(\rho)]^{\frac{2\omega+3}{2(\omega+1)}}} + \frac{(2\omega^2+4\omega+3)b^2\alpha^4}{2(\omega+1)^4[\alpha^2 r^2(\rho)]^{\frac{2\omega+3}{\omega+1}}} \\
&+\frac{(\omega-1)}{(\omega+1)^2}\frac{8k\chi_m^2\alpha^4}{[\alpha^2 r^2(\rho)]^{\frac{\omega+2}{\omega+1}}} - \frac{(\omega^2+2\omega+2)}{(\omega+1)^4}\frac{k\chi_m^2 b\alpha^4}{[\alpha^2 r^2(\rho)]^{\frac{4\omega+7}{2(\omega+1)}}} \\
&-\frac{(\omega^2+2\omega+3)}{(\omega+1)^4}\frac{k^2\chi_m^4\alpha^4}{[\alpha^2 r^2(\rho)]^{\frac{2(\omega+2)}{\omega+1}}} + 12\alpha^4 .
\end{aligned} \tag{3.105}$$

This scalar does not diverge for any value of ρ (if $\omega > -1$). Therefore, spacetime (3.103) has no curvature singularities. However, it has a conic geometry with a conical singularity at $\rho = 0$. In fact, in the vicinity of $\rho = 0$, metric (3.103) is written as

$$ds^2 \sim -\alpha^2 r_+^2 dt^2 + \frac{\nu}{\alpha r_+}d\rho^2 + (\alpha r_+\nu)^{-1}\rho^2 d\varphi^2 , \tag{3.106}$$

with ν given by

$$\nu = \left[\alpha r_+ - \frac{b(\alpha r_+)^{-\frac{\omega+2}{\omega+1}}}{2(\omega+1)} + \frac{k\chi_m^2}{\omega+1}(\alpha r_+)^{-\frac{\omega+3}{\omega+1}}\right]^{-1} . \tag{3.107}$$

So, there is indeed a conical singularity at $\rho = 0$ since as the radius ρ tends to zero, the limit of the ratio "circumference/radius" is not 2π. The period of coordinate φ associated with this conical singularity is

$$\text{Period}_\varphi = 2\pi \left[\lim_{\rho\to 0}\frac{1}{\rho}\sqrt{\frac{g_{\varphi\varphi}}{g_{\rho\rho}}}\right]^{-1} = 2\pi\nu . \tag{3.108}$$

From (3.106)-(3.108) one concludes that in the vicinity of the origin, metric (3.103) describes a spacetime which is locally flat but has a conical singularity with an angle deficit $\delta\varphi = 2\pi(1-\nu)$.

Before closing this case, one should mention the particular $\omega = 0$ case of Brans-Dicke theory since this theory is related (through dimensional reduction) to 4D General Relativity with one Killing vector studied in [8].

(ii) Brans-Dicke theory with $\omega = \pm\infty$

The Brans-Dicke theory defined by $\omega = \pm\infty$ reduces to the spacetime generated by a static magnetic point source in 3D Einstein-Maxwell theory with $\Lambda < 0$ studied in detail in [48], [51]-[53]. The behavior of this spacetime is quite similar to those described in case **(i)**. It has a conical singularity at the origin and no horizons.

(iii) Brans-Dicke theories with $-\infty < \omega < -2$

For this range of the Brans-Dicke parameter we have to consider separately the case (1) $b > 0$ and (2) $b < 0$, where b is the mass parameter.

(1) If $b > 0$ the shape of the $e^{2\mu(r)}$ function is drawn in Fig. 1(b). Both g_{rr} and $g_{\varphi\varphi}$ are always positive (except at $r = 0$) and there is no apparent change of signature. Hence, for this range

of parameters, the spacetime is correctly described by equations (3.87) and (3.98). There are no horizons and so no magnetic black holes, but at $r = 0$ the scalar $R_{\mu\nu}R^{\mu\nu}$ diverges (in equation (3.105) put $r_+ = 0$ and replace ρ by r). Therefore, at $r = 0$ one has the presence of a naked curvature singularity.

(2) If $b < 0$ the shape of the $e^{2\mu(r)}$ function defined in (3.98) is sketched in Fig. 1(c). There occurs an apparent change of signature for $0 < r < r_+$. Proceeding exactly as we did in case (i) one can however introduce the new radial coordinate ρ defined in (3.102) and obtain the geodesically complete spacetime described by (3.103) and (3.104) (where now $\omega < -2$). This spacetime has no horizons and the scalar $R_{\mu\nu}R^{\mu\nu}$ given by (3.105) does not diverge for any value of ρ and so no curvature singularities are present. The spacetime has a conical singularity at $\rho = 0$ corresponding to an angle deficit $\delta\varphi = 2\pi(1 - \nu)$, where ν is defined in (3.107).

(iv) Brans-Dicke theory with $\omega = -2$

The shape of the $e^{2\mu(r)}$ function is drawn in Fig. 2(a). There is an apparent change of signature for $r > r_+$, where r_+ is the zero of $e^{2\mu(r)}$. We can however introduce a new coordinate system that will allow us to conclude that the spacetime is complete for $0 \le r \le r_+$. First, we introduce the radial coordinate $R = 1/r$. With this new coordinate $[g_{RR}(R)]^{-1}$ has a shape similar to the one shown in Fig. 1(a). Finally, we set a second coordinate transformation given by $\rho^2 = R^2 - R_+^2$, where $R_+ = 1/r_+$ is the zero of $(g_{RR})^{-1}$. Use of these coordinate transformations, together with equations (3.87) and (3.99), allows us to write the spacetime generated by the static magnetic point source as

$$ds^2 = -\frac{\alpha^2}{R^2(\rho)}dt^2 + \frac{\rho^2}{[R^2(\rho)]^3}\frac{1}{h(\rho)}d\rho^2 + \frac{h(\rho)}{\alpha^2}d\varphi^2 \,, \tag{3.109}$$

where $0 \le \rho < \infty$ and the function $h(\rho)$ is given by

$$h(\rho) = \left(1 + \frac{\chi_{\mathrm{m}}^2}{8}\ln[R^2(\rho)]\right)R^{-2}(\rho) - bR^{-1}(\rho) \,. \tag{3.110}$$

This function $h(\rho)$ is always positive except at $\rho = 0$ where it is zero. Hence, the spacetime described by equation (3.109) and (3.110) has no horizon. Along this section 3.3.2.b, in cases (iv)-(vii) we will use the definition $R^2(\rho) \equiv \rho^2 + R_+^2$ in order to shorten the formulas.

The scalar $R_{\mu\nu}R^{\mu\nu}$ is given by

$$\begin{aligned}
R_{\mu\nu}R^{\mu\nu} &= \chi_{\mathrm{m}}^4\left[\frac{3}{4}\ln^2[R(\rho)] + \frac{5}{4}\ln[R(\rho)] + 9\right] - \chi_{\mathrm{m}}^2\left[6\ln[R(\rho)] + \frac{4\ln[R(\rho)]}{R(\rho)} + \frac{3}{R(\rho)} + 5\right] + \\
&\quad + 8 + \frac{32}{R(\rho)} + \frac{6}{R^2(\rho)} \,.
\end{aligned} \tag{3.111}$$

This scalar diverges for $\rho = +\infty$ and so there is a curvature singularity at $\rho = +\infty$. Besides, the spacetime described by (3.109) and (3.110) has a conical singularity at $\rho = 0$ with coordinate φ having a period defined in equation (3.108),

$$\mathrm{Period}_\varphi = 2\pi\left[r_+\left(\frac{\chi_{\mathrm{m}}^2}{8} - 1 + \frac{b}{2r_+} - \frac{\chi_{\mathrm{m}}^2}{4}\ln r_+\right)\right]^{-1} \,. \tag{3.112}$$

So, near the origin, metric (3.109) and (3.110) describe a spacetime which is locally flat but has a conical singularity at $\rho = 0$ with an angle deficit $\delta\varphi = 2\pi - \mathrm{Period}_\varphi$.

(v) Brans-Dicke theories with $-2 < \omega < -3/2$

For this range of the Brans-Dicke parameter we have again to consider separately the case (1) $b > 0$ and (2) $b < 0$, where b is the mass parameter.

(1) If $b > 0$ the shape of the $e^{2\mu(r)}$ function defined in (3.98) is similar to the one of case **(iv)** and sketched in Fig. 2(a). So, proceeding as in case **(iv)**, we find that the spacetime generated by the static magnetic point source is given by (3.109) with function $h(\rho)$ defined by

$$h(\rho) = \frac{\alpha^2}{R^2(\rho)} + b\left(\frac{\alpha^2}{R^2(\rho)}\right)^{-\frac{1}{2(\omega+1)}} - k\chi_{\mathrm{m}}^2\left(\frac{\alpha^2}{R^2(\rho)}\right)^{-\frac{1}{\omega+1}}, \tag{3.113}$$

which is always positive except at $\rho = 0$ where it is zero. Hence, the spacetime described by equations (3.109) and (3.113) has no horizons.

The scalar $R_{\mu\nu}R^{\mu\nu}$ is given by (3.105) as long as we replace function $r^2(\rho)$ by $R^{-2}(\rho) \equiv (\rho^2 + R_+^2)^{-1}$. There is a curvature singularity at $\rho = +\infty$.

Near the origin, equations (3.109) and (3.113) describe a spacetime which is locally flat but has a conical singularity at $\rho = 0$ with an angle deficit $\delta\varphi = 2\pi - \mathrm{Period}_\varphi$, with Period_φ defined in equation (3.108),

$$\mathrm{Period}_\varphi = 2\pi\left[\alpha r_+ - \frac{b(\alpha r_+)^{-\frac{\omega+2}{\omega+1}}}{2(\omega+1)} + \frac{k\chi_{\mathrm{m}}^2}{\omega+1}(\alpha r_+)^{-\frac{\omega+3}{\omega+1}}\right]^{-1}. \tag{3.114}$$

(2) If $b < 0$ the $e^{2\mu(r)}$ function can have a shape similar to the one sketched in Fig. 2(b) or similar to Fig. 2(c), depending on the values of the range. We will not proceed further with the study of this case since it has a rather exotic spacetime structure.

(vi) Brans-Dicke theory with $\omega = -3/2$

The shape of the $e^{2\mu(r)}$ function defined in (3.100) is similar to the one of case **(iv)** and sketched in Fig. 2(a). So, proceeding as in case **(iv)**, we conclude that the spacetime generated by the static magnetic point source is given by (3.109) with function $h(\rho)$ defined by

$$h(\rho) = R^{-2}(\rho)\left(\frac{\Lambda}{2}\ln[b^{-2}R^2(\rho)] - \chi_{\mathrm{m}}^2 R^{-2}(\rho)\right), \tag{3.115}$$

which is always positive except at $\rho = 0$ where it is zero. Hence, the spacetime described by equations (3.109) and (3.115) has no horizons.

The scalar $R_{\mu\nu}R^{\mu\nu}$ is

$$R_{\mu\nu}R^{\mu\nu} = \Lambda^2\left[12\ln^2[bR(\rho)] + 20\ln[bR(\rho)] + 9\right] + -\Lambda\chi_{\mathrm{m}}^2 R^2(\rho)\left[5\ln[bR(\rho)] + \tfrac{9}{2}\right] + \tfrac{9}{16}\chi_{\mathrm{m}}^4 R^4(\rho). \tag{3.116}$$

There is a curvature singularity at $\rho = +\infty$.

Near the origin, equations (3.109) and (3.115) describe a spacetime which is locally flat but has a conical singularity at $\rho = 0$ with an angle deficit $\delta\varphi = 2\pi - \mathrm{Period}_\varphi$, with Period_φ defined in equation (3.108),

$$\mathrm{Period}_\varphi = 2\pi\left[r_+\left(\frac{\Lambda}{2} + \chi_{\mathrm{m}}^2 r_+^2\right)\right]^{-1}. \tag{3.117}$$

(vii) Brans-Dicke theories with $-3/2 < \omega < -1$

The shape of the $e^{2\mu(r)}$ function is sketched in Fig. 2(a) and is similar to the one of case **(iv)**. So, proceeding as in case **(iv)**, we find that the spacetime generated by the static magnetic point source is given by (3.109) with function $h(\rho)$ defined by (3.113). There are no horizons and there is no curvature singularity [the scalar $R_{\mu\nu}R^{\mu\nu}$ is given by (3.105) if we replace function $r^2(\rho)$ by $R^{-2}(\rho)$]. The spacetime has a conical singularity at $\rho = 0$ corresponding to an angle deficit $\delta\varphi = 2\pi - \mathrm{Period}_\varphi$, where Period_φ is defined in (3.114).

3.3.2.c Geodesic structure

We want to confirm that the spacetimes described by (3.87), (3.103) and (3.109) are both null and timelike geodesically complete. The equations governing the geodesics can be derived from the Lagrangian

$$\mathcal{L} = \frac{1}{2} g_{\mu\nu} \frac{dx^\mu}{d\tau} \frac{dx^\nu}{d\tau} = -\frac{\delta}{2}, \tag{3.118}$$

where τ is an affine parameter along the geodesic which, for a timelike geodesic, can be identified with the proper time of the particle along the geodesic. For a null geodesic one has $\delta = 0$ and for a timelike geodesic $\delta = +1$. From the Euler-Lagrange equations one gets that the generalized momentums associated with the time coordinate and angular coordinate are constants: $p_t = E$ and $p_\varphi = L$. The constant E is related to the timelike Killing vector $(\partial/\partial t)^\mu$ which reflects the time translation invariance of the metric, while the constant L is associated to the spacelike Killing vector $(\partial/\partial\varphi)^\mu$ which reflects the invariance of the metric under rotation. Note that since the spacetime is not asymptotically flat, the constants E and L cannot be interpreted as the energy and angular momentum at infinity.

From the metric we can derive the radial geodesic,

$$\dot{\rho}^2 = -\frac{1}{g_{\rho\rho}} \frac{E^2 g_{\varphi\varphi} + L^2 g_{tt}}{g_{tt} g_{\varphi\varphi}} - \frac{\delta}{g_{\rho\rho}}. \tag{3.119}$$

Next, we analyse this geodesic equation for each of the seven cases defined in the last section. Cases **(i)**, **(ii)** and **(iii)** have identical geodesic structure, and cases **(iv)**-**(vii)** also.

(i) Brans-Dicke theories with $-1 < \omega < +\infty$

Using the two useful relations $g_{tt} g_{\varphi\varphi} = -\rho^2/g_{\rho\rho}$ and $g_{\varphi\varphi} = [\rho^2/(\rho^2 + r_+^2)](\alpha^2 g_{\rho\rho})^{-1}$, we can write equation (3.119) as

$$\rho^2 \dot{\rho}^2 = \left[\frac{E^2}{\alpha^2} \frac{1}{\rho^2 + r_+^2} - \delta \right] \frac{\rho^2}{g_{\rho\rho}} + L^2 g_{tt}. \tag{3.120}$$

Noticing that $1/g_{\rho\rho}$ is always positive for $\rho > 0$ and zero for $\rho = 0$, and that $g_{tt} < 0$ we conclude the following about the null geodesic motion ($\delta = 0$). The first term in (3.120) is positive (except at $\rho = 0$ where it vanishes), while the second term is always negative. We can then conclude that spiraling ($L \neq 0$) null particles coming in from an arbitrary point are scattered at the turning point $\rho_{\text{tp}} > 0$ and spiral back to infinity. If the angular momentum L of the null particle is zero it hits the origin (where there is a conical singularity) with vanishing velocity.

Now we analyze the timelike geodesics ($\delta = +1$). Timelike geodesic motion is possible only if the energy of the particle satisfies $E > \alpha r_+$. In this case, spiraling timelike particles are bounded between two turning points that satisfy $\rho_{\text{tp}}^a > 0$ and $\rho_{\text{tp}}^b < \sqrt{E^2/\alpha^2 - r_+^2}$, with $\rho_{\text{tp}}^b \geq \rho_{\text{tp}}^a$. When the timelike particle has no angular momentum ($L = 0$) there is a turning point located exactly at $\rho_{\text{tp}}^b = \sqrt{E^2/\alpha^2 - r_+^2}$ and it hits the origin $\rho = 0$. Hence, we confirm that the spacetime described by equation (3.103) is both timelike and null geodesically complete.

(ii) Brans-Dicke theory with $\omega = \pm\infty$

The geodesic structure of the spacetime generated by a static magnetic point source in 3D Einstein-Maxwell theory with $\Lambda < 0$ has been studied in detail in [53]. The behavior of this geodesic structure is quite similar to the one described in case **(i)**. In particular, the spacetime is both timelike and null geodesically complete.

(iii) Brans-Dicke theories with $-\infty < \omega < -2$

For this range of the Brans-Dicke parameter we have to consider separately the case (1) $b > 0$ and (2) $b < 0$, where b is the mass parameter.

(1) If $b > 0$ the motion of null and timelike geodesics is correctly described by equation (3.120) if we replace ρ by r and put $r_+ = 0$. Hence, the null and timelike geodesic motion has the same feature as the one described in the above case **(i)**. In the above statements we just have to replace ρ by r, put $r_+ = 0$ and remember that at the origin there is now a naked curvature singularity rather than a conical singularity.

(2) If $b < 0$ the motion of null and timelike geodesics is exactly described by (3.120) and the statements presented in case **(i)** apply directly to this case.

(iv), (v), (vi), (vii) Brans-Dicke theories with $-2 \leq \omega < -1$

In order to study the geodesic motion of spacetime described by equations (3.109), one first notices that $g_{tt}g_{\varphi\varphi} = -[g_{\rho\rho}(\rho^2 + R_+^2)^2/\rho^2]^{-1}$ and $g_{\varphi\varphi} = [\rho^2/(\rho^2 + R_+^2)^3](\alpha^2 g_{\rho\rho})^{-1}$. Hence we can write equation (3.119) as

$$\rho^2 \dot{\rho}^2 = \left[\frac{E^2}{\alpha^2} \frac{1}{\rho^2 + R_+^2} - \delta\right] \frac{\rho^2}{g_{\rho\rho}} + (\rho^2 + R_+^2)^2 L^2 g_{tt} . \tag{3.121}$$

One concludes that the geodesic motion of null and timelike particles has the same feature as the one described in case **(i)** after (3.120) if in the statements we replace r_+ by R_+. The only difference is that on $\rho = +\infty$ there is now a curvature singularity for cases **(iv)** $\omega = -2$, **(v)** $-2 < \omega < -3/2$ and **(vi)** $\omega = -3/2$. In case **(v)** $-2 < \omega < -3/2$, if $b < 0$ (as we saw in last section) the spacetime has an exotic structure and so we do not study it.

So, we confirm that the spacetimes described by equations (3.109) are also both timelike and null geodesically complete.

3.3.3 The general rotating solution

3.3.3.a The generating technique

Now, we want to endow our spacetime solution with a global rotation, i.e., we want to add angular momentum to the spacetime. In order to do so we perform the following rotation boost in the t-φ plane (see e.g. [70, 7, 232])

$$
\begin{aligned}
t &\mapsto \gamma t - \frac{\varpi}{\alpha^2}\varphi , \\
\varphi &\mapsto \gamma\varphi - \varpi t ,
\end{aligned}
\tag{3.122}
$$

where γ and ϖ are constant parameters.

(i) Brans-Dicke theories with $-1 < \omega < +\infty$

Use of equation (3.122) and (3.103) gives the gravitational field generated by the rotating magnetic source

$$ds^2 = -\alpha^2(\rho^2 + r_+^2)(\gamma dt - \frac{\varpi}{\alpha^2}d\varphi)^2 +$$
$$+\frac{\rho^2}{(\rho^2 + r_+^2)} \frac{1}{f(\rho)} d\rho^2 + \frac{f(\rho)}{\alpha^2}(\gamma d\varphi - \varpi dt)^2, \tag{3.123}$$

where $f(\rho)$ is defined in (3.104).

The 1-form electromagnetic vector potential, $A = A_\mu(\rho)dx^\mu$, of the rotating solution is

$$A = -\varpi A(\rho)dt + \gamma A(\rho)d\varphi , \tag{3.124}$$

where

$$A(\rho) = -\frac{1}{4\alpha^2}\chi_{\mathrm{m}}(\omega + 1)[\alpha^2(\rho^2 + r_+^2)]^{-\frac{1}{2(\omega+1)}} . \tag{3.125}$$

(ii) Brans-Dicke theory with $\omega = \pm\infty$

The spacetime generated by a rotating magnetic point source in 3D Einstein-Maxwell theory with $\Lambda < 0$ has been obtained and studied in detail in [53].

(iii) Brans-Dicke theories with $-\infty < \omega < -2$

Proceeding exactly as in case **(i)**, we conclude that the gravitational and electromagnetic fields generated by the rotating magnetic source are also described by equations (3.123)-(3.125).

If $b > 0$ we have to set $r_+ = 0$ in equations (3.123) and (3.125).

(iv) Brans-Dicke theory with $\omega = -2$

Use of equations (3.122) and (3.109) yields the gravitational field generated by the rotating magnetic source

$$ds^2 = -\frac{\alpha^2}{(\rho^2 + R_+^2)}(\gamma dt - \frac{\varpi}{\alpha^2}d\varphi)^2 +$$

$$+\frac{\rho^2}{(\rho^2 + R_+^2)^3}\frac{1}{h(\rho)}d\rho^2 + \frac{h(\rho)}{\alpha^2}(\gamma d\varphi - \varpi dt)^2, \tag{3.126}$$

where $h(\rho)$ is defined in (3.110).

The 1-form vector potential is also given by (3.124) but now one has

$$A(\rho) = -\frac{1}{4\alpha^2}\chi_{\rm m}(\omega + 1)[\alpha^{-2}(\rho^2 + R_+^2)]^{\frac{1}{2(\omega+1)}} . \tag{3.127}$$

(v) Brans-Dicke theories with $-2 < \omega < -3/2$

If $b > 0$, the gravitational and electromagnetic fields generated by the rotating magnetic source are described by equations (3.126) and (3.127), with $h(\rho)$ defined in (3.113).

(vi) Brans-Dicke theory with $\omega = -3/2$

The gravitational and electromagnetic fields generated by the rotating magnetic source are described by equations (3.126) and (3.127), with $h(\rho)$ defined in (3.115).

(vii) Brans-Dicke theories with $-3/2 < \omega < -1$

The gravitational and electromagnetic fields generated by the rotating magnetic source are described by equations (3.126) and (3.127), with $h(\rho)$ defined in (3.113).

In equations (3.123), (3.124) and (3.126) we choose $\gamma^2 - \varpi^2/\alpha^2 = 1$ because in this way when the angular momentum vanishes ($\varpi = 0$) we have $\gamma = 1$ and so we recover the static solution.

Solutions (3.123)-(3.127) represent magnetically charged stationary spacetimes and also solve (3.83). Analyzing the Einstein-Rosen bridge of the static solution one concludes that spacetime is not simply connected which implies that the first Betti number of the manifold is one, i.e., closed curves encircling the horizon cannot be shrunk to a point. So, transformations (3.122) generate a new metric because they are not permitted global coordinate transformations [233]. Transformations (3.122) can be done locally, but not globally. Therefore metrics (3.103), (3.109) and (3.123)-(3.127) can be locally mapped into each other but not globally, and such they are distinct.

3.3.3.b   Mass, angular momentum and charge of the solutions

As we shall see the spacetime solutions describing the cases **(i)** $-1 < \omega < +\infty$, **(ii)** $\omega = \pm\infty$ and **(iii)** $-\infty < \omega < -2$ are asymptotically anti-de Sitter. This fact allows us to calculate the mass, angular momentum and the electric charge of the static and rotating solutions. To obtain these quantities we apply the formalism of Regge and Teitelboim [234].

(i) Brans-Dicke theories with $-1 < \omega < +\infty$

We first write (3.123) in the canonical form involving the lapse function $N^0(\rho)$ and the shift function $N^\varphi(\rho)$

$$ds^2 = -(N^0)^2 dt^2 + \frac{d\rho^2}{f^2} + H^2(d\varphi + N^\varphi dt)^2 \,, \tag{3.128}$$

where $f^{-2} = g_{\rho\rho}$, $H^2 = g_{\varphi\varphi}$, $H^2 N^\varphi = g_{t\varphi}$ and $(N^0)^2 - H^2(N^\varphi)^2 = g_{tt}$. Then, the action can be written in the Hamiltonian form as a function of the energy constraint $\mathcal{H}$, momentum constraint $\mathcal{H}_\varphi$ and Gauss constraint G

$$
\begin{aligned}
S = &- \int dt d^2x [N^0 \mathcal{H} + N^\varphi \mathcal{H}_\varphi + A_t G] + \mathcal{B} \\
= &-\Delta t \int d\rho N \nu \left[\frac{2\pi^2 e^{-2\phi}}{H^3} - 4f^2(H\phi_{,\rho}e^{-2\phi})_{,\rho} \right. \\
&-2H\phi_{,\rho}(f^2)_{,\rho}e^{-2\phi} + 2f(fH_{,\rho})_{,\rho}e^{-2\phi} \\
&\left. +4\omega H f^2(\phi_{,\rho})^2 e^{-2\phi} - \Lambda H e^{-2\phi} + \frac{2H}{f}e^{-2\phi}(E^2 + B^2) \right] \\
&+\Delta t \int d\rho N^\varphi \nu \left[(2\pi e^{-2\phi})_{,\rho} + \frac{4H}{f}e^{-2\phi}E^\rho B \right] \\
&+\Delta t \int d\rho A_t \nu \left[-\frac{4H}{f}e^{-2\phi}\partial_\rho E^\rho \right] + \mathcal{B} \,,
\end{aligned}
\tag{3.129}
$$

where $N = \frac{N^0}{f}$, $\pi \equiv \pi_\varphi{}^\rho = -\frac{fH^3(N^\varphi)_{,\rho}}{2N^0}$ (with $\pi^{\rho\varphi}$ being the momentum conjugate to $g_{\rho\varphi}$), E^ρ and B are the electric and magnetic fields and $\mathcal{B}$ is a boundary term. The factor ν [defined in (3.107)] comes from the fact that, due to the angle deficit, the integration over φ is between 0 and $2\pi\nu$. Upon varying the action with respect to $f(\rho)$, $H(\rho)$, $\pi(\rho)$, $\phi(\rho)$ and $E^\rho(\rho)$ one picks up additional surface terms. Indeed,

$$
\begin{aligned}
\delta S = &-\Delta t N \nu \left[(H_{,\rho} - 2H\phi_{,\rho})e^{-2\phi}\delta f^2 - (f^2)_{,\rho}e^{-2\phi}\delta H \right. \\
&-4f^2 H e^{-2\phi}\delta(\phi_{,\rho}) + 2f^2 e^{-2\phi}\delta(H_{,\rho}) \\
&\left. +2H[(f^2)_{,\rho} + 4(\omega + 1)f^2\phi_{,\rho}]e^{-2\phi}\delta\phi \right] \\
&+\Delta t N^\varphi \nu \left[2e^{-2\phi}\delta\pi - 4\pi e^{-2\phi}\delta\phi \right] \\
&+\Delta t A_t \nu \left[-\frac{4H}{f}e^{-2\phi}\delta E^\rho \right] + \delta\mathcal{B} \\
&+(\text{terms vanishing when equations of motion hold}).
\end{aligned}
\tag{3.130}
$$

In order that the Hamilton's equations are satisfied, the boundary term $\mathcal{B}$ has to be adjusted so that it cancels the above additional surface terms. More specifically one has

$$\delta\mathcal{B} = -\Delta t N \delta M + \Delta t N^\varphi \delta J + \Delta t A_t \delta Q_{\text{e}} \,, \tag{3.131}$$

where one identifies M as the mass, J as the angular momentum and Q_{e} as the electric charge since they are the terms conjugate to the asymptotic values of N, N^φ and A_t, respectively.

To determine the mass, the angular momentum and the electric charge of the solutions one must take the spacetime that we have obtained and subtract the background reference spacetime contribution, i.e., we choose the energy zero point in such a way that the mass, angular momentum and charge vanish when the matter is not present.

Now, note that for $\omega > -1$ (and $\omega < -2$), spacetime (3.123) has an asymptotic metric given by

$$-\left(\gamma^2 - \frac{\varpi^2}{\alpha^2}\right)\alpha^2\rho^2 dt^2 + \frac{d\rho^2}{\alpha^2\rho^2} + \left(\gamma^2 - \frac{\varpi^2}{\alpha^2}\right)\rho^2 d\varphi^2 , \tag{3.132}$$

where $\gamma^2 - \varpi^2/\alpha^2 = 1$ so, it is asymptotically an anti-de Sitter spacetime. For $\omega > -1$ (and $\omega < -2$) the anti-de Sitter spacetime is also the background reference spacetime, since the metric (3.123) reduces to (3.132) if the matter is not present ($b = 0$ and $\chi_{\rm m} = 0$).

Taking the subtraction of the background reference spacetime into account and noting that $\phi - \phi_{\rm ref} = 0$ and that $\phi_{,\rho} - \phi_{,\rho}^{\rm ref} = 0$ we have that the mass, angular momentum and electric charge are given by

$$
\begin{aligned}
M &= \nu\left[(2H\phi_{,\rho} - H_{,\rho})e^{-2\phi}(f^2 - f_{\rm ref}^2) + (f^2)_{,\rho}e^{-2\phi}(H - H_{\rm ref}) - 2f^2 e^{-2\phi}(H_{,\rho} - H_{,\rho}^{\rm ref})\right] , \\
J &= -2\nu e^{-2\phi}(\pi - \pi_{\rm ref}) , \\
Q_{\rm e} &= \frac{4H}{f}\nu e^{-2\phi}(E^\rho - E_{\rm ref}^\rho) .
\end{aligned}
\tag{3.133}
$$

Then, we finally have that the mass and angular momentum are (after taking the asymptotic limit, $\rho \to +\infty$)

$$M = b\nu\left[\gamma^2 + \frac{\omega + 2}{\omega + 1}\frac{\varpi^2}{\alpha^2}\right] + {\rm Div_M}(\chi_{\rm m}, \rho) , \tag{3.134}$$

$$J = \frac{\gamma\varpi}{\alpha^2}b\nu\frac{2\omega + 3}{\omega + 1} + {\rm Div_J}(\chi_{\rm m}, \rho) , \tag{3.135}$$

where ${\rm Div_M}(\chi_{\rm m}, \rho)$ and ${\rm Div_J}(\chi_{\rm m}, \rho)$ are terms proportional to the magnetic source $\chi_{\rm m}$ that diverge as $\rho \to +\infty$. The presence of these kind of divergences in the mass and angular momentum is a usual feature present in charged solutions. They can be found for example in the electrically charged point source solution [23], in the electric counterpart of the BTZ black hole [49], in the pure electric black holes of 3D Brans-Dicke action [71] and in the magnetic counterpart of the BTZ solution [53]. Following [23, 49], the divergences on the mass can be treated as follows. One considers a boundary of large radius ρ_0 involving the system. Then, one sums and subtracts ${\rm Div_M}(\chi_{\rm m}, \rho_0)$ to (3.134) so that the mass (3.134) is now written as

$$M = M(\rho_0) + \left[{\rm Div_M}(\chi_{\rm m}, \rho) - {\rm Div_M}(\chi_{\rm m}, \rho_0)\right] , \tag{3.136}$$

where $M(\rho_0) = M_0 + {\rm Div_M}(\chi_{\rm m}, \rho_0)$, i.e.,

$$M_0 = M(\rho_0) - {\rm Div_M}(\chi_{\rm m}, \rho_0) . \tag{3.137}$$

The term between brackets in (3.136) vanishes when $\rho \to \rho_0$. Then $M(\rho_0)$ is the energy within the radius ρ_0. The difference between $M(\rho_0)$ and M_0 is $-{\rm Div_M}(\chi_{\rm m}, \rho_0)$ which is interpreted as the electromagnetic energy outside ρ_0 apart from an infinite constant which is absorbed in $M(\rho_0)$. The sum (3.137) is then independent of ρ_0, finite and equal to the total mass. In practice the treatment of the mass divergence amounts to forgetting about ρ_0 and take as zero the asymptotic limit: $\lim {\rm Div_M}(\chi_{\rm m}, \rho) = 0$.

To handle the angular momentum divergence, one first notices that the asymptotic limit of the angular momentum per unit mass (J/M) is either zero or one, so the angular momentum diverges at a rate slower or equal to the rate of the mass divergence. The divergence on the angular momentum can then be treated in a similar way as the mass divergence. So, one can again consider a boundary of large radius ρ_0 involving the system. Following the procedure applied for the mass divergence one concludes that the divergent term $-{\rm Div_J}(\chi_{\rm m}, \rho_0)$ can be interpreted as the electromagnetic angular momentum outside ρ_0 up to an infinite constant that is absorbed in $J(\rho_0)$.

Hence, in practice the treatment of both the mass and angular divergences amounts to forgetting about ρ_0 and take as zero the asymptotic limits : $\lim {\rm Div_M}(\chi_{\rm m}, \rho) = 0$ and $\lim {\rm Div_J}(\chi_{\rm m}, \rho) = 0$ in (3.134) and (3.135).

Now, we calculate the electric charge of the solutions. To determine the electric field we must consider the projections of the Maxwell field on spatial hypersurfaces. The normal to such hypersurfaces is $n^\nu = (1/N^0, 0, -N^\varphi/N^0)$ and the electric field is given by $E^\mu = g^{\mu\sigma} F_{\sigma\nu} n^\nu$. Then, from (3.133), the electric charge is

$$Q_{\rm e} = -\frac{4Hf}{N^0} \nu e^{-2\phi} (\partial_\rho A_t - N^\varphi \partial_\rho A_\varphi) = \frac{\varpi}{\alpha^2} \nu \chi_{\rm m} . \tag{3.138}$$

Note that the electric charge is proportional to $\varpi \chi_{\rm m}$. In section 3.3.4 we will propose a physical interpretation for the origin of the magnetic field source and discuss the result obtained in (3.138).

The mass, angular momentum and electric charge of the static solutions can be obtained by putting $\gamma = 1$ and $\varpi = 0$ on the above expressions [see (3.122)].

(ii) Brans-Dicke theory with $\omega = \pm\infty$

The mass, angular momentum and electric charge of the spacetime generated by a magnetic point source in 3D Einstein-Maxwell theory with $\Lambda < 0$ have been calculated in [53]. Both the static and rotating solutions have negative mass and there is an upper bound for the intensity of the magnetic source and for the value of the angular momentum.

(iii) Brans-Dicke theories with $-\infty < \omega < -2$

The mass, angular momentum and electric charge of the $\omega < -2$ solutions are also given by (3.134), (3.135) and (3.138), respectively. If $b < 0$ the factor ν is defined in (3.107) and if $b > 0$ one has $\nu = 1$.

For $-2 \leq \omega \leq -1$ [cases (iv)-(vii)], the asymptotic and background reference spacetimes have a very peculiar form. In particular, they are not an anti-de Sitter spacetime. Therefore, there are no conserved quantities for these solutions.

3.3.3.c   The rotating magnetic solution in final form

For cases (i) $-1 < \omega < +\infty$, (ii) $\omega = \pm\infty$ and (iii) $-\infty < \omega < -2$ we may cast the metric in terms of M, J and $Q_{\rm e}$.

(i) Brans-Dicke theories with $-1 < \omega < +\infty$

Use of (3.134) and (3.135) allows us to solve a quadratic equation for γ^2 and ϖ^2/α^2. It gives two distinct sets of solutions

$$\gamma^2 = \frac{M(2-\Omega)}{2\nu b} , \qquad \frac{\varpi^2}{\alpha^2} = \frac{\omega+1}{2(\omega+2)} \frac{M\Omega}{\nu b} , \tag{3.139}$$

$$\gamma^2 = \frac{M\Omega}{2\nu b} , \qquad \frac{\varpi^2}{\alpha^2} = \frac{\omega+1}{2(\omega+2)} \frac{M(2-\Omega)}{\nu b} , \tag{3.140}$$

where we have defined a rotating parameter Ω as

$$\Omega \equiv 1 - \sqrt{1 - \frac{4(\omega+1)(\omega+2)}{(2\omega+3)^2} \frac{J^2\alpha^2}{M^2}} . \tag{3.141}$$

When we take $J = 0$ (which implies $\Omega = 0$), (3.139) gives $\gamma \neq 0$ and $\varpi = 0$ while (3.140) gives the nonphysical solution $\gamma = 0$ and $\varpi \neq 0$ which does not reduce to the static original metric. Therefore we will study the solutions found from (3.139).

For $\omega > -1$ (and $\omega < -2$), the condition that Ω remains real imposes a restriction on the allowed values of the angular momentum

$$|\alpha J| \leq \frac{|2\omega + 3|M}{2\sqrt{(\omega+1)(\omega+2)}} . \tag{3.142}$$

The parameter Ω ranges between $0 \leq \Omega \leq 1$. The condition $\gamma^2 - \varpi^2/\alpha^2 = 1$ fixes the value of b as a function of $M, \Omega, \chi_{\mathrm{m}}$,

$$b = \frac{M}{\nu}\left[1 - \frac{2\omega + 3}{2(\omega + 2)}\Omega\right], \tag{3.143}$$

where

$$\nu = \frac{2(\omega + 1)(\alpha r_+)^{\frac{\omega+2}{\omega+1}} + M\left(1 - \frac{2\omega+3}{2(\omega+2)}\Omega\right)}{2(\omega + 1)(\alpha r_+)^{\frac{2\omega+3}{\omega+1}} + 2k\chi_{\mathrm{m}}^2(\alpha r_+)^{-\frac{1}{\omega+1}}}. \tag{3.144}$$

The gravitational field (3.123) generated by the rotating point source may now be cast in the form

$$
\begin{aligned}
ds^2 &= -\left[\alpha^2(\rho^2 + r_+^2) - \frac{\omega + 1}{2(\omega + 2)}\frac{M\Omega/\nu}{[\alpha^2(\rho^2 + r_+^2)]^{\frac{1}{2(\omega+1)}}} + \frac{(\omega+1)^2}{8(\omega+2)}\frac{Q_{\mathrm{e}}^2/\nu^2}{[\alpha^2(\rho^2 + r_+^2)]^{\frac{1}{\omega+1}}}\right]dt^2 \\
&\quad -\frac{\omega+1}{2\omega+3}\frac{J}{\nu}\left[[\alpha^2(\rho^2 + r_+^2)]^{-\frac{1}{2(\omega+1)}} - \frac{(\omega+1)Q_{\mathrm{e}}^2}{4M\Omega\nu}[\alpha^2(\rho^2 + r_+^2)]^{\frac{1}{\omega+1}}\right]2dtd\varphi \\
&\quad +\frac{\rho^2/(\rho^2 + r_+^2)}{\left[\alpha^2(\rho^2 + r_+^2) + \frac{M}{\nu}\frac{1-2(\omega+3)\Omega/[2(\omega+2)]}{[\alpha^2(\rho^2+r_+^2)]^{\frac{1}{2(\omega+1)}}} - \frac{k\chi_{\mathrm{m}}^2}{[\alpha^2(\rho^2+r_+^2)]^{\frac{1}{\omega+1}}}\right]}d\rho^2 \\
&\quad +\frac{1}{\alpha^2}\left[\alpha^2(\rho^2 + r_+^2) + \frac{M(2-\Omega)/(2\nu)}{[\alpha^2(\rho^2 + r_+^2)]^{\frac{1}{2(\omega+1)}}} - \frac{(\omega+2)(2-\Omega)}{2(\omega+2)-(2\omega+3)\Omega}\frac{k\chi_{\mathrm{m}}^2}{[\alpha^2(\rho^2 + r_+^2)]^{\frac{1}{\omega+1}}}\right]d\varphi^2,
\end{aligned}
\tag{3.145}
$$

with $0 \leq \rho < \infty$ and the electromagnetic field generated by the rotating point source can be written as

$$A = \frac{A(\rho)}{\sqrt{2(\omega + 2) - (2\omega + 3)\Omega}}\left[-\alpha\sqrt{(\omega + 1)\Omega}\,dt + \sqrt{(\omega + 2)(2 - \Omega)}\,d\varphi\right], \tag{3.146}$$

with $A(\rho)$ defined in (3.125).

The static solution can be obtained by putting $\Omega = 0$ (and thus $J = 0$ and $Q_{\mathrm{e}} = 0$) on the above expression [see (3.122)].

(ii) Brans-Dicke theory with $\omega = \pm\infty$

The spacetime generated by a rotating magnetic point source in 3D Einstein-Maxwell theory with $\Lambda < 0$ is written as a function of its hairs in [53].

(iii) Brans-Dicke theories with $-\infty < \omega < -2$

For this range of ω, the gravitational and electromagnetic fields generated by a rotating magnetic point source are also given by (3.145) and (3.146). If $b < 0$ the factor ν is defined in (3.144) and if $b > 0$ one has $\nu = 1$.

3.3.3.d   Geodesic structure

The geodesic structure of the rotating spacetime is similar to the static spacetime (see section 3.3.2.c), although there are now direct (corotating with $L > 0$) and retrograde (counter-rotating with $L < 0$) orbits. The most important result that spacetime is geodesically complete still holds for the stationary spacetime.

3.3.4 Physical interpretation of the magnetic source

When we look back to the electric charge given in (3.138), we see that it is zero when $\varpi = 0$, i.e., when the angular momentum J of the spacetime vanishes. This is expected since in the static solution we have imposed that the electric field is zero (F_{12} is the only non-null component of the Maxwell tensor).

Still missing is a physical interpretation for the origin of the magnetic field source. The magnetic field source is not a Nielson-Oleson vortex solution since we are working with the Maxwell theory and not with an Abelian-Higgs model. We might then think that the magnetic field is produced by a Dirac point-like monopole. However, this is not also the case since a Dirac monopole with strength g_{m} appears when one breaks the Bianchi identity [235], yielding $\partial_\mu(\sqrt{-g}\tilde{F}^\mu e^{-2\phi}) = g_{\mathrm{m}}\delta^2(\vec{x})$ (where $\tilde{F}^\mu = \epsilon^{\mu\nu\gamma}F_{\nu\gamma}/2$ is the dual of the Maxwell field strength), whereas in this work we have that $\partial_\mu(\sqrt{-g}\tilde{F}^\mu e^{-2\phi}) = 0$. Indeed, we are clearly dealing with the Maxwell theory which satisfies Maxwell equations and the Bianchi identity

$$\frac{1}{\sqrt{-g}}\partial_\nu(\sqrt{-g}F^{\mu\nu}e^{-2\phi}) = \frac{\pi}{2}\frac{1}{\sqrt{-g}}j^\mu \,, \tag{3.147}$$

$$\partial_\mu(\sqrt{-g}\tilde{F}^\mu e^{-2\phi}) = 0 \,, \tag{3.148}$$

respectively. In (3.147) we have made use of the fact that the general relativistic current density is $1/\sqrt{-g}$ times the special relativistic current density $j^\mu = \sum q\delta^2(\vec{x} - \vec{x}_0)\dot{x}^\mu$.

We then propose that the magnetic field source can be interpreted as composed by a system of two symmetric and superposed electric charges (each with strength q). One of the electric charges is at rest with positive charge (say), and the other is spinning with an angular velocity $\dot{\varphi}_0$ and negative electric charge. Clearly, this system produces no electric field since the total electric charge is zero and the magnetic field is produced by the angular electric current. To confirm our interpretation, we go back to (3.147). In our solution, the only non-vanishing component of the Maxwell field is $F^{\varphi\rho}$ which implies that only j^φ is not zero. According to our interpretation one has $j^\varphi = q\delta^2(\vec{x} - \vec{x}_0)\dot{\varphi}$, which one inserts in (3.147). Finally, integrating over ρ and φ we have

$$\chi_{\mathrm{m}} \propto q\dot{\varphi}_0 \,. \tag{3.149}$$

So, the magnetic source strength, χ_{m}, can be interpreted as an electric charge times its spinning velocity.

Looking again to the electric charge given in (3.138), one sees that after applying the rotation boost in the t-φ plane to endow the initial static spacetime with angular momentum, there appears a net electric charge. This result was already expected since now, besides the scalar magnetic field ($F_{\rho\varphi} \neq 0$), there is also an electric field ($F_{t\rho} \neq 0$) [see (3.146)]. A physical interpretation for the appearance of the net electric charge is now needed. To do so, we return to the static spacetime. In this static spacetime there is a static positive charge and a spinning negative charge of equal strength at the center. The net charge is then zero. Therefore, an observer at rest (S) sees a density of positive charges at rest which is equal to the density of negative charges that are spinning. Now, we perform a local rotational boost $t' = \gamma t - (\varpi/\alpha^2)\varphi$ and $\varphi' = \gamma\varphi - \varpi t$ to an observer (S') in the static spacetime, so that S' is moving relatively to S. This means that S' sees a different charge density since a density is a charge over an area and this area suffers a Lorentz contraction in the direction of the boost. Hence, the two sets of charge distributions that had symmetric charge densities in the frame S will not have charge densities with equal magnitude in the frame S'. Consequently, the charge densities will not cancel each other in the frame S' and a net electric charge appears. This was done locally. When we turn into the global rotational Lorentz boost of (3.122) this interpretation still holds. The local analysis above is similar to the one that occurs when one has a copper wire with an electric current and we apply a translation Lorentz boost to the wire: first, there is only a magnetic field but, after the Lorentz boost, one also has an electric field. The difference is that in the present situation the Lorentz boost is a rotational one and not a translational one.

3.4 Summary and discussion

We have added the Maxwell action to the action of a generalized 3D dilaton gravity specified by the Brans-Dicke parameter ω introduced in [69, 70] and discussed in section 3.1. We have concluded that for the static spacetime the electric and magnetic fields cannot be simultaneously non-zero, i.e. there is no static dyonic solution. Notice that, in oppose to what occurs in 4-dimensions where the the Maxwell tensor and its dual are 2-forms, in 3-dimensions the Maxwell tensor is still a 2-form, but its dual is a 1-form (in practice, the Maxwell tensor has only three independent components: two for the electric vector field, and one for the scalar magnetic field). As a consequence, the magnetic solutions are radically different from the electric solutions in 3-dimensions.

In section 3.2 we have considered the electrically charged case alone. We have found the static and rotating black hole solutions of this theory. It contains eight different cases that appear naturally from the solutions. For $\omega = 0$ one gets a theory related (through dimensional reduction) to electrically charged four dimensional AdS general relativity with one Killing vector [7], and for $\omega = \pm\infty$ one obtains electrically charged three dimensional general relativity [48, 49]. For $\omega > -3/2$ the ADM mass and angular momentum of the solutions are finite, well-behaved and equal to the ADM masses of the uncharged solutions. However, for $\omega < -3/2$ the ADM mass and angular momentum of the solutions have terms proportional to the charge that diverge at the asymptotic limit, as frequently occurs in the 3-dimensional theories including a Maxwell field (see, e.g. [23, 49, 53, 71, 55]). We have shown how to treat this problem. For each range of ω we have determined what conditions must be imposed on the ADM hairs of the solutions in order to be possible the existence of black holes. Our results show that there is no upper bound on the electric charge. The causal and geodesic structure of the charged solutions has been analyzed in detail.

In section 3.3 we have found geodesically complete spacetimes generated by static and rotating magnetic point sources. These spacetimes are horizonless and many of them have a conical singularity at the origin. These features are common in spacetimes generated by point sources in 3D gravity theories [18]-[31]. The static solution generates a scalar magnetic field while the rotating solution produces, in addition, a radial electric field. The source for the magnetic field can be interpreted as composed by a system of two symmetric and superposed electric charges. One of the electric charges is at rest and the other is spinning. This system produces no electric field since the total electric charge is zero and the scalar magnetic field is produced by the angular electric current. When we apply a rotational Lorentz boost to add angular momentum to the spacetime, there appears a net electric charge and a radial electric field. The $\omega = \pm\infty$ solution reduces to the magnetic counterpart of the BTZ solution studied in chapter 2. The solutions corresponding to the theories described by a Brans-Dicke parameter that belongs to the range $-1 < \omega < +\infty$ or $-\infty < \omega < -2$ have a behavior quite similar to the magnetic counterpart of the BTZ solution. For this range of the Brans-Dicke parameter, the solutions are asymptotically anti-de Sitter. This allowed us to calculate the mass, angular momentum and charge of the solutions, and once again in we found divergencies at spatial infinity.

The relation between spacetimes generated by sources in 3D and cylindrically symmetric 4D solutions has been noticed by many authors (see e.g. [20, 16, 50, 6, 8]). The $\omega = 0$ solutions (electric and magnetic) considered in this chapter are the 3D counterparts of the 4D cylindrical or toroidal solutions studied in [6, 7, 8], and that will be discussed in chapter 5. Indeed, the dimensional reduction of 4D general relativity with one Killing vector yields the $\omega = 0$ case of Brans-Dicke theory.

Chapter 4

Pair creation of black holes in three dimensions

In chapters 9 and 11 we will analyze in detail the pair creation process of 4-dimensional black holes and of higher dimensional black holes, respectively. The process of quantum pair creation of black holes in an external field in a 3-dimensional background has not been analyzed yet, as far as we know. We will not do it here. However, we will try to understand the difficulties associated with this issue, and we will also propose a possible background in which the pair creation process in 3-dimensions might be analyzed.

When we want to analyze analytically the gravitational pair creation process, our first task is to ask if there is an exact solution of Einstein gravity that represents a pair of accelerated black holes. This solution is important for the analysis of the process since it describes the subsequent motion of the pair, after its creation. In 4-dimensions and higher dimensions these solutions exist (see, respectively, chapters 6 and 10), however in 3-dimensions these solutions are not known. In order to understand this lack recall that in 3-dimensional Einstein gravity the only black hole that exists is the BTZ one, and it lives in an AdS background (see chapter 2). So, black hole pair creation in 3-dimensional Einstein gravity, if possible, must occur in an AdS background. However, from the studies on 4-dimensional spacetimes (see chapter 9), we know that it is much more difficult in a sense to create a pair in an AdS background than in a dS or flat background. Indeed, the AdS background is attractive, i.e., it furnishes a cosmological constant acceleration that pulls in the particles. Moreover, as we saw in detail in chapter 2, the BTZ black hole has constant curvature and thus its construction is topological, i.e., it is obtained from the pure AdS_3 solution through identifications along an isometry of the AdS_3 spacetime. Therefore, a possible exact solution describing an accelerating pair of BTZ black holes would probably have to be also constructed using a similar topological procedure.

Now, in what concerns the acceleration source of the black holes, we could in principle manage a way to overcome the repulsive AdS acceleration. Using again our knowledge from pair creation in 4-dimensions, we could try an external source such as (i) an electromagnetic field, (ii) a string with its tension, or (iii) the 3-dimensional analogue of a domain wall with its repulsive gravitational field. In what concerns the hypothesis (i), even in 4-dimensions, there is no AdS exact solution that describes a pair of AdS black holes accelerated by an external Lorentz force. Thus, we expect also serious difficulties when we try to find it in 3-dimensions. The hypothesis (ii) cannot be discarded since there are string solutions in 3-dimensions. Hypothesis (iii) is discarded since the analogue of a domain wall does not exist in 3-dimensions. The reason is simple: in 3-dimensional Einstein gravity a matter distribution produces no gravitational field.

Another possibility, is to try to analyze the black hole pair creation process in the context of an effective 3-dimensional gravity theory, e.g., in the dilaton Brans-Dicke theory discussed in chapter 3. In particular, the case with $\omega = 0$ (where ω is the Brans-Dicke parameter) might be interesting for our purposes. Indeed, recall that this $\omega = 0$ case can be obtained through dimensional reduction from 4-dimensional AdS general relativity with one Killing vector [6, 7, 8]. This is, the cylindrical or toroidal 4-dimensional black hole found in [6] yields, through dimensional reduction, the $\omega = 0$ black hole. Now, in section 7.4.2 we study the planar, cylindrical or toroidal AdS C-metric [86], which describes a pair of accelerated 4-dimensional black holes with planar symmetry (i.e., with

planar, cylindrical or toroidal topology). The solution with planar black holes, or black walls, is the most useful for our present discussion. Indeed, it is possible that the dimensional reduction of this planar AdS C-metric yields a 3-dimensional exact solution that describes a pair of accelerated $\omega = 0$ Brans-Dicke black strings (this is sketched in Fig. 4.1). We will not do this here. We leave it for future work. In chapter 9 we will analyze in detail the pair creation process of 4-dimensional black holes, and in chapter 11 we will study the pair creation process of higher dimensional black holes.
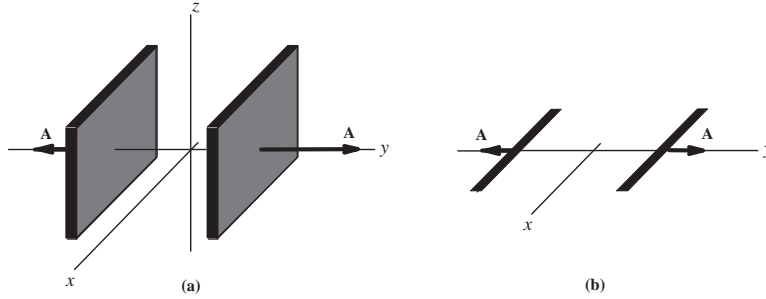
Figure 4.1: (a) Schematic representation of the planar AdS C-metric that describes a pair of accelerated 4-dimensional black holes with planar topology (black walls). (b) After dimensional reduction the above solution might yield a 3-dimensional exact solution that describes a pair of accelerated $\omega = 0$ Brans-Dicke black strings.

We have been discussing pair creation of black holes in 3-dimensions, and gave reasons for the difficulty in studying the problem. One could ask if there are works discussing particle pair creation in 3-dimensions. As far as we know, the literarture is also void in this subject. Some of the remarks gathered for the difficulties in black hole pair creation also apply here. Although point particle solutions in flat 3-dimensional general relativity exist, perhaps there are still difficulties in finding exact solutions with an accelerating field where the point particles could be boxed in. We would like to mention that 2-dimensional pair creation of particles has not been totally neglected. Indeed, Brown and Teitelboim have discussed this problem [243].

Part II

Black holes and pair creation in 4 dimensions

Chapter 5

Black holes in a generalized Λ background

Contents

In this chapter we will briefly describe the main features of the black hole solutions of the Einstein-Maxwell theory in a background with a generalized cosmological constant Λ. We stress that this description is by no way a complete one. We will only focus on those properties that will be needed to better understand the processes that will be discussed in later chapters. Mainly, we shall discuss the range of parameters for which one has black holes, we will analyze the causal structure of the solutions, and we will briefly discuss the main difference between the geodesic motion in an anti-de Sitter (AdS), in a flat, and in a de Sitter (dS) background.

In sections 5.1.1, 5.2 and 5.3 we will describe black holes with spherical topology in an AdS, flat and dS background, respectively. Their properties will be useful for us in chapter 6, where we will analyze solutions that describe a pair of accelerated black holes with spherical topology in an AdS, flat and dS background. Then, in chapter 9 we will discuss the pair creation process of these black holes in an external field. Moreover, in chapter 7 we will see that the solutions studied in sections 5.1.3, 5.2 and 5.3 of this chapter allows us to generate the so called Nariai, Bertotti-Robinson and anti-Nariai solutions. Subsection 5.1.2.b discusses work developed by us [8]. We thus think that this introductory chapter is well justified.

In what concerns the causal structure, the main difference between the Carter-Penrose diagrams of the $\Lambda < 0$ (AdS), of the $\Lambda = 0$ (flat), and of the $\Lambda > 0$ (dS) is at the level of the line that represents infinity ($r = +\infty$). In the AdS case the infinity is a timelike line (vertical line in the diagrams), in the flat case it is represented by a null line (a 45° line), and in the dS case it is represented by a spacelike line (an horizontal line in the diagram). These features are represented in Fig. 5.1 for the pure AdS, Minkowski and dS backgrounds (the character of the infinity line does not change when a mass or a charge is added to the system). The infinity line is then a signature of the cosmological background.
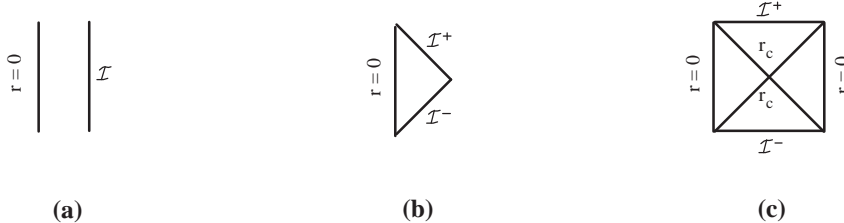
Figure 5.1: Carter-Penrose diagram of the: (a) AdS solution, (b) Minkowski solution, and (c) dS solution. $\mathcal{I}$ represents the infinity ($r = \infty$). The infinity line is a timelike line in the AdS case, a null line in the Minkowski case, and a spacelike line in the dS case.

Note that in these Carter-Penrose diagrams, a null particle (e.g., a light ray) moves necessarily along 45° lines, while timelike particles can move only into the top of the diagrams along a curve whose tangent vector must do an angle less than 45° with the vertical line. As a typical example of the kind of information that can be withdrawn from the Carter-Penrose diagrams, let us analyze the evolution of these diagrams in a $\Lambda = 0$ background when we start with the empty spacetime (Minkowski solution with $M = 0$, $Q = 0$), and then progressively add a mass M (Schwarzschild solution) and then also a charge Q (Reissner-Nordström solution) to the background spacetime. This evolution is sketched in Fig. 5.2. In Fig. 5.2.(a), we have the diagram of the Minkowski solution. The past infinity ($\mathcal{I}^-$) and the future infinity ($\mathcal{I}^+$) are both represented by a null line, and the origin of the radial coordinate, $r = 0$, is represented by a timelike line. A null ray that is emitted from a point a is free to move towards $r = 0$ or into the future infinity $\mathcal{I}^+$. When we add a mass M to the system [see Fig. 5.2.(b)], several changes occur. First of all, $r = 0$ supports now a curvature singularity (since any scalar polynomial of the curvature, e.g. the square of the Riemann tensor, diverges there). The presence of this curvature singularity is indicated by a zigzag line. Moreover, when compared with Fig. 5.2.(a), we see that $r = 0$ suffers a 90° rotation and is now represented by a spacelike line. This rotation is accompanied by the appearance of two mutually perpendicular lines at 45° that represent the black hole event horizon r_+. The region IV is equivalent to region I [that was already present in diagram (a)] and both represent the region outside the black hole horizon, $r_+ < r < +\infty$. A null ray that is sent from a point a in these regions can move towards $r = 0$, after crossing r_+, but it is also free to move into the future infinity $\mathcal{I}^+$ [see Fig. 5.2.(c)]. Note that regions I and IV are casually disconnected: no null or timelike particle can start in region I and reach region IV. The adding of the mass also leads to the appearance of two new regions, represented by regions II and III in figure (b). Region II is interpreted as the interior of the black hole horizon, since a null ray emitted from a point in its interior [e.g., point b in Fig. 5.2.(c)] necessarily hits the future curvature singularity, and cannot cross the horizon towards region I or IV (the discussion also applies to timelike particles). Region III is interpreted as the interior of the white hole, since any particle, e.g. the light ray that is emitted from point c in Fig. 5.2.(c), is necessarily expelled out from region III, i.e., it necessarily crosses the horizon towards region I or IV. In Fig. 5.2.(d) we show the causal diagram of the solution when a charge is added to the solution. Again, several changes occur. When compared with Fig. 5.2.(b), we see that the curvature singularity $r = 0$ suffers again a 90° rotation and is now represented by a timelike zigzag line. This rotation is accompanied by the appearance of two new mutually perpendicular lines at 45°, that represent the black hole Cauchy horizon r_-, together with two new equivalent regions that are represented as region V in the figure. The properties of this Cauchy horizon are quite interesting. As an example note that the full history of the regions I, II and IV is in the causal past of the Cauchy horizon, i.e., this horizon can have access to all the information that is generated in those regions.
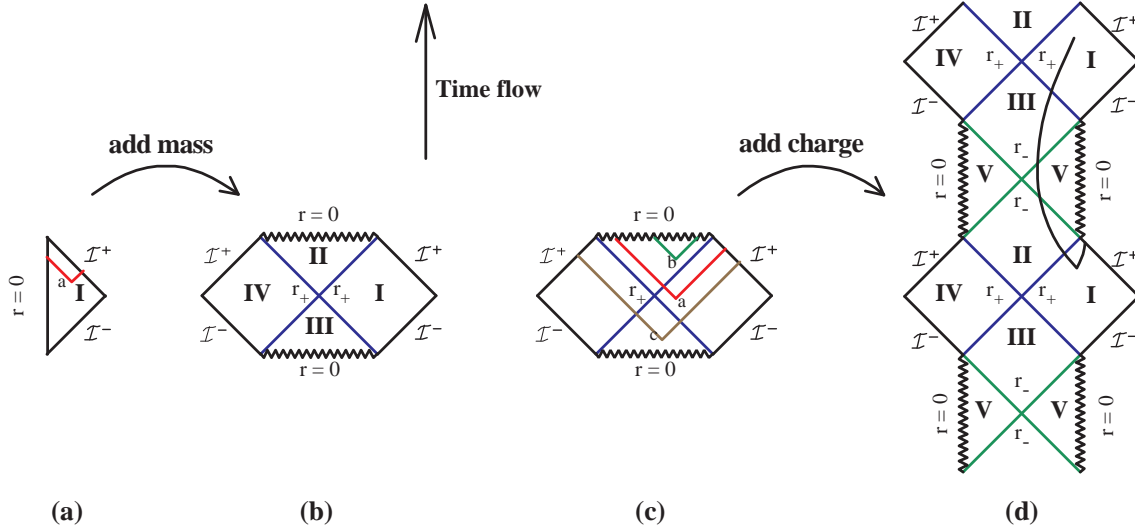
Figure 5.2: Carter-Penrose diagram of the: (a) Minkowski solution, $M = 0$, $Q = 0$; (b) Schwarzschild ($Q = 0$) black hole; and (c) Reissner-Nordström black hole. The zigzag line represents a curvature singularity, $\mathcal{I}$ represents the infinity ($r = \infty$), r_+ represents a black hole event horizon, and r_- represents the Cauchy or inner black hole horizon.

The causal diagrams provide a lot of information about the solution, but there are also relevant features that cannot be withdrawn from them. The study of the geodesic structure of the solution provides some more information, that will be useful for us in later chapters. The geodesic equation of motion, for a general non-rotating black hole, can be written as

$$\dot{r}^2 = E^2 - \left(\delta + \frac{L^2}{g_{\varphi\varphi}}\right)\frac{1}{g_{rr}} = E^2 - V(r)\,, \tag{5.1}$$

where

$$V(r) = \left(\delta + \frac{L^2}{r^2}\right)\left(1 - \frac{2M}{r} + \frac{Q^2}{r^2} - \frac{\Lambda}{3}r^2\right)\,, \tag{5.2}$$

and $\dot{r} = \frac{dr}{d\tau}$, with τ being an affine parameter along the geodesic which, for a timelike geodesic, can be identified with the proper time of the particle along the geodesic. For a null geodesic one has $\delta = 0$ and for a timelike geodesic $\delta = +1$. M and Q are respectively the mass and charge of the black holes, and L is the angular momentum of the particle subjected to the gravitational field of the black hole.

In later chapters we will make a reference to the information withdrawn from Fig. 5.3, where we draw the general form of $V(r)$ for timelike geodesics in a pure anti-de Sitter, Minkowski and de Sitter spacetimes ($M = 0$, $Q = 0$, $\delta = 1$ and $L = 0$). From it we conclude that the AdS spacetime is attractive, in the sense that particles in this background are subjected to a potential well that attracts them, i.e., if a particle tries to escape to infinity, it will be reflected back, no matter how big its energy. On the other side, the dS spacetime is repulsive: if a low-energy particle tries to approach the origin, it will be reflected back to infinity.

V(r) V(r) V(r)

AdS Flat dS

(a) (b) (c)
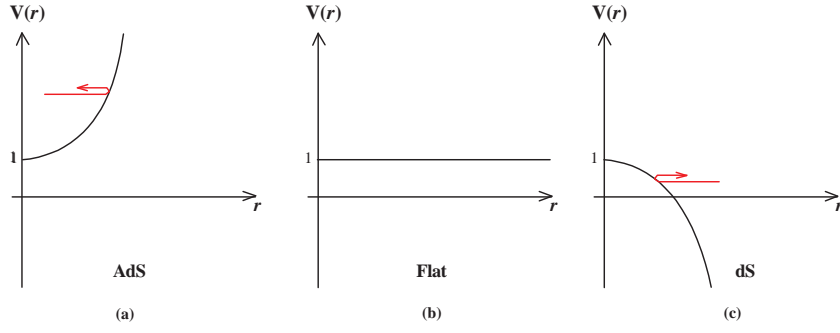
Figure 5.3: Timelike geodesics for the black hole parameters $M = 0$, and $Q = 0$. (a) Anti-de Sitter case ($\Lambda < 0$), (b) flat case ($\Lambda = 0$), and (c) de Sitter case ($\Lambda = 0$).

For massless particles, this information concerning the attractive/repulsive character of the AdS/dS backgrounds could also be withdrawn from the corresponding Carter-Penrose diagrams, Fig. 5.1. Indeed, we see that a null ray (45° line) that hits the timelike AdS infinity is necessarily reflected back, and that a null ray that is sent towards the dS spacelike infinity can never return back (unless we act on the ray through an external process, a mirror, for example).

As another example of the utility of the geodesic analysis, and of the limitations associated with the causal diagrams, the general form of $V(r)$ for $L = 0$ timelike geodesics in a Schwarzschild black hole and Reissner-Nordström black hole is sketched, respectively, in Figs. 5.4 and 5.5 for the three cosmological backgrounds (AdS, flat, dS). The important fact that we want to stress is that, in the Schwarzschild black hole (AdS, flat or dS), when a massive particle crosses inward the $r = r_+$ sphere it cannot come back, as already expected. However, in the Reissner-Nordström black hole (AdS, flat or dS), a massive particle can never hit the curvature singularity (note that this does not apply in the case of massless particles). This information could not be withdrawn from the analysis of the Carter-Penrose diagram.

V(r) V(r) V(r)

AdS Flat dS

(a) (b) (c)
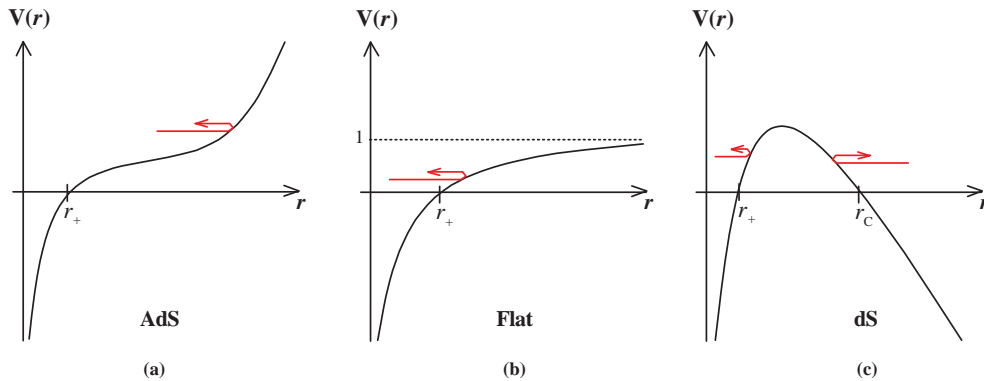
Figure 5.4: Timelike geodesics with vanishing angular momentum ($L = 0$) for the black hole parameters $M \neq 0$, and $Q = 0$. (a) AdS case ($\Lambda < 0$), (b) flat case ($\Lambda = 0$), and (c) dS case ($\Lambda = 0$).
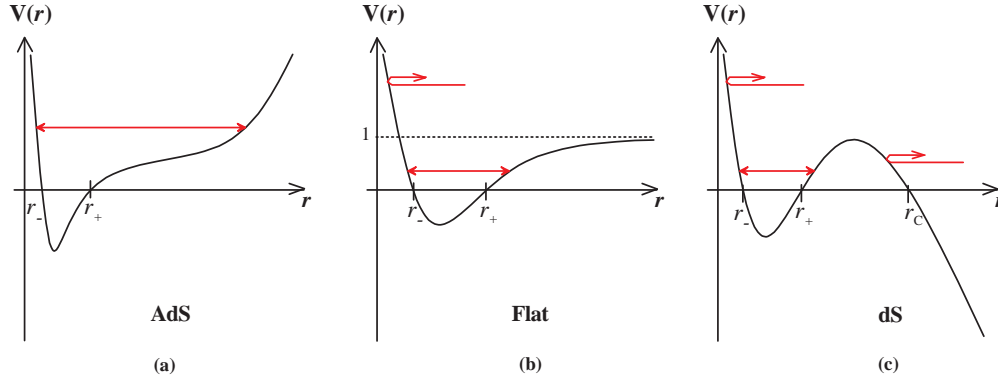
Figure 5.5: Timelike geodesics with vanishing angular momentum $(L = 0)$ for the black hole parameters $M \neq 0$, and $Q \neq 0$. (a) AdS case $(\Lambda < 0)$, (b) flat case $(\Lambda = 0)$, and (c) dS case $(\Lambda = 0)$.

5.1 Black holes in an anti-de Sitter background

The Einstein-Maxwell equations in an AdS background $(\Lambda < 0)$ admit a three-family of black hole solutions whose gravitational field is described by

$$ds^2 = -\left(b - \frac{2M}{r} + \frac{Q^2}{r^2} - \frac{\Lambda}{3}r^2\right)dt^2 + \frac{dr^2}{b - \frac{2M}{r} + \frac{Q^2}{r^2} - \frac{\Lambda}{3}r^2} + r^2 d\Omega_b^2, \qquad (5.3)$$

where b can take the values $1, 0, -1$ and

$$\begin{cases} d\Omega_b^2 = d\theta^2 + \sin^2\theta\,d\phi^2 & \text{for } b = 1\,, \\ d\Omega_b^2 = d\theta^2 + d\phi^2 & \text{for } b = 0\,, \\ d\Omega_b^2 = d\theta^2 + \sinh^2\theta\,d\phi^2 & \text{for } b = -1\,. \end{cases} \qquad (5.4)$$

These three solutions describe three different kind of AdS black holes. The black holes with $b = 1$ are the usual AdS black holes with spherical topology. The black holes with $b = 0$ have planar, cylindrical or toroidal (with genus $g \geq 1$) topology and were introduced and analyzed in [6, 7, 8]. The topology of the $b = -1$ black holes is hyperbolic or, upon compactification, toroidal with genus $g \geq 2$, and they have been analyzed in [11]. In the following subsections we shall describe briefly which one of these families of black holes. The solutions with non-spherical topology (cases $b = 0$ and $b = -1$) do not have counterparts in a $\Lambda = 0$ or in a $\Lambda > 0$ background.

5.1.1 Black holes with spherical topology

In this subsection we will briefly present the black hole solutions with spherical symmetry of the Einstein-Maxwell equations in a negative cosmological background $(\Lambda < 0)$. The gravitational field of the electrically charged black hole solution is given by

$$ds^2 = -\left(1 - \frac{\Lambda}{3}r^2 - \frac{2M}{r} + \frac{Q^2}{r^2}\right)dt^2 + \frac{dr^2}{1 - \frac{\Lambda}{3}r^2 - \frac{2M}{r} + \frac{Q^2}{r^2}} + r^2(d\theta^2 + \sin^2\theta\,d\phi^2)\,, \qquad (5.5)$$

where M and Q are, respectively, the ADM mass and charge of the solution, while the electromagnetic field is

$$A = -\frac{Q}{r}\,dt\,, \qquad A = Q\cos\theta\,d\phi\,, \qquad (5.6)$$

in the pure electric and in the pure magnetic cases, respectively. The Carter-Penrose diagram of the nonextreme AdS−Reissner-Nordström black hole is sketched in Fig. (5.6).(a), of the extreme AdS−Reissner-Nordström black hole in Fig. (5.6).(b), and the naked particle in Fig. (5.6).(c). The Carter-Penrose diagram of the AdS-Schwarzschild is drawn in Fig. (5.7).
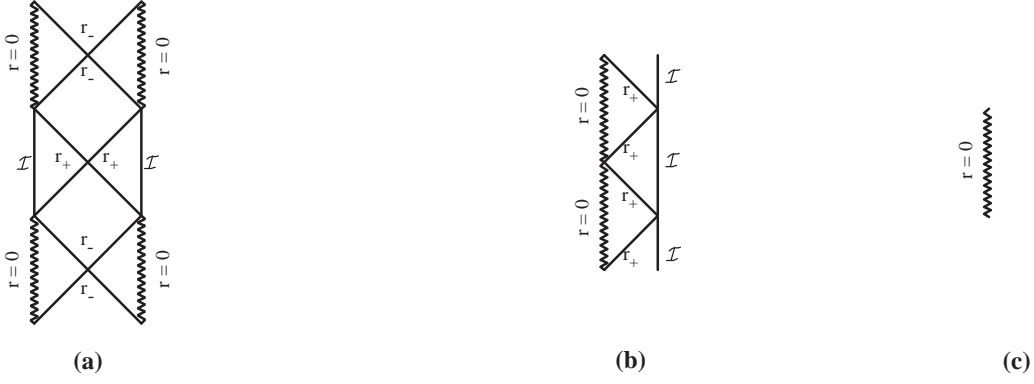
Figure 5.6: Carter-Penrose diagrams of the AdS−Reissner-Nordström ($Q \neq 0$) black holes (with spherical topology) discussed in the text of section 5.1.1. The zigzag line represents a curvature singularity, $\mathcal{I}$ represents the infinity ($r = \infty$), r_+ represents a black hole event horizon, and r_- represents a Cauchy horizon.
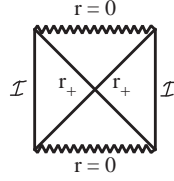
Figure 5.7: Carter-Penrose diagrams of the AdS-Schwarzschild ($Q = 0$) black hole (with spherical topology) discussed in the text of section 5.1.1. The zigzag line represents a curvature singularity, $\mathcal{I}$ represents the infinity ($r = \infty$), r_+ represents a black hole event horizon, and r_- represents a Cauchy horizon.

5.1.2 Black holes with toroidal or cylindrical topology

In this subsection we will consider solutions of the Einstein-Maxwell equations with cylindrical symmetry in a negative cosmological background ($\Lambda < 0$). The topology of the two dimensional angular space can be (i) $R \times S^1$, the standard cylindrically symmetric model, (ii) $S^1 \times S^1$ the flat torus T^2 model , and (iii) R^2. We will focus upon (i) and (ii). In the cylindrical model (i), we work with the cylindrical coordinate system (t, r, φ, z) with $-\infty < t < +\infty$, $0 \le r < +\infty$, $-\infty < z < +\infty$, $0 \le \varphi < 2\pi$. In the toroidal model (ii), the range of the coordinate z is $0 \le \alpha z < 2\pi$, with $\alpha^2 \equiv -\frac{1}{3}\Lambda$.

5.1.2.a Neutral and electric charged black holes

The gravitational field of the rotating electrically charged black hole solution can be written as [6, 7]

$$ds^2 = -\left(\alpha^2 r^2 - \frac{4M(1-\frac{a^2\alpha^2}{2})}{\alpha r} + \frac{4Q^2}{\alpha^2 r^2}\right)dt^2 - \frac{4aM\sqrt{1-\frac{a^2\alpha^2}{2}}}{\alpha r}\left(1 - \frac{Q^2}{M(1-\frac{a^2\alpha^2}{2})\alpha r}\right)2dtd\varphi+$$

$$+\left(\alpha^2 r^2 - \frac{4M(1-\frac{3}{2}a^2\alpha^2)}{\alpha r} + \frac{4Q^2}{\alpha^2 r^2}\frac{(1-\frac{3}{2}a^2\alpha^2)}{(1-\frac{a^2\alpha^2}{2})}\right)^{-1}dr^2 + \left[r^2 + \frac{4Ma^2}{\alpha r}\left(1 - \frac{Q^2}{(1-\frac{a^2\alpha^2}{2})M\alpha r}\right)\right]d\varphi^2 + \alpha^2 r^2 dz^2,$$

$$(5.7)$$

where $\alpha^2 \equiv -\frac{1}{3}\Lambda$, M is the mass per unit length, Q is the electric charge per unit length, and parameter a (with units of angular momentum per unit mass, and with range $0 \le a\alpha \le 1$) is related to the angular momentum per unit length of the black hole by

$$a = \frac{2}{3}\frac{J}{M}\left(1 - \frac{a^2\alpha^2}{2}\right)^{-1/2}. \qquad (5.8)$$

The electromagnetic vector potential of the solution is given by

$$A = \frac{2Q}{\alpha r}\left(-dt + \frac{a}{\sqrt{1 - \frac{1}{2}\alpha^2 a^2}}d\varphi\right), \tag{5.9}$$

At $r = 0$ is located a curvature singularity. Depending on the value of Q and of J, there are five distinct cases to consider, namely: (i) $0 \le a^2\alpha^2 \le \frac{2}{3} - \frac{128}{81}\frac{Q^6}{M^4(1-\frac{1}{2}a^2\alpha^2)^3}$, which yields a black hole solution with event and Cauchy horizons; (ii) $a^2\alpha^2 = \frac{2}{3} - \frac{128}{81}\frac{Q^6}{M^4(1-\frac{1}{2}a^2\alpha^2)^3}$, which corresponds to the extreme case of the above black hole, where the two horizons merge; (iii) $\frac{2}{3} - \frac{128}{81}\frac{Q^6}{M^4(1-\frac{1}{2}a^2\alpha^2)^3} < a^2\alpha^2 < \frac{2}{3}$, which yields a naked singularity solution; (iv) $a^2\alpha^2 = \frac{2}{3}$, which gives a null topological singularity; and (v) $\frac{2}{3} < a^2\alpha^2 < 1$, which gives a pathological black hole solution with a single horizon. The most interesting solutions are given by cases (i) and (ii), which present features similar to the $\Lambda = 0$ Kerr-Newman solution. For example, the curvature singularity at $r = 0$ has a ring structure, and closed timelike curves are present but inside the inner horizon of the solution. Solutions (iv) and (v) do not have partners in the Kerr-Newman family. The black hole (v) is pathological since there are closed timelike curves outside the horizon. The Carter-Penrose diagrams of these solutions (i)-(v) are respectively sketched in items (a)-(e) of Fig. 5.8.

When we turn off the rotation, $J = 0$ or $a = 0$, only the counterparts of the solutions (i)-(iii) survive. We then have (i) a black hole solution with event and Cauchy horizons if $Q^6 < 3^3 M^4/4^3$, (ii) an extreme black hole if $Q^6 = 3^3 M^4/4^3$, and (iii) a naked singularity if $Q^6 > 3^3 M^4/4^3$. All these three solutions are free of closed timelike curves and the curvature singularity at $r = 0$ looses the ring structure. The Carter-Penrose diagrams of these solutions are identical to the ones sketched in items (a)-(c) of Fig. 5.8.

When we set $Q = 0$ we have to consider three cases. If $0 \le a^2\alpha^2 < \frac{2}{3}$, we have a black hole solution with a single horizon and without closed timelike curves. The Carter-Penrose diagrams of this solution is sketched in Fig. 5.8.(e), and it also describes the solution with $J = 0$. If $a^2\alpha^2 = \frac{2}{3}$ we have a null topological singularity without an horizon [see Fig. 5.8.(d)]. This solution can be considered the extreme uncharged black hole of the later black hole. Finally, when $a^2\alpha^2 > \frac{2}{3}$ we have a naked timelike singularity [see Fig. 5.8.(c)].

(a) (b) (c) (d) (e)
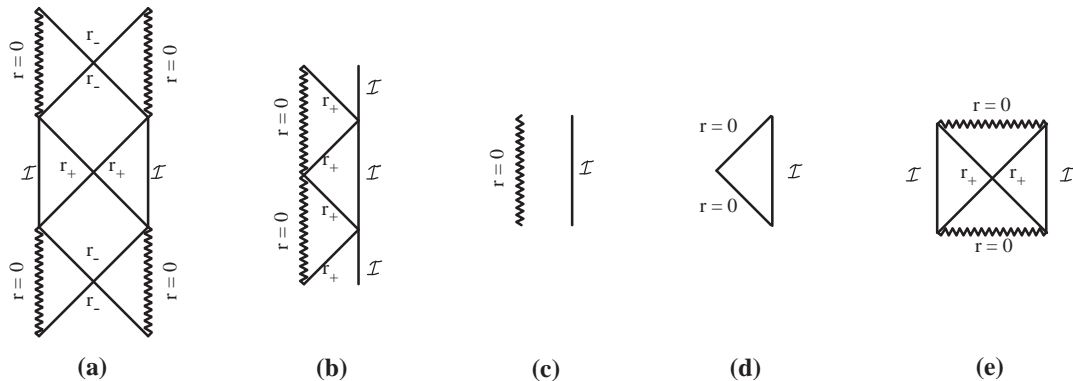
Figure 5.8: Carter-Penrose diagrams of the AdS black holes toroidal or cylindrical topology discussed in the text of section 5.1.2.a. The zigzag line represents a curvature singularity, $\mathcal{I}$ represents the infinity ($r = \infty$), r_+ represents a black hole event horizon, and r_- represents a Cauchy horizon.

5.1.2.b   Magnetic solutions

The gravitational field of the rotating magnetic solution is given by [8]

$$ds^2 = -\left[\alpha^2(r^2+\rho_0^2) - \tfrac{2M\Omega}{1-4\mu}[\alpha^2(r^2+\rho_0^2)]^{-1/2} + \tfrac{4Q_e^2}{(1-4\mu)^2}[\alpha^2(r^2+\rho_0^2)]^{-1}\right]dt^2$$

$$-\tfrac{8}{3}\tfrac{J}{1-4\mu}\left[[\alpha^2(r^2+\rho_0^2)]^{-1/2} - \tfrac{2Q_e^2}{M\Omega(1-4\mu)}[\alpha^2(r^2+\rho_0^2)]^{-1}\right]2dtd\varphi$$

$$+\cfrac{r^2/(r^2+\rho_0^2)}{\left[\alpha^2(r^2+\rho_0^2)+\tfrac{2M(4-3\Omega)}{1-4\mu}[\alpha^2(r^2+\rho_0^2)]^{-1/2}-4\chi_m^2[\alpha^4(r^2+\rho_0^2)]^{-1}\right]}dr^2$$

$$+\tfrac{1}{\alpha^2}\left[\alpha^2(r^2+\rho_0^2) + \tfrac{4M(2-\Omega)/(1-4\mu)}{[\alpha^2(r^2+\rho_0^2)]^{1/2}} - \tfrac{8(2-\Omega)}{4-3\Omega}\tfrac{\chi_m^2}{[\alpha^4(r^2+\rho_0^2)]}\right]d\varphi^2 + \alpha^2(r^2+\rho_0^2)dz^2 , \quad (5.10)$$

and the vector potential is given by

$$A = -\frac{2\chi_m}{\alpha^3\sqrt{r^2+\rho_0^2}}\frac{1}{\sqrt{8-6\Omega}}\left[-\sqrt{2\Omega}dt + 2\sqrt{2-\Omega}d\varphi\right] . \qquad (5.11)$$

In these equations we have $\alpha^2 \equiv -\tfrac{1}{3}\Lambda$, ρ_0 is the highest root of the equation $\alpha^2\rho_0^2+\tfrac{8M/(1-4\mu)}{\alpha\rho_0}-\tfrac{4\chi_m^2}{\alpha^4\rho_0^2} = 0$, M is the mass per unit length, Q_e is the electric charge per unit length, , χ_m is a constant that measures the intensity of the magnetic field source, and we have defined a rotating parameter Ω, which ranges between $0 \le \Omega < 1$, as

$$\Omega \equiv 1 - \sqrt{1 - \frac{8}{9}\frac{J^2\alpha^2}{M^2}} . \qquad (5.12)$$

The condition that Ω remains real imposes a restriction on the allowed values of the angular momentum: $\alpha^2J^2 \le \tfrac{8}{9}M^2$. Note also that (5.11) indicates that the static solution ($\Omega = 0$) produces only a longitudinal magnetic field, while the rotating solution ($\Omega \ne 0$) generates in addition a radial electric field.

The static solution can be obtained by setting $\Omega = 0$ (and thus $J = 0$; this also implies that $Q_e = 0$, as we shall see just below) on (5.10) and (5.11). This static solution has no horizons and no curvature singularity. However, it has a conical singularity at $r = 0$ with a deficit angle given by

$$\delta = 2\pi\left(1 - \lim_{r\to 0}\frac{1}{r}\sqrt{\frac{g_{\varphi\varphi}}{g_{rr}}}\right) . \qquad (5.13)$$

This conical deficit implies that the period of φ is $\Delta\varphi = 2\pi - \delta$, and its presence is associated with a string with mass density $\mu = \delta/(8\pi)$. The range of the other coordinates is $-\infty < t < +\infty$, $0 \le r < +\infty$, and $-\infty < z < +\infty$ (cylindrical model). In the toroidal model, the range of the coordinate z is $0 \le \alpha z < 2\pi$.

Now, the electric charge of the solution described by (5.10) and (5.11) can be written as a function of the other parameters of the solution as

$$Q_e = \frac{1-4\mu}{\alpha}\sqrt{\frac{\Omega}{4-3\Omega}}\chi_m . \qquad (5.14)$$

Thus we see that $\Omega = 0$ implies $Q_e = 0$. This feature agrees with the conclusions withdrawn from (5.11): the static solution produces no electric field because its electric charge is zero.

In [8], and following [251], we have interpreted the magnetic field source as being composed by a system of two symmetric and superposed electrically charged lines along the z direction. One of the electrically charged lines is at rest with positive charge (say), and the other is spinning around the z direction with a negative electric charge. Clearly, this system produces no electric field since the total electric charge is zero and the magnetic field is produced by the angular electric current.

The value of the electric charge per unit length (5.14), says that after applying a rotation boost in the t-φ plane to endow our initial static spacetime with angular momentum, there appears a net electric charge. This result was once again expected since now, besides the magnetic field along the z direction ($F_{r\varphi} \neq 0$), there is also a radial electric field ($F_{tr} \neq 0$). In the same spirit of the explanation presented in subsection 2.4.3, we can show that the rotational boost induces an asymmetry in the charge densities of the two above strings that is responsible for the appearance of the radial electric field. This physical situation is similar to the one that occurs when one has a copper wire with an electric current and we apply a translation Lorentz boost to the wire: first, there is only a magnetic field but, after the Lorentz boost, one also has an electric field. The difference is that in the present situation the Lorentz boost is a rotational one and not a translational one.

5.1.3 Black holes with hyperbolic topology

In this subsection we will briefly present the black hole solutions of the $\Lambda < 0$ Einstein-Maxwell equations with hyperbolic topology or, upon compactification, with toroidal topology with genus $g \geq 2$. The gravitational field of the electrically charged black hole solution is given by [11]

$$ds^2 = -\left(-1 - \frac{\Lambda}{3}r^2 - \frac{2M}{r} + \frac{Q^2}{r^2}\right) dt^2 + \frac{dr^2}{-1 - \frac{\Lambda}{3}r^2 - \frac{2M}{r} + \frac{Q^2}{r^2}} + r^2(d\theta^2 + \sinh^2\theta\, d\phi^2), \quad (5.15)$$

while the electromagnetic field is still given by (5.6). M and Q are respectively the ADM mass and charge of the solution.

In order to describe the basic properties of these solutions let us first define the quantity

$$M_{\text{ext}} = \frac{1}{3\sqrt{2}|\Lambda|} \left(\sqrt{1 + \frac{4}{3}|\Lambda|Q^2} - 2\right) \left(\sqrt{1 + \frac{4}{3}|\Lambda|Q^2} + 1\right)^{1/2}, \quad (5.16)$$

which is negative when $Q = 0$. When $M = 0$ and $Q = 0$, the solution has an horizon that we identify as a cosmological horizon (r_{c}) since it is present when the mass and charge vanish. In this case $r = 0$ is not a curvature singularity, but can be regarded as a topological singularity (see Brill, Louko, and Peldan in [11] for a detailed discussion). The Carter-Penrose diagram of this solution is drawn in Fig. 5.9.(a). When $Q = 0$ and $M > 0$, the solution still has a single horizon, the same cosmological horizon that is present in the latter case. However, now a curvature singularity is present at $r = 0$. The corresponding Carter-Penrose diagram of this solution is represented in Fig. 5.9.(b). The most interesting $Q = 0$ solutions are present when the mass of the solution is negative. We have three distinct cases, namely: (i) $M_{\text{ext}} < M < 0$, which yields a black hole solution with an event horizon and a cosmological horizon; (ii) $M = M_{\text{ext}}$, which corresponds to the extreme case of the above black hole, where the two horizons merge; (iii) $M < M_{\text{ext}}$, which yields a naked timelike singularity solution. The Carter-Penrose diagrams of these solutions (i)-(iii) are sketched in items (c)-(e) of Fig. 5.9. When $Q \neq 0$, one has three cases, namely: (i) $M > M_{\text{ext}}$, which yields a black hole solution with an event horizon and a cosmological horizon; (ii) $M = M_{\text{ext}}$, which corresponds to the extreme case of the above black hole; (iii) $M < M_{\text{ext}}$, which yields a naked timelike singularity solution. Note that the presence of the charge does not introduce an extra horizon, contrary to what usually occurs in other black hole solutions. The Carter-Penrose diagrams of these charged solutions (i)-(iii) are also identical to the ones sketched in items (c)-(e) of Fig. 5.9.
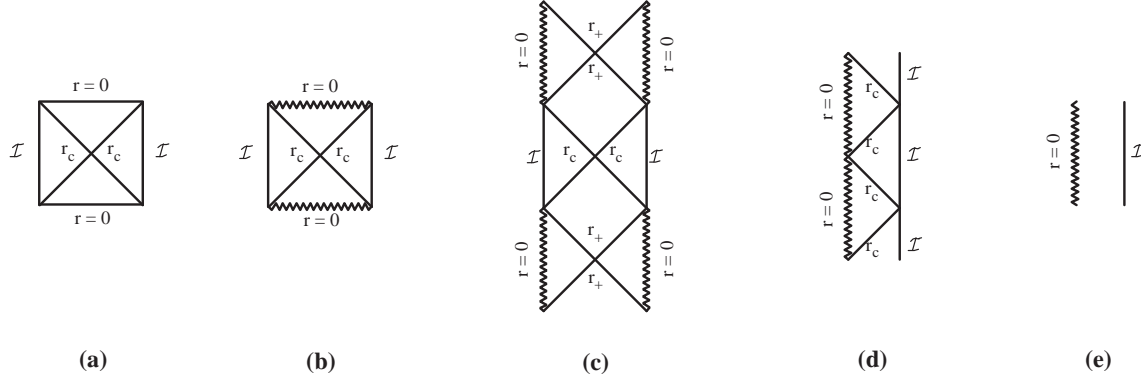
Figure 5.9: Carter-Penrose diagrams of the AdS black holes with hyperbolic topology discussed in the text of section 5.1.3. The zigzag line represents a curvature singularity, $\mathcal{I}$ represents the infinity $(r = \infty)$, r_+ represents a black hole event horizon, and r_c represents a cosmological horizon.

5.2 Black holes in a flat background

In this section we will briefly present the black hole solutions of the Einstein-Maxwell equations in a flat background ($\Lambda = 0$). These black holes have a spherical topology and the gravitational field of the electrically charged black hole solution is given by (5.5), as long as we set $\Lambda = 0$. The electromagnetic field is given by (5.6). In these equations M and Q are still the ADM mass and charge of the solution. The Reissner-Nordström solution ($Q \neq 0$) has three distinct cases, namely: (i) $Q < M$, which yields a nonextreme black hole solution with event and Cauchy horizons; (ii) $Q = M$, which corresponds to the extreme case of the above black hole, where the two horizons merge; and (iii) $Q > M$, which yields a naked singularity solution. The Carter-Penrose diagrams of these solutions (i)-(iii) are respectively sketched in items (a)-(c) of Fig. 5.10. The Schwarzschild solution ($Q = 0$) has a Carter-Penrose diagram sketched in Fig. 5.11.
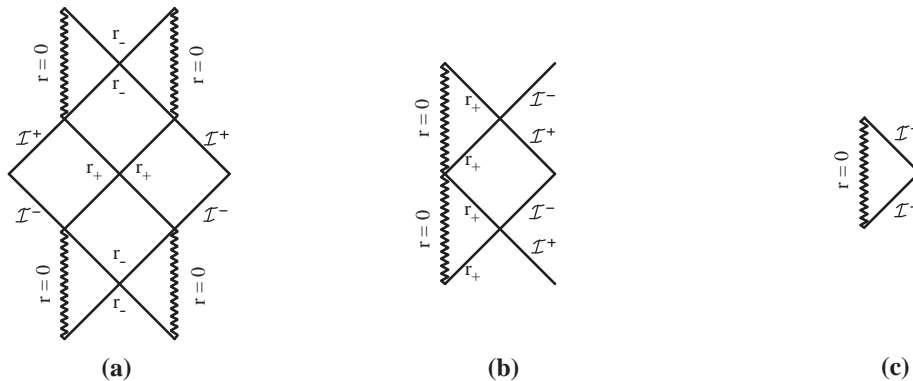
Figure 5.10: Carter-Penrose diagrams of the Reissner-Nordström ($Q \neq 0$) black holes discussed in the text of section 5.2. The zigzag line represents a curvature singularity, $\mathcal{I}$ represents the infinity $(r = \infty)$, r_+ represents a black hole event horizon, and r_- represents a Cauchy horizon.
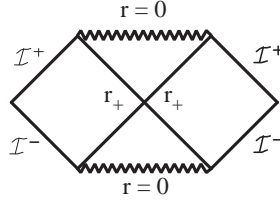
Figure 5.11: Carter-Penrose diagram of the Schwarzschild ($Q = 0$) black hole discussed in the text of section 5.2. The zigzag line represents a curvature singularity, $\mathcal{I}$ represents the infinity ($r = \infty$), and r_+ represents a black hole event horizon.

5.3   Black holes in a de Sitter background

In this section we will briefly present the black hole solutions of the Einstein-Maxwell equations in a de Sitter background ($\Lambda > 0$). These black holes have a spherical topology and the gravitational field of the charged black hole solution is given by (5.5), as long as we set $\Lambda > 0$. The electromagnetic field is given by (5.6). In these equations M and Q are still the ADM mass and charge of the solution. The dS−Reissner-Nordström solution ($Q \neq 0$) has four distinct cases, namely: (a) a nonextreme black hole solution with a cosmological horizon (r_c), and with an event (r_+) and Cauchy horizons (r_-), where $r_- < r_+ < r_c$; (b) an extreme case in which the cosmological horizon merges with the black hole event horizon ($r_+ = r_c$); (c) an extreme case in which the Cauchy horizon merges with the black hole event horizon ($r_- = r_+$); and (d) a naked singularity solution. The ranges of M and Q that represent which one of the above black holes is sketched in Fig. 5.12. The Carter-Penrose diagrams of these solutions (a)-(d) are respectively sketched in items (a)-(d) of Fig. 5.13. The dS-Schwarzschild solution ($Q = 0$) has three distinct cases, namely: (a) a nonextreme black hole solution with a cosmological horizon (r_c), and with an event horizon (r_+); (b) an extreme case in which the cosmological horizon merges with the black hole event horizon ($r_+ = r_c$); and (c) a naked singularity solution. The Carter-Penrose diagrams of these solutions (a)-(c) are respectively sketched in items (a)-(c) of Fig. 5.14. Case (b) of Figs. 5.13 and 5.14 is sometimes called as Nariai black hole, although the this nomenclature is not the most appropriate (see chapter 7).
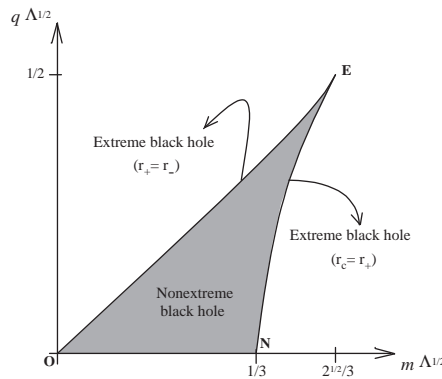
Figure 5.12: Range of M and Q for which one has a nonextreme black hole, an extreme black hole with $r_+ = r_c$, and an extreme black hole with $r_- = r_+$. The black holes represented by line NE are sometimes called as Nariai Reissner-Nordström black holes. The line ON represents the nonextreme dS-Schwarzschild, and point N represents the extreme Nariai Schwarzschild black hole. Point E represents an extreme black hole with $r_- = r_+ = r_c$.
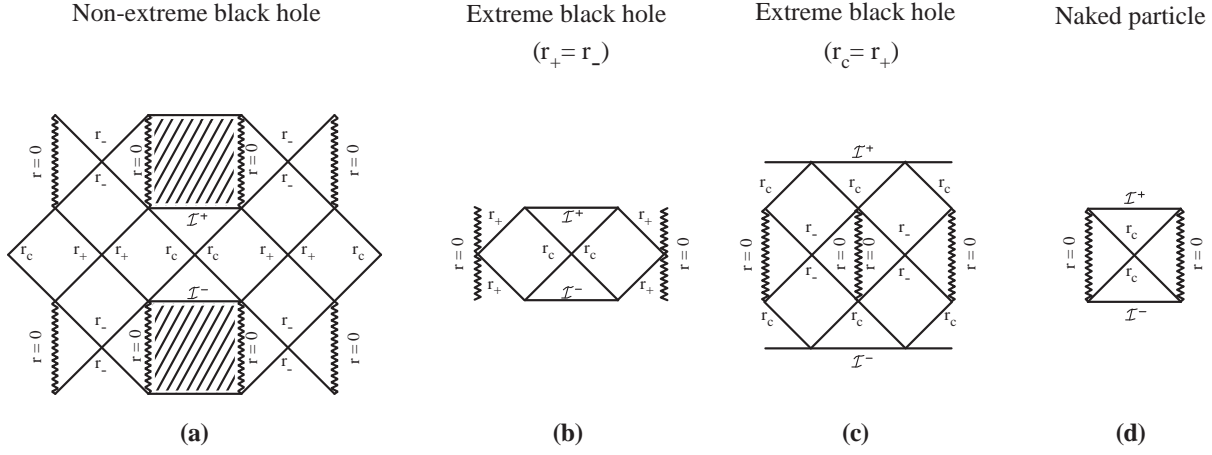
Figure 5.13: Carter-Penrose diagrams of the dS−Reissner-Nordström ($Q \neq 0$) black holes discussed in the text of section 5.3. The zigzag line represents a curvature singularity, $\mathcal{I}$ represents the infinity ($r = \infty$), r_c represents a cosmological horizon, r_+ represents a black hole event horizon, and r_- represents a Cauchy horizon.
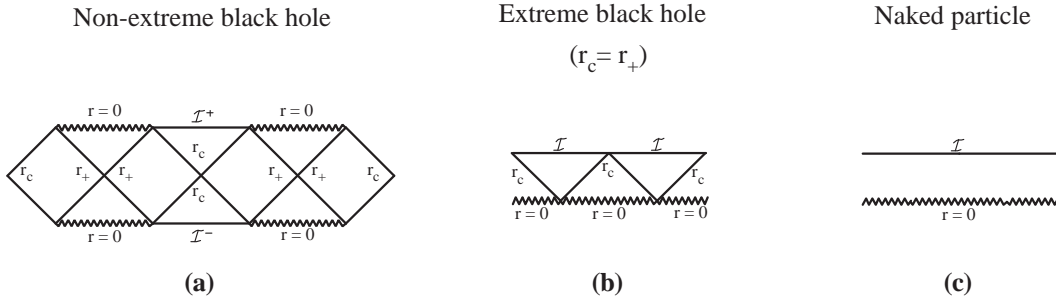
Figure 5.14: Carter-Penrose diagram of the dS−Schwarzschild ($Q = 0$) black hole discussed in the text of section 5.3. The zigzag line represents a curvature singularity, $\mathcal{I}$ represents the infinity ($r = \infty$), and r_+ represents a black hole event horizon.

Chapter 6

Pair of accelerated black holes:
the C-metric in a generalized Λ background

Contents

Kinnersley and Walker [84], in 1970, have interpreted the C-metric, found by Levi-Civita [82] and by Weyl [83] in 1918-1919, has describing a pair of accelerated black holes, with the energy being provided by the tension of the strings or strut that are present in the solution. We will review their interpretation in section 6.2. From the charged C-metric, Ernst [85] has generated a knew exact solution in which the black hole pair is accelerated by an external electromagnetic field. This solution will also be reviewed in section 6.2. These are one of the few exact solutions that contain already a radiative term. I.e., being accelerated, the black holes necessarily release radiation and the information concerning the radiative properties are already included in the metric. The cosmological C-metric has been found by Plebański and Demiański in 1976 [86]. In section 6.1 we will study in detail the properties and physical interpretation of the C-metric in an anti-de Sitter (AdS) background. We follow our work [87] which complements earlier work done by Emparan, Horowitz and Myers [121] and by Podolský [122]. Then, in section 6.3 we will discuss in detail the C-metric in a de Sitter (dS) background, following our work [88] (which has complemented previous work of Podolský and Griffiths [120]). The analysis of this chapter will be supported by a thorough analysis of the causal structure of the solution, together with the description of the solution in the AdS and dS 4-hyperboloid, and the study of the strings and strut's physics. We follow the approach of Kinnersley and Walker [84] and Ashtekar and Dray [104]. Although the alternative approach of Bonnor simplifies in a way the interpretation, we cannot use the case of the AdS C-metric and dS C-metric, since the cosmological constant prevents the coordinate transformation of Bonnor into the Weyl form. In section 6.4 we will summarize the results, and in particular we will compare the C-metric in the three cosmological backgrounds, AdS, flat and dS.

For a more complete historical overview on the C-metric we ask the reader to go back to subsection 1.3.3. In chapter 9 we will use the solutions analyzed in this chapter to construct the instantons that describe the quantum process of black hole pair creation in an external field.

6.1 Pair of accelerated black holes in an anti-de Sitter background: the AdS C-metric

The plan of this section is as follows. In subsection 6.1.1 we present the AdS C-metric and analyze its curvature and conical singularities. In subsection 6.1.2 we study the causal diagrams of the solution.

6.1 Pair of accelerated black holes in an anti-de Sitter background: the AdS C-metric

In subsection 6.1.3 we give and justify a physical interpretation to the solution. The description of the solution in the AdS 4-hyperboloid and the physics of the strut are analyzed. These two subsections, 6.1.2 and 6.1.3, are highly related and so, in order to fully understand each of them, the reading of the other is required.

6.1.1 General properties of the AdS C-metric

6.1.1.a The AdS C-metric

The AdS C-metric, i.e., the C-metric with negative cosmological constant Λ, has been obtained by Plebański and Demiański [86]. For zero rotation and zero NUT parameter it is given, according to [86] (see also [178]), by

$$ds^2 = 1/(\tilde{x} + \tilde{y})^2 (-\mathcal{F}d\tilde{t}^2 + \mathcal{F}^{-1}d\tilde{y}^2 + \mathcal{G}^{-1}d\tilde{x}^2 + \mathcal{G}d\tilde{z}^2) , \tag{6.1}$$

where

$$\begin{aligned} \mathcal{F}(\tilde{y}) &= -\Lambda/6 - \tilde{A}^2 + \tilde{y}^2 - 2m\tilde{y}^3 + q^2\tilde{y}^4, \\ \mathcal{G}(\tilde{x}) &= -\Lambda/6 + \tilde{A}^2 - \tilde{x}^2 - 2m\tilde{x}^3 - q^2\tilde{x}^4. \end{aligned} \tag{6.2}$$

The meaning of parameters $\tilde{A}$, m, and q will be clarified soon. For the benefit of comparison with the flat C-metric, we note that when Λ vanishes we have $\mathcal{F}(\tilde{y}) = -\mathcal{G}(-\tilde{y})$. It is now convenient to redefine the parameter $\tilde{A}$ as $-\Lambda/6 + \tilde{A}^2 \equiv A^2$, together with the coordinate transformations: $\tilde{t} = t/A, \tilde{y} = Ay, \tilde{x} = Ax$ and $\tilde{z} = \phi/A$. With these redefinitions, the gravitational field of the AdS C-metric is written as

$$ds^2 = [A(x + y)]^{-2} (-\mathcal{F}dt^2 + \mathcal{F}^{-1}dy^2 + \mathcal{G}^{-1}dx^2 + \mathcal{G}d\phi^2) , \tag{6.3}$$

where

$$\begin{aligned} \mathcal{F}(y) &= \left(\frac{1}{\ell^2 A^2} - 1 \right) + y^2 - 2mAy^3 + q^2A^2y^4, \\ \mathcal{G}(x) &= 1 - x^2 - 2mAx^3 - q^2A^2x^4 , \end{aligned} \tag{6.4}$$

and the Maxwell field in the magnetic case is given by

$$F_{\mathrm{mag}} = -q \, dx \wedge d\phi , \tag{6.5}$$

while in the electric case it is given by

$$F_{\mathrm{el}} = -q \, dt \wedge dy . \tag{6.6}$$

This solution depends on four parameters namely, A which is the acceleration of the black hole, m which is interpreted as the ADM mass of the non-accelerated black hole, q which is interpreted as the ADM electromagnetic charge of the non-accelerated black hole and, in general, $q^2 = e^2 + g^2$ with e and g being the electric and magnetic charges, respectively, and finally the cosmological length $\ell^2 \equiv 3/|\Lambda|$. The meaning attributed to the parameter A will be understood in section 6.1.3, while the physical interpretation given to the parameters m and q is justified in the Appendix. We will consider the case $A > 0$.

The coordinates used in (6.3)-(6.6) to describe the AdS C-metric are useful to understand the geometrical properties of the spacetime, but they hide the physical interpretation of the solution. In order to understand the physical properties of the source and gravitational field we will introduce progressively new coordinates more suitable to this propose, following the approach of Kinnersley and Walker [84] and Ashtekar and Dray [104]. Although the alternative approach of Bonnor simplifies in a way the interpretation, we cannot use it were since the cosmological constant prevents such a coordinate transformation into the Weyl form.

6.1.1.b   Radial Coordinate. Curvature Singularities

We start by defining a coordinate r as

$$r = [A(x+y)]^{-1} \,. \tag{6.7}$$

In order to interpret this coordinate as being a radial coordinate, we calculate a curvature invariant of the metric, namely the Kretschmann scalar,

$$
\begin{aligned}
R_{\mu\nu\alpha\beta}R^{\mu\nu\alpha\beta} &= \frac{24}{\ell^2} + \frac{8}{r^8}\Big[6m^2r^2 + 12mq^2(2Axr - 1)r \\
&\quad + q^4(7 - 24Axr + 24A^2x^2r^2)\Big] \,.
\end{aligned} \tag{6.8}
$$

Clearly, this curvature invariant is equal to $24/\ell^2$ when the mass m and charge q are both zero. When at least one of these parameters is not zero, the curvature invariant diverges at $r = 0$, revealing the presence of a curvature singularity. Moreover, when we take the limit $r \to \infty$, the curvature singularity approaches the expected value for a spacetime which is asymptotically AdS. Therefore it is justified that r is interpreted as a radial coordinate.

6.1.1.c   Angular Surfaces. Conical Singularities

To gain more insight into the physical nature of the AdS C-metric we now turn our attention into the angular surfaces $t =$constant and $r =$constant, onwards labelled by Σ. In this section we follow [84]. In order to have the AdS C-metric with correct signature, $(- + ++)$, one must restrict the coordinate x to a domain on which the function $\mathcal{G}(x)$ is non-negative [see (6.3)]. The shape of this function depends crucially on the three parameters A, m, and q. In this work we will select only the ranges of these three parameters for which $\mathcal{G}(x)$ has at least two real roots, x_s and x_n (say), and demand x to belong to the range $[x_s, x_n]$ where $\mathcal{G}(x) \geq 0$. This restriction has the important advantage of allowing us to endow the angular surfaces Σ with the topology of a compact surface. In these surfaces we now define two new coordinates,

$$
\begin{aligned}
\theta &= \int_x^{x_n} \mathcal{G}^{-1/2}dx \,, \\
\tilde{\phi} &= \phi/\kappa \,,
\end{aligned} \tag{6.9}
$$

where $\tilde{\phi}$ ranges between $[0, 2\pi]$ and κ is an arbitrary positive constant which will be needed later when regularity conditions at the poles are discussed. The coordinate θ ranges between the north pole, $\theta = \theta_n = 0$, and the south pole, $\theta = \theta_s$ (not necessarily at π). With these transformations the metric restricted to the surfaces Σ, $d\sigma^2 = r^2(\mathcal{G}^{-1}dx^2 + \mathcal{G}d\phi^2)$, takes the form

$$d\sigma^2 = r^2\big(d\theta^2 + \kappa^2\mathcal{G}d\tilde{\phi}^2\big) \,. \tag{6.10}$$

When $A = 0$ or when both $m = 0$ and $q = 0$, (6.9) gives $x = \cos\theta$, $\mathcal{G} = 1 - x^2 = \sin^2\theta$ and if we use the freedom to put $\kappa \equiv 1$, the metric restricted to Σ is given by $d\sigma^2 = r^2(d\theta^2 + \sin^2\theta\,d\tilde{\phi}^2)$. This implies that in this case the angular surface is a sphere and justifies the label given to the new angular coordinates defined in (6.9). In this case the north pole is at $\theta_n = 0$ or $x_n = +1$ and the south pole is at $\theta_s = \pi$ or $x_s = -1$. In the other cases x and $\sqrt{\mathcal{G}}$ can always be expressed as elliptic functions of θ. The explicit form of these functions is of no need in this work. All we need to know is that these functions have a period given by $2\theta_s$.

As we shall see, the regularity analysis of the metric in the region $[0, \theta_s]$ will play an essential role in the physical interpretation of the AdS C-metric. The function $\mathcal{G}$ is positive and bounded in $]0, \theta_s[$ and thus, the metric is regular in this region between the poles. We must be more careful with the regularity analysis at the poles, i.e., at the roots of $\mathcal{G}$. Indeed, if we draw a small circle around the north pole, in general, as the radius goes to zero, the limit circumference/radius is not

2π. Therefore, in order to avoid a conical singularity at the north pole one must require that $\delta_{\mathrm{n}} = 0$, where

$$\delta_{\mathrm{n}} \equiv 2\pi \left(1 - \lim_{\theta \to 0} \frac{1}{\theta} \sqrt{\frac{g_{\phi\phi}}{g_{\theta\theta}}} \right) = 2\pi \left(1 - \frac{\kappa}{2} \left| \frac{d\mathcal{G}}{dx} \right|_{x_{\mathrm{n}}} \right). \tag{6.11}$$

Repeating the procedure, this time for the south pole, x_{s}, we conclude that the conical singularity at this pole can also be avoid if

$$\delta_{\mathrm{s}} \equiv 2\pi \left(1 - \frac{\kappa}{2} \left| \frac{d\mathcal{G}}{dx} \right|_{x_{\mathrm{s}}} \right) = 0. \tag{6.12}$$

The so far arbitrary parameter κ introduced in (6.9) plays its important role here. Indeed, if we choose

$$\kappa^{-1} = \frac{1}{2} \left| \frac{d\mathcal{G}}{dx} \right|_{x=x_{\mathrm{s}}}, \tag{6.13}$$

Eq. (6.12) is satisfied. However, since we only have a single constant κ at our disposal and this has been fixed to remove the conical singularity at the south pole, we conclude that the conical singularity will be present at the north pole. There is another alternative. We can choose instead $2\kappa^{-1} = |d_x\mathcal{G}|_{x=x_{\mathrm{n}}}$ (where d_x means derivative in order to x) and by doing so we avoid the deficit angle at the north pole and leave a conical singularity at the south pole. In section 6.1.3 we will see that in the extended Kruskal solution the north pole points towards the other black hole, while the south pole points towards infinity. The first choice of κ corresponds to a strut between the black holes while the alternative choice corresponds to two strings from infinity into each black hole. When we choose κ such that $\delta_s = 0$, the period of ϕ is given by

$$\Delta\phi = \frac{4\pi}{|\mathcal{G}'(x_{\mathrm{s}})|}, \tag{6.14}$$

while the choice $\delta_n = 0$ implies that the period of ϕ is given by

$$\Delta\phi = \frac{4\pi}{|\mathcal{G}'(x_{\mathrm{n}})|}. \tag{6.15}$$

We leave a further discussion on the physical nature of the conical singularities and on the two possible choices for the value of κ to section 6.1.3.a. There is a small number of very special cases for which the very particular condition, $|d_x\mathcal{G}|_{x_{\mathrm{n}}} = |d_x\mathcal{G}|_{x_{\mathrm{s}}}$ is verified. In these special cases, the solution is free of conical singularities. They will be mentioned bellow.

Since we have managed to put $\mathcal{G}(x)$ in a form equal to [84], we can now, following [84] closely, describe the behavior of $\mathcal{G}(x)$ for different values of the parameters A, m, and q. We can divide this discussion in three cases.

1. *Massless uncharged solution* ($m = 0$, $q = 0$): in this case, we have $x = \cos\theta$, $\mathcal{G} = 1 - x^2 = \sin^2\theta$, and $\kappa = 1$. The angular surface Σ is a sphere and this is a particular case for which both the north and south poles are free of conical singularities.

2. *Massive uncharged solution* ($m > 0$, $q = 0$): the massive uncharged case must be divided into $mA < 3^{-3/2}$, and $mA \geq 3^{-3/2}$. When $mA < 3^{-3/2}$, $\mathcal{G}(x)$ has three roots and, as justified above, we require x to lie between the two roots for which $\mathcal{G}(x) \geq 0$. In doing so we maintain the metric with the correct signature and have an angular surface Σ which is compact. Setting the value of κ given in (6.13) one avoids the conical singularity at the south pole but leave one at the north pole. When $mA \geq 3^{-3/2}$, Σ is an open angular surface. For this reason, onwards we will analyze only the case $mA < 3^{-3/2}$.

3. *Massive charged solution* ($m > 0$, $q \neq 0$): for a general massive charged solution, depending on the values of the parameters A, m and q, $\mathcal{G}(x)$ can be positive in a single compact interval, $]x_{\mathrm{s}}, x_{\mathrm{n}}[$, or in two distinct compact intervals, $]x'_{\mathrm{s}}, x'_{\mathrm{n}}[$ and $]x_{\mathrm{s}}, x_{\mathrm{n}}[$, say. In this latter case we will work only with the interval $[x_{\mathrm{s}}, x_{\mathrm{n}}]$ (say) for which the charged solutions reduce to the uncharged solutions when $q = 0$. These solutions have a conical singularity at one of the poles. The only

massive charged solutions that are totally free of conical singularities are those which satisfy the particular conditions $m = |q|$ and $mA > 1/4$. This indicates that in this case the AdS C-metric is an AdS black hole written in an accelerated coordinate frame. In the massless charged solution ($m = 0$ and $q \neq 0$), $\mathcal{G}(x)$ is an even function, has two symmetric roots and is positive between them. The angular surface Σ is therefore compact and there are no conical singularities at both poles. Once again, this suggests that the solution is written in an accelerated coordinate frame.

6.1.1.d   Coordinate ranges

In this section we analyze the important issue of the coordinate ranges. Rewritten in terms of the new coordinates introduced in (6.7) and (6.9), the AdS C-metric is given by

$$ds^2 = r^2[-\mathcal{F}(y)dt^2 + \mathcal{F}^{-1}(y)dy^2 + d\theta^2 + \kappa^2\mathcal{G}(x_{(\theta)})d\tilde\phi^2]\,, \tag{6.16}$$

where $\mathcal{F}(y)$ and $\mathcal{G}(x_{(\theta)})$ are given by (6.4). The time coordinate t can take any value from the interval $]-\infty, +\infty[$ and $\tilde\phi$ ranges between $[0, 2\pi]$. As we saw in section 6.1.1.b, when m or q are not zero there is a curvature singularity at $r = 0$. Therefore, we restrict the radial coordinate to the range $[0, +\infty[$. On the other hand, in section 6.1.1.c we have decided to consider only the values of A, m, and q for which $\mathcal{G}(x)$ has at least two real roots, $x_{\rm s}$ and $x_{\rm n}$ (say) and have demanded x to belong to the range $[x_{\rm s}, x_{\rm n}]$ where $\mathcal{G}(x) \geq 0$. By doing this we guarantee that the metric has the correct signature $(-+++)$ and that the angular surfaces Σ ($t =$constant and $r =$constant) are compact. From $Ar = (x + y)^{-1}$ we then conclude that y must belong to the range $-x \leq y < +\infty$. Indeed, $y = -x$ corresponds to $r = +\infty$, and $y = +\infty$ to $r = 0$. Note however, that when both m and q vanish there are no restrictions on the ranges of r and y (i.e., $-\infty < r < +\infty$ and $-\infty < y < +\infty$) since in this case there is no curvature singularity at the origin of r to justify the constraint on the coordinates.

6.1.1.e   Mass and charge parameters

In this subsection, one gives the physical interpretation of parameters m and q that appear in the AdS C-metric. Applying the coordinate transformations to (6.3) (see [122]),

$$T = \sqrt{1 - \ell^2 A^2} A^{-1} t\,, \quad R = \sqrt{1 - \ell^2 A^2}(Ay)^{-1}\,,$$
$$\theta = \int_x^{x_{\rm n}} \mathcal{G}^{-1/2} dx\,, \quad \tilde\phi = \phi/\kappa\,, \tag{6.17}$$

and setting $A = 0$ (and $\kappa = 1$) one obtains

$$ds^2 = -F(R)\,dT^2 + F^{-1}(R)\,dR^2 + R^2(d\theta^2 + \sin^2\theta\,d\tilde\phi^2)\,, \tag{6.18}$$

where $F(R) = 1 + R^2/\ell^2 - 2m/R + q^2/R^2$. So, when the acceleration parameter vanishes, the AdS C-metric, (6.3), reduces to the AdS-Schwarzschild and AdS−Reissner-Nordström black holes and the parameters m and q that are present in the AdS C-metric are precisely the ADM mass and ADM electromagnetic charge of these non-accelerated black holes. It should however be emphasized that the accelerated black holes lose mass through radiative processes and so the determination of the mass of the accelerated black holes would require the calculation of the Bondi mass, which we do not here.

6.1.2   Causal Structure of the AdS C-metric

In this section we analyze the causal structure of the solution. As occurs with the original flat C-metric [84, 104], the original AdS C-metric, (6.16), is not geodesically complete. To obtain the maximal analytic spacetime, i.e., to draw the Carter-Penrose diagrams we will introduce the usual null Kruskal coordinates.

6.1 Pair of accelerated black holes in an anti-de Sitter background: the AdS C-metric

We now look carefully to the AdS C-metric, (6.16), with $\mathcal{F}(y)$ given by (6.4). We first notice that, contrarily to what happens in the $\Lambda \geq 0$ background where the causal structure and physical nature of the corresponding C-metric is independent of the relation between the acceleration A and $\ell \equiv \sqrt{3/|\Lambda|}$, in the $\Lambda < 0$ case we must distinguish and analyze separately the cases $A > 1/\ell$, $A = 1/\ell$ and $A < 1/\ell$. Later, in section 6.1.3, we will justify physically the reason for this distinction. The mathematical reason for this difference is clearly identified by setting $m = 0$ and $q = 0$ in (6.4) giving $\mathcal{F}(y) = y^2 - [1 - 1/(\ell^2 A^2)]$. Since the horizons of the solution are basically given by the real roots of $\mathcal{F}(y)$, we conclude that we have to treat separately the cases (A) $A > 1/\ell$ for which $\mathcal{F}(y)$ can have two real roots, (B) $A = 1/\ell$ for which $y = 0$ is double root and (C) $A < 1/\ell$ for which $\mathcal{F}(y)$ has no real roots (see discussion in the text of Fig. 6.1). We will consider each of these three cases separately in subsections 6.1.2.a and 6.1.3.a ($A > 1/\ell$ case), 6.1.2.b and 6.1.3.b ($A = 1/\ell$ case), and 6.1.2.c and 6.1.3.c ($A < 1/\ell$ case). The description of the solution depends crucially on the values of m and q. In each subsection, we will consider the three most relevant solutions, namely: *1. Massless uncharged solution* ($m = 0$, $q = 0$), *2. Massive uncharged solution* ($m > 0$, $q = 0$), and *3. Massive charged solution* ($m > 0$, $q \neq 0$).

6.1.2.a   Causal Structure of the $A > 1/\ell$ solutions

• Massless uncharged solution ($m = 0, q = 0$)

In this case we have

$$\mathcal{F}(y) = y^2 - y_+^2 \quad \text{with} \quad y_+ = \sqrt{1 - \frac{1}{\ell^2 A^2}}, \tag{6.19}$$

and $x \in [x_s = -1, x_n = +1]$, $x = \cos\theta$, $\mathcal{G} = 1 - x^2 = \sin^2\theta$, $\kappa = 1$ and $\tilde{\phi} = \phi$, with $0 \leq \phi \leq 2\pi$. The shapes of $\mathcal{F}(y)$ and $\mathcal{G}(x)$ are represented in Fig. 6.1.
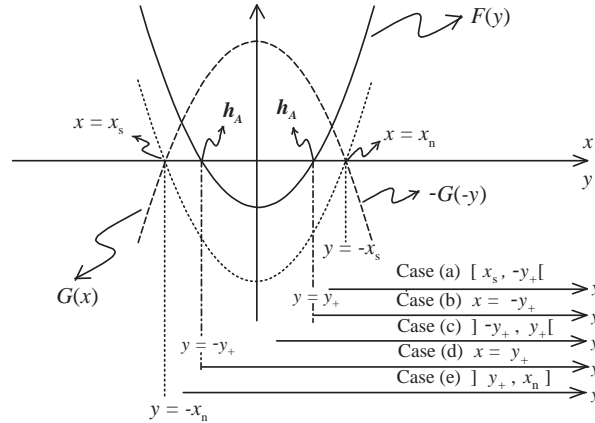
Figure 6.1: Shape of $\mathcal{G}(x)$ and $\mathcal{F}(y)$ for the $A > 1/\ell$, $m = 0$ and $q = 0$ C-metric studied in sections 6.1.2.a and 6.1.3.a. The allowed range of x is between $x_s = -1$ and $x_n = +1$ where $\mathcal{G}(x)$ is positive and compact. The permitted range of y depends on the angular direction x ($-x \leq y < +\infty$) and is sketched for the five cases (a)-(e) discussed in the text. The presence of an accelerated horizon is indicated by h_A. [For completeness we comment here on two other cases not represented in the figure but analyzed in the text: for $A = 1/\ell$, $m = 0$ and $q = 0$ (this case is studied in sections 6.1.2.b and 6.1.3.b), $\mathcal{F}(y)$ is zero at its minimum and positive elsewhere. For $A < 1/\ell$, $m = 0$ and $q = 0$ (this case is studied in sections 6.1.2.c and 6.1.3.c), $\mathcal{F}(y)$ is always positive and only case (a) survives.]

The angular surfaces Σ ($t =$constant and $r =$constant) are spheres and both the north and south poles are free of conical singularities. The origin of the radial coordinate, $r = 0$, has no curvature singularity and therefore both r and y are in the range $]-\infty, +\infty[$. However, in the general case,

Chapter 6. Pair of accelerated black holes: the C-metric in a generalized Λ background

where m or q are non-zero, there is a curvature singularity at $r = 0$. Since the discussion of the present section is only a preliminary to that of the massive general case, following [104], the origin $r = 0$ will treat as if it had a curvature singularity and thus we admit that r belongs to the range $[0, +\infty[$ and y lies in the region $-x \leq y < +\infty$. We leave a discussion on the extension to negative values of r to section 6.1.3.a.

The general procedure to draw the Carter-Penrose diagrams is as follows. First, we make use of the null condition $g_{\mu\nu}k^\mu k^\nu = 0$ (where k^μ is a geodesic tangent) to introduce the advanced and retarded Finkelstein-Eddington null coordinates,

$$u = t - y_* ; \qquad v = t + y_* , \tag{6.20}$$

where the tortoise coordinate is

$$y_* = \int \mathcal{F}^{-1} dy = \frac{1}{2y_+} \ln \left| \frac{y - y_+}{y + y_+} \right| . \tag{6.21}$$

and both u and v belong to the range $] -\infty, +\infty[$. In these coordinates the metric is given by

$$ds^2 = r^2 [-\mathcal{F} du dv + d\theta^2 + \sin^2\theta \, d\phi^2] . \tag{6.22}$$

The metric still has coordinate singularities at the roots of $\mathcal{F}$. To overcome this unwanted feature we have to introduce Kruskal coordinates. Now, due to the lower restriction on the value of y $(-x \leq y)$, the choice of the Kruskal coordinates (and therefore the Carter-Penrose diagrams) depends on the angular direction x we are looking at. In fact, depending on the value of x, the region accessible to y might contain two, one or zero roots of $\mathcal{F}$ (see Fig. 6.1) and so the solution may have two, one or zero horizons, respectively. This angular dependence of the causal diagram is not new. The Schwarzschild and Reissner-Nordström solutions being spherically symmetric do not present this feature but, in the Kerr solution, the Carter-Penrose diagram along the pole direction is different from the diagram along the equatorial direction. Such a dependence occurs also in the flat C-metric [84]. Back again to the AdS C-metric, we have to consider separately five distinct sets of angular directions, namely (a) $x_s \leq x < -y_+$, (b) $x = -y_+$, (c) $-y_+ < x < y_+$, (d) $x = +y_+$ and (e) $y_+ < x \leq x_n$, where $x_s = -1$ and $x_n = +1$ (see Fig. 6.1).

(a) $x_s \leq x < -y_+$: within this interval of the angular direction, the restriction on the range of y, $-x \leq y < +\infty$, implies that the function $\mathcal{F}(y)$ is always positive in the accessible region of y (see Fig. 6.1), and thus the solution has no horizons. Introducing the null coordinates defined in (6.20) followed by the Kruskal coordinates $u' = -e^{-y_+ u} < 0$ and $v' = +e^{+y_+ v} > 0$ gives $u'v' = -e^{2y_+ y_*} = -(y - y_+)/(y + y_+) < 0$, and (6.22) becomes

$$ds^2 = r^2 \left[-\frac{(y + y_+)^2}{y_+^2} du' dv' + d\theta^2 + \sin^2\theta \, d\phi^2 \right] , \tag{6.23}$$

where y and $r = A^{-1}(x + y)^{-1}$ are regarded as functions of u' and v',

$$y = y_+ \frac{1 - u'v'}{1 + u'v'} , \qquad r = \frac{1}{A} \frac{1 + u'v'}{(y_+ + x) - u'v'(y_+ - x)} . \tag{6.24}$$

Now, let us find the values of the product $u'v'$ at $r = 0$ and $r = +\infty$,

$$\lim_{r \to 0} u'v' = -1 , \qquad \lim_{r \to +\infty} u'v' = \frac{y_+ + x}{y_+ - x} < 0 \text{ and finite} . \tag{6.25}$$

So, for $x_s \leq x < -y_+$, the original massless uncharged AdS C-metric is described by (6.23) subjected to the following coordinates ranges,

$$0 \leq \phi < 2\pi , \quad -1 \leq x \leq +1 , \quad u' < 0 , \quad v' > 0 , \tag{6.26}$$

$$-1 \leq u'v' < \frac{y_+ + x}{y_+ - x} . \tag{6.27}$$

6.1 Pair of accelerated black holes in an anti-de Sitter background: the AdS C-metric

This spacetime is however geodesically incomplete. To obtain the maximal analytical extension one allows the Kruskal coordinates to take also the values $u' \geq 0$ and $v' \leq 0$ as long as (6.27) is satisfied.

Finally, to construct the Carter-Penrose diagram one has to define the Carter-Penrose coordinates by the usual arc-tangent functions of u' and v': $\mathcal{U} = \arctan u'$ and $\mathcal{V} = \arctan v'$, that bring the points at infinity into a finite position. In general, to find what kind of curve describes the lines $r = 0$ or $r = +\infty$ one has to take the limit of $u'v'$ as $r \to 0$ (in the case of $r = 0$) and the limit of $u'v'$ as $r \to +\infty$ (in the case of $r = +\infty$). If this limit is 0 or ∞ the corresponding line is mapped into a curved null line. If the limit is -1, or a negative and finite constant, the corresponding line is mapped into a curved timelike line and finally, when the limit is $+1$, or a positive and finite constant, the line is mapped into a curved spacelike line. The asymptotic lines are drawn as straight lines although in the coordinates $\mathcal{U}$ and $\mathcal{V}$ they should be curved outwards, bulged. It is always possible to change coordinates so that the asymptotic lines are indeed straight lines. So, from (6.25) we draw the Carter-Penrose diagram sketched in Fig. 6.2.(a). There are no horizons and both $r = 0$ and $r = +\infty$ ($\mathcal{I}$) are timelike lines.
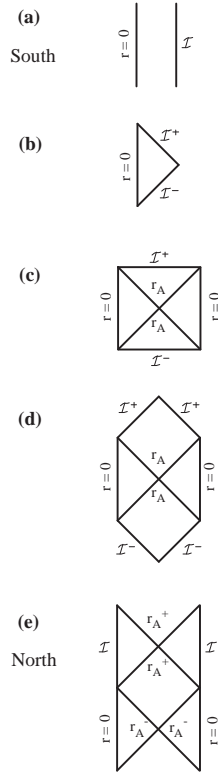
Figure 6.2: Carter-Penrose diagrams of cases (a)-(e) discussed in the text of section 6.1.2.a concerning the $A > 1/\ell$, $m = 0$, $q = 0$ C-metric. Case (a) describes the solution seen from the vicinity of the south pole, case (c) applies to the equatorial vicinity, and case (e) describes the solution seen from the vicinity of the north pole. An accelerated horizon is represented by r_A, and $\mathcal{I}^-$ and $\mathcal{I}^+$ represent respectively the past and future infinity ($r = +\infty$). $r = 0$ corresponds to $y = +\infty$ and $r = +\infty$ corresponds to $y = -x$.

(b) $x = -y_+$: for this particular angular direction, y is restricted to be on $+y_+ \leq y < +\infty$ and $\mathcal{F}(y)$ is always positive except at $y = +y_+$ (which corresponds to $r = +\infty$) where it is zero (see Fig. 6.1). Therefore, the solution has no horizon and the Kruskal construction is similar to the one described above in case (a). The only difference is that now $\lim_{r \to +\infty} u'v' = 0$ and thus $r = +\infty$ ($\mathcal{I}$) is represented by a null line in the Carter-Penrose diagram which is shown in Fig. 6.2.(b).

(c) $-y_+ < x < y_+$: the demand that y must belong to the range $[-x; +\infty[$ implies, for this range of the angular direction, that we have a region I, $-x \leq y < +y_+$, where $\mathcal{F}(y)$ is negative and

a region II, $+y_+ < y < +\infty$, where $\mathcal{F}(y)$ is positive (see Fig. 6.1). There is a single Rindler-like acceleration horizon (r_A) at $y = +y_+$, so called because it is is absent when $A = 0$ and present even when $m = 0$ and $q = 0$. In region I one sets the Kruskal coordinates $u' = +e^{-\alpha u}$ and $v' = +e^{+\alpha v}$ so that $u'v' = +e^{2\alpha y_*}$. In region II one defines $u' = -e^{-\alpha u}$ and $v' = +e^{+\alpha v}$ in order that $u'v' = -e^{2\alpha y_*}$. We set $\alpha \equiv y_+$. Thus, in both regions the product $u'v'$ is given by

$$u'v' = -\frac{y - y_+}{y + y_+} \,, \tag{6.28}$$

and (6.22) expressed in terms of the Kruskal coordinates is given by

$$\begin{aligned}
ds^2 &= r^2\left[\frac{1}{y_+^2}\frac{\mathcal{F}}{u'v'}du'dv' + d\theta^2 + \sin^2\theta\,d\phi^2\right] \tag{6.29}\\
&= r^2\left[-\frac{(y + y_+)^2}{y_+^2}du'dv' + d\theta^2 + \sin^2\theta\,d\phi^2\right]. \tag{6.30}
\end{aligned}$$

The Kruskal coordinates in both regions were chosen in order to obtain a negative value for the factor $\mathcal{F}/(u'v')$, which appears in the metric coefficient $g_{u'v'}$. The value of constant α was selected in order that the limit of $\mathcal{F}/(u'v')$ as $y \to y_+$ stays finite and different from zero. By doing this, we have removed the coordinate singularity that was present at the root y_+ of $\mathcal{F}$ [see (6.22)]. So, the metric is now well-behaved in the whole range $-x \leq y < +\infty$ or $0 \leq r < +\infty$. The coordinates y and r are expressed as functions of u' and v' by (6.24) and at the edges of the interval allowed to r, the product $u'v'$ takes the values

$$\lim_{r\to 0} u'v' = -1\,, \qquad \lim_{r\to+\infty} u'v' = \frac{y_+ + x}{y_+ - x} > 0 \text{ and finite}\,. \tag{6.31}$$

Once again, the maximal analytical extension is achieved by allowing the Kruskal coordinates u' and v' to take all the values on the range $]-\infty; +\infty[$, as soon as the condition $-1 \leq u'v' < (y_+ + x)/(y_+ - x)$ is satisfied. The Carter-Penrose diagram for this range of the angular direction is drawn in Fig. 6.2.(c). $r = 0$ is represented by a timelike line while $r = +\infty$ ($\mathcal{I}$) is a spacelike line. The two mutual perpendicular straight null lines at 45°, $u'v' = 0$, represent the accelerated horizon at $y_A = +y_+$ or $r_A = [A(x + y_+)]^{-1}$.

(d) $x = +y_+$: in this particular direction, the region accessible to y is $-y_+ \leq y < +\infty$. $\mathcal{F}(y)$ is negative in region I, $-y_+ < y < y_+$ and positive in region II, $y > y_+$. It is zero at $y = +y_+$ where is located the only horizon (r_A) of the solution and $\mathcal{F}(y)$ vanishes again at $y = -y_+$ which corresponds to $r = +\infty$ (see Fig. 6.1). The Kruskal construction follows directly the procedure described in case (c). The only difference is that now $\lim_{r\to+\infty} u'v' = +\infty$ and thus the $r = +\infty$ line ($\mathcal{I}$) is now represented by a null line in the Carter-Penrose diagram which is shown in Fig. 6.2.(d).

(e) $y_+ < x \leq x_n$: the region accessible to y must be separated into three regions (see Fig. 6.1). In region I, $-x < y < -y_+$, $\mathcal{F}(y)$ is positive; in region II, $-y_+ < y < +y_+$, $\mathcal{F}(y)$ is negative and finally in region III, $y > +y_+$, $\mathcal{F}(y)$ is positive again. We have two Rindler-like acceleration horizons, more specifically, an outer horizon at $y = -y_+$ or $r_A^+ = [A(x - y_+)]^{-1}$ and an inner horizon at $y = +y_+$ or $r_A^- = [A(x + y_+)]^{-1}$. Therefore one must introduce a Kruskal coordinate patch around each of the horizons. The first patch constructed around $-y_+$ is valid for $-x \leq y < +y_+$ (thus, it includes regions I and II). In region I we define $u' = -e^{+\alpha_- u}$ and $v' = +e^{-\alpha_- v}$ so that $u'v' = -e^{-2\alpha_- y_*}$. In region II one defines $u' = +e^{\alpha_- u}$ and $v' = +e^{-\alpha_- v}$ in order that $u'v' = +e^{-2\alpha_- y_*}$. We set $\alpha_- \equiv y_+$. Thus, in both regions, I and II, the product $u'v'$ is given by

$$u'v' = -\frac{y + y_+}{y - y_+} \,, \tag{6.32}$$

and (6.22) expressed in terms of the Kruskal coordinates is given by

$$ds^2 = r^2\left[-\frac{(y-y_+)^2}{y_+^2}du'dv' + d\theta^2 + \sin^2\theta\,d\phi^2\right],\tag{6.33}$$

which is regular in this patch $-x \leq y < +y_+$ and, in particular, it is regular at the root $y = -y_+$ of $\mathcal{F}(y)$. However, it is singular at the second root, $y = +y_+$, of $\mathcal{F}(y)$. To regularize the metric around $y = +y_+$, one has to introduce new Kruskal coordinates for the second patch which is built around y_+ and is valid for $-y_+ < y < +\infty$ (thus, it includes regions II and III). In region II we set $u' = +e^{-\alpha_+ u}$ and $v' = +e^{+\alpha_+ v}$ so that $u'v' = +e^{+2\alpha_+ y_*}$. In region III one defines $u' = -e^{-\alpha_+ u}$ and $v' = +e^{+\alpha_+ v}$ in order that $u'v' = -e^{+2\alpha_+ y_*}$. We set $\alpha_+ \equiv y_+$. Thus, in both regions, II and III, the product $u'v'$ is given by

$$u'v' = -\frac{y-y_+}{y+y_+},\tag{6.34}$$

and, in this second Kruskal patch, (6.22) is given by

$$ds^2 = r^2\left[-\frac{(y+y_+)^2}{y_+^2}du'dv' + d\theta^2 + \sin^2\theta\,d\phi^2\right],\tag{6.35}$$

which is regular in $y > -y_+$ and, in particular, at the second root $y = +y_+$ of $\mathcal{F}(y)$. Once again, in both patches, the Kruskal coordinates were chosen in order to obtain a factor $\mathcal{F}/(u'v')$ negative [see (6.29)]. The values of constants α_- and α_+ were selected in order that the limit of $\mathcal{F}/(u'v')$ as $y \to \mp y_+$ stays finite and different from zero. To end the construction of the Kruskal diagram of this solution with two horizons, the two patches have to be joined together in an appropriate way first defined by Carter in the Reissner-Nordström solution.

From (6.34) and (6.32) we find the values of product $u'v'$ at the edges $r = 0$ and $r = +\infty$ of the radial coordinate,

$$\lim_{r\to 0} u'v' = -1\,,\qquad \lim_{r\to+\infty} u'v' = \frac{y_+ - x}{y_+ + x} < 0 \text{ and finite}\,.\tag{6.36}$$

and conclude that both $r = 0$ and $r = +\infty$ ($\mathcal{I}$) are represented by timelike lines in the Carter-Penrose diagram sketched in Fig. 6.2.(e). The two accelerated horizons of the solution are both represented as perpendicular straight null lines at $45°$ ($u'v' = 0$).

● **Massive uncharged solution ($m > 0$, $q = 0$)**

Now that the causal structure of the AdS C-metric with $m = 0$ and $q = 0$ has been studied, the construction of the Carter-Penrose diagrams for the $m > 0$ case follows up directly. As has justified in detail in section 6.1.1.c, we will consider only the case with small mass or acceleration, i.e., we require $mA < 3^{-3/2}$, in order to have compact angular surfaces (see discussion on the text of Fig. 6.3). We also demand x to belong to the range $[x_s, x_n]$ (see Fig. 6.3) where $\mathcal{G}(x) \geq 0$ and such that $x_s \to -1$ and $x_n \to +1$ when $mA \to 0$. By satisfying the two above conditions we endow the $t = $constant and $r = $constant surfaces with the topology of a compact surface.
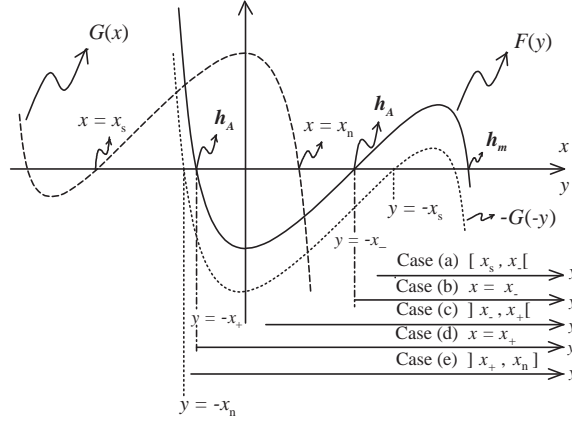
Figure 6.3: Shape of $\mathcal{G}(x)$ and $\mathcal{F}(y)$ for the $A > 1/\ell, mA < 3^{-3/2}$, and $q = 0$ C-metric studied in sections 6.1.2.a and 6.1.3.a. The allowed range of x is between $x_{\rm s}$ and $x_{\rm n}$ where $\mathcal{G}(x)$ is positive and compact. The permitted range of y depends on the angular direction x $(-x \leq y < +\infty)$ and is sketched for the five cases (a)-(e) discussed in the text. The presence of an accelerated horizon is indicated by h_A and the Schwarzschild-like horizon by h_m. [For completeness we comment on two other cases not represented in the figure: for $A = 1/\ell, mA < 3^{-3/2}$ and $q = 0$ (this case is studied in sections 6.1.2.b and 6.1.3.b), $\mathcal{F}(y)$ is zero at its local minimum. For $A < 1/\ell, mA < 3^{-3/2}$ and $q = 0$ (this case is studied in sections 6.1.2.c and 6.1.3.c), the local minimum of $\mathcal{F}(y)$ is positive and only case (a) survives. For $mA = 3^{-3/2}$, $\mathcal{G}(x)$ is zero at its local minimum on the left and for $mA > 3^{-3/2}$ $\mathcal{G}(x)$ is positive between $-\infty$ and $x_{\rm n}$. These two last cases are not studied in the text.]

The technical procedure to obtain the Carter-Penrose diagrams is similar to the one described along section 6.1.2.a. In what concerns the physical conclusions, we will see that the essential difference is the presence of an extra horizon, a Schwarzschild-like horizon (r_+), due to the non-vanishing mass parameter, in addition to the accelerated Rindler-like horizon (r_A) which has due to non-vanishing A. Another important difference, as stated in section 6.1.1.b, is the presence of a curvature singularity at $r = 0$ and the existence of a conical singularity at the north pole (see section 6.1.1.c).

Once more the Carter-Penrose diagrams depend on the angular direction we are looking at (see Fig. 6.3). We have to analyze separately five distinct cases, namely (a) $x_{\rm s} \leq x < x_-$, (b) $x = x_-$, (c) $x_- < x < x_+$, (d) $x = x_+$ and (e) $x_+ < x \leq x_{\rm n}$, which are the massive counterparts of cases (a)-(e) that were considered in section 6.1.2.a. When $m \to 0$ we have $x_{\rm s} \to -1$, $x_{\rm n} \to +1$, $x_- \to -y_+$ and $x_+ \to +y_+$.

(a) $x_{\rm s} \leq x < x_-$: the Carter-Penrose diagram [Fig. 6.4.(a)] for this range of the angular direction has a spacelike curvature singularity at $r = 0$, a timelike line that represents $r = +\infty$ $(\mathcal{I})$ and a Schwarzschild-like horizon (r_+) that was not present in the $m = 0$ corresponding diagram Fig. 6.2.(a). The diagram is similar to the one of the AdS-Schwarzschild solution, although now the curvature singularity has an acceleration A, as will be seen in section 6.1.3.

(b) $x = x_-$: the curvature singularity $r = 0$ is also a spacelike line in the Carter-Penrose diagram [see Fig 6.4.(b)] and there is a Schwarzschild-like horizon (r_+). The infinity, $r = +\infty$ $(\mathcal{I})$, is represented by a null line. The origin is being accelerated (see section 6.1.3).

(c) $x_- < x < x_+$: the Carter-Penrose diagram [Fig. 6.4.(c)] has a more complex structure that can be divided into left, middle and right regions. The middle region contains the spacelike infinity $(\mathcal{I})$ and an accelerated Rindler-like horizon, $r_A = [A(x - x_-)]^{-1}$, that is already present in the $m = 0$ corresponding diagram [see Fig. 6.2.(c)]. The left and right regions both contain a spacelike curvature singularity and a Schwarzschild-like horizon, r_+.

(d) $x = x_+$: the Carter-Penrose diagram [Fig. 6.4.(d)] for this particular value of the angular

direction is similar to the one of above case (c). The only difference is that $r = +\infty$ ($\mathcal{I}$) is represented by a null line rather than a spacelike line.

(e) $x_+ < x \leq x_{\mathrm{n}}$: the Carter-Penrose diagram [Fig. 6.4.(e)] can again be divided into left, middle and right regions. The middle region consists of a timelike line representing $r = +\infty$ ($\mathcal{I}$) and two accelerated Rindler-like horizons, an inner one ($r_A^- = [A(x - x_-)]^{-1}$) and an outer one ($r_A^+ = [A(x - x_+)]^{-1}$), that were already present in the $m = 0$ corresponding diagram [Fig. 6.2.(e)]. The left and right regions both contain a spacelike curvature singularity and a Schwarzschild-like horizon (r_+).

Figure 6.4: Carter-Penrose diagrams of cases (a)-(e) discussed in the text of section 6.1.2.a concerning the $A > 1/\ell, mA < 3^{-3/2}$, and $q = 0$ C-metric. Case (a) describes the solution seen from the vicinity of the south pole, case (c) applies to the equatorial vicinity, and case (e) describes the solution seen from the vicinity of the north pole. The zigzag line represents a curvature singularity, an accelerated horizon is represented by r_A, the Schwarzschild-like horizon is sketched as r_+. $r = 0$ corresponds to $y = +\infty$ and $r = +\infty$ ($\mathcal{I}$) corresponds to $y = -x$. The hatched region does not belong to the solution. In diagrams (c)-(e) we have to glue indefinitely copies of the represented figure in the left and right sides of it. In diagram (e) a similar gluing must be done in the top and bottom regions.

● **Massive charged solution ($m > 0$, $q \neq 0$)**

When both the mass and charge parameters are non-zero, depending on the values of the parameters A, m and q, $\mathcal{G}(x)$ can be positive in a single compact interval, $]x_{\mathrm{s}}, x_{\mathrm{n}}[$, or in two distinct compact intervals, $]x'_{\mathrm{s}}, x'_{\mathrm{n}}[$ and $]x_{\mathrm{s}}, x_{\mathrm{n}}[$, say (see Fig. 6.5). In this latter case we will work only with

the interval $[x_s, x_n]$ (say) for which the charged solutions are in the same sector of those we have analyzed in the last two subsections when $q \to 0$.

Depending also on the values of A, m and q, the function $\mathcal{F}(y)$ can have four roots, three roots (one of them degenerated) or two roots (see the discussion on the text of Fig. 6.5). As will be seen, the first case describes a pair of accelerated AdS−Reissner-Nordström (AdS-RN) black holes, the second case describes a pair of extremal AdS-RN black holes and the third case describes a pair of naked AdS-RN singularities.
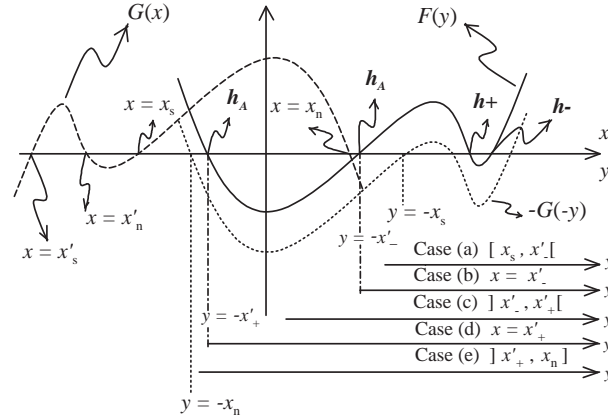
Figure 6.5: Shape of $\mathcal{G}(x)$ and $\mathcal{F}(y)$ for the non-extremal charged massive C-metric (with $A > 1/\ell$) studied in sections 6.1.2.a and 6.1.3.a. The allowed range of x is between x_s and x_n where $\mathcal{G}(x)$ is positive and compact. The permitted range of y depends on the angular direction x ($-x \leq y < +\infty$) and is sketched for the five cases (a)-(e) discussed in the text. The presence of an accelerated horizon is indicated by h_A and the inner and outer charged horizons by $h-$ and $h+$. In the extremal case, $h-$ and $h+$ superpose each other and in the naked case $\mathcal{F}(y) > 0$ in the local minimum on the right. [For completeness we comment on two other cases not represented in the figure: for $A = 1/\ell$ (this case is studied in sections 6.1.2.b and 6.1.3.b), $\mathcal{F}(y)$ is zero at its local minimum on the left. For $A < 1/\ell$ (this case is studied in sections 6.1.2.c and 6.1.3.c), the local minimum on the left of $\mathcal{F}(y)$ is positive and only case (a) survives.]

The essential differences between the Carter-Penrose diagrams of the massive charged solutions and those of the massive uncharged solutions are: (i) the curvature singularity is now represented by a timelike line rather than a spacelike line, (ii) excluding the extremal and naked cases, there are now (in addition to the accelerated Rindler-like horizon, r_A) not one but two extra horizons, the expected inner (r_-) and outer (r_+) horizons associated to the charged character of the solution.

Below, we study the causal structure of the electric or magnetic counterparts of cases (a)-(e) discussed in the two last sections (see Fig. 6.5), namely (a) $x_s \leq x < x'_-$, (b) $x = x'_-$, (c) $x'_- < x < x'_+$, (d) $x = x'_+$ and (e) $x'_+ < x \leq x_n$. When $q \to 0$ we have $x'_- \to x_-$ and $x'_+ \to x_+$. The Carter-Penrose diagrams are drawn in Fig. 6.6. In these diagrams, the left column represents the non-extremal case, the middle column represents the extremal case and the right column represents the naked charged case. The row (a) describes the solution seen from the vicinity of the south pole, row (c) applies to the equatorial vicinity, and row (e) describes the solution seen from the vicinity of the north pole. The zigzag line represents a curvature singularity, an accelerated horizon is represented by r_A, the inner and outer charge associated horizons are sketched as r_- and r_+. $\mathcal{I}^-$ and $\mathcal{I}^+$ represent respectively the past and future infinity ($r = +\infty$). $r = 0$ corresponds to $y = +\infty$ and $r = +\infty$ corresponds to $y = -x$. The hatched region does not belong to the solution. In diagrams (c)-(e) we have to glue indefinitely copies of the represented figure in the left and right sides of it. In some of the diagrams, a similar gluing must be done in the top and bottom regions.

6.1 Pair of accelerated black holes in an anti-de Sitter background: the AdS C-metric

(a) $x_{\rm s} \leq x < x'_-$: both the curvature singularity, $r = 0$, and $r = +\infty$ ($\mathcal{I}$) are represented by a spacelike line in the Carter-Penrose diagram [Fig. 6.6.(a)]. Besides, in the non-extremal case, there is an inner horizon (r_-) and an outer horizon (r_+) associated to the charged character of the solution. In the extremal case the two horizons r_- and r_+ become degenerate and so there is a single horizon, r_+ (say), and in the naked case there is no horizon. The diagram is similar to the one of the AdS$-$Reissner-Nordström solution, although now the curvature singularity has an acceleration A, as will be seen in section 6.1.3.

(b) $x = x'_-$: the curvature singularity $r = 0$ is a spacelike line in the Carter-Penrose diagram [see Fig. 6.6.(b)] and $r = +\infty$ ($\mathcal{I}$) is represented by a null line. Again, in the non-extremal case, there is an inner horizon (r_-) and an outer horizon (r_+) associated to the charged character of the solution. In the extremal case there is a single horizon, r_+, and in the naked case there is no horizon. The origin is being accelerated (see section 6.1.3).

(c) $x'_- < x < x'_+$: the Carter-Penrose diagram [Fig. 6.6.(c)] has a complex structure. As before [see Fig 6.4.(c)], it can be divided into left, middle and right regions. The middle region contains the spacelike infinity ($\mathcal{I}$) and an accelerated Rindler-like horizon, $r_A = [A(x - x'_-)]^{-1}$, that was already present in the $m = 0$, $q = 0$ corresponding diagram [see Fig. 6.2.(c)]. The left and right regions both contain a timelike curvature singularity ($r = 0$). In addition, these left and right regions contain, in the non-extremal case, an inner horizon (r_-) and an outer horizon (r_+), in the extremal case they contain is a single horizon (r_+), and in the naked case they have no horizon.

(d) $x = x'_+$: the Carter-Penrose diagram [Fig. 6.6.(d)] for this particular value of the angular direction is similar to the one of above case (c). The only difference is that $r = +\infty$ ($\mathcal{I}$) is represented by a null line rather than a spacelike line.

(e) $x'_+ < x \leq x_{\rm n}$: the Carter-Penrose diagram [Fig. 6.6.(e)]. As before [see Fig 6.4.(e)], it can be divided into left, middle and right regions. The middle region consists of a timelike line representing $r = +\infty$ ($\mathcal{I}$) and two accelerated Rindler-like horizon, $r_A^- = [A(x - x'_-)]^{-1}$ and $r_A^+ = [A(x - x'_+)]^{-1}$, that were already present in the $m = 0$ and $q = 0$ corresponding diagram [see Fig. 6.2.(e)]. The left and right regions both contain a timelike curvature singularity ($r = 0$). In addition, these left and right regions contain, in the non-extremal case, an inner horizon (r_-) and an outer horizon (r_+), in the extremal case they contain is a single horizon (r_+), and in the naked case they have no horizon (see however the physical interpretation of this case as a black hole in the end of subsection 6.1.3).
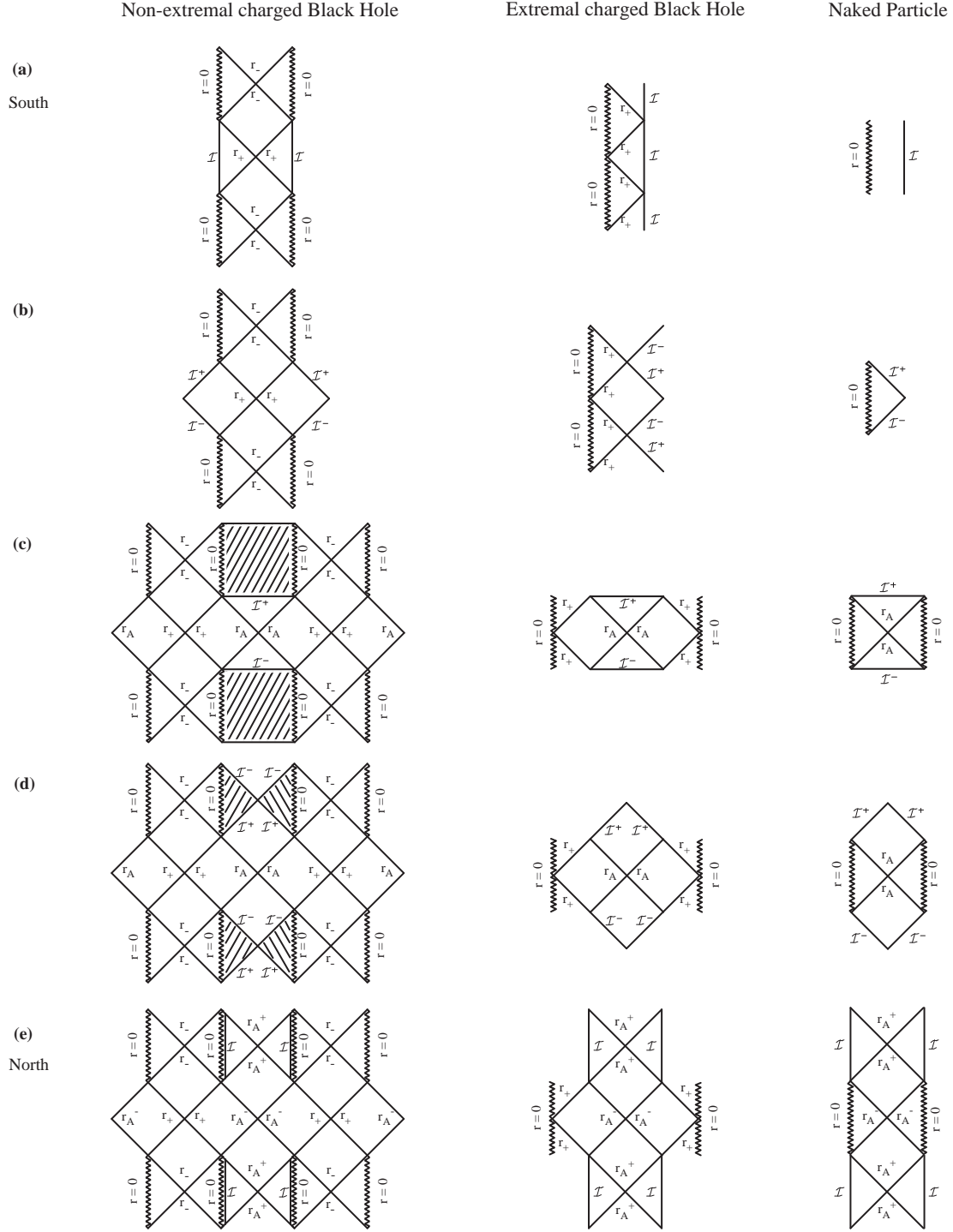
Figure 6.6: Carter-Penrose diagrams of cases (a)-(e) discussed in the text of section 6.1.2.a concerning the charged massive C-metric. The left column represents the non-extremal case, the middle column represents the extremal case and the right column represents the naked charged case. The row (a) describes the solution seen from the vicinity of the south pole, row (c) applies to the equatorial vicinity, and row (e) describes the solution seen from the vicinity of the north pole.

6.1.2.b   Causal Structure of the $A = 1/\ell$ solutions

The $A = 1/\ell$ case was studied in detail in [121]. In particular, the causal structure of the massive uncharged solution was discussed. For completeness, we will also present the causal diagrams of the massless uncharged solution and of the massive charged solution.

Once more, due to the lower restriction on the value of y $(-x \leq y)$, the causal diagrams depend

on the angular direction x we are looking at. We have to consider separately three distinct sets of angular directions (see discussion on the text of Figs. 6.1, 6.3 and 6.5), namely (a) $x_{\mathrm{s}} \leq x < 0$, (b) $x = 0$ and (c) $0 < x \leq x_{\mathrm{n}}$, where $x_{\mathrm{s}} = -1$ and $x_{\mathrm{n}} = +1$ when $m = 0$ and $q = 0$.

● Massless uncharged solution ($m = 0, q = 0$)

In this case we have $x \in [x_{\mathrm{s}} = -1, x_{\mathrm{n}} = +1]$, $x = \cos\theta$, $\mathcal{G} = 1 - x^2 = \sin^2\theta$, $\kappa = 1$ and $\mathcal{F}(y) = y^2$ (see discussion on the text of Fig. 6.1). The angular surfaces Σ ($t =$constant and $r =$constant) are spheres free of conical singularities. The origin of the radial coordinate r has no curvature singularity and therefore both r and y can lie in the range $] - \infty, +\infty[$. However, in the general case, where m or q are non-zero, there is a curvature singularity at $r = 0$. Since the discussion of the present section is only a preliminary to that of the massive general case, following [104], we will treat the origin $r = 0$ as if it had a curvature singularity and thus we admit that r belongs to the range $[0, +\infty[$ and y lies in the region $-x \leq y < +\infty$. The Carter-Penrose diagrams are drawn in Fig. 6.7. In case (c) $0 < x \leq x_{\mathrm{n}}$, and only in this case, there is an accelerated horizon, $r_A = (Ax)^{-1}$.
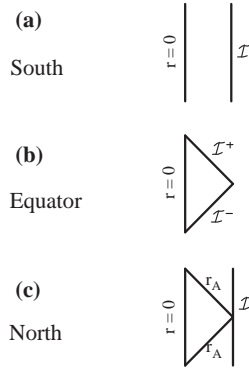
Figure 6.7: Carter-Penrose diagrams of cases (a)-(c) discussed in the text of section 6.1.2.b concerning the $A = 1/\ell$, $m = 0$, and $q = 0$ C-metric. $r_A = (Ax)^{-1}$. In diagrams (a) and (c) we have to glue indefinitely copies of the represented figure in the top and bottom regions of it.

● Massive uncharged solution ($m > 0, q = 0$)

The causal diagrams of this solution were first presented in [121] and are drawn in Fig. 6.8. In the case (c) $0 < x \leq x_{\mathrm{n}}$, and only in this case, there is an accelerated horizon, $r_A = (Ax)^{-1}$ which is degenerated (see [121]). The Schwarzschild-like horizon is at $r_+ = A^{-1}[x + 1/(2mA)]^{-1}$.
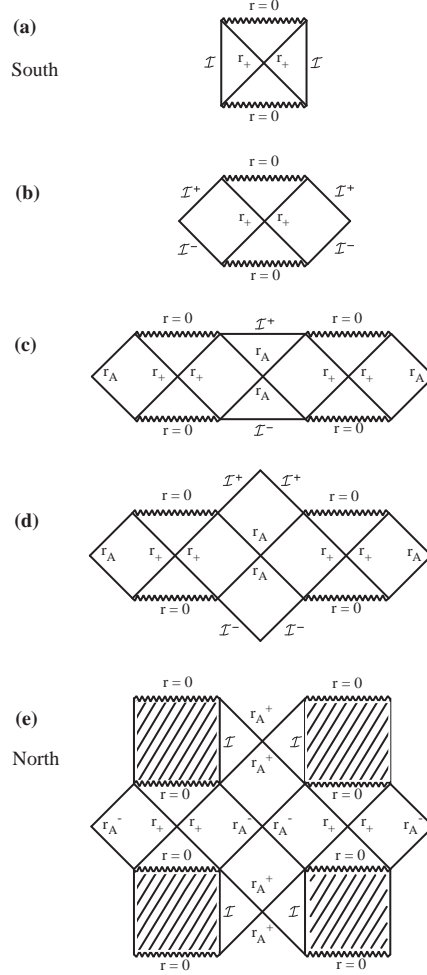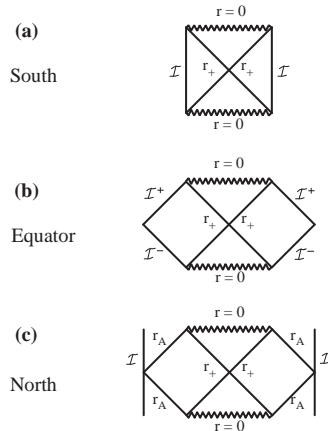

Figure 6.8: Carter-Penrose diagrams of cases (a)-(c) discussed in the text of section 6.1.2.b concerning the $A = 1/\ell, mA < 3^{-3/2}$, and $q = 0$ C-metric. $r_A = (Ax)^{-1}$ is a degenerated horizon (see [121]). In diagram (c) we have to glue indefinitely copies of the represented figure in the top and bottom regions of it.

Chapter 6. Pair of accelerated black holes: the C-metric in a generalized Λ background

• Massive charged solution ($m > 0$, $q \neq 0$)

The Carter-Penrose diagrams of the solution for this range of parameters is sketched in Fig. 6.9. In these diagrams, the left column represents the non-extremal black hole, the middle column represents the extremal black hole and the right column represents the naked charged particle. The row (a) describes the solution seen from an angle that is between the south pole (including) and the equator (excluding), row (b) applies only to the equatorial direction, and row (c) describes the solution seen from an angle between the equator (excluding) and the north pole (including).
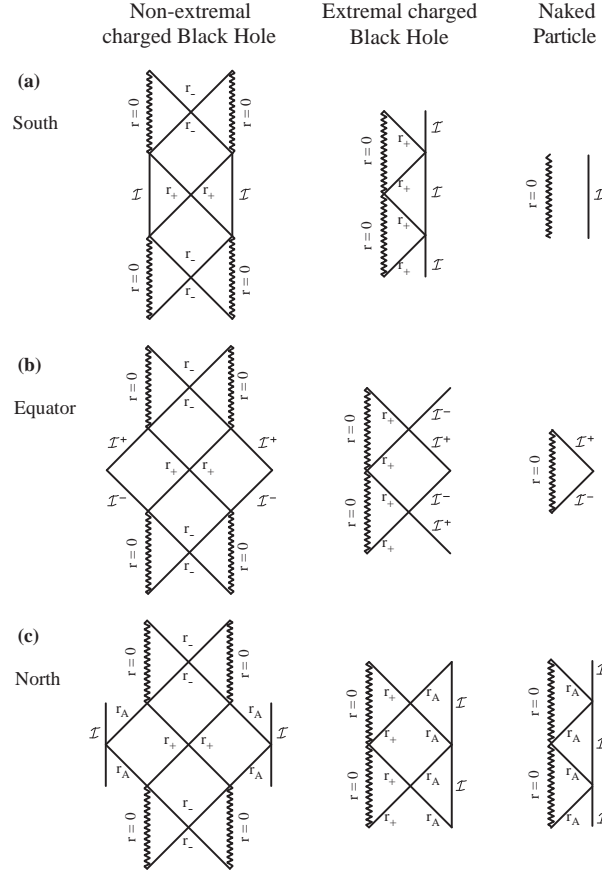
Figure 6.9: Carter-Penrose diagrams of cases (a)-(c) discussed in the text of section 6.1.2.b concerning the charged massive C-metric with $A = 1/\ell$. The left column represents the non-extremal black hole, the middle column represents the extremal black hole and the right column represents the naked charged particle. $r_A = (Ax)^{-1}$ is an accelerated horizon and r_- and r_+ are charged associated horizons. In these diagrams we have to glue indefinitely copies of the represented figure in the top and bottom regions of it.

6.1.2.c   Causal Structure of the $A < 1/\ell$ solutions

The $A < 1/\ell$ case was first analyzed in [122]. We complement it with the analysis of the causal structure. Contrarily to the cases $A > 1/\ell$ and $A = 1/\ell$, the causal diagrams of this spacetime do not depend on the angular direction we are looking at. The reason for this feature is clearly identified and explained in the discussion on the text of Figs. 6.1, 6.3 and 6.5.

• Massless uncharged solution ($m = 0, q = 0$)

The Carter-Penrose diagram is identical to the one of the AdS solution ($A = 0$, $m = 0$, $q = 0$) and is sketched in Fig. 6.7.(a). The origin has an acceleration A, as will be seen in section 6.1.3.

• Massive uncharged solution ($m > 0$, $q = 0$)

The Carter-Penrose diagram is identical to the one of the AdS-Schwarzschild solution ($A = 0$, $m > 0$, $q = 0$) and is drawn in Fig. 6.8.(a). The origin has an acceleration A, as will be seen in section 6.1.3.

• Massive charged solution ($m > 0$, $q \neq 0$)

The Carter-Penrose diagrams are identical to those of the AdS$-$Reissner-Nordström solution ($A = 0$, $m > 0$, $q \neq 0$) and is represented in Fig. 6.9.(a). In this figure, the non-extremal black hole is represented in the left column, the extremal black hole is represented in the middle column, and the naked charged particle is represented in the right column. The origin has an acceleration A, as will be seen in section 6.1.3.

6.1.3   Physical interpretation of the AdS C-metric

The parameter A that is found in the AdS C-metric is interpreted as being an acceleration and the AdS C-metric with $A > 1/\ell$ describes a pair of black holes accelerating away from each other in an AdS background, while the AdS C-metric with $A \leq 1/\ell$ describes a single accelerated black hole. In this section we will justify this statement.

In subsection 6.1.1.e we saw that, when $A = 0$, the general AdS C-metric, (6.16), reduces to the AdS ($m = 0$, $q = 0$), to the AdS-Schwarzschild ($m > 0$, $q = 0$), and to the AdS$-$Reissner-Nordström solutions ($m = 0$, $q \neq 0$). Therefore, the parameters m and q are, respectively, the ADM mass and ADM electromagnetic charge of the non-accelerated black holes. Moreover, if we set the mass and charge parameters equal to zero, even when $A \neq 0$, the Kretschmann scalar [see (6.8)] reduces to the value expected for the AdS spacetime. This indicates that the massless uncharged AdS C-metric is an AdS spacetime in disguise.

6.1.3.a $A > 1/\ell$. Pair of accelerated black holes

In this section, we will first interpret case *1. Massless uncharged solution* ($m = 0$, $q = 0$), which is the simplest, and then with the acquired knowledge we interpret cases *2. Massive uncharged solution* ($m > 0$, $q = 0$) and *3. Massive charged solution* ($m > 0$, $q \neq 0$). We will interpret the solution following two complementary descriptions, the four dimensional (4D) one and the five dimensional (5D).

• The 4-Dimensional description ($m = 0$, $q = 0$)

As we said in 6.1.2.a, when $m = 0$ and $q = 0$ the origin of the radial coordinate r defined in (6.7) has no curvature singularity and therefore r has the range $]-\infty, +\infty[$. However, in the realistic general case, where m or q are non-zero, there is a curvature singularity at $r = 0$ and since the discussion of the massless uncharged solution was only a preliminary to that of the massive general case, following [104], we have treated the origin $r = 0$ as if it had a curvature singularity and thus we admitted that r belongs to the range $[0, +\infty[$. In these conditions we obtained the causal diagrams of Fig. 6.2. Note however that one can make a further extension to include the negative values of r, enlarging in this way the range accessible to the Kruskal coordinates u' and v'. By doing this procedure we obtain the causal diagram of the AdS spacetime. In Fig. 6.10 we show the extension to negative values of coordinate r (so $-\infty < y < +\infty$) of the Carter-Penrose diagrams of Fig. 6.2. This diagram indicates that the origin of the AdS spacetime, $r = 0$, is accelerating. The situation is analogous to the one that occurs in the usual Rindler spacetime, $ds^2 = -X^2 dT^2 + dX^2$. If one restricts the coordinate X to be positive one obtains an accelerated origin that approaches a Rindler accelerated horizon. However, by making an extension to negative values of X one obtains the Minkowski spacetime.
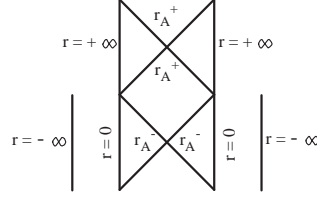
Figure 6.10: Extending the Carter-Penrose diagrams of Fig. 6.2 to negative values of r, we obtain the AdS spacetime with its origin being accelerated. $r_A^+ = [A(x-y_+)]^{-1} > 0$ and $r_A^- = [A(x+y_+)]^{-1} > 0$. We have to glue indefinitely copies of the represented figure in the top and bottom regions.

Now, we want to clearly identify the parameter A that appears in the AdS C-metric with the acceleration of its origin. To achieve this aim, we recover the massless uncharged AdS C-metric defined by (6.3) and (6.4) (with $m = 0$ and $q = 0$), and after performing the following coordinate transformation

$$\tau = \frac{\sqrt{\ell^2 A^2 - 1}}{A} t, \qquad \rho = \frac{\sqrt{\ell^2 A^2 - 1}}{A}\frac{1}{y},$$
$$\theta = \arccos x, \qquad \phi = \tilde\phi, \tag{6.37}$$

we can rewrite the massless uncharged AdS C-metric as

$$ds^2 = \frac{1}{\gamma^2}\left[-(1 - \rho^2/\ell^2)d\tau^2 + \frac{d\rho^2}{1 - \rho^2/\ell^2} + \rho^2 d\Omega^2\right], \tag{6.38}$$

with $d\Omega^2 = d\theta^2 + \sin^2\theta d\phi^2$ and

$$\gamma = \sqrt{\ell^2 A^2 - 1} + A\rho\cos\theta. \tag{6.39}$$

The causal diagram of this spacetime is drawn in Fig. 6.11.
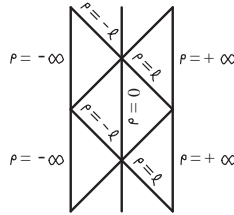
Figure 6.11: Carter-Penrose diagram of metric (6.38). We have to glue indefinitely copies of the represented figure in the top and bottom regions.

Notice that the origin of the radial coordinate ρ corresponds to $y = +\infty$ and therefore to $r = 0$, where r has been introduced in (6.7). So, when we consider the massive AdS C-metric there will be a curvature singularity at $\rho = 0$ (see section 6.1.1.b).

To discover the meaning of parameter A we consider the 4D timelike worldlines described by an observer with $\rho =$ constant, $\theta = 0$ and $\phi = 0$ (see [252]). These are given by $x^\mu(\lambda) = (\gamma\ell\lambda/\sqrt{\ell^2 - \rho^2}, \rho, 0, 0)$, were λ is the proper time of the observer since the 4-velocity $u^\mu = dx^\mu/d\lambda$ satisfies $u_\mu u^\mu = -1$. The 4-acceleration of these observers, $a^\mu = (\nabla_\nu u^\mu)u^\nu$, has a magnitude given by

$$|a_4| = \sqrt{a_\mu a^\mu} = \frac{\rho\sqrt{\ell^2 A^2 - 1} + \ell^2 A}{\ell\sqrt{\ell^2 - \rho^2}}. \tag{6.40}$$

Since $a_\mu u^\mu = 0$, the value $|a_4|$ is also the magnitude of the 3-acceleration in the rest frame of the observer. From (6.40) we achieve the important conclusion that the origin of the AdS C-metric,

6.1 Pair of accelerated black holes in an anti-de Sitter background: the AdS C-metric

$\rho = 0$ (or $r = 0$), is being accelerated with a constant acceleration whose value is precisely given by the parameter A that appears in the AdS C-metric. Moreover, at radius $\rho = \ell$ [or $y = y_+$ defined in equation (6.19)] the acceleration is infinite which corresponds to the trajectory of a null ray. Thus, observers held at $\rho =$ constant see this null ray as an acceleration horizon and they will never see events beyond this null ray.

● **The 5-Dimensional description ($m = 0$, $q = 0$)**

In order to improve and clarify the physical aspects of the AdS C-metric we turn now into the 5D representation of the solution.

The AdS spacetime can be represented as the 4-hyperboloid,

$$-(z^0)^2 + (z^1)^2 + (z^2)^2 + (z^3)^2 - (z^4)^2 = -\ell^2, \tag{6.41}$$

in the 5D Minkowski (with two timelike coordinates) embedding spacetime,

$$ds^2 = -(dz^0)^2 + (dz^1)^2 + (dz^2)^2 + (dz^3)^2 - (dz^4)^2. \tag{6.42}$$

Now, the massless uncharged AdS C-metric is an AdS spacetime in disguise and therefore our next task is to understand how the AdS C-metric can be described in this 5D picture. To do this we first recover the massless uncharged AdS C-metric described by (6.38) and apply to it the coordinate transformation

$$
\begin{aligned}
z^0 &= \gamma^{-1}\sqrt{\ell^2 - \rho^2}\,\sinh(\tau/\ell)\,, & z^2 &= \gamma^{-1}\rho\sin\theta\cos\phi\,, \\
z^1 &= \gamma^{-1}\sqrt{\ell^2 - \rho^2}\,\cosh(\tau/\ell)\,, & z^3 &= \gamma^{-1}\rho\sin\theta\sin\phi\,, \\
z^4 &= \gamma^{-1}[\sqrt{\ell^2 A^2 - 1}\,\rho\cos\theta + \ell^2 A]\,,
\end{aligned}
\tag{6.43}
$$

where γ is defined in (6.39). Transformations (6.43) define an embedding of the massless uncharged AdS C-metric into the 5D description of the AdS spacetime since they satisfy (6.41) and take directly (6.38) into (6.42).

(a) (b)
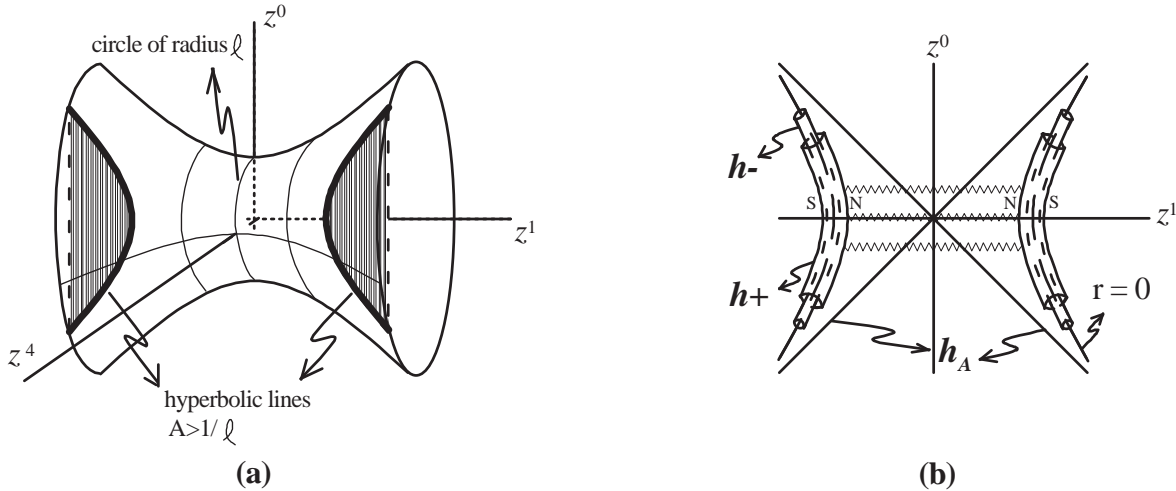
Figure 6.12: (a) AdS 4-hyperboloid embedded in the 5D Minkowski spacetime with two timelike coordinates, z^0 and z^4. The directions z^2 and z^3 are suppressed. The two hyperbolic lines lying on the AdS hyperboloid result from the intersection of the hyperboloid surface with the z^4=constant$> \ell$ plane. They describe the motion of the origin of the AdS C-metric with $A > 1/\ell$. (b) Schematic diagram representing the 5D hyperbolic motion of two uniformly accelerating massive charged black holes approaching asymptotically the Rindler-like accelerated horizon (h_A). The inner and outer charged horizons are represented by $h-$ and $h+$. The strut that connects the two black holes is represented by the zigzag lines. The north pole direction is represented by N and the south pole direction by S.

Chapter 6. Pair of accelerated black holes: the C-metric in a generalized Λ background

So, the massless uncharged AdS C-metric is an AdS spacetime, but we can extract more information from this 5D analysis. Indeed, let us analyze with some detail the properties of the origin of the radial coordinate, $\rho = 0$ (or $r = 0$). This origin moves in the 5D Minkowski embedding spacetime according to [see (6.43)]

$$z^2 = 0 , \quad z^3 = 0 , \quad z^4 = \ell^2 A / \sqrt{\ell^2 A^2 - 1} > \ell \quad \text{and}$$
$$(z^1)^2 - (z^0)^2 = (A^2 - 1/\ell^2)^{-1} \equiv a_5^{-2} . \tag{6.44}$$

These equations define two hyperbolic lines lying on the AdS hyperboloid which result from the intersection of this hyperboloid surface defined by (6.41) and the z^4=constant$> \ell$ plane [see Fig. 6.12.(a)]. They tell us that the origin is subjected to a uniform 5D acceleration, a_5, and consequently moves along a hyperbolic worldline in the 5D embedding space, describing a Rindler-like motion (see Fig. 6.12) that resembles the well-known hyperbolic trajectory, $X^2 - T^2 = a^{-2}$, of an accelerated observer in Minkowski space. But uniformly accelerated radial worldlines in the 5D Minkowski embedding space are also uniformly accelerated worldlines in the 4D AdS space [253], with the 5D acceleration a_5 being related to the associated 4D acceleration a_4 by $a_5^2 = a_4^2 - 1/\ell^2$. Comparing this last relation with (6.44) we conclude that $a_4 \equiv A$. Therefore, and once again, we conclude that the origin of the AdS C-metric is uniformly accelerating with a 4D acceleration whose value is precisely given by the parameter A that appears in the AdS C-metric, (6.3), and this solution describes a AdS space whose origin is not at rest as usual but is being accelerated. Note that the origin of the usual AdS spacetime describes the circle $(z^0)^2 + (z^4)^2 = \ell^2$ in the AdS hyperboloid in contrast to the origin of the AdS C-metric with $A > 1/\ell$ whose motion is described by (6.44). This discussion allowed us to find the physical interpretation of parameter A and to justify its label. Notice also that the original AdS C-metric coordinates introduced in (6.3) cover only the half-space $z^1 > -z^0$. The Kruskal construction done in section 6.1.2.a extended this solution to include also the $z^1 < -z^0$ region and so, in the extended solution, $r = 0$ is associated to two hyperbolas that represent two accelerated points (see Fig. 6.12). These two hyperbolas approach asymptotically the Rindler-like acceleration horizon (r_A), so called because it is is absent when $A = 0$ and present even when $A \neq 0$, $m = 0$ and $q = 0$.

• Pair of accelerated black holes ($m > 0$, $q \neq 0$)

Now, we are in position to interpret the massive and charged solutions that describe two black holes accelerating away from each other. To see clearly this, let us look to the Carter-Penrose diagrams near the equator, Fig. 6.2.(c), Fig. 6.4.(c) and Fig. 6.6.(c) (for the discussion that follows we could, as well, look at the diagrams of case (d) on these figures). Looking at these figures we can compare the different features that belong to the massless uncharge case [Fig. 6.2.(c)], to the massive uncharged case [Fig. 6.4.(c)], and ending in the massive charged case [Fig. 6.6.(c)]. In Fig. 6.2.(c) we identify the two hyperbolas $r = 0$ (represented by two timelike lines) approaching asymptotically the Rindler-like acceleration horizon (r_A). When we add a mass to the solution we conclude that each of these two simple hyperbolas $r = 0$ are replaced by the more complex structure that represents a Schwarzschild black hole with its spacelike curvature singularity and its horizon (these are represented by r_+ in the left and right regions of Fig. 6.4.(c)). So, the two accelerating points $r = 0$ have been replaced by two Schwarzschild black holes that approach asymptotically the Rindler-like acceleration horizon (represented by r_A in the middle region of Fig. 6.4.(c)). The same interpretation can be assigned to the massive charged solution. The two hyperbolas $r = 0$ of Fig. 6.2.(c) are replaced by two Reissner-Nordström black holes (with its timelike curvature singularity and its inner r_- and outer r_+ horizons; see the left and right regions of Fig. 6.6.(c)) that approach asymptotically the Rindler-like acceleration horizon already present in the $m = 0$ and $q = 0$ causal diagram.

The Carter-Penrose diagrams of cases (a) and (b) of Fig. 6.4 and Fig. 6.6 indicate that an observer that is looking through an angular direction which is in the vicinity of the south pole does not see the acceleration horizon and notices the presence of a single black hole. This is in agreement with Fig. 6.12.(b). Indeed, in this schematic figure, coordinates z^0 and z^1 can be seen as Kruskal

coordinates and we conclude that an observer, initially located at infinity ($z^1 = \infty$) and moving inwards into the black hole along the south pole, passes through the black hole horizons and hits eventually its curvature singularity. Therefore, he never has the opportunity of getting in contact with the acceleration horizon and with the second black hole. This is no longer true for an observer that moves into the black hole along an angular direction that is in the vicinity of the north pole. In Fig. 6.12.(b) this observer would be between the two black holes, at one of the points of the $z^0 < 0$ semi-axis (say) and moving into the black hole. Clearly, this observer passes through the acceleration horizon before crossing the black hole horizons and hitting its curvature singularity. This description agrees with cases (c), (d) and (e) of Fig. 6.4 and Fig. 6.6 which describe the solution along an angular direction which includes the equatorial plane [case (c)] as well as the north pole [case (e)].

The diagrams of the third column of Fig. 6.6 concerning the naked case of the $A > 1/\ell$ massive charged C-metric deserve a comment. First, we stress that the term naked is employed in this situation because the values of parameters m and q are such that the solution has no charged associated horizons, i.e., in the notation used along this paper, r_- and r_+ are not present in these diagrams. However, these diagrams present an interesting new feature. Indeed, looking at at rows (a) and (b) we have a single accelerated naked particle, in rows (c)-(d) we find two naked singularities approaching asymptotically the acceleration horizon r_A but in row (e) we have no longer two naked singularities. More precisely, we have a kind of a single AdS−Reissner-Nordström black hole with the curvature singularity being provided by the mass and charge but with the horizons having their origin in the acceleration and cosmological constant.

● **Source of acceleration. The strut or the strings**

We can now ask what entity is causing the acceleration and where it is localized. To achieve this aim, let us go back to the massless uncharged AdS C-metric and consider radial worldlines motions with $z^2 = 0$, $z^3 = 0$ and $z^4 =$ constant or, equivalently, with $\theta = 0$, $\phi =$constant and $\rho =$constant. These observers move along a Rindler-like hyperbola described by [see (6.43)]

$$(z^1)^2 - (z^0)^2 = \frac{\ell^2 - \rho^2}{(\sqrt{\ell^2 A^2 - 1} + A\rho)^2}. \tag{6.45}$$

Since the right hand side of (6.45) is smaller than a_5^{-2} defined in (6.44), the north pole $\theta_n = 0$ is localized between the hyperbolas $(z^1)^2 - (z^0)^2 = a_5^{-2}$ in the z^0, z^1 diagram [see Fig. 6.12.(b)]. What does this means? When we put m or q different from zero, each of the two hyperbolas assigned to $r = 0$ represent the accelerated motion of a black hole. Thus, (6.45) tells us that the $\theta_n = 0$ axis points toward the other black hole, i.e., it is in the region between the two black holes [see Fig. 6.12.(b)]. The south pole points along the symmetry axis towards spatial infinity. Now, in section 6.1.1.c, we saw that parameter κ has been chosen in order to avoid a conical singularity at the south pole [see (6.13)] and, by doing so, at the north pole is localized a conical singularity. This is associated to a strut that joins the two black holes and provides the acceleration of the black holes. To confirm this, recall that either a straight string or a strut have a metric described by [98]

$$ds^2 = -dt^2 + dZ^2 + d\varrho^2 + \varrho^2 d\tilde{\varphi}^2, \tag{6.46}$$

where $\tilde{\varphi} = [1 - \delta/(2\pi)]\varphi$ and $0 \leq \varphi < 2\pi$. A string has $\delta > 0$ and the geometry around it is conic, i.e., it is a plane with a deficit angle δ, while a strut has $\delta < 0$. Their mass per unit length is $\mu = \delta/(8\pi)$ and their interior energy-momentum tensor is

$$T_\alpha{}^\beta = \mu\delta(X)\delta(Y)\text{diag}(-1, 0, 0, -1), \tag{6.47}$$

where $X = \varrho\cos\tilde{\varphi}$ and $Y = \varrho\sin\tilde{\varphi}$ are the directions normal to the strut, and $\delta(X)$ and $\delta(Y)$ are Dirac delta-functions. The pressure on the string or in the strut satisfies $p = -\mu$. If $\mu > 0$ we have a string, if $\mu < 0$ we have a strut. Now, turning to our case, the AdS C-metric, (6.16), near the

north pole is given by

$$ds^2 \sim -r^2\mathcal{F}dt^2 + r^2\mathcal{F}^{-1}dy^2 + \left(r^2d\theta^2 + \frac{\kappa^2}{4}\left|\frac{dG}{dx}\right|_{x_{\rm n}} r^2\theta^2 d\tilde{\phi}^2 \right), \tag{6.48}$$

where κ is defined in (6.13) and the term between the curved brackets is the induced metric in the plane normal to the strut that connects the two black holes (along the y direction) and will be labelled as $dX^2 + dY^2$. The C-metric strut has a mass per unit length given by

$$\mu = \frac{1}{4}\frac{\delta_{\rm n}}{2\pi} = \frac{1}{4}\left(1 - \left|\frac{dG}{dx}\right|_{x_{\rm s}}^{-1}\left|\frac{dG}{dx}\right|_{x_{\rm n}} \right). \tag{6.49}$$

We have $|d_x\mathcal{G}|_{x_{\rm s}} < |d_x\mathcal{G}|_{x_{\rm n}}$ and so μ is negative. To obtain the pressure of the C-metric strut, we write (6.48) in a Minkowski frame, $ds^2 = -\theta^{(0)2} + \theta^{(1)2} + \theta^{(2)2} + \theta^{(3)2}$, with $\theta^{(A)} = e^{(A)}{}_\alpha dx^\alpha$ and $e^{(0)}{}_0 = r\sqrt{\mathcal{F}}$, $e^{(1)}{}_1 = r$, $e^{(2)}{}_2 = r\theta k|d_x\mathcal{G}|_{x_{\rm n}}/2$ and $e^{(3)}{}_3 = r/\sqrt{\mathcal{F}}$. In this Minkowski frame the energy-momentum tensor, $T_{(A)}{}^{(B)}$, of the C-metric strut is given by (6.47). In order to come back to the coordinate basis frame and write the energy-momentum tensor of the C-metric strut in this basis we use $T^{\alpha\beta} = e^{(A)\alpha}e_{(B)}{}^\beta T_{(A)}{}^{(B)}$ and obtain

$$T^{\alpha\beta} = \mu(r^2\mathcal{F})^{-1}\delta(X)\delta(Y)\mathrm{diag}(1,0,0,-\mathcal{F}^2). \tag{6.50}$$

Defining the unit vector $\zeta = \partial/\partial y$ [so, $\zeta^\alpha = (0,0,0,1)$], the pressure along the strut is $T^{\alpha\beta}\zeta_\alpha\zeta_\beta$ and the pressure on the C-metric strut is given by the integration over the X-Y plane normal to the strut,

$$p = \int dX dY \sqrt{{}^{(2)}g}\, T^{\alpha\beta}\zeta_\alpha\zeta_\beta = -\mu. \tag{6.51}$$

So, the pressure and mass density of the C-metric strut satisfy the relation $p = -\mu$. Since μ is negative, at both ends of the strut, one has a positive pressure pushing away the two black holes.

Alternatively, instead of (6.13), we could have chosen for κ the value $\kappa^{-1} = (1/2)|d_x\mathcal{G}|_{x_{\rm n}}$. By doing so we would avoid the deficit angle at the north pole ($\delta_{\rm n} = 0$) and leave a conical singularity at the south pole ($\delta_{\rm s} > 0$). This option would lead to the presence of a semi-infinite string extending from each of the black holes towards infinity along the south pole direction, which would furnish the acceleration. The mass density of both strings is $\mu = (1/4)(1 - |d_x\mathcal{G}|_{x_{\rm n}}^{-1}|d_x\mathcal{G}|_{x_{\rm s}}) > 0$ and the pressure on the string, $p = -\mu$, is negative which means that each string is pulling the corresponding black hole towards infinity.

At this point, we briefly remark that when we take the limit $A = 0$ the AdS C-metric does not reduce to a static solution describing two AdS black holes whose inward gravitational attraction is cancelled by an outward pressure exerted by the strut or strings. Indeed, when the acceleration parameter A vanishes, the AdS C-metric reduces into a single non-accelerated black hole free of struts or strings (see subsection 6.1.1.e and section 6.1.3.c). We shall return to this issue in subsection 6.2.3.b, where we will discuss this note in detail and explain that the reason for this behavior is due to the fact that the black holes do not interact gravitationally. This conclusion is withdrawn from the Carter-Penrose diagrams of the AdS C-metric.

Ernst [85] has employed a Harrison-type transformation to the $\Lambda = 0$ charged C-metric in order to append a suitably chosen external electromagnetic field (see discussion of this solution in subsection 6.2.1.b). With this procedure the so called Ernst solution is free of conical singularities at both poles and the acceleration that drives away the two oppositely charged Reissner-Nordström black holes is totally provided by the external electromagnetic field. In the AdS background we cannot remove the conical singularities through the application of the Harrison transformation [124]. Indeed, the Harrison transformation does not leave invariant the cosmological term in the action. Therefore,

applying the Harrison transformation to (6.3)-(6.6) does not yield a new solution of the Einstein-Maxwell-AdS theory.

• **Radiative properties**

The C-metric (either in the flat, de Sitter or anti-de Sitter background) is an exact solution that is radiative. As noticed in [84], the gravitational radiation is present since the complex scalar of the Newman-Penrose formalism, $\Psi^4 = -C_{\mu\nu\alpha\beta}n^\mu\bar{m}^\nu n^\alpha\bar{m}^\beta$ (where $C_{\mu\nu\alpha\beta}$ is the Weyl tensor and $\{l, n, m, \bar{m}\}$ is the usual null tetrad of Newman-Penrose), contains a term proportional to r^{-1}. Similarly, the charged version of the C-metric includes, in addition, electromagnetic radiation. In [104], it has been shown that the Bondi news functions of the flat C-metric are indeed non-zero. These Bondi news functions appear in the context of the Bondi method introduced to study gravitational radiative systems. They are needed to determine the evolution of the radiative gravitational field since they carry the information concerning the changes of the system. When at least one of them is not zero, the total Bondi mass of the system decreases due to the emission of gravitational waves. The Bondi news functions of the flat C-metric have been explicitly calculated in [112, 113]. For a detailed review on the radiative properties of the C-metric and other exact solutions see [113]. In an AdS background the energy released by a pair of accelerated black holes has been discussed in detail by Podolský, Ortaggio and Krtouš [190].

6.1.3.b $A = 1/\ell$. Single accelerated black hole

When $A = 1/\ell$ the AdS C-metric describes a single accelerated black hole. The absence of a second black hole is clearly indicated by the Carter-Penrose diagrams of Figs. 6.8 and 6.9.

This case has been studied in detail in [121] where the Randall-Sundrum model in a lower dimensional scenario has analyzed. In this scenario, the brane-world is a 2-brane moving in a 4D asymptotically AdS background. They have shown that the AdS C-metric with $A = 1/\ell$ describes a black hole bound to the Minkowski 2-brane. The brane tension is fine tuned relative to the cosmological background acceleration and thus, $A = 1/\ell$ is precisely the acceleration that the black hole has to have in order to comove with the 2-brane. They concluded that the AdS C-metric describes the final state of gravitational collapse on the brane-world. The causal structure of the massive uncharged solution (Fig. 6.8) has been first discussed in [121]. For completeness, we have also presented the causal diagrams of the massless uncharged solution in Fig. 6.7 and of the non-extremal, extremal, and naked massive charged solutions in Fig. 6.9.

In [121] the coordinate transformation that takes the massless uncharged AdS C-metric with $A = 1/\ell$ into the known description of the AdS spacetime in Poincaré coordinates is given. From there one can easily go to the 5D description on the AdS hyperboloid. This 5D description can be also understood directly from the limits on the solutions $A > 1/\ell$ and $A < 1/\ell$ when $A \to 1/\ell$. Indeed, if we take the limit $A \to 1/\ell$ in section 6.1.3.a (where we have studied the 5D description of case $A > 1/\ell$), one sees that the cut that generates the two hyperbolic lines degenerates into two half circles which, on identifying the ends of the AdS hyperboloid at both infinities, yields one full circle. This means that the trajectory of the origin of the AdS C-metric in the $A = 1/\ell$ case is a circle (which when one unwraps the hyperboloid to its universal cover yields a straight accelerated line). As we will see in the next subsection, for $A < 1/\ell$ the trajectory of the origin is a circle which, on taking the limit $A \to 1/\ell$, still yields a circle. The two limits give the same result as expected.

6.1.3.c $A < 1/\ell$. Single accelerated black hole

The $A < 1/\ell$ case was first analyzed in [122]. We have complemented this work with the analysis of the causal structure. The causal diagrams of this spacetime are identical to the ones of the AdS ($m = 0$, $q = 0$) [see Fig. 6.7.(a)], of the AdS-Schwarzschild ($m > 0$, $q = 0$) [see Fig. 6.8.(a)], and of the AdS−Reissner-Nordström solutions ($m > 0$, $q \neq 0$) [see Fig. 6.9.(a)]. However, the curvature singularity of the single black hole of the solution is not at rest but is being accelerated, with the acceleration A provided by an open string that extends from the pole into asymptotic infinity.

Chapter 6. Pair of accelerated black holes: the C-metric in a generalized Λ background

As was done with the $A > 1/\ell$ case, it is useful to interpret the solution following two complementary descriptions, the 4D one and the 5D. One first recovers the massless uncharged AdS C-metric defined by (6.3) and (6.4) (with $A < 1/\ell$, $m = 0$ and $q = 0$), and after performing the following coordinate transformation [122]

$$T = \frac{\sqrt{1 - \ell^2 A^2}}{A} t \,, \qquad R = \frac{\sqrt{1 - \ell^2 A^2}}{A} \frac{1}{y} \,,$$

$$\theta = \arccos x \,, \qquad \phi = \tilde{\phi} \,, \tag{6.52}$$

we can rewrite the massless uncharged AdS C-metric as

$$ds^2 = \frac{1}{\eta^2} \left[-(1 + R^2/\ell^2) dT^2 + \frac{dR^2}{1 + R^2/\ell^2} + R^2 d\Omega^2 \right], \tag{6.53}$$

with $\eta^{-1} = \sqrt{1 - \ell^2 A^2} + AR \cos \theta$ and $d\Omega^2 = d\theta^2 + \sin^2 \theta d\phi^2$. A procedure similar to the one used to obtain (6.40) indicates that an observer describing 4D timelike worldlines with $R =$constant, $\theta = 0$ and $\phi = 0$ suffers a 4-acceleration with magnitude given by

$$|a_4| = \frac{\ell^2 A - R\sqrt{1 - \ell^2 A^2}}{\ell \sqrt{\ell^2 + R^2}} \,. \tag{6.54}$$

Therefore, the origin of the AdS C-metric, $R = 0$, is being accelerated with a constant acceleration whose value is precisely given by A. The causal diagram of this spacetime is drawn in Fig. 6.13. Notice that when we set $A = 0$, (6.53) reduces to the usual AdS spacetime written in static coordinates.
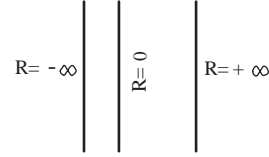
Figure 6.13: Carter-Penrose diagram of metric (6.53).

Now, to obtain the 5D description, one applies to (6.53) the coordinate transformation [122],

$$z^0 = \eta^{-1} \sqrt{\ell^2 + R^2} \sin(T/\ell) \,, \qquad z^2 = \eta^{-1} R \sin \theta \cos \phi \,,$$

$$z^4 = \eta^{-1} \sqrt{\ell^2 + R^2} \cos(T/\ell) \,, \qquad z^3 = \eta^{-1} R \sin \theta \sin \phi \,,$$

$$z^1 = \eta^{-1} [\sqrt{1 - \ell^2 A^2} R \cos \theta - \ell^2 A] \,. \tag{6.55}$$

Transformations (6.55) define an embedding of the massless uncharged AdS C-metric with $A < 1/\ell$ into the 5D description of the AdS spacetime since they satisfy (6.41) and take directly (6.53) into (6.42).

The origin of the radial coordinate, $R = 0$ moves in the 5D Minkowski embedding spacetime according to [see (6.55)]

$$z^1 = -\ell^2 A / \sqrt{1 - \ell^2 A^2} \,, \quad z^2 = 0 \,, \quad z^3 = 0 \quad \text{and}$$

$$(z^0)^2 + (z^4)^2 = (1/\ell^2 - A^2)^{-1} \equiv a_5^{-2} \,. \tag{6.56}$$

So, contrarily to the case $A > 1/\ell$ where the origin described a Rindler-like hyperbolic trajectory [see (6.44)] that suggests the presence of two black holes driving away from each other in the extended diagram, in the $A < 1/\ell$ case the origin describes a circle (a uniformly accelerated worldline) in the 5D embedding space (see Fig. 6.14), indicating the presence of a single trapped black hole in the AdS background.
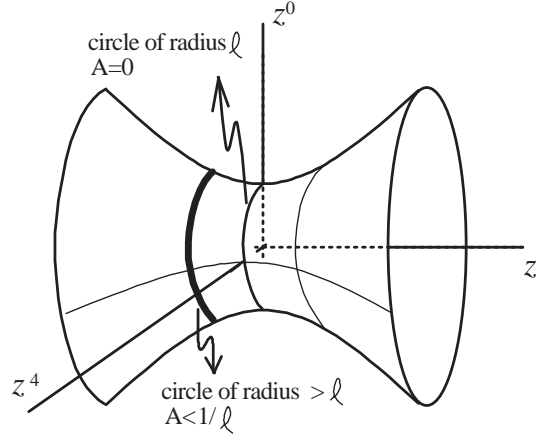
Figure 6.14: AdS 4-hyperboloid embedded in the 5D Minkowski spacetime. The origin of the AdS C-metric with $A < 1/\ell$ moves in the hyperboloid along the circle with z^1=constant< 0. When $A = 0$ this circle is at the plane $z^1 = 0$ and has a radius ℓ.

To summarize and conclude, we present the global description on the AdS hyperboloid of the AdS C-metric origin when the acceleration A varies from $+\infty$ to zero. When $A = +\infty$ the origin of the solution is represented in the hyperboloid by two mutual perpendicular straight null lines at 45° that result from the intersection of the hyperboloid surface defined by (6.41) and the $z^4 = \ell$ plane (see Fig. 6.12). When A belongs to $]1/\ell, +\infty[$, the origin of the solution is represented by two hyperbolic lines [see (6.44)] lying on the AdS hyperboloid and result from the intersection of (6.41) and the z^4=constant$> \ell$ plane [see Fig. 6.12.(a)]. As the acceleration approaches the value $A = 1/\ell$ the separation between the two hyperbolic lines increases. When $A = 1/\ell$ the separation between the two hyperbolic lines becomes infinite and they collapse into two half circles which, on identifying the ends of the AdS hyperboloid at both infinities, yields one full circle in the $z^0 - z^4$ plane at infinite z^1. At this point we see again that the value $A = 1/\ell$ sets a transition stage between $A > 1/\ell$ and $A < 1/\ell$. When A belongs to $]0, 1/\ell[$ the origin of the solution is described again by a circle [see (6.56)] in the $z^0 - z^4$ plane but now at a constant $z^1 < 0$. As the acceleration approaches the value $A = 0$, the radius of this circle decreases and when $A = 0$ the circle has a radius with value ℓ and is at $z^1 = 0$ (see Fig. 6.14) and we recover the usual AdS solution whose origin is at rest.

6.2 Pair of accelerated black holes in a flat background: the flat C-metric and Ernst solution

6.2.1 General properties of the flat C-metric and Ernst solution

The original flat C-metric has been found Levi-Civita [82] and by Weyl [83] in 1918-1919. In 1963 Ehlers and Kundt [100] have given the actual name to this solution. The physical interpretation of the flat C-metric remained unknown until 1970 when Kinnersley and Walker [84], in a pathbreaking work, have shown that the solution describes two uniformly accelerated black holes in opposite directions, with the acceleration being provided by strings or by a strut. In this section we will review the work of Kinnersley and Walker [84]. In this way, in the end of this chapter we will be able to make a comparison between the C-metric in an AdS, flat and dS background. From the charged flat C-metric, Ernst [85] has generated a knew exact solution in which the black hole pair is accelerated by an external electromagnetic field. We will also review briefly this solution.

Chapter 6. Pair of accelerated black holes: the C-metric in a generalized Λ background

6.2.1.a The flat C-metric

The gravitational field of the flat C-metric can be written as [84]

$$ds^2 = [A(x+y)]^{-2}(-\mathcal{F}dt^2 + \mathcal{F}^{-1}dy^2 + \mathcal{G}^{-1}dx^2 + \mathcal{G}d\phi^2)\,, \tag{6.57}$$

where

$$\begin{aligned}
\mathcal{F}(y) &= -1 + y^2 - 2mAy^3 + q^2A^2y^4, \\
\mathcal{G}(x) &= 1 - x^2 - 2mAx^3 - q^2A^2x^4\,,
\end{aligned} \tag{6.58}$$

and therefore we have now $\mathcal{F}(y) = -\mathcal{G}(-y)$. Note that when $\Lambda = 0$, the function $\mathcal{G}(x)$ behaves in the same manner described in the AdS case. The Maxwell field in the magnetic case is given by (6.5), while in the electric case it is given by (6.6). This solution depends on three parameters namely, $A > 0$ which is the acceleration of the black holes (see section 6.2.3), and m and q which are interpreted as the ADM mass and electromagnetic charge of the non-accelerated black holes, respectively. To justify this interpretation of m and q, apply to (6.57) the coordinate transformations [114], $\tau = A^{-1}t$, $\rho = (Ay)^{-1}$, together with (6.9) and setting $A = 0$ (and $\kappa = 1$, $\tilde{\phi} = \phi$) one obtains

$$ds^2 = -F(\rho)\,d\tau^2 + F^{-1}(\rho)\,d\rho^2 + \rho^2(d\theta^2 + \sin^2\theta\,d\phi^2)\,, \tag{6.59}$$

where $F(\rho) = 1 - 2m/\rho + q^2/\rho^2$. So, when the acceleration parameter vanishes, the flat C-metric, (6.57), reduces to the Schwarzschild and Reissner-Nordström black holes and the parameters m and q that are present in the flat C-metric are precisely the ADM mass and ADM electromagnetic charge of these non-accelerated black holes. The physical properties and interpretation of the flat C-metric have been analyzed in detail by Kinnersley and Walker [84].

Now, the general properties of the flat C-metric, in what concerns the issues of radial coordinate and curvature singularities, the analysis of the angular surfaces and conical singularities, and the issue of coordinate ranges are straightforwardly similar to the corresponding properties of the AdS C-metric analyzed in subsections 6.1.1.b, 6.1.1.c, and 6.1.1.d. For this reason we will not analyze again these properties in detail. We ask the reader to go back to subsection 6.1.1.b or to see [84] for details.

6.2.1.b The Ernst solution

Ernst [85] has employed a Harrison-type transformation to the charged flat C-metric in order to append a suitably chosen external electromagnetic field. With this procedure the Ernst solution is free of conical singularities at both poles and the acceleration that drives away the two oppositely charged Reissner-Nordström black holes is provided by the external electromagnetic field. The gravitational field of the Ernst solution is [85]

$$ds^2 = \frac{\Sigma^2(-\mathcal{F}dt^2 + \mathcal{F}^{-1}dy^2 + \mathcal{G}^{-1}dx^2 + \Sigma^{-4}\mathcal{G}\,d\phi^2)}{[A(x+y)]^2}\,, \tag{6.60}$$

where $\mathcal{F}(y)$ and $\mathcal{G}(x)$ are given by (6.58), and

$$\Sigma(x,y) = \left(1 + \frac{1}{2}q\,\mathcal{E}_0\,x\right)^2 + \frac{\mathcal{E}_0^2\,\mathcal{G}(x)}{4A^2\,(x+y)^2}\,. \tag{6.61}$$

In the electric solution one has $q \equiv e$ and $\mathcal{E}_0 \equiv E_0$, i.e., q and $\mathcal{E}_0$ are respectively the electric charge and the external electric field. In the magnetic solution one has $q \equiv g$ and $\mathcal{E}_0 \equiv B_0$, i.e., q and $\mathcal{E}_0$ are respectively the magnetic charge and the external magnetic field. The electromagnetic potential of the magnetic Ernst solution is [85]

$$A_\phi = -\frac{2}{\Sigma B_0}\left(1 + \frac{1}{2}g\,B_0\,x\right)\,. \tag{6.62}$$

while for the electric Ernst solution it is given by [101]

$$
\begin{aligned}
A_t &= qy - \frac{E_0}{2A^2}\frac{\mathcal{F}(y)}{(x+y)^2}\left(1 + e\,E_0\,x - \frac{1}{2}e\,E_0\,y\right)\\
&\quad - \frac{E_0}{2A^2}(1 + r_- Ay)(1 + r_+ Ay)(1 - e\,E_0\,y/2)\,,
\end{aligned}
\tag{6.63}
$$

with $r_+ r_- = e^2$ and $r_+ + r_- = 2m$. This exact solution describes two oppositely charged Reissner-Nordström black holes accelerating away from each other in a magnetic Melvin [102] or in an electric Melvin-like background, respectively.

Technically, the Harrison-type transformation employed to generate the Ernst solution introduces, in addition to the parameter κ, a new parameter, the external field $\mathcal{E}_0$ that when appropriately chosen allow us to eliminate the conical singularities at both poles. Indeed, applying a procedure analogous to the one employed in subsection 6.1.1.c, but now focused in spacetime (6.60), one introduces the new angular coordinates

$$
\bar{\theta} = \int_{x_{\mathrm{n}}}^{x}\tilde{\mathcal{G}}^{-1/2}dx\,,\qquad \bar{\phi} = \phi/\bar{\kappa}\,,
\tag{6.64}
$$

where $\tilde{\mathcal{G}}(x,y) = \Sigma^{-2}(x,y)\mathcal{G}(x)$. As before, the conical singularity at the south pole is avoided by choosing

$$
\bar{\kappa}^{-1} = \frac{1}{2}\left|\tilde{\mathcal{G}}'(x_{\mathrm{s}})\right|\,,
\tag{6.65}
$$

while the conical singularity at the north pole can now be also eliminated by choosing the value of the external field $\mathcal{E}_0$ to satisfy

$$
\left|\tilde{\mathcal{G}}'(x_{\mathrm{n}})\right| = \left|\tilde{\mathcal{G}}'(x_{\mathrm{s}})\right|\,.
\tag{6.66}
$$

An interesting support to the physical interpretation given to the Ernst solution is the fact that in the particle limit, i.e., for small values of mA, the condition (6.66) implies the classical Newton's law [85]

$$
q\,\mathcal{E}_0 \approx m\,A\,.
\tag{6.67}
$$

So, in this regime, the acceleration is indeed provided by the Lorentz force.

Remark that in a cosmological background we cannot remove the conical singularities through the application of the Harrison transformation [124]. Indeed, the Harrison transformation applied by Ernst does not leave invariant the cosmological term in the action. Therefore, applying the Harrison transformation to the cosmological C-metric solutions does not yield a new solution of the Einstein-Maxwell theory in a cosmological background.

6.2.2   Causal Structure of the flat C-metric

For a similar reason to the one that occurs in the AdS C-metric, due to the lower restriction on the value of y ($-x \leq y$), the choice of the Kruskal coordinates (and therefore the Carter-Penrose diagrams) for the flat C-metric depends on the angular direction x we are looking at [84, 104]. In fact, depending on the value of x, the region accessible to y might contain a different number roots of $\mathcal{F}$ (see Figs. 6.15, 6.17, and 6.19) and so the solution may have a different number of horizons. We have to consider separately three distinct sets of angular directions, namely (a) $x = x_{\mathrm{s}}$, (c) $x_{\mathrm{s}} < x < x_{\mathrm{n}}$, and (c) $x = x_{\mathrm{n}}$, where $x_{\mathrm{s}} = -1$ and $x_{\mathrm{n}} = +1$ when $A \to 0$. These three cases are perfectly identified in Figs. 6.15, 6.17, and 6.19. The technical procedures to obtain the Carter-Penrose diagrams of these flat cases (a), (b) and (c) is equal to the ones presented in the AdS cases (b), (c) and (d) of subsection 6.1.2.a, respectively. Hence, we will not present again the construction process that leads to the diagrams. We will only draw the diagrams, and even the discussion of their main features follows now directly from the analysis of subsection 6.1.2.a. Once again, the description of

the solution depends crucially on the values of m and q. We will consider the three most relevant solutions, namely: *A. Massless uncharged solution* $(m = 0, q = 0)$, *B. Massive uncharged solution* $(m > 0, q = 0)$, and *C. Massive charged solution* $(m \geq 0, q \neq 0)$. The causal diagrams of the Ernst solution are equal to the ones that describe the flat C-metric.

6.2.2.a   Massless uncharged solution ($m = 0$, $q = 0$)

In this case we have $x \in [x_s = -1, x_n = +1]$, $x = \cos\theta$, $\mathcal{G} = 1 - x^2 = \sin^2\theta$, $\kappa = 1$, $\tilde{\phi} = \phi$, and $\mathcal{F}(y) = y^2 - 1$. The general behavior of these functions for this case is represented in Fig. 6.15.
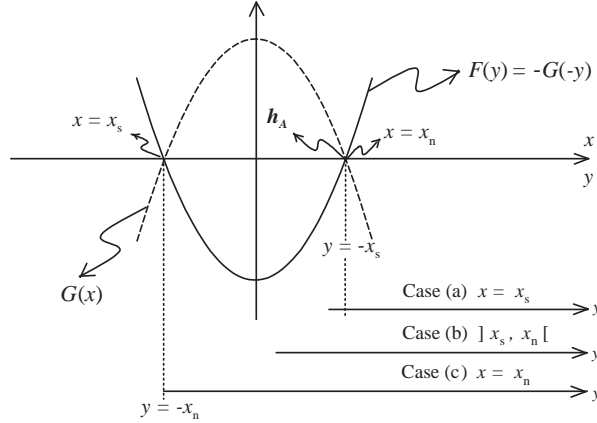
Figure 6.15: Shape of $\mathcal{G}(x)$ and $\mathcal{F}(y)$ for the $m = 0, q = 0$ flat C-metric and Ernst solution. The allowed range of x is between $x_s = -1$ and $x_n = +1$ where $\mathcal{G}(x)$ is positive and compact. The range of y is restricted to $-x \leq y < +\infty$. The presence of an accelerated horizon is indicated by h_A.

The Carter-Penrose diagrams of the massless uncharged flat C-metric and Ernst solution are sketched in Fig. 6.16 for the three angular directions, (a), (b) and (c), specified above.
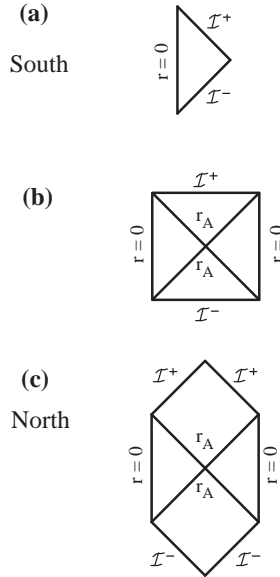
Figure 6.16: Carter-Penrose diagrams concerning the $m = 0, q = 0$ flat C-metric and Ernst solution studied in section 6.2.2.a. Case (a) describes the solution seen from the south pole, case (c) applies to the equatorial vicinity, and case (c) describes the solution seen from the north pole. The accelerated horizon is represented by r_A. $\mathcal{I}^-$ and $\mathcal{I}^+$ represent respectively the past and future infinity ($r = +\infty$). $r = 0$ corresponds to $y = +\infty$ and $r = +\infty$ corresponds to $y = -x$.

6.2.2.b   Massive uncharged solution ($m > 0$, $q = 0$)

As occurs with the AdS case (see subsection 6.1.2.a), we will consider only the case with small mass or acceleration, i.e., we require $mA < 3^{-3/2}$, in order to have compact angular surfaces (see discussion on the text of Fig. 6.17). We also demand x to belong to the range $[x_\mathrm{s}, x_\mathrm{n}]$ (see Fig. 6.17) where $\mathcal{G}(x) \geq 0$ and such that $x_\mathrm{s} \to -1$ and $x_\mathrm{n} \to +1$ when $mA \to 0$. By satisfying the two above conditions we endow the $t =$constant and $r =$constant surfaces with the topology of a compact surface.
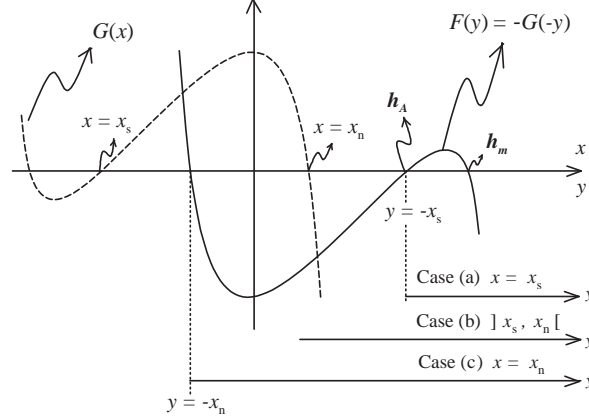
Figure 6.17: Shape of $\mathcal{G}(x)$ and $\mathcal{F}(y)$ for the $27m^2A^2 < 1 - 9m^2\Lambda$, and $q = 0$ flat C-metric and Ernst solution. The allowed range of x is between x_s and x_n where $\mathcal{G}(x)$ is positive and compact. The range of y is restricted to $-x \leq y < +\infty$. The presence of an accelerated horizon is indicated by h_A and the Schwarzschild-like horizon by h_m. For completeness we comment on two other cases not studied in the text: for $27m^2A^2 = 1 - 9m^2\Lambda$, $\mathcal{F}(y)$ is zero at its local maximum, i.e., h_A and h_m coincide. For $27m^2A^2 > 1 - 9m^2\Lambda$, $\mathcal{F}(y)$ is always negative in the allowed range of y.

The Carter-Penrose diagrams of the $27m^2A^2 < 1 - 9m^2\Lambda$, and $q = 0$ flat C-metric are sketched in Fig. 6.18 for the three angular directions, (a), (b) and (c), specified above.
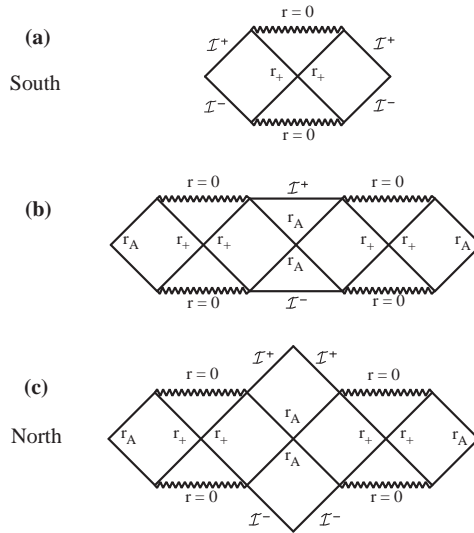
Figure 6.18: Carter-Penrose diagrams of the $27m^2A^2 < 1 - 9m^2\Lambda$, and $q = 0$ flat C-metric discussed in section 6.2.2.b. Case (a) describes the solution seen from the south pole, case (c) applies to the equatorial vicinity, and case (c) describes the solution seen from the north pole. The zigzag line represents a curvature singularity, the accelerated horizon is represented by r_A. It coincides with the cosmological horizon and has a non-spherical shape. The Schwarzschild-like horizon is sketched as r_+. $r = 0$ corresponds to $y = +\infty$ and $r = +\infty$ ($\mathcal{I}^-$ and $\mathcal{I}^+$) corresponds to $y = -x$.

6.2.2.c   Massive charged solution ($m > 0$, $q \neq 0$)

When both the mass and charge parameters are non-zero, depending on the values of the parameters A, m and q, $\mathcal{G}(x)$ can be positive in a single compact interval, $]x_\mathrm{s}, x_\mathrm{n}[$, or in two distinct compact intervals, $]x'_\mathrm{s}, x'_\mathrm{n}[$ and $]x_\mathrm{s}, x_\mathrm{n}[$, say (see Fig. 6.19). In this latter case we will work only with the interval $[x_\mathrm{s}, x_\mathrm{n}]$ (say) for which the charged solutions are in the same sector of those we have analyzed in the last two subsections when $q \to 0$.
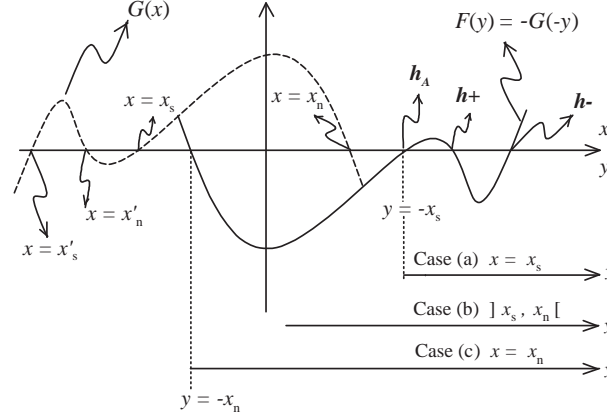
Figure 6.19: Shape of $\mathcal{G}(x)$ and $\mathcal{F}(y)$ for the non-extreme charged massive flat C-metric and Ernst solution. The allowed range of x is between x_s and x_n where $\mathcal{G}(x)$ is positive and compact. The presence of an accelerated horizon is indicated by h_A and the inner and outer charged horizons by $h-$ and $h+$. In the extreme cases, $h-$ and $h+$ superpose each other. Note that when y_+ and y_A coincide, the same occurs with x_s and x_0.

The Carter-Penrose diagrams of the charged massive flat C-metric and Ernst solution are sketched in Fig. 6.20 for the three angular directions, (a), (b) and (c), specified above.

6.2.3   Physical interpretation of the flat C-metric

The parameter A that is found in the flat C-metric is interpreted as being an acceleration and the flat C-metric describes a pair of black holes accelerating away from each other. In this section we will justify this statement.

6.2.3.a   Description of the $m = 0$, $q = 0$ solution

Use of (6.7), (6.9) with $\kappa = 1$ and $\tilde{\phi} = \phi$, together with $u = t + \int \mathcal{F}(y)^{-1}dy$ on (6.57) yields [84]

$$ds^2 = \left(1 - 2Ar\cos\theta - A^2 r^2 \sin^2\theta\right) du^2 + 2dudr - 2Ar^2 \sin\theta\, dud\theta - r^2\left(d\theta^2 + \sin^2\theta d\phi^2\right). \quad (6.68)$$

As noticed by Kinnersly and Walker [84] this spacetime is closely related to the ones discussed by Newman and Unti. There is a coordinate transformation that allows to recast (6.68) into a Minkowski form, namely

$$
\begin{aligned}
T &= (A^{-1} - r\cos\theta)\sinh(Au) + r\cosh(Au)\,, \\
Z &= (A^{-1} - r\cos\theta)\cosh(Au) + r\sinh(Au)\,, \\
X &= r\sin\theta\cos\phi\,, \\
Y &= r\sin\theta\sin\phi\,.
\end{aligned}
\quad (6.69)
$$
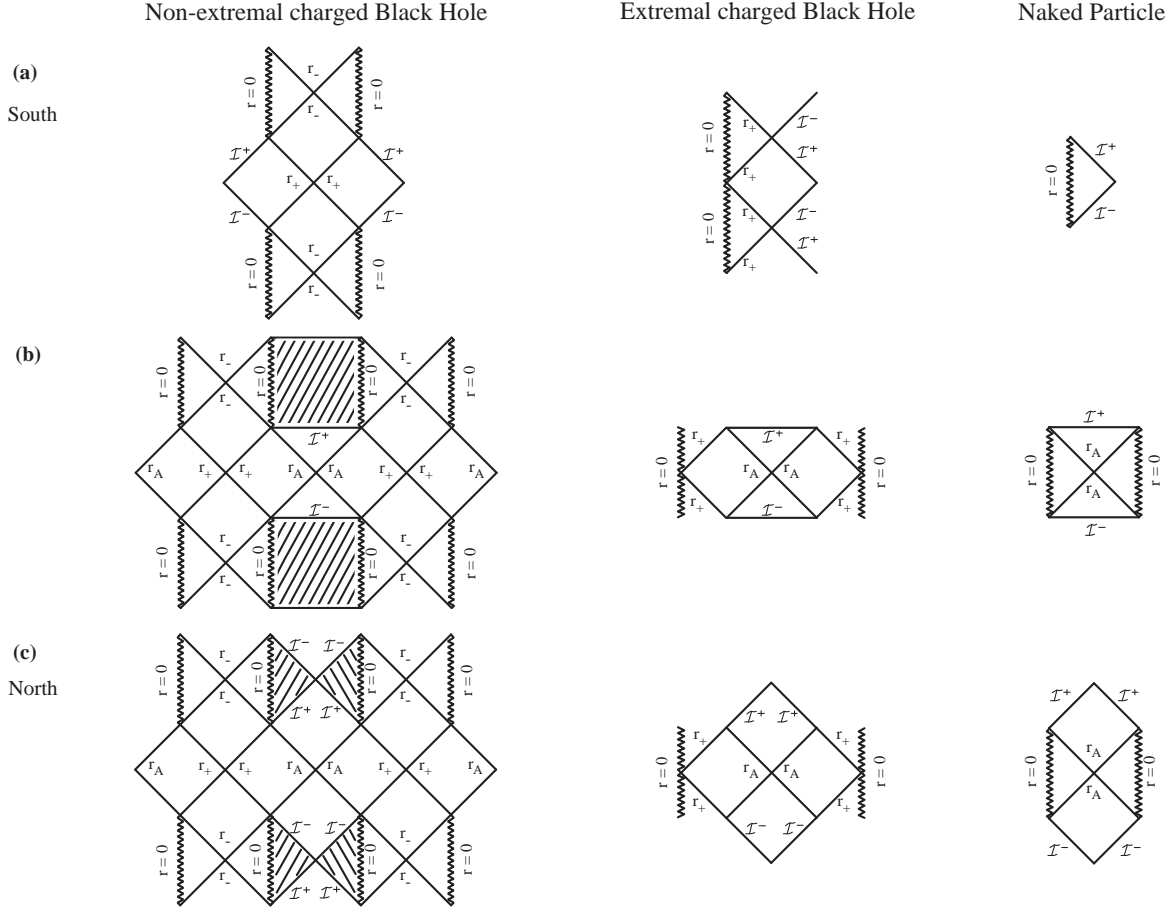
Figure 6.20: Carter-Penrose diagrams of the charged massive flat C-metric and Ernst solution . Case (a) describes the solution seen from the south pole, case (c) applies to the equatorial vicinity, and case (c) describes the solution seen from the north pole. The zigzag line represents a curvature singularity, an accelerated horizon is represented by r_A, the inner and outer charge associated horizons are sketched as r_- and r_+. $\mathcal{I}^-$ and $\mathcal{I}^+$ represent respectively the past and future infinity $(r = +\infty)$. $r = 0$ corresponds to $y = +\infty$ and $r = +\infty$ corresponds to $y = -x$.

Indeed, under this transformation the massless neutral flat C-metric transforms into

$$ds^2 = -dT^2 + dX^2 + dY^2 + dZ^2 \,, \tag{6.70}$$

and hence, the $m = 0$ and $q = 0$ flat C-metric is a Minkowski spacetime. But we can extract more information from this analysis. Indeed, let us analyze with some detail the properties of the origin of the radial coordinate, $r = 0$. This origin moves according to [see (6.69)]

$$X = 0 \,, \quad Y = 0 \,, \quad \text{and} \quad Z^2 - T^2 = A^{-2} \,. \tag{6.71}$$

These equations define two hyperbolic lines that tell us that the origin is subjected to a uniform acceleration, A, and consequently moves along a hyperbolic worldline, describing a Rindler motion.

Let us now address the issue of the acceleration source and its localization. In the massless uncharged dS C-metric, observers that move along radial worldlines with $r =$ const and $\theta =$ const describe the Rindler-like hyperbola [see (6.84)]

$$Z^2 - T^2 = (A^{-1} - r\cos\theta)^2 - r^2 \,. \tag{6.72}$$

Thus, observers that move in the region $\theta = 0$ describe the the hyperbolic line $Z^2 - T^2 < A^{-2}$ (which is in between the two $r = 0$ hyperbolas, $Z^2 - T^2 = A^{-2}$), while observers in the region $\theta = \pi$ follow the curve $Z^2 - T^2 > A^{-2}$. When we put m or q different from zero, each of the

two hyperbolas assigned to $r = 0$ represents the accelerated motion of a black hole. Hence, from (6.72) we conclude that the north pole axis is in the region between the two black holes [see Fig. 6.12.(b)]. When the conical singularity is at the north pole we then have a strut in between the black holes, while when we choose the parameters such that the conical singularity is at the south pole we have two strings from each of the black holes into infinity that accelerates them. Notice also that the original flat C-metric coordinates introduced in (6.57) cover only the half-space $Z > -T$. The Kruskal construction extends this solution to include also the $Z < -T$ region and so, in the extended solution, $r = 0$ is associated to two hyperbolas that represent two accelerated points [see Fig. 6.12.(b)] that approach asymptotically the Rindler acceleration horizon (r_A).

6.2.3.b   Pair of accelerated black holes ($m > 0$, $q \neq 0$)

The massive and charged solutions describe two black holes accelerating away from each other. This interpretation follows directly from the Carter-Penrose diagrams, Fig. 6.16, Fig. 6.18 and Fig. 6.20, in a way already explained in subsection 6.1.3.a. In Fig. 6.16 we identify the two hyperbolas $r = 0$ (represented by two timelike lines) approaching asymptotically the Rindler acceleration horizon (r_A). When we add a mass or a charge to the solution we conclude that each of these two simple hyperbolas $r = 0$ are replaced by the more complex structure that represents a Schwarzschild black hole (see Fig. 6.18) or a Reissner-Nordström black hole (see Fig. 6.20).

At this point, a remark is relevant. Israel and Khan [90] (see also Bach and Weyl [91], Aryal, Ford and Vilenkin [92], and Costa and Perry [93]) have found a $\Lambda = 0$ solution that represents two (or more) collinear Schwarzschild black holes interacting with each other in such a way that allows dynamical equilibrium. In this solution, the two black holes are connected by a strut that exerts an outward pressure which cancels the inward gravitational attraction and so the distance between the two black holes remains fixed [90]. Now, the C-metric solution reduces to a single non-accelerated black hole free of struts or strings when the acceleration parameter A vanishes (see subsection 6.2.1.a). Thus, when we take the limit $A = 0$, the C-metric does not reduce to the static solution of Israel and Khan. The reason for this behavior can be found in the Carter-Penrose diagrams of the C-metric. For example, looking into Fig. 6.18.(c) [redrawn again in Fig. 6.21.(a) with the motion of a light ray that will be described just below] which represents the massive uncharged flat C-metric along the north pole, we conclude that a null ray sent from the vicinity of one of the black holes can never cross the acceleration horizon (r_A) into the other black hole. Indeed, recall that in these diagrams the vertical axes represents the time flow and that light rays move along 45° lines. Thus, a null ray that is emitted from a region next to the horizon r_+ of the left black hole of Fig. 6.21.(a) can pass through the acceleration horizon r_A and, once it has done this, we will necessarily proceed into infinity $\mathcal{I}^+$ [see Fig. 6.21.(a)]. This null ray cannot enter the right region of Fig. 6.21.(a) and, in particular, it cannot hit the horizon r_+ of the right black hole. So, if the two black holes cannot communicate through a null ray they cannot interact gravitationally. The only interaction that is present in the system is between the strut and each one of the black holes, that suffer an acceleration which is only furnished by the strut's pressure. That the limit $A = 0$ does not yield the solution [90] can also be inferred from [107], where the flat C-metric is obtained from the the two black hole solution of [90] but through a singular limit in which several quantities go appropriately to infinity. The situation is completely different in the case of the Israel-Khan solution, whose causal diagram is sketched in Fig. 6.21.(b). In this case, a null ray that is emitted from a region next to the horizon r_+ of the left black hole can hit the horizon r_+ of the right black hole. Hence, in the Israel-Khan solution the two black holes can communicate through a null ray and so they interact gravitationally. Note also that the acceleration horizon is absent in the causal diagram of the Israel-Khan solution, as expected for a static solution.

The Israel-Khan solution [90] is valid for $\Lambda = 0$ but, although it has not been done, it can be extended in principle for generic Λ. Hence, the above remark holds also for generic Λ, as has already briefly mentioned in the end of subsection 6.1.3.a.

A similar discussion also applies to the Ernst solution. In this solution, there is no gravitational

force between the two Reissner-Nordtröm black holes. They accelerate apart only subjected to the Lorentz force provided for the external electromagnetic field, and when $A = 0$ the Ernst solution reduces to a single non-accelerated Reissner-Nordtröm black hole. On the other side, Tomimatsu [94] has found a solution, that is the charged counterpart of the neutral Israel-Khan solution [90], in which two Reissner-Nordtröm black holes are held in equilibrium. In this case the gravitational attraction between the black holes is cancelled by the Coulomb repulsion, and this occurs only when the black holes are extreme, $M_i = Q_i$. Tomimatsu has generalized for the black hole case, the relativistic treatment used by Bonnor [95] and Ohta and Kimura [96] to study the equilibrium system of two charged particles.
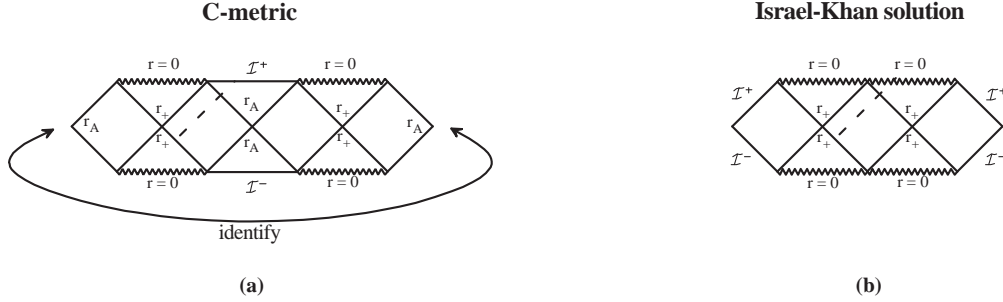
Figure 6.21: The dashed line represents a null ray that is sent from the vicinity of the event horizon of one of the black holes towards the other black hole. (a) In the case of the C-metric this ray can never reach the other black. (b) In the Israel-Khan solution the null ray can reach the second black hole.

6.3 Pair of accelerated black holes in a de Sitter background: the dS C-metric

The plan of this section is as follows. In section 6.3.1 we present the dS C-metric and analyze its curvature and conical singularities. In section 6.3.2 we study the causal diagrams of the solution. In section 6.3.3 we give and justify a physical interpretation to the solution. The description of the solution in the dS 4-hyperboloid and the physics of the strut are analyzed.

6.3.1   General properties of the dS C-metric

6.3.1.a   The dS C-metric

The dS C-metric, i.e., the C-metric with positive cosmological constant Λ, has been obtained by Plebański and Demiański [86]. For zero rotation and zero NUT parameter, the gravitational field of the dS C-metric can be written as

$$ds^2 = [A(x+y)]^{-2}(-\mathcal{F}dt^2 + \mathcal{F}^{-1}dy^2 + \mathcal{G}^{-1}dx^2 + \mathcal{G}d\phi^2)\,, \tag{6.73}$$

where

$$\mathcal{F}(y) = -\left(\frac{1}{\ell^2 A^2} + 1\right) + y^2 - 2mAy^3 + q^2 A^2 y^4,$$
$$\mathcal{G}(x) = 1 - x^2 - 2mAx^3 - q^2 A^2 x^4\,. \tag{6.74}$$

The Maxwell field in the magnetic case is given by (6.5), while in the electric case it is given by (6.6). This solution depends on four parameters namely, the cosmological length $\ell^2 \equiv 3/\Lambda$, $A > 0$ which is the acceleration of the black holes (see subsection 6.3.3), and m and q which are interpreted as the ADM mass and electromagnetic charge of the non-accelerated black holes, respectively (see subsection 6.3.1.b). The physical properties and interpretation of this solution have been analyzed by Dias and Lemos [88], and by Podolský and Griffiths [120].

Now, the general properties of the dS C-metric, in what concerns the issues of radial coordinate and curvature singularities, the analysis of the angular surfaces and conical singularities, and the issue of coordinate ranges are straightforwardly similar to the corresponding properties of the AdS C-metric analyzed in subsections 6.1.1.b, 6.1.1.c, and 6.1.1.d. For this reason we will not analyze again these properties in detail. We will only briefly mention the main features, and we ask the reader to go back to subsection 6.1.1.b or to see [88] for details.

As occurs with the AdS C-metric (see subsection 6.1.1.b), we can define a radial coordinate given by (6.7). The Kretschmann scalar is also given by (6.8), and indicates that the dS C-metric has a curvature singularity at $y = +\infty$, and y must belong to the range $-x \leq y < +\infty$. The point $y = -x$ corresponds to a point that is infinitely far away from the curvature singularity, thus as y increases we approach the curvature singularity and $y + x$ is the inverse of a radial coordinate. At most, $\mathcal{F}(y)$ can have four real zeros which we label in ascending order by $y_{\text{neg}} < 0 < y_A \leq y_+ \leq y_-$. The roots y_- and y_+ are respectively the inner and outer charged black hole horizons, and y_A is an acceleration horizon which coincides with the cosmological horizon and has a non-spherical shape, although the topology is spherical. The negative root y_{neg} satisfies $y_{\text{neg}} < -x$ and has no physical significance, i.e., it does not belong to the range accessible to y.

As occurs with the AdS C-metric (see subsection 6.1.1.c), we will demand that x belongs to the interval $x_{\text{s}} \leq x \leq x_{\text{n}}$, sketched onwards in the appropriate figures, where $\mathcal{G}(x) \geq 0$. By doing this we guarantee that the metric has the correct signature $(- + + +)$ [see (6.73)] and that the angular surfaces $t =$const and $y =$const are compact. In these angular surfaces we can also define, through (6.9), two new coordinates, θ and $\tilde{\phi}$, where $\tilde{\phi}$ ranges between $[0, 2\pi]$ and κ is an arbitrary positive constant which will be discussed later. The coordinate θ ranges between the north pole, $\theta = \theta_{\text{n}} = 0$, and the south pole, $\theta = \theta_{\text{s}}$ (not necessarily at π). Rewritten as a function of these new coordinates, the angular part of the metric becomes $d\theta^2 + \kappa^2 \mathcal{G} \, d\tilde{\phi}^2$. Note that when we set $A = 0$ we have $x_{\text{s}} \leq x \leq x_{\text{n}}$, with $x_{\text{s}} = -1$ and $x_{\text{n}} = 1$, $x = \cos\theta$, $\mathcal{G} = 1 - x^2 = \sin^2\theta$, and $\kappa = 1$. Therefore, in this case the compact angular surface $\tilde{S}^2$ is a round S^2 sphere which justifies the label given to the new angular coordinates. When we set $A \neq 0$ the compact angular surface turns into a deformed 2-sphere that we represent onwards by $\tilde{S}^2$.

Finally, note again that when m or q are not zero there is a curvature singularity at $r = 0$. Therefore, we restrict the radial coordinate to the range $[0, +\infty[$. On the other hand, we have restricted x to belong to the range $[x_{\text{s}}, x_{\text{n}}]$ where $\mathcal{G}(x) \geq 0$. From $Ar = (x + y)^{-1}$ we then conclude that y must belong to the range $-x \leq y < +\infty$. Indeed, $y = -x$ corresponds to $r = +\infty$, and $y = +\infty$ to $r = 0$. However, when both m and q vanish there are no restrictions on the ranges of r and y (i.e., $-\infty < r < +\infty$ and $-\infty < y < +\infty$) since in this case there is no curvature singularity at the origin of r to justify the constraint on the coordinates.

6.3.1.b   Mass and charge parameters

In this subsection, one gives the physical interpretation of parameters m and q that appear in the dS C-metric. Applying to (6.73) the coordinate transformations [120], $\tau = \sqrt{1 + \ell^2 A^2} A^{-1} t$, $\rho = \sqrt{1 + \ell^2 A^2} (Ay)^{-1}$, together with (6.9) and setting $A = 0$ (and $\kappa = 1$, $\tilde{\phi} = \phi$) one obtains

$$ds^2 = -F(\rho) \, d\tau^2 + F^{-1}(\rho) \, d\rho^2 + \rho^2 (d\theta^2 + \sin^2\theta \, d\phi^2) \,, \tag{6.75}$$

where $F(\rho) = 1 - \rho^2/\ell^2 - 2m/\rho + q^2/\rho^2$. So, when the acceleration parameter vanishes, the dS C-metric, (6.73), reduces to the dS-Schwarzschild and dS−Reissner-Nordström black holes and the parameters m and q that are present in the dS C-metric are precisely the ADM mass and ADM electromagnetic charge of these non-accelerated black holes.

6.3.2   Causal Structure of the dS C-metric

In this section we analyze the causal structure of the solution. The original dS C-metric, (6.73), is not geodesically complete. To obtain the maximal analytic spacetime, i.e., to draw the Carter-Penrose diagrams we have to introduce the usual null Kruskal coordinates. The technical procedure

to obtain the Carter-Penrose diagram is similar to the one presented in subsection 6.1.2. Hence, we will not present again the construction process that leads to the diagrams. We will only discuss the main features and the diagrams. The description of the solution depends crucially on the values of m and q. We will consider the three most relevant solutions, namely: *A. Massless uncharged solution ($m = 0$, $q = 0$)*, *B. Massive uncharged solution ($m > 0$, $q = 0$)*, and *C. Massive charged solution ($m \geq 0$, $q \neq 0$)*.

6.3.2.a   Massless uncharged solution ($m = 0$, $q = 0$)

In this case we have $x \in [x_s = -1, x_n = +1]$, $x = \cos\theta$, $\mathcal{G} = 1 - x^2 = \sin^2\theta$, $\kappa = 1$ (and so $\tilde{\phi} = \phi$) and

$$\mathcal{F}(y) = y^2 - y_+^2 \quad \text{with} \quad y_+ = \sqrt{1 + \frac{1}{\ell^2 A^2}} \,. \tag{6.76}$$

The general behavior of these functions for this case is represented in Fig. 6.22.

The angular surfaces Σ (t =const and r =const) are spheres and both the north and south poles are free of conical singularities. The origin of the radial coordinate r has no curvature singularity and therefore both r and y can lie in the range $]-\infty, +\infty[$. However, in the realistic general case, where m or q are non-zero, there is a curvature singularity at $r = 0$. Since the discussion of the present section is only a preliminary to that of the massive general case we will treat the origin $r = 0$ as if it had a curvature singularity and thus we admit that r belongs to the range $[0, +\infty[$ and y lies in the region $-x \leq y < +\infty$. We leave a discussion on the extension to negative values of r to section 6.3.3.a.
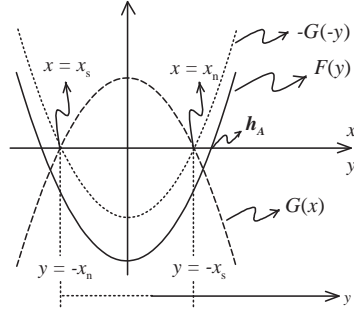
Figure 6.22: Shape of $\mathcal{G}(x)$ and $\mathcal{F}(y)$ for the $m = 0, q = 0$ dS C-metric. The allowed range of x is between $x_s = -1$ and $x_n = +1$ where $\mathcal{G}(x)$ is positive and compact. The range of y is restricted to $-x \leq y < +\infty$. The presence of an accelerated horizon is indicated by h_A. It coincides with the cosmological horizon of the solution and has a non-spherical shape.

The construction of the Carter-Penrose diagram follows directly the one given in case (c) of subsection 6.1.2.a. The Carter-Penrose diagram of the massless uncharged dS C-metric is sketched in Fig. 6.23. $r = 0$ is represented by a timelike line while $r = +\infty$ is a spacelike line (with $\mathcal{I}^-$ and $\mathcal{I}^+$ representing, respectively, the past and future infinity). The two mutual perpendicular straight null lines at $45°$, $u'v' = 0$, represent a Rindler-like accelerated horizon.
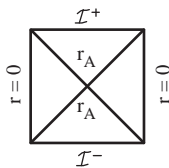
Figure 6.23: Carter-Penrose diagram concerning the $m = 0, q = 0$ dS C-metric studied in section 6.3.2.a. The accelerated horizon is represented by r_A. It coincides with the cosmological horizon and has a non-spherical shape. $\mathcal{I}^-$ and $\mathcal{I}^+$ represent respectively the past and future infinity ($r = +\infty$). $r = 0$ corresponds to $y = +\infty$ and $r = +\infty$ corresponds to $y = -x$.

To end this subsection it is important to remark that, contrary to what happens in the C-metric
with $\Lambda < 0$ [87] and with $\Lambda = 0$ [84], the presence of the acceleration in the $\Lambda > 0$ C-metric does
not introduce an extra horizon relatively to the $A = 0$ solution. Indeed, in the dS C-metric the
acceleration horizon coincides with the cosmological horizon that is already present in the $A = 0$
solution. However, in the $A = 0$ solution the cosmological horizon has the topology of a round sphere,
while in the dS C-metric ($A \neq 0$) the presence of the acceleration induces a non-spherical shape in
the acceleration (cosmological) horizon. This conclusion is set from the expression of the radius of
the horizon, $r_A = A^{-1}(x + y_+)^{-1}$. It varies with the angular direction $x = \cos\theta$ and depends on the
value of A [see (6.76)]. Another important difference between the causal structure of the dS C-metric
and the causal structure of the $\Lambda = 0$ and the $\Lambda < 0$ cases is the fact that the general features of
the Carter-Penrose diagram of the dS C-metric are independent of the angular coordinate $x = \cos\theta$.
Indeed, in the $\Lambda < 0$ case (see subsection 6.1.2.a and [87]) and in the $\Lambda = 0$ case (see subsection 6.2.2
and [84]), the Carter-Penrose diagram at the north pole direction is substantially different from the
one along the south pole direction and different from the diagram along the equator direction (see
[84, 87]).

6.3.2.b   Massive uncharged solution ($m > 0$, $q = 0$)
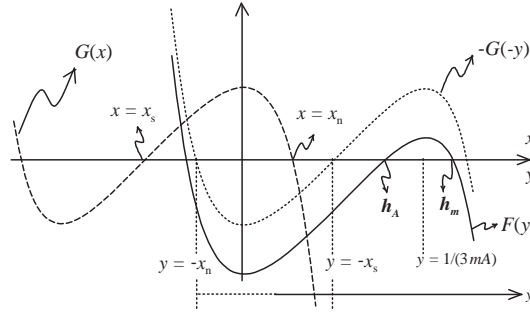
Figure 6.24: Shape of $\mathcal{G}(x)$ and $\mathcal{F}(y)$ for the $27m^2A^2 < 1 - 9m^2\Lambda$, and $q = 0$ dS C-metric (case
(i) in the text). The allowed range of x is between x_s and x_n where $\mathcal{G}(x)$ is positive and compact.
The range of y is restricted to $-x \leq y < +\infty$. The presence of an accelerated horizon (which
coincides with the cosmological horizon and has a non-spherical shape) is indicated by h_A and the
Schwarzschild-like horizon by h_m. For completeness we comment on two other cases studied in the
text: for $27m^2A^2 = 1 - 9m^2\Lambda$ (case (ii) in the text), $\mathcal{F}(y)$ is zero at its local maximum, i.e., h_A and
h_m coincide. For $27m^2A^2 > 1 - 9m^2\Lambda$ (case (iii) in the text), $\mathcal{F}(y)$ is always negative in the allowed
range of y.

The construction of the Carter-Penrose diagram for the $m > 0$ dS C-metric follows up directly from
the last subsection. We will consider the small mass or acceleration case, i.e., we require $27m^2A^2 < 1$
and we also demand x to belong to the range $[x_n, x_s]$ (represented in Fig. 6.24 and such that $x_s \to -1$
and $x_n \to +1$ when $mA \to 0$) where $\mathcal{G}(x) \geq 0$. By satisfying the two above conditions we endow
the $t =$const and $r =$const surfaces Σ with the topology of a compact surface. For $27m^2A^2 \geq 1$ this
surface is an open one and will not be discussed.

Now we turn our attention to the behavior of function $\mathcal{F}(y)$. We have to consider three distinct
cases (see Fig. 6.25), namely: (i) pair of non-extreme dS-Schwarzschild black holes ($27m^2A^2 <
1 - 9m^2\Lambda$) for which $\mathcal{F}(y = 1/3mA) > 0$ (see Fig. 6.24), (ii) pair of extreme dS-Schwarzschild black
holes ($27m^2A^2 = 1 - 9m^2\Lambda$) for which $\mathcal{F}(y = 1/3mA) = 0$, and (iii) case $27m^2A^2 > 1 - 9m^2\Lambda$
for which $\mathcal{F}(y)$ is always negative in the allowed range for y. This last case represents a naked
particle and will not be discussed further. Notice that when we set $A = 0$ in the above relations we
get the known results [254] for the non-accelerated dS spacetime, namely: for $9m^2\Lambda < 1$ we have
the non-extreme dS-Schwarzschild solution and for $9m^2\Lambda = 1$ we get the extreme dS-Schwarzschild
solution. In what follows we will draw the Carter-Penrose diagrams of cases (i) and (ii).
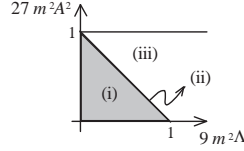
Figure 6.25: Allowed ranges of the parameters Λ, A, and m for the cases (i), (ii), and (iii) of the uncharged massive dS C-metric discussed in the text of section 6.3.2.b.

(i) Non-extreme Black Hole

(ii) Extreme Black Hole
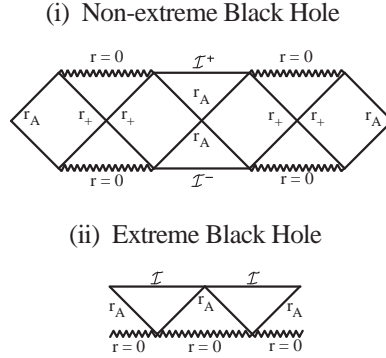
Figure 6.26: (i) Carter-Penrose diagram of the $27m^2A^2 < 1 - 9m^2\Lambda$, and $q = 0$ dS C-metric discussed in case (i) of section 6.3.2.b. The zigzag line represents a curvature singularity, the accelerated horizon is represented by r_A. It coincides with the cosmological horizon and has a non-spherical shape. The Schwarzschild-like horizon is sketched as r_+. $r = 0$ corresponds to $y = +\infty$ and $r = +\infty$ ($\mathcal{I}^-$ and $\mathcal{I}^+$) corresponds to $y = -x$. (ii) Carter-Penrose diagram of the degenerate case (ii), $27m^2A^2 = 1 - 9m^2\Lambda$ and $q = 0$, discussed in the text of section 6.3.2.b. The accelerated horizon r_A coincides with the Schwarzschild-like horizon r_+.

(i) *Pair of non-extreme dS-Schwarzschild black holes* $(27m^2A^2 < 1 - 9m^2\Lambda)$: the technical procedure to obtain the Carter-Penrose diagram is similar to the one described along section 6.3.2.a. In what concerns the physical conclusions, we will see that the essential difference is the presence of an extra horizon, a Schwarzschild-like horizon (r_+) due to the non-vanishing mass parameter, in addition to the accelerated Rindler-like horizon (r_A). Another important difference is the presence of a curvature singularity at the origin of the radial coordinate and the existence of a conical singularity at one of the poles. The Carter-Penrose diagram is drawn in Fig. 6.26.(i) and has a structure that can be divided into left, middle and right regions. The middle region contains the spacelike infinity (with $\mathcal{I}^-$ and $\mathcal{I}^+$ representing, respectively, the past and future infinity) and an accelerated Rindler-like horizon, $r_A = [A(x - x_-)]^{-1}$, that was already present in the $m = 0$ corresponding diagram [see Fig. 6.23]. The left and right regions both contain a spacelike curvature singularity at $r = 0$ and a Schwarzschild-like horizon, r_+. This diagram is analogous to the one of the non-accelerated $(A = 0)$ dS-Schwarzschild solution. However, in the $A = 0$ solution the cosmological and black hole horizons have the topology of a round sphere, while in the dS C-metric $(A \neq 0)$ the presence of the acceleration induces a non-spherical shape in the acceleration horizon (that coincides with the cosmological horizon) and in the black hole horizon. Indeed, notice that once we find the zero, y_h, of $\mathcal{F}(y)$ that corresponds to an accelerated or black hole horizon, the position of these horizons depends on the angular coordinate x since $r_h = [A(x + y_h)]^{-1}$. In section 6.3.3.b we will justify that this solution describes a pair of accelerated dS-Schwarzschild black holes.

(ii) *Pair of extreme dS-Schwarzschild black holes* $(27m^2A^2 = 1 - 9m^2\Lambda)$: for this range of values, we have a degenerate case in which the size of the black hole horizon approaches and equals the size of the acceleration horizon. In this case, as we shall see in section 6.3.3.b, the dS C-metric describes a pair of accelerated extreme dS-Schwarzschild black holes. The Carter-Penrose diagram of this solution is sketched in Fig. 6.26.(ii). It should be noted that for this sector of the solution,

and as occurs with the $A = 0$ case, there is an appropriate limiting procedure (see chapter 7 and [89]) that takes this solution into the Nariai C-metric, i.e., the accelerated counterpart of the Nariai solution [125].

6.3.2.c   Massive charged solution ($m > 0$, $q \neq 0$)

When both the mass and charge parameters are non-zero, depending on the values of the parameters, $\mathcal{G}(x)$ can be positive in a single compact interval, $]x_{\mathrm{s}}, x_{\mathrm{n}}[$, or in two distinct compact intervals, $]x_{\mathrm{s}}, x_{\mathrm{n}}[$ and $]x'_{\mathrm{s}}, x'_{\mathrm{n}}[$, say. We require that x belongs to the interval $[x_{\mathrm{s}}, x_{\mathrm{n}}]$ (sketched in Fig. 6.27) for which the charged solutions are in the same sector of those we have analyzed in the last two subsections when $q \to 0$. Defining

$$\beta \equiv \frac{q^2}{m^2}, \quad 0 < \beta \leq \frac{9}{8}, \quad \alpha_{\pm} \equiv 1 \pm \sqrt{1 - \frac{8}{9}\beta},$$

$$\sigma(\beta, \alpha_{\pm}) = \frac{(4\beta)^2(3\alpha_{\pm})^2 - 8\beta(3\alpha_{\pm})^3 + \beta(3\alpha_{\pm})^4}{(4\beta)^4},$$

$$(6.77)$$

the above requirement is fulfilled by the parameter range $m^2 A^2 < \sigma(\beta, \alpha_-)$. Now we look into the behavior of the function $\mathcal{F}(y)$. Depending on the sign of $\mathcal{F}(y)$ at y_{t} and y_{b} (with $y_{\mathrm{t}} = \frac{3\alpha_-}{4\beta m A}$ and $y_{\mathrm{b}} = \frac{3\alpha_+}{4\beta m A}$ being the points represented in Fig. 6.27 where the derivative of $\mathcal{F}(y)$ vanishes) we can group the solutions into five different relevant physical classes, namely: (i) $\mathcal{F}(y_{\mathrm{t}}) > 0$ and $\mathcal{F}(y_{\mathrm{b}}) < 0$, (ii) $\mathcal{F}(y_{\mathrm{t}}) > 0$ and $\mathcal{F}(y_{\mathrm{b}}) = 0$, (iii) $\mathcal{F}(y_{\mathrm{t}}) = 0$ and $\mathcal{F}(y_{\mathrm{b}}) < 0$, (iv) $\mathcal{F}(y_{\mathrm{t}}) > 0$ and $\mathcal{F}(y_{\mathrm{b}}) > 0$, and (v) $\mathcal{F}(y_{\mathrm{t}}) < 0$ and $\mathcal{F}(y_{\mathrm{b}}) < 0$. The ranges of parameters Λ, A, m, and β that correspond to these five cases are identified in Fig. 6.28.

Condition $\mathcal{F}(y_{\mathrm{t}}) \geq 0$ requires $m^2 A^2 \leq \sigma(\beta, \alpha_-) - m^2 \Lambda/3$ and $\mathcal{F}(y_{\mathrm{b}}) \leq 0$ is satisfied by $m^2 A^2 \geq \sigma(\beta, \alpha_+) - m^2 \Lambda/3$. We have $\sigma(\beta, \alpha_-) > \sigma(\beta, \alpha_+)$ except at $\beta = 9/8$ where these two functions are equal; $\sigma(\beta, \alpha_-)$ is always positive; and $\sigma(\beta, \alpha_+) < 0$ for $0 < \beta < 1$ and $\sigma(\beta, \alpha_+) > 0$ for $1 < \beta \leq 9/8$. Case (i) has three horizons, the acceleration horizon h_A and the inner (h_-) and outer (h_+) charged horizons and is the one that is exactly represented in Fig. 6.27 ($h_A \neq h_+ \neq h_-$); in case (ii) the inner horizon and outer horizon coincide ($h_+ \equiv h_-$) and are located at y_{b} (h_A is also present); in case (iii) the acceleration horizon and outer horizon coincide ($h_A \equiv h_+$) and are located at y_{t} (h_- is also present); finally in cases (iv) and (v) there is a single horizon $h_A \equiv h_+ \equiv h_-$. As will be seen, case (i) describes a pair of accelerated dS$-$Reissner-Nordström (dS-RN) black holes, case (ii) describes a pair of extreme dS-RN black holes in which the inner and outer charged horizons become degenerated, case (iii) describes a pair of extreme dS-RN black holes in which acceleration horizon and outer charged horizon become degenerated, and cases (iv) and (v) describe a pair of naked charged particles. In chapter 7 we will return to the study of the properties of the extreme cases of the dS C-metric. We will give explicit expressions that give the mass and charge of these extreme black holes as a function of Λ and A. Moreover, we will see that for the sector (ii) of the solution, and as occurs with the $A = 0$ case, there is an appropriate limiting procedure [89] that takes this solution into the Bertotti-Robinson C-metric, i.e., the accelerated counterpart of the Bertotti-Robinson solution [127]. We will also show that for the sector (iii) of the solution, and as occurs with the $A = 0$ case, there is also an appropriate limiting procedure [89] that takes this solution into the charged Nariai C-metric, i.e., the accelerated counterpart of the charged Nariai solution [169, 125].
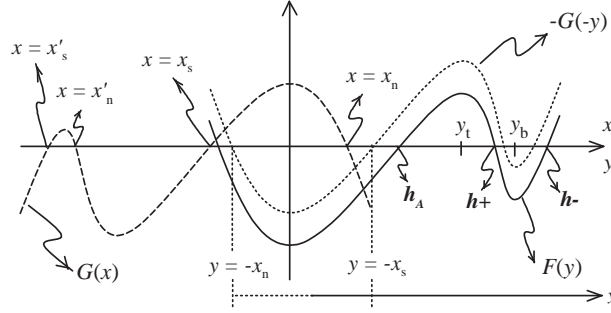
Figure 6.27: Shape of $\mathcal{G}(x)$ and $\mathcal{F}(y)$ for the non-extreme charged massive dS C-metric (case (i) in the text of section 6.3.2.c). The allowed range of x is between x_s and x_n where $\mathcal{G}(x)$ is positive and compact. The presence of an accelerated horizon is indicated by h_A and the inner and outer charged horizons by $h-$ and $h+$. In the extreme cases, $h-$ and $h+$ [case (ii)] or $h-_A$ and $h+$ [case (iii)] superpose each other and in the naked case [case (iv) and (v)] $\mathcal{F}(y)$ has only one zero in the allowed range of y.
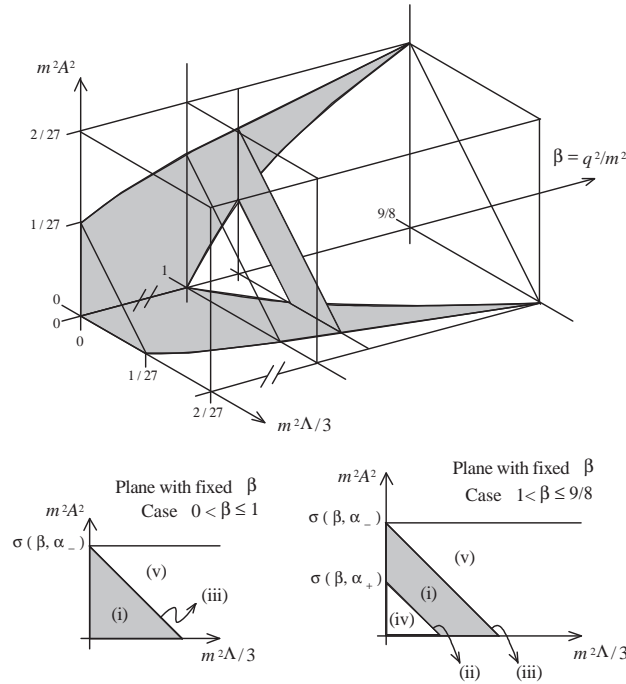
Figure 6.28: Allowed ranges of the parameters $\Lambda, A, m, \beta \equiv q^2/m^2$ for the cases (i), (ii), (iii), (iv), and (v) of the charged massive dS C-metric discussed in the text of section 6.3.2.c.

The essential differences between the Carter-Penrose diagram of the massive charged solutions and the diagram of the massive uncharged solutions are: (1) the curvature singularity is now represented by a timelike line rather than a spacelike line, (2) excluding the extreme and naked cases, there are now (in addition to the accelerated Rindler-like horizon, r_A) not one but two extra horizons, the expected inner (r_-) and outer (r_+) horizons associated to the charged character of the solution.

The Carter-Penrose diagram of case (i) is drawn in Fig. 6.29.(i) and has a structure that, as occurs in the massive uncharged case, can be divided into left, middle and right regions. The middle region contains the spacelike infinity and an accelerated Rindler-like horizon, r_A, that was already present in the $q = 0 = m$ corresponding diagram (see Fig. 6.23). The left and right regions both contain a timelike curvature singularity ($r = 0$), and an inner (r_-) and an outer (r_+) horizons associated to the charged character of the solution. This diagram is analogous the the one of the

non-accelerated ($A = 0$) dS−Reissner-Nordström solution. However, in the $A = 0$ solution the cosmological and black hole horizons have the topology of a round sphere, while in the dS C-metric ($A \neq 0$) the presence of the acceleration induces a non-spherical shape in the accelerated horizon (that coincides with the cosmological horizon) and in the black hole horizons. Indeed, notice that once we find the zero, y_h, of $\mathcal{F}(y)$ that corresponds to an accelerated or black hole horizon, the position of these horizons depends on the angular coordinate x since $r_h = [A(x + y_h)]^{-1}$. In Fig. 6.29 are also represented the other cases (ii)-(v). Again the accelerated horizon is in between two (extreme) black holes in cases (ii) and (iii) and in between two naked particles in cases (iv) and (v).

(i) Non-extreme charged Black Hole
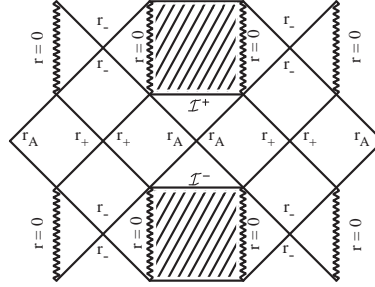
(ii) Extreme charged Black Hole ($r_+ = r_-$)
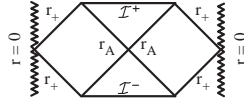
(iii) Extreme charged Black Hole ($r_A = r_+$)
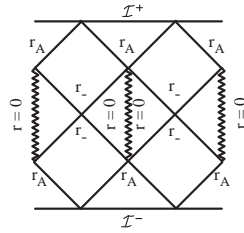
(iv) and (v) Naked Particle
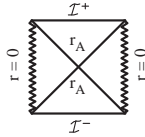
Figure 6.29: Carter-Penrose diagrams of cases (i), (ii), (iii), and (iv) and (v) of the charged massive dS C-metric. The zigzag line represents a curvature singularity, an accelerated horizon is represented by r_A, the inner and outer charge associated horizons are sketched as r_- and r_+. $\mathcal{I}^-$ and $\mathcal{I}^+$ represent respectively the past and future infinity ($r = +\infty$). $r = 0$ corresponds to $y = +\infty$ and $r = +\infty$ corresponds to $y = -x$.

6.3.3   Physical interpretation of the dS C-metric

The parameter A that is found in the dS C-metric is interpreted as being an acceleration and the dS C-metric describes a pair of black holes accelerating away from each other in a dS background. In this section we will justify this statement.

In subsection 6.3.1.b we saw that, when $A = 0$, the general dS C-metric, (6.73), reduces to the dS ($m = 0$, $q = 0$), to the dS-Schwarzschild ($m > 0$, $q = 0$), and to the dS−Reissner-Nordström

solutions ($m = 0$, $q \neq 0$). Therefore, the parameters m and q are, respectively, the ADM mass and ADM electromagnetic charge of the non-accelerated black holes. Moreover, if we set the mass and charge parameters equal to zero, even when $A \neq 0$, the Kretschmann scalar [see (6.8)] reduces to the value expected for the dS spacetime. This indicates that the massless uncharged dS C-metric is a dS spacetime in disguise.

In this section, we will first interpret case *A. Massless uncharged solution* ($m = 0$, $q = 0$), which is the simplest, and then with the acquired knowledge we interpret cases *B. Massive uncharged solution* ($m > 0$, $q = 0$) and *C. Massive charged solution* ($m > 0$, $q \neq 0$). We will interpret the solution following two complementary descriptions, the four dimensional (4D) one and the five dimensional (5D).

6.3.3.a   Description of the $m = 0$, $q = 0$ solution

The 4-Dimensional description:

As we said in 6.3.2.a, when $m = 0$ and $q = 0$ the origin of the radial coordinate r defined in (6.7) has no curvature singularity and therefore r has the range $]-\infty, +\infty[$. However, in the realistic general case, where m or q are non-zero, there is a curvature singularity at $r = 0$ and since the discussion of the massless uncharged solution was only a preliminary to that of the massive general case, following [104], we have treated the origin $r = 0$ as if it had a curvature singularity and thus we admitted that r belongs to the range $[0, +\infty[$. In these conditions we obtained the causal diagram of Fig. 6.23. Note however that one can make a further extension to include the negative values of r, enlarging in this way the range accessible to the Kruskal coordinates u' and v'. By doing this procedure we obtain the causal diagram of the dS spacetime, represented in Fig. 6.30.
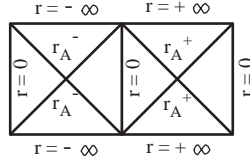
Figure 6.30: Extending the Carter-Penrose diagram of Fig. 6.23 to negative values of r, we obtain the dS spacetime with its origin being accelerated. $r_A^- = [A(x - y_+)]^{-1} < 0$ and $r_A^+ = [A(x + y_+)]^{-1} > 0$.

Now, we want to clearly identify the parameter A that appears in the dS C-metric with the acceleration of its origin. To achieve this aim, we recover the massless uncharged dS C-metric defined by (6.73) and (6.74) (with $m = 0$ and $q = 0$), and after performing the following coordinate transformation [120]

$$\tau = \frac{\sqrt{1 + \ell^2 A^2}}{A} t, \qquad \rho = \frac{\sqrt{1 + \ell^2 A^2}}{A} \frac{1}{y},$$
$$\theta = \arccos x, \qquad \tilde{\phi} = \phi, \tag{6.78}$$

we can rewrite the massless uncharged dS C-metric as

$$ds^2 = \frac{1}{\gamma^2} \left[-(1 - \rho^2/\ell^2)d\tau^2 + \frac{d\rho^2}{1 - \rho^2/\ell^2} + \rho^2 d\Omega^2 \right], \tag{6.79}$$

with $d\Omega^2 = d\theta^2 + \sin^2\theta d\phi^2$ and

$$\gamma = \sqrt{1 + \ell^2 A^2} + A\rho \cos\theta. \tag{6.80}$$

At this point some remarks are convenient. The origin of the radial coordinate ρ corresponds to $y = +\infty$ and therefore to $r = 0$, where r has been introduced in (6.7). So, when we consider the

massive dS C-metric there will be a curvature singularity at $\rho = 0$. Moreover, when we set $A = 0$, (6.79) reduces to the usual dS spacetime written in static coordinates.

To discover the meaning of the parameter A we consider the 4D timelike worldlines described by an observer with $\rho =$const, $\theta = 0$ and $\phi = 0$ (see [120]). These are given by $x^\mu(\lambda) = (\gamma \ell \lambda / \sqrt{\ell^2 - \rho^2}, \rho, 0, 0)$, were λ is the proper time of the observer and the 4-velocity $u^\mu = dx^\mu/d\lambda$ satisfies $u_\mu u^\mu = -1$. The 4-acceleration of these observers, $a^\mu = (\nabla_\nu u^\mu) u^\nu$, has a magnitude given by

$$|a_4| = \sqrt{a_\mu a^\mu} = \frac{\rho \sqrt{1 + \ell^2 A^2} + \ell^2 A}{\ell \sqrt{\ell^2 - \rho^2}} \ . \tag{6.81}$$

Since $a_\mu u^\mu = 0$, the value $|a_4|$ is also the magnitude of the 3-acceleration in the rest frame of the observer. From (6.81) we achieve the important conclusion that the origin of the dS C-metric, $\rho = 0$ (or $r = 0$), is being accelerated with a constant acceleration $|a_4|$ whose value is precisely given by the parameter A that appears in the dS C-metric. Moreover, at radius $\rho = \ell$ [or $y = y_+$ defined in equation (6.76)] the acceleration is infinite which corresponds to the trajectory of a null ray. Thus, observers held at $\rho =$const see this null ray as an acceleration horizon and they will never see events beyond this null ray. This acceleration horizon coincides with the dS cosmological horizon and has a non-spherical shape. For the benefit of comparison with the $A = 0$ dS spacetime, we note that when we set $A = 0$, (6.81) says that the origin, $\rho = 0$, has zero acceleration and at radius $\rho = \ell$ the acceleration is again infinite but now this is due only to the presence of the usual dS cosmological horizon which has a spherical shape.

The 5-Dimensional description:

In order to improve and clarify the physical aspects of the dS C-metric we turn now into the 5D representation of the solution.

The dS spacetime can be represented as the 4-hyperboloid,

$$-(z^0)^2 + (z^1)^2 + (z^2)^2 + (z^3)^2 + (z^4)^2 = \ell^2, \tag{6.82}$$

in the 5D Minkowski embedding spacetime,

$$ds^2 = -(dz^0)^2 + (dz^1)^2 + (dz^2)^2 + (dz^3)^2 + (dz^4)^2. \tag{6.83}$$

Now, the massless uncharged dS C-metric is a dS spacetime in disguise and therefore our next task is to understand how the dS C-metric can be described in this 5D picture. To do this we first recover the massless uncharged dS C-metric described by (6.79) and apply to it the coordinate transformation [120]

$$
\begin{aligned}
z^0 &= \gamma^{-1} \sqrt{\ell^2 - \rho^2} \, \sinh(\tau/\ell) \,, & z^2 &= \gamma^{-1} \rho \sin\theta \cos\phi \,, \\
z^1 &= \gamma^{-1} \sqrt{\ell^2 - \rho^2} \, \cosh(\tau/\ell) \,, & z^3 &= \gamma^{-1} \rho \sin\theta \sin\phi \,, \\
z^4 &= \gamma^{-1} [\sqrt{1 + \ell^2 A^2} \, \rho \cos\theta + \ell^2 A] \,,
\end{aligned}
\tag{6.84}
$$

where γ is defined in (6.80). Transformations (6.84) define an embedding of the massless uncharged dS C-metric into the 5D description of the dS spacetime since they satisfy (6.82) and take directly (6.79) into (6.83).

So, the massless uncharged dS C-metric is a dS spacetime, but we can extract more information from this 5D analysis. Indeed, let us analyze with some detail the properties of the origin of the radial coordinate, $\rho = 0$ (or $r = 0$). This origin moves in the 5D Minkowski embedding spacetime according to [see (6.84)]

$$
\begin{aligned}
z^2 &= 0 \,, \quad z^3 = 0 \,, \quad z^4 = \ell^2 A / \sqrt{1 + \ell^2 A^2} \ < \ell \quad \text{and} \\
(z^1)^2 &- (z^0)^2 = (A^2 + 1/\ell^2)^{-1} \equiv a_5^{-2} \,.
\end{aligned}
\tag{6.85}
$$

These equations define two hyperbolic lines lying on the dS hyperboloid which result from the intersection of this hyperboloid surface defined by (6.82) and the z^4=constant$< \ell$ plane (see Fig. 6.31). They tell us that the origin is subjected to a uniform 5D acceleration, a_5, and consequently moves along a hyperbolic worldline in the 5D embedding space, describing a Rindler-like motion [see Figs. 6.31.(a) and 6.31.(b)] that resembles the well-known hyperbolic trajectory, $X^2 - T^2 = a^{-2}$, of an accelerated observer in Minkowski space.

(a)   **(b)**
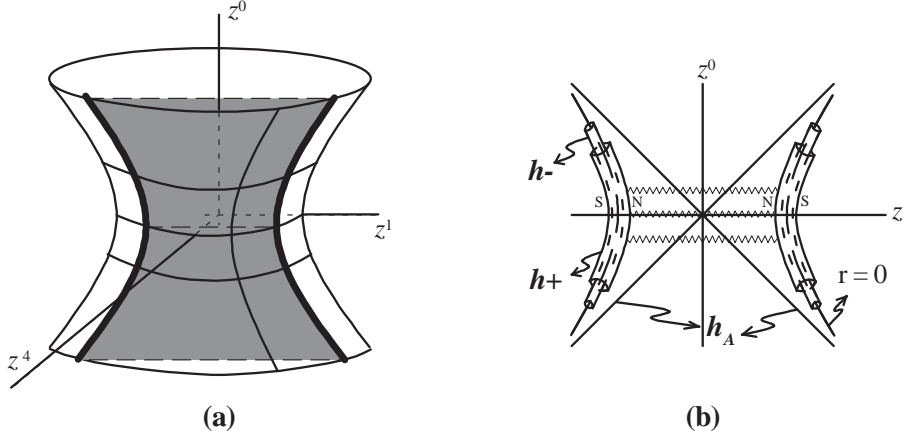
Figure 6.31: (a) The dS 4-hyperboloid embedded in the 5D Minkowski spacetime. The directions z^2 and z^3 are suppressed. The two hyperbolic lines lying on the dS hyperboloid result from the intersection of the hyperboloid surface with the z^4=constant$< \ell$ plane. They describe the motion of the origin of the dS C-metric ($A \neq 0$). For $A = 0$ the intersecting plane is $z^4 = 0$. (b) Schematic diagram representing the 5D hyperbolic motion of two uniformly accelerating massive charged black holes approaching asymptotically the Rindler-like accelerated horizon (h_A). This horizon coincides with the cosmological horizon. The inner and outer charged horizons are represented by $h-$ and $h+$. The strut that connects the two black holes is represented by the zigzag lines. The north pole direction is represented by N and the south pole direction by S.

But uniformly accelerated radial worldlines in the 5D Minkowski embedding space are also uniformly accelerated worldlines in the 4D dS space [253], with the 5D acceleration a_5 being related to the associated 4D acceleration a_4 by $a_5^2 = a_4^2 + 1/\ell^2$. Comparing this last relation with (6.85) we conclude that $a_4 \equiv A$. Therefore, and once again, we conclude that the origin of the dS C-metric is uniformly accelerating with a 4D acceleration whose value is precisely given by the parameter A that appears in the dS C-metric, (6.73), and this solution describes a dS space whose origin is not at rest as usual but is being accelerated. For the benefit of comparison with the $A = 0$ dS spacetime, note that the origin of the $A = 0$ spacetime describes the hyperbolic lines $(z^1)^2 - (z^0)^2 = \ell^2$ which result from the intersection of the $z^4 = 0$ plane with the dS hyperboloid. In this case we can say that we have two antipodal points on the spatial 3-sphere of the dS space accelerating away from each other due only to the cosmological background acceleration. When $A \neq 0$ these two points suffer an extra acceleration. This discussion allowed us to find the physical interpretation of parameter A and to justify its label. Notice also that the original dS C-metric coordinates introduced in (6.73) cover only the half-space $z^1 > -z^0$. The Kruskal construction done in section 6.3.2 extended this solution to include also the $z^1 < -z^0$ region and so, in the extended solution, $r = 0$ is associated to two hyperbolas that represent two accelerated points (see Fig. 6.31.(b)). These two hyperbolas approach asymptotically the Rindler-like acceleration horizon (r_A).

6.3.3.b   Pair of accelerated black holes ($m > 0$, $q \neq 0$)

Now, we are in a position to interpret the massive and charged solutions that describe two black holes accelerating away from each other. To see clearly this, let us look to the Carter-Penrose

diagrams, Fig. 6.23, Fig. 6.26 and Fig. 6.29. Looking at these diagrams we can compare the different features that belong to the massless uncharge case (Fig. 6.23), to the non-extreme massive uncharged case [Fig. 6.26.(i)], and ending in the non-extreme massive charged case [Fig. 6.29).(i)]. In Fig. 6.23 we identify the two hyperbolas $r = 0$ (represented by two timelike lines) approaching asymptotically the Rindler-like acceleration horizon (r_A). When we add a mass to the solution we conclude that each of these two simple hyperbolas $r = 0$ are replaced by the more complex structure that represents a Schwarzschild black hole with its spacelike curvature singularity and its horizon [this is represented by r_+ in the left and right regions of Fig. 6.26.(i)]. So, the two accelerating points $r = 0$ have been replaced by two Schwarzschild black holes that approach asymptotically the Rindler-like acceleration horizon [represented by r_A in the middle region of Fig. 6.26.(i)]. The same interpretation can be assigned to the massive charged solution. The two hyperbolas $r = 0$ of Fig. 6.23 are replaced by two Reissner-Nordström black holes [with its timelike curvature singularity and its inner r_- and outer r_+ horizons; see the left and right regions of Fig. 6.29.(i)] that approach asymptotically the Rindler-like acceleration horizon already present in the $m = 0$ and $q = 0$ causal diagram. An issue that is relevant here, is whether the Cauchy horizons of the charged dS C-metric are stable. The Cauchy horizon of the non-accelerated dS−Reissner-Nordström black holes is stable to small perturbations, as shown in [255] (for a review on Cauchy horizon instabilities see, e.g., Burko and Ori [256]). Moreover, in [257] it has been shown that nearly extremal accelerating black holes in the flat background have stable Cauchy horizons, unlike the Cauchy horizon of the non-accelerated flat Reissner-Nordström black hole which is unstable. Therefore, we expect that the Cauchy horizons of the accelerated dS−Reissner-Nordström black holes are stable, although we do not have confirmed this result. The discussion of this subsection also applies directly to the extreme cases of the dS C-metric.

6.3.3.c   Source of acceleration and radiative properties

In this subsection we address the issue of the acceleration source and its localization. In the massless uncharged dS C-metric, observers that move along radial worldlines with $\rho =$const and $\theta = 0$ describe the Rindler-like hyperbola [see (6.84)]

$$(z^1)^2 - (z^0)^2 \;\; = \;\; \frac{\ell^2 - \rho^2}{(\sqrt{1 + \ell^2 A^2} + A\rho)^2} \, . \tag{6.86}$$

Moreover, when we put m or q different from zero, each of the two hyperbolas assigned to $r = 0$ represents the accelerated motion of a black hole. Thus, from (6.86) we conclude [87] that the north pole axis is in the region between the two black holes (see Fig. 6.31.(b)). Now, the value of the arbitrary parameter κ introduced in (6.9) can be chosen in order to avoid a conical singularity at the south pole ($\delta_s = 0$), leaving a conical singularity at the north pole ($\delta_n < 0$). This is associated to a strut that joins the two black holes along their north poles and provides their acceleration [87]. This strut satisfies the relation $p = -\mu > 0$, where p and μ are respectively its pressure and its mass density [87]. Alternatively, we can choose κ such that avoids the deficit angle at the north pole ($\delta_n = 0$) and leaves a conical singularity at the south pole ($\delta_s > 0$). This option leads to the presence of a string (with $p = -\mu < 0$) that connects the two black holes along their south poles, and furnishes the acceleration.

The C-metric is an exact solution that emits gravitational and electromagnetic radiation. In the flat background the Bondi news functions have been explicitly calculated in [104, 112, 113]. In dS background these calculations have been carried in [188, 189].

Finally, recall (see subsection 6.60) that in a dS background we cannot remove the conical singularities through Ernst's trick.

6.4   Summary and concluding remarks

The C-metric in an AdS, flat, and dS backgrounds share many common properties, but there are also many features that differentiate them. In the flat ($\Lambda = 0$) and dS ($\Lambda > 0$) backgrounds, the corresponding C-metric always describes a pair of accelerated black holes. However, the AdS C-metric only describes a pair of accelerated black holes if the acceleration parameter A satisfies $A > 1/\ell$, where $\ell = \sqrt{3/|\Lambda|}$ is the cosmological length. We can interpret this as due to the fact that the AdS background is attractive, i.e., an analysis of the geodesic equations indicates that particles in this background are subjected to a potential well that attracts them (see Fig. 5.3 and the associated discussion in the text). Therefore, if we want to have a pair of black holes accelerating apart, we will have to furnish a sufficient force that overcomes this cosmological background attraction. We then expect that a pair of accelerated black holes in an asymptotically AdS spacetime is possible only if acceleration A is higher than a critical value ($1/\ell$). For $A \leq 1/\ell$ the analysis of the solution clearly indicates the absence of a second black hole and so the solution describes a single accelerated black hole.

Among the properties that are shared by the three C-metrics, we first point that the two black holes described by the solutions cannot interact gravitationally. This feature is best displayed in the Carter-Penrose diagram of the solutions, with one clarifying example sketched in Fig. 6.21.(a). In this figure one sees that a null ray sent from the vicinity of a black hole can never reach the horizon of the second black hole. So, if the two black holes cannot communicate through a null ray they cannot interact gravitationally. The black holes accelerate away from each other only due to the pressure of the strut/strings without opposition from gravitational attraction. In particular this also explains why the C-metric does not reduce to the Israel-Khan when the acceleration vanishes. In the Israel-Khan solution [see Fig. 6.21.(b)], the null ray sent from one of the black holes can reach the second black hole, and so they attract each other gravitationally. In this solution, the two black holes are connected by a strut that exerts an outward pressure which exactly cancels the inward gravitational attraction, and so the distance between the two black holes remains fixed.

Another common feature between the three cases concerns the physical source of the acceleration. This source is associated with a conical singularity in the angular poles of the solutions. The conical singularity can be located in between the two black holes and along the symmetry axis (or alternatively from the black holes out to infinity). When it is between the two black holes, it is associated to a strut satisfying the relation $p = -\mu > 0$, where p and μ are respectively the pressure on the strut and its mass density. The pressure is positive, so it points outwards into infinity and pulls the black holes apart, furnishing their acceleration. When the conical singularity points from each of the black holes into infinity, it is associated to a string from each one of the black holes towards infinity with negative pressure that pushes the black holes into infinity (to be more accurate, in the dS case, there is only one string that connects the two black holes along their south poles, but this difference is due to the fact that the dS space is closed).

When we set the mass and charge to zero, the AdS C-metric and the dS C-metric have a clarifying geometric interpretation in the 4-hyperboloids that represent the AdS and dS solutions in a 5-dimensional (5D) Minkowski spacetime. Indeed, the origin of the AdS C-metric (with $A > 1/\ell$) and the origin of the dS C-metric, are subjected to a uniform acceleration, and describe a hyperbolic Rindler-like worldline in the AdS/dS 4-hyperboloid embedded in the 5D Minkowski space. To be more precise, the origin is represented by two hyperbolic lines that approach asymptotically the Rindler-like accelerated horizon, so called because it is is absent when $A = 0$ and present even when $A \neq 0$, $m = 0$ and $q = 0$. When we add a mass or a charge to the system the causal diagrams indicate (see the clarifying explanation sketched in Fig. 1.6) that now we have two AdS/dS-Schwarzschild or two AdS/dS$-$Reissner-Nordström black holes approaching asymptotically the Rindler-like accelerated horizon. In the case of the AdS C-metric with $A \leq 1/\ell$ the above procedure indicates the absence of a second black hole and so the solution describes a single black hole. In the AdS 4-hyperboloid, the origin of these solutions describes a circle in the plane defined by the two timelike coordinates.

Chapter 6. Pair of accelerated black holes: the C-metric in a generalized Λ background

The general features of the Carter-Penrose diagram of the dS C-metric are independent of the angular coordinate. This sets a great difference between the causal diagrams of the dS C-metric and the ones of the AdS case and of the flat case. Indeed, for the $\Lambda \leq 0$ C-metric, the Carter-Penrose diagram at the north pole direction is substantially different from the one along the south pole direction and different from the diagram along the equator direction. These angular differences between the causal diagrams between the AdS, flat and dS cases are identified by comparing the Figs. 6.4, 6.18 and 6.26 (in the neutral black hole case), and by comparing Figs. 6.6, 6.20 and 6.29 (in the charged black hole case).

In the AdS and flat backgrounds, when $A \to 0$, the acceleration horizon disappears, and the C-metric reduces to a single black hole with the usual features. In the dS case, when $A \to 0$, the solution still reduces to the usual dS-Schwarzschild or dS$-$Reissner-Nordström black holes. These $A = 0$ solutions, however, can also be interpreted as a pair of black holes accelerated by the positive cosmological constant. The cosmological horizon of the $A = 0$ dS black hole plays the role of a acceleration horizon. In the $A = 0$ dS solution the cosmological horizon has the topology of a round sphere, while in the dS C-metric ($A \neq 0$) the presence of the acceleration induces a non-spherical shape in the acceleration horizon which coincides with the cosmological horizon.

Ernst has removed the conical singularities of the flat charged C-metric through the introduction of an appropriate external electromagnetic field. Its new exact solution then describes a pair of black holes accelerated by the external Lorentz force. In a cosmological background we cannot remove the conical singularities through the application of the Harrison transformation used by Ernst in the flat case. Indeed, the Harrison transformation applied by Ernst does not leave invariant the cosmological term in the action. Therefore, applying the Harrison transformation to the cosmological C-metric solutions does not yield a new solution of the Einstein-Maxwell theory in a cosmological background.

Chapter 7

The extremal limits of the C-metric:
Nariai, Bertotti-Robinson and anti-Nariai C-metrics

Contents

Three important exact solutions of general relativity are de Sitter (dS) spacetime which is a spacetime with positive cosmological constant ($\Lambda > 0$), Minkowski (or flat) spacetime with $\Lambda = 0$, and anti-de Sitter (AdS) spacetime with negative cosmological constant ($\Lambda < 0$). These stainless spacetimes, with trivial topology $\mathbb{R}^4$, have nonetheless a rich internal structure best displayed through the Carter-Penrose diagrams [258]. They also serve as the background to spacetimes containing black holes which are then asymptotically dS, flat, or AdS. These black holes in background spacetimes with a cosmological constant - Schwarzschild, Reissner-Nordström, Kerr, and Kerr-Newman - have a complex causal and topological structure well described in [259].

There are other very interesting solutions of general relativity with generic cosmological constant, that are neither pure nor contain a black hole, and somehow can be considered intermediate type solutions. These are the Nariai, Bertotti-Robinson, and anti-Nariai solutions [81]. The Nariai solution [125, 126] solves exactly the Einstein equations with $\Lambda > 0$, without or with a Maxwell field, and has been discovered by Nariai in 1951 [125]. It is the direct topological product of $dS_2 \times S^2$, i.e., of a (1+1)-dimensional dS spacetime with a round 2-sphere of fixed radius. The Bertotti-Robinson solution [127] is an exact solution of the Einstein-Maxwell equations with any Λ, and was found independently by Bertotti and Robinson in 1959. It is the direct topological product of $AdS_2 \times S^2$, i.e., of a (1+1)-dimensional AdS spacetime with a round 2-sphere of fixed radius. The anti-Nariai solution, i.e., the AdS counterpart of the Nariai solution, also exists [128] and is an exact solution of the Einstein equations with $\Lambda < 0$, without or with a Maxwell field. It is the direct topological product of $AdS_2 \times H_2$, with H_2 being a 2-hyperboloid.

Three decades after Nariai's paper, Ginsparg and Perry [97] connected the Nariai solution with the Schwarzschild-dS solution. They showed that the Nariai solution can be generated from a near-extreme dS black hole, through an appropriate limiting procedure in which the black hole horizon approaches the cosmological horizon. A similar extremal limit generates the Bertotti-Robinson solution and the anti-Nariai solution from an appropriate near extreme black hole (see, e.g. [128]). One of the aims of Ginsparg and Perry was to study the quantum stability of the Nariai and the Schwarzschild-dS solutions [97]. It was shown that the Nariai solution is in general unstable and, once created, decays through a quantum tunnelling process into a slightly non-extreme black hole pair

(for a complete review and references on this subject see, e.g., Bousso [129], and later discussions on our paper). The same kind of process happens for the Bertotti-Robinson and anti-Nariai solutions.

There is yet another class of related metrics, the C-metric class, which represent not one, but two black holes, being accelerate apart from each other. These black holes can also inhabit a dS, flat or AdS background, as we saw in the last chapter. It is therefore of great interest to apply the Ginsparg-Perry procedure to these metrics in order to find a new set of exact solutions with a clear physical and geometrical interpretation. In this chapter, following our work [89], we address this issue of the extremal limits of the C-metric with a generic Λ following [97], in order to generate the C-metric counterparts ($A \neq 0$) of the Nariai, Bertotti-Robinson and anti-Nariai solutions ($A = 0$), among others.

These C-metric counterparts are conformal to the product of two 2-dimensional manifolds of constant curvature, the conformal factor depending on the angular coordinate. In addition, the C-metric extremal solutions have a conical singularity at least at one of the poles of their angular surfaces. We give a physical interpretation to these solutions, e.g., in the Nariai C-metric (with topology $dS_2 \times \tilde{S}^2$) to each point in the deformed 2-sphere $\tilde{S}^2$ corresponds a dS_2 spacetime, except for one point which corresponds a dS_2 spacetime with an infinite straight strut or string. There are other important new features that appear. One expects that the solutions found in this chapter are unstable and decay into a slightly non-extreme black hole pair accelerated by a strut or by strings. Moreover, the Euclidean version of some of these solutions mediate the quantum process of black hole pair creation, that accompanies the decay of the dS and AdS spaces, as we shall see in chapter 9.

The plan of this chapter is as follows. In section 7.1, we describe the main features of the Nariai, Bertotti-Robinson and anti-Nariai solutions. In section 7.2, we analyze the extremal limits of the dS C-metric. We generate the Nariai C-metric, the Bertotti-Robinson dS C-metric, and the Nariai Bertotti-Robinson dS C-metric. We study the topology and the causal structure of these solutions, and we give a physical interpretation. In section 7.3 we present the extremal limits of the flat C-metric and Ernst solution, which are obtained from the solutions of section 7.2 by taking the direct $\Lambda = 0$ limit. The Euclidean version of one of these $\Lambda = 0$ solutions has already been used previously, but we discuss two new solutions that have not been discussed previously. In section 7.4, we discuss the extremal limits of the AdS C-metric and, in particular, we generate the anti-Nariai C-metric. Finally, in section 7.6 concluding remarks are presented.

7.1 Extremal limits of black hole solutions in dS, flat, and AdS spacetimes: The Nariai, Bertotti-Robinson and anti-Nariai solutions

In this section we will describe the main features of the Nariai, Bertotti-Robinson and anti-Nariai solutions. The extremal limits of the C-metric that will be generated in later sections reduce to these solutions when the acceleration parameter A is set to zero.

7.1.1 The Nariai solution

The neutral Nariai solution has been first introduced by Nariai [125, 126]. It satisfies the Einstein field equations in a positive cosmological constant Λ background, $G_{\mu\nu} + \Lambda g_{\mu\nu} = 0$, and is given by

$$ds^2 = \Lambda^{-1}(-\sin^2 \chi \, d\tau^2 + d\chi^2 + d\theta^2 + \sin^2 \theta \, d\phi^2), \tag{7.1}$$

where χ and θ both run from 0 to π, and ϕ has period 2π.

The electromagnetic extension of the Nariai solution has been introduced by Bertotti and Robinson [127]. Its gravitational field is given by

$$ds^2 = \frac{\mathcal{R}_0^2}{\mathcal{K}_0} \left(-\sin^2 \chi \, d\tau^2 + d\chi^2\right) + \mathcal{R}_0^2 \left(d\theta^2 + \sin^2 \theta \, d\phi^2\right) \tag{7.2}$$

where $\mathcal{R}_0$ is a positive constant and constant $\mathcal{K}_0$ satisfies $0 < \mathcal{K}_0 \leq 1$, while the electromagnetic field of the Nariai solution is

$$F = q \sin\theta \, d\theta \wedge d\phi \tag{7.3}$$

in the purely magnetic case, and

$$F = \frac{q}{\mathcal{K}_0} \sin\chi \, d\tau \wedge d\chi \tag{7.4}$$

in the purely electric case, with q being the electric or magnetic charge, respectively. The cosmological constant and the charge of the Nariai solution are related to $\mathcal{R}_0$ and $\mathcal{K}_0$ by

$$\Lambda = \frac{1 + \mathcal{K}_0}{2\mathcal{R}_0^2}, \qquad \text{and} \qquad q^2 = \frac{1 - \mathcal{K}_0}{2} \mathcal{R}_0^2. \tag{7.5}$$

Note that $0 < \mathcal{K}_0 \leq 1$, otherwise the charge is a complex number. The charged Nariai solution satisfies the field equations of the Einstein-Maxwell action in a positive cosmological constant background, $G_{\mu\nu} + \Lambda g_{\mu\nu} = 8\pi T_{\mu\nu}$, with $T_{\mu\nu}$ being the energy-momentum tensor of the Maxwell field. The neutral Nariai solution (7.1) is obtained from the charged solution (7.2)-(7.3) when one sets $\mathcal{K}_0 = 1$. The $\Lambda = 0$ limit of the Nariai solution, which is Minkowski spacetime, is taken in subsection 7.1.4. Through a redefinition of coordinates, $\sin^2\chi = 1 - \frac{\mathcal{K}_0}{\mathcal{R}_0^2} R^2$ and $\tau = \sqrt{\frac{\mathcal{K}_0}{\mathcal{R}_0^2}} T$, the spacetime (7.2) can be rewritten in new static coordinates as

$$ds^2 = -N(R) \, dT^2 + \frac{dR^2}{N(R)} + \mathcal{R}_0^2 \left(d\theta^2 + \sin^2\theta \, d\phi^2 \right), \tag{7.6}$$

with

$$N(R) = 1 - \frac{\mathcal{K}_0}{\mathcal{R}_0^2} R^2, \tag{7.7}$$

and the electromagnetic field changes also accordingly to the coordinate transformation. Written in these coordinates, we clearly see that the Nariai solution is the direct topological product of $dS_2 \times S^2$, i.e., of a (1+1)-dimensional dS spacetime with a round 2-sphere of fixed radius $\mathcal{R}_0$. This spacetime is homogeneous with the same causal structure as (1+1)-dimensional dS spacetime, but it is not an asymptotically 4-dimensional dS spacetime since the radius of the 2-spheres is constant ($\mathcal{R}_0$), contrarily to what happens in the dS solution where this radius increases as one approaches infinity.

Another way [126, 260] to see clearly the topological structure of the Nariai solution is achieved by defining it through its embedding in the flat manifold $\mathbb{M}^{1,5}$, with metric

$$ds^2 = -dz_0^2 + dz_1^2 + dz_2^2 + dz_3^2 + dz_4^2 + dz_5^2. \tag{7.8}$$

The Nariai 4-submanifold is determined by the two constraints

$$-z_0^2 + z_1^2 + z_2^2 = \ell^2,$$
$$z_3^2 + z_4^2 + z_5^2 = \mathcal{R}_0^2, \tag{7.9}$$

where $\ell^2 = \mathcal{R}_0^2/\mathcal{K}_0$. The first of these constraints defines the dS_2 hyperboloid and the second defines the 2-sphere of radius $\mathcal{R}_0$. The parametrization of $\mathbb{M}^{1,5}$ given by $z_0 = \sqrt{\ell^2 - R^2} \sinh(T/\ell)$, $z_1 = \sqrt{\ell^2 - R^2} \cosh(T/\ell)$, $z_2 = R$, $z_3 = \mathcal{R}_0 \sin\theta \cos\phi$, $z_4 = \mathcal{R}_0 \sin\theta \sin\phi$ and $z_5 = \mathcal{R}_0 \cos\theta$, induces the metric (7.6) on the Nariai hypersurface (7.9).

Quite remarkably, Ginsparg and Perry [97] (see also [170]) have shown that the neutral Nariai solution (7.1) can be obtained from the near-extreme Schwarzschild-dS black hole through an appropriate limiting procedure. By extreme we mean that the black hole horizon and the cosmological

horizon coincide. Hawking and Ross [181], and Mann and Ross [169] have concluded that a similar limiting approach takes the near-extreme dS−Reissner-Nordström black hole into the charged Nariai solution (7.2). In this case, by extreme we mean that the cosmological and outer charged black hole horizons coincide. We will make heavy use of this Ginsparg-Perry procedure later, so we will not sketch it here. These relations between the near-extreme dS black holes and the Nariai solutions are a priori quite unexpected since (i) the dS black holes have a curvature singularity while the Nariai solutions do not, (ii) the Nariai spacetime is homogeneous unlike the dS black holes spacetimes, (iii) the dS black holes approach asymptotically the 4-dimensional dS spacetime while the Nariai solutions do not. The Carter-Penrose diagram of the Nariai solution is equivalent to the diagram of the (1+1)-dimensional dS solution, as will be discussed in subsection 7.2.1.

An important role played by the Nariai solution in physics is at the quantum level (see Bousso [129] for a detailed review of what follows). First, there is the issue of the stability of the solution when perturbed quantically. Ginsparg and Perry [97], in the neutral case, and Bousso and Hawking [170] and Bousso [174], in the charged case, have shown that the Nariai solutions are quantum mechanically unstable. Indeed, due to quantum fluctuations, the radius $\mathcal{R}_0$ of the 2-spheres oscillates along the non-compact spatial coordinate χ and the degenerate horizon splits back into a black hole and a cosmological horizon. Those 2-spheres whose radius fluctuates into a radius smaller than $\mathcal{R}_0$ will collapse into the dS black hole interior, while the 2-spheres that have a radius greater than $\mathcal{R}_0$ will suffer an exponential expansion that generates an asymptotic dS region. Therefore, the Nariai solutions are unstable and, once created, they decay through the quantum tunnelling process into a slightly non-extreme dS−Reissner-Nordström black hole pair. This issue of the Nariai instability against perturbations and associated evaporation process has been further analyzed by Bousso and Hawking [261], by Nojiri and Odintsov [262], and by Kofman, Sahni, and Starobinski [263]. Second, the Nariai Euclidean solution plays a further role as an instanton, in the quantum decay of the dS space. This decay of the dS space is accompanied by the creation of a dS black hole pair, in a process that is the gravitational analogue of the Schwinger pair production of charged particles in an external electromagnetic field. Here, the energy necessary to materialize the black hole pair and to accelerate the black holes apart comes from the cosmological constant background. It is important to note that not all of the dS black holes can be pair produced through this quantum process of black hole pair creation. Only those black holes that have regular Euclidean sections can be pair created (the term regular is applied here in the context of the analysis of the Hawking temperature of the horizons). The Nariai instanton (regular Euclidean Nariai solution, that is obtained from (7.1) and (7.2) by setting $\tau = i\bar{\tau}$), belongs to the very restrictive class of solutions that are regular [167, 168, 169, 170, 173, 172], and can therefore mediate the pair creation process in the dS background. In the uncharged case the Nariai instanton is even the only solution that can describe the pair creation of neutral black holes. Another result at the quantum level by Medved [264] indicates that quantum back-reaction effects prevent a near extreme dS black hole from ever reaching a Nariai state of precise extremality.

Other extensions of the Nariai solution are the dilaton charged Nariai solution found by Bousso [174], the rotating Nariai solution studied by Mellor and Moss [167, 168], and by Booth and Mann [173], and solutions that describe non-expanding impulsive waves propagating in the Nariai universe studied by Ortaggio [260].

7.1.2   The Bertotti-Robinson solution

The simplest Bertotti-Robinson solution [127] (see also [128, 265]) is a solution of the $\Lambda = 0$ Einstein-Maxwell equations. Its gravitational field is given by

$$ds^2 = q^2(-\sinh^2 \chi \, d\tau^2 + d\chi^2 + d\theta^2 + \sin^2 \theta \, d\phi^2),$$

$$(7.10)$$

where q is the charge of the solution, and χ is unbounded, θ runs from 0 to π and ϕ has period 2π. The electromagnetic field of the Bertotti-Robinson solution is

$$F = q \sin\theta \, d\theta \wedge d\phi \,, \tag{7.11}$$

and

$$F = -q \, \sinh\chi \, d\tau \wedge d\chi \,, \tag{7.12}$$

in the magnetic and electric cases, respectively. Through a redefinition of coordinates, $\sinh^2\chi = R^2/q^2 - 1$ and $\tau = T/q$, the spacetime (7.10) can be rewritten in new static coordinates as

$$ds^2 = -N(R) \, dT^2 + \frac{dR^2}{N(R)} + q^2(d\theta^2 + \sin^2\theta \, d\phi^2), \tag{7.13}$$

with

$$N(R) = R^2/q^2 - 1 \,, \tag{7.14}$$

and the electromagnetic field changes also accordingly to the coordinate transformation. Written in these coordinates, we clearly see that the Bertotti-Robinson solution is the direct topological product of $AdS_2 \times S^2$, i.e., of a (1+1)-dimensional AdS spacetime with a round 2-sphere of fixed radius q. Another way to see clearly the topological structure of the Bertotti-Robinson solution is achieved by defining it through its embedding in the flat manifold $\mathbb{M}^{2,4}$, with metric

$$ds^2 = -dz_0{}^2 + dz_1{}^2 - dz_2{}^2 + dz_3{}^2 + dz_4{}^2 + dz_5{}^2 \,. \tag{7.15}$$

The Bertotti-Robinson 4-submanifold is determined by the two constraints

$$\begin{aligned} -z_0{}^2 + z_1{}^2 - z_2{}^2 &= -q^2 \,, \\ z_3{}^2 + z_4{}^2 + z_5{}^2 &= q^2 \,. \end{aligned} \tag{7.16}$$

The first of these constraints defines the AdS_2 hyperboloid and the second defines the 2-sphere of radius q. The parametrization of $\mathbb{M}^{2,4}$, $z_0 = \sqrt{R^2 - q^2}\,\sinh{(T/q)}$, $z_1 = \sqrt{R^2 - q^2}\,\cosh{(T/q)}$, $z_2 = R$, $z_3 = q\sin\theta\cos\phi$, $z_4 = q\sin\theta\sin\phi$ and $z_5 = q\cos\theta$, induces the metric (7.13) on the Bertotti-Robinson hypersurface (7.16). Note that since the parametrization $z_0 = \sqrt{q^2 + \tilde{R}^2}\,\sin(\tilde{T}/q)$, $z_1 = \tilde{R}$ and $z_2 = \sqrt{q^2 + \tilde{R}^2}\,\cos(\tilde{T}/q)$, also obeys (7.15) and the first constraint of (7.16), the Bertotti-Robinson solution (7.13) can also be written as $ds^2 = -N(\tilde{R})\,d\tilde{T}^2 + d\tilde{R}^2/N(\tilde{R}) + q^2(d\theta^2 + \sin^2\theta \, d\phi^2)$, with $N(\tilde{R}) = \tilde{R}^2/q^2 + 1$.

Following a similar procedure to the one applied in the Nariai solution, the Bertotti-Robinson solution can be obtained from the near-extreme Reissner-Nordström black hole through an appropriate limiting procedure (here, by extreme we mean that the inner black hole horizon and the outer black hole horizon coincide). Later on, we will make heavy use of the Ginsparg-Perry procedure, so we will not sketch it here. Generalizations of the Bertotti-Robinson solution to include a cosmological constant background also exist [127], and are an extremal limit of the near-extreme Reissner-Nordström black holes with a cosmological constant. The Carter-Penrose diagram of the Bertotti-Robinson solution (with or without Λ) is equivalent to the diagram of the (1+1)-dimensional AdS solution, as will be discussed in subsection 7.2.2.

The Hawking effect in the Bertotti-Robinson universe has been studied by Lapedes [265], and its thermodynamic properties have been analyzed by Zaslavsky [266], and by Mann and Solodukhin [267]. In [268] the authors have shown that quantum back-reaction effects prevent a near extreme charged black hole from ever reaching a Berttoti-Robinson state of precise extremality. Recently, Ortaggio and Podolský [269] have found exact solutions that describe non-expanding impulsive waves propagating in the Bertotti-Robinson universe.

7.1.3 The anti-Nariai solution

The anti-Nariai solution has a gravitational field given by [128]

$$ds^2 = \frac{\mathcal{R}_0^2}{\mathcal{K}_0}\left(-\sinh^2\chi\, d\tau^2 + d\chi^2\right) + \mathcal{R}_0^2\left(d\theta^2 + \sinh^2\theta\, d\phi^2\right),$$

$$(7.17)$$

where χ and θ are unbounded, ϕ has period 2π, $\mathcal{R}_0$ is a positive constant, and the constant $\mathcal{K}_0$ satisfies $1 \leq \mathcal{K}_0 < 2$. The electromagnetic field of the anti-Nariai solution is

$$F = q\sinh\theta\, d\theta \wedge d\phi$$

$$(7.18)$$

in the purely magnetic case, and

$$F = -\frac{q}{\mathcal{K}_0}\sinh\chi\, d\tau \wedge d\chi$$

$$(7.19)$$

in the purely electric case, with q being the magnetic or electric charge, respectively. The cosmological constant, $\Lambda < 0$, and the charge of the anti-Nariai solution are related to $\mathcal{R}_0$ and $\mathcal{K}_0$ by

$$\Lambda = -\frac{1 + \mathcal{K}_0}{2\mathcal{R}_0^2} < 0, \qquad \text{and} \qquad q^2 = \frac{\mathcal{K}_0 - 1}{2}\mathcal{R}_0^2.$$

$$(7.20)$$

The neutral anti-Nariai solution ($q = 0$) is obtained from the charged solution (7.17) when one sets $\mathcal{K}_0 = 1$ which implies $\mathcal{R}_0^2 = |\Lambda|^{-1}$. The $\Lambda = 0$ limit of the anti-Nariai solution, which is Minkowski spacetime, is taken in subsection 7.1.4. The charged anti-Nariai solution satisfies the field equations of the Einstein-Maxwell action in a negative cosmological constant background. Through a redefinition of coordinates, $\sinh^2\chi = 1 - \frac{\mathcal{K}_0}{\mathcal{R}_0^2}R^2$ and $\tau = \sqrt{\frac{\mathcal{K}_0}{\mathcal{R}_0^2}}\,T$, the spacetime (7.17) can be rewritten in static coordinates as

$$ds^2 = -N(R)\,dT^2 + \frac{dR^2}{N(R)} + \mathcal{R}_0^2\left(d\theta^2 + \sinh^2\theta\, d\phi^2\right),$$

$$(7.21)$$

with

$$N(R) = -1 + \frac{\mathcal{K}_0}{\mathcal{R}_0^2}R^2,$$

$$(7.22)$$

and the electromagnetic field changes also accordingly to the coordinate transformation. Written in these coordinates, we clearly see that the anti-Nariai solution is the direct topological product of $AdS_2 \times H_2$, i.e., of a (1+1)-dimensional AdS spacetime with a 2-hyperboloid of radius $\mathcal{R}_0$. It is a homogeneous spacetime with the same causal structure as (1+1)-dimensional AdS spacetime, but it is not an asymptotically 4-dimensional AdS spacetime since the size of the 2-hyperboloid is constant ($\mathcal{R}_0$), contrarily to what happens in the AdS solution where this radius increases as one approaches infinity. Another way to see clearly the topological structure of the anti-Nariai solution is achieved by defining it through its embedding in the flat manifold $\mathbb{M}^{3,3}$ with metric

$$ds^2 = -dz_0{}^2 + dz_1{}^2 - dz_2{}^2 + dz_3{}^2 + dz_4{}^2 - dz_5{}^2.$$

$$(7.23)$$

The anti-Nariai 4-submanifold is determined by the two constraints

$$-z_0{}^2 + z_1{}^2 - z_2{}^2 = -\ell^2,$$
$$z_3{}^2 + z_4{}^2 - z_5{}^2 = -\mathcal{R}_0^2.$$

$$(7.24)$$

where $\ell^2 = \mathcal{R}_0^2/\mathcal{K}_0$. The first of these constraints defines the AdS_2 hyperboloid and the second defines the 2-hyperboloid of radius $\mathcal{R}_0$. The parametrization of $\mathbb{M}^{3,3}$, $z_0 = \sqrt{R^2 - \ell^2} \sinh(T/\ell)$, $z_1 = \sqrt{R^2 - \ell^2} \cosh(T/\ell)$, $z_2 = R$, $z_3 = \mathcal{R}_0 \sinh\theta \cos\theta$, $z_4 = \mathcal{R}_0 \sinh\theta \sin\theta$ and $z_5 = \mathcal{R}_0 \cosh\theta$ induces the metric (7.21) on the anti-Nariai hypersurface (7.24).

Having in mind the example of the Nariai solution, we may ask if the anti-Nariai solution can be obtained, through a similar limiting Ginsparg-Perry procedure, from a near-extreme AdS black hole. As we saw in subsection 5.1, in the AdS background, there are black holes whose horizons have topologies different from spherical, such as toroidal horizons [6, 7, 10, 8], and hyperbolical horizons [11], also called topological black holes. The AdS black hole that generates the anti-Nariai solution is the hyperbolic one [as is clear from the angular part of (7.21)], and has a cosmological horizon. Indeed, the hyperbolic topology together with the presence of the cosmological horizon turn the hyperbolic black holes (studied in subsection 5.1.3) into the appropriate solutions that allow the generation of the anti-Nariai solution (7.17) with the limiting Ginsparg-Perry procedure, when the black hole horizon approaches the cosmological horizon.

A further study of the anti-Nariai solution was done in [269] where non-expanding impulsive waves propagating in the anti-Nariai universe are described.

7.1.4 $\Lambda = 0$ limit of the Nariai and anti-Nariai solutions

In this subsection we find the $\Lambda = 0$ limit of the Nariai solution, (7.2), and of the anti-Nariai solution, (7.17). In this limit the line element of both solutions goes apparently to infinity since $\mathcal{R}_0^2 \to \infty$. To achieve the suitable limit of the Nariai solution, we first make the coordinate rescales: $\tilde{x} = (\mathcal{R}_0/\sqrt{\mathcal{K}_0})\chi$, and $\varrho = \mathcal{R}_0\theta$. Then, taking the $\Lambda = 0$ limit, the solution becomes

$$ds^2 = (-\tilde{x}^2 d\tau^2 + d\tilde{x}^2) + (d\varrho^2 + \varrho^2 d\phi^2). \tag{7.25}$$

The spacetime sector is a Rindler factor, and the angular sector is a cylinder. Therefore, under the usual coordinate transformation $\tilde{x} = \sqrt{\bar{x}^2 - \bar{t}^2}$ and $\tau = \operatorname{arctanh}(\bar{t}/\bar{x})$, and unwinding the cylinder ($\bar{y} = \varrho \cos\phi$ and $\bar{z} = \varrho \sin\phi$), we have

$$ds^2 = (-d\bar{t}^2 + d\bar{x}^2) + (d\bar{y}^2 + d\bar{z}^2). \tag{7.26}$$

Therefore, while the Nariai solution is topologically $dS_2 \times S^2$, its $\Lambda = 0$ limit is topologically $\mathbb{M}^{1,1} \times \mathbb{R}^2$, i.e., $\mathbb{R}^4$.

A similar procedure shows that taking the $\Lambda = 0$ limit of the anti-Nariai solution (7.17) ($AdS_2 \times H_2$) leads to (7.26).

7.2 Extremal limits of the dS C-metric

In the last section we saw that there is an appropriate extremal limiting procedure, introduced by Ginsparg and Perry [97], that generates from the near-extreme black hole solutions the Nariai, Bertotti-Robinson and anti-Nariai solutions. Analogously, we shall apply the procedure of [97] to generate new exact solutions from the near-extreme cases of the dS C-metric. Specifically the C-metric counterparts of the Nariai and Bertotti-Robinson solutions are found using this method. When the acceleration parameter A is set to zero in these new solutions, we will recover the Nariai and Bertotti-Robinson solutions. To achieve our propose we will analyze with more detail the extreme cases of the dS C-metric already discussed in subsections 6.3.2.b and 6.3.2.c. Recall that the gravitational field of the dS C-metric is given by (6.73) and (6.74), and its electromagnetic field is given by (6.5) and (6.6).

7.2.1 The Nariai C-metric

We will generate the Nariai C-metric from a special extremal limit of the dS C-metric. First we will describe this particular near-extreme solution and then we will generate the Nariai C-metric.

We are interested in a particular extreme dS C-metric, for which the size of the acceleration horizon y_A is equal to the size of the outer charged horizon y_+. Let us label this degenerated horizon by ρ, i.e., $y_A = y_+ \equiv \rho$ with $\rho < y_-$. In this case, the function $\mathcal{F}(y)$ given by (6.74) can be written as

$$\mathcal{F}(y) = \frac{\rho^2 - 3\gamma}{\rho^4}(y - y_{\text{neg}})(y - y_-)(y - \rho)^2 \,, \tag{7.27}$$

where

$$\gamma = \frac{\Lambda + 3A^2}{3A^2} \,, \tag{7.28}$$

and the roots ρ, y_{neg} and y_- are given by

$$\rho = \frac{3m}{4q^2 A}\left(1 - \sqrt{1 - \frac{8}{9}\frac{q^2}{m^2}}\right) \,, \tag{7.29}$$

$$y_{\text{neg}} = \frac{\gamma\rho}{\rho^2 - 3\gamma}\left(1 - \sqrt{\frac{\rho^2 - 2\gamma}{\gamma}}\right) \,, \tag{7.30}$$

$$y_- = \frac{\gamma\rho}{\rho^2 - 3\gamma}\left(1 + \sqrt{\frac{\rho^2 - 2\gamma}{\gamma}}\right) \,. \tag{7.31}$$

The mass and the charge of the solution are written as functions of ρ as

$$m = \frac{1}{A\rho}\left(1 - \frac{2\gamma}{\rho^2}\right) \,,$$
$$q^2 = \frac{1}{A^2\rho^2}\left(1 - \frac{3\gamma}{\rho^2}\right) \,. \tag{7.32}$$

The conditions $\rho < y_-$ and $q^2 \geq 0$ require that the allowed range of ρ is

$$\sqrt{3\gamma} \leq \rho < \sqrt{6\gamma} \,. \tag{7.33}$$

The value of y_- decreases monotonically with ρ and we have $\sqrt{6\gamma} < y_- < +\infty$. The mass and the charge of the Nariai solution, denoted now as m_{N} and q_{N} respectively, are monotonically increasing functions of ρ, and as we go from $\rho = \sqrt{3\gamma}$ into $\rho = \sqrt{6\gamma}$ we have

$$\frac{1}{3}\frac{1}{\sqrt{\Lambda + 3A^2}} \leq m_{\text{N}} < \frac{\sqrt{2}}{3}\frac{1}{\sqrt{\Lambda + 3A^2}} \,,$$
$$0 \leq q_{\text{N}} < \frac{1}{2}\frac{1}{\sqrt{\Lambda + 3A^2}} \,, \tag{7.34}$$

so the $A \neq 0$ extreme ($y_A = y_+$) solution has a lower maximum mass and charge, and has a lower minimum mass than the corresponding $A = 0$ solution [167, 168, 169, 173], and, for a fixed Λ, as the acceleration parameter A grows these extreme values decrease monotonically. For a fixed Λ and for a fixed mass between $\sqrt{1/(9\Lambda)} \leq m < \sqrt{2/(9\Lambda)}$, the allowed acceleration varies as $\sqrt{1/(27m^2) - \Lambda/3} \leq A < \sqrt{2/(27m^2) - \Lambda/3}$.

We are now ready to obtain the Nariai C-metric. In order to generate it from the above near-extreme dS C-metric we first set

$$y_A = \rho - \varepsilon, \quad y_+ = \rho + \varepsilon, \quad \text{with } \varepsilon \ll 1 \,, \tag{7.35}$$

in order that ε measures the deviation from degeneracy, and the limit $y_A \to y_+$ is obtained when $\varepsilon \to 0$. Now, we introduce a new time coordinate τ and a new radial coordinate χ,

$$t = \frac{1}{\varepsilon\mathcal{K}}\tau, \quad y = \rho + \varepsilon\cos\chi \,, \tag{7.36}$$

where

$$\mathcal{K} = -\frac{\rho^2 - 3\gamma}{\rho^4}(\rho - y_{\text{neg}})(\rho - y_-) = \frac{2(\Lambda + 3A^2)}{A^2 \rho^2} - 1 \,,$$

(7.37)

and condition (7.33) implies $0 < \mathcal{K} \leq 1$ with $q = 0 \Rightarrow \mathcal{K} = 1$. In the limit $\varepsilon \to 0$, from (6.73) and (7.27), we get the gravitational field of the Nariai C-metric

$$ds^2 = \frac{\mathcal{R}^2(x)}{\mathcal{K}}\left(-\sin^2\chi\, d\tau^2 + d\chi^2\right) + \mathcal{R}^2(x)\left[\mathcal{G}^{-1}(x)dx^2 + \mathcal{G}(x)dz^2\right] \,,$$

(7.38)

where χ runs from 0 to π and

$$\mathcal{R}^2(x) = \left(Ax + \sqrt{\tfrac{2(\Lambda+3A^2)}{1+\mathcal{K}}}\right)^{-2} \,,$$

$$\mathcal{G}(x) = 1 - x^2 - \tfrac{2A}{3}\sqrt{\tfrac{(1+\mathcal{K})(2-\mathcal{K})^2}{2(\Lambda+3A^2)}}\, x^3 - \tfrac{A^2}{4}\tfrac{1-\mathcal{K}^2}{\Lambda+3A^2}\, x^4 \,.$$

(7.39)

$\mathcal{G}(x)$ has only two real roots, the south pole x_{s} and the north pole x_{n}. The angular coordinate x can range between these two poles, whose values are calculated in section 7.5. Under the coordinate transformation (7.36), the Maxwell field for the magnetic case is still given by (6.5), while in the electric case, (6.6) becomes

$$F = \frac{q}{\mathcal{K}}\sin\chi\, d\tau \wedge d\chi \,.$$

(7.40)

So, if we give the parameters Λ, A, and q we can construct the Nariai C-metric. The Nariai C-metric is conformal to the topological product of two 2-dimensional manifolds, $dS_2 \times \tilde{S}^2$, with the conformal factor $\mathcal{R}^2(x)$ depending on the angular coordinate x, and $\tilde{S}^2$ being a deformed 2-sphere.

In order to obtain the $A = 0$ limit, we first set $\tilde{\rho} = A\rho$ [see (7.29)], a parameter that has a finite and well-defined value when $A \to 0$. Then when $A \to 0$ we have $\mathcal{K} \to \mathcal{K}_0 = 2\Lambda/\tilde{\rho}^2 - 1$ and $\mathcal{R}^2(x) \to \mathcal{R}_0^2 = \tilde{\rho}^{-2}$, with $\mathcal{R}_0^2$ and $\mathcal{K}_0$ satisfying relations (7.5). This, together with transformations (6.9), show that the Nariai C-metric transforms into the Nariai solution (7.2) when $A = 0$.

The limiting procedure that has been applied in this subsection has generated a new exact solution that satisfies the Maxwell-Einstein equations in a positive cosmological constant background.

In order to give a physical interpretation to this extremal limit of the dS C-metric, we first recall the physical interpretation of the dS C-metric. This solution describes a pair of uniformly accelerated black holes in a dS background, with the acceleration being provided by the cosmological constant and by a strut between the black holes that pushes them away or, alternatively, by a string that connects and pulls the black holes in. The presence of the strut or of the string is associated to the conical singularities that exist in the C-metric (see, e. g., [88]). Indeed, in general, if we draw a small circle around the north or south pole, as the radius goes to zero, the limit circunference/radius is not 2π. There is a deficit angle at the north pole given by (see [87, 88]), $\delta_{\text{n}} = 2\pi\left(1 - \frac{\kappa}{2}|\mathcal{G}'(x_{\text{n}})|\right)$ (where the prime means derivative with respect to x) and, analogously, a similar conical singularity (δ_{s}) is present at the south pole. The so far arbitrary parameter κ introduced in (6.9) plays its important role here. Indeed, if we choose $\kappa^{-1} = \frac{1}{2}|\mathcal{G}'(x_{\text{s}})|$ we remove the conical singularity at the south pole ($\delta_{\text{s}} = 0$). However, since we only have a single constant κ at our disposal and this has been fixed to avoid the conical singularity at the south pole ($\delta_{\text{s}} = 0$), we conclude that a conical singularity will be present at the north pole with $\delta_{\text{n}} < 0$. This is associated to a strut (since $\delta_{\text{n}} < 0$) that joins the two black holes along their north poles and provides their acceleration. This strut satisfies the relation $p = -\mu > 0$, where p and $\mu = \delta_{\text{n}}/(8\pi)$ are respectively its pressure and its mass density (see [87]). There is another alternative. We can choose instead $\kappa^{-1} = \frac{1}{2}|\mathcal{G}'(x_{\text{n}})|$ and by doing so we avoid the deficit angle at the north pole ($\delta_{\text{n}} = 0$), and leave a conical singularity at the

south pole ($\delta_s > 0$). This option leads to the presence of a string (with $p = -\mu < 0$) connecting the black holes along their south poles that furnishes the acceleration. Summarizing, when the conical singularity is at the north pole, the pressure of the strut is positive, so it points outwards and pushes the black holes apart, furnishing their acceleration. When the conical singularity is at the south pole, it is associated to a string between the two black holes with negative pressure that pulls the black holes away from each other.

The causal structure of the dS C-metric has been analyzed in detail in [88]. The Carter-Penrose diagram of the non-extreme charged dS C-metric is sketched in Fig. 7.1.(a) (whole figure) and has a structure that, loosely speaking, can be divided into left, middle and right regions. The middle region contains the null infinity, the past infinity, $\mathcal{I}^-$, and the future infinity, $\mathcal{I}^+$, and an accelerated Rindler-like horizon, h_A (that coincides with the cosmological horizon). The left and right regions both contain a timelike curvature singularity (the zig-zag line), and an inner (h_-) and an outer (h_+) horizons associated to the charged character of the solution. This diagram represents two dS$-$Reissner-Nordström black holes that approach asymptotically the Rindler-like acceleration horizon (for a more detailed discussion see [88]). This is also schematically represented in Fig. 7.1.(c) (whole figure), where we explicitly show the strut that connects the two black holes and provides their acceleration.

Now, as we have just seen, the Nariai C-metric can be appropriately obtained from the vicinity of the black hole and acceleration horizons in the limit in which the size of these two horizons approach each other. We now will see that the conical singularity of the dS C-metric survives the near-extremal limiting procedure that generates the Nariai C-metric. Following an elucidative illustration shown in [270] for the Bertotti-Robinson solution (with $\Lambda < 0$ and $A = 0$), this near-horizon region is sketched in Fig. 7.1.(a) as a shaded area, and from it we can identify some of the features of the Nariai C-metric, e.g., the curvature singularity of the original dS black hole is lost in the near-extremal limiting procedure. But, more important, this shaded near-horizon region also allows us to construct straightforwardly the Carter-Penrose diagram of the Nariai C-metric drawn in Fig. 7.1.(b). The construction steps are as follows. First, as indicated by (7.35) and the second relation of (7.36), we let the cross lines that represent the black hole horizon [h_+ in Fig. 7.1.(a)] join together with the cross lines that represent the acceleration horizon [h_A in Fig. 7.1.(a)], and so on, i.e., we do this joining ad infinitum with all the cross lines h_+ and h_A. After this step all that is left from the original diagram is a single cross line, i.e, all the spacetime that has originally contained in the shaded area of Fig. 7.1.(a) has collapsed into two mutually perpendicular lines at 45° at $y = \rho$. Now, as indicated by the first relation of (7.36), when $\varepsilon \to 0$ the time suffers an infinite blow up. To this blow up in the time corresponds an infinite expansion in the Carter-Penrose diagram in the vicinity of $y = \rho$. We then get again the shaded area of Fig. 7.1.(a), but now the cross lines of this shaded area are all identified into a single horizon, and they no longer have the original signature associated to h_+ and h_A that differentiated them. This is, in the shaded area of Fig. 7.1.(a) we must now erase the original labels h_+ and h_A. The Carter-Penrose diagram of the Nariai C-metric is then given by Fig. 7.1.(b), which is equivalent to the diagram of the (1+1)-dimensional dS solution. Note that the diagram of the $A = 0$ dS$-$Reissner-Nordström solution is identical to the one of Fig. 7.1.(a), as long as we replace h_A (acceleration horizon) by h_c (cosmological horizon). Applying the same construction process described just above we find that the Carter-Penrose diagram of the Nariai solution ($A = 0$), described in subsection 7.1.1, is also given by Fig. 7.1.(b).
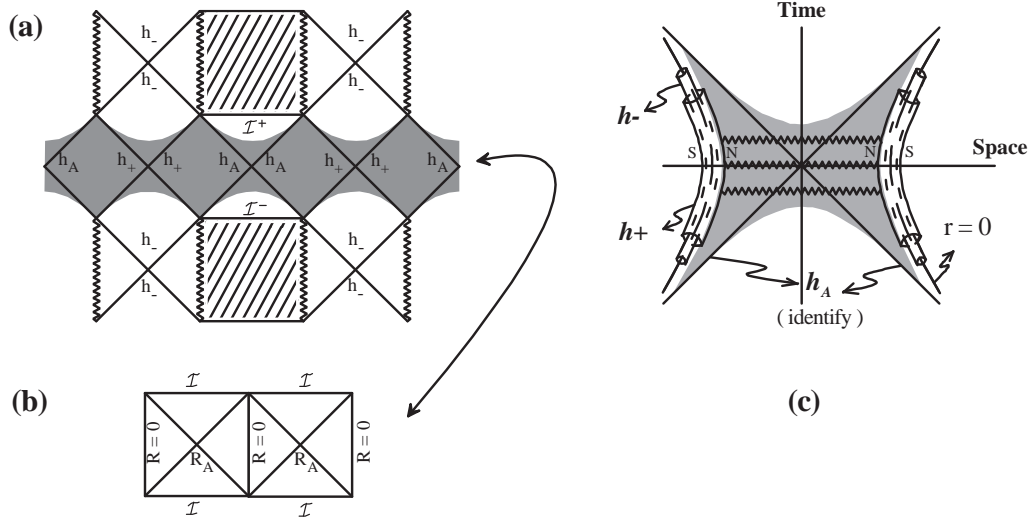
Figure 7.1: (a) The whole figure is the Carter-Penrose diagram of the dS C-metric. The shaded region represents the near-horizon area that, when the black hole horizon (h_+) approaches the acceleration horizon (h_+), gives the dS_2 manifold of the Nariai C-metric solution. See discussion in the text. (b) Carter-Penrose diagram of the Nariai C-metric. (c) The whole figure represents schematically the two black holes of the dS C-metric approaching asymptotically the Rindler-like acceleration horizon. They are accelerated by a strut that joins them along their north poles. The shaded region represents the near-horizon area that, when the black hole horizon approaches the acceleration horizon, gives the Nariai C-metric solution [compare with Fig. 7.1.(a)]. The strut survives to the limiting process.

   The Nariai near-horizon region is also sketched in Fig. 7.1.(c) as a shaded area. This schematic figure is clarifying in the sense that it indicates that the strut that connects the two original black holes along their north pole directions survives to the near-extremal limiting process and will be present in the final result of the process, i.e., in the Nariai C-metric. Indeed, note that the endpoints of the strut are at the north pole of the event horizons of the two black holes and crosses the acceleration horizon. As we saw just above, this region suffers first a collapse followed by an infinite blow up and during the process the strut is not lost. Thus the Nariai C-metric (7.38)-(7.39) describes a spacetime that is conformal to the product $dS_2 \times \tilde{S}^2$. To each point in the deformed 2-sphere corresponds a dS_2 spacetime, except for one point which corresponds a dS_2 spacetime with an infinite straight strut. This strut has negative mass density given by

$$\mu = \frac{1}{4}\left(1 - \left|\frac{\mathcal{G}'(x_{\mathrm{n}})}{\mathcal{G}'(x_{\mathrm{s}})}\right|\right), \tag{7.41}$$

where $\mathcal{G}'(x)$ is the derivative of (7.39), and with a positive pressure $p = -\mu > 0$. Alternatively, if we remove the conical singularity at the north pole, the Nariai C-metric describes a string with positive mass density $\mu = (1/4)\left(1 - |\mathcal{G}'(x_{\mathrm{s}})/\mathcal{G}'(x_{\mathrm{n}})|\right)$ and negative pressure $p = -\mu < 0$.
   As we have said in subsection 7.1.1, the Nariai solution ($A = 0$) is unstable and, once created, it decays through the quantum tunnelling process into a slightly non-extreme black hole pair. We then expect that the Nariai C-metric is also unstable and that it will decay into a slightly non-extreme pair of black holes accelerated by a strut or by a string. The Nariai C-metric instanton also plays an important role in the decay of the dS space, since it can mediate the Schwinger-like quantum process of pair creation of black holes in a dS background [131]. Indeed, as we said in subsection 7.1.1, the Nariai instanton ($A = 0$) has been used [167, 168, 169, 173, 172] to study the pair creation of dS black holes materialized and accelerated by the cosmological background field. Moreover, the Euclidean "Nariai" flat C-metric and Ernst solution (see section 6.3) have been used to analyze the process of pair production of $\Lambda = 0$ black holes, accelerated by a string or by an electromagnetic external field, respectively. Therefore, it is natural to expect that the Euclidean Nariai limit of the

dS C-metric mediates the process of pair creation of black holes in a cosmological background, that are then accelerated by a string, in addition to the cosmological background field. The picture would be that of the nucleation, in a dS background, of a Nariai C universe, whose string then breaks down and a pair of dS black holes is created at the endpoints of the string. This expectation is confirmed in [131].

7.2.2 The Bertotti-Robinson dS C-metric

Now, we are interested in another particular extreme dS C-metric (usually called cold solution when $A = 0$ [167, 168, 169, 173]) for which the size of the outer charged black hole horizon y_+ is equal to the size of the inner charged horizon y_-. Let us label this degenerated horizon by ρ, such that, $y_+ = y_- \equiv \rho$ and $\rho > y_A$. This solution requires the presence of the electromagnetic charge. In this case, the function $\mathcal{F}(y)$ given by (6.74) can be written as

$$\mathcal{F}(y) = \frac{\rho^2 - 3\gamma}{\rho^4}(y - y_{\text{neg}})(y - y_A)(y - \rho)^2 , \tag{7.42}$$

with γ given by (7.28), the roots ρ and y_{neg} are defined by (7.29) and (7.30), respectively, and y_A is given by

$$y_A = \frac{\gamma\rho}{\rho^2 - 3\gamma}\left(1 + \sqrt{\frac{\rho^2 - 2\gamma}{\gamma}}\right) . \tag{7.43}$$

Eq. (7.32) defines the mass and the charge of the solution as a function of ρ, and, for a fixed A and Λ, the ratio q/m is higher than 1. The conditions $\rho > y_A$ and $q^2 > 0$ require that the allowed range of ρ is

$$\rho > \sqrt{6\gamma} . \tag{7.44}$$

The value of y_A decreases monotonically with ρ and we have $\sqrt{\gamma} < y_A < \sqrt{6\gamma}$. Contrary to the Nariai case, the mass and the charge of the Bertotti-Robinson solution, m_{BR} and q_{BR}, respectively, are monotonically decreasing functions of ρ, and as we come from $\rho = +\infty$ into $\rho = \sqrt{6\gamma}$ we have

$$0 < m_{\text{BR}} < \frac{\sqrt{2}}{3}\frac{1}{\sqrt{\Lambda + 3A^2}} ,$$
$$0 < q_{\text{BR}} < \frac{1}{2}\frac{1}{\sqrt{\Lambda + 3A^2}} , \tag{7.45}$$

so the $A \neq 0$ extreme ($y_+ = y_-$) solution has a lower maximum mass and charge than the corresponding $A = 0$ solution [167, 168, 169, 173] and, for a fixed Λ, as the acceleration parameter A grows this maximum value decreases monotonically. For a fixed Λ and for a fixed mass below $\sqrt{2/(9\Lambda)}$, the maximum value of the acceleration is $\sqrt{2/(27m^2) - \Lambda/3}$.

We are now ready to generate the Bertotti-Robinson dS C-metric from the above cold dS C-metric. We first set

$$y_+ = \rho - \varepsilon, \quad y_- = \rho + \varepsilon, \quad \text{with } \varepsilon << 1 , \tag{7.46}$$

in order that ε measures the deviation from degeneracy, and the limit $y_+ \to y_-$ is obtained when $\varepsilon \to 0$. Now, we introduce a new time coordinate τ and a new radial coordinate χ,

$$t = \frac{1}{\varepsilon \mathcal{K}}\tau , \qquad y = \rho + \varepsilon \cosh\chi , \tag{7.47}$$

where

$$\mathcal{K} = \frac{\rho^2 - 3\gamma}{\rho^4}(\rho - y_{\text{neg}})(\rho - y_A) = 1 - \frac{2(\Lambda + 3A^2)}{A^2\rho^2} , \tag{7.48}$$

and condition (7.44) implies $0 < \mathcal{K} < 1$. In the limit $\varepsilon \to 0$, from (6.73) and (7.42), the metric becomes

$$ds^2 = \frac{\mathcal{R}^2(x)}{\mathcal{K}}\left(-\sinh^2\chi\, d\tau^2 + d\chi^2\right) + \mathcal{R}^2(x)\left[\mathcal{G}^{-1}(x)dx^2 + \mathcal{G}(x)dz^2\right], \qquad (7.49)$$

where χ is unbounded and

$$\mathcal{R}^2(x) = \left(Ax + \sqrt{\tfrac{2(\Lambda+3A^2)}{1-\mathcal{K}}}\right)^{-2},$$

$$\mathcal{G}(x) = 1 - x^2 - \tfrac{2A}{3}\sqrt{\tfrac{(1-\mathcal{K})(2+\mathcal{K})^2}{2(\Lambda+3A^2)}}\, x^3 - \tfrac{A^2}{4}\tfrac{1-\mathcal{K}^2}{\Lambda+3A^2}\, x^4.$$

$$(7.50)$$

$\mathcal{G}(x)$ has only two real roots, the south pole $x_{\rm s}$ and the north pole $x_{\rm n}$. The angular coordinate x can range between these two poles whose value is calculated in section 7.5. Under the coordinate transformation (7.47), the Maxwell field for the magnetic case is still given by (6.5), while in the electric case, (6.6) becomes

$$F = -\frac{q}{\mathcal{K}}\sinh\chi\, d\tau \wedge d\chi. \qquad (7.51)$$

So, if we give the parameters Λ, A, and q we can construct the Bertotti-Robinson dS C-metric. This solution is conformal to the topological product of two 2-dimensional manifolds, $AdS_2 \times \tilde{S}^2$, with the conformal factor $\mathcal{R}^2(x)$ depending on the angular coordinate x.

In order to obtain the $A = 0$ limit, we first set $\tilde{\rho} = A\rho$ [see (7.29)], a parameter that has a finite and well-defined value when $A \to 0$. Then when $A \to 0$ we have $\mathcal{K} \to \mathcal{K}_0 = 1 - 2\Lambda/\tilde{\rho}^2$ and $\mathcal{R}^2(x) \to \mathcal{R}_0^2 = \tilde{\rho}^{-2}$. This, together with transformations (6.9), show that the Bertotti-Robinson dS C-metric transforms into the dS counterpart of the Bertotti-Robinson solution discussed in subsection 7.1.2, when $A = 0$. The limiting procedure that has been applied in this subsection has generated a new exact solution that satisfies the Maxwell-Einstein equations in a positive cosmological constant background.

Figure 7.2: (a) The whole figure is the Carter-Penrose diagram of the dS C-metric. The shaded region represents the near-horizon area that, when the inner black hole horizon (h_-) approaches the outer black hole horizon (h_+), gives the AdS_2 manifold of the Bertotti-Robinson C-metric. See discussion in the text. (b) Carter-Penrose diagram of the Bertotti-Robinson C-metric. (c) The whole figure represents schematically the two accelerated black holes of the dS C-metric. The shaded region represents the near-horizon area that, when the inner black hole horizon approaches the outer black hole horizon, gives the Bertotti-Robinson C-metric [compare with Fig. 7.2.(a)]. The strut does not survive to the limiting process.

We have just seen that the Bertotti-Robinson dS C-metric can be appropriately obtained from the vicinity of the inner and outer black hole horizons in the limit in which the size of these two

horizons approach each other. This near-horizon region is sketched in Fig. 7.2.(a) as a shaded area, and from it we can construct straightforwardly the Carter-Penrose diagram of the Bertotti-Robinson dS C-metric drawn in Fig. 7.2.(b). The construction steps are as follows. First, as indicated by (7.46) and the second relation of (7.47), we let the cross lines that represent the black hole Cauchy horizon [h_- in Fig. 7.2.(a)] join together with the cross lines that represent the black hole event horizon [h_+ in Fig. 7.2.(a)], and so on, i.e., we do this junction ad infinitum with all the cross lines h_- and h_+. After this step all that is left from the original diagram is a single cross line, i.e, all the spacetime that has originally contained in the shaded area of Fig. 7.2.(a) has collapsed into two mutually perpendicular lines at $45°$ at $y = \rho$. Now, as indicated by the first relation of (7.47), when $\varepsilon \to 0$ the time suffers an infinite blow up. To this blow up in the time corresponds an infinite expansion in the Carter-Penrose diagram in the vicinity of $y = \rho$ that generates an AdS_2 region. We then get again the shaded area of Fig. 7.2.(a), but now the cross lines of this shaded area are all identified into a single line, and they no longer have the original labels associated to h_- and h_+ that differentiated them. This is, in the shaded area of Fig. 7.2.(a) we must now erase the original labels h_- and h_+. The Carter-Penrose diagram of the Bertotti-Robinson dS C-metric is then given by Fig. 7.2.(b), which is equivalent to the diagram of the (1+1)-dimensional AdS solution. Note that the diagram of the $A = 0$ Reissner-Nordström$-$dS solution is identical to the one of Fig. 7.2.(a). Therefore, applying the same construction process described just above we find that the Carter-Penrose diagram of the Bertotti-Robinson dS solution ($A = 0$) is similar to the one of Fig. 7.2.(b). The diagram of the Bertotti-Robinson solution with $\Lambda = 0$ described by (7.10) is also given by Fig. 7.2.(b).

The Bertotti-Robinson near-horizon region is also sketched in Fig. 7.2.(c) as a shaded area. This schematic figure is clarifying in the sense that it indicates that the strut that connects the two original black holes along their north pole directions does not survive to the near-extremal limiting process and will not be present in the final result of the process, i.e., in the Bertotti-Robinson dS C-metric. However, a reminiscence of this strut remains in the final solution. Indeed, the angular factor of the Bertotti-Robinson dS C-metric [which, remind, describes a deformed 2-sphere $\tilde{S}^2$ with a fixed size $\mathcal{R}^2(x)$ given by (7.50)] has a conical singularity at least at one of its poles. We can choose the parameter κ, introduced in (6.9), in order to have a conical singularity only at the north pole ($\delta_{\rm s} = 0$), or only at the south pole ($\delta_{\rm n} = 0$), however we cannot eliminate both. When the parameter A is set to zero, the conical singularities disappear, the angular factor describes a round 2-sphere with fixed radius, and the Bertotti-Robinson dS C-metric reduces into the Bertotti-Robinson dS solution with topology $AdS_2 \times S^2$.

7.2.3 The Nariai Bertotti-Robinson dS C-metric

As the previous sections and the label suggest, the Nariai Bertotti-Robinson dS C-metric will be generated from the extremal limit of a very particular dS C-metric (usually called ultracold solution when $A = 0$ [167, 168, 169, 173]) for which the size of the three horizons (y_A, y_+ and y_-) are equal, and let us label this degenerated horizon by ρ: $y_A = y_+ = y_- \equiv \rho$. In this case, the function $\mathcal{F}(y)$ is given by (7.27) with $y_- = \rho$, and γ defined in (7.28). The negative root $y_{\rm neg}$ is given by (7.30) and

$$\rho = \sqrt{6\gamma} \,. \tag{7.52}$$

The mass and the charge of the Nariai Bertotti-Robinson dS C-metric solution , $m_{\rm NBR}$ and $q_{\rm NBR}$, respectively, are given by

$$m_{\rm NBR} = \frac{\sqrt{2}}{3}\sqrt{\frac{1}{\Lambda + 3A^2}} \,,$$

$$q_{\rm NBR} = \frac{1}{2}\sqrt{\frac{1}{\Lambda + 3A^2}} \,, \tag{7.53}$$

and these values are the maximum values of the mass and charge of both the Nariai C and Bertotti-Robinson C solutions, (7.34) and (7.45), respectively. To clarify the nature of these solutions, a

diagram $m\sqrt{\Lambda + 3A^2} \times q\sqrt{\Lambda + 3A^2}$ is plotted in Fig. 7.3. For a fixed value of A and Λ, the allowed range of the mass and charge of the Nariai C-metric, of the Bertotti-Robinson dS C-metric, and of the Nariai Bertotti-Robinson dS C-metric is shown.
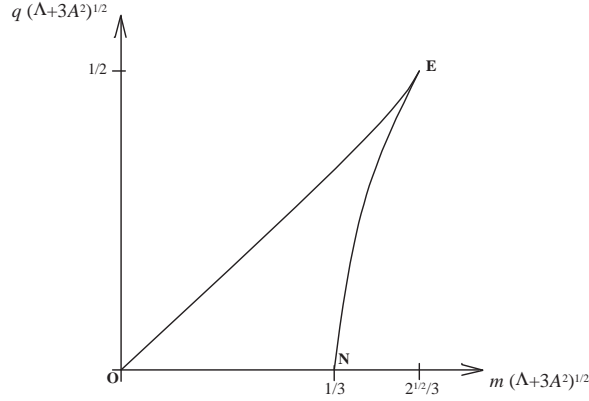
Figure 7.3: Relation $m\sqrt{\Lambda + 3A^2} \times q\sqrt{\Lambda + 3A^2}$, for a fixed value of A and Λ, for the extremal limits of the dS C-metric. NE represents the Nariai C-metric (with point N representing the neutral case), OE represents the Bertotti-Robinson dS C-metric, and point E represents the Nariai Bertotti-Robinson dS C-metric.

We are now ready to generate the Nariai Bertotti-Robinson dS C-metric from the above ultracold dS C-metric. We first set

$$\rho = \sqrt{6\gamma} - \varepsilon, \quad y_- = \sqrt{6\gamma} + \varepsilon, \quad \text{with } \varepsilon << 1. \tag{7.54}$$

Now, we introduce a new time coordinate τ and a new radial coordinate χ,

$$t = \frac{1}{2\varepsilon^2\mathcal{K}}\,\tau, \qquad y = \sqrt{6\gamma} + \varepsilon\cosh(\sqrt{2\varepsilon\mathcal{K}}\,\chi), \tag{7.55}$$

where

$$\mathcal{K} = \frac{\rho^2 - 3\gamma}{\rho^4}(\rho - y_{\text{neg}}) = \frac{1}{3}\sqrt{\frac{2A^2}{\Lambda + 3A^2}}. \tag{7.56}$$

In the limit $\varepsilon \to 0$ the metric (6.73) becomes

$$ds^2 = \mathcal{R}^2(x)\left[-\chi^2\,d\tau^2 + d\chi^2 + \mathcal{G}^{-1}(x)dx^2 + \mathcal{G}(x)dz^2\right], \tag{7.57}$$

with

$$\mathcal{R}^2(x) = \left(Ax + \sqrt{2(\Lambda + 3A^2)}\right)^{-2},$$

$$\mathcal{G}(x) = 1 - x^2 - \frac{2A}{3}\sqrt{\frac{2}{\Lambda + 3A^2}}\,x^3 - \frac{A^2}{4(\Lambda + 3A^2)}\,x^4. \tag{7.58}$$

$\mathcal{G}(x)$ has only two real roots, the south pole x_{s} and the north pole x_{n}. The angular coordinate x can range between these two poles whose value is calculated in section 7.5. Notice that the spacetime factor $-\chi^2\,d\tau^2 + d\chi^2$ is just $\mathbb{M}^{1,1}$ in Rindler coordinates. Therefore, under the usual coordinate transformation $\chi = \sqrt{\bar{x}^2 - \bar{t}^2}$ and $\tau = \text{arctanh}(\bar{t}/\bar{x})$, this factor transforms into $-d\bar{t}^2 + d\bar{x}^2$. Under the coordinate transformation (7.55), the Maxwell field for the magnetic case is still given by (6.5), while in the electric case, (6.6) becomes

$$F = -q\,\chi\,d\tau \wedge d\chi. \tag{7.59}$$

The Nariai Bertotti-Robinson dS C-metric is conformal to the topological product of two 2-dimensional manifolds, $\mathbb{M}^{1,1} \times \tilde{S}^2$, with the conformal factor $\mathcal{R}^2(x)$ depending on the angular coordinate x.

In the $A = 0$ limit, $\mathcal{R}^2(x) \to (2\Lambda)^{-1}$, and one obtains the Nariai Bertotti-Robinson solution $ds^2 = (2\Lambda)^{-1}(-d\bar{t}^2 + d\bar{x}^2 + d\theta^2 + \sin^2\theta\, d\phi^2)$, which has the topology $\mathbb{M}^{1,1} \times S^2$ [167, 168, 169, 173]).
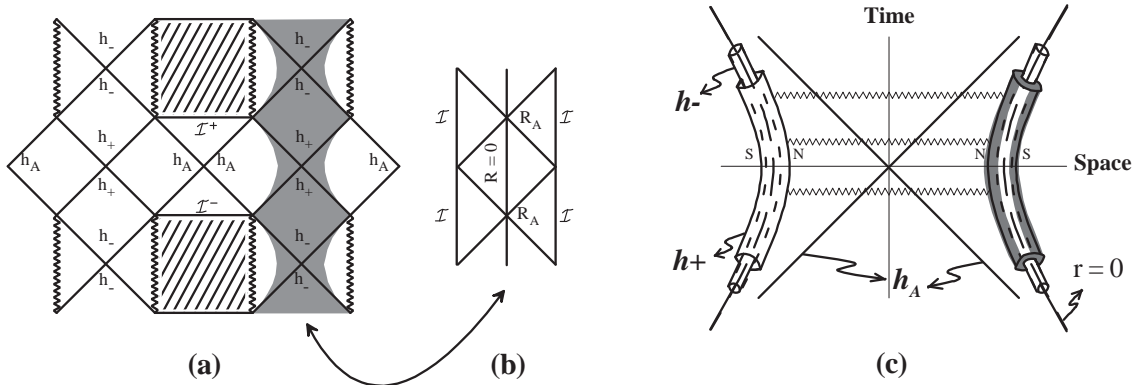

(a) **(b)**
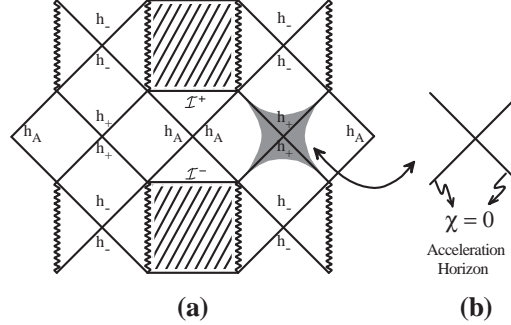
Figure 7.4: (a) The whole figure is the Carter-Penrose diagram of the dS C-metric. The shaded region represents the near-horizon area that, when the inner black hole horizon (h_-) and the acceleration horizon (h_A) approach the outer black hole horizon (h_+), gives the Rindler manifold of the Nariai Bertotti-Robinson C-metric. This shaded region is the intersection of the shaded areas of Figs. 7.1.(a) and 7.2.(a). See discussion in the text. (b) Kruskal diagram of the Nariai Bertotti-Robinson dS C-metric.

We have just seen that the Nariai Bertotti-Robinson dS C-metric can be appropriately obtained from the vicinity of the accelerated and black hole horizons in the limit in which the size of these three horizons approach each other. This near-horizon region is sketched in Fig. 7.4.(a) as a shaded area, and can be viewed as the intersection of the shaded areas of Figs. 7.1.(a) and 7.2.(a). From it we can construct straightforwardly, following the construction steps already sketched in subsections 7.2.1 and 7.2.2, the Kruskal diagram of the Nariai Bertotti-Robinson dS C-metric drawn in Fig. 7.4.(b). This diagram is equivalent to the Kruskal diagram of the Rindler solution. The strut that connects the two original black holes along their north pole directions survives to the near-extremal limiting process. Thus the Nariai Bertotti-Robinson dS C-metric describes a spacetime that is conformal to the product $\mathbb{M}^{1,1} \times \tilde{S}^2$. To each point in the deformed 2-sphere corresponds a $\mathbb{M}^{1,1}$ spacetime, except for one point which corresponds a $\mathbb{M}^{1,1}$ spacetime with an infinite straight strut or string, with a mass density and pressure satisfying $p = -\mu$. In an analogous way to the one that occurs with the Nariai C universe (see section 7.3.1), we expect that the Nariai Bertotti-Robinson dS C universe is unstable and, once created, it decays through the quantum tunnelling process into a slightly non-extreme black hole pair. The picture would be that of the nucleation, in a dS background, of a Nariai Bertotti-Robinson dS C universe, whose string then breaks down and a pair of dS black holes is created at the endpoints of the string. This expectation is confirmed in [131]. When the parameter A is set to zero, the conical singularities disappear (and so the strut or string are no longer present) and the angular factor describes a round 2-sphere with fixed radius, and the topology of the Nariai Bertotti-Robinson dS C-metric reduces into $\mathbb{M}^{1,1} \times S^2$.

7.3 Extremal limits of the flat C-metric and of the Ernst solution

The Euclidean version of the "Nariai" flat C-metric that will be discussed in subsection 7.3.1 has already been used previously, [158]-[166] and [133], in the study of the quantum process of pair creation of black holes. However, as far as we know, the Bertotti-Robinson flat C-metric (discussed in subsection 7.3.2) and the Nariai Bertotti-Robinson flat C-metric (discussed in subsection 7.3.3) have not been written explicitly.

7.3.1 The "Nariai" flat C-metric

The Nariai solution [125] is originally a solution in the $\Lambda > 0$ background which can be obtained from a near-extremal limit of the dS black hole when the outer black horizon approaches the cosmological horizon. Therefore, it would seem not appropriate to use the name Nariai to label a $\Lambda = 0$ solution. However, in the flat C-metric the acceleration horizon plays the role of the cosmological horizon. Moreover, the limit $A = 0$ of the solution discussed in this subsection is equal to the limit $\Lambda = 0$ of the Nariai solution (see subsection 7.1.4). In this context, we find appropriate to label this solution by "Nariai" in between commas, in order to maintain the nomenclature of the paper.

This solution can be obtained from a near-extremal limit of the flat C-metric when the outer black horizon approaches the acceleration horizon. This is the way it has been first constructed in [158]-[166]. However, given the Nariai C-metric ($\Lambda > 0$) generated in subsection 7.2.1, we can construct the "Nariai" flat C-metric ($\Lambda = 0$) by taking directly the $\Lambda = 0$ limit of (7.38)-(7.39). The gravitational field of the "Nariai" flat C-metric is then given by (7.38) with

$$\mathcal{R}^2(x) = A^{-2} \left(x + \sqrt{\tfrac{6}{1+\mathcal{K}}} \right)^{-2} ,$$

$$\mathcal{G}(x) = 1 - x^2 - \sqrt{\tfrac{2(1+\mathcal{K})(2-\mathcal{K})^2}{27}} \, x^3 - \tfrac{1-\mathcal{K}^2}{12} \, x^4 , \tag{7.60}$$

where $0 < \mathcal{K} \le 1$ and $\mathcal{K} = 1$ when $q = 0$. $\mathcal{G}(x)$ has only two real roots, the south pole x_s and the north pole x_n. The angular coordinate x can range between these two poles whose value is calculated in section 7.5.

There is a great difference between the Nariai C solution of the $\Lambda > 0$ case and the "Nariai" C solution of the $\Lambda = 0$ case. In subsection 7.2.1 we saw that the Nariai C-metric ($\Lambda > 0$) has a conical singularity at one of the poles of its deformed 2-sphere. This feature is no longer present in the "Nariai" flat C-metric, i.e., it is free of conical singularities. Indeed, in the flat C-metric we have $\mathcal{F}(y) = -\mathcal{G}(-y)$. Therefore, if the outer black hole horizon coincides with the acceleration horizon then the roots x_0 and x_s of $\mathcal{G}(x)$ also coincide (see Fig. 6.19). This implies that the range of the angular coordinate x becomes $x_s < x \le x_n$ since the proper distance between x_s and x_n goes to infinity [114],[158]-[166]. The point x_s disappears from the x, z angular section which is no longer compact but becomes topologically $\mathbb{R} \times S^1$ or $\mathbb{R}^2$. So, we have a conical singularity only at $x = x_n$ which can be avoided by choosing $2\kappa^{-1} = |\mathcal{G}'(x_n)|$. Therefore, while the Nariai C-metric ($\Lambda > 0$) is topologically conformal to $dS_2 \times \tilde{S}^2$, the "Nariai" flat C-metric is topologically conformal to $dS_2 \times \mathbb{R}^2$. Its Carter-Penrose diagram is given by Fig. 7.1(b). We could construct the "Nariai" Ernst solution, however since its main motivation is related to the removal of the conical singularities present in the C-metric solution and in this case our "Nariai" flat C-metric is free of conical singularities, we will not do it.

At this point, it is appropriate to find the $A = 0$ limit of the "Nariai" flat C-metric. This limit is not direct [see (7.60)]. To achieve the suitable limit we first make the coordinate rescales: $\tilde{x} = \chi/A$, $\bar{y} = x/A$, and $\bar{z} = z/A$. Then, setting $A = 0$, the solution becomes $ds^2 = (1 + \mathcal{K})/6 \, [\mathcal{K}^{-1}(-\tilde{x}^2 d\tau^2 + d\tilde{x}^2) + d\bar{y}^2 + d\bar{z}^2]$. This limit agrees with the one taken from the $A = 0$ Nariai solution (written in subsection 7.1.1) in the limit $\Lambda = 0$ (see subsection 7.1.4). Therefore, while the limit $A = 0$ of the Nariai C-metric ($\Lambda > 0$) is topologically $dS_2 \times S^2$, the $A = 0$ limit of the "Nariai" flat C-metric is topologically $\mathbb{M}^{1,1} \times \mathbb{R}^2$. This is a reminiscence of the fact that with $\Lambda = 0$ when A goes to zero there is no acceleration horizon to play the role of cosmological horizon that supports the extremal limit taken in this subsection. As a final remark in this subsection, we note that Horowitz and Sheinblatt [271] have taken a different extremal limit, which differs from the one discussed in this subsection mainly because it preserves the asymptotic behavior and topology of the original flat C-metric solution.

7.3.2 The Bertotti-Robinson flat C-metric

Given the Bertotti-Robinson dS C-metric generated in subsection 7.2.2, we can construct the Bertotti-Robinson flat C-metric by taking the direct $\Lambda = 0$ limit of (7.49)-(7.50). The gravita-

tional field of the Bertotti-Robinson flat C-metric is then given by (7.49) with

$$\mathcal{R}^2(x) = \left(A x + \sqrt{\tfrac{6A^2}{1-\mathcal{K}}} \right)^{-2} ,$$

$$\mathcal{G}(x) = 1 - x^2 - \sqrt{\tfrac{2(1-\mathcal{K})(2+\mathcal{K})^2}{27}}\, x^3 - \tfrac{1-\mathcal{K}^2}{12}\, x^4 , \qquad (7.61)$$

and $0 < \mathcal{K} < 1$. $\mathcal{G}(x)$ has only two real roots, the south pole x_{s} and the north pole x_{n}. The angular coordinate x can range between these two poles whose value is calculated in section 7.5. As in the Bertotti-Robinson dS C-metric, this solution has topology conformal to $AdS_2 \times \tilde{S}^2$, and a Carter-Penrose diagram drawn in Fig. 7.2.(b). The solution has a conical singularity at one of the poles of its deformed 2-sphere $\tilde{S}^2$. In the $A = 0$ limit, we have $\mathcal{K} \to 1$ and $\mathcal{R}^2(x) \to q^2$ and we obtain the Bertotti-Robinson solution (7.10) discussed in subsection 7.1.2.

From the above solution we can generate the Bertotti-Robinson Ernst solution whose gravitational field is given by

$$ds^2 = \Sigma^2(x) \frac{\mathcal{R}^2(x)}{\mathcal{K}} \left(- \sinh^2 \chi\, d\tau^2 + d\chi^2 \right) + \mathcal{R}^2(x) \left[\frac{\Sigma^2(x)}{\mathcal{G}(x)} dx^2 + \frac{\mathcal{G}(x)}{\Sigma^2(x)}\, dz^2 \right] . \qquad (7.62)$$

with $\mathcal{R}^2(x)$ and $\mathcal{G}(x)$ given by (7.61), and with

$$\Sigma(x) = \left(1 + \frac{1}{2}\, q\, \mathcal{E}_0\, x \right)^2 + \frac{1}{4}\mathcal{E}_0^2\, \mathcal{G}(x)\mathcal{R}^2(x) . \qquad (7.63)$$

Its electromagnetic field is given by (6.62), in the pure magnetic case, and by (6.63), in the pure electric case. Choosing $\tilde{\kappa}$ satisfying (6.65), with $\tilde{\mathcal{G}}(x) = \Sigma^{-2}(x)\mathcal{G}(x)$, and $\mathcal{E}_0$ such that condition (6.66) is satisfied, the Bertotti-Robinson Ernst solution is free of conical singularities. As a final remark in this subsection, we note that Dowker, Gauntlett, Kastor and Traschen [114] have taken a different extremal limit, which differs from the one discussed in this subsection mainly because it preserves the asymptotic behavior and topology of the original flat C-metric solution.

7.3.3 The "Nariai" Bertotti-Robinson flat C-metric

From the Nariai Bertotti-Robinson dS C-metric generated in subsection 7.2.3, we can construct the "Nariai" Bertotti-Robinson flat C-metric by taking the direct $\Lambda = 0$ limit of (7.57)-(7.58). We can also construct the "Nariai" Bertotti-Robinson Ernst solution. We do not do these limits here because they are now straightforward.

7.4 Extremal limits of the AdS C-metric

In the AdS background there are three different families of C-metrics. When we set $A = 0$, each one of these families reduces to a different single AdS black hole. The main features of each one of these three families of AdS black holes (the spherical, the toroidal and the hyperbolic families) have been described in section 5.1).

Now, to each one of these families corresponds a different AdS C-metric which has been found by Plebański and Demiański [86]. In what follows we will then describe each one of these solutions and, in particular, we will generate a new solution - the anti-Nariai C-metric.

7.4.1 Extremal limits of the AdS C-metric with spherical horizons

The spherical AdS C-metric has already been discussed in detail in section 6.1. Its gravitational field is given by (6.3) with $\mathcal{F}(y)$ and $\mathcal{G}(x)$ given by 6.4. Recall that this solution describes a pair of accelerated black holes in the AdS background [87] when the acceleration A and the cosmological constant are related by $A > |\Lambda|/3$. When we set $A = 0$ [121, 122, 87] we obtain a single non-accelerated AdS black hole with spherical topology described subsection 5.1.1.

Chapter 7. The extremal limits of the C-metric:
Nariai, Bertotti-Robinson and anti-Nariai C-metrics

In a way analogous to the one described in last sections we can generate new solutions from the extremal limits of the AdS C-metric. Since this follows straightforwardly, we do not do it here. The new relevant feature of this case is the fact that the Nariai-like extremal solution only exists when $A > |\Lambda|/3$. In this case, and only in this one, the acceleration horizon is present in the AdS C-metric and we can have the outer black hole horizon approaching it.

7.4.2 Extremal limits of the AdS C-metric with toroidal horizons

The gravitational field of the massive charged toroidal AdS C-metric (see [86, 178]) is given by (6.3) with

$$
\begin{aligned}
\mathcal{F}(y) &= \frac{|\Lambda| - 3A^2}{3A^2} - 2mAy^3 + q^2A^2y^4, \\
\mathcal{G}(x) &= 1 - 2mAx^3 - q^2A^2x^4 ,
\end{aligned}
\tag{7.64}
$$

and the electromagnetic field is given by (6.5) and (6.6). When we set $A = 0$ we obtain the AdS black hole with planar, cylindrical or toroidal topology [6, 7, 10, 8] described in subsection 5.1.2.a.
In a way analogous to the one described in section 7.2 we can generate new solutions from the extremal limits of the toroidal AdS C-metric, that are the toroidal AdS counterparts of the Nariai and Bertotti-Robinson C-metrics. Since this follows straightforwardly, we do not do it here.

7.4.3 Extremal limits of the AdS C-metric with hyperbolic horizons

The gravitational field of the massive charged AdS C-metric with hyperbolic horizons, the hyperbolic AdS C-metric, is given by (6.3) with [86, 178]

$$
\begin{aligned}
\mathcal{F}(y) &= \frac{|\Lambda| + 3A^2}{3A^2} - y^2 - 2mAy^3 + q^2A^2y^4, \\
\mathcal{G}(x) &= -1 + x^2 - 2mAx^3 - q^2A^2x^4
\end{aligned}
\tag{7.65}
$$

(represented in Fig. 7.5), and the electromagnetic field is given by (6.5) and (6.6).
This solution depends on four parameters namely, the cosmological constant $\Lambda < 0$, the acceleration parameter $A > 0$, and m and q which are mass and electromagnetic charge parameters, respectively. When $A = 0$ this solution reduces to the hyperbolic black holes [11] studied in subsection 5.1.3.
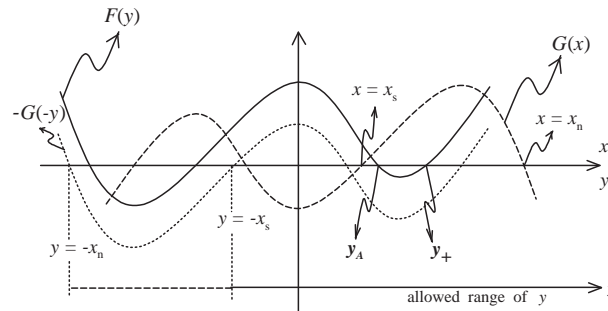
Figure 7.5: Shape of $\mathcal{G}(x)$ and $\mathcal{F}(y)$ for a general non-extremal charged massive hyperbolic AdS C-metric studied in section 7.4.3. The allowed range of x is between x_{s} and x_{n} where $\mathcal{G}(x)$ is positive and compact. The permitted range of y is $-x \leq y < +\infty$. The presence of an accelerated horizon is indicated by y_A and the black hole horizon by y_+. In the anti-Nariai case considered in subsection 7.4.3.a, y_A and y_+ coincide. [For completeness we comment on a case not represented in the figure but discussed on the text: when $q = 0$, the zero x_{n} of $\mathcal{G}(x)$ disappears, and $\mathcal{G}(x)$ grows monotonically from $x = x_{\mathrm{s}}$ into $x = +\infty$.]

7.4.3.a The anti-Nariai C-metric

We are interested in a particular extreme hyperbolic AdS C-metric, for which $y_A = y_+$ (see Fig. 7.5), and let us label this degenerated horizon by ρ: $y_A = y_+ \equiv \rho$. In this case, the function $\mathcal{F}(y)$ can be written as

$$\mathcal{F}(y) = -\frac{\rho^2 - 3\gamma}{\rho^4}(y - y_{\mathrm{neg}})(y - y'_{\mathrm{neg}})(y - \rho)^2 \,, \tag{7.66}$$

where

$$\gamma = \frac{|\Lambda| + 3A^2}{3A^2} \,, \tag{7.67}$$

and the degenerate root ρ, and the negative roots y_{neg} and y'_{neg} are given by

$$\rho = \frac{3m}{4q^2 A}\left(1 + \sqrt{1 + \frac{8}{9}\frac{q^2}{m^2}}\right) \,,$$

$$y_{\mathrm{neg}} = -\frac{\gamma\rho}{3\gamma - \rho^2}\left(1 + \sqrt{\frac{\rho^2 - 2\gamma}{\gamma}}\right) \,,$$

$$y'_{\mathrm{neg}} = -\frac{\gamma\rho}{3\gamma - \rho^2}\left(1 - \sqrt{\frac{\rho^2 - 2\gamma}{\gamma}}\right) \,. \tag{7.68}$$

The mass parameter and the charge parameter of the solution are written as a function of ρ as

$$m = -\frac{1}{A\rho}\left(1 - \frac{2\gamma}{\rho^2}\right) \,,$$

$$q^2 = \frac{1}{A^2\rho^2}\left(\frac{3\gamma}{\rho^2} - 1\right) \,. \tag{7.69}$$

The requirement that y_{neg} and y'_{neg} are real roots and the condition $q^2 \geq 0$ require that the allowed range of ρ is

$$2\gamma < \rho^2 \leq 3\gamma \,. \tag{7.70}$$

The mass and the charge of the anti-Nariai type solution, m_{aN} and q_{aN}, respectively, are both monotonically decreasing functions of ρ, and as one comes from $\rho = \sqrt{3\gamma}$ into $\rho = \sqrt{2\gamma}$ one has,

$$-\frac{1}{3}\frac{1}{\sqrt{|\Lambda| + 3A^2}} \leq m_{\mathrm{aN}} < 0 \,,$$

$$0 \leq q_{\mathrm{aN}} < \frac{\sqrt{3}}{2}\frac{1}{\sqrt{|\Lambda| + 3A^2}} \,. \tag{7.71}$$

In order to generate the anti-Nariai C-metric from the near-extreme topological AdS C-metric we first set

$$y_A = \rho - \varepsilon, \quad y_+ = \rho + \varepsilon, \quad \text{with } \varepsilon << 1 \,, \tag{7.72}$$

in order that ε measures the deviation from degeneracy, and the limit $y_A \to y_+$ is obtained when $\varepsilon \to 0$. Now, we introduce a new time coordinate τ and a new radial coordinate χ,

$$t = \frac{1}{\varepsilon\mathcal{K}}\tau \,, \qquad y = \rho + \varepsilon\cosh\chi \,, \tag{7.73}$$

where

$$\mathcal{K} = \frac{3\gamma - \rho^2}{\rho^4}(\rho - y_{\text{neg}})(\rho - y_{\text{neg}}') = \frac{2(|\Lambda| + 3A^2)}{A^2\rho^2} - 1 \, ,$$

(7.74)

and $2\gamma < \rho^2 \leq 3\gamma$ implies $1 \leq \mathcal{K} < 2$ with $q = 0 \Rightarrow \mathcal{K} = 1$. In the limit $\varepsilon \to 0$, from (6.3) and (7.66), the metric becomes

$$ds^2 = \frac{\mathcal{R}^2(x)}{\mathcal{K}}\left(-\sinh^2\chi \, d\tau^2 + d\chi^2\right) + \mathcal{R}^2(x)\left[\mathcal{G}^{-1}(x)dx^2 + \mathcal{G}(x)dz^2\right] \, .$$

(7.75)

where

$$\mathcal{R}^2(x) = \left(Ax + \sqrt{\frac{2(|\Lambda| + 3A^2)}{1 + \mathcal{K}}}\right)^{-2} \, ,$$

(7.76)

$$\mathcal{G}(x) = -1 + x^2 + \frac{A}{3}\sqrt{\frac{2(1+\mathcal{K})(2-\mathcal{K})^2}{(|\Lambda| + 3A^2)}}\, x^3 + \frac{A^2}{4}\frac{\mathcal{K}^2 - 1}{|\Lambda| + 3A^2}\, x^4 \, ,$$

(7.77)

Under the coordinate transformation (7.73), the Maxwell field for the magnetic case is still given by (6.5), while in the electric case, (6.6) becomes

$$F = -\frac{q}{\mathcal{K}}\sinh\chi \, d\tau \wedge d\chi \, .$$

(7.78)

The Carter-Penrose diagram of the anti-Nariai C-metric is also given by Fig. 7.2.(b).

At this point, let us focus our attention on the angular surfaces with $\tau =$ constant and $\chi =$ constant. When $q \neq 0$, we choose x such that it belongs to the range $[x_{\text{s}}, x_{\text{n}}]$ (sketched in Fig. 7.5) where $\mathcal{G}(x) \geq 0$. In this way, the metric has the correct signature, the angular surfaces are compact, and the allowed range of y includes the acceleration (y_A) and black hole (y_+) horizons (if we had chosen the other possible interval of x where $\mathcal{G}(x) \geq 0$, sketched in Fig. 7.5, this last condition would not be satisfied). We unavoidably have a conical singularity at least at one of the poles of this compact surface (that we label by $\tilde{S}^2$, say). Thus, the charged anti-Nariai C-metric has a compact angular surface of fixed size with a conical singularity at one of its poles. It is topologically conformal to $AdS_2 \times \tilde{S}^2$. When $q = 0$, the zero x_{n} of $\mathcal{G}(x)$ disappears, and $\mathcal{G}(x)$ grows monotonically from $x = x_{\text{s}}$ into $x = +\infty$. Then, the angular surfaces are not compact, and we have a single pole $(x = x_{\text{s}})$ with a conical singularity, which can be eliminated. Thus, the neutral anti-Nariai C-metric has a non-compact angular surface of fixed size (a kind of a deformed 2-hyperboloid that we label by $\tilde{H}_2$, say) which is free of conical singularities. It is topologically conformal to $AdS_2 \times \tilde{H}_2$.

In order to obtain the $A = 0$ limit, we first set $\hat{\rho} = A\rho$ [see first relation of (7.68)], a parameter that has a finite and well-defined value when $A \to 0$. Then when $A \to 0$ we have $\mathcal{K} \to \mathcal{K}_0 = 2|\Lambda|/\hat{\rho}^2 - 1$ and $\mathcal{R}^2 \to \mathcal{R}_0^2 = \hat{\rho}^{-2}$, with $\mathcal{R}_0^2$ and $\mathcal{K}_0$ satisfying relations (7.20). Moreover, when we set $A = 0$, $m \neq 0$ and $q \neq 0$, the coordinate transformations $\theta = \int_{x_{\text{s}}}^x \mathcal{G}^{-1/2}dx$ and $\phi = z$ imply that $x \in [x_{\text{s}} = +1, +\infty[$, $x = \cosh\theta$, and $\mathcal{G} = -1 + x^2 = \sinh^2\theta$. The angular surface then reduces to a 2-hyperboloid, H_2, of fixed size with line element $d\theta^2 + \sinh^2\theta \, d\phi^2$. Therefore, when $A = 0$ the anti-Nariai C-metric reduces to the anti-Nariai solution (7.17) described in subsection 7.1.3, with topology $AdS_2 \times H_2$. The limiting procedure that has been applied in this subsection has generated a new exact solution that satisfies the Maxwell-Einstein equations in a negative cosmological constant background.

7.4.3.b Other extremal limits

We could also discuss other extremal limits of the charged topological AdS C-metric (see Fig. 7.5), but these do not seem to be so interesting.

7.5 Determination of the north and south poles

In this section we discuss the zeros of the function $\mathcal{G}(x)$ that appears in the extremal limits of the dS C-metric, and in the extremal limits of the flat C-metric. This function $\mathcal{G}(x)$ has only two real zeros in the cases discussed in this paper, namely the Nariai, the Bertotti-Robinson, and the Nariai Bertotti-Robinson (both for $\Lambda > 0$ and $\Lambda = 0$). These two roots are the south pole and the north pole, and are respectively given by

$$
\begin{aligned}
x_{\rm s} &= -p + \frac{h}{2} - \frac{a}{4b} < 0, \\
x_{\rm n} &= +p + \frac{h}{2} - \frac{a}{4b} > 0,
\end{aligned}
\tag{7.79}
$$

with

$$
\begin{aligned}
p &= \frac{1}{2}\left(-\frac{s}{3} + \frac{a^2}{2b^2} - \frac{1-12b}{3sb^2} - \frac{4}{3b} + n\right)^{1/2}, \\
n &= \frac{-a^3 + 4ab}{4hb^3}, \\
h &= \sqrt{\frac{s}{3} + \frac{a^2}{4b^2} + \frac{1-12b}{3sb^2} - \frac{2}{3b}}, \\
s &= \frac{1}{2^{1/3}b}\left(\lambda - \sqrt{\lambda^2 - 4(1-12b)^3}\right)^{1/3}, \\
\lambda &= 2 - 27a^2 + 72b,
\end{aligned}
\tag{7.80}
$$

where a and b are, respectively, the absolute values of the coefficients of x^3 and x^4 in (7.39), (7.50), (7.58), (7.60), and (7.61). For the function $\mathcal{G}(x)$ written in a different polynomial form that facilitates the determination of its zeros see Hong and Teo [272].

7.6 Summary and discussion

Following the limiting approach first introduced by Ginsparg and Perry [97], we have analyzed the extremal limits of the dS, flat and AdS C-metrics. Among other new exact solutions, we have generated the Nariai C-metric, the Bertotti-Robinson C-metric, the Nariai Bertotti-Robinson C-metric and the anti-Nariai C-metric. These solutions are the C-metric counterparts of the well know solutions found in the 1950's. They are specified by an extra parameter: the acceleration parameter A of the C-metric from which they are generated. When we set $A = 0$ the solutions found in this paper reduce to the Nariai, the Bertotti-Robinson, the Nariai Bertotti-Robinson and the anti-Nariai solutions.

One of the features of these $A = 0$ solutions is the fact that they are topologically the direct product of two 2-dimensional manifolds of constant curvature. Their C-metric counterparts are conformal to this topology, with the conformal factor depending on the angular coordinate. Moreover, the angular surfaces of these new C-solutions have a fixed size, but they lose the symmetry of the $A = 0$ counterparts. For example, while the angular surfaces of the Nariai and Bertotti-Robinson solutions are round 2-spheres, the angular surfaces of their C-metric counterparts are deformed 2-spheres - they are compact but not round. Another important difference between the $A = 0$ and $A \neq 0$ solutions is the fact that the $A \neq 0$ solutions have, in general, a conical singularity at least at one of the poles of their angular surfaces. This conical singularity is a reminiscence of the conical singularity that is present in the C-metric from which they were generated. In the C-metric these conical singularities are associated to the presence of a strut or string that furnishes the acceleration of the near-extremal black holes. In this context, we find that the Nariai C-metric generated from a extremal limit of the dS C-metric describes a spacetime that is conformal to the product $dS_2 \times \tilde{S}^2$. To each point in the deformed 2-sphere corresponds a dS_2 spacetime, except for one point

which corresponds a dS_2 spacetime with an infinite straight strut or string, with a mass density and pressure satisfying $p = -\mu$. Analogously, the Nariai Bertotti-Robinson dS C-metric describes a spacetime that is conformal to the product $\mathbb{M}^{1,1} \times \tilde{S}^2$. To each point in the deformed 2-sphere corresponds a $\mathbb{M}^{1,1}$ spacetime, except for one point which corresponds a $\mathbb{M}^{1,1}$ spacetime with an infinite straight strut or string. In the case of the Bertotti-Robinson dS C-metric (topologically conformal to $AdS_2 \times \tilde{S}^2$), the strut or string does not survive to the Ginsparg-Perry limiting procedure, and thus in the end of the process we only have a conical singularity.

In what concerns the causal structure, the Carter-Penrose diagrams of the $A \neq 0$ solutions are equal to those of the $A = 0$ solutions. For example, the diagram of the Nariai C-metric is equal to the one that describes the (1+1)-dimensional dS solution, the diagram of the Bertotti-Robinson C-metric and of the anti-Nariai C-metric is equal to the one that describes the (1+1)-dimensional AdS solution, and the diagram of the Nariai Bertotti-Robinson C-metric is given by the Rindler diagram.

Some of these solutions, perhaps all, are certainly of physical interest. Indeed, it is known that the Nariai solution ($A = 0$) is unstable and, once created, it decays through the quantum tunnelling process into a slightly non-extreme black hole pair [129]. We then expect that the Nariai C-metric is also unstable and that it will decay into a slightly non-extreme pair of black holes accelerated by a strut or by a string. The solutions found in this paper also play an important role in the decay of the dS or AdS spaces, and therefore can mediate the Schwinger-like quantum process of pair creation of black holes. Indeed, the Nariai, and the dS Nariai Bertotti-Robinson instantons ($A = 0$) are one of the few Euclidean solutions that are regular, and have thus been used [167, 168, 169, 173, 172] to study the pair creation of dS black holes materialized and accelerated by the cosmological constant background field (an instanton is a solution of the Euclidean field equations that smoothly connects the spacelike sections of the initial state, the pure dS space in this case, and the final state, the dS black hole pair in this case). Moreover, the Euclidean "Nariai" flat C-metric and Ernst solution (see section 9.2) have been used to analyze the process of pair production of $\Lambda = 0$ black holes, accelerated by a string or by an electromagnetic external field, respectively. Therefore, its natural to expect that the Euclidean extremal limits of the dS C-metric and AdS C-metric found in this paper mediate the process of pair creation of black holes in a cosmological background, that are then accelerated by a string, in addition to the cosmological field acceleration. For the Nariai case, e.g., the picture would be that of the nucleation, in a dS background, of a Nariai C universe, whose string then breaks down and a pair of dS black holes is created at the endpoints of the string. This expectation is confirmed in [131].

Chapter 8

False vacuum decay:
effective one-loop action for pair creation of domain walls

Contents

This chapter can be seen as an introductory toy model for the black hole pair creation analysis that will be done in chapter 9. We propose an effective one-loop action to describe the domain wall pair creation process that accompanies the false vacuum decay of a scalar field (in the absence of gravity). We compute the pair creation rate of the process, including the one-loop contribution, using the instanton method that is also applied in the computation of black hole pair creation rates.

8.1   The false vacuum decay process

Stone [144] has studied the problem of a scalar field theory in (1+1)-dimensions with a metastable vacuum, i.e., with a scalar potential that has a false vacuum, ϕ_+, and a true vacuum, ϕ_-, separated by an energy density difference, ϵ. Stone has noticed that the decay process can be interpreted as the false vacuum decaying into the true vacuum plus a creation of a soliton-antisoliton pair: $\phi_+ \to \phi_- + s + \bar{s}$. The energy necessary for the materialization of the pair comes from the energy density difference between the two vacua. The soliton-antisoliton pair production rate per unit time and length, Γ/L, can then be identified with the decay rate of the false vacuum and is given by ($\hbar = c = 1$) [144]:

$$\Gamma/L = A\,\mathrm{e}^{-S_0} = A\,\mathrm{e}^{-\frac{\pi m^2}{\epsilon}}\,, \tag{8.1}$$

where m is the soliton mass and prefactor A is a functional determinant whose value was first calculated by Kiselev and Selivanov [145, 146] and later by Voloshin [148]. Extensions to this decay problem, such as induced false vacuum decay, have been studied by several authors (for a review and references see, e.g., [149, 147]).

The method used in [144, 145, 146, 148] is based on the instanton method introduced by Langer in his work about decay of metastable termodynamical states [139]. This powerful method has been applied to several different studies, namely: Coleman and Callan [140, 141] have computed the bubble production rate that accompanies the cosmological phase transitions in a (3+1)-dimensional scalar theory (this was indeed previously calculated by other methods by Voloshin, Kobzarev and Okun [143]); Affleck and Manton [152] have studied monopole pair production in a weak external magnetic field and Affleck, Alvarez and Manton [153], have studied e^+e^- boson pair production in a weak external electric field. Recent developments studying pair production of boson and spinorial

particles in external Maxwell's fields have been performed by several authors using different methods [274, 275, 276]. Similar results in the Euler-Heisenberg theory, a modified Maxwell theory, have been also obtained [277].

In this chapter, following our work [150], we propose an effective one-loop action built from the soliton field itself to study the problem of Stone [144], Kiselev and Selivanov [145, 146] and Voloshin [148]. The action consists of the usual mass term and a kinetic term in which the simple derivative of the soliton field is replaced by a kind of covariant derivative. In this effective action the soliton charge is treated no longer as a topological charge but as a Noether charge. This procedure of working with an effective action for the soliton field itself has been introduced by Coleman [273] where the equivalence between the Sine-Gordon model and the Thirring model was shown, and by Montonen and Olive [278] who have proposed an equivalent dual field theory for the Prasad-Sommerfield monopole soliton. More connected to our problem, Manton [279] has proposed an effective action built from the soliton field itself which reproduces the soliton physical properties of (1+1)-dimensional nonlinear scalar field theories having symmetric potentials with degenerate minima. In this paper we deal instead with a potential with non-degenerate minima in a (1+1)-dimensional scalar field theory. Thus, our effective action is new since Manton was not dealing with the soliton pair production process.

Using the effective one-loop action and the method presented in [153], we calculate the soliton-antisoliton pair production rate, (8.1). One recovers Stone's exponential factor S_0 [144] and the prefactor A of Kiselev and Selivanov [145, 146] and Voloshin [148].

8.2 Effective one-loop action

In order to present some useful soliton properties let us consider a scalar field theory in a (1+1)-dimensional spacetime, whose dynamics is governed by the action (see, e.g., [280]),

$$S[\phi(x,t)] = \int d^2x \left[\frac{1}{2}\partial_\mu\phi\partial^\mu\phi - U(\phi) \right], \tag{8.2}$$

where U is a generic potential. A particular important case is when U is a symmetric potential, $U = U_{\rm s}(\phi)$, with two or more degenerate minima. In the ϕ^4 theory the potential is $U_{\rm s}(\phi) = \frac{1}{4}\lambda\big(\phi^2 - \mu^2/\lambda\big)^2$, with $\mu \geq 0$ and $\lambda \geq 0$. Stationarizing the action one obtains the solutions of the theory which have finite and localized energy. The solutions are the soliton

$$\psi \equiv \phi_{\rm sol} = +\frac{\mu}{\sqrt{\lambda}}\tanh\left[\frac{\mu}{\sqrt{2}}\frac{(x-x_0)-vt}{\sqrt{1-v^2}} \right], \tag{8.3}$$

and the antisoliton $-\psi$. From the hamiltonian density, $\mathcal{H} = \frac{1}{2}(\partial_x\phi)^2 + U_{\rm s}(\phi)$, one can calculate the mass of the soliton and antisoliton

$$m = \int_{-\infty}^{+\infty} dx\,\mathcal{H}(x) = \frac{2\sqrt{2}}{3}\frac{\mu^3}{\lambda}. \tag{8.4}$$

One can also define the topological charge, $Q = \frac{1}{2}\big[\psi(x = +\infty) - \psi(x = -\infty)\big]$, (conserved in time) which has the positive value $Q_{\rm s} = +\mu/\sqrt{\lambda}$ in the case of the soliton and the negative value $Q_{\bar{\rm s}} = -\mu/\sqrt{\lambda}$ in the case of the antisoliton. To this charge one associates the topological current $k^\mu = \frac{1}{2}\varepsilon^{\mu\nu}\partial_\nu\psi$ which is conserved, $\partial_\mu k^\mu = 0$, and such that $Q = \int_{-\infty}^{+\infty} dx k^0$.

Now, let us consider a non-degenerate potential U in action (8.2) by adding to $U_{\rm s}$ a small term that breaks its symmetry [144, 141]: $U(\phi) = U_{\rm s}(\phi) + \frac{\epsilon}{2\mu/\sqrt{\lambda}}(\phi - \mu/\sqrt{\lambda})$, where ϵ is the energy density (per unit length) difference between the true ($\phi_- = -\mu/\sqrt{\lambda}$) and false ($\phi_+ = +\mu/\sqrt{\lambda}$) vacua. As noticed in [144, 145, 146], ϵ is responsible for both the decay of false vacuum and soliton-antisoliton pair creation.

We want to find an effective one-loop action built from the soliton field itself and that describes the above pair creation process. The soliton field should be a charged field since the system admits

two charges, Q_s and $Q_{\bar{s}}$. Therefore, the action should contain the mass term $m^2 \psi \psi^*$, where m is the soliton mass given in (8.4), and the kinetic term $(\partial_\mu \psi)(\partial^\mu \psi^*)$. Thus, the free field effective action is $\int d^2 x [(\partial_\mu \psi)(\partial^\mu \psi^*) - m^2 \psi \psi^*]$. However, if one demands local gauge invariance one has to introduce an "electromagnetic" 2-vector potential A_μ which transforms the common derivative $\partial_\mu \psi$ into a covariant derivative $(\partial_\mu + i Q_s A_\mu)\psi$. As is well known, the field A_μ itself should contribute to the action. This contribution must be gauge invariant since the covariant kinetic term plus the mass term are already gauge invariant. This is achieved by defining the invariant 2-form field, $F_{\mu\nu} = \partial_\mu A_\nu - \partial_\nu A_\mu$. In two dimensions, an anti-symmetric field can only be of the form: $F_{\mu\nu} = \sigma(t,x)\varepsilon_{\mu\nu}$, where $\varepsilon_{\mu\nu}$ is the Levi-Civita tensor and $\sigma(t,x)$ a function. Therefore the effective one-loop action should be $S^{\text{eff}} = \int d^2 x [(\partial_\nu \psi + i Q_s A_\nu \psi)(\partial^\nu \psi^* - i Q_s A^\nu \psi^*) - m^2 \psi \psi^* - \frac{1}{4} F_{\mu\nu} F^{\mu\nu}]$.

Note now that the charged soliton acts also as a source, thus modifying the surrounding field. As a first approximation we shall neglect this effect and assume A_μ fixed by external conditions. This allows us to drop the contribution of the term $F_{\mu\nu} F^{\mu\nu}$ in the effective action. Moreover, the external field responsible for the pair creation is essentially represented by the energy density difference ϵ so we postulate that $F^{\text{ext}}_{\mu\nu} = \frac{\epsilon}{\mu/\sqrt{\lambda}} \varepsilon_{\mu\nu}$. Therefore, A^{ext}_μ is given by $A^{\text{ext}}_\mu = \frac{1}{2} \frac{\epsilon}{\mu/\sqrt{\lambda}} \varepsilon_{\mu\nu} x^\nu$.

Finally, if the system is analytically continued to Euclidean spacetime ($t_{\text{Min}} \to -it_{\text{Euc}}$; $A_0 \to iA_2$) one obtains the Euclidean effective one-loop action for the soliton pair creation problem

$$S^{\text{eff}}_{\text{Euc}} = \int d^2 x \left[\left|(\partial_\mu - \frac{1}{2} \epsilon \, \varepsilon_{\mu\nu} x_\nu)\psi\right|^2 + m^2 |\psi|^2 \right]. \tag{8.5}$$

In the next section this Euclidean effective one-loop action is going to be used to calculate the soliton-antisoliton pair production rate (8.1). Although the calculations are now similar to those found in Affleck, Alvarez and Manton pair creation problem [153], we present some important steps and results since in two dimensions they are slightly different.

8.3 Pair production rate

The soliton-antisoliton pair production rate per unit time is equal to the false vacuum decay rate per unit time

$$\Gamma = -2 \, \text{Im} E_0 \,, \tag{8.6}$$

where the vacuum energy, E_0, is given by the Euclidean functional integral

$$e^{-E_0 T} = \lim_{T \to \infty} \int [\mathcal{D}\psi][\mathcal{D}\psi^*] e^{-S^{\text{eff}}_{\text{Euc}}(\psi; \psi^*)} \,. \tag{8.7}$$

As it will be verified, E_0 will receive a small imaginary contribution from the negative-mode associated to the quantum fluctuations about the instanton (which stationarizies the action) and this fact is responsible for the decay. Combining (8.6) and (8.7) one has

$$\Gamma = \lim_{T \to \infty} \frac{2}{T} \text{Im} \ln \int [\mathcal{D}\psi][\mathcal{D}\psi^*] e^{-S^{\text{eff}}_{\text{Euc}}(\psi; \psi^*)} \,, \tag{8.8}$$

where $S^{\text{eff}}_{\text{Euc}}$ is given by (8.5). Integrating out ψ and ψ^* in (8.8) one obtains

$$\Gamma = -\lim_{T \to \infty} \frac{2}{T} \, \text{Im} \, \text{tr} \, \ln \left[(\partial_\mu - \frac{1}{2} \epsilon \, \varepsilon_{\mu\nu} x_\nu)^2 + m^2 \right]. \tag{8.9}$$

The logarithm in (8.9) can be written as a "Schwinger proper time integral", $\ln u = -\int_0^\infty \frac{d\mathcal{T}}{\mathcal{T}} \exp \left(-\frac{1}{2} u \mathcal{T} \right)$. Taking $u = [(\partial_\mu - \frac{1}{2} \epsilon \, \varepsilon_{\mu\nu} x_\nu)^2 + m^2]$, yields

$$\Gamma = \lim_{T \to \infty} \frac{2}{T} \, \text{Im} \int_0^\infty \frac{d\mathcal{T}}{\mathcal{T}} e^{-\frac{1}{2} m^2 \mathcal{T}} \, \text{tr} \, \exp \left[-\frac{1}{2} \left(P_\mu - \frac{1}{2} \epsilon \, \varepsilon_{\mu\nu} x_\nu \right)^2 \mathcal{T} \right]. \tag{8.10}$$

Notice that now the trace is of the form $\text{tr}\,e^{-H\mathcal{T}}$, with $H = \frac{1}{2}\left[P_\mu - \frac{1}{2}\epsilon\varepsilon_{\mu\nu}x_\nu\right]^2$ being the Hamiltonian for a particle subjected to the interaction with the external scalar field in a (2+1)-dimensional spacetime, and the proper time playing the role of a time coordinate. One has started with a scalar field theory in a Euclidean 2-dimensional spacetime and now one has found an effective theory for particles in a 3D spacetime. It is in this new context that the pair production rate is going to be calculated. The gain in having the trace in the given form is that it can be written as a path integral $\text{tr}\,e^{-H\mathcal{T}} = \int [dx]\exp\left[-\int d\mathcal{T}\,L\right]$, where $L = \frac{1}{2}\dot{x}_\mu\dot{x}_\mu + \frac{1}{2}\epsilon\,\varepsilon_{\mu\nu}x_\nu\dot{x}_\mu$ is the Lagrangian associated with our Hamiltonian. Thus,

$$\Gamma = \lim_{T\to\infty}\frac{2}{T}\,\text{Im}\int_0^\infty \frac{d\mathcal{T}}{\mathcal{T}}e^{-\frac{1}{2}m^2\mathcal{T}}\int[dx]\exp\left[-\int_0^{\mathcal{T}}d\mathcal{T}\left(\frac{1}{2}\dot{x}_\mu\dot{x}_\mu + \frac{1}{2}\epsilon\,\varepsilon_{\mu\nu}x_\nu\dot{x}_\mu\right)\right]. \tag{8.11}$$

Rescaling the proper time variable, $d\mathcal{T} \to \frac{d\tau}{\mathcal{T}}$, and noticing that the path integral is over all the paths, $x_\mu(\tau)$, such that $x_\mu(1) = x_\mu(0)$, one has

$$\Gamma = \lim_{T\to\infty}\frac{2}{T}\,\text{Im}\int[dx]e^{-\frac{1}{2}\epsilon\oint \varepsilon_{\mu\nu}x_\nu dx_\mu}\int_0^\infty \frac{d\mathcal{T}}{\mathcal{T}}\exp\left[-\left(\frac{1}{2}m^2\mathcal{T} + \frac{1}{2\mathcal{T}}\int_0^1 d\tau\,\dot{x}_\mu\dot{x}_\mu\right)\right]. \tag{8.12}$$

The $\mathcal{T}$ integral can be calculated expanding the function about the stationary point $\mathcal{T}_0^2 = \frac{\int_0^1 d\tau\dot{x}^2}{m^2}$:

$$\int \frac{d\mathcal{T}}{\mathcal{T}}e^{-f(\mathcal{T})} \sim e^{-f(\mathcal{T}_0)}\frac{1}{\mathcal{T}_0}\sqrt{\frac{\pi}{\frac{1}{2}f''(\mathcal{T}_0)}} \sim e^{-m\sqrt{\int_0^1 d\tau\dot{x}^2}}\frac{1}{m}\sqrt{\frac{2\pi}{\mathcal{T}_0}}. \tag{8.13}$$

Then (8.12) can be written as

$$\Gamma = \lim_{T\to\infty}\frac{1}{T}\frac{2}{m}\sqrt{\frac{2\pi}{\mathcal{T}_0}}\,\text{Im}\int[dx]e^{-S_{\text{Euc}}[x_\mu(\tau)]}, \tag{8.14}$$

where $S_{\text{Euc}} = m\sqrt{\int_0^1 d\tau\dot{x}_\mu\dot{x}_\mu} + \frac{1}{2}\epsilon\oint \varepsilon_{\mu\nu}x_\nu dx_\mu$. This integral can be solved using the instanton method. Stationarizing the action, one gets the equation of motion in the (2+1)D spacetime

$$\frac{m\ddot{x}_\mu(\tau')}{\sqrt{\int_0^1 d\tau\dot{x}^2}} = -\epsilon\,\varepsilon_{\mu\nu}\dot{x}_\nu(\tau')\,;\quad \text{with } \mu = 1,2 \text{ and } \dot{x}_\mu = \frac{dx_\mu}{d\tau}. \tag{8.15}$$

The instanton, $x_\mu^{\text{cl}}(\tau)$, i.e., the solution of the Euclidean equation of motion that obeys the boundary conditions $x_\mu(\tau=1) = x_\mu(\tau=0)$ is

$$x_\mu^{\text{cl}}(\tau) = R(\cos 2\pi\tau, \sin 2\pi\tau)\,;\quad \text{with } R = \frac{m}{\epsilon}. \tag{8.16}$$

The instanton represents a particle describing a loop of radius R in the plane defined by the time x_2 and by the direction x_1. The loop is a thin wall that separates the true vacuum located inside the loop from the false vacuum outside.

The Euclidean action of the instanton is given by $S_0 = S_{\text{Euc}}[x_\mu^{\text{cl}}(\tau)] = m2\pi R - \epsilon\pi R^2$. The first term is the rest energy of the particle times the orbital length and the second term represents the interaction of the particle with the external scalar field. The loop radius, $R = m/\epsilon$, stationarizies the instanton action. The action is then $S_0 = \pi m^2/\epsilon$.

The second order variation operator is given by

$$M_{\mu\nu} \equiv \left.\frac{\delta^2 S}{\delta x_\nu(\tau')\delta x_\mu(\tau)}\right|_{x^{\text{cl}}} =$$

$$= \left[-\left(\frac{m\delta_{\mu\nu}}{\sqrt{\int_0^1 d\tau\dot{x}^2}}\frac{d^2}{d\tau^2} + \epsilon\,\varepsilon_{\mu\nu}\frac{d}{d\tau}\right)\delta(\tau-\tau') - \frac{m\ddot{x}_\mu(\tau)\ddot{x}_\nu(\tau')}{\left[\int_0^1 d\tau\dot{x}^2\right]^{3/2}}\right]_{x^{\text{cl}}} =$$

$$= -\left[\frac{\epsilon}{2\pi}\delta_{\mu\nu}\frac{d^2}{d\tau^2} + \epsilon\,\varepsilon_{\mu\nu}\frac{d}{d\tau}\right]\delta(\tau-\tau') - \frac{2\pi\epsilon x_\mu^{\text{cl}}(\tau)x_\nu^{\text{cl}}(\tau')}{R^2}. \tag{8.17}$$

The eigenvectors η_μ^n, and the eigenvalues λ_n, associated with the operator $M_{\mu\nu}$ are such that

$$M_{\mu\nu}\, \eta_\nu^n(\tau') = \lambda_n\, \eta_\mu^n(\tau')\, \delta(\tau - \tau') . \tag{8.18}$$

From this one concludes that:

(**i**) the positive eigenmodes are:

$(\cos 2n\pi\tau, \sin 2n\pi\tau)$ and $(\sin 2n\pi\tau, -\cos 2n\pi\tau)$ with $\lambda_n = 2\pi\epsilon(n^2 - n)$, $n = 2, 3, 4...$;

$(\sin 2n\pi\tau, \cos 2n\pi\tau)$ and $(\cos 2n\pi\tau, -\sin 2n\pi\tau)$ with $\lambda_n = 2\pi\epsilon(n^2 + n)$, $n = 1, 2, 3...$;

(**ii**) there are two zero-modes associated with the translation of the loop along the x_1 and x_2 directions: $(1,0)$ and $(0,1)$ with $\lambda = 0$;

(**iii**) there is a zero-mode associated with the translation along the proper time, τ: $(\sin 2\pi\tau, -\cos 2\pi\tau) = -\frac{\dot{x}_\mu^{\rm cl}}{2\pi R}$ with $\lambda = 0$;

(**iv**) there is a single negative mode associated to the change of the loop radius R: $(\cos 2\pi\tau, \sin 2\pi\tau) = \frac{x_\mu^{\rm cl}}{R}$ with $\lambda_- = -2\pi\epsilon$.
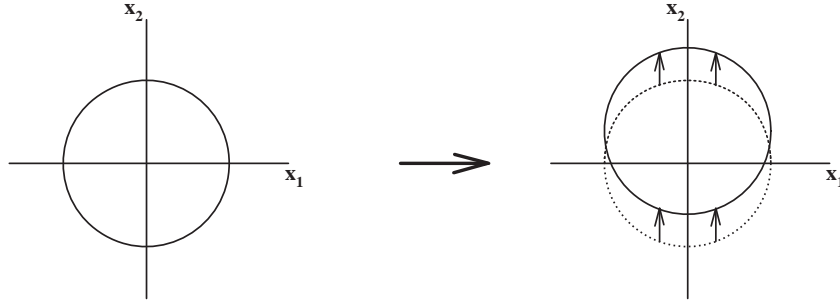
Figure 8.1: The zero-mode $\eta_\mu^n(\tau) = (0,1)$ is associated with the translation of the loop along the x_2 direction: $x_\mu^{\rm cl}(\tau) \to x_\mu^{\rm cl}(\tau) + \alpha\, \eta_\mu^n(\tau) = R(\cos 2\pi\tau, \sin 2\pi\tau) + \alpha(0, 1)$
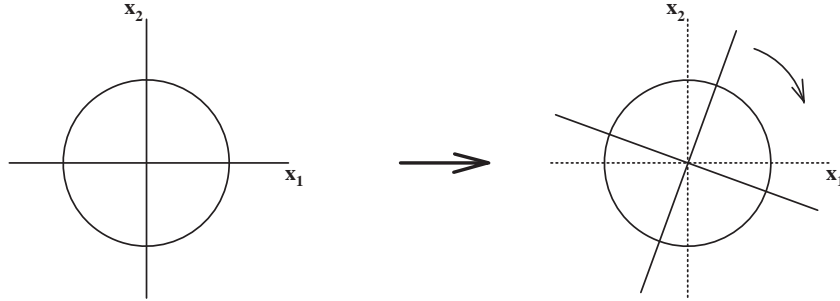
Figure 8.2: The zero-mode $\eta_\mu^n(\tau) = -\dot{x}_\mu^{\rm cl}/(2\pi R)$ is associated with the translation of the loop along the proper time τ: $x_\mu^{\rm cl}(\tau) \to x_\mu^{\rm cl}(\tau) + \alpha\, \eta_\mu^n(\tau) = x_\mu^{\rm cl}(\tau) + \alpha\dot{x}_\mu^{\rm cl}$
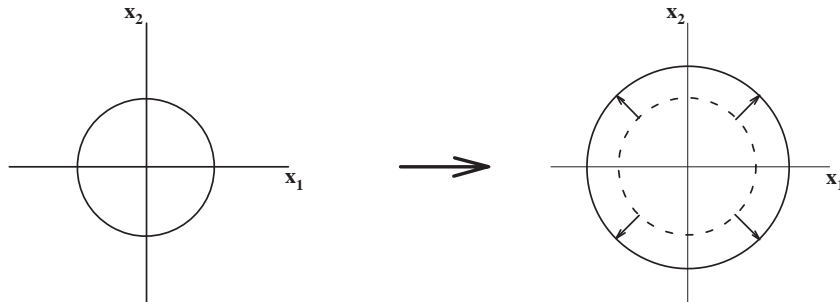
Figure 8.3: The zero-mode $\eta_\mu^n(\tau) = x_\mu^{\rm cl}/R$ is associated with the change of the loop radius R: $x_\mu^{\rm cl}(\tau) \to x_\mu^{\rm cl}(\tau) + \alpha\, \eta_\mu^n(\tau) = (1 + \alpha)x_\mu^{\rm cl}(\tau)$

Now, we consider small fluctuations about the instanton, i.e., we do $x_\mu(\tau) = x_\mu^{\text{cl}}(\tau) + \eta_\mu(\tau)$. The Euclidean action is expanded to second order so that the path integral (8.14) can be approximated by

$$\Gamma \simeq \lim_{T\to\infty} \frac{1}{T} \frac{2}{m} \sqrt{\frac{2\pi}{\mathcal{T}_0}} \, e^{-S_0} \, \text{Im} \int [d\eta(\tau)] \exp\left[-\frac{1}{2} \int d\tau d\tau' \, \eta_\mu(\tau) \, M_{\mu\nu} \, \eta_\nu(\tau')\right]. \tag{8.19}$$

The path integral in equation (8.19) is the one-loop factor and is given by $\mathcal{N} \left(\text{Det} M\right)^{-\frac{1}{2}} = \mathcal{N} \prod (\lambda_n)^{-\frac{1}{2}}$, where λ_n are the eigenvalues of $M_{\mu\nu}$ and $\mathcal{N}$ is a normalization factor that will not be needed. To overcome the problem that arises from having an infinite product of eigenvalues, one compares our system with the free particle system

$$\int [d\eta] \exp\left[-\frac{1}{2} \int d\tau d\tau' \, \eta_\mu(\tau) \, M_{\mu\nu} \, \eta_\nu(\tau')\right] =$$

$$= \int [d\eta] \exp\left[-\frac{1}{2} \int d\tau d\tau' \, \eta_\mu(\tau) \, M_{\mu\nu}^0 \, \eta_\nu(\tau')\right] \frac{\prod (\lambda_n)^{-\frac{1}{2}}}{\prod (\lambda_n')^{-\frac{1}{2}}}, \tag{8.20}$$

where $M_{\mu\nu}^0 = -\frac{1}{\mathcal{T}_0} \delta_{\mu\nu} \frac{d^2}{d\tau^2} \delta(\tau - \tau')$ is the second variation operator of the free system with eigenvalues $\lambda_n' = 2\pi\epsilon n^2$, $n = 0, 1, 2, 3...$ (each with multiplicity 4). In equation (8.20) the first factor is the path integral of a free particle in a 3-dimensional Euclidean spacetime

$$\int [d\eta] \exp\left[-\frac{1}{2} \int d\tau d\tau' \, \eta_\mu \, M_{\mu\nu}^0 \, \eta_\nu\right] = \int [d\eta] \exp\left[-\frac{1}{2\mathcal{T}_0} \int d\tau \, \dot\eta_\mu \, \dot\eta_\mu\right] = \frac{1}{2\pi\mathcal{T}_0}. \tag{8.21}$$

In the productory, one omits the zero eigenvalues, but one has to introduce the normalization factor $\frac{||dx_\mu^{\text{cl}}/d\tau||}{||\eta_\mu^0||} \sqrt{\frac{1}{2\pi}} = \sqrt{2\pi} R$ which is associated with the proper time eigenvalue. In addition, associated with the negative eigenvalue one has to introduce a factor of $1/2$ which accounts for the loops that do expand. The other half contracts (representing the annihilation of recently created pairs) and so does not contribute to the creation rate. So, the one-loop factor becomes

$$\frac{1}{2\pi\mathcal{T}_0} \frac{\prod (\lambda_n)^{-\frac{1}{2}}}{\prod (\lambda_n')^{-\frac{1}{2}}} = \frac{1}{2\pi\mathcal{T}_0} \frac{1}{2} \frac{i}{\sqrt{2\pi\epsilon}} \sqrt{2\pi} R \frac{\prod_{\lambda>0} (\lambda_n)^{-\frac{1}{2}}}{\prod_{\lambda'>0} (\lambda_n')^{-\frac{1}{2}}} = i \frac{1}{2\pi\mathcal{T}_0} \frac{1}{2} \sqrt{2\pi\epsilon} \sqrt{2\pi} R. \tag{8.22}$$

Written like this, the one loop factor accounts only for the contribution of the instanton centered in $(x_1, x_2) = (0, 0)$. The translational invariance in the x_1 and x_2 directions requires that one multiplies (8.22) by the spacetime volume factor $\int dx_2 \int dx_1 = TL$, which represents the spacetime region where the instanton might be localized. So, the correct one-loop factor is given by

$$\int [d\eta(\tau)] \exp\left[-\frac{1}{2} \int d\tau d\tau' \, \eta_\mu(\tau) \, M_{\mu\nu} \, \eta_\nu(\tau')\right] = i \frac{LT}{2\pi\mathcal{T}_0} \frac{1}{2} \sqrt{2\pi\epsilon} \sqrt{2\pi} R. \tag{8.23}$$

Putting (8.23) into (8.19), using $\mathcal{T}_0^2 = \frac{\int d\tau \dot x^2}{m^2} = \frac{(2\pi R)^2}{m^2}$, $R = \frac{m}{\epsilon}$ and $S_0 = \pi m^2/\epsilon$, one finally has that the soliton-antisoliton pair production rate per unit time and length is given by

$$\Gamma/L = \frac{\epsilon}{2\pi} \, e^{-\frac{\pi m^2}{\epsilon}}. \tag{8.24}$$

We have recovered Stone's exponential factor $e^{-\frac{\pi m^2}{\epsilon}}$ [144] as well as the prefactor $A = \epsilon/2\pi$ of Kiselev and Selivanov [145, 146] and Voloshin [148].

Note the difference to the 4D problem of Affleck *et al* [153] and Schwinger [130], who have found for the factor A the value $(eE)^2/(2\pi)^3$ which is quadratic in eE and not linear, as in our case. This difference has to do with the dimensionality of the problems.

It is well known that a one-particle system in 2D can be transformed straightforwardly to a thin line in 3D and a thin wall in 4D, where now the mass m of the soliton should be interpreted as a line density and surface density, respectively. In fact, a particle in (1+1)D, as well as an infinite line in (2+1)D, can be considered as walls as seen from within the intrinsic space dimension, justifying the use of the name wall for any dimension. Our calculations apply directly to the domain wall pair creation problem in any dimension.

8.4 Summary and discussion

The equation for the loop of radius R in 2-dimensional Euclidean spacetime is given by $x^2 + \tau^2 = R^2$, where we have put $x = x_1$ and $\tau = x_2$. One can make an analytical continuation of the Euclidean time (τ) to the Minkowskian time $(\tau = it)$ and obtain the solution in 2-dimensional Minkowski spacetime

$$x^2 - t^2 = R^2. \tag{8.25}$$

At $\tau = t = 0$ the system makes a quantum jump and a soliton-antisoliton pair materializes at $x = \pm R = \pm m/\epsilon$. After the materialization, the soliton and antisoliton are accelerated, driving away from each other, as (8.25) shows. To check these statements note first that the energy necessary for the materialization of the pair at rest is $E = 2m$, where m is the soliton mass. This energy comes from the conversion of false vacuum into true vacuum. Since ϵ is the energy difference per unit length between the two vacua, we conclude that an energy of value $E = 2R\epsilon$ is released when this conversion occurs in the region $(2R)$ within the pair. So, the pair materialization should occur only when R is such that the energy released is equal to the rest energy: $2R\epsilon = 2m \Rightarrow R = m/\epsilon$. This value agrees with the one that has been determined in section 8.3.

After the materialization the pair is accelerated so that its energy is now $E = 2m/\sqrt{1 - v^2}$. Differentiating (8.25), we get the velocity $v = \sqrt{1 - R^2/x^2}$. The energy of the pair is then given by $E = 2\frac{m}{R}|x| = \epsilon\, 2|x|$. Notice now that $\epsilon\, 2|x|$ is the energy released in the conversion of false vacuum into true vacuum. So, after pair creation, all the energy released in the conversion between the two vacua is used to accelerate the soliton-antisoliton pair.

This discussion agrees with the interpretation of the process as being the false vacuum decaying to the true vacuum plus a creation of a soliton-antisoliton pair. It also justifies the presence of the interaction term $\epsilon\, \varepsilon_{\mu\nu} x_\nu \psi$ present in the covariant derivative of the proposed effective one-loop action, (8.5), since $\epsilon\, x$ is the energy released in the decay and responsible for the creation and acceleration of the pair.

With the proposed effective one-loop action (8.5) we have recovered Stone's exponential factor S_0 [144] of the pair creation rate in (8.1), and the prefactor A of Kiselev and Selivanov [145, 146] and Voloshin [148]. In the proposed effective one-loop action the soliton charge is treated no longer as a topological charge but as a Noether charge. Such an interchange between the topological and the Noether charges was already present in [273, 278].

The problem of false vacuum decay coupled to gravity has been introduced in [142] and also discussed in [281, 282]. With the proposed effective one-loop action (8.5) it would be interesting to further analyze this problem.

Chapter 9

Pair creation of black holes on a cosmic string background

Contents

A process that allows the formation of black holes (even with Plank sizes) is the gravitational analogue of the Schwinger quantum process of pair creation of particles in an external electric field. This gravitational black hole pair creation process has first proposed by Gibbons (1986). In order to turn the pair of virtual black holes real one needs a background field that provides the energy needed to materialize the pair, and that provides the force necessary to accelerate away the black holes once they are created. This background field can be: (i) an external electromagnetic field with its Lorentz force [157]-[181], (ii) the positive cosmological constant Λ, or inflation [181]-[174], (iii) a cosmic string with its tension [133]-[166], (iv) a domain wall with its gravitational repulsive energy [176]-[178]. One can also have a combination of the above fields, for example, a process involving cosmic string breaking in a background magnetic field [175], or a scenario in which a cosmic string breaks in a cosmological background [132, 131]. We have already made a historical overview of these processes in section 1.3.3, and we will now analyze some of these processes in great detail. To study these processes we must have exact solutions of the Einstein equations that describe the pair of uniformly accelerated black holes in the external field, after they are created. These solutions, the C-metric and Ernst solution, exist and we have already studied them in chapters 6 and 7. Finally, an important process that accompanies the production of the black hole pair is the emission of radiation. An estimate for the amount of gravitational radiation released during the pair creation period will be explicitly computed in chapter 12.

The particular process we are going to study in this chapter is the quantum process in which a cosmic string breaks, and a pair of black holes is created at the ends of the string (see Fig. 1.9). In a flat background this process has been analyzed by Hawking and Ross [133], with the support provided by [134, 135, 136]. We will discuss the main results of [133] in section 9.2, including the explicit values of the pair creation rates which have not been written in [133]. In section 9.1, we will discuss in detail the same process but in an AdS background, following your work [132]. Finally, in section 9.3, we will analyze the black hole pair creation probability when a string breaks in an dS background, following your work [131].

The energy to materialize and accelerate the black holes comes from the strings' tension. In the dS case the cosmological background acceleration also makes a positive contribution to the process, while in the AdS case the cosmological background acceleration contributes negatively. Thus, pair creation of black holes in a dS background is possible even when there is no string, and this process has been analyzed in [167, 168, 169, 170, 172, 173]. Due to the negative cosmological background contribution, in the AdS case, pair creation of black holes is possible only when the acceleration provided by the strings tension is higher than $\sqrt{|\Lambda|/3}$.

We remark that in principle our explicit values for the pair creation rates [132, 131] also apply to the process of pair creation in an external electromagnetic field, with the acceleration being provided in this case by the Lorentz force instead of being furnished by the string tension. There is no Ernst solution in a cosmological constant background, and thus we cannot discuss analytically the process. However, physically we could in principle consider an external electromagnetic field that supplies the same energy and acceleration as our strings and, from the results of the $\Lambda = 0$ case (where the pair creation rates in the string and electromagnetic cases agree), we expect that the results found in [131, 132] do not depend on whether the energy is being provided by an external electromagnetic field or by strings.

9.1 Pair creation of anti-de Sitter black holes on a cosmic string background

In this section we want to analyze the process in which a cosmic string breaks and a pair of black holes is produced at the ends of the string, in an anti-de Sitter (AdS) background ($\Lambda < 0$). Therefore, the energy to materialize and accelerate the pair comes from the strings' tension. In an AdS background this will be the only study done in the process of production of a pair of correlated black holes with spherical topology. The instantons for this process can be constructed by analytically continuing the AdS C-metric found in [86] and analyzed in detail in [121]-[87]. Contrary to the $\Lambda = 0$ [84] and $\Lambda > 0$ [88] cases, the AdS describes a pair of accelerated black holes only when the acceleration supplied by the strings is greater than $\sqrt{|\Lambda|/3}$ [87]. Hence we expect that pair creation of black holes in an AdS background is possible only when $A > \sqrt{|\Lambda|/3}$. We will confirm this expectation. The quantum production of uncorrelated AdS black holes has been studied in [180], and the pair creation process of correlated topological AdS black holes (with hyperbolic topology) has been analyzed in [178] in a domain wall background.

The plan of this chapter is as follows. The AdS C-metric represents two accelerating black holes in an AdS background (see previous section 6.1), and in section 9.1.1 we construct, from the AdS C-metric, the regular instantons that describe the pair creation process. We find an instanton that mediates pair creation of nonextreme black holes and other that mediates the production of extreme black holes. Then, in section 9.1.2, we explicitly evaluate the pair creation rate for each one of the cases discussed in section 9.1.1.

9.1.1 The AdS C-metric instantons

The AdS C-metric has been discussed in detail in section 6.1. When $A > \sqrt{|\Lambda|/3}$, and only in this case, the AdS C-metric describes a pair of uniformly accelerated black holes in an anti-de Sitter background, with the acceleration being provided by two strings, from each one of the black holes towards infinity, that pulls them away. Since we are interested in black hole pair creation, onwards we will deal only with the $A > \sqrt{|\Lambda|/3}$ case. The presence of the string is associated to the conical singularity that exists in the south pole of the AdS C-metric (see subsections 6.1.1.c and 6.1.3.a).

Before we proceed, let us refresh some basic properties that will be really needed later. The AdS C-metric (6.3)-(6.6) has a curvature singularity at $y = +\infty$ where the matter source is and, in the Lorentzian sector, y must belong to the range $-x \leq y < +\infty$. The point $y = -x$ corresponds to a point that is infinitely far away from the curvature singularity, thus as y increases we approach the curvature singularity and $y + x$ is the inverse of a radial coordinate. The south pole, $x = x_s$, points towards the infinity, while the north pole points towards the other black hole. At most, $\mathcal{F}(y)$ can have four real zeros which we label in ascending order by $y'_A < 0 < y_A \leq y_+ \leq y_-$. The roots y_- and y_+ are, respectively, the inner and outer charged black hole horizons, and y_A and y'_A are acceleration horizons. Later on it will be crucial to note that the number and nature of the horizons crossed by an observer that travels into the black hole singularity depends on the angular direction x that he is following. This peculiar feature is due to the lower restriction on the value of y ($-x \leq y$). Thus, for $A > \sqrt{|\Lambda|/3}$, we have to consider separately five distinct sets of angular directions, namely (a)

$x_s \leq x < -y_A$, (b) $x = -y_A$, (c) $-y_A < x < -y'_A$, (d) $x = -y'_A$ and (e) $-y'_A < x \leq x_n$. For example, when the observer is travelling towards the the black hole singularity following an angular direction in the vicinity of the south pole [case (a)] we will cross only the outer (y_+) and inner (y_-) black hole horizons. When he does this trip following an angular direction in the vicinity of the equator [case (c)], he crosses the acceleration horizon y_A before passing through the black hole horizons y_+ and y_-. If this trip is done following an angular direction in the vicinity of the north pole [case (e)] we will cross two accelerations horizons, y'_A and y_A and then the black hole horizons y_+ and y_-. The angular coordinate x belongs to the range $[x_s, x_n]$ for which $\mathcal{G}(x) \geq 0$. By doing this we guarantee that the Euclidean metric has the correct signature $(+ + ++)$, and that the angular surfaces are compact. In order to avoid a conical singularity in the north pole, the period of ϕ must be given by

$$\Delta\phi = \frac{4\pi}{|\mathcal{G}'(x_n)|}, \tag{9.1}$$

and this leaves a conical singularity in the south pole given by

$$\delta = 2\pi \left(1 - \frac{\mathcal{G}'(x_s)}{|\mathcal{G}'(x_n)|} \right), \tag{9.2}$$

that signals the presence of a string with mass density, $\mu = \frac{1}{4}(1 - |\mathcal{G}'(x_s)/\mathcal{G}'(x_n)|)$, and with pressure $p = -\mu < 0$.

Now, in order to evaluate the black hole pair creation rate we need to find the instantons of the theory. I.e., we must look into the euclidean section of the AdS C-metric and choose only those euclidean solutions which are regular in a way that will be explained soon. To obtain the euclidean section of the AdS C-metric from the lorentzian AdS C-metric we simply introduce an imaginary time coordinate $\tau = -it$ in (6.3), (6.5), and (6.6). Then the gravitational field of the euclidean AdS C-metric is given by

$$ds^2 = [A(x + y)]^{-2}(\mathcal{F}d\tau^2 + \mathcal{F}^{-1}dy^2 + \mathcal{G}^{-1}dx^2 + \mathcal{G}d\phi^2), \tag{9.3}$$

with

$$\mathcal{F}(y) = -\frac{3A^2 - |\Lambda|}{3A^2} + y^2 - 2mAy^3 + q^2A^2y^4,$$
$$\mathcal{G}(x) = 1 - x^2 - 2mAx^3 - q^2A^2x^4, \tag{9.4}$$

and the euclidean Maxwell field in the magnetic case is still given by (6.5), while in the electric case it is now given by $F_{el} = -i\,q\,d\tau \wedge dy$.

To have a positive definite euclidean metric we must require that y belongs to $y_A \leq y \leq y_+$. In general, when $y_+ \neq y_-$, one then has conical singularities at the horizons $y = y_A$ and $y = y_+$. In order to obtain a regular solution we have to eliminate the conical singularities at both horizons, ensuring in this way that the system is in thermal equilibrium. This is achieved by imposing that the period of τ is the same for the two horizons, and is equivalent to requiring that the Hawking temperature of the two horizons be equal. To eliminate the conical singularity at $y = y_A$ the period of τ must be $\beta = 2\pi/k_A$ (where k_A is the surface gravity of the acceleration horizon),

$$\beta = \frac{4\pi}{|\mathcal{F}'(y_A)|}. \tag{9.5}$$

This choice for the period of τ also eliminates simultaneously the conical singularity at the outer black hole horizon, y_+, if and only if the parameters of the solution are such that the surface gravities of the black hole and acceleration horizons are equal $(k_+ = k_A)$, i.e.

$$\mathcal{F}'(y_+) = -\mathcal{F}'(y_A). \tag{9.6}$$

This condition is satisfied by a regular euclidean solution with $y_A \neq y_+$ that will be referred to as nonextreme AdS instanton. This solution requires the presence of an electromagnetic charge.

We now turn our attention to the case $y_+ = y_-$ (and $y_A \neq y_+$), which obviously requires the presence of charge. When this happens the allowed range of y in the euclidean sector is simply $y_A \leq y < y_+$. This occurs because when $y_+ = y_-$ the proper distance along spatial directions between y_A and y_+ goes to infinity. The point y_+ disappears from the τ, y section which is no longer compact but becomes topologically $S^1 \times \mathbb{R}$. Thus, in this case we have a conical singularity only at y_A, and so we obtain a regular euclidean solution by simply requiring that the period of τ be equal to (9.5). We will label this solution by extreme AdS instanton.

In a de Sitter background there is another $y_+ \neq y_-$ instanton which satisfies $y_A = y_+$. It is called Nariai instanton and exists with or without charge. Moreover, in the dS background, there is also a special solution that satisfies $y_A = y_+ = y_-$. It is called ultracold instanton. In the AdS C-metric case, the counterparts of these dS instantons are of no interest for the pair creation process because they are out of the allowed range of the angular direction x.

Below, we will describe in detail the nonextreme AdS instanton with $m = q$ and the extreme AdS instanton. These instantons are the natural AdS C-metric counterparts of the lukewarm dS C and cold dS C instantons constructed in [88]. Thus, these instantons could also be labelled as lukewarm AdS C and cold AdS C instantons. These two families of instantons will allow us to calculate the pair creation rate of accelerated AdS−Reissner-Nordström black holes in section 9.1.2.

As is clear from the above discussion, when the charge vanishes we have no regular instanton available. Therefore, in the instanton context, we cannot discuss the pair creation of accelerated AdS-Schwarzschild black holes. In the dS background the instanton that describes this process is the neutral Nariai instanton [97, 169, 170, 172], whose AdS counterpart is not well-behaved as we said.

9.1.1.a The nonextreme AdS instanton with $m = q$

As we said above, for the nonextreme AdS instanton the gravitational field is given by (6.73) with the requirement that $\mathcal{F}(y)$ satisfies $\mathcal{F}(y_+) = 0 = \mathcal{F}(y_A)$ and $\mathcal{F}'(y_+) = -\mathcal{F}'(y_A)$. In this case we can then write

$$
\begin{aligned}
\mathcal{F}(y) &= -\left(\frac{y_A \, y_+}{y_A + y_+}\right)^2 \left(1 - \frac{y}{y_A}\right)\left(1 - \frac{y}{y_+}\right) \\
&\times \left(1 + \frac{y_A + y_+}{y_A \, y_+} y - \frac{y^2}{y_A \, y_+}\right),
\end{aligned}
\tag{9.7}
$$

with

$$
y_A = \frac{1 - \alpha}{2mA}, \qquad y_+ = \frac{1 + \alpha}{2mA},
$$
$$
\text{and} \quad \alpha = \sqrt{1 - \frac{4m}{\sqrt{3}}\sqrt{3A^2 - |\Lambda|}}.
\tag{9.8}
$$

The parameters A, Λ, m and q, written as a function of y_A and y_+, are

$$
\frac{|\Lambda|}{3A^2} = \left(\frac{y_A \, y_+}{y_A + y_+}\right)^2,
$$
$$
mA = (y_A + y_+)^{-1} = qA.
\tag{9.9}
$$

Thus, the mass and the charge of the nonextreme AdS instanton are necessarily equal, $m = q$, as occurs with its flat [114, 160, 181] and dS counterparts [167, 169, 88]. The demand that α is real requires that

$$
0 < m \leq \frac{1}{4}\sqrt{\frac{3}{3A^2 - |\Lambda|}},
\tag{9.10}
$$

and that

$$
A > \sqrt{|\Lambda|/3}.
\tag{9.11}
$$

Therefore, as already anticipated, the nonextreme AdS instanton is available only when (9.11) is satisfied.

As we said, the allowed range of y in the Euclidean sector is $y_A \le y \le y_+$. Then, the period of τ, (9.5), that avoids the conical singularity at both horizons is

$$\beta = \frac{8\pi \, mA}{\alpha(1-\alpha^2)} \, , \tag{9.12}$$

and $T = 1/\beta$ is the common temperature of the two horizons.

Using the fact that $\mathcal{G}(x) = |\Lambda|/(3A^2) - \mathcal{F}(-x)$ [see (9.4)] we can write

$$\mathcal{G}(x) = 1 - x^2 \, (1 + mA\,x)^2 \, , \tag{9.13}$$

and the roots of $\mathcal{G}(x)$ we are interested in are the south and north pole (represented, respectively, as x_{s} and x_{n} in Fig. 6.5),

$$x_{\mathrm{s}} = \frac{-1+\omega_-}{2mA} < 0 \, , \qquad x_{\mathrm{n}} = \frac{-1+\omega_+}{2mA} > 0 \, ,$$
$$\text{with} \quad \omega_\pm = \sqrt{1 \pm 4mA} \, . \tag{9.14}$$

When m and q go to zero we have $x_{\mathrm{s}} \to -1$ and $x_{\mathrm{n}} \to +1$. This is the reason why we decided to work in between the roots x_{s} and x_{n}, instead of working in between the roots x'_{s} and x'_{n} also represented in Fig. 6.5. Indeed, when $m \to 0$ and $q \to 0$ these two last roots disappear, and our instanton has no vacuum counterpart. Now, the requirement that ω_- is real demands that $mA < 1/4$ [note that $1/(4A) < (1/4)\sqrt{3/(3A^2 - |\Lambda|)}$, see (9.10)]. If this requirement is not fulfilled then $\mathcal{G}(x)$ has only two real roots that are represented as x'_{s} and x_{n} in Fig. 6.5 and, as we have just said, in this case the solution has no counterpart in the $m = 0$ and $q = 0$ case. Therefore we discard the solutions that satisfy $\frac{1}{4A} \le m \le \frac{1}{4}\sqrt{\frac{3}{3A^2 - |\Lambda|}}$, and hereafter when we refer to the mass of the nonextreme AdS instanton we will be working in the range

$$0 < m \le \frac{1}{4A} \, , \tag{9.15}$$

The period of ϕ, (9.76), that avoids the conical singularity at the north pole (and leaves one at the south pole responsible for the presence of the string) is

$$\Delta\phi = \frac{8\pi \, mA}{\omega_+(\omega_+^2 - 1)} < 2\pi \, . \tag{9.16}$$

When m and q go to zero we have $\Delta\phi \to 2\pi$ and the conical singularity disappears.

The topology of the nonextreme AdS instanton is $S^2 \times S^2 - \{region\}$, where $S^2 \times S^2$ represents $0 \le \tau \le \beta$, $y_A \le y \le y_+$, $x_{\mathrm{s}} \le x \le x_{\mathrm{n}}$, and $0 \le \phi \le \Delta\phi$, but we have to remove the region, $\{region\} = \{\{x,y\} : x_{\mathrm{s}} \le x \le -y_A \ \wedge \ y + x = 0\}$. The Lorentzian sector of this nonextreme instanton describes two charged AdS black holes being accelerated by the strings, so this instanton describes pair creation of nonextreme black holes with $m = q$.

9.1.1.b   The extreme AdS instanton with $y_+ = y_-$

The gravitational field of the extreme AdS instanton is given by (6.73) with the requirement that the size of the outer charged black hole horizon y_+ is equal to the size of the inner charged horizon y_-. Let us label this degenerated horizon by ρ: $y_+ = y_- \equiv \rho$ and $\rho > y_A$. In this case, the function $\mathcal{F}(y)$ can be written as

$$\mathcal{F}(y) = \frac{\rho^2 - 3\gamma}{\rho^4}(y - y'_A)(y - y_A)(y - \rho)^2 \, , \tag{9.17}$$

with

$$\gamma = \frac{3A^2 - |\Lambda|}{3A^2} , \qquad \text{and} \quad A > \sqrt{|\Lambda|/3} . \tag{9.18}$$

Note that, as occurred with the nonextreme AdS instanton, the extreme AdS instanton is also available only when $A > \sqrt{|\Lambda|/3}$. The roots ρ, y'_A and y_A are given by

$$\rho = \frac{3m}{4q^2 A} \left(1 + \sqrt{1 - \frac{8}{9} \frac{q^2}{m^2}} \right) , \tag{9.19}$$

$$y'_A = \frac{\gamma \rho}{\rho^2 - 3\gamma} \left(1 - \sqrt{\frac{\rho^2 - 2\gamma}{\gamma}} \right) , \tag{9.20}$$

$$y_A = \frac{\gamma \rho}{\rho^2 - 3\gamma} \left(1 + \sqrt{\frac{\rho^2 - 2\gamma}{\gamma}} \right) . \tag{9.21}$$

The mass and the charge of the solution are written as a function of ρ as

$$m = \frac{1}{A\rho} \left(1 - \frac{2\gamma}{\rho^2} \right) ,$$
$$q^2 = \frac{1}{A^2 \rho^2} \left(1 - \frac{3\gamma}{\rho^2} \right) , \tag{9.22}$$

and, for a fixed A and Λ, the ratio q/m is higher than 1. The conditions $\rho > y_A$ and $q^2 > 0$ require that, for the extreme AdS instanton, the allowed range of ρ is

$$\rho > \sqrt{6\gamma} . \tag{9.23}$$

The value of y_A decreases monotonically with ρ and we have $\sqrt{\gamma} < y_A < \sqrt{6\gamma}$. The mass and the charge of the extreme AdS instanton are also monotonically decreasing functions of ρ, and as we come from $\rho = +\infty$ into $\rho = \sqrt{6\gamma}$ we have

$$0 < m < \frac{\sqrt{2}}{3} \frac{1}{\sqrt{3A^2 - |\Lambda|}} , \tag{9.24}$$

$$0 < q < \frac{1}{2} \frac{1}{\sqrt{3A^2 - |\Lambda|}} , \tag{9.25}$$

so, for a fixed Λ, as the acceleration parameter A grows the maximum value of the mass and of the charge decreases monotonically. For a fixed Λ and for a fixed mass below $\sqrt{2/(9|\Lambda|)}$, the maximum value of the acceleration is $\sqrt{2/(27m^2) + |\Lambda|/3}$.

As we have already said, the allowed range of y in the Euclidean sector is $y_A \leq y < y_+$ and does not include $y = y_+$. Then, the period of τ, (9.5), that avoids the conical singularity at the only horizon of the extreme AdS instanton is

$$\beta = \frac{2\pi \rho^3}{(y_A - \rho)^2 \sqrt{\gamma(\rho^2 - 2\gamma)}} , \tag{9.26}$$

and $T = 1/\beta$ is the temperature of the acceleration horizon.

In what concerns the angular sector of the extreme AdS instanton, $\mathcal{G}(x)$ is given by (9.4), and its only real zeros are the south and north pole (represented, respectively, as x_s and x_n in Fig. 6.5; x'_s and x'_n also represented in this figure become complex roots in the extreme case),

$$x_s = -p + \frac{h}{2} - \frac{m}{2q^2 A} < 0 ,$$

$$x_n = +p + \frac{h}{2} - \frac{m}{2q^2 A} > 0 , \tag{9.27}$$

with

$$
p = \frac{1}{2}\left(-\frac{s}{3} + \frac{2m^2}{q^4 A^2} - \frac{1 - 12q^2 A^2}{3sq^4 A^4} - \frac{4}{3q^2 A^2} + n\right)^{1/2},
$$

$$
n = \frac{-m^3 + mq^2}{2hq^6 A^3},
$$

$$
h = \sqrt{\frac{s}{3} + \frac{m^2}{q^4 A^2} + \frac{1 - 12q^2 A^2}{3sq^4 A^4} - \frac{2}{3q^2 A^2}},
$$

$$
s = \frac{1}{2^{1/3}q^2 A^2}\left(\lambda - \sqrt{\lambda^2 - 4(1 - 12q^2 A^2)^3}\right)^{1/3},
$$

$$
\lambda = 2 - 108m^2 A^2 + 72q^2 A^2, \tag{9.28}
$$

where m and q are fixed by (9.22), for a given A, Λ and ρ. When $m \to 0$ and $q \to 0$ we have $x_{\mathrm{s}} \to -1$ and $x_{\mathrm{n}} \to +1$. The period of ϕ that avoids the conical singularity at the north pole (and leaves one at the south pole responsible for the presence of the strings) is given by (9.76) with x_{n} defined in (9.27).

The topology of the extreme AdS instanton is $\mathbb{R}^2 \times S^2 - \{region\}$, where $\mathbb{R}^2 \times S^2$ represents $0 \leq \tau \leq \beta$, $y_A \leq y < y_+$, $x_{\mathrm{s}} \leq x \leq x_{\mathrm{n}}$, and $0 \leq \phi \leq \Delta\phi$, but we have to remove the region, $\{region\} = \{\{x, y\} : x_{\mathrm{s}} \leq x \leq -y_A \wedge y + x = 0\}$. Since $y = y_+ = \rho$ is at an infinite proper distance, the surface $y = y_+ = \rho$ is an internal infinity boundary. The Lorentzian sector of this extreme case describes two extreme ($y_+ = y_-$) charged AdS black holes being accelerated by the strings, and the extreme AdS instanton describes the pair creation of these extreme black holes.

9.1.1.c The nonextreme AdS instanton with $m \neq q$

The AdS C-metric instantons studied in the two last subsections, namely the nonextreme instantons with $m = q$ and the extreme instantons with $y_+ = y_-$, are saddle point solutions free of conical singularities both in the y_+ and y_A horizons. The corresponding black holes may then nucleate in the AdS background when a cosmic string breaks, and we will compute their pair creation rates in Sec. 9.1.2. However, these particular black holes are not the only ones that can be pair created. Indeed, it has been shown in [155, 156] that Euclidean solutions with conical singularities may also be used as saddle points for the pair creation process. These nonextreme instantons have $m \neq q$ and describe pair creation of nonextreme black holes with $m \neq q$.

In what follows we will find the range of parameters for which one has nonextreme black holes with conical singularities, i.e., with $m \neq q$. First, when $m \neq 0$ and $q \neq 0$, we require that x belongs to the interval $[x_{\mathrm{s}}, x_{\mathrm{n}}]$ (sketched in Fig. 6.5) for which the charged solutions are in the same sector of the $m = 0$ and $q = 0$ solutions. Defining

$$
\chi \equiv \frac{q^2}{m^2}, \quad 0 < \chi \leq \frac{9}{8}, \quad \gamma_{\pm} \equiv 1 \pm \sqrt{1 - \frac{8}{9}\chi},
$$

$$
\sigma(\chi, \gamma_{\pm}) = \frac{(4\chi)^2 (3\gamma_{\pm})^2 - 8\chi(3\gamma_{\pm})^3 + \chi(3\gamma_{\pm})^4}{(4\chi)^4},
$$

$$
\tag{9.29}
$$

the above requirement is fulfilled by the parameter range

$$
m^2 A^2 < \sigma(\chi, \gamma_-), \tag{9.30}
$$

for which $\mathcal{G}(x = x_0) < 0$, with $x_0 = -\frac{3\gamma_-}{4\chi}\frac{1}{mA}$ being the less negative x where the derivative of $\mathcal{G}(x)$ vanishes. Second, in order to insure that one has a nonextreme solution we must require that

$$
m^2 A^2 > \sigma(\chi, \gamma_+) + m^2|\Lambda|/3, \tag{9.31}
$$

for which $\mathcal{F}(y = y_0) < 0$, with $y_0 = \frac{3\gamma_+}{4\chi}\frac{1}{mA}$ being the point in between y_+ and y_- where the derivative of $\mathcal{F}(y)$ vanishes. We have $\sigma(\chi, \gamma_-) > \sigma(\chi, \gamma_+)$ except at $\chi = 9/8$ where these two functions are equal; $\sigma(\chi, \gamma_-)$ is always positive; and $\sigma(\chi, \gamma_+) < 0$ for $0 < \chi < 1$ and $\sigma(\chi, \gamma_+) > 0$ for $1 < \chi \leq 9/8$. The nonextreme black holes with conical singularities are those that satisfy (9.30), (9.31) and $A > \sqrt{|\Lambda|/3}$. The range of parameters of these nonextreme black holes with $m \neq q$ are sketched in Fig. 9.1.
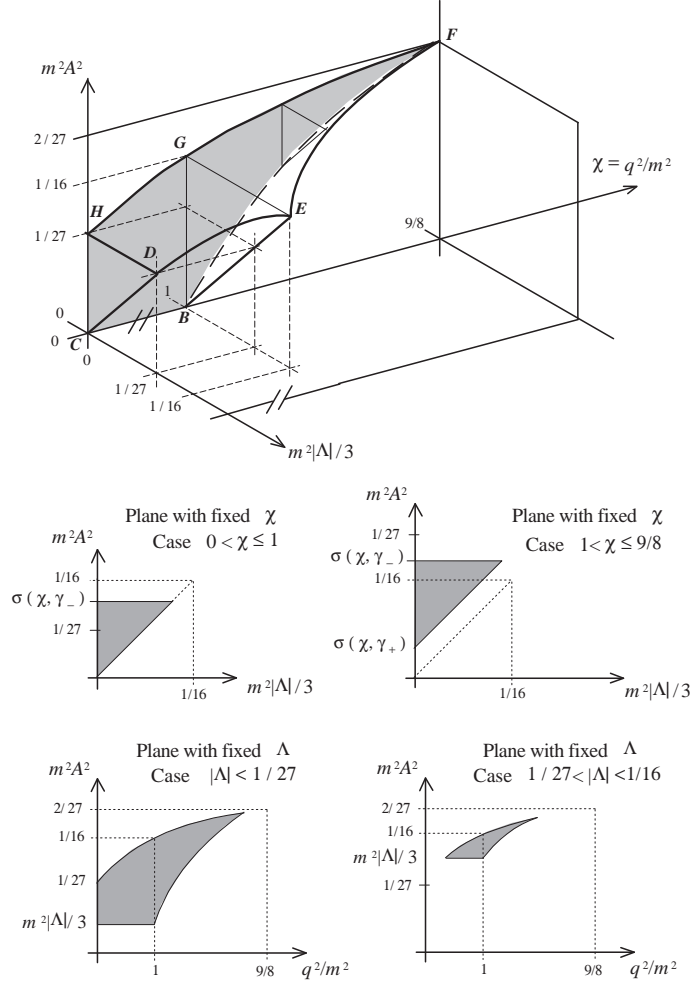
Figure 9.1: Allowed ranges of the parameters $\Lambda, A, m, \chi \equiv q^2/m^2$ for which one has a solution representing a pair of accelerated black holes. The planar surface whose frontier is the triangle BEG represents the nonextreme AdS instanton with $m = q$. The curved surface delimitated by the closed line BEF represents the extreme AdS instanton with $y_+ = y_-$ and satisfies $m^2A^2 = \sigma(\chi, \gamma_+) + m^2|\Lambda|/3$. The curved surface whose frontier is $DEFGH$ satisfies $m^2A^2 = \sigma(\chi, \gamma_-)$ [see (9.30)]. The plane surface with boundary given by $BCDE$ satisfies $A = \sqrt{|\Lambda|/3}$. Neutral AdS instantons ($q = 0$) are those that belong to the planar surface with the triangle boundary CDH. The nonextreme AdS instantons with $m \neq q$ are those whose parameters are in the volume with boundary defined by $BCDE$, BEF, $CBFGH$, CDH and $DEFGH$.

In order to compute the pair creation rate of the nonextreme black holes with $m \neq q$, we will need the relation between the parameters A, Λ, m, q, and the horizons y_A, y_+ and y_-. In general, for a nonextreme solution with horizons $y_A < y_+ < y_-$, one has

$$\mathcal{F}(y) = -\frac{1}{d}(y - y_A)(y - y_+)(y - y_-)(ay + b), \tag{9.32}$$

with

$$
\begin{aligned}
d &= y_A y_+ y_- (y_A + y_+ + y_-) + (y_A y_+ + y_A y_- + y_+ y_-)^2 \\
a &= (y_A y_+ + y_A y_- + y_+ y_-) \\
b &= y_A y_+ y_- \,.
\end{aligned}
\tag{9.33}
$$

The parameters A, Λ, m and q can be expressed as a function of y_A, y_+ and y_- by

$$
\begin{aligned}
\frac{|\Lambda|}{3A^2} &= 1 - d^{-2}(y_A y_+ y_-)^2 \\
q^2 A^2 &= d^{-1}(y_A y_+ + y_A y_- + y_+ y_-) \\
mA &= (2\,\sigma)^{-1}(y_A + y_+)(y_A + y_-)(y_+ + y_-) \\
\sigma &= y_A^2 y_+ y_- + y_A y_+^2 y_- + y_A y_+ y_-^2 + (y_A y_+)^2 \\
&\quad + (y_A y_-)^2 + (y_+ y_-)^2 \,.
\end{aligned}
\tag{9.34}
$$

The allowed values of parameters m and q are those contained in the interior region sketched in Fig. 9.1.

The topology of these nonextreme AdS instantons with $m \neq q$ is $S^2 \times S^2 - \{region\}$, where $S^2 \times S^2$ represents $0 \leq \tau \leq \beta$, $y_A \leq y \leq y_+$, $x_\mathrm{s} \leq x \leq x_\mathrm{n}$, and $0 \leq \phi \leq \Delta\phi$, but we have to remove the region, $\{region\} = \{\{x,y\} : x_\mathrm{s} \leq x \leq -y_A \ \wedge \ y + x = 0\}$. These instantons describe the pair creation of nonextreme black holes with $m \neq q$.

9.1.1.d   Initial system: AdS background with a string

So far, we have described the solution that represents a pair of black holes accelerated by the strings tension. This solution describes the evolution of the black hole pair after its creation. Now, we want to find a solution that represents a string in a AdS background. This solution will describe the initial system, before the breaking of the cosmic string that leads to the formation of the black hole pair. In order to achieve our aim we note that at spatial infinity the gravitational field of the Euclidean AdS C-metric reduces to

$$
ds^2 = \frac{1}{[A_0(x+y)]^2}\left[-\left(\frac{|\Lambda|}{3A_0^2} - 1 + y^2\right)dt^2 + \frac{dy^2}{\frac{|\Lambda|}{3A_0^2} - 1 + y^2} + \frac{dx^2}{1-x^2} + (1-x^2)d\phi_0^2 \right],
\tag{9.35}
$$

and the Maxwell field goes to zero. A_0 is a constant that represents a freedom in the choice of coordinates, and $-1 \leq x \leq 1$. We want that this metric also describes the solution before the creation of the black hole pair, i.e., we demand that it describes a string with its conical deficit in an AdS background. Now, if we want to maintain the intrinsic properties of the string during the process we must impose that its mass density and thus its conical deficit remains constant. After the pair creation we already know that the conical deficit is given by (9.2). Hence, the requirement that the background solution describes an AdS spacetime with a conical deficit angle given exactly by (9.2) leads us to impose that in (9.35) one has

$$
\Delta\phi_0 = 2\pi - \delta = 2\pi \frac{\mathcal{G}'(x_\mathrm{s})}{|\mathcal{G}'(x_\mathrm{n})|} \,.
\tag{9.36}
$$

The arbitrary parameter A_0 can be fixed as a function of A by imposing a matching between (6.73) and (9.35) at large spatial distances. We will do this matching in the following section.

9.1.2   Calculation of the black hole pair creation rates

The black hole pair creation rate is given by the path integral

$$
\Gamma(g_{ij}, A_i) = \int d[g_{\mu\nu}]d[A_\mu] e^{-\left[I(g_{\mu\nu}, A_\mu) - I_0(g_{\mu\nu}^0, A_\mu^0)\right]} ,
\tag{9.37}
$$

where g_{ij} and A_i are the induced metric and electromagnetic potential on the boundary $\partial\mathcal{M}$ of a compact manifold $\mathcal{M}$, $d[g_{\mu\nu}]$ is a measure on the space of the metrics $g_{\mu\nu}$ and $d[A_\mu]$ is a measure on the space of Maxwell field A_μ, and $I(g_{\mu\nu}, A_\mu)$ is the Euclidean action of the instanton that mediates the process. In our case this action is the Einstein-Maxwell action with a negative cosmological constant Λ. The path integral is over all compact metrics and potentials on manifolds $\mathcal{M}$ with boundary $\partial\mathcal{M}$, which agree with the boundary data on $\partial\mathcal{M}$. $I_0(g^0_{\mu\nu}, A^0_\mu)$ is the action for the background reference spacetime, the AdS background with the string, specified by $g^0_{\mu\nu}$ and A^0_μ (see Sec. 9.1.1.d). Its presence is required because it describes the initial system. Moreover, the geometry of the final system with the black hole pair is noncompact, that is $I(g_{\mu\nu}, A_\mu)$ diverges. However, the physical action $I(g_{\mu\nu}, A_\mu) - I_0(g^0_{\mu\nu}, A^0_\mu)$ is finite for fields $g_{\mu\nu}$, A_μ that approach asymptotically $g^0_{\mu\nu}$, A^0_μ in an appropriate way [165]. Specifically, one fixes a boundary near infinity, Σ^∞, and demands that $g_{\mu\nu}$, A_μ and $g^0_{\mu\nu}$, A^0_μ induce fields on this boundary that agree to sufficient order, so that their difference does not contribute to the action in the limit that Σ^∞ goes to infinity [165].

In the semiclassical instanton approximation, the dominant contribution to the path integral (9.37) comes from metrics and Maxwell fields which are near the solutions (instantons) that extremalize the Euclidean action and satisfy the boundary conditions. In this approximation, the pair creation rate of AdS black holes is then given by

$$\Gamma \sim \eta\, e^{-I_{\text{inst}}}\,, \tag{9.38}$$

where $I_{\text{inst}} \equiv I - I_0$ includes already the contribution from the background reference spacetime. η is the one-loop prefactor that accounts for the fluctuations in the gravitational and matter fields, and its evaluation will not be considered in this paper (see [171, 172, 138, 162] [284]-[288] for a treatment of this factor in some backgrounds).

Hawking and Horowitz [165] (see also Brown and York [289]) have shown that the Euclidean action of the instanton that mediates pair creation of nonextreme black holes can be written in the form

$$I_{\text{inst}} = \beta H - \frac{1}{4}\left(\Delta\mathcal{A}_{\text{ac}} + \mathcal{A}_{\text{bh}}\right)\,, \tag{9.39}$$

where $\Delta\mathcal{A}_{\text{ac}}$ is the difference in area of the acceleration horizon between the AdS C-metric and the background, and $\mathcal{A}_{\text{bh}}$ is the area of the black hole horizon present in the instanton. The Euclidean action of the instanton that describes pair creation of extreme black holes can be written as

$$I_{\text{inst}} = \beta H - \frac{1}{4}\Delta\mathcal{A}_{\text{ac}}\,. \tag{9.40}$$

In these relations, β is the period of the Euclidean time, and H represents the Hamiltonian of the system which, for static solutions, is given by [165, 289]

$$H = \int_{\Sigma_t} d^3x\sqrt{h}\, N\mathcal{H} - \frac{1}{8\pi}\int_{\Sigma_t^\infty} d^2x\sqrt{\sigma}\left(N\,^2K - N_0\,^2K_0\right)\,. \tag{9.41}$$

The boundary ∂M consists of an initial and final spacelike surface, Σ_t, of constant t with unit normal u^μ ($u\cdot u = -1$) and with intrinsic metric $h_{\mu\nu} = g_{\mu\nu} + u_\mu u_\nu$ plus a timelike surface near infinity, Σ^∞, with unit normal n^μ ($n\cdot n = 1$, and $u\cdot n = 0$) and with intrinsic metric $\sigma_{\mu\nu} = h_{\mu\nu} - n_\mu n_\nu$. This surface Σ^∞ needs not to be at infinity. It can also be at a black hole horizon or at an internal infinity, but we will generally label it by Σ^∞. This surface Σ^∞ is foliated by a family of 2-surfaces Σ_t^∞ that result from the intersection between Σ^∞ and Σ_t. In (9.41), N and N_0 are the lapse functions of the system with the pair and of the background, respectively, and $N = N_0$ in the boundary near infinity, Σ^∞. $\mathcal{H}$ is the hamiltonian constraint that contains contributions from the gravitational and Maxwell fields, and vanishes for solutions of the equations of motion. Then, the Hamiltonian is simply given by the boundary surface term. In this surface term, ^2K represents the trace of the

extrinsic curvature of the surface imbedded in the AdS C-metric, and $^2K_0$ is the extrinsic curvature of the surface imbedded in the background spacetime.

We will now verify that the boundary surface term in the Hamiltonian (9.41) is also zero, and thus the Hamiltonian makes no contribution to (9.39) and (9.40). We follow the technical procedure applied by Hawking, Horowitz and Ross [164] in the Ernst solution and by Hawking and Ross [133] in the flat C-metric. As we said above, one will require that the intrinsic metric $ds^2_{(\Sigma_t^\infty)}$ on the boundary Σ_t^∞ as embedded in the AdS C-metric agrees (to sufficient order) with the intrinsic metric on the boundary Σ_t^∞ as embedded in the background spacetime, in order to be sure that one is taking the same near infinity boundary in the evaluation of the quantities in the two spacetimes. In the AdS C-metric one takes this boundary to be at $x + y = \varepsilon_c$, where $\varepsilon_c \ll 1$. The background reference spacetime is described by (9.35), subjected to $-1 \leq x \leq 1$, $y \geq -x$ and (9.36). In this background spacetime we take the boundary Σ_t^∞ to be at $x + y = \varepsilon_0$, where $\varepsilon_0 \ll 1$.

We are now interested in writing the intrinsic metric in the boundary Σ_t^∞ (the 2-surface $t = $ const and $x + y = \varepsilon$). In the AdS C-metric (6.73) one performs the coordinate transformation

$$\phi = \frac{2}{|\mathcal{G}'(x_{\rm n})|} \tilde{\phi}, \qquad t = \frac{2}{\mathcal{F}'(y_A)} \tilde{t} \tag{9.42}$$

in order that $\Delta\tilde{\phi} = 2\pi$, and the analytic continuation of $\tilde{t}$ has period 2π, i.e., $\Delta\tilde{\tau} = 2\pi$. Furthermore, one takes

$$x = x_{\rm s} + \varepsilon_c \chi, \qquad y = -x_{\rm s} + \varepsilon_c(1 - \chi) \tag{9.43}$$

where $0 \leq \chi \leq 1$. By making the evaluations up to second order in ε_c (since higher order terms will not contribute to the Hamiltonian in the final limit $\varepsilon_c \to 0$), the intrinsic metric on the boundary Σ_t^∞ is then

$$ds^2_{(\Sigma_t^\infty)} \sim \frac{2}{A^2 \varepsilon_c \mathcal{G}'(x_{\rm s})} \left[\frac{d\chi^2}{2\chi} + \left| \frac{\mathcal{G}'(x_{\rm s})}{\mathcal{G}'(x_{\rm n})} \right|^2 \left(2\chi + \varepsilon_c \frac{\mathcal{G}''(x_{\rm s})}{\mathcal{G}'(x_{\rm s})} \chi^2 \right) d\tilde{\phi}^2 \right]. \tag{9.44}$$

Analogously, for the background spacetime (9.35) one sets

$$x = -1 + \varepsilon_0 \chi, \qquad y = 1 + \varepsilon_0(1 - \chi) \tag{9.45}$$

and the intrinsic metric on the boundary Σ_t^∞ yields

$$ds^2_{(\Sigma_t^\infty)} \sim \frac{1}{A_0^2 \varepsilon_0} \left[\frac{d\chi^2}{2\chi} + \left(2\chi - \varepsilon_0 \chi^2 \right) d\phi_0^2 \right] \tag{9.46}$$

These two intrinsic metrics on the boundary will agree (up to second order in ε) as long as we take the period of ϕ_0 to be given by (9.36) and the following matching conditions are satisfied,

$$\varepsilon_0 = -\frac{\mathcal{G}''(x_{\rm s})}{\mathcal{G}'(x_{\rm s})} \varepsilon_c, \tag{9.47}$$

$$A_0^2 = -\frac{[\mathcal{G}'(x_{\rm s})]^2}{2\mathcal{G}''(x_{\rm s})} A^2. \tag{9.48}$$

Note that the Maxwell fields of the two solutions agree trivially at the near infinity boundary Σ_t^∞.

In what concerns the lapse function of the AdS C-metric, we evaluate it with respect to the time coordinate $\tilde{t}$ defined in (9.42) and, using $[A(x + y)]^{-2} \mathcal{F} dt^2 = N^2 d\tilde{t}^2$, we find

$$N \sim \sqrt{\frac{|\Lambda|}{3}} \frac{2}{A^2 \varepsilon_c \mathcal{F}'(y_A)} \left(1 + \frac{1}{2} \frac{3}{|\Lambda|} (1 - \chi) A^2 \varepsilon_c \, \mathcal{G}'(x_{\rm s}) \right). \tag{9.49}$$

Analogously, an evaluation with respect to the time coordinate t defined in (9.35) yields

$$N_0 \sim \frac{\mathcal{G}'(x_{\mathrm{s}})}{\mathcal{F}'(y_A)} \sqrt{\frac{|\Lambda|}{3}} \frac{1}{A_0^2 \varepsilon_0} \left(1 + \frac{3}{|\Lambda|} (1 - \chi) A_0^2 \varepsilon_0 \right). \tag{9.50}$$

Note that these two lapse functions are also matched by the conditions (9.47) and (9.48).

The extrinsic curvature to Σ_t^∞ as embedded in Σ_t is ${}^2K_{\mu\nu} = \sigma_\mu{}^\alpha h_\alpha{}^\beta \nabla_\beta n_\nu$ (where ∇_β represents the covariant derivative with respect to $g_{\mu\nu}$), and the trace of the extrinsic curvature is ${}^2K = g^{\mu\nu}\, {}^2K_{\mu\nu} = A\sqrt{\mathcal{F}(y)}$. The extrinsic curvature of the boundary embedded in the AdS C-metric is then

$$^2K \sim \sqrt{\frac{|\Lambda|}{3}} \left(1 + \frac{1}{2} \frac{3}{|\Lambda|} (1 - \chi) A^2 \varepsilon_c \, \mathcal{G}'(x_{\mathrm{s}}) \right), \tag{9.51}$$

while the extrinsic curvature of the boundary embedded in the background reference spacetime is

$$^2K_0 \sim \sqrt{\frac{|\Lambda|}{3}} \left(1 + \frac{3}{|\Lambda|} (1 - \chi) A_0^2 \varepsilon_0 \right). \tag{9.52}$$

We are now in position to compute the contribution from the surface boundary term in (9.41). The evaluation in the AdS C-metric yields

$$\int_{\Sigma_t^\infty} d\chi d\tilde{\phi} \sqrt{\sigma}\, N\, {}^2K \sim \frac{8\pi}{|\mathcal{G}'(x_{\mathrm{n}})| \mathcal{F}'(y_A)} \frac{|\Lambda|}{3} \frac{1}{(A^2 \varepsilon_c)^2} \left(1 - \frac{1}{2} \frac{3}{|\Lambda|} A^2 \varepsilon_c \, \mathcal{G}'(x_{\mathrm{s}}) \right), \tag{9.53}$$

while for the background reference spacetime we have

$$\int_{\Sigma_t^\infty} \sqrt{\sigma_0}\, d\chi d\phi_0 N_0\, {}^2K_0 \sim \frac{8\pi [\mathcal{G}'(x_{\mathrm{s}})]^2}{|\mathcal{G}'(x_{\mathrm{n}})| \mathcal{F}'(y_A)} \frac{|\Lambda|}{3} \frac{1}{(2A_0^2 \varepsilon_0)^2} \left(1 - \frac{3}{|\Lambda|} A_0^2 \varepsilon_0 \right). \tag{9.54}$$

From the matching conditions (9.47) and (9.48) we conclude that these two boundary terms are equal. Hence, the surface term and the Hamiltonian (9.41) vanish. The Euclidean action (9.39) of the nonextreme AdS instanton that mediates pair creation of nonextreme black holes is then simply

$$I_{\mathrm{nonext}} = -\frac{1}{4} \left(\Delta\mathcal{A}_{\mathrm{ac}} + \mathcal{A}_{\mathrm{bh}} \right), \tag{9.55}$$

while the Euclidean action (9.39) of the extreme AdS instanton that mediates pair creation of nonextreme black holes is just given by

$$I_{\mathrm{ext}} = -\frac{1}{4} \Delta\mathcal{A}_{\mathrm{ac}}. \tag{9.56}$$

Thus as occurs in the Ernst case, in the flat C-metric case, in the de Sitter case and in the dS C-metric case, the pair creation of nonextreme black holes is enhanced relative to the pair creation of extreme black holes by a factor of $e^{\mathcal{A}_{\mathrm{bh}}}$.

In the next two subsections we will explicitly compute (9.55) using the results of subsection 9.1.1.a, and (9.56) using the results of subsection 9.1.1.b. In subsection 9.1.2.c we analyze the pair creation rate of black holes discussed in subsection 9.1.1.c. Remark that the only horizons that contribute with their areas to (9.55) and (9.56) are those that belong to the instanton responsible for the pair creation, i.e, only those horizons that are in the Euclidean sector of the instanton will make a contribution.

The domain of validity of our results is the particle limit, $mA \ll 1$, for which the radius of the black hole, $r_+ \sim m$, is much smaller than the typical distance between the black holes at the creation moment, $\ell \sim 1/A$ (this value follows from the Rindler motion $x^2 - t^2 = 1/A^2$ that describes the uniformly accelerated motion of the black holes).

9.1.2.a   Pair creation rate in the nonextreme case with $m = q$

In the nonextreme case, the instanton has two horizons in its Euclidean section, namely the acceleration horizon at $y = y_A$ and the black hole horizon at $y = y_+$ (the horizons y'_A and y_- do not belong to the instanton, see Fig. 6.5). The black hole horizon covers the whole range of the angular coordinate x, $x_{\rm s} \le x \le x_{\rm n}$, and its area is

$$
\begin{aligned}
\mathcal{A}_{\rm bh} &= \int_{y=y_+} \sqrt{g_{xx}g_{\phi\phi}}\, dx\, d\phi \\
&= \frac{1}{A^2} \int_{\Delta\phi} d\phi \int_{x_{\rm s}}^{x_{\rm n}} \frac{dx}{(x+y_+)^2} \\
&= \frac{4\pi}{A^2|\mathcal{G}'(x_{\rm n})|} \frac{x_{\rm n} - x_{\rm s}}{(x_{\rm n}+y_+)(x_{\rm s}+y_+)}\,,
\end{aligned}
\tag{9.57}
$$

where y_+ is given in (9.8), $x_{\rm s}$ and $x_{\rm n}$ are defined by (9.14), and $\Delta\phi$ is given by (9.16).

   The acceleration horizon, y_A defined in (9.8), of the nonextreme AdS instanton covers the angular range $-y_A \le x \le x_{\rm n}$ (i.e., it is not present in the vicinity of the south pole), and is noncompact, i.e., its area is infinite. We have to deal appropriately with this infinity. In order to do so, we first introduce a boundary at $x = -y_A + \varepsilon_c$ ($\varepsilon_c \ll 1$), and compute the area inside of this boundary, which yields

$$
\begin{aligned}
\mathcal{A}_{\rm ac}^c &= \int_{y=y_A} \sqrt{g_{xx}g_{\phi\phi}}\, dx\, d\phi \\
&= \frac{1}{A^2} \int_{\Delta\phi} d\phi \int_{-y_A+\varepsilon_c}^{x_{\rm n}} \frac{dx}{(x+y_A)^2} \\
&= -\frac{4\pi}{A^2|\mathcal{G}'(x_{\rm n})|} \left(\frac{1}{x_{\rm n}+y_A} - \frac{1}{\varepsilon_c} \right)\,,
\end{aligned}
\tag{9.58}
$$

When we let $\varepsilon_c \to 0$, the term $1/\varepsilon_c$ diverges, and the acceleration horizon has an infinite area. This area is renormalized with respect to the area of the acceleration horizon of the background reference spacetime (9.35). This background reference spacetime has an acceleration horizon at $y = \sqrt{1 - |\Lambda|/(3A_0^2)}$ which is the direct counterpart of the above acceleration horizon of the nonextreme AdS instanton, and it covers the angular range $-\sqrt{1 - |\Lambda|/(3A_0^2)} \le x \le 1$. The area inside a boundary at $x = -\sqrt{1 - |\Lambda|/(3A_0^2)} + \varepsilon_0$ is

$$
\begin{aligned}
\mathcal{A}_{\rm ac}^0 &= \int_{y=\sqrt{1-\frac{|\Lambda|}{3A_0^2}}} \sqrt{g_{xx}g_{\phi_0\phi_0}}\, dx\, d\phi_0 \\
&= \frac{1}{A_0^2} \int_{\Delta\phi_0} d\phi_0 \int_{-\sqrt{1-\frac{|\Lambda|}{3A_0^2}}+\varepsilon_0}^{1} \frac{dx}{\left(x + \sqrt{1-\frac{|\Lambda|}{3A_0^2}}\right)^2} \\
&= -\frac{2\pi}{A_0^2} \frac{\mathcal{G}'(x_{\rm s})}{|\mathcal{G}'(x_{\rm n})|} \left(\frac{1}{1+\sqrt{1-\frac{|\Lambda|}{3A_0^2}}} - \frac{1}{\varepsilon_0} \right)\,,
\end{aligned}
\tag{9.59}
$$

where in the last step we have replaced $\Delta\phi_0$ by (9.36). When $\varepsilon_0 \to 0$, the term $1/\varepsilon_0$ diverges, and thus the area of this background acceleration horizon is also infinite. Now, we have found that the intrinsic metrics at the near infinity boundary match together if (9.47) and (9.48) are satisfied. Our next task is to verify that these matching conditions between (ε_c, A) and (ε_0, A_0) are such that the divergent terms in (9.58) and (9.59) cancel each other. It is straightforward to show that $\Delta\mathcal{A}_{\rm ac} = \mathcal{A}_{\rm ac}^c - \mathcal{A}_{\rm ac}^0$ yields a finite value if

$$
2A_0^2\varepsilon_0 = A^2\varepsilon_c\mathcal{G}'(x_{\rm s})\,.
\tag{9.60}
$$

Thus, the matching conditions (9.47) and (9.48) satisfy condition (9.60), i.e., they indeed eliminate the divergencies in $\Delta\mathcal{A}_{\text{ac}}$. It is worthy to remark that with the choices (9.47) and (9.48) the proper lengths of the boundaries $x = -y_A + \varepsilon_c$ and $x = -\sqrt{1 - |\Lambda|/(3A_0^2)} + \varepsilon_0$, (given, respectively, by $l_c = \int \sqrt{g_{\phi\phi}}d\phi$ and $l_0 = \int \sqrt{g_{\phi_0\phi_0}}d\phi_0$) do not match. This is in contrast with the flat case [133], where the choice of the matching parameters that avoids the infinities in $\Delta\mathcal{A}_{\text{ac}}$, also leads to $l_c = l_0$. In the AdS case, our main goal was to remove the infinities in $\Delta\mathcal{A}_{\text{ac}}$. We have achieved this aim by comparing the appropriate acceleration horizons in the instanton and in the reference background. The fact that the matching relations then lead to $l_c \neq l_0$ is not a problem at all[a]. Replacing (9.47) and (9.48) in (9.59) yields for $\Delta\mathcal{A}_{\text{ac}} = \mathcal{A}_{\text{ac}}^c - \mathcal{A}_{\text{ac}}^0$ the result

$$\Delta\mathcal{A}_{\text{ac}} = -\frac{4\pi}{A^2|\mathcal{G}'(x_{\text{n}})|}\left(\frac{1}{x_{\text{n}} + y_A} + \frac{1}{1 + \sqrt{1 - \frac{|\Lambda|}{3A^2}\frac{2|\mathcal{G}''(x_{\text{s}})|}{[\mathcal{G}'(x_{\text{s}})]^2}}}\frac{\mathcal{G}''(x_{\text{s}})}{\mathcal{G}'(x_{\text{s}})}\right), \tag{9.61}$$

where $2|\mathcal{G}''(x_{\text{s}})|/[\mathcal{G}'(x_{\text{s}})]^2 < 1$.

Adding (9.57) and (9.61), and using the results of Sec. 9.1.1.a yields finally the total area of the nonextreme AdS instanton with $m = q$,

$$\mathcal{A}_{\text{bh}}^{\text{nonext}} + \Delta\mathcal{A}_{\text{ac}}^{\text{nonext}} =$$
$$-\frac{16\pi m^2}{\omega_+(\omega_+^2 - 1)}\left(-\frac{\omega_+ - \omega_-}{(\omega_+ + \alpha)(\omega_- + \alpha)} + \frac{1}{\omega_+ - \alpha} + \frac{1}{1 + \sqrt{1 - \frac{8|\Lambda|m^2}{3}\frac{3\omega_-^2 - 1}{\omega_-^2(1-\omega_-^2)^2}}}\frac{1 - 3\omega_-^2}{\omega_-(1 - \omega_-^2)}\right), \tag{9.62}$$

where ω_+ and ω_- are defined in (9.14), α is given by (9.8), and condition (9.15) must be satisfied. The pair creation rate of nonextreme AdS black holes with $m = q$ is then

$$\Gamma_{\text{nonext}} \sim e^{\frac{1}{4}\left(\mathcal{A}_{\text{bh}}^{\text{nonext}} + \Delta\mathcal{A}_{\text{ac}}^{\text{nonext}}\right)}. \tag{9.63}$$

Fixing A and Λ one concludes that the pair creation rate decreases as the mass of the black holes increases (see Fig. 9.2). Moreover, fixing m and Λ, in the domain of validity of our results, $mA \ll 1$ and $A > \sqrt{|\Lambda|/3}$, as A increases the pair creation rate increases (see Fig. 9.2). Hence, the general behavior of the pair creation rate of nonextreme black holes with $m = q$ in the AdS case is analogous to the corresponding behavior in the flat case [133] (see also section 9.2).

---

[a]This question deserves a physical interpretation. Both in the flat and AdS cases, the proper lengths in the C-metric instanton and in the background are equal, $l_c = l_0$, at the south pole boundaries, $x = x_{\text{s}} + \varepsilon_c$ and $x = -1 + \varepsilon_0$, respectively. Now, a string is present when the ratio between the perimeter of a circle and its radius is not 2π, i.e., one has a deficit angle. The fact that for a same radius one has $l_c = l_0$ at the south pole confirms that the string before and after the pair creation has the same properties, as expected from the discussion of subsection 9.1.1.d. In the flat case, but not in the AdS one, the south pole boundary coincides with the acceleration boundary, i.e., $x = x_{\text{s}} + \varepsilon_c \equiv -y_A + \varepsilon_c$, and this is the reason why in the flat case one has $l_c = l_0$ at the horizon boundary.

(a) **(b)**
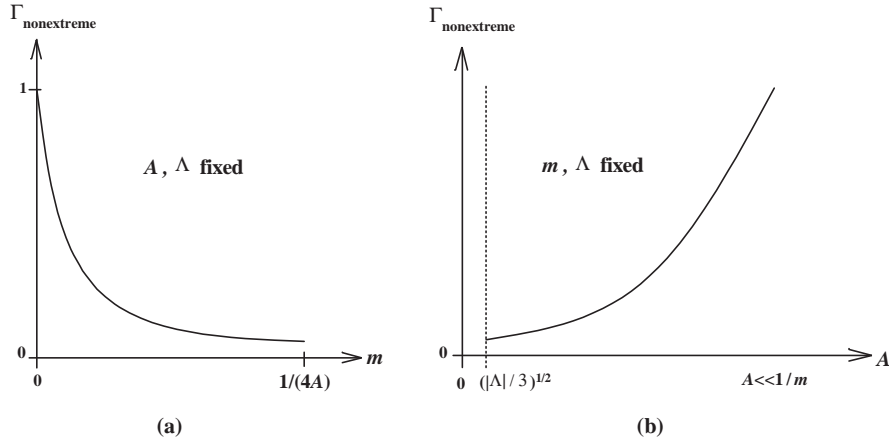
Figure 9.2: (a) Plot of the pair creation rate of nonextreme black holes, Γ_{nonext}, as a function of m for a fixed A and Λ. The range of m is $0 < m < \frac{1}{4m}$. (b) Plot of the pair creation rate of nonextreme black holes, Γ_{nonext}, as a function of A for a fixed m and Λ. The range of A is $\sqrt{\frac{|\Lambda|}{3}} < A < \frac{1}{4m}$. See text of subsection 9.1.2.a.

9.1.2.b Pair creation rate in the extreme case ($y_+ = y_-$)

In the extreme AdS case, the instanton has a single horizon, the acceleration horizon at $y = y_A$, in its Euclidean section, since $y = y_+$ is an internal infinity. The pair creation rate of extreme AdS black holes with $y_+ = y_-$ is then

$$\Gamma_{\text{ext}} \sim e^{\frac{1}{4}\Delta\mathcal{A}_{\text{ac}}^{\text{ext}}}, \tag{9.64}$$

where $\Delta\mathcal{A}_{\text{ac}}^{\text{ext}}$ is given by (9.61), with y_A defined in (9.21), x_{s} and x_{n} given by (9.27), and condition (9.25) must be satisfied. The pair creation rate decreases as the mass of the black holes increases, and the pair creation rate increases when A increases (see Fig. 9.3). The general behavior of the pair creation rate of extreme black holes as a function of m and A in the AdS case is also analogous to the behavior of the flat case, discussed in [133] (see also section 9.2).

(a) **(b)**
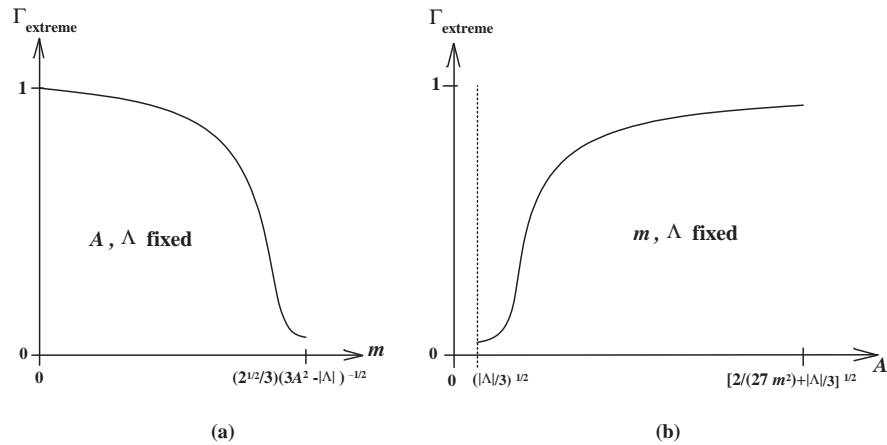
Figure 9.3: (a) Plot of the pair creation rate of extreme black holes, Γ_{ext}, as a function of m for a fixed A and Λ. The range of m is $0 < m < \frac{\sqrt{2}}{3}\frac{1}{\sqrt{3A^2-|\Lambda|}}$. (b) Plot of the pair creation rate of nonextreme black holes, Γ_{ext}, as a function of A for a fixed m and Λ. The range of A is $\sqrt{\frac{|\Lambda|}{3}} < A < \sqrt{\frac{2}{27m^2} + \frac{|\Lambda|}{3}}$. See text of subsection 9.1.2.b.

9.1.2.c   Pair creation rate in the nonextreme case with $m \neq q$

The nonextreme instantons, that mediate the pair creation of nonextreme black holes with $m \neq q$ (including the case $q = 0$), have two horizons in their Euclidean section, namely the acceleration horizon at $y = y_A$ and the black hole horizon at $y = y_+$. The pair creation rate of nonextreme AdS black holes with $m \neq q$ is then $\Gamma \sim e^{(\mathcal{A}_{\text{bh}}^{\text{nonext}} + \Delta \mathcal{A}_{\text{ac}}^{\text{nonext}})/4}$, with $\mathcal{A}_{\text{bh}}^{\text{nonext}}$ given by (9.57) and $\Delta \mathcal{A}_{\text{ac}}^{\text{nonext}}$ given by (9.61), subjected to the results found in Sec. 9.1.1.c. The pair creation rate decreases as the mass of the black holes increases, and the pair creation rate increases when A increases.

9.1.3   Heuristic derivation of the nucleation rates

In order to clarify the physical interpretation of the results, in this subsection we heuristically derive some results discussed in the main body of section 9.1. In particular, we find heuristically the pair creation rates.

In an AdS background, pair creation of black holes is possible only when the acceleration provided by the strings satisfies $A > \sqrt{|\Lambda|/3}$. To understand this result one can argue as follows. In general, the time-time component of the gravitational field is given by $g_{00} = 1 - 2\Phi$, where Φ is the Newtonian potential. In the AdS spacetime, one has $\Phi = -|\Lambda| r^2/6$ and its derivative yields the force per unit mass or acceleration of the AdS spacetime, $A_{\text{AdS}} = -|\Lambda| r/3 \sim -\sqrt{|\Lambda|/3}$, where we have replaced r by the characteristic AdS radius $(|\Lambda|/3)^{-1/2}$. The minus sign indicates that the AdS background is attractive and thus, if one wants to have a pair of accelerated black holes driving away from each other, the cosmic string will have to provide a sufficient acceleration A that overcomes the AdS background attraction, i.e., $A > |A_{\text{AdS}}|$.

An estimate for the black hole pair creation probability can be given by the Boltzmann factor, $\Gamma \sim e^{-E_0/W_{\text{ext}}}$, where E_0 is the energy of the system that nucleates and $W_{\text{ext}} = F\ell$ is the work done by the external force F, that provides the energy for the nucleation, through the typical distance ℓ separating the created pair. First we ask what is the probability that a black hole pair is created in a $\Lambda = 0$ background when a string breaks. This process has been discussed in [133] (see also section 9.2) where it was found that the pair creation rate is $\Gamma \sim e^{-m/A}$. In this case, $E_0 \sim 2m$, where m is the rest energy of the black hole, and $W_{\text{ext}} \sim A$ is the work provided by the strings. To derive $W_{\text{ext}} \sim A$ one can argue as follows. The acceleration provided by the string is A, the characteristic distance that separates the pair at the creation moment is $1/A$ (this value follows from the Rindler motion $x^2 - t^2 = 1/A^2$ that describes the uniformly accelerated motion of the black holes), and the characteristic mass of the system is A by the Compton relation. Thus, the characteristic work is $W_{\text{ext}} = \text{mass} \times \text{acceleration} \times \text{distance} \sim AAA^{-1}$. So, from the Boltzmann factor we indeed expect that the creation rate of a black hole pair when a string breaks in a $\Lambda = 0$ background is given by $\Gamma \sim e^{-m/A}$.

Now we ask what is the probability that a string breaks in an AdS background and a pair of black holes is produced. As we saw just above, the presence of the AdS background leads in practice to a problem in which we have a net acceleration that satisfies $A' \equiv \sqrt{A^2 - |\Lambda|/3}$, this is, Λ makes a negative contribution to the process. Heuristically, we may then apply the same arguments that have been used in the last paragraph, with the replacement $A \to A'$. At the end, the Boltzmann factor tells us that the creation rate for the process is $\Gamma \sim e^{-m/\sqrt{A^2 - |\Lambda|/3}}$. So, given m and Λ, when the acceleration provided by the string grows the pair creation rate increases, as the explicit calculations done in the main body of section 9.2.

9.1.4   Summary and discussion

We have studied in detail the quantum process in which a cosmic string breaks in an anti-de Sitter (AdS) background and a pair of black holes is created at the ends of the string. The energy to materialize and accelerate the black holes comes from the strings' tension. The analysis of this process in a flat background ($\Lambda = 0$) has been carried in [133], while in a de Sitter background ($\Lambda > 0$) it has been done in [131]. In an AdS background this is the only study done in the process

of production of a pair of correlated black holes with spherical topology. Note that in a cosmological background, the transformation used by Ernst to generate an exact solution in an electromagnetic background does not work, since it does not leave invariant the cosmological term in the action. Thus Ernst's trick cannot be used, and we do not have an exact AdS Ernst solution available to study analytically the process in which a pair of black holes is produced and accelerated by the electromagnetic force. However, in principle, we could find a perturbative AdS Ernst solution that supplies the same energy and acceleration as our strings and, from the results of the $\Lambda = 0$ case we expect that the results found in this paper would not depend on whether the energy is being furnished by an external electromagnetic field or by strings.

It is well known that the AdS background is attractive, i.e., an analysis of the geodesic equations indicates that particles in this background are subjected to a potential well that attracts them. Therefore, if we have a virtual pair of black holes and we want to turn them real, we will have to furnish a sufficient force that overcomes this cosmological background attraction. We then expect that pair creation is possible only if the strings' tension and the associated acceleration A is higher than a critical value. We have confirmed that this is indeed the case: in the AdS background, black holes with spherical topology can be produced only with an acceleration higher than $\sqrt{|\Lambda|/3}$. This result was also expected from the AdS C-metric properties, which describes the evolution of the system after the creation process. Indeed, in [87] we have shown that it only describes a pair of black holes if $A > \sqrt{|\Lambda|/3}$, otherwise it represents a single accelerated black hole.

We have constructed the instantons that mediate the pair creation process through the analytic continuation of some special cases of the AdS C-metric. The regularity condition imposed to these instantons restricts the mass m and the charge q of the black holes that are produced, and physically it means that the only black holes that can be pair produced are those that are in thermodynamic equilibrium. Concretely, we have found two charged regular instantons. One mediates the pair creation of nonextreme black holes with $m = q$, and the other mediates the pair creation of extreme black holes. These instantons are the natural AdS C-metric counterparts of the instantons found in previous works on the subject. We note that the Nariai instanton, and the ultracold instanton that are available in the de Sitter background, are not present in the AdS case since they are out of the allowed range of the angular direction x. The instantons constructed from the $\Lambda < 0$ and $\Lambda = 0$ C-metric are noncompact (contrary to what occurs with the $\Lambda > 0$ instantons), in the sense that they have an acceleration horizon with an infinite area. Thus when dealing with them, we have to eliminate this infinity by normalizing this area relative to the acceleration horizon area of an appropriate background reference spacetime.

We have explicitly computed the pair creation rate for the nonextreme and extreme black holes. In both cases, the AdS pair creation rate reduces to the corresponding ones of the flat case when we set $\Lambda = 0$ [133] (see also section 9.2). In the two cases, the pair creation rate decreases monotonically, as the mass (and charge) of the black holes increases (see Figs. 9.2.(a) and 9.3.(a) for the nonextreme and extreme cases, respectively). This is the physically expected result since an higher mass demands an higher energy. In what concerns the evolution of the pair creation rate with the acceleration A, we found that the pair creation rate increases monotonically with A (see Figs. 9.2.(b) and 9.3.(b) for the nonextreme and extreme cases, respectively). The physical interpretation of this result is clear: the acceleration A of the black hole pair is provided by the string. When the energy of the string is higher (i.e., when its mass density or the acceleration that it provides is higher), the probability that it breaks and produces a black hole pair with a given mass is also higher. This behavior is better understood if we make a analogy with a thermodynamical system, with the mass density of the string being the analogue of the temperature T. Indeed, from the Boltzmann factor, $e^{-E_0/(k_B T)}$ (where k_B is the Boltzmann constant), one knows that a higher background temperature T turns the nucleation of a particle with energy E_0 more probable. Similarly, a background string with a higher mass density turns the creation of a black hole pair with mass $2m$ more probable.

We have also verified that (as occurs with pair creation in other backgrounds) the pair production of nonextreme black holes is enhanced relative to the pair creation of extreme black holes by a factor of $e^{S_{bh}}$, where $S_{bh} = \mathcal{A}_{bh}/4$ is the gravitational entropy of the black hole.

9.2   Pair creation of flat black holes on a cosmic string background

In a flat background ($\Lambda = 0$), the analysis of the process of pair creation of black holes when a cosmic string breaks has been analyzed by Hawking and Ross [133]. In this case, there is a direct $\Lambda = 0$ counterpart of the nonextreme AdS instanton and of the extreme AdS instanton discussed in our AdS case. These instantons describe pair creation of nonextreme (with $m = q$) and extreme black holes with $y_+ = y_-$, respectively [133]. The total area of these $\Lambda = 0$ instantons can be found in [133], and can be obtained by taking the direct $\Lambda = 0$ limit of (9.57) and (9.61), together with the replacement $y_A \mapsto -x_{\mathrm{s}}$. This procedure yields that (9.57) also holds in the $\Lambda = 0$ case, while $\Delta\mathcal{A}_{\mathrm{ac}}$ becomes

$$\Delta\mathcal{A}_{\mathrm{ac}} = -\frac{4\pi}{A^2|\mathcal{G}'(x_{\mathrm{n}})|}\left(\frac{1}{x_{\mathrm{n}} - x_{\mathrm{s}}} + \frac{1}{2}\frac{\mathcal{G}''(x_{\mathrm{s}})}{\mathcal{G}'(x_{\mathrm{s}})}\right). \tag{9.65}$$

In [133] the explicit numerical value of $\mathcal{A}_{\mathrm{bh}}$ and $\Delta\mathcal{A}_{\mathrm{ac}}$ has not been computed. We will do it here.

For the $\Lambda = 0$ nonextreme case, the discussion of Sec. 9.1.1.a applies generically, as long as we set $\Lambda = 0$ in the corresponding equations. With this data we find the explicit value of the total area of the nonextreme flat instanton

$$\mathcal{A}_{\mathrm{bh}} + \Delta\mathcal{A}_{\mathrm{ac}} = -\frac{\pi}{A^2}\frac{-1 + 4mA + \sqrt{1 - (4mA)^2}}{\sqrt{1 - (4mA)^2}}. \tag{9.66}$$

In the particle limit, $mA \ll 1$, the above relation reduces to $-\pi m/(4A)$ and the mass density of the string is given by $\mu \sim mA$. The pair creation rate is then $\Gamma \sim e^{-\pi m^2/\mu}$. Thus, as occurs with the AdS case, the pair creation rate decreases when m increases and the rate increases when A or μ increase [see Fig. 9.4].

We remark that for $mA \sim 1$, and as occurs in the corresponding AdS case, the pair creation rate associated to (9.66) starts decreasing when A increases. This is a physically unexpected result since a higher acceleration provided by the string background should favor the nucleation of a fixed black hole mass. The sector $mA \sim 1$ must then be discarded and the reason is perfectly identified: the domain of validity of the rates is $mA \ll 1$, for which the radius of the black hole, $r_+ \sim m$, is much smaller than the typical distance between the black holes at the creation moment, $\ell \sim 1/A$ (this value follows from the Rindler motion $x^2 - t^2 = 1/A^2$ that describes the uniformly accelerated motion of the black holes). So, for $mA \sim 1$ one has $r_+ \sim \ell$ and the black holes start interacting with each other.

In what concerns the pair creation rate of extreme and nonextreme with $m = q$ $\Lambda = 0$ black holes, an explicit computation shows that its general behavior with A and m is also similar to the one of the AdS case, i.e., the rate decreases when m or q increase, and the rate increases when A increases.
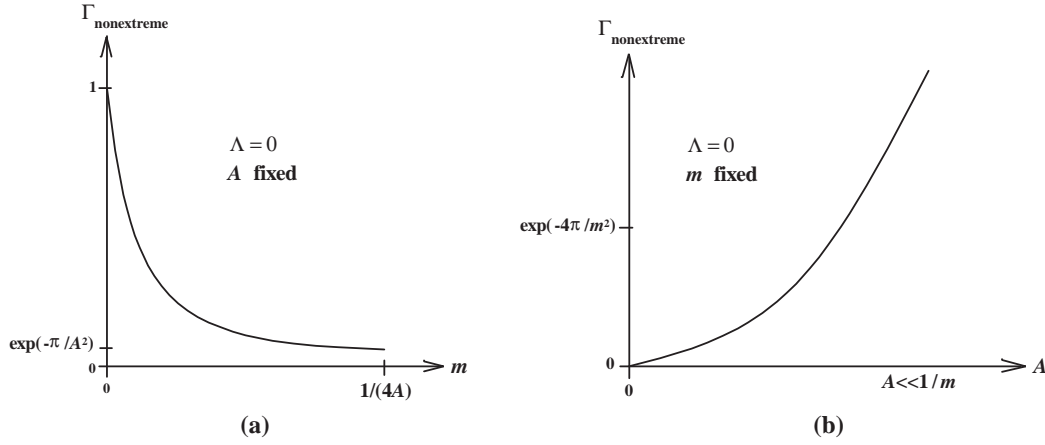
Figure 9.4: (a) Plot of the pair creation rate of nonextreme $\Lambda = 0$ black holes, $\Gamma_{\rm nonext}$, as a function of m for a fixed A. (b) Plot of the pair creation rate of nonextreme $\Lambda = 0$ black holes, $\Gamma_{\rm nonext}$, as a function of A for a fixed m.

9.3 Pair creation of de Sitter black holes on a cosmic string background

In this section we want to analyze the process in which a cosmic string breaks and a pair of black holes is produced at the ends of the string, in a de Sitter (dS) background. Therefore, the energy to materialize and accelerate the pair comes from the positive cosmological constant and, in addition, from the string tension. This process is a combination of the processes considered in [167]-[172] and in [133]-[136]. The instantons for this process can be constructed by analytically continuing the dS C-metric found by Plebański and Demiański [86] and analyzed by Podolský and Griffiths [120], and in detail by Dias and Lemos [88].

The plan of this section is as follows. In section 9.3.1, we describe the semiclassical instanton method used to evaluate the pair creation rate. In section 9.3.2 we construct, from the dS C-metric studied in section 6.3, the regular instantons that describe the pair creation process. Then, in section 9.3.3, we explicitly evaluate the pair creation rate for each one of the cases discussed in section 9.3.2. In section 9.3.4 we verify that the usual relation between pair creation rate, entropy and total area holds also for the pair creation process discussed in this section. Finally, in section 9.3.6 concluding remarks are presented.

9.3.1 Black hole pair creation rate: the instanton method

The pair creation of black holes in a de Sitter (dS) background is described, according to the no-boundary proposal of Hartle and Hawking [283], by the propagation from nothing to a 3-surface boundary Σ. The amplitude for this process is given by the wave function

$$\Psi(h_{ij}, A_i) = \int d[g_{\mu\nu}]d[A_\mu]e^{-I(g_{\mu\nu}, A_\mu)} , \qquad (9.67)$$

where h_{ij} and A_i are the induced metric and electromagnetic potential on the boundary $\Sigma = \partial\mathcal{M}$ of a compact manifold $\mathcal{M}$, $d[g_{\mu\nu}]$ is a measure on the space of the metrics $g_{\mu\nu}$ and $d[A_\mu]$ is a measure on the space of the Maxwell field A_μ, and $I(g_{\mu\nu}, A_\mu)$ is their Euclidean action. The path integral is over all compact metrics and potentials on manifolds $\mathcal{M}$ with boundary Σ, which agree with the boundary data on Σ. For a nice detailed discussion of the no-boundary proposal applied to the study of black hole pair creation see Bousso and Chamblin [177].

In the semiclassical instanton approximation, the dominant contribution to the path integral comes from metrics and Maxwell fields which are near the solutions (instantons) that extremalize

the Euclidean action and satisfy the boundary conditions. Thus, considering small fluctuations around this solution, $g_{\mu\nu} \to g_{\mu\nu} + \tilde{g}_{\mu\nu}$ and $A_\mu \to A_\mu + \tilde{A}_\mu$, the action expands as

$$I = I_{\text{inst}}(g_{\mu\nu}, A_\mu) + \delta^2 I(\tilde{g}_{\mu\nu}) + \delta^2 I(\tilde{A}_\mu) + \cdots , \tag{9.68}$$

where $\delta^2 I$ are quadratic in $\tilde{g}_{\mu\nu}$ and $\tilde{A}_\mu$, and dots denote higher order terms. The wave function, that describes the creation of a black hole pair from nothing, is then given by $\Psi_{\text{inst}} = B e^{-I_{\text{inst}}}$, where I_{inst} is the classical action of the gravitational instanton that mediates the pair creation of black holes, and the prefactor B is the one loop contribution from the quantum quadratic fluctuations in the fields, $\delta^2 I$. Similarly, the wave function that describes the nucleation of a dS space with a string from nothing is $\Psi_{\text{string}} \propto e^{-I_{\text{string}}}$, and the wave function describing the nucleation of a dS space from nothing is $\Psi_{\text{dS}} \propto e^{-I_{\text{dS}}}$. The nucleation probability of the dS space from nothing, of the dS space with a string from nothing, and of a space with a pair of black holes from nothing is then given by $|\Psi_{\text{dS}}|^2$, $|\Psi_{\text{string}}|^2$ and $|\Psi_{\text{inst}}|^2$, respectively.

We may now ask four questions: what is the probability for (i) pair creation of black holes in a dS spacetime, (ii) the nucleation of a string in a dS background, (iii) the process in which a string in a dS background breaks and a pair of black holes is created, and (iv) the combined process (ii)+(iii). In the process (i) the energy to materialize the pair comes only from the positive cosmological constant background, Λ. The system does not contain a string and the probability for this process has been found in [169]. The aim of the present paper is to compute explicitly the probability for processes (ii)-(iv). It is important to note that in the process (iii), one assumes that the initial background contains a string, i.e. , the question that is being asked is: given that the string is already present in our initial system, what is the probability that it breaks and a pair of black holes is produced and accelerated apart by Λ and by the string tension? On the other side, in (iv) one is asking: starting from a pure dS background, what is the probability that a string nucleates on it and then breaks forming a pair of black holes? Naturally, the probability for process (iv) is the product of the probability for process (ii) and the probability for process (iii).

According to the no-boundary proposal, the nucleation rate of a string in a dS background is proportional to $|\Psi_{\text{string}}|^2/|\Psi_{\text{dS}}|^2$, i.e.,

$$\Gamma_{\text{string/dS}} \simeq \eta\bar{\eta}\, e^{-2I_{\text{string}}+2I_{\text{dS}}} . \tag{9.69}$$

The pair creation rate of black holes when a string breaks in a dS background is given by

$$\Gamma_{\text{BHs/string}} \simeq \eta\, e^{-2I_{\text{inst}}+2I_{\text{string}}} , \tag{9.70}$$

and the pair creation rate of black holes when process (iv) occurs is given by the product of (9.69) and (9.70), i.e.,

$$\Gamma_{\text{BHs/dS}} \simeq \tilde{\eta}\, e^{-2I_{\text{inst}}+2I_{\text{dS}}} . \tag{9.71}$$

We will find I_{inst} and I_{string} in the next subsections. In the three relations above, $\bar{\eta}$, η and $\tilde{\eta}$ are one-loop prefactors which will not be considered in this paper. The evaluation of this one-loop prefactor has been done only in a small number of cases, namely for the vacuum background by Gibbons, Hawking and Perry [284], for the Schwarzschild instanton by Gross, Perry and Yaffe [138], for other asymptotically flat instantons by Young [287], for the dS background by Gibbons and Perry [285] and Christensen and Duff [286], for the dS-Schwarzschild instanton by Ginsparg and Perry [97], Young [288], Volkov and Wipf [172] and Garattinni [171], and for the Ernst instanton by Yi [162].

At this point we must specify the Euclidean action needed to compute the path integral (9.67). This issue was analyzed and clarified in detail by Hawking and Ross [181] and by Brown [163]. Now, due to its relevance for the present paper, we briefly discuss the main results of [181, 163]. One wants to use an action for which it is natural to fix the boundary data on Σ specified in (9.67). That is, one wants to use an action whose variation gives the Euclidean equations of motion when

the variation fixes these boundary data on Σ [289]. In the magnetic case this Euclidean action is the Einstein-Maxwell action with a positive cosmological constant Λ given by

$$I = -\frac{1}{16\pi} \int_{\mathcal{M}} d^4x \sqrt{g} \, (R - 2\Lambda - F^{\mu\nu}F_{\mu\nu}) - \frac{1}{8\pi} \int_{\Sigma=\partial\mathcal{M}} d^3x \sqrt{h} \, K \, , \qquad (9.72)$$

where g is the determinant of the Euclidean metric, h is the determinant of the induced metric on the boundary Σ, R is the Ricci scalar, K is the trace of the extrinsic curvature K_{ij} of the boundary, and $F_{\mu\nu} = \partial_\mu A_\nu - \partial_\nu A_\mu$ is the Maxwell field strength of the gauge field A_ν. Variation of (9.72) yields $\delta I = (\cdots) + \frac{1}{4\pi} \int_\Sigma d^3x \sqrt{h} \, F^{\mu\nu} n_\mu \delta A_\nu$, where $(\cdots)$ represents terms giving the equations of motion plus gravitational boundary terms that are discussed in [289], and n_μ is the unit outward normal to Σ. Thus, variation of (9.72) gives the equations of motion as long as it is at fixed gauge potential A_i on the boundary. Now, for magnetic black hole solutions, fixing the potential fixes the charge on each of the black holes, since the magnetic charge is just given by the integral of F_{ij} over a 2-sphere lying in the boundary. However, in the electric case, fixing A_i can be regarded as fixing a chemical potential ω which is conjugate to the charge [181]. Holding the electric charge fixed is equivalent to fixing $n_\mu F^{\mu i}$ on Σ, as the electric charge is given by the integral of the dual of F over a 2-sphere lying in Σ. Therefore in the electric case the appropriate Euclidean action is [181]

$$I_{\rm el} = I - \frac{1}{4\pi} \int_{\Sigma=\partial\mathcal{M}} d^3x \sqrt{h} \, F^{\mu\nu} n_\mu A_\nu \, , \qquad (9.73)$$

where I is defined in (9.72). Variation of action (9.73) yields $\delta I_{\rm el} = (\cdots) + \frac{1}{4\pi} \int_\Sigma d^3x \delta(\sqrt{h} \, F^{\mu\nu} n_\mu) A_\nu$, and thus it gives the equations of motion when $\sqrt{h} \, n_\mu F^{\mu i}$, and so the electric charge, is held fixed. Since $\int_{\mathcal{M}} d^4x \sqrt{g} F^{\mu\nu} F_{\mu\nu}$ has opposite signs for dual magnetic and electric solutions, if we took (9.72) to evaluate both the magnetic and electric actions we would conclude that the pair creation of electric black holes would be enhanced relative to the pair creation of magnetic black holes. This physically unexpected result does not occur when one considers the appropriate boundary conditions and includes the extra Maxwell boundary term in (9.73).

We have to be careful [290, 181] when computing the extra Maxwell boundary term in the electric action (9.73). Indeed, we have to find a vector potential, A_ν, that is regular everywhere in the instanton, including at the horizons. Usually, as we shall see, this requirement leads to unusual choices for A_ν. The need of this requirement is easily understood if we take the example of the electric Reissner-Nordström solution [290, 181]. In this case, normally, the gauge potential in Schwarzschild coordinates is taken to be $A = -\frac{q}{r} dt$. However, this potential is not regular at the horizon $r = r_+$, since dt diverges there. An appropriate choice that yields a regular electromagnetic potential everywhere, including at the horizon is $A = -q(\frac{1}{r} - \frac{1}{r_+}) dt$ or, alternatively, $A = -\frac{q}{r^2} t \, dr$. To all these potentials corresponds the field strength $F = -\frac{q}{r^2} dt \wedge dr$.

Before we finish this section, note that since the dS C-metric instantons that we will consider in this paper are all compact we do not have to define their action relative an appropriate background solution, contrarily to what happens with the non-compact $\Lambda = 0$ instantons [159]-[166].

9.3.2   The dS C-metric instantons

The dS C-metric has been studied in detail in section 6.3. It describes a pair of uniformly accelerated black holes in a dS background, with the acceleration being provided by the cosmological constant and, in addition, by a string that connects the two black holes along their south poles and pulls them away. The presence of the string is associated to the conical singularity that exists in the south pole of the dS C-metric.

Following section 9.3.1, in order to evaluate the black hole pair creation rate we need to find the instantons of the theory, i.e., we must look into the Euclidean section of the dS C-metric and choose only those Euclidean solutions which are regular in a way that will be explained soon. To obtain the Euclidean section of the dS C-metric from the Lorentzian dS C-metric we simply introduce an

imaginary time coordinate $\tau = -it$. Then the gravitational field of the Euclidean dS C-metric is given by (see, e.g., [88])

$$ds^2 = [A(x+y)]^{-2}(\mathcal{F}d\tau^2 + \mathcal{F}^{-1}dy^2 + \mathcal{G}^{-1}dx^2 + \mathcal{G}d\phi^2) \,, \tag{9.74}$$

with $\mathcal{F}(y)$ and $\mathcal{G}(x)$ given by (6.74). The Maxwell field in the magnetic case is still given by (6.5), while in the electric case it is given by

$$F_{\mathrm{el}} = -i\,q\,d\tau \wedge dy \,. \tag{9.75}$$

Recall some basic properties that will be needed. The solution has a curvature singularity at $y = +\infty$ where the matter source is. The point $y = -x$ corresponds to a point that is infinitely far away from the curvature singularity, thus as y increases we approach the curvature singularity and $y + x$ is the inverse of a radial coordinate. At most, $\mathcal{F}(y)$ can have four real zeros which we label in ascending order by $y_{\mathrm{neg}} < 0 < y_A \leq y_+ \leq y_-$. The roots y_- and y_+ are respectively the inner and outer charged black hole horizons, and y_A is an acceleration horizon which coincides with the cosmological horizon and has a non-spherical shape. The negative root y_{neg} satisfies $y_{\mathrm{neg}} < -x$ and thus has no physical significance. The angular coordinate x belongs to the range $[x_{\mathrm{s}}, x_{\mathrm{n}}]$ for which $\mathcal{G}(x) \geq 0$ (when we set $A = 0$ we have $x_{\mathrm{s}} = -1$ and $x_{\mathrm{n}} = +1$). In order to avoid a conical singularity in the north pole, the period of ϕ must be given by

$$\Delta\phi = \frac{4\pi}{|\mathcal{G}'(x_{\mathrm{n}})|} \,, \tag{9.76}$$

and this leaves a conical singularity in the south pole with deficit angle

$$\delta = 2\pi\left(1 - \frac{\mathcal{G}'(x_{\mathrm{s}})}{|\mathcal{G}'(x_{\mathrm{n}})|}\right) \,. \tag{9.77}$$

that signals the presence of a string with mass density $\mu = \delta/(8\pi)$, and with pressure $p = -\mu < 0$. When we set the acceleration parameter A equal to zero, the dS C-metric reduces to the usual dS$-$Reissner-Nordström or dS-Schwarzschild solutions without conical singularities.

So far, we have described the solution that represents a pair of black holes accelerated by the cosmological constant and by the string tension. This solution describes the evolution of the black hole pair after its creation. Now, we want to find a solution that represents a string in a dS background. This solution will describe the initial system, before the breaking of the cosmic string that leads to the formation of the black hole pair. In order to achieve our aim we note that at spatial infinity the gravitational field of the Euclidean dS C-metric reduces to

$$\begin{aligned}ds^2 &= \frac{1}{[A_0(x+y)]^2}\left[\left(-\frac{\Lambda}{3A_0^2} - 1 + y^2\right)dt^2 \right.\\ &\quad \left. + \frac{dy^2}{-\frac{\Lambda}{3A_0^2} - 1 + y^2} + \frac{dx^2}{1 - x^2} + (1 - x^2)d\phi_0^2\right],\end{aligned} \tag{9.78}$$

and the Maxwell field goes to zero. A_0 is a constant that represents a freedom in the choice of coordinates, and $-1 \leq x \leq 1$. We want that this metric also describes the solution before the creation of the black hole pair, i.e., we demand that it describes a string with its conical deficit in a dS background. Now, if we want to maintain the intrinsic properties of the string during the process we must impose that its mass density and thus its conical deficit remains constant. After the pair creation we already know that the conical deficit is given by (9.77). Hence, the requirement that the background solution describes a dS spacetime with a conical deficit angle given exactly by (9.77) leads us to impose that in (9.78) one has

$$\Delta\phi_0 = 2\pi - \delta = 2\pi\frac{\mathcal{G}'(x_{\mathrm{s}})}{|\mathcal{G}'(x_{\mathrm{n}})|} \,. \tag{9.79}$$

The arbitrary parameter A_0 can be fixed by imposing a matching between (9.74) and (9.78) at large spatial distances [164, 133], yielding $A_0^2 = -A^2[\mathcal{G}'(x_s)]^2/[2\mathcal{G}''(x_s)]$.

Returning back to the euclidean dS C-metric (9.74), in order to have a positive definite Euclidean metric we must require that y belongs to $y_A \leq y \leq y_+$. In general, when $y_+ \neq y_-$, one then has conical singularities at the horizons $y = y_A$ and $y = y_+$. In order to obtain a regular solution we have to eliminate the conical singularities at both horizons. This is achieved by imposing that the period of τ is the same for the two horizons, and is equivalent to requiring that the Hawking temperature of the two horizons be equal. To eliminate the conical singularity at $y = y_A$ the period of τ must be $\beta = 2\pi/k_A$ (where k_A is the surface gravity of the acceleration horizon),

$$\beta = \frac{4\pi}{|\mathcal{F}'(y_A)|} \,. \tag{9.80}$$

This choice for the period of τ also eliminates simultaneously the conical singularity at the outer black hole horizon, y_+, if and only if the parameters of the solution are such that the surface gravities of the black hole and acceleration horizons are equal ($k_+ = k_A$), i.e.

$$\mathcal{F}'(y_+) = -\mathcal{F}'(y_A) \,. \tag{9.81}$$

There are two ways to satisfy this condition. One is a regular Euclidean solution with $y_A \neq y_+$, and will be called lukewarm C instanton. This solution requires the presence of an electromagnetic charge. The other way is to have $y_A = y_+$, and will be called Nariai C instanton. This last solution exists with or without charge. When we want to distinguish them, they will be labelled by charged Nariai and neutral Nariai C instantons, respectively.

We now turn our attention to the case $y_+ = y_-$ and $y_A \neq y_+$, which obviously requires the presence of charge. When this happens the allowed range of y in the Euclidean sector is simply $y_A \leq y < y_+$. This occurs because when $y_+ = y_-$ the proper distance along spatial directions between y_A and y_+ goes to infinity. The point y_+ disappears from the τ, y section which is no longer compact but becomes topologically $S^1 \times \mathbb{R}$. Thus, in this case we have a conical singularity only at y_A, and so we obtain a regular Euclidean solution by simply requiring that the period of τ be equal to (9.80). We will label this solution by cold C instanton. Finally, we have a special solution that satisfies $y_A = y_+ = y_-$ and that is regular when condition (9.80) is satisfied. This instanton will be called ultracold C instanton and can be viewed as a limiting case of both the charged Nariai C instanton and cold C instanton.

Below, we will describe in detail each one of these four C instantons, following the order: (A) lukewarm C instanton, (B) cold C instanton, (C) Nariai C instanton, and (D) ultracold C instanton. These instantons are the C-metric counterparts ($A \neq 0$) of the $A = 0$ instantons that have been constructed from the Euclidean section of the dS$-$Reissner-Nordström solution ($A = 0$) [167, 168, 169, 173]. The original name of the $A = 0$ instantons is associated to the relation between their temperatures: $T_{\text{lukewarm}} > T_{\text{cold}} > T_{\text{ultracold}} > T_{\text{Nariai}} = 0$. This relation is preserved by their C-metric counterparts discussed in this paper, and we preserve the $A = 0$ nomenclature. The ultracold instanton could also, very appropriately, be called Nariai Bertotti-Robinson instanton (see [89]). These four families of instantons will allow us to calculate the pair creation rate of accelerated dS$-$Reissner-Nordström black holes in section 9.3.3.

As is clear from the above discussion, when the charge vanishes the only regular Euclidean solution that can be constructed is the neutral Nariai C instanton. The same feature is present in the $A = 0$ case where only the neutral Nariai instanton is available [97, 169, 170, 172].

9.3.2.a   The lukewarm C instanton

For the lukewarm C instanton the gravitational field is given by (9.74) with the requirement that $\mathcal{F}(y)$ satisfies $\mathcal{F}(y_+) = 0 = \mathcal{F}(y_A)$ and $\mathcal{F}'(y_+) = -\mathcal{F}'(y_A)$. In this case we can then write (onwards the subscript "ℓ" means lukewarm)

$$\mathcal{F}_\ell(y) = -\left(\frac{y_A\, y_+}{y_A + y_+}\right)^2 \left(1 - \frac{y}{y_A}\right)\left(1 - \frac{y}{y_+}\right)\left(1 + \frac{y_A + y_+}{y_A\, y_+}\, y - \frac{y^2}{y_A\, y_+}\right), \tag{9.82}$$

with

$$y_A = \frac{1 - \alpha}{2mA}, \qquad y_+ = \frac{1 + \alpha}{2mA}, \quad \text{and} \quad \alpha = \sqrt{1 - \frac{4m}{\sqrt{3}}\sqrt{\Lambda + 3A^2}}\,. \tag{9.83}$$

The parameters A, Λ, m and q, written as a function of y_A and y_+, are

$$\frac{\Lambda}{3A^2} = \left(\frac{y_A\, y_+}{y_A + y_+}\right)^2,$$

$$mA = (y_A + y_+)^{-1} = qA\,. \tag{9.84}$$

Thus, the mass and the charge of the lukewarm C instanton are necessarily equal, $m = q$, as occurs with its $A = 0$ counterpart, the lukewarm instanton [167, 168, 169, 173]. The demand that α is real requires that

$$0 < m_\ell \leq \frac{\sqrt{3}}{4}\frac{1}{\sqrt{\Lambda + 3A^2}}\,, \tag{9.85}$$

so the lukewarm C instanton has a lower maximum mass and a lower maximum charge than the $A = 0$ lukewarm instanton [167, 168, 169, 173] and, for a fixed Λ, as the acceleration parameter A grows this maximum value decreases monotonically. For a fixed Λ and for a fixed mass below $\sqrt{3/(16\Lambda)}$, the maximum value of the acceleration is $\sqrt{1/(4m)^2 - \Lambda/3}$.

As we said, the allowed range of y in the Euclidean sector is $y_A \leq y \leq y_+$. Then, the period of τ, (9.80), that avoids the conical singularity at both horizons is

$$\beta_\ell = \frac{8\pi\, mA}{\alpha(1 - \alpha^2)}\,, \tag{9.86}$$

and $T_\ell = 1/\beta_\ell$ is the common temperature of the two horizons.

Using the fact that $\mathcal{G}(x) = -\Lambda/(3A^2) - \mathcal{F}(-x)$ [see (6.74)] we can write

$$\mathcal{G}_\ell(x) = 1 - x^2\,(1 + mA\,x)^2\,, \tag{9.87}$$

and the only real zeros of $\mathcal{G}_\ell(x)$ are the south and north pole

$$x_{\mathrm{s}} = \frac{-1 + \omega_-}{2mA} < 0\,, \qquad x_{\mathrm{n}} = \frac{-1 + \omega_+}{2mA} > 0\,, \quad \text{with} \quad \omega_\pm \equiv \sqrt{1 \pm 4mA}\,. \tag{9.88}$$

When A goes to zero we have $x_{\mathrm{s}} \to -1$ and $x_{\mathrm{n}} \to +1$. The period of ϕ, (9.76), that avoids the conical singularity at the north pole (and leaves one at the south pole responsible for the presence of the string) is

$$\Delta\phi_\ell = \frac{8\pi\, mA}{\omega_+(\omega_+^2 - 1)} \leq 2\pi\,. \tag{9.89}$$

When A goes to zero we have $\Delta\phi_\ell \to 2\pi$ and the conical singularity disappears.

The topology of the lukewarm C instanton is $S^2 \times S^2$ ($0 \leq \tau \leq \beta_\ell$, $y_A \leq y \leq y_+$, $x_{\mathrm{s}} \leq x \leq x_{\mathrm{n}}$, and $0 \leq \phi \leq \Delta\phi_\ell$). The Lorentzian sector describes two dS black holes being accelerated by the cosmological background and by the string, so this instanton describes pair creation of nonextreme black holes with $m = q$.

9.3.2.b The cold C instanton

The gravitational field of the cold C instanton is given by (9.74) with the requirement that the size of the outer charged black hole horizon y_+ is equal to the size of the inner charged horizon y_-. Let us label this degenerated horizon by ρ: $y_+ = y_- \equiv \rho$ and $\rho > y_A$. In this case, the function $\mathcal{F}(y)$ can be written as (onwards the subscript "c" means cold)

$$\mathcal{F}_{\mathrm{c}}(y) = \frac{\rho^2 - 3\gamma}{\rho^4}(y - y_{\mathrm{neg}})(y - y_A)(y - \rho)^2\,, \tag{9.90}$$

with

$$\gamma = \frac{\Lambda + 3A^2}{3A^2} \,, \tag{9.91}$$

and the roots ρ, y_{neg} and y_A are given by

$$\rho = \frac{3m}{4q^2 A} \left(1 + \sqrt{1 - \frac{8}{9}\frac{q^2}{m^2}} \right) \,, \tag{9.92}$$

$$y_{\mathrm{neg}} = \frac{\gamma\rho}{\rho^2 - 3\gamma} \left(1 - \sqrt{\frac{\rho^2 - 2\gamma}{\gamma}} \right) \,, \tag{9.93}$$

$$y_A = \frac{\gamma\rho}{\rho^2 - 3\gamma} \left(1 + \sqrt{\frac{\rho^2 - 2\gamma}{\gamma}} \right) \,. \tag{9.94}$$

The mass and the charge parameters of the solution are written as a function of ρ as

$$m = \frac{1}{A\rho} \left(1 - \frac{2\gamma}{\rho^2} \right) \,,$$
$$q^2 = \frac{1}{A^2 \rho^2} \left(1 - \frac{3\gamma}{\rho^2} \right) \,, \tag{9.95}$$

and, for a fixed A and Λ, the ratio q/m is higher than 1. The conditions $\rho > y_A$ and $q^2 > 0$ require that, for the cold C instanton, the allowed range of ρ is

$$\rho > \sqrt{6\gamma} \,. \tag{9.96}$$

The value of y_A decreases monotonically with ρ and we have $\sqrt{\gamma} < y_A < \sqrt{6\gamma}$. The mass and the charge of the cold C instanton are also monotonically decreasing functions of ρ, and as we come from $\rho = +\infty$ into $\rho = \sqrt{6\gamma}$ we have

$$0 < m_{\mathrm{c}} < \frac{\sqrt{2}}{3} \frac{1}{\sqrt{\Lambda + 3A^2}} \,, \tag{9.97}$$

$$0 < q_{\mathrm{c}} < \frac{1}{2} \frac{1}{\sqrt{\Lambda + 3A^2}} \,, \tag{9.98}$$

so the cold C instanton has a lower maximum mass and a lower maximum charge than the $A = 0$ cold instanton, and, for a fixed Λ, as the acceleration parameter A grows this maximum value decreases monotonically. For a fixed Λ and for a fixed mass below $\sqrt{2/(9\Lambda)}$, the maximum value of the acceleration is $\sqrt{2/(27m^2) - \Lambda/3}$.

As we have already said, the allowed range of y in the Euclidean sector is $y_A \leq y < y_+$ and does not include $y = y_+$. Then, the period of τ, (9.80), that avoids the conical singularity at the only horizon of the cold C instanton is

$$\beta_{\mathrm{c}} = \frac{2\pi\rho^3}{(y_A - \rho)^2 \sqrt{\gamma(\rho^2 - 2\gamma)}} \,, \tag{9.99}$$

and $T_{\mathrm{c}} = 1/\beta_{\mathrm{c}}$ is the temperature of the acceleration horizon.

In what concerns the angular sector of the cold C instanton, $\mathcal{G}(x)$ is given by (6.74), and its only real zeros are the south and north pole,

$$x_{\mathrm{s}} = -p + \frac{h}{2} - \frac{m}{2q^2 A} < 0 \,,$$
$$x_{\mathrm{n}} = p + \frac{h}{2} - \frac{m}{2q^2 A} > 0 \,, \tag{9.100}$$

with

$$p = \frac{1}{2}\left(-\frac{s}{3} + \frac{2m^2}{q^4 A^2} - \frac{1 - 12q^2 A^2}{3sq^4 A^4} - \frac{4}{3q^2 A^2} + n\right)^{1/2},$$

$$n = \frac{-m^3 + mq^2}{2hq^6 A^3},$$

$$h = \sqrt{\frac{s}{3} + \frac{m^2}{q^4 A^2} + \frac{1 - 12q^2 A^2}{3sq^4 A^4} - \frac{2}{3q^2 A^2}},$$

$$s = \frac{1}{2^{1/3}q^2 A^2}\left(\lambda - \sqrt{\lambda^2 - 4(1 - 12q^2 A^2)^3}\right)^{1/3},$$

$$\lambda = 2 - 108m^2 A^2 + 72q^2 A^2, \tag{9.101}$$

where m and q are fixed by (9.95), for a given A, Λ and ρ. When A goes to zero we have $x_s \to -1$ and $x_n \to +1$. The period of ϕ, $\Delta\phi_c$, that avoids the conical singularity at the north pole (and leaves one at the south pole responsible for the presence of the string) is given by (9.76) with x_n defined in (9.100).

The topology of the cold C instanton is $\mathbb{R}^2 \times S^2$, since $y = y_+ = \rho$ is at an infinite proper distance ($0 \le \tau \le \beta_c$, $y_A \le y < y_+$, $x_s \le x \le x_n$, and $0 \le \phi \le \Delta\phi_c$). The surface $y = y_+ = \rho$ is then an internal infinity boundary that will have to be taken into account in the calculation of the action of the cold C instanton (see section 9.3.3.b). The Lorentzian sector of this cold case describes two extreme ($y_+ = y_-$) dS black holes being accelerated by the cosmological background and by the string, and the cold C instanton describes pair creation of these extreme black holes.

9.3.2.c The Nariai C instanton

In the case of the Nariai C instanton, we require that the size of the acceleration horizon y_A is equal to the size of the outer charged horizon y_+. Let us label this degenerated horizon by ρ: $y_A = y_+ \equiv \rho$ and $\rho < y_-$. In this case, the function $\mathcal{F}(y)$ can be written as (onwards the subscript "N" means Nariai)

$$\mathcal{F}_N(y) = \frac{\rho^2 - 3\gamma}{\rho^4}(y - y_{neg})(y - y_-)(y - \rho)^2, \tag{9.102}$$

where γ is defined by (9.91), the roots ρ and y_{neg} are given by (9.92) and (9.93), and y_- is given by $y_- = \frac{\gamma\rho}{\rho^2 - 3\gamma}\left(1 + \sqrt{\frac{\rho^2 - 2\gamma}{\gamma}}\right)$. The mass and the charge of the solution are defined as a function of ρ by (9.95). The conditions $\rho < y_-$ and $q^2 \ge 0$ require that for the Nariai C instanton, the allowed range of ρ is

$$\sqrt{3\gamma} \le \rho < \sqrt{6\gamma}. \tag{9.103}$$

The value of y_- decreases monotonically with ρ and we have $\sqrt{6\gamma} < y_- < +\infty$. Contrary to the cold C instanton, the mass and the charge of the Nariai C instanton are monotonically increasing functions of ρ, and as we go from $\rho = \sqrt{3\gamma}$ to $\rho = \sqrt{6\gamma}$ we have

$$\frac{1}{3}\frac{1}{\sqrt{\Lambda + 3A^2}} \le m_N < \frac{\sqrt{2}}{3}\frac{1}{\sqrt{\Lambda + 3A^2}},$$

$$0 \le q_N < \frac{1}{2}\frac{1}{\sqrt{\Lambda + 3A^2}}. \tag{9.104}$$

Note that $\rho = \sqrt{3\gamma}$ implies $q = 0$. For a fixed Λ and for a mass fixed between $\sqrt{1/(9\Lambda)} \le m < \sqrt{2/(9\Lambda)}$, the acceleration varies as $\sqrt{1/(27m^2) - \Lambda/3} \le A < \sqrt{2/(27m^2) - \Lambda/3}$.

At this point, one has apparently a problem that is analogous to the one that occurs with the $A = 0$ neutral Nariai instanton [97] and with the $A = 0$ charged Nariai instanton [169, 181].

Indeed, as we said in the beginning of this section, the allowed range of y in the Euclidean sector is $y_A \leq y \leq y_+$ in order to obtain a positive definite metric. But in the Nariai case $y_A = y_+$, and so it seems that we are left with no space to work with in the Euclidean sector. However, as in [97, 169, 181], the proper distance between y_A and y_+ remains finite as $y_A \to y_+$, as is shown in detail in [89] where the Nariai C-metric is constructed and analyzed. In what follows we briefly exhibit the construction. We first set $y_A = \rho - \varepsilon$ and $y_+ = \rho + \varepsilon$, in order that $\varepsilon << 1$ measures the deviation from degeneracy, and the limit $y_A \to y_+$ is obtained when $\varepsilon \to 0$. Now, we introduce a new time coordinate $\tilde{\tau}$, $\tau = \frac{1}{\varepsilon \mathcal{K}} \tilde{\tau}$, and a new radial coordinate χ, $y = \rho + \varepsilon \cos \chi$, where $\chi = 0$ and $\chi = \pi$ correspond, respectively, to the horizons y_+ and y_A, and

$$\mathcal{K} = \frac{2(\Lambda + 3A^2)}{A^2 \rho^2} - 1 \,. \tag{9.105}$$

Condition (9.103) implies $0 < \mathcal{K} \leq 1$ with $q = 0 \Rightarrow \mathcal{K} = 1$. Then, in the limit $\varepsilon \to 0$, from (9.74) and (9.102), we obtain the gravitational field of the Nariai C instanton

$$ds^2 = \frac{\mathcal{R}^2(x)}{\mathcal{K}} \left(\sin^2 \chi \, d\tilde{\tau}^2 + d\chi^2 \right) + \mathcal{R}^2(x) \left[\mathcal{G}^{-1}(x) dx^2 + \mathcal{G}(x) d\phi^2 \right] \,. \tag{9.106}$$

where χ runs from 0 to π, and

$$\mathcal{R}^2(x) \;=\; [A(x + \rho)]^{-2} \,. \tag{9.107}$$

In the new coordinates $\tilde{\tau}$ and χ, the Maxwell field for the magnetic case is still given by (6.5), while in the electric case we have now

$$F_{\mathrm{el}} = i \frac{q}{\mathcal{K}} \sin \chi \, d\tilde{\tau} \wedge d\chi \,. \tag{9.108}$$

The period of $\tilde{\tau}$ of the Nariai C instanton is simply $\beta_{\mathrm{N}} = 2\pi$. The function $\mathcal{G}(x)$ is given by (6.74), with m and q fixed by (9.95) for a given A, Λ and $\sqrt{3\gamma} < \rho < \sqrt{6\gamma}$. Under these conditions the south and north pole (which are the only real roots) are also given by (9.100) and (9.101). The period of ϕ, $\Delta\phi_{\mathrm{N}}$, that avoids the conical singularity at the north pole (and leaves one at the south pole responsible for the presence of the string) is given by (9.76) with x_{n} defined in (9.100).

The topology of the Nariai C instanton is $S^2 \times S^2$ ($0 \leq \tilde{\tau} \leq \beta_{\mathrm{N}}$, $0 \leq \chi \leq \pi$, $x_{\mathrm{s}} \leq x \leq x_{\mathrm{n}}$, and $0 \leq \phi \leq \Delta\phi_{\mathrm{N}}$). The Nariai C instanton transforms into the Nariai instanton when we take the limit $A = 0$ [89]. The Lorentzian sector is conformal to the direct topological product of $dS_2 \times S^2$, i.e., of a (1+1)-dimensional de Sitter spacetime with a deformed 2-sphere of fixed size. To each point in the sphere corresponds a dS_2 spacetime, except for one point - the south pole - which corresponds a dS_2 spacetime with a string [89]. When we set $A = 0$ the S^2 is a round 2-sphere free of the conical singularity and so, without the string. In this case it has been shown [97, 170] that the Nariai solution decays through the quantum tunnelling process into a slightly non-extreme dS black hole pair (for a complete review on this subject see, e.g., Bousso [129] and chapter chapter 7 on this thesis). We then naturally expect that an analogous quantum instability is present in the Nariai C-metric. Therefore, the Nariai C instanton describes the creation of a Nariai C universe that then decays into a slightly non-extreme ($y_A \sim y_+$) pair of black holes accelerated by the cosmological background and by the string.

We recall again that the neutral Nariai C instanton with $m = \frac{1}{3} \frac{1}{\sqrt{\Lambda + 3A^2}}$ is the only regular Euclidean solution that can be constructed from the dS C-metric when the charge vanishes. The same feature is present in the $A = 0$ case where only the neutral Nariai instanton with $m = \frac{1}{3} \frac{1}{\sqrt{\Lambda}}$ is available [97, 169, 170, 172].

9.3.2.d   The ultracold C instanton

In the case of the ultracold C instanton, we require that the size of the three horizons (y_A, y_+ and y_-) is equal, and let us label this degenerated horizon by ρ: $y_A = y_+ = y_- \equiv \rho$. In this case, the

function $\mathcal{F}(y)$ can be written as (onwards the subscript "u" means ultracold)

$$\mathcal{F}_\mathrm{u}(y) = \frac{\rho^2 - 3\gamma}{\rho^4}(y - y_\mathrm{neg})(y - \rho)^3 \, , \tag{9.109}$$

where γ is defined by (9.91) and the roots ρ and y_neg are given by (9.92) and (9.93), respectively. Given the values of A and Λ, ρ can take only the value

$$\rho = \sqrt{6\gamma} \, . \tag{9.110}$$

The mass and the charge of the solution, defined by (9.98), are then given by

$$m_\mathrm{u} = \frac{\sqrt{2}}{3}\sqrt{\frac{1}{\Lambda + 3A^2}} \, ,$$
$$q_\mathrm{u} = \frac{1}{2}\sqrt{\frac{1}{\Lambda + 3A^2}} \, , \tag{9.111}$$

and these values are the maximum values of the mass and charge of both the cold and charged Nariai instantons.

Being a limiting case of both the cold C instanton and of the charged Nariai C instanton, the ultracold C instanton presents similar features. The appropriate analysis of this solution (see [89] for a detailed discussion) requires that we first set $\rho = \sqrt{6\gamma} - \varepsilon$ and $y_- = \sqrt{6\gamma} + \varepsilon$, with $\varepsilon \ll 1$. Then, we introduce a new time coordinate $\tilde{\tau}$, $\tau = \frac{1}{2\varepsilon^2\mathcal{K}}\tilde{\tau}$, and a new radial coordinate χ, $y = \sqrt{6\gamma} + \varepsilon\cosh(\sqrt{2\varepsilon\mathcal{K}}\,\chi)$, where $\mathcal{K} = \frac{1}{3}\sqrt{\frac{2A^2}{\Lambda + 3A^2}}$. Finally, in the limit $\varepsilon \to 0$, from (9.74) and (9.109), we obtain the gravitational field of the ultracold C instanton

$$ds^2 = \mathcal{R}^2(x)\left[\chi^2\,d\tilde{\tau}^2 + d\chi^2 + \mathcal{G}^{-1}(x)dx^2 + \mathcal{G}(x)d\phi^2\right] \, ,$$
$$\text{with} \quad \mathcal{R}^2(x) = \left(Ax + \sqrt{2(\Lambda + 3A^2)}\right)^{-2} \, . \tag{9.112}$$

Notice that the spacetime factor $\chi^2\,d\tilde{\tau}^2 + d\chi^2$ is just Euclidean space in Rindler coordinates, and therefore, under the usual coordinate transformation, it can be putted in the form $dT^2 + dX^2$. $\chi = 0$ corresponds to the Rindler horizon and $\chi = +\infty$ corresponds an internal infinity boundary. In the new coordinates $\tilde{\tau}$ and χ, the Maxwell field for the magnetic case is still given by (6.5), while in the electric case we have now

$$F_\mathrm{el} = -i\,q\,\chi\,d\tilde{\tau} \wedge d\chi \, . \tag{9.113}$$

The period of $\tilde{\tau}$ of the ultracold C instanton is simply $\beta_\mathrm{u} = 2\pi$.

The function $\mathcal{G}(x)$ is given by (6.74), with m and q fixed by (9.111) for a given A and Λ. Under these conditions the south and north pole (which are the only real roots) are also given by (9.100) and (9.101). The period of ϕ, $\Delta\phi_\mathrm{u}$, that avoids the conical singularity at the north pole is given by (9.76) with x_n defined in (9.100).

The topology of the ultracold C instanton is $\mathbb{R}^2 \times S^2$, since $\chi = +\infty$ is at an infinite proper distance ($0 \leq \tilde{\tau} \leq \beta_\mathrm{u}$, $0 \leq \chi \leq \infty$, $x_\mathrm{s} \leq x \leq x_\mathrm{n}$, and $0 \leq \phi \leq \Delta\phi_\mathrm{u}$). The surface $\chi = +\infty$ is then an internal infinity boundary that will have to be taken into account in the calculation of the action of the ultracold C instanton (see section 9.3.3.d). The ultracold C instanton transforms into the ultracold instanton when we take the limit $A = 0$ [89]. The Lorentzian sector is conformal to the direct topological product of $\mathbb{M}^{1,1} \times S^2$, i.e., of a (1+1)-dimensional Minkowski spacetime with a deformed 2-sphere of fixed size. To each point in the sphere corresponds a $\mathbb{M}^{1,1}$ spacetime, except for one point - the south pole - which corresponds a $\mathbb{M}^{1,1}$ spacetime with a string [89]. We can, appropriately, label this solution as Nariai Bertotti-Robinson C universe (see [89]). When we set $A = 0$ the S^2 is a round 2-sphere free of the conical singularity and so, without the string. In an analogous way to the Nariai C universe, the Nariai Bertotti-Robinson C universe is unstable

and decays into a slightly non-extreme ($y_A \sim y_+ \sim y_-$) pair of black holes accelerated by the cosmological background and by the string. The ultracold C instanton mediates this decay.

The allowed range of m and q for each one of the four C instantons is sketched in Fig. 9.5.
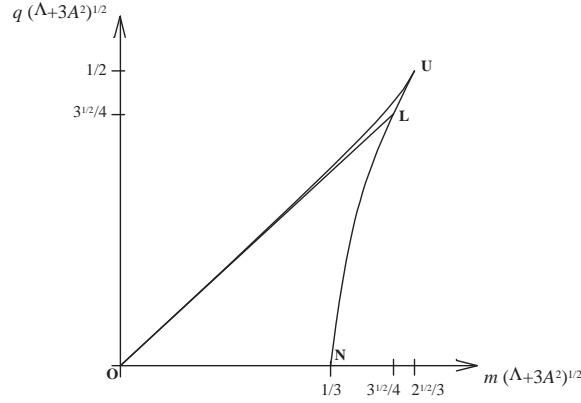
Figure 9.5: Relation $q\sqrt{\Lambda + 3A^2}$ vs $m\sqrt{\Lambda + 3A^2}$ for a fixed value of A and Λ for the four dS C instantons. OL represents the lukewarm C instanton ($m = q$), OU represents the cold C instanton, NLU represents the Nariai C instanton, and U represents the ultracold C instanton. Point N represents the neutral Nariai C instanton, the only instanton for the uncharged case. When we set $\Lambda = 0$ we obtain the charge/mass relation of the flat C-metric and flat Ernst instantons, and setting $A = 0$ yields the charge/mass relation for the dS instantons [169]. This reveals the close link that exists between the instantons that describe the pair creation process in different backgrounds. $c_1 = 1/3$, $c_2 = \sqrt{3}/4$ and $c_3 = \sqrt{2}/3$.

9.3.3 Calculation of the black hole pair creation rates

In the last section we have found the regular dS C instantons that can be interpreted as describing a circular motion in the Euclidean sector of the solution with a period β. These instantons are the Euclidean continuation of a Lorentzian solution which describes a pair of black holes that start at rest at the creation moment, and then run hyperbolically in opposite directions by the strings that accelerate them. Now, in order to compute the pair creation rate of the corresponding black holes, we have to slice the instanton, the Euclidean trajectory, in half along $\tau = 0$ and $\tau = \beta/2$, where the velocities vanish. The resulting geometry is precisely that of the moment of closest approach of the black holes in the Lorentzian sector of the dS C-metric, and in this way the Euclidean and Lorentzian solutions smoothly match together. In particular, the extrinsic curvature vanishes for both surfaces and therefore, they can be glued to each other.

In this section, we will compute the black hole pair creation rates given in (9.71) for each one of the four cases considered in section 9.3.2. Moreover, we will also compute the pair creation rate of black holes whose nucleation process is described by sub-maximal instantons. For the reason explained in section 9.3.1, the magnetic action will be evaluated using (9.72), while the electric action will be computed using (9.73). In general, in (9.72) and (9.73) we identify $\Sigma = \partial\mathcal{M}$ with the surfaces of zero extrinsic curvature discussed just above. It then follows that the boundary term $\int_\Sigma d^3x \sqrt{h}\, K$ vanishes. However, as we already mentioned in sections 9.3.2.b and 9.3.2.d, in the cold and ultracold case we have in addition an internal infinity boundary, $\Sigma_\infty^{\text{int}}$, for which the boundary action term does not necessarily vanish.

The domain of validity of our results is the particle limit, $mA \ll 1$, for which the radius of the black hole, $r_+ \sim m$, is much smaller than the typical distance between the black holes at the creation moment, $\ell \sim 1/A$.

In order to compute the black hole pair creation rate given by (9.70) or (9.71), we need to find I_{string} and I_{dS}. The evaluation of the action of the string instanton that mediates the nucleation of

a string in the dS spacetime is done using (9.78) and (9.79), yielding

$$
\begin{aligned}
I_{\text{string}} &= -\frac{1}{16\pi} \int_{\mathcal{M}} d^4 x \sqrt{g} \left(R - 2\Lambda\right) \\
&= -\frac{3\pi}{2\Lambda} \frac{\mathcal{G}'(x_{\text{s}})}{|\mathcal{G}'(x_{\text{n}})|} ,
\end{aligned}
\tag{9.114}
$$

where the integration over τ has been done in the interval $[0, \beta_0/2]$ with $\beta_0 = 2\pi/\sqrt{1 + \Lambda/(3A_0^2)}$, the integration range of x was $[-1, 1]$, the integration interval of y was $[\sqrt{1 + \Lambda/(3A_0^2)}, \infty]$, and $R = 4\Lambda$.

The action of the S^4 gravitational instanton that mediates the nucleation of the dS spacetime is [170, 172]

$$
I_{\text{dS}} = -\frac{3\pi}{2\Lambda} .
\tag{9.115}
$$

The nucleation rate of a string in a dS background is then given by (9.69). For the particle limit, $mA \ll 1$, the mass density of the string, μ, is given by $\mu \simeq mA$ and

$$
\Gamma_{\text{string/dS}} \sim e^{-12\pi \frac{\mu}{\Lambda}} .
\tag{9.116}
$$

Thus, the nucleation probability of a string in the dS background decreases when its mass density increases.

9.3.3.a The lukewarm C pair creation rate

We first consider the magnetic case, whose Euclidean action is given by (9.72), and then we consider the electric case, using (9.73), and we verify that these two quantities give the same numerical value. The boundary $\Sigma = \partial \mathcal{M}$ that appears in (9.72) consists of an initial spatial surface at $\tau = 0$ plus a final spatial surface at $\tau = \beta_\ell/2$. We label these two 3-surfaces by Σ_τ. Each one of these two spatial 3-surfaces is delimitated by a 2-surface at the acceleration horizon and by a 2-surface at the outer black hole horizon. The two surfaces Σ_τ are connected by a timelike 3-surface that intersects Σ_τ at the frontier y_A and by a timelike 3-surface that intersects Σ_τ at the frontier y_+. We label these two timelike 3-surfaces by Σ_h. Thus $\Sigma = \Sigma_\tau + \Sigma_h$, and the region $\mathcal{M}$ within it is compact. With the analysis of section 9.3.2.a, we can compute all the terms of action (9.72). We start with

$$
-\frac{1}{16\pi} \int_{\mathcal{M}} d^4 x \sqrt{g} \left(R - 2\Lambda\right) = -\frac{1}{16\pi} \int_{\Delta\phi_\ell} d\phi \int_0^{\beta_\ell/2} d\tau \int_{x_{\text{s}}}^{x_{\text{n}}} dx \int_{y_A}^{y_+} dy \frac{2\Lambda}{[A(x+y)]^4} ,
\tag{9.117}
$$

where we have used $R = 4\Lambda$, and y_A and y_+ are given by (9.83), x_{s} and x_{n} are defined by (9.88), and β_ℓ and $\Delta\phi_\ell$ are respectively given by (9.86) and (9.89). The Maxwell term in the action yields

$$
\frac{1}{16\pi} \int_{\mathcal{M}} d^4 x \sqrt{g} \, F_{\text{mag}}^2 = \frac{q^2}{16\pi} \Delta\phi_\ell \, \beta_\ell \, (x_{\text{n}} - x_{\text{s}})(y_+ - y_A) ,
\tag{9.118}
$$

where we have used $F_{\text{mag}}^2 = 2q^2 A^4 (x+y)^4$ [see (6.5)], and $\int_{\Sigma} d^3 x \sqrt{h} \, K = 0$. Adding all these terms yields for the magnetic action (9.72)

$$
I_{\text{mag}}^\ell = -\frac{3\pi}{16\Lambda} \frac{1}{8mA} \left(1 - \sqrt{\frac{1 - 4mA}{1 + 4mA}}\right) \left(1 + \sqrt{1 - (4mA)^2} - \frac{4m}{\sqrt{3}} \sqrt{\Lambda + 3A^2}\right) ,
\tag{9.119}
$$

and, given that the string is already present in the initial system, the pair creation rate of nonextreme lukewarm black holes when the cosmic string breaks is

$$
\Gamma_{\text{BHs/string}}^\ell = \eta \, e^{-2I_{\text{mag}}^\ell + 2I_{\text{string}}} ,
\tag{9.120}
$$

where (9.114) yields $I_{\text{string}} = -\frac{3\pi}{2\Lambda}\frac{\sqrt{1-4mA}}{\sqrt{1+4mA}}$, and η is the one-loop contribution not computed here. I_{mag}^{ℓ} is a monotonically increasing function of both m and A (for a fixed Λ). When we take the limit $A = 0$ on (9.119) we get

$$ I_{\text{mag}}^{\ell}\Big|_{A\to 0} = -\frac{3\pi}{2\Lambda} + \pi m\sqrt{\frac{3}{\Lambda}}, \tag{9.121} $$

recovering the action for the $A = 0$ lukewarm instanton [169], that describes the pair creation of two non-extreme dS−Reissner-Nordström black holes accelerated only by the cosmological constant.

In the electric case, the Euclidean action is given by (9.73) with $F_{\text{el}}^2 = -2q^2 A^4 (x + y)^4$ [see (9.75)]. Thus,

$$ \frac{1}{16\pi} \int_{\mathcal{M}} d^4x\sqrt{g}\, F_{\text{el}}^2 = -\frac{1}{16\pi} \int_{\mathcal{M}} d^4x\sqrt{g}\, F_{\text{mag}}^2 \,. \tag{9.122} $$

In order to compute the extra Maxwell boundary term in (9.73) we have to find a vector potential, A_ν, that is regular everywhere including at the horizons. An appropriate choice in the lukewarm case is $A_y = -i\,q\,\tau$, which obviously satisfies (9.75). The integral over Σ consists of an integration between y_A and y_+ along the $\tau = 0$ surface and back along $\tau = \beta_\ell/2$, and of an integration between $\tau = 0$ and $\tau = \beta_\ell/2$ along the $y = y_+$ surface and back along the $y = y_A$ surface. The normal to Σ_τ is $n_\mu = (\sqrt{\mathcal{F}}/[A(x + y)], 0, 0, 0)$, and the normal to Σ_h is $n_\mu = (0, \sqrt{\mathcal{F}}/[A(x + y)], 0, 0)$. Thus $F^{\mu\nu} n_\mu A_\nu = 0$ on Σ_h, and the non-vanishing contribution comes only from the integration along the $\tau = \beta_\ell/2$ surface. The Maxwell boundary term in (9.73), $-\frac{1}{4\pi}\int_\Sigma d^3x\sqrt{h}\, F^{\mu\nu} n_\mu A_\nu$, is then

$$ -\frac{1}{4\pi} \int_{\Sigma_{\tau=\beta_\ell/2}} d^3x\sqrt{g_{yy}g_{xx}g_{\phi\phi}}\, F^{\tau y} n_\tau A_y = \frac{q^2}{8\pi} \Delta\phi_\ell\, \beta_\ell\, (x_{\text{n}} - x_{\text{s}})(y_+ - y_A)\,. \tag{9.123} $$

Adding (9.117), (9.122) and (9.123) yields for the electric action (9.73)

$$ I_{\text{el}}^{\ell} = I_{\text{mag}}^{\ell}\,, \tag{9.124} $$

where I_{mag}^{ℓ} is given by (9.119).

In Fig. 9.6 we show a plot of I^{ℓ}/I_{dS} as a function of m and A for a fixed Λ, where $I_{\text{dS}} = -\frac{3\pi}{2\Lambda}$ is the action of de Sitter space. Given the pair creation rate, $\Gamma_{\text{BHs/string}}^{\ell} \propto e^{-2I_{\text{mag}}^{\ell}+2I_{\text{string}}}$, we conclude that, for a fixed Λ and A, as the mass and charge of the lukewarm black holes increase, the probability they have to be pair created decreases monotonically. Moreover, for a fixed mass and charge, this probability increases monotonically as the acceleration provided by the string increases. Alternatively, we can discuss the behavior of $\Gamma_{\text{BHs/dS}}^{\ell} \propto e^{-2I_{\text{mag}}^{\ell}+2I_{\text{dS}}}$. In this case, for a fixed mass and charge, the probability decreases monotonically as the acceleration of the black holes increases.
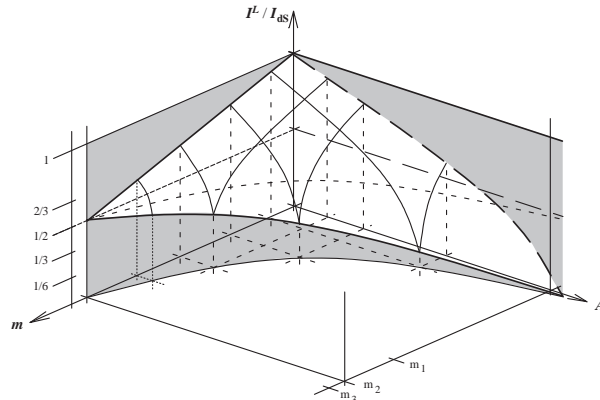
Figure 9.6: Plot of I^{ℓ}/I_{dS} as a function of m and A for a fixed Λ, where I^{ℓ} is the action of the lukewarm C instanton, given in (9.119), and $I_{\text{dS}} = -\frac{3\pi}{2\Lambda}$ is the action of de Sitter space. See text of section 9.3.3.a. $m_1 = 1/(3\sqrt{\Lambda})$, $m_2 = \sqrt{3}/(4\sqrt{\Lambda})$ and $m_3 = \sqrt{2}/(3\sqrt{\Lambda})$.

9.3.3.b   The cold C pair creation rate

We first consider the magnetic case, whose Euclidean action is given by (9.72). The boundary that appears in (9.72) is given by $\Sigma = \Sigma_\tau + \Sigma_h + \Sigma_\infty^{\text{int}}$, where Σ_τ is a spatial surface at $\tau = 0$ and $\tau = \beta_c/2$, Σ_h is a timelike 3-surface at $y = y_A$, and the timelike 3-surface $\Sigma_\infty^{\text{int}}$ is an internal infinity boundary at $y = y_+ = \rho$. With the analysis of section 9.3.2.b, we can compute all the terms of action (9.72). We start with

$$-\frac{1}{16\pi} \int_{\mathcal{M}} d^4 x \sqrt{g}\, (R - 2\Lambda) = -\frac{1}{16\pi} \int_{\Delta\phi_c} d\phi \int_0^{\beta_c/2} d\tau \int_{x_s}^{x_n} dx \int_{y_A}^{\rho} dy \frac{2\Lambda}{[A(x+y)]^4} \,, \tag{9.125}$$

where we used $R = 4\Lambda$, and ρ and y_A are respectively given by (9.92) and (9.94), x_s and x_n are defined by (9.100), and β_c and $\Delta\phi_c$ are, respectively, given by (9.99) and (9.76). The Maxwell term in the action yields

$$\frac{1}{16\pi} \int_{\mathcal{M}} d^4 x \sqrt{g}\, F_{\text{mag}}^2 = \frac{q^2}{16\pi} \Delta\phi_c\, \beta_c\, (x_n - x_s)(\rho - y_A) \,, \tag{9.126}$$

where we used $F_{\text{mag}}^2 = 2q^2 A^4 (x+y)^4$ [see (6.5)], and $\int_\Sigma d^3 x \sqrt{h}\, K = 0$. Adding all these terms yields for the magnetic action (9.72) of the cold case

$$I_{\text{mag}}^c = -\frac{\Delta\phi_c}{8A^2} \frac{x_n - x_s}{(x_n + y_A)(x_s + y_A)} \,, \tag{9.127}$$

where y_A is given by (9.94), x_s and x_n are defined by (9.100), and $\Delta\phi_c$ is given by (9.76). Given that the string is already present in the initial system, the pair creation rate of extreme cold black holes when the string breaks is $\Gamma_{\text{BHs/string}}^c = \eta\, e^{-2I_{\text{mag}}^c + 2I_{\text{string}}}$, where I_{string} is given by (9.114), and η is the one-loop contribution not computed here. In Fig. 9.7 we show a plot of $I_{\text{mag}}^c / I_{\text{dS}}$ as a function of m and A for a fixed Λ. Given the pair creation rate, $\Gamma_{\text{BHs/string}}^c$, we conclude that for a fixed Λ and A as the mass and charge of the cold black holes increases, the probability they have to be pair created decreases monotonically. Moreover, for a fixed mass and charge, this probability increases monotonically as the acceleration of the black holes increases. Alternatively, we can discuss the behavior of $\Gamma_{\text{BHs/dS}}^c \propto e^{-2I_{\text{mag}}^c + 2I_{\text{dS}}}$. In this case, for a fixed mass and charge, the probability decreases monotonically as the acceleration of the black holes increases. When we take the limit $A = 0$ we recover the action for the $A = 0$ cold instanton [169], which lies in the range $-\frac{3\pi}{2\Lambda} \le I_{\text{mag}}^c \big|_{A \to 0} \le -\frac{\pi}{4\Lambda}$, and which describes the pair creation of extreme dS$-$Reissner-Nordström black holes accelerated only by the cosmological constant.

In the electric case, the Euclidean action is given by (9.73) with $F_{\text{el}}^2 = -2q^2 A^4 (x+y)^4$ [see (9.75)]. Thus,

$$\frac{1}{16\pi} \int_{\mathcal{M}} d^4 x \sqrt{g}\, F_{\text{el}}^2 = -\frac{1}{16\pi} \int_{\mathcal{M}} d^4 x \sqrt{g}\, F_{\text{mag}}^2 \,. \tag{9.128}$$

In order to compute the extra Maxwell boundary term in (9.73) we have to find a vector potential, A_ν, that is regular everywhere including at the horizons. An appropriate choice in the cold case is $A_y = -i\, q\, \tau$, which obviously satisfies (9.75). Analogously to the lukewarm case, the non-vanishing contribution to the Maxwell boundary term in (9.73) comes only from the integration along the $\tau = \beta_c/2$ surface, and is given by

$$-\frac{1}{4\pi} \int_{\Sigma_{\tau = \beta_c/2}} d^3 x \sqrt{g_{yy} g_{xx} g_{\phi\phi}}\, F^{\tau y} n_\tau A_y = \frac{q^2}{8\pi} \Delta\phi_c\, \beta_c\, (x_n - x_s)(\rho - y_A) \,. \tag{9.129}$$

Adding (9.128) and (9.129) yields (9.126). Thus, the electric action (9.73) of the cold instanton is equal to the magnetic action, $I_{\text{el}}^c = I_{\text{mag}}^c$, and therefore electric and magnetic cold black holes have the same probability of being pair created.

Figure 9.7: Plot of I^c/I_{dS} as a function of m and A for a fixed Λ, where I^c is the action of the cold C instanton, given in (9.127), and $I_{\mathrm{dS}} = -\frac{3\pi}{2\Lambda}$ is the action of de Sitter space (see text of section 9.3.3.b). The plot for the ultracold C action, given in (9.138), is also represented by the curve BC (see text of section 9.3.3.d). $m_1 = 1/(3\sqrt{\Lambda})$, $m_2 = \sqrt{3}/(4\sqrt{\Lambda})$ and $m_3 = \sqrt{2}/(3\sqrt{\Lambda})$.

9.3.3.c   The Nariai C pair creation rate

The Nariai C instanton is the only one that can have zero charge. We will first consider the charged Nariai C instanton and then the neutral Nariai C instanton.

We start with the magnetic case, whose Euclidean action is given by (9.72). The boundary that appears in (9.72) is given by $\Sigma = \Sigma_{\tilde{\tau}} + \Sigma_h$, where $\Sigma_{\tilde{\tau}}$ is a spatial surface at $\tilde{\tau} = 0$ and $\tilde{\tau} = \pi$, and Σ_h is a timelike 3-surface at $\chi = 0$ and $\chi = \pi$. With the analysis of section 9.3.2.c, we can compute all the terms of action (9.72). We start with

$$-\frac{1}{16\pi} \int_{\mathcal{M}} d^4x \sqrt{g}\, (R - 2\Lambda) = -\frac{1}{16\pi} \int_{\Delta\phi_N} d\phi \int_0^\pi d\tilde{\tau} \int_{x_s}^{x_n} dx \int_0^\pi d\chi\, \frac{2\Lambda \sin\chi}{[A(x + \rho)]^4 \mathcal{K}}\,, \tag{9.130}$$

where we have used $R = 4\Lambda$, x_s and x_n are defined by (9.100), and $\Delta\phi_N$ is given by (9.76). The Maxwell term in the action yields

$$\frac{1}{16\pi} \int_{\mathcal{M}} d^4x \sqrt{g}\, F_{\mathrm{mag}}^2 = \frac{q^2}{4\mathcal{K}} \Delta\phi_N\, (x_n - x_s)\,, \tag{9.131}$$

where we have used $F_{\mathrm{mag}}^2 = 2q^2 A^4(x + \rho)^4$ [see (6.5)], and $\int_\Sigma d^3x \sqrt{h}\, K = 0$. Adding these three terms yields the magnetic action (9.72) of the Nariai case

$$I_{\mathrm{mag}}^{\mathrm{N}} = -\frac{\Delta\phi_N}{4A^2} \frac{x_n - x_s}{(x_n + \rho)(x_s + \rho)}\,, \tag{9.132}$$

where $\sqrt{3\gamma} \le \rho < \sqrt{6\gamma}$, x_s and x_n are defined by (9.100), and $\Delta\phi_N$ is given by (9.76), with m and q subjected to (9.104). Given that the string is already present in the initial system, the pair creation rate of extreme Nariai black holes when the string breaks is $\Gamma_{\mathrm{BHs/string}}^{\mathrm{N}} = \eta\, e^{-2I_{\mathrm{mag}}^{\mathrm{N}} + 2I_{\mathrm{string}}}$, where I_{string} is given by (9.114), and η is the one-loop contribution not computed here. In Fig. 9.8 we show a plot of $I_{\mathrm{mag}}^{\mathrm{N}}/I_{\mathrm{dS}}$ as a function of m and A for a fixed Λ. Given the pair creation rate, $\Gamma_{\mathrm{BHs/string}}^{\mathrm{N}}$, we conclude that for a fixed Λ and A as the mass and charge of the Nariai black holes increases, the probability they have to be pair created decreases monotonically. Moreover, for a fixed mass and charge, this probability increases monotonically as the acceleration of the black holes increases. Alternatively, we can discuss the behavior of $\Gamma_{\mathrm{BHs/dS}}^{\mathrm{N}} \propto e^{-2I_{\mathrm{mag}}^{\mathrm{N}} + 2I_{\mathrm{dS}}}$. In this case, for a fixed mass and charge, the probability decreases monotonically as the acceleration of the black holes increases. When we take the limit $A = 0$ we recover the action for the $A = 0$ Nariai instanton [169, 181], which lies in the range $-\frac{\pi}{\Lambda} \le I_{\mathrm{mag}}^{\mathrm{N}}|_{A \to 0} \le -\frac{\pi}{2\Lambda}$, and that describes the nucleation of a Nariai universe that

is unstable [97, 170, 129] and decays through the pair creation of extreme dS−Reissner-Nordström black holes accelerated only by the cosmological constant.

In the electric case, the Euclidean action is given by (9.73) with $F_{\text{el}}^2 = -2q^2 A^4 (x + \rho)^4$ [see (9.108)]. Thus,

$$\frac{1}{16\pi} \int_{\mathcal{M}} d^4x \sqrt{g}\, F_{\text{el}}^2 = -\frac{1}{16\pi} \int_{\mathcal{M}} d^4x \sqrt{g}\, F_{\text{mag}}^2 \,. \tag{9.133}$$

In order to compute the extra Maxwell boundary term in (9.73), the appropriate vector potential, A_ν, that is regular everywhere including at the horizons is $A_\chi = i\, \frac{q}{\mathcal{K}} \tilde{\tau} \sin \chi$, which obviously satisfies (9.108). The integral over Σ consists of an integration between $\chi = 0$ and $\chi = \pi$ along the $\tilde{\tau} = 0$ surface and back along $\tilde{\tau} = \pi$, and of an integration between $\tilde{\tau} = 0$ and $\tilde{\tau} = \pi$ along the $\chi = 0$ surface, and back along the $\chi = \pi$ surface. The unit normal to $\Sigma_{\tilde{\tau}}$ is $n_\mu = (\frac{\sin \chi}{\sqrt{\mathcal{K}} A(x+\rho)}, 0, 0, 0)$, and $F^{\mu\nu} n_\mu A_\nu = 0$ on Σ_h. Thus, the non-vanishing contribution to the Maxwell boundary term in (9.73), $-\frac{1}{4\pi} \int_\Sigma d^3x \sqrt{h}\, F^{\mu\nu} n_\mu A_\nu$, comes only from the integration along the $\tilde{\tau} = \pi$ surface and is given by

$$-\frac{1}{4\pi} \int_{\Sigma_{\tilde{\tau}=\pi}} d^3x \sqrt{h}\, F^{\tilde{\tau}\chi} n_{\tilde{\tau}} A_\chi = \frac{q^2}{2\mathcal{K}} \Delta\phi_{\text{N}} (x_{\text{n}} - x_{\text{s}}) \,. \tag{9.134}$$

Adding (9.133) and (9.134) yields (9.131). Therefore, the electric action (9.73) of the charged Nariai instanton is equal to the magnetic action, $I_{\text{el}}^{\text{N}} = I_{\text{mag}}^{\text{N}}$, and therefore electric and magnetic charged Nariai black holes have the same probability of being pair created.

Now, we discuss the neutral Nariai C instanton. This instanton is particulary important since it is the only regular Euclidean solution available when we want to evaluate the pair creation of neutral black holes. The same feature is present in the $A = 0$ case where only the neutral Nariai instanton is available [97, 169, 170, 172]. The action of the neutral Nariai C instanton is simply given by (9.130) and, for a fixed Λ and A, it is always smaller than the action of the charged Nariai C instanton (see line DE in Fig. 9.8): $I_{\text{charged}}^{\text{N}} > I_{\text{neutral}}^{\text{N}} > I_{\text{dS}}$. Thus the pair creation of charged Nariai black holes is suppressed relative to the pair creation of neutral Nariai black holes, and both are suppressed relative to the dS space.
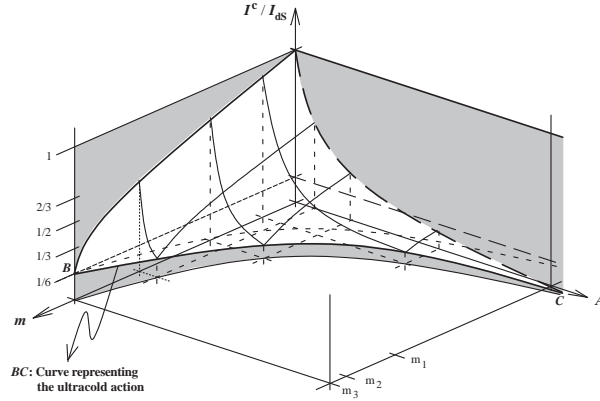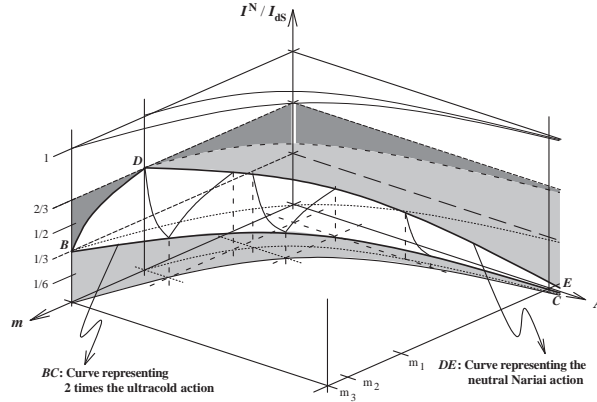

Figure 9.8: Plot of $I^{\text{N}}/I_{\text{dS}}$ as a function of m and A for a fixed Λ, where I^{N} is the action of the cold C instanton, given in (9.132), and $I_{\text{dS}} = -\frac{3\pi}{2\Lambda}$ is the action of de Sitter space. The neutral Nariai plot is sketched by the curve DE (see text of section 9.3.3.c). The curve BC represents two times the ultracold C action, given in (9.138). $m_1 = 1/(3\sqrt{\Lambda})$, $m_2 = \sqrt{3}/(4\sqrt{\Lambda})$ and $m_3 = \sqrt{2}/(3\sqrt{\Lambda})$.

9.3.3.d   The ultracold C pair creation rate

We first consider the magnetic case, whose Euclidean action is given by (9.72). The boundary that appears in (9.72) is given by $\Sigma = \Sigma_{\tilde{\tau}} + \Sigma_h + \Sigma_\infty^{\text{int}}$, where $\Sigma_{\tilde{\tau}}$ is a spatial surface at $\tilde{\tau} = 0$ and $\tilde{\tau} = \pi$, Σ_h is a timelike 3-surface at the Rindler horizon $\chi = 0$, and the timelike 3-surface $\Sigma_\infty^{\text{int}}$ is an internal

infinity boundary at $\chi = \infty$. With the analysis of section 9.3.2.d, we can compute all the terms of action (9.72). We start with $-\frac{1}{16\pi}\int_{\mathcal{M}} d^4x\sqrt{g}\,(R - 2\Lambda)$ which yields (using $R = 4\Lambda$)

$$-\frac{1}{16\pi}\int_{\Delta\phi_u} d\phi \int_0^\pi d\tilde{\tau} \int_{x_s}^{x_n} dx \int_0^{\chi_0} d\chi\, \frac{2\Lambda\chi}{(Ax+\rho)^4} = -\frac{\Lambda}{16}\,\Delta\phi_u\,\chi_0^2 \int_{x_s}^{x_n} dx \frac{1}{(Ax+A\rho)^4}\bigg|_{\chi_0\to\infty}, \qquad (9.135)$$

where x_s and x_n are defined by (9.100) and (9.111), and $\Delta\phi_u$ is given by (9.76). The Maxwell term in the action yields

$$\frac{1}{16\pi}\int_{\mathcal{M}} d^4x\sqrt{g}\,F_{\text{mag}}^2 = \frac{q^2}{16}\,\Delta\phi_u\,\chi_0^2\,(x_n - x_s)\bigg|_{\chi_0\to\infty}, \qquad (9.136)$$

where we used $F_{\text{mag}}^2 = 2q^2A^4(x+\rho)^4$ [see (6.5)] with $\rho = \sqrt{2(\Lambda + 3A^2)}$. Due to the fact that $\chi_0 \to \infty$ it might seem that the contribution from (9.135) and (9.136) diverges. Fortunately this is not the case since these two terms cancel each other. Trying to verify this analytically is cumbersome, but for our purposes we can simply fix any numerical value for Λ and A, and using (9.111) and (9.100) we indeed verify that (9.135) and (9.136) cancel each other.

Now, contrary to the other instantons, the ultracold C instanton has a non-vanishing extrinsic curvature boundary term, $-\frac{1}{16\pi}\int_\Sigma d^3x\sqrt{h}\,K \neq 0$, due to the internal infinity boundary ($\Sigma_\infty^{\text{int}}$ at $\chi = \infty$) contribution. The extrinsic curvature to $\Sigma_\infty^{\text{int}}$ is $K_{\mu\nu} = h_\mu{}^\alpha\nabla_\alpha n_\nu$, where $n_\nu = (0, \frac{1}{A(x+\rho)}, 0, 0)$ is the unit outward normal to $\Sigma_\infty^{\text{int}}$, $h_\mu{}^\alpha = g_\mu{}^\alpha - n_\mu n^\alpha = (1, 0, 1, 1)$ is the projection tensor onto $\Sigma_\infty^{\text{int}}$, and ∇_α represents the covariant derivative with respect to $g_{\mu\nu}$. Thus the trace of the extrinsic curvature to $\Sigma_\infty^{\text{int}}$ is $K = g^{\mu\nu}K_{\mu\nu} = A(x+\rho)/\chi$, and

$$-\frac{1}{8\pi}\int_\Sigma d^3x\sqrt{h}\,K = -\frac{1}{8\pi}\int_{\Delta\phi_u} d\phi \int_0^\pi d\tilde{\tau} \int_{x_s}^{x_n} dx\, \frac{1}{(Ax+A\rho)^2}. \qquad (9.137)$$

The magnetic action (9.72) of the ultracold C instanton is then

$$I_{\text{mag}}^u = -\frac{\pi}{4}\left[x_n\left(1 + A\sqrt{\frac{2}{\Lambda + 3A^2}}\,x_n + \frac{A^2}{2(\Lambda + 3A^2)}x_n^2\right)\right]^{-1}$$

$$\times \frac{x_n - x_s}{\left[Ax_n + \sqrt{2(\Lambda + 3A^2)}\right]\left[Ax_s + \sqrt{2(\Lambda + 3A^2)}\right]}, \qquad (9.138)$$

where x_s and x_n are defined by (9.100) and (9.111). When we take the limit $A = 0$ we get $x_s = -1$ and $x_n = 1$, and

$$I_{\text{mag}}^u\bigg|_{A\to 0} = -\frac{\pi}{4\Lambda}, \qquad (9.139)$$

and therefore we recover the action for the $A = 0$ ultracold instanton [169], that describes the pair creation of ultracold black holes accelerated only by the cosmological constant.

In Fig. 9.6 we show a plot of $I_{\text{mag}}^u/I_{\text{dS}}$ as a function of m and A for a fixed Λ. When we fix Λ and A we also fix the mass and charge of the ultracold black holes. For a fixed Λ, when A increases the probability of pair creation of ultracold black holes, $\Gamma_{\text{BHs/string}}^u$, increases monotonically and they have a lower mass and charge. Alternatively, we can discuss the behavior of $\Gamma_{\text{BHs/dS}}^u$. In this case, the probability decreases monotonically as the acceleration of the black holes increases.

In the electric case, the Euclidean action is given by (9.73) with $F_{\text{el}}^2 = -2q^2A^4(x + \rho)^4$ [see (9.113)]. Thus,

$$\frac{1}{16\pi}\int_{\mathcal{M}} d^4x\sqrt{g}\,F_{\text{el}}^2 = -\frac{1}{16\pi}\int_{\mathcal{M}} d^4x\sqrt{g}\,F_{\text{mag}}^2. \qquad (9.140)$$

In the ultracold case the vector potential A_ν, that is regular everywhere including at the horizon, needed to compute the extra Maxwell boundary term in (9.73) is $A_{\tilde{\tau}} = i\frac{q}{2}\chi^2$, which obviously

satisfies (9.113). The integral over Σ consists of an integration between $\chi = 0$ and $\chi = \infty$ along the $\tilde{\tau} = 0$ surface and back along $\tilde{\tau} = \pi$, and of an integration between $\tilde{\tau} = 0$ and $\tilde{\tau} = \pi$ along the $\chi = 0$ surface, and back along the internal infinity surface $\chi = \infty$. The non-vanishing contribution to the Maxwell boundary term in (9.73) comes only from the integration along the internal infinity boundary $\Sigma_\infty^{\mathrm{int}}$, and is given by

$$-\frac{1}{4\pi} \int_{\Sigma_\infty^{\mathrm{int}}} d^3x \sqrt{g_{\tilde{\tau}\tilde{\tau}} g_{xx} g_{\phi\phi}} \, F^{\chi\tilde{\tau}} n_\chi A_{\tilde{\tau}} = \frac{q^2}{8} \Delta\phi_{\mathrm{u}} \, \chi_0^2 \, (x_{\mathrm{n}} - x_{\mathrm{s}}) \bigg|_{\chi_0 \to \infty} . \tag{9.141}$$

Adding (9.140) and (9.141) yields (9.136). Thus, the electric action (9.73) of the ultracold C instanton is equal to the magnetic action, $I_{\mathrm{el}}^{\mathrm{u}} = I_{\mathrm{mag}}^{\mathrm{u}}$, and therefore electric and magnetic ultracold black holes have the same probability of being pair created.

9.3.3.e Pair creation rate of nonextreme sub-maximal black holes

The lukewarm, cold, Nariai and ultracold C-metric instantons are saddle point solutions free of conical singularities both in the y_+ and y_A horizons. The corresponding black holes may then nucleate in the dS background when a cosmic string breaks, and we have computed their pair creation rates in the last four subsections. However, these particular black holes are not the only ones that can be pair created. Indeed, it has been shown in [155, 156] that Euclidean solutions with conical singularities may also be used as saddle points for the pair creation process. In this way, pair creation of nonextreme sub-maximal black holes is allowed (by this nomenclature we mean all the nonextreme black holes other than the lukewarm ones that are in the region interior to the close line $NOUN$ in Fig. 9.5), and their pair creation rate may be computed. In order to calculate this rate, the action is given by (9.72) and (9.73) (in the magnetic and electric cases respectively) and, in addition, it has now an extra contribution from the conical singularity (c.s.) that is present in one of the horizons (y_+, say) given by [291, 97]

$$\frac{1}{16\pi} \int_{\mathcal{M}} d^4x \sqrt{g} \, (R - 2\Lambda) \bigg|_{\mathrm{c.s.\ at\ } y_+} = \frac{\mathcal{A}_+ \, \delta}{16\pi} , \tag{9.142}$$

where $\mathcal{A}_+ = \int_{y=y_+} \sqrt{g_{xx} g_{\phi\phi}} \, dx \, d\phi$ is the area of the 2-surface spanned by the conical singularity, and

$$\delta = 2\pi \left(1 - \frac{\beta_A}{\beta_+} \right) \tag{9.143}$$

is the deficit angle associated to the conical singularity at the horizon y_+, with $\beta_A = 4\pi/|\mathcal{F}'(y_A)|$ and $\beta_+ = 4\pi/|\mathcal{F}'(y_+)|$ being the periods of τ that avoid a conical singularity in the horizons y_A and y_+, respectively. The contribution from (9.72) and (9.73) follows straightforwardly in a similar way as the one shown in subsection 9.3.3.a with the period of τ, β_A, chosen in order to avoid the conical singularity at the acceleration horizon, $y = y_A$. The full Euclidean action for general nonextreme sub-maximal black holes is then

$$I = \frac{\Delta\phi}{A^2} \left(\frac{x_{\mathrm{n}} - x_{\mathrm{s}}}{(x_{\mathrm{n}} + y_A)(x_{\mathrm{s}} + y_A)} + \frac{x_{\mathrm{n}} - x_{\mathrm{s}}}{(x_{\mathrm{n}} + y_+)(x_{\mathrm{s}} + y_+)} \right) , \tag{9.144}$$

where $\Delta\phi$ is given by (9.76), and the pair creation rate of nonextreme sub-maximal black holes is $\Gamma = \eta \, e^{-2I + 2I_{dS}}$, where $I_{dS} = -\frac{3\pi}{2\Lambda}$ is the action of de Sitter space, and η is the one-loop contribution not computed here. In order to compute (9.144), we need the relation between the parameters A, Λ, m, q, and the horizons y_A, y_+ and y_-. In general, for a nonextreme solution with horizons $y_A < y_+ < y_-$, one has

$$\mathcal{F}(y) = -\frac{1}{\mu}(y - y_A)(y - y_+)(y - y_-)(ay + b) , \tag{9.145}$$

with

$$
\begin{aligned}
\mu &= y_A y_+ y_- (y_A + y_+ + y_-) + (y_A y_+ + y_A y_- + y_+ y_-)^2 \\
a &= (y_A y_+ + y_A y_- + y_+ y_-) \\
b &= y_A y_+ y_- \,.
\end{aligned}
\tag{9.146}
$$

The parameters A, Λ, m and q can be expressed as a function of y_A, y_+ and y_- by

$$
\begin{aligned}
\frac{\Lambda}{3A^2} &= \mu^{-2}(y_A y_+ y_-)^2 - 1 \\
q^2 A^2 &= \mu^{-1}(y_A y_+ + y_A y_- + y_+ y_-) \\
mA &= (2\,\sigma)^{-1}(y_A + y_+)(y_A + y_-)(y_+ + y_-) \\
\sigma &= y_A^2 y_+ y_- + y_A y_+^2 y_- + y_A y_+ y_-^2 + (y_A y_+)^2 + (y_A y_-)^2 + (y_+ y_-)^2 \,.
\end{aligned}
\tag{9.147}
$$

The allowed values of parameters m and q are those contained in the interior region defined by the close line $NOUN$ in Fig. 9.5.

9.3.4   Entropy, area and pair creation rate

In previous works on black hole pair creation in general background fields it has been well established that the pair creation rate is proportional to the exponential of the gravitational entropy S of the system, $\Gamma \propto e^S$, with the entropy being given by one quarter of the the total area $\mathcal{A}$ of all the horizons present in the instanton, $S = \mathcal{A}/4$. In what follows we will verify that these relations also hold for the instantons of the dS C-metric.

9.3.4.a   The lukewarm C case. Entropy and area

In the lukewarm case, the instanton has two horizons in its Euclidean section, namely the acceleration horizon at $y = y_A$ and the black hole horizon at $y = y_+$. So, the total area of the lukewarm C instanton is

$$
\begin{aligned}
\mathcal{A}^\ell &= \int_{y=y_A} \sqrt{g_{xx} g_{\phi\phi}}\, dx\, d\phi + \int_{y=y_+} \sqrt{g_{xx} g_{\phi\phi}}\, dx\, d\phi = \\
&\quad \frac{\Delta\phi_\ell}{A^2}\left(\frac{x_{\mathrm{n}} - x_{\mathrm{s}}}{(x_{\mathrm{n}} + y_A)(x_{\mathrm{s}} + y_A)} + \frac{x_{\mathrm{n}} - x_{\mathrm{s}}}{(x_{\mathrm{n}} + y_+)(x_{\mathrm{s}} + y_+)}\right),
\end{aligned}
\tag{9.148}
$$

where y_A and y_+ are given by (9.83), x_{s} and x_{n} are defined by (9.88), and $\Delta\phi_\ell$ is given by (9.89). It is straightforward to verify that $\mathcal{A}^\ell = -8 I^\ell$, where I^ℓ is given by (9.119), and thus $\Gamma^\ell \propto e^{S^\ell}$, where $S^\ell = \mathcal{A}^\ell/4$.

9.3.4.b   The cold C case. Entropy and area

In the cold case, the instanton has a single horizon, the acceleration horizon at $y = y_A$, in its Euclidean section, since $y = y_+$ is an internal infinity. So, the total area of the cold C instanton is

$$
\mathcal{A}^{\mathrm{c}} = \int_{y=y_A} \sqrt{g_{xx} g_{\phi\phi}}\, dx\, d\phi = \frac{\Delta\phi_{\mathrm{c}}}{A^2}\frac{x_{\mathrm{n}} - x_{\mathrm{s}}}{(x_{\mathrm{n}} + y_A)(x_{\mathrm{s}} + y_A)},
\tag{9.149}
$$

where y_A is given by (9.94), x_{s} and x_{n} are defined by (9.100), and $\Delta\phi_{\mathrm{c}}$ is given by (9.76). Thus, $\mathcal{A}^{\mathrm{c}} = -8 I^{\mathrm{c}}$, where I^{c} is given by (9.127), and thus $\Gamma^{\mathrm{c}} \propto e^{S^{\mathrm{c}}}$, where $S^{\mathrm{c}} = \mathcal{A}^{\mathrm{c}}/4$.

9.3.4.c   The Nariai C case. Entropy and area

In the Nariai case, the instanton has two horizons in its Euclidean section, namely the acceleration horizon y_A and the black hole horizon y_+, both at $y = \rho$, and thus they have the same area. So, the total area of the Nariai C instanton is

$$\mathcal{A}^{\mathrm{N}} = 2 \int_{y=\rho} \sqrt{g_{xx}g_{\phi\phi}} \, dx \, d\phi = 2 \frac{\Delta\phi_{\mathrm{N}}}{A^2} \frac{x_{\mathrm{n}} - x_{\mathrm{s}}}{(x_{\mathrm{n}} + \rho)(x_{\mathrm{s}} + \rho)} \,, \qquad (9.150)$$

where $\sqrt{3\gamma} \leq \rho < \sqrt{6\gamma}$, x_{s} and x_{n} are defined by (9.100), and $\Delta\phi_{\mathrm{N}}$ is given by (9.76), with m and q subjected to (9.104). Thus, $\mathcal{A}^{\mathrm{N}} = -8I^{\mathrm{N}}$, where I^{N} is given by (9.132), and thus $\Gamma^{\mathrm{N}} \propto e^{S^{\mathrm{N}}}$, where $S^{\mathrm{N}} = \mathcal{A}^{\mathrm{N}}/4$.

9.3.4.d   The ultracold C case. Entropy and area

In the ultracold case, the instanton has a single horizon, the Rindler horizon at $\chi = 0$, in its Euclidean section, since $\chi = \infty$ is an internal infinity. So, the total area of the ultracold C instanton is

$$\mathcal{A}^{\mathrm{u}} = \int_{\chi=0} \sqrt{g_{xx}g_{\phi\phi}} \, dx \, d\phi = \frac{\Delta\phi_{\mathrm{u}}}{A^2} \frac{x_{\mathrm{n}} - x_{\mathrm{s}}}{(x_{\mathrm{n}} + \rho)(x_{\mathrm{s}} + \rho)} \,, \qquad (9.151)$$

with $\rho = \sqrt{2(\Lambda + 3A^2)}$ [see (9.110)], x_{s} and x_{n} are defined by (9.100), and $\Delta\phi_{\mathrm{c}}$ is given by (9.76), with m and q subjected to (9.111). It straightforward to verify that $\mathcal{A}^{\mathrm{u}} = -8I^{\mathrm{u}}$, where I^{u} is given by (9.138), and thus $\Gamma^{\mathrm{u}} \propto e^{S^{\mathrm{u}}}$, where $S^{\mathrm{u}} = \mathcal{A}^{\mathrm{u}}/4$.

As we have already said, the ultracold C instanton is a limiting case of both the charged Nariai C instanton and the cold C instanton (see, e.g., Fig. 9.5). Then, as expected, the action of the cold C instanton gives, in this limit, the action of the ultracold C instanton (see Fig. 9.7). However, the ultracold frontier of the Nariai C action is given by two times the ultracold C action (see Fig. 9.8). From the results of this section we clearly understand the reason for this behavior. Indeed, in the ultracold case and in the cold case, the respective instantons have a single horizon (the other possible horizon turns out to be an internal infinity). This horizon gives the only contribution to the total area, $\mathcal{A}$, and therefore to the pair creation rate. In the Nariai case, the instanton has two horizons with the same area, and thus the ultracold limit of the Nariai action is doubled with respect to the true ultracold action.

9.3.4.e   The nonextreme sub-maximal case. Entropy and area

In the lukewarm case, the instanton has two horizons in its Euclidean section, namely the acceleration horizon at $y = y_A$ and the black hole horizon at $y = y_+$. So, the total area of the saddlepoint solution is

$$\mathcal{A} = \int_{y=y_A} \sqrt{g_{xx}g_{\phi\phi}} \, dx \, d\phi + \int_{y=y_+} \sqrt{g_{xx}g_{\phi\phi}} \, dx \, d\phi \,, \qquad (9.152)$$

and once again one has $\mathcal{A} = -8I$, where I is given by (9.144), and thus $\Gamma \propto e^{S}$, where $S = \mathcal{A}/4$.

9.3.5   Heuristic derivation of the nucleation rates

The physical interpretation of our exact results of section 9.3 can be clarified with a heuristic derivation of the nucleation rates. An estimate for the nucleation probability is given by the Boltzmann factor, $\Gamma \sim e^{-E_0/W_{\mathrm{ext}}}$, where E_0 is the energy of the system that nucleates and $W_{\mathrm{ext}} = F\ell$ is the work done by the external force F, that provides the energy for the nucleation, through the typical distance ℓ separating the created pair.

Forget for a moment the string, and ask what is the probability that a black hole pair is created in a dS background. This process has been discussed in [169] where it was found that the pair

creation rate is $\Gamma \sim e^{-m/\sqrt{\Lambda}}$. In this case, $E_0 \sim 2m$, where m is the rest energy of the black hole, and $W_{\text{ext}} \sim \sqrt{\Lambda}$ is the work provided by the cosmological background. To derive $W_{\text{ext}} \sim \sqrt{\Lambda}$ one can argue as follows. In the dS case, the Newtonian potential is $\Phi = \Lambda r^2/3$ and its derivative yields the force per unit mass or acceleration, Λr, where r is the characteristic dS radius, $\Lambda^{-1/2}$. The force can then be written as $F = \text{mass} \times \text{acceleration} \sim \sqrt{\Lambda}\sqrt{\Lambda}$, where the characteristic mass of the system is $\sqrt{\Lambda}$. Thus, the characteristic work is $W_{\text{ext}} = \text{force} \times \text{distance} \sim \Lambda\Lambda^{-1/2} \sim \sqrt{\Lambda}$, where the characteristic distance that separates the pair at the creation moment is $\Lambda^{-1/2}$. So, from the Boltzmann factor we indeed expect that the creation rate of a black hole pair in a dS background is given by $\Gamma \sim e^{-m/\sqrt{\Lambda}}$ [169].

A question that has been answered in the present section 9.3 was: given that a string is already present in our initial system, what is the probability that it breaks and a pair of black holes is produced and accelerated apart by Λ and by the string tension? The presence of the string leads in practice to a problem in which we have an effective cosmological constant that satisfies $\Lambda' \equiv \Lambda + 3A^2$, that is, the acceleration A provided by the string makes a positive contribution to the process. Heuristically, we may then apply the same arguments that have been used in the last paragraph, with the replacement $\Lambda \to \Lambda'$. At the end, the Boltzmann factor tells us that the creation rate for the process is $\Gamma \sim e^{-m/\sqrt{\Lambda+3A^2}}$. So, for a given black hole mass, m, and for a given cosmological constant, Λ, the black hole pair creation process is enhanced when a string is present, as the explicit calculations done in section 9.3 show. For $\Lambda = 0$ this heuristic derivation yields $\Gamma \sim e^{-m/A}$ which is the pair creation rate found in [133].

Another question that we have dealt with in the present section 9.3 was: what is the probability for the nucleation of a string in a dS background? Heuristically, the energy of the string that nucleates is $E_0 \sim \mu\Lambda^{-1/2}$, i.e., its mass per unit length times the dS radius, while the work provided by the cosmological background is still given by $W_{\text{ext}} \sim \sqrt{\Lambda}$. The Boltzmann factor yields for nucleation rate the value $\Gamma \sim e^{-\mu/\Lambda}$, in agreement with (9.116).

9.3.6 Summary and discussion

We have studied in detail the quantum process in which a cosmic string breaks in a de Sitter (dS) background and a pair of black holes is created at the ends of the string. The energy to materialize and accelerate the pair comes from the positive cosmological constant and from the string tension. This process is a combination of the processes considered in [167]-[172], where the creation of a black hole pair in a dS background has been analyzed, and in [133]-[136], where the breaking of a cosmic string accompanied by the creation of a black hole pair in a flat background has been studied.

We have constructed the saddle point solutions that mediate the pair creation process through the analytic continuation of the dS C-metric [86, 120, 88], and we have explicitly computed the nucleation rate of the process (see also a heuristic derivation of the rate in the Appendix). Globally our results state that the dS space is stable against the nucleation of a string, or against the nucleation of a string followed by its breaking and consequent creation of a black hole pair. In particular, we have answered three questions. First, we have concluded that the nucleation rate of a cosmic string in a dS background $\Gamma_{\text{string/dS}}$ decreases when the mass density of the string increases. Second, given that the string is already present in our initial system, the probability $\Gamma_{\text{BHs/string}}$ that it breaks and a pair of black holes is produced and accelerated apart by Λ and by the string tension increases when the mass density of the string increases. In other words, a string with a higher mass density makes the process more probable, for a fixed black hole mass. Third, if we start with a pure dS background, the probability $\Gamma_{\text{BHs/dS}}$ that a string nucleates on it and then breaks forming a pair of black holes decreases when the mass density of the string increases. These processes have a clear analogy with a thermodynamical system, with the mass density of the string being the analogue of the temperature T. Indeed, from the Boltzmann factor, $e^{-E_0/(k_B T)}$ (where k_B is the Boltzmann constant), one knows that a higher background temperature turns the nucleation of a particle with energy E_0 more probable. However, in order to have a higher temperature we have first to furnish more energy to the background, and thus the global process (increasing the temperature to the final

value T plus the nucleation of the particle) becomes energetically less favorable as T increases.

We have also verified that the relation between the rate, entropy and area, which is satisfied for all the black hole pair creation processes analyzed so far, also holds in the process studied in this paper. Indeed, the pair creation rate is proportional to e^S, where S is the gravitational entropy of the system, and is given by one quarter of the total area of all the horizons present in the saddle point solution that mediates the pair creation.

9.4 Pair creation in AdS, flat and dS backgrounds: a comparing discussion

We have reviewed in detail the studies on the quantum process in which a cosmic string breaks in an anti-de Sitter [132], in a flat [133, 134, 135, 136] and in a de Sitter background [131], and a pair of black holes is created at the ends of the string (see Fig. 1.9). The energy to materialize and accelerate the black holes comes from the strings' tension, and we have explicitly computed the pair creation rates. In the dS case the cosmological background acceleration makes a positive contribution to the process, while in the AdS case the cosmological background acceleration contributes negatively. In particular, in the AdS case, pair creation of black holes is possible only when the acceleration provided by the string tension is higher than $\sqrt{|\Lambda|/3}$: if we have a virtual pair of black holes and we want to turn them real, we have to furnish a sufficient force that overcomes the AdS background attraction.

We remark that in principle our explicit values for the pair creation rates [132] in an AdS and dS [131] background also apply to the process of pair creation in an external electromagnetic field, with the acceleration being provided in this case by the Lorentz force instead of being furnished by the string tension. Indeed, there is no Ernst solution in a cosmological constant background, and thus we cannot discuss analytically the process. However, physically we could in principle consider an external electromagnetic field that supplies the same energy and acceleration as our strings and, from the results of the $\Lambda = 0$ case (where the pair creation rates in the string and electromagnetic cases agree), we expect that the results found in [131, 132] do not depend on whether the energy is being provided by an external electromagnetic field or by strings.

For the benefit of comparison, in Fig. 9.9 we schematically represent the general behavior of the black hole pair creation rate Γ as a function of the acceleration A provided by the strings, when a cosmic string breaks in the three cosmological constant backgrounds. In a flat background [see Fig. 9.9.(a)], the pair creation rate is zero when $A = 0$ [133]. In this case, the flat C-metric reduces to a single black hole, and since we are studying the probability of pair creation, the corresponding rate is naturally zero. This does not mean that a single black hole cannot be materialized from the quantum vacuum, it only means that this latter process is not described by the C-metric. The creation probability of a single black hole in a hot bath has been considered in [138]. In a dS background [see Fig. 9.9.(b)], the pair creation rate is not zero when $A = 0$ [131]. This means that even in the absence of the string, the positive cosmological constant is enough to provide the energy to materialize the black hole pair [169]. If in addition one has an extra energy provided by the string, the process becomes more favorable [131]. In the AdS case [see Fig. 9.9.(c)], the negative cosmological constant makes a negative contribution to the process, and black hole pair creation is possible only when the acceleration provided by the strings overcomes the AdS background attraction. The branch $0 < A \leq \sqrt{|\Lambda|/3}$ represents the creation probability of a single black hole when the acceleration provided by the broken string is not enough to overcome the AdS attraction, and was not studied in this thesis. We can also fix Λ and A, and describe the evolution of the pair creation rates when the mass and charge of the black holes increase. In the three cases, $\Lambda < 0$, $\Lambda = 0$ and $\Lambda > 0$, we conclude that as the mass and charge of the black holes increase, the probability they have to be pair created decreases monotonically. This is the expected result since the materialization of a higher mass implies the need of a higher energy.

In order to study the pair creation processes, we had to construct the instantons that mediate
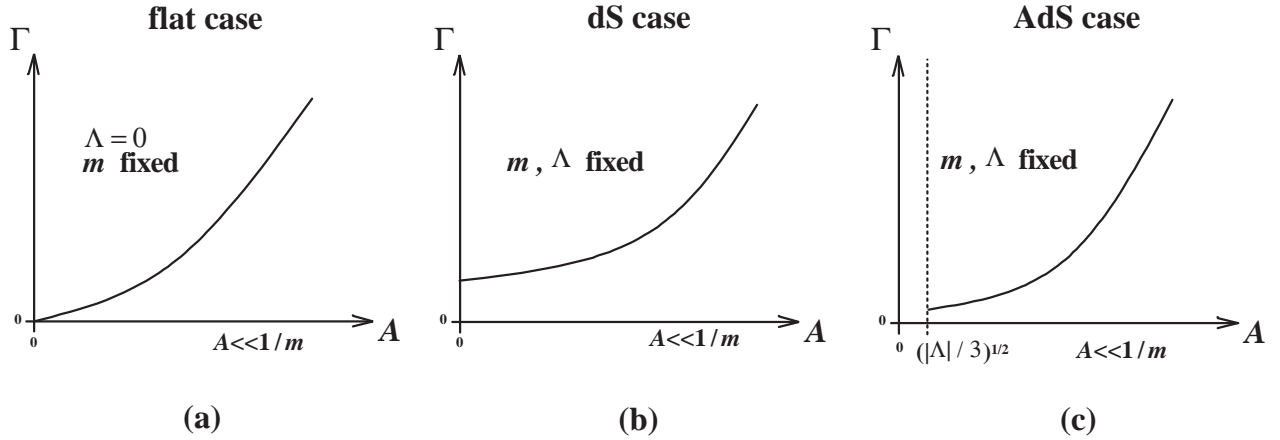
Figure 9.9: General behavior of the black hole pair creation rate Γ as a function of the acceleration A provided by the strings, when a cosmic string breaks: (a) in a flat background ($\Lambda = 0$) [133], (b) in a dS background ($\Lambda > 0$) [131], and (c) in an AdS background ($\Lambda < 0$) [132].

the process. This has done through the analytic continuation of some special cases of the AdS, flat and dS C-metrics. The regularity condition imposed to these instantons restricts the mass m and the charge q of the black holes that are produced, and physically it means that the only black holes that can be pair produced are those that are in thermodynamic equilibrium. Concretely, in the three cases, AdS, flat and dS, we have found two charged regular instantons. One mediates the pair creation of nonextreme black holes with $m = q$, and the other mediates the pair creation of extreme black holes ($y_+ = y_-$). The instantons constructed from the AdS and flat C-metric are noncompact (contrary to what occurs with the $\Lambda > 0$ instantons), in the sense that they have an acceleration horizon with an infinite area. Thus when dealing with them, we had to eliminate this infinity by normalizing this area relative to the acceleration horizon area of an appropriate background reference spacetime. In the dS case, the acceleration horizon has a finite area, and the above nonextreme instanton is also called lukewarm and the extreme instanton is also called cold. Moreover, in the dS case there are two other instantons available: the Nariai instanton, and the ultracold instanton, which are not present in the AdS and flat cases since they are out of the allowed range of the angular direction x. The Nariai C instanton describes the creation of a Nariai C universe (see section 7.2.1) that is unstable and, once created, it decays through the quantum tunnelling process into a slightly non-extreme ($y_A \sim y_+$) pair of black holes accelerated by the cosmological background and by the string. Finally, the ultracold C instanton describes the creation of a Nariai Bertotti-Robinson C universe (see section 7.2.3) that is unstable and, once created, it decays into a slightly non-extreme ($y_A \sim y_+ \sim y_-$) pair of black holes accelerated by the cosmological background and by the string.

In all the cases studied in this chapter, the pair creation rate is proportional to e^S, where S is the gravitational entropy of the system, and is given by one quarter of the total area of all the horizons present in the instanton that mediates the pair creation.

To conclude let us recall that the C-metric allows two distinct physical interpretations. In one of them one removes the conical singularity at the north pole and leaves one at the south pole. In this way the C-metric describes a pair of black holes accelerated away by two strings with positive mass density from each one of the black holes towards infinity. Alternatively, we can avoid the conical singularity at the south pole and in this case the black holes are pushed away by a strut (with negative mass density) in between them, along their north poles. In this chapter, as in we have adopted the first choice. Technically, the second choice introduces minor changes. Essentially it changes the period of the angular coordinate ϕ: it would be given by $\Delta\phi = \frac{4\pi}{|\mathcal{G}'(x_s)|}$ instead of (9.76). We have chosen the first choice essentially for two reasons. First, the string has a positive mass density and, in this sense, it is a more physical solution than the strut. Second, in order to get

the above string/pair configuration we only have to cut the string in a point. The strings tension does the rest of the work. However, if we desire the strut/pair system described above we would have to cut the strut in two different points. Then we would have to discard somehow the parts that join each one of the black holes towards infinity along their south poles.

Part III

Black holes and pair creation in higher dimensions

Chapter 10

Black holes in higher dimensional spacetimes

Contents

In this chapter we will describe the main features of the static higher dimensional black hole solutions of the Einstein-Maxwell theory in a background with a generalized cosmological constant Λ. Some of these black holes were found by Tangherlini [202], and are the higher dimensional cousins of the Schwarzschild and of the Reissner-Nordström black holes. We work in the context of the Einstein-Maxwell action with a cosmological constant Λ,

$$I = \frac{1}{16\pi} \int_{\mathcal{M}} d^D x \sqrt{-g} \, (R - 2\lambda) - \frac{1}{16\pi} \int_{\mathcal{M}} d^D x \sqrt{-g} F^{\mu\nu} F_{\mu\nu} \,, \tag{10.1}$$

where D is the dimension of the spacetime, g is the determinant of the metric, R is the Ricci scalar, $F_{\mu\nu} = \partial_\mu A_\nu - \partial_\nu A_\mu$ is the Maxwell field strength of the gauge field A_ν, and we have defined

$$\lambda = \frac{(D-1)(D-2)\Lambda}{6} \,. \tag{10.2}$$

The coefficient of the Λ term was chosen in order to insure that, for any dimension D, the pure dS or AdS spacetime is described by $g_{tt} = 1 - (\Lambda/3)r^2$, as occurs with $D = 4$. We set the D-dimensional Newton's constant equal to one, and $c = 1$. The variation of (10.1), $\delta I = 0$, yields the equations for the gravitational field and for the Maxwell field, respectively,

$$R_{\mu\nu} - \frac{1}{2}R\,g_{\mu\nu} + \lambda g_{\mu\nu} = 8\pi\,T_{\mu\nu} \,, \tag{10.3}$$

$$\nabla_\mu F^{\mu\nu} = 0 \,, \tag{10.4}$$

where $R_{\mu\nu}$ is the Ricci tensor and $T_{\mu\nu}$ is the electromagnetic energy-momentum tensor,

$$T_{\mu\nu} = \frac{1}{4\pi} \left(g^{\alpha\beta} F_{\alpha\mu} F_{\beta\nu} - \frac{1}{4} g_{\mu\nu} F_{\alpha\beta} F^{\alpha\beta} \right) \,. \tag{10.5}$$

The contraction of (10.3) with $g^{\mu\nu}$ yields for the Ricci tensor

$$R = \frac{D(D-1)}{3} \Lambda - \frac{16\pi}{D-2} T \,, \tag{10.6}$$

where T is the trace of $T_{\mu\nu}$. We remark that in a general D-dimensional background the electromagnetic energy-momentum tensor is not traceless. Indeed, the contraction of (10.5) with $g^{\mu\nu}$ yields

$$T = -\frac{D-4}{4\pi} F_{\mu\nu} F^{\mu\nu} \,, \tag{10.7}$$

which vanishes only for $D = 4$.

10.1   Higher dimensional black holes in a flat background

In a flat background, $\Lambda = 0$, the most general static solution with spherical symmetry is given by [202] (see also [203])

$$ds^2 = -f(r)dt^2 + f(r)^{-1}dr^2 + r^2\,d\Omega_{D-2}^2 \tag{10.8}$$

where $d\Omega_{D-2}^2$ is the line element on an unit $(D-2)$-sphere,

$$d\Omega_{D-2}^2 = d\theta_1^2 + \sin^2\theta_1\,d\theta_2^2 + \sin^2\theta_1\sin^2\theta_2\,d\theta_3^2 + \cdots + \prod_{i=1}^{D-3}\sin^2\theta_i\,d\theta_{D-2}^2\,, \tag{10.9}$$

and the function $f(r)$ is given by

$$f(r) = 1 - \frac{M}{r^{D-3}} + \frac{Q^2}{r^{2(D-3)}}\,. \tag{10.10}$$

The mass parameter M and the charge parameter Q are related to the ADM mass, M_{ADM}, and ADM electric charge, Q_{ADM}, of the solution by [203]

$$M_{\mathrm{ADM}} = \frac{(D-2)\Omega_{D-2}}{16\pi}\,M\,, \quad \text{and}\quad Q_{\mathrm{ADM}} = \sqrt{\frac{(D-3)(D-2)}{2}}\,Q\,, \tag{10.11}$$

where Ω_{D-2} is the area of an unit $(D-2)$-sphere,

$$\Omega_{D-2} = \frac{2\pi^{(D-1)/2}}{\Gamma[(D-1)/2]}\,. \tag{10.12}$$

Here, $\Gamma[z]$ is the Gamma function, whose definition and properties are listed in [292]. For our purposes we need to know that

$$\begin{aligned}\Gamma[z] &= (z-1)!\,, \qquad \text{when } z \text{ is a positive integer,}\\ \Gamma[1/2] &= \sqrt{\pi}\,, \qquad \text{and}\qquad \Gamma[z+1] = z\Gamma[z]\,, \qquad \text{when } z \text{ is a multiple of } 1/2\,,\end{aligned} \tag{10.13}$$

The radial electromagnetic field produced by the electric charge Q_{ADM} is given by

$$F = -\frac{Q_{\mathrm{ADM}}}{r^{D-2}}\,dt \wedge dr\,. \tag{10.14}$$

When $Q^2 < \frac{M^2}{4}$ the solution (10.8) (10.14) represents a black hole solution with a curvature singularity at the origin, and with an event horizon, r_+, and a Cauchy horizon, r_- which satisfy

$$r_\pm^{D-3} = \frac{M}{2} \pm \sqrt{\frac{M^2}{4} - Q^2}. \tag{10.15}$$

such that $r_+^{D-3} + r_-^{D-3} = M$, and $r_+^{D-3}r_-^{D-3} = Q^2$. When $Q^2 = \frac{M^2}{4}$, one has an extreme black hole with $r_+ = r_- = (M/2)^{\frac{1}{D-3}}$, and when $Q^2 > \frac{M^2}{4}$, one has a naked singularity. When $Q = 0$ we have a neutral black hole with an event horizon at $r_+ = M^{\frac{1}{D-3}}$.

Now, any D-dimensional geometry can be embedded into a higher dimensional Minkowski spacetime [293], with one or more timelike coordinates. This process is usually called as global embedding Minkowskian spacetime procedure (GEMS). This procedure allows, for example, to verify that the Hawking temperature and the Unruh temperature can be matched (see, e.g., [294, 210]). The neutral Tangherlini black hole ($Q = 0$) admits the following embedding in a $(D+1)$-dimensional Minkowski

spacetime [210],

$$
\begin{aligned}
z_0 &= k_+^{-1}\sqrt{f(r)}\sinh(k_+ t) \\
z_1 &= k_+^{-1}\sqrt{f(r)}\cosh(k_+ t) \\
z_2 &= r\prod_{i=1}^{D-2}\sin\theta_i \\
&\cdots \\
z_j &= r\left(\prod_{i=1}^{D-j}\sin\theta_i\right)\cos\theta_{D+1-j}\,, \quad \text{for } 3\le j < D \\
&\cdots \\
z_D &= r\cos\theta_1 \\
z_{D+1} &= \int dr\left(\frac{\sum_{i=1}^{D-1}M^{\frac{(D-3)+(i-1)}{D-3}}r^{(D-1)-i}}{\sum_{i=1}^{D-3}M^{\frac{i-1}{D-3}}r^{(D-3)-i}}\frac{1}{r^{D-1}}\right)^{\frac{1}{2}},
\end{aligned}
\tag{10.16}
$$

where k_+ is the surface gravity of the event horizon r_+ given by $k_+ = \frac{D-3}{2}M^{-\frac{1}{D-3}}$. Starting with the $(D+1)$-dimensional Minkowski spacetime, $ds^2 = -dz_0^2 + \sum_{i=1}^{D+1}dz_i^2$, the transformations (10.16) map it into the neutral Tangherlini black hole (10.8). When $D=4$, (10.16) yields the global embedding of the Schwarzschild black hole found in [294].

Analogously the charged Tangherlini black hole ($Q\ne 0$) admits the following embedding in a $(D+2)$-dimensional Minkowski spacetime with two timelike coordinates ($ds^2 = -dz_0^2 + \sum_{i=1}^{D+1}dz_i^2 - dz_{D+2}^2$) [210],

$$
\begin{aligned}
z^{D+1} &= \int dr\ \left(\frac{W(r_+^{D-3}+r_-^{D-3})+rr_+^{2(D-3)}+r^{2D-5}}{r^2(r^{D-3}-r_-^{D-3})W}\right)^{\frac{1}{2}}; \\
z^{D+2} &= \int dr\ \left(\frac{4r_+^{3D-7}r_-^{D-3}}{(r_+^{D-3}-r_-^{D-3})^2 r^{2(D-2)}}\right)^{\frac{1}{2}};
\end{aligned}
\tag{10.17}
$$

with the coordinates z^0 to z^D being the same as those defined in (10.16), and we have defined $W = \sum_{i=1}^{D-3}r_+^{i-1}r^{D-3-i}$. When $D=4$, (10.17) yields the global embedding of the Reissner-Nordström black hole found in [294].

10.2 Higher dimensional exact solutions in a dS background

10.2.1 Higher dimensional black holes in an asymptotically dS background

In an asymptotically de Sitter background, $\Lambda > 0$, the static higher dimensional black hole solutions with spherical topology were also found by Tangherlini [202]. The gravitational field and the electromagnetic field are still given by (10.8) and by (10.14), respectively, but now the function $f(r)$ is given by

$$
f(r) = 1 - \frac{\Lambda}{3}r^2 - \frac{M}{r^{D-3}} + \frac{Q^2}{r^{2(D-3)}}\,.
\tag{10.18}
$$

The mass parameter M and the charge parameter Q are related to the ADM hairs, M_{ADM} and Q_{ADM}, by (10.11). The causal structure of the dS-Tangherlini black holes is similar to the one of their 4-dimensional counterparts (see chapter 5). In particular, these solutions have a curvature singularity at the origin, and the black holes can have at most three horizons with one of them being the cosmological horizon.

In section 10.2.2 and in chapter 11, we will need to have the range of parameters for which one has an extreme dS black hole. We start with the five-dimensional case, $D=5$ [211]. The non-extreme dS black hole has three horizons, namely the Cauchy horizon, r_-, the event horizon,

r_+, and the cosmological horizon r_c, with $r_- \leq r_+ \leq r_c$. We are interested in the extreme dS black holes, for which two of the above horizons coincide. Let us label this degenerated horizon by ρ. In this case (and for $D = 5$), the function $f(r)$ given by (10.18) can be written as [211]

$$f(r) = -\frac{\Lambda}{3}\frac{1}{r^4}(r - \rho)^2(r + \rho)^2 \left(r - \sqrt{\frac{3}{\Lambda} - 2\rho^2}\right)\left(r + \sqrt{\frac{3}{\Lambda} - 2\rho^2}\right), \qquad (10.19)$$

and thus the other horizon of the extreme black hole is

$$\sigma = \sqrt{\frac{3}{\Lambda} - 2\rho^2} \,. \qquad (10.20)$$

The mass parameter M and the charge parameter Q of the black holes are written as functions of ρ as

$$M = \rho^2(2 - \Lambda\rho^2), \qquad \text{and} \ \ Q^2 = \rho^4\left(1 - \frac{2\Lambda}{3}\rho^2\right). \qquad (10.21)$$

The condition $Q^2 \geq 0$ implies that $\rho \leq \sqrt{\frac{3}{2\Lambda}}$. At this point we note that M and Q first increase with ρ (this stage corresponds to $\sigma > \rho$), until ρ reaches the critical value $\rho = \sqrt{1/\Lambda}$ (this stage corresponds to $\sigma = \rho$), and then M and Q start decreasing until ρ reaches its maximum allowed value (this stage corresponds to $\sigma < \rho$). These three stages are associated to three distinct extreme dS black holes: the cold, the ultracold and the Nariai[a] black holes, respectively (here we follow the nomenclature used in the analogous 4-dimensional black holes [168]). More precisely, for $0 < \rho < \frac{1}{\sqrt{\Lambda}}$ one has the cold black hole with $r_- = r_+ \equiv \rho$ and $r_c \equiv \sigma$. The ranges of the mass and charge parameters for the cold black hole are $0 < M < \frac{1}{\Lambda}$ and $0 < Q < \frac{1}{\sqrt{3\Lambda}}$. The case $\rho = \frac{1}{\sqrt{\Lambda}}$ gives the ultracold black hole in which the three horizons coincide, $r_- = r_+ = r_c$. Its mass and charge parameters are $M = \frac{1}{\Lambda}$ and $Q = \frac{1}{\sqrt{3\Lambda}}$. For $\frac{1}{\sqrt{\Lambda}} < \rho \leq \sqrt{\frac{3}{2\Lambda}}$ one has the Nariai black hole with $r_+ = r_c \equiv \rho$ and $r_- \equiv \sigma$. The ranges of the mass and charge parameters for the Nariai black hole are $\frac{3}{4\Lambda} \leq M < \frac{1}{\Lambda}$ and $0 \leq Q < \frac{1}{\sqrt{3\Lambda}}$.

Now, the above construction can be extended for D-dimensional extreme dS black holes. In the extreme case the function $f(r)$ given by (10.18) can be written as [211]

$$f(r) = (r - \rho)^2\frac{1}{r^2}\left[1 - \frac{\Lambda}{3}\left[r^2 + h(r)\right]\right], \qquad (10.22)$$

where $r = \rho$ is the degenerated horizon of the black hole, and

$$h(r) = a + br + \frac{c_1}{r} + \frac{c_2}{r^2} + \cdots + \frac{c_{2(D-4)}}{r^{2(D-4)}}, \qquad (10.23)$$

where $a, b, c_1, ..., c_{2(D-4)}$ are constants that can be found through the matching between (10.18) and (10.23). This procedure yields the mass parameter M and the charge parameter Q of the black holes as functions of ρ,

$$M = 2\rho^{D-3}\left(1 - \frac{D-2}{D-3}\frac{\Lambda}{3}\rho^2\right), \qquad \text{and} \qquad Q^2 = \rho^{2(D-3)}\left(1 - \frac{D-1}{D-3}\frac{\Lambda}{3}\rho^2\right). \qquad (10.24)$$

The condition $Q^2 \geq 0$ implies that $\rho \leq \rho_{\max}$ with

$$\rho_{\max} = \sqrt{\frac{D-3}{D-1}\frac{3}{\Lambda}}\,. \qquad (10.25)$$

---

[a]Please note that in this section we deal with the Nariai black hole while in the next section we will generate the Nariai solution which is not a black hole solution.

For the D-dimensional cold black hole ($r_- = r_+$), M and Q increase with ρ, and one has

$$0 < \rho < \rho_{\rm u}\,, \qquad 0 < M < \frac{4}{D-1}\,\rho_{\rm u}^{D-3}\,, \qquad \text{and} \qquad 0 < Q < \frac{1}{\sqrt{D-2}}\,\rho_{\rm u}^{D-3}\,, \qquad (10.26)$$

where we have defined

$$\rho_{\rm u} = \sqrt{\frac{3}{\Lambda}}\,\frac{D-3}{\sqrt{(D-2)(D-1)}}\,. \qquad (10.27)$$

For the D-dimensional ultracold black hole ($r_- = r_+ = r_{\rm c}$), one has

$$\rho = \rho_{\rm u}\,, \qquad M = \frac{4}{D-1}\,\rho_{\rm u}^{D-3}\,, \qquad \text{and} \qquad Q = \frac{1}{\sqrt{D-2}}\,\rho_{\rm u}^{D-3}\,. \qquad (10.28)$$

Finally, for the D-dimensional Nariai black hole ($r_+ = r_{\rm c}$), M and Q decrease with ρ, and one has

$$\rho_{\rm u} < \rho \leq \rho_{\rm max}\,, \qquad \frac{2}{D-1}\,\rho_{\rm max}^{D-3} \leq M < \frac{4}{D-1}\,\rho_{\rm u}^{D-3}\,, \qquad \text{and} \quad 0 \leq Q < \frac{1}{\sqrt{D-2}}\,\rho_{\rm u}^{D-3}\,. \qquad (10.29)$$

The ranges of M and Q that represent which one of the above black holes are sketched in Fig. 10.1.
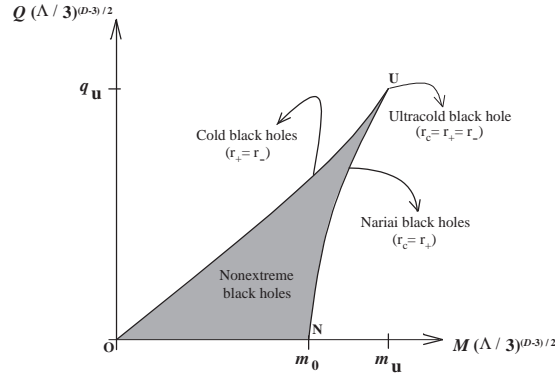
Figure 10.1: Range of M and Q for which one has a nonextreme black hole (region interior to the closed line $ONUO$), an extreme Nariai black hole with $r_+ = r_{\rm c}$ (line NU), an extreme cold black hole with $r_- = r_+$ (line OU), and an extreme ultracold black hole with $r_- = r_+ = r_{\rm c}$ (point U). The line ON represents the nonextreme dS-Schwarzschild black hole, and point N represents the extreme Nariai Schwarzschild black hole. $m_0 = \frac{2}{D-1}\left(\frac{D-3}{D-1}\right)^{(D-3)/2}$, $m_{\rm u} = \frac{4}{D-1}\left(\frac{(D-3)^2}{(D-2)(D-1)}\right)^{(D-3)/2}$, and $q_{\rm u} = \frac{1}{\sqrt{D-2}}\left(\frac{(D-3)^2}{(D-2)(D-1)}\right)^{(D-3)/2}$.

10.2.2 Extremal limits of the higher dimensional dS black holes

In chapter 7, we saw that Ginsparg and Perry [97] have connected the extreme Nariai black hole with the Nariai solution [125] in a 4-dimensional spacetime. This is, they have shown that the already known Nariai solution (which is not a black hole solution) could be generated from an extremal limit of a near-Nariai black hole. They realized this connection while they were studying the quantum stability of the Nariai and the Schwarzschild-dS solutions [97, 129]. A similar procedure allows to generate the Bertotti-Robinson solution and the Nariai−Bertotti-Robinson solution from the near-cold black hole Bland near-ultracold black hole, respectively. In this section, we will apply the near extremal procedure of [97] to the extreme black holes discussed in the last subsection, in order to find the higher dimensional Nariai, dS−Bertotti-Robinson, Bertotti-Robinson and Nariai−Bertotti-Robinson solutions [211].

10.2.2.a   Higher dimensional Nariai solution

In order to generate the higher dimensional Nariai solution from the near-Nariai black hole we first go back to (10.22) and rewrite it in the form $f(r) = -A(r)(r - \rho)^2$, where $r = \rho$ is the degenerated horizon of the black hole, and $A(r)$ is a polynomial function of r. Then, we set $r_+ = \rho - \varepsilon$ and $r_c = \rho + \varepsilon$, in order that $\varepsilon << 1$ measures the deviation from degeneracy, and the limit $r_+ \to r_c$ is obtained when $\varepsilon \to 0$. Now, we introduce a new time coordinate T, $t = \frac{1}{\varepsilon A} T$, and a new radial coordinate χ, $r = \rho + \varepsilon \cos \chi$, where $\chi = 0$ and $\chi = \pi$ correspond, respectively, to the horizons r_c and r_+, and $A \equiv A(\rho) = \frac{1}{\rho^2} \left[1 - \frac{\Lambda}{3} \left(\rho^2 + h(\rho) \right) \right] > 0$, with $h(\rho)$ is defined in (10.23). Then, in the limit $\varepsilon \to 0$, from (10.8) and (10.22), we obtain the gravitational field of the Nariai solution [211]

$$ds^2 = \frac{1}{A} \left(-\sin^2 \chi \, dT^2 + d\chi^2 \right) + \frac{1}{B} d\Omega_{D-2}^2 \,. \tag{10.30}$$

where χ runs from 0 to π, and A and $B = \frac{1}{\rho^2}$ are related to Λ and Q by

$$\Lambda = \frac{3}{(D-2)(D-1)} \left[A + (D-3)^2 B \right] \,, \quad \text{and} \quad Q^2 = \frac{(D-3)B - A}{(D-3)(D-2)B^{D-2}} \,. \tag{10.31}$$

The Maxwell field (10.14) of the higher dimensional Nariai solution is

$$F = Q_{\text{ADM}} \frac{B^{(D-2)/2}}{A} \sin \chi \, dT \wedge d\chi \,. \tag{10.32}$$

So, if we give the parameters Λ, and Q we can construct the higher dimensional Nariai solution. This solution is the direct topological product of $dS_2 \times S^{D-2}$, i.e., of a (1+1)-dimensional dS spacetime with a $(D-2)$-sphere of fixed radius $B^{-1/2}$, and is an exact solution of Einstein-Maxwell equations with $\Lambda > 0$ in D-dimensions.

The neutral Nariai solution $(Q = 0)$ satisfies $A = \frac{D-1}{3} \Lambda$ and $B = \frac{D-1}{3(D-3)} \Lambda$. The $\Lambda = 0$ limit of the Nariai solution is D-dimensional Minkowski spacetime as occurs with the $D = 4$ solution (see subsection 7.1.4).

10.2.2.b   Higher dimensional dS Bertotti-Robinson solution

In order to generate the higher dimensional dS Bertotti-Robinson solution from the near-cold black hole we first go back to (10.22) and rewrite it in the form $f(r) = C(r)(r - \rho)^2$, where $r = \rho$ is the degenerated horizon of the black hole, and $C(r)$ is a polynomial function of r. Then, we set $r_- = \rho - \varepsilon$ and $r_+ = \rho + \varepsilon$, in order that $\varepsilon << 1$ measures the deviation from degeneracy, and the limit $r_- \to r_+$ is obtained when $\varepsilon \to 0$. Now, we introduce a new time coordinate T, $t = \frac{1}{\varepsilon C} T$, and a new radial coordinate χ, $r = \rho + \varepsilon \cosh \chi$, where $C \equiv C(\rho) = \frac{1}{\rho^2} \left[1 - \frac{\Lambda}{3} \left(\rho^2 + h(\rho) \right) \right] > 0$, with $h(\rho)$ is defined in (10.23). Then, in the limit $\varepsilon \to 0$, from (10.8) and (10.22), we obtain the gravitational field of the dS Bertotti-Robinson solution [211]

$$ds^2 = \frac{1}{C} \left(-\sinh^2 \chi \, dT^2 + d\chi^2 \right) + \frac{1}{B} d\Omega_{D-2}^2 \,. \tag{10.33}$$

where C and $B = \frac{1}{\rho^2}$ are related to Λ and Q by

$$\Lambda = \frac{3}{(D-2)(D-1)} \left[-C + (D-3)^2 B \right] \,, \quad \text{and} \quad Q^2 = \frac{(D-3)B + C}{(D-3)(D-2)B^{D-2}} \,. \tag{10.34}$$

The Maxwell field (10.14) of the higher dimensional dS Bertotti-Robinson solution is

$$F = -Q_{\text{ADM}} \frac{B^{(D-2)/2}}{C} \sinh \chi \, dT \wedge d\chi \,. \tag{10.35}$$

So, if we give the parameters Λ, and Q we can construct the higher dimensional dS Bertotti-Robinson solution. This solution is the direct topological product of $AdS_2 \times S^{D-2}$, i.e., of a (1+1)-dimensional AdS spacetime with a $(D-2)$-sphere of fixed radius $B^{-1/2}$, and is an exact solution of Einstein-Maxwell equations with $\Lambda > 0$ in D-dimensions. There is no neutral $(Q = 0)$ Bertotti-Robinson solution.

10.2.2.c   Higher dimensional flat Bertotti-Robinson solution

From the $\Lambda = 0$ limit of the dS Bertotti-Robinson, one can generate the $\Lambda = 0$ Bertotti-Robinson solution. It is described by (10.33) and (10.35) with C and B being related to Q by [211]

$$B = Q^{-2/(D-3)}, \quad \text{and} \quad C = (D-3)^2 \, Q^{-2/(D-3)}. \tag{10.36}$$

Topologically this solution is also $AdS_2 \times S^{D-2}$, and is an exact solution of Einstein-Maxwell equations with $\Lambda = 0$ in D-dimensions.

10.2.2.d   Higher dimensional Nariai$-$Bertotti-Robinson solution

In order to generate the higher dimensional Nariai$-$Bertotti-Robinson solution from the near-ultracold black hole we first go back to (10.22) and rewrite it in the form $f(r) = -P(r)(r-\rho)^2(r-\sigma)$, where $r = \rho$ is a degenerated horizon of the black hole, $\sigma > \rho$ is the other horizon, and $P(r)$ is a polynomial function of r. Then, we set $\rho = \rho_\mathrm{u} - \varepsilon$ and $\sigma = \rho_\mathrm{u} + \varepsilon$, with ρ_u defined in (10.27), in order that $\varepsilon << 1$ measures the deviation from degeneracy, and the limit $\rho \to \sigma$ is obtained when $\varepsilon \to 0$. Now, we introduce a new time coordinate T, $t = \frac{1}{2\varepsilon^2 P} T$, and a new radial coordinate χ, $r = \rho_\mathrm{u} + \varepsilon \cos\left(\sqrt{2\varepsilon P}\,\chi\right)$, where $P \equiv P(\rho_\mathrm{u}) > 0$. Then, in the limit $\varepsilon \to 0$, from (10.8) we obtain the gravitational field of the Nariai$-$Bertotti-Robinson solution [211]

$$ds^2 = -\chi^2 \, dT^2 + d\chi^2 + \rho_\mathrm{u}^2 \, d\Omega_{D-2}^2. \tag{10.37}$$

where χ runs from 0 to $+\infty$, and ρ_u defined in (10.27). The Maxwell field (10.14) of the higher dimensional Nariai$-$Bertotti-Robinson solution is

$$F = \frac{Q_\mathrm{ADM}}{\rho_\mathrm{u}^{D-2}} \chi \, dT \wedge d\chi, \tag{10.38}$$

where Q_ADM is given by (10.11) and (10.28). So, if we give Λ we can construct the higher dimensional Nariai$-$Bertotti-Robinson solution. Notice that the spacetime factor $-\chi^2 \, dT^2 + d\chi^2$ is just $\mathbb{M}^{1,1}$ (2-dimensional Minkowski spacetime) in Rindler coordinates. Therefore, under the usual coordinate transformation $\chi = \sqrt{x^2 - t^2}$ and $T = \mathrm{arctanh}(\mathrm{t/x})$, this factor transforms into $-dt^2 + dx^2$. The higher dimensional Nariai$-$Bertotti-Robinson solution is the direct topological product of $\mathbb{M}^{1,1} \times S^{D-2}$, and is an exact solution of Einstein-Maxwell equations with $\Lambda > 0$ in D-dimensions.

10.3   Higher dimensional exact solutions in an AdS background

10.3.1   Higher dimensional black holes in an asymptotically AdS background

In a higher dimensional asymptotically anti-de Sitter background, $\Lambda < 0$, the Einstein-Maxwell equations allow a three-family of static black hole solutions, parameterized by the constant k which can take the values $1, 0, -1$, and whose gravitational field is described by

$$ds^2 = -f(r) \, dt^2 + f(r)^{-1} \, dr^2 + r^2 (d\,\Omega_{D-2}^k)^2, \tag{10.39}$$

where

$$f(r) = k - \frac{\Lambda}{3} r^2 - \frac{M}{r^{D-3}} + \frac{Q^2}{r^{2(D-3)}}, \tag{10.40}$$

and

$$(d\Omega_{D-2}^k)^2 = d\theta_1^2 + \sin^2\theta_1 \, d\theta_2^2 + \sin^2\theta_1 \sin^2\theta_2 \, d\theta_3^2 + \cdots + \prod_{i=1}^{D-3} \sin^2\theta_i \, d\theta_{D-2}^2, \quad \text{for } k = 1,$$

$$(d\Omega_{D-2}^k)^2 = d\theta_1^2 + d\theta_2^2 + d\theta_3^2 + \cdots + d\theta_{D-2}^2, \quad \text{for } k = 0,$$

$$(d\Omega_{D-2}^k)^2 = d\theta_1^2 + \sinh^2\theta_1 \, d\theta_2^2 + \sinh^2\theta_1 \sin^2\theta_2 \, d\theta_3^2 + \cdots + \sinh^2\theta_1 \prod_{i=2}^{D-3} \sin^2\theta_i \, d\theta_{D-2}^2, \quad \text{for } k = -1.$$

$$\tag{10.41}$$

Thus, the family with $k = 1$ yields AdS black holes with spherical topology found in [202]. The family with $k = 0$ yields AdS black holes with planar, cylindrical or toroidal (with genus $g \geq 1$) topology that are the higher dimensional counterparts (introduced in [295] in the neutral case, and in [296] in the charged case) of the 4-dimensional black holes found and analyzed in [6, 7, 8]. Finally, the family with $k = -1$ yields AdS black holes with hyperbolic, or toroidal topology with genus $g \geq 2$ that are the higher dimensional counterparts (introduced in [295] in the neutral case) of the 4-dimensional black holes analyzed in [11]. The solutions with non-spherical topology (i.e., with $k = 0$ and $k = -1$) do not have counterparts in a $\Lambda = 0$ or in a $\Lambda > 0$ background.

The mass parameter M and the charge parameter Q are related to the ADM hairs, M_{ADM} and Q_{ADM}, by (10.11). The causal structure of these higher dimensional AdS black holes is similar to the one of their 4-dimensional counterparts (see chapter 5). In particular, these black holes can have at most two horizons. Following a similar procedure as the one sketched in section 10.2.1, we find the mass parameter M and the charge parameter Q of the extreme black holes as functions of the degenerated horizon at $r = \rho$ [211]

$$M = 2\rho^{D-3}\left(k - \frac{D-2}{D-3}\frac{\Lambda}{3}\rho^2\right), \qquad \text{and} \qquad Q^2 = \rho^{2(D-3)}\left(k - \frac{D-1}{D-3}\frac{\Lambda}{3}\rho^2\right). \qquad (10.42)$$

10.3.1.a   Higher dimensional AdS black holes with spherical topology

When $k = 1$, one has $0 < \rho < +\infty$ and M and Q in (10.42) are always positive. The ranges of M and Q that represent extreme and nonextreme black holes are sketched in Fig. 10.2.

For $D = 5$, the function $f(r)$ in the extreme case can be written as

$$f(r) = -\frac{\Lambda}{3}\frac{1}{r^4}(r-\rho)^2(r+\rho)^2\left(r^2 + 2\rho^2 - \frac{3}{\Lambda}\right). \qquad (10.43)$$
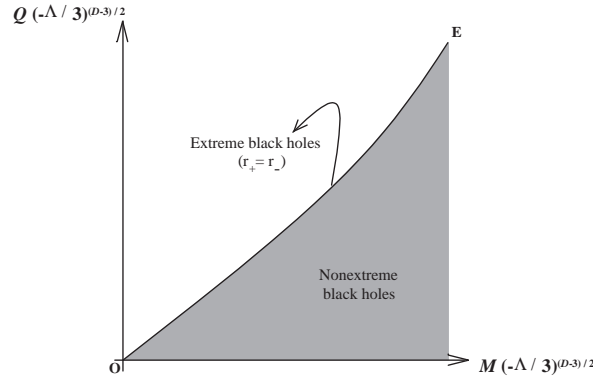
Figure 10.2: Range of M and Q for which one has a nonextreme black hole (region below the line OE), and an extreme black hole with $r_+ = r_-$ (line OE) in the AdS case with spherical topology ($k = 1$) or with planar, cylindrical or toroidal topology ($k = 0$). The region above the line OE represents a naked singularity.

10.3.1.b   Higher dimensional AdS black holes with toroidal or cylindrical topology

When $k = 0$, one has $0 < \rho < +\infty$ and M and Q in (10.42) are also always positive. The ranges of M and Q that represent extreme and nonextreme black holes are sketched in Fig. 10.2.

For $D = 5$, the function $f(r)$ in the extreme case can be written as

$$f(r) = -\frac{\Lambda}{3}\frac{1}{r^4}(r-\rho)^2(r+\rho)^2(r^2 + 2\rho^2). \qquad (10.44)$$

10.3.1.c   Higher dimensional AdS black holes with hyperbolic topology

When $k = -1$, the condition that $Q^2 \geq 0$ demands that $-\frac{D-3}{D-1}\frac{3}{\Lambda} \leq \rho < +\infty$. For $\rho = -\frac{D-3}{D-1}\frac{3}{\Lambda}$, the extreme black hole has no electric charge ($Q = 0$) and its mass is negative, $M = -\frac{4}{D-1}\left(-\frac{D-3}{D-1}\right)^{(D-3)/2}$. For $\rho = -\frac{D-3}{D-2}\frac{3}{\Lambda}$, the extreme black hole has no mass ($M = 0$) and its charge is given by $Q = \frac{1}{\sqrt{D-2}}\left(-\frac{D-3}{D-2}\right)^{(D-3)/2}$. The ranges of M and Q that represent extreme and nonextreme black holes are sketched in Fig. 10.3.

For $D = 5$, the function $f(r)$ in the extreme case can be written as

$$f(r) = -\frac{\Lambda}{3}\frac{1}{r^4}(r-\rho)^2(r+\rho)^2\left(r - \sqrt{-\frac{3}{\Lambda} - 2\rho^2}\right)\left(r + \sqrt{-\frac{3}{\Lambda} - 2\rho^2}\right). \tag{10.45}$$

The condition $Q^2 \geq 0$ requires $\rho^2 \geq -3/(2\Lambda)$ which implies that $r = \rho$ is the only real root of the solution.
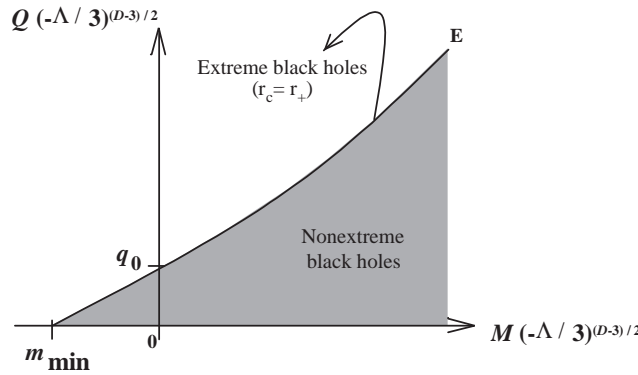
Figure 10.3: Range of M and Q for which one has a nonextreme black hole (region below the line OE), and an extreme black hole with $r_c = r_+$ (line OE) in the AdS case with hyperbolic topology ($k = -1$). The region above the line OE represents a naked singularity. $m_{\min} = -\frac{4}{D-1}\left(-\frac{D-3}{D-1}\right)^{(D-3)/2}$, and $q_0 = \frac{1}{\sqrt{D-2}}\left(-\frac{D-3}{D-2}\right)^{(D-3)/2}$.

10.3.2   Extremal limits of the higher dimensional AdS black holes

In this subsection, we will consider the extremal limits of the near-extreme higher dimensional AdS black holes. This procedure leads to the generation of the higher dimensional anti-Nariai solution and higher dimensional AdS Bertotti-Robinson solution. To achieve our aim, we first go back to the extreme case of (10.40) and rewrite it in the form $f(r) = A(r)(r - \rho)^2$, where $r = \rho$ is the degenerated horizon of the black hole, and $A(r)$ is a polynomial function of r. Then, we introduce a new time coordinate T, $t = \frac{1}{\varepsilon A}T$, and a new radial coordinate χ, $r = \rho + \varepsilon \cosh \chi$, where $A \equiv A(\rho)$, and $\varepsilon << 1$ measures the deviation from degeneracy. Finally, taking the limit $\varepsilon \to 0$ in (10.39) yields the gravitational field of the new higher dimensional solutions [211],

$$ds^2 = \frac{1}{A}\left(-\sinh^2\chi\,dT^2 + d\chi^2\right) + \frac{1}{B}(d\Omega_{D-2}^k)^2, \tag{10.46}$$

where $k = 1, 0, -1$ in the spherical, cylindrical and hyperbolic cases, respectively, and A and B are constants related to Λ and Q by

$$\Lambda = -\frac{3}{(D-2)(D-1)}\left[A - k(D-3)^2B\right], \quad \text{and} \quad Q^2 = \frac{A + k(D-3)B}{(D-3)(D-2)B^{D-2}}, \tag{10.47}$$

In the new coordinate system, the Maxwell field (10.14) of the solutions is

$$F = -Q_{\text{ADM}}\frac{B^{(D-2)/2}}{A}\sinh\chi\,dT \wedge d\chi. \tag{10.48}$$

Equations (10.46)-(10.48) describe three exact solutions of the Einstein-Maxwell theory with $\Lambda < 0$ in D-dimensions. The $k = +1$ case describes the AdS Bertotti-Robinson solution with spherical topology. This solution is the direct topological product of $AdS_2 \times S^{D-2}$, i.e., of a (1+1)-dimensional AdS spacetime with a $(D-2)$-sphere of fixed radius $B^{-1/2}$. The $k = 0$ case describes the AdS Bertotti-Robinson solution with toroidal or cylindrical topology. This solution is the direct topological product of $AdS_2 \times \mathbb{E}^{D-2}$, i.e., of a (1+1)-dimensional AdS spacetime with a $(D-2)$ Euclidean space. Finally, the $k = -1$ case describes the the higher dimensional anti-Nariai solution. This solution is the direct topological product of $AdS_2 \times H^{D-2}$, i.e., of a (1+1)-dimensional AdS spacetime with a $(D-2)$-hyperboloid with a fixed size, $B^{-1/2}$. The $k = -1$ case is the only one that admits a solution with $Q = 0$. This neutral anti-Nariai solution satisfies $A = -\frac{D-1}{3}\Lambda$ and $B = -\frac{D-1}{3(D-3)}\Lambda$. The $\Lambda = 0$ limit of the anti-Nariai solution is D-dimensional Minkowski spacetime as occurs with the $D = 4$ solution (see subsection 7.1.4).

Chapter 11

Pair creation of black holes in higher dimensional spacetimes

Contents

In this chapter, we discuss in detail the creation of a higher dimensional Tangherlini black hole pair in a dS background [210, 212]. The instantons that describe the process are constructed from the dS Tangherlini solution, which describes a pair of higher dimensional dS black holes accelerated apart by the cosmological constant expansion. We compute the pair creation rates of the process. This study is the only one discussing the black hole pair creation process in a higher dimensional spacetime.

11.1 The higher dimensional dS instantons

In order to evaluate the black hole pair creation rate we need to find the instantons of the theory, i.e., we must look into the Euclidean section of the higher dimensional dS solution and choose only those Euclidean solutions which are regular in a way that will be explained soon. To obtain the Euclidean section of the dS solution from the Lorentzian dS solution, (10.8), (10.14) and (10.18), we simply introduce an imaginary time coordinate $\tau = -it$.

To have a positive definite Euclidean metric we must require that r belongs to $r_+ \leq r \leq r_{\rm c}$. In general, when $r_- \neq r_+$, one then has conical singularities at the horizons $r = r_+$ and $r = r_{\rm c}$. In order to obtain a regular solution we have to eliminate the conical singularities at both horizons. This is achieved by imposing that the period of τ is the same for the two horizons, and is equivalent to requiring that the Hawking temperature of the two horizons be equal. To eliminate the conical singularity at $r = r_{\rm c}$ the period of τ must be $\beta = 2\pi/k_{\rm c}$ (where $k_{\rm c}$ is the surface gravity of the cosmological horizon),

$$\beta = \frac{4\pi}{|f'(r_{\rm c})|} \,. \tag{11.1}$$

This choice for the period of τ also eliminates simultaneously the conical singularity at the outer black hole horizon, $r = r_+$, if and only if the parameters of the solution are such that the surface gravities of the black hole and acceleration horizons are equal ($k_+ = k_{\rm c}$), i.e.,

$$f'(r_+) = -f'(r_{\rm c}) \,. \tag{11.2}$$

There are two ways to satisfy this condition. One is a regular Euclidean solution with $r_+ \neq r_{\rm c}$, and will be called lukewarm instanton. This solution requires the presence of an electromagnetic charge. The other way is to have $r_+ = r_{\rm c}$, and will be called Nariai instanton. This last solution exists with or without charge. When we want to distinguish them, they will be labelled by charged Nariai and neutral Nariai instantons, respectively.

We now turn our attention to the case $r_- = r_+$ and $r_c \neq r_+$, which obviously requires the presence of charge. When this happens the allowed range of r in the Euclidean sector is simply $r_+ < r \leq r_c$. This occurs because when $r_- = r_+$ the proper distance along spatial directions between r_+ and r_c goes to infinity. The point r_+ disappears from the τ, r section which is no longer compact but becomes topologically $S^1 \times \mathbb{R}$. Thus, in this case we have a conical singularity only at r_c, and so we obtain a regular Euclidean solution by simply requiring that the period of τ be equal to (11.1). We will label this solution by cold instanton. Finally, we have a special solution that satisfies $r_- = r_+ = r_c$ and that is regular when condition (11.1) is satisfied. This instanton will be called ultracold instanton and can be viewed as a limiting case of both the charged Nariai instanton and cold instanton.

Below, we will describe each one of these four instantons, following the order: (A) cold instanton, (B) Nariai instanton, (C) ultracold instanton, and (D) lukewarm instanton. These instantons are the higher dimensional counterparts of the 4-dimensional instantons that have been constructed [167, 168, 169, 173] from the Euclidean section of the dS−Reissner-Nordström solution, and thus we preserve the 4-dimensional nomenclature. The cold instanton, the Nariai instanton, and the ultracold instanton are obtained by euclideanizing solutions found chapter in 10. These four families of instantons will allow us to calculate the pair creation rate of accelerated dS−Reissner-Nordström black holes in section 11.2.

As is clear from the above discussion, when the charge vanishes the only regular Euclidean solution that can be constructed is the neutral Nariai instanton. The same feature is present in the 4-dimensional case where only the neutral Nariai instanton is available [97, 169, 170, 172].

11.1.1   The higher dimensional cold instanton

The gravitational field of the higher dimensional cold instanton is given by (10.8) and (10.18), while its Maxwell field is given by (10.14), with the replacement $\tau = -it$. Moreover, the degenerated horizon ρ, the mass parameter M, and the charge parameter Q satisfy relations (10.24) and (10.26). The topology of the higher dimensional cold instanton is $\mathbb{R}^2 \times S^{D-2}$, since $r = r_+ = \rho$ is at an infinite proper distance ($0 \leq \tau \leq \beta$, $r_+ < r \leq r_c$). The surface $r = r_+ = \rho$ is then an internal infinity boundary that will have to be taken into account in the calculation of the action of the cold instanton (see section 11.2.1). The Lorentzian sector of this cold case describes two extreme ($r_- = r_+$) dS black holes being accelerated by the cosmological background, and the higher dimensional cold instanton describes pair creation of these extreme black holes. To compute the pair creation rate of cold black holes we need to know the location of the cosmological horizon, r_c. This location can be explicitly determined for $D = 4$ and $D = 5$. Specifically, for $D = 4$ one has $r_c = \sqrt{3/\Lambda - 2\rho^2} - \rho$, where, from (10.26), one has $0 < \rho < 1/\sqrt{2\Lambda}$. For $D = 5$ one has $r_c = \sqrt{3/\Lambda - 2\rho^2}$, where, from (10.26), one has $0 < \rho < 1/\sqrt{\Lambda}$. For $D \geq 6$ finding explicitly r_c requires solving a polynomial of degree higher than four.

11.1.2   The higher dimensional Nariai instanton

The gravitational field of the higher dimensional Nariai instanton is given by (10.30), while the Maxwell field is given by (10.32), with the replacement $\tau = -iT$. Moreover, the parameter A and $B = \rho^{-2}$ satisfy relations (10.31) and (10.29). The topology of the Nariai instanton is $S^2 \times S^{D-2}$ ($0 \leq \tau \leq \beta$, $0 \leq \chi \leq \pi$). The Lorentzian sector of this solution is the direct topological product of $dS_2 \times S^{D-2}$, i.e., of a (1+1)-dimensional de Sitter spacetime with a (D-2)-sphere of fixed size. To each point in the sphere corresponds a dS_2 spacetime. In the $D = 4$ case it has been shown [97, 170] that the Nariai solution decays through the quantum tunnelling process into a slightly non-extreme dS black hole pair (for a complete review on this subject see [129]). We then naturally expect that an analogous quantum instability is present in the higher dimensional Nariai solution. Therefore, the Nariai instanton describes the creation of a higher dimensional Nariai universe that then decays into a slightly non-extreme ($r_+ \sim r_c$) pair of black holes accelerated by the cosmological constant background.

11.1.3 The higher dimensional ultracold instanton

The gravitational field of the higher dimensional ultracold instanton is given by (10.37) while the Maxwell field is given by (10.38), with the replacement $\tau = -iT$. Moreover the parameters ρ_{u} and Q are defined in (10.27) and (10.28), respectively. The topology of the ultracold instanton is $\mathbb{E}^2 \times S^{D-2}$. The Lorentzian sector of this solution is the direct topological product of $\mathbb{M}^{(1,1)} \times S^{D-2}$, i.e., of a $(1+1)$-dimensional Minkowski spacetime with a (D-2)-sphere of fixed size. The ultracold instanton describes the creation of a higher dimensional Nariai$-$Bertotti-Robinson universe that then decays into a slightly non-extreme ($r_- \sim r_+ \sim r_{\mathrm{c}}$) pair of black holes accelerated by the cosmological constant background.

11.1.4 The higher dimensional lukewarm instanton

The gravitational field of the higher dimensional lukewarm instanton is given by (10.8) with the requirement that $f(r)$ satisfies condition (11.2) and $f(r_+) = 0 = f(r_{\mathrm{c}})$. To find the properties of the lukewarm instanton we note that the function $f(r)$, given by (10.8), can also be written as

$$f(r) = -\frac{\Lambda}{3}r^2 \left(1 - \frac{r_+}{r}\right)\left(1 - \frac{r_{\mathrm{c}}}{r}\right)$$
$$\times \left(1 + \frac{a_1}{r} + \frac{a_2}{r^2} + \cdots + \frac{a_{2(D-3)}}{r^{2(D-3)}}\right), \tag{11.3}$$

where a_i ($i = 1, \cdots, 2(D-3)$) are constants that can be found from the matching between (10.8) and (11.3). This matching, together with the extra condition (11.2), lead to unique relations between the parameters Λ, M, Q and the position of the horizons, r_+ and r_{c}. Since this procedure involves polynomials with a high degree, we have not been able to find the general relations between (Λ, M, Q) and (r_+, r_{c}) for any D. So, we have to carry this procedure for each D. As examples, we specifically discuss now the $D = 4$ and the $D = 5$ lukewarm instantons. For $D = 4$, the above procedure yields the relations

$$\Lambda = \frac{3}{(r_{\mathrm{c}} + r_+)^2},$$
$$M = 2\frac{r_{\mathrm{c}}r_+}{r_{\mathrm{c}} + r_+},$$
$$Q = \frac{r_{\mathrm{c}}r_+}{r_{\mathrm{c}} + r_+}. \tag{11.4}$$

For $D = 5$, the relations are

$$\Lambda = 3\left(2r_{\mathrm{c}} + r_+ - \frac{r_{\mathrm{c}}^3(r_{\mathrm{c}} + r_+)}{r_{\mathrm{c}}^2 + r_{\mathrm{c}}r_+ + r_+^2}\right)^{-1},$$
$$M = \frac{r_{\mathrm{c}}^2 r_+^2(2r_{\mathrm{c}}^2 + r_{\mathrm{c}}r_+ + 2r_+^2)}{r_{\mathrm{c}}^4 + r_{\mathrm{c}}^3 r_+ + 3r_{\mathrm{c}}^2 r_+^2 + r_{\mathrm{c}}r_+^3 + r_+^4},$$
$$Q^2 = \frac{r_{\mathrm{c}}^4 r_+^4}{r_{\mathrm{c}}^4 + r_{\mathrm{c}}^3 r_+ + 3r_{\mathrm{c}}^2 r_+^2 + r_{\mathrm{c}}r_+^3 + r_+^4}. \tag{11.5}$$

These two examples indicate an important difference between the lukewarm instanton in $D = 4$ dimensions and in $D \geq 5$: for $D = 4$ the lukewarm instanton has a ADM mass, $M_{\mathrm{ADM}} = M/2$, equal to its ADM charge, $Q_{ADM} = Q$, while for $D \geq 5$ one has $M_{\mathrm{ADM}} \neq Q_{ADM}$. Note also that relations (11.4) and (11.5) and their higher dimensional counterparts define implicitly r_{c} and r_+ as a function of Λ, M, and Q. The location of r_{c} and r_+ can be explicitly determined for $D = 4$ and $D = 5$. For $D \geq 6$ finding explicitly r_{c} requires solving a polynomial of degree higher than four.

The topology of the lukewarm instanton is $S^2 \times S^{D-2}$ ($0 \leq \tau \leq \beta$, $r_+ \leq r \leq r_{\mathrm{c}}$). The Lorentzian sector of the lukewarm solution describes two higher dimensional dS black holes being accelerated apart by the cosmological constant, so this instanton describes pair creation of nonextreme black holes.

11.2 Calculation of the black hole pair creation rates

The pair creation rate of higher dimensional black holes in a dS background is given, according to the no-boundary proposal of [283], by (see subsection 9.3.1)

$$\Gamma \sim \eta \, e^{-2I_{\text{inst}}+2I_{\text{dS}}} , \tag{11.6}$$

where η is the one-loop contribution from the quantum quadratic fluctuations in the fields that will not be considered here. I_{inst} is the classical Euclidean action of the gravitational instanton that mediates the pair creation of black holes, given by [101, 181]

$$
\begin{aligned}
I_{\text{inst}} &= -\frac{1}{16\pi} \int_{\mathcal{M}} d^D x \sqrt{g} \, (R - 2\lambda - F^{\mu\nu} F_{\mu\nu}) \\
&\quad - \frac{1}{8\pi} \int_{\Sigma=\partial\mathcal{M}} d^{D-1} x \sqrt{h} \, K \\
&\quad - \frac{1}{4\pi} \int_{\Sigma=\partial\mathcal{M}} d^{D-1} x \sqrt{h} \, F^{\mu\nu} n_\mu A_\nu ,
\end{aligned}
\tag{11.7}
$$

where $\Sigma = \partial\mathcal{M}$ is the boundary of a compact manifold $\mathcal{M}$, g is the determinant of the Euclidean metric, h is the determinant of the induced metric on the boundary Σ, λ is proportional to the cosmological constant as defined in (10.2), R is the Ricci scalar defined in (10.6), K is the trace of the extrinsic curvature K_{ij} of the boundary, $F_{\mu\nu} = \partial_\mu A_\nu - \partial_\nu A_\mu$ is the Maxwell field strength of the gauge field A_ν, and n_μ is the unit outward normal to Σ

We note again, since this fact is important for the computation of the pair creation rates, that in a general D-dimensional background the electromagnetic energy-momentum tensor is not traceless. Indeed, it is given by (10.7), which vanishes only for $D = 4$.

I_{dS} is the Euclidean action of the S^D gravitational instanton that mediates the nucleation of a dS space from nothing, given by

$$
\begin{aligned}
I_{\text{dS}} &= -\frac{1}{16\pi} \int d^D x \sqrt{g} \, (R - 2\lambda) \\
&= -\frac{3^{D/2}}{12 \, \Lambda^{(D-2)/2}} \frac{\pi^{(D-1)/2}}{\Gamma[(D-1)/2]} .
\end{aligned}
\tag{11.8}
$$

11.2.1 The higher dimensional cold pair creation rate

The Maxwell field of the higher dimensional cold is $F = -i\frac{Q_{\text{ADM}}}{r^{D-2}} \, d\tau \wedge dr$. With this information we are able to compute all the terms of the Euclidean action (11.7). We start with

$$
\begin{aligned}
&-\frac{1}{16\pi} \int_{\mathcal{M}} d^D x \sqrt{g} \, (R - 2\lambda) \\
&= \left(-\frac{D-1}{24\pi} \Lambda + \frac{(D-4)(D-3)}{16\pi} Q^2 \right) \int d\Omega_{D-2} \int_0^{\beta/2} d\tau \int_\rho^{r_c} dr \, r^{D-2} \\
&= \frac{\pi^{(D-3)/2}}{\Gamma[(D-1)/2]} \frac{\beta}{8} \left[-\frac{\Lambda}{3} \left(r_c^{D-1} - \rho^{D-1} \right) + \frac{(D-4) Q^2}{2} \left(\rho^{-(D-3)} - r_c^{-(D-3)} \right) \right] ,
\end{aligned}
\tag{11.9}
$$

where $\int d\Omega_{D-2} = \Omega_{D-2}$ is defined in (10.12). The Maxwell term in the action yields

$$
\frac{1}{16\pi} \int_{\mathcal{M}} d^D x \sqrt{g} \, F^2 = -\frac{(D-2) Q^2 \beta}{16} \frac{\pi^{(D-3)/2}}{\Gamma[(D-1)/2]} \left[\rho^{-(D-3)} - r_c^{-(D-3)} \right],
\tag{11.10}
$$

and $\int_\Sigma d^{D-1} x \sqrt{h} \, K = 0$. In order to compute the extra Maxwell boundary term in (11.7) we have to find a vector potential, A_ν, that is regular everywhere including at the horizons. An appropriate

choice in the cold case is $A_r = -i \frac{Q_{\text{ADM}}}{r^{D-2}} \tau$. The integral over Σ consists of an integration between ρ and r_c along the $\tau = 0$ surface and back along $\tau = \beta/2$, and of an integration between $\tau = 0$ and $\tau = \beta/2$ along the $r = r_c$ surface and back along the $r = \rho$ surface. The normal to Σ_τ is $n_\mu = \left(\sqrt{f(r)}, 0, \cdots, 0\right)$, and the normal to Σ_h is $n_\mu = \left(0, \sqrt{f(r)}, 0, \cdots, 0\right)$. Thus the non-vanishing contribution comes only from the integration along the $\tau = \beta/2$ surface. The Maxwell boundary term in (11.7) is then

$$-\frac{1}{4\pi} \int_{\Sigma_{\tau=\beta/2}} d^{D-1}x \sqrt{h}\, F^{\tau r} n_\tau A_r = -\frac{1}{8\pi} \int_{\mathcal{M}} d^D x \sqrt{g}\, F^2. \tag{11.11}$$

Adding all these terms yields the action (11.7) of the higher dimensional cold instanton (onwards the subscript "c" means cold)

$$I_c = -r_c^{D-2} \frac{\pi^{(D-1)/2}}{4\,\Gamma[(D-1)/2]}, \tag{11.12}$$

which, for $D = 4$, reduces to the result of [169]. The allowed interval of ρ is defined in (10.26). As ρ varies from $\rho = \rho_u$, defined in (10.27), to $\rho = 0$, the cold action (11.12) varies according to

$$-\frac{\rho_u^{D-2}}{4} \frac{\pi^{(D-1)/2}}{\Gamma[(D-1)/2]} < I_c < I_{\text{dS}}, \tag{11.13}$$

where the lower limit of this relation is the ultracold action, as we shall see in (11.25), and I_{dS} is defined in (11.8).

The pair creation rate of extreme cold black holes is given by (11.6),

$$\Gamma_c = \eta\, e^{-2I_c + 2I_{\text{dS}}}, \tag{11.14}$$

where η is the one-loop contribution not computed here.

11.2.2   The higher dimensional Nariai pair creation rate

The first term of the Euclidean action (11.7) gives in the Nariai case

$$-\frac{1}{16\pi} \int_{\mathcal{M}} d^D x \sqrt{g}\,(R - 2\lambda)$$

$$= \left(-\frac{\Lambda\,(D-1)}{24\pi} + \frac{(D-4)(D-3)}{16\pi} Q^2 B^{D-2}\right) \int d\Omega_{D-2} \int_0^{2\pi/2} d\tau \int_0^\pi d\chi\, \frac{\sin\chi}{A\, B^{(D-2)/2}}$$

$$= \frac{\pi^{(D-1)/2}}{\Gamma[(D-1)/2]} \left[-\frac{\Lambda\,(D-1)}{6} \frac{1}{A\, B^{(D-2)/2}} + \frac{Q^2\,(D-4)(D-3)}{4} \frac{B^{(D-2)/2}}{A}\right]. \tag{11.15}$$

The Maxwell term in the action yields

$$\frac{1}{16\pi} \int_{\mathcal{M}} d^D x \sqrt{g}\, F^2 = -\frac{(D-2)(D-3)\,Q^2}{4} \frac{B^{(D-2)/2}}{A} \frac{\pi^{(D-1)/2}}{\Gamma[(D-1)/2]}, \tag{11.16}$$

and $\int_\Sigma d^{D-1}x \sqrt{h}\, K = 0$. In order to compute the extra Maxwell boundary term in (11.7) we have to find a vector potential, A_ν, that is regular everywhere including at the horizons. An appropriate choice in the lukewarm case is $A_\chi = i\, Q_{\text{ADM}} \frac{B^{(D-2)/2}}{A} \sin\chi\, \tau$. The integral over Σ consists of an integration between $\chi = 0$ and $\chi = \pi$ along the $\tau = 0$ surface and back along $\tau = \pi$, and of an integration between $\tau = 0$ and $\tau = \pi$ along the $\chi = 0$ surface, and back along the $\chi = \pi$ surface. The non-vanishing contribution to the Maxwell boundary term in (11.7), $-\frac{1}{4\pi} \int_\Sigma d^3x \sqrt{h}\, F^{\mu\nu} n_\mu A_\nu$, comes only from the integration along the $\tau = \pi$ surface and is given by

$$-\frac{1}{4\pi} \int_{\Sigma_{\tau=\pi}} d^{D-1}x \sqrt{h}\, F^{\tau\chi} n_\tau A_\chi = -\frac{1}{8\pi} \int_{\mathcal{M}} d^D x \sqrt{g}\, F^2. \tag{11.17}$$

Adding all these terms yields the action (11.7) of the higher dimensional Nariai instanton (onwards the subscript "N" means Nariai)

$$I_{\mathrm{N}} = -\frac{1}{2\,B^{(D-2)/2}}\frac{\pi^{(D-1)/2}}{\Gamma[(D-1)/2]}\,, \tag{11.18}$$

which, for $D = 4$, reduces to the result of [181, 169]. One has $B = \rho^{-2}$, where ρ lies in the range defined in (10.29). Thus, the Nariai action (11.18) lies in the range

$$-\frac{\pi^{(D-1)/2}\,\rho_{\mathrm{max}}^{D-2}}{2\,\Gamma[(D-1)/2]} \leq I_{\mathrm{N}} < -\frac{\pi^{(D-1)/2}\,\rho_{\mathrm{u}}^{D-2}}{2\,\Gamma[(D-1)/2]}\,, \tag{11.19}$$

where the quantities ρ_{max} and ρ_{u} are defined, respectively, in (10.25) and (10.27). The equality holds in the neutral Nariai case ($Q = 0$), while the upper limit of (11.19) is the double of the ultracold action, which will be defined in (11.25).

The pair creation rate of extreme Nariai black holes is given by (11.6),

$$\Gamma_{\mathrm{N}} = \eta\,e^{-2I_{\mathrm{N}}+2I_{\mathrm{dS}}}\,, \tag{11.20}$$

where I_{dS} is given by (11.8), and η is the one-loop contribution not computed here. The process studied in this subsection describes the nucleation of a higher dimensional Nariai universe that is unstable [97, 170, 129] and decays through the pair creation of extreme Nariai black holes.

11.2.3 The higher dimensional ultracold pair creation rate

The boundary $\Sigma = \partial\mathcal{M}$ that appears in (11.7) consists of an initial spatial surface at $\tau = 0$ plus a final spatial surface at $\tau = \pi$. We label these two 3-surfaces by Σ_τ. Each one of these two spatial $(D-1)$-surfaces is delimitated by a $(D-2)$-surface at the Rindler horizon $\chi = 0$ and by a $(D-2)$-surface at the internal infinity $\chi = \infty$. The two surfaces Σ_τ are connected by a timelike $(D-1)$-surface, Σ_h, that intersects Σ_τ at the frontier $\chi = 0$ and by a timelike $(D-1)$-surface, $\Sigma_\infty^{\mathrm{int}}$, that intersects Σ_τ at the internal infinity boundary $\chi = \infty$. Thus $\Sigma = \Sigma_\tau + \Sigma_h + \Sigma_\infty^{\mathrm{int}}$, and the region $\mathcal{M}$ within it is compact. The first term of the Euclidean action (11.7) yields

$$-\frac{1}{16\pi}\int_{\mathcal{M}} d^D x \sqrt{g}\,(R - 2\lambda)$$

$$= \frac{1}{16\pi}\left[\Lambda\frac{2(D-1)}{3}\rho_{\mathrm{u}}^{D-2} + Q^2\,(D-4)(D-3)\frac{1}{\rho_{\mathrm{u}}^{D-2}}\right]\int d\Omega_{D-2}\int_0^{2\pi/2} d\tau \int_0^{\chi_0\to\infty} d\chi\,\chi$$

$$= \left[-\frac{D-1}{24}\Lambda\,\rho_{\mathrm{u}}^{D-2} + \frac{(D-4)(D-3)}{16}\frac{Q^2}{\rho_{\mathrm{u}}^{D-2}}\right]\frac{\pi^{(D-1)/2}}{\Gamma[(D-1)/2]}\,\chi_0^2\bigg|_{\chi_0\to\infty}\,. \tag{11.21}$$

The Maxwell term in the action yields

$$\frac{1}{16\pi}\int_{\mathcal{M}} d^D x \sqrt{g}\,F^2 = -\frac{(D-3)(D-2)\,Q^2}{16\,\rho_{\mathrm{u}}^{D-2}}\frac{\pi^{(D-1)/2}}{\Gamma[(D-1)/2]}\chi_0^2\bigg|_{\chi_0\to\infty}\,. \tag{11.22}$$

Now, contrary to the other instantons, the ultracold instanton has a non-vanishing extrinsic curvature boundary term, $-\frac{1}{16\pi}\int_\Sigma d^{D-1}x\sqrt{h}\,K \neq 0$, due to the internal infinity boundary ($\Sigma_\infty^{\mathrm{int}}$ at $\chi = \infty$) contribution. The extrinsic curvature to $\Sigma_\infty^{\mathrm{int}}$ is $K_{\mu\nu} = h_\mu{}^\alpha \nabla_\alpha n_\nu$, where $n_\nu = (0, 1, 0, \cdots, 0)$ is the unit outward normal to $\Sigma_\infty^{\mathrm{int}}$, $h_\mu{}^\alpha = g_\mu{}^\alpha - n_\mu n^\alpha = (1, 0, 1, \cdots, 1)$ is the projection tensor onto $\Sigma_\infty^{\mathrm{int}}$, and ∇_α represents the covariant derivative with respect to $g_{\mu\nu}$. Thus the trace of the extrinsic curvature to $\Sigma_\infty^{\mathrm{int}}$ is $K = g^{\mu\nu}K_{\mu\nu} = \frac{1}{\chi}$, and

$$-\frac{1}{8\pi}\int_\Sigma d^{D-1}x\sqrt{h}\,K = -\frac{\rho_{\mathrm{u}}^{D-2}}{4}\frac{\pi^{(D-1)/2}}{\Gamma[(D-1)/2]}\,. \tag{11.23}$$

In the ultracold case the vector potential A_ν, that is regular everywhere including at the horizon, needed to compute the extra Maxwell boundary term in (11.7) is $A_\tau = -i\frac{Q_{\text{ADM}}}{\rho^{D-2}}\chi^2/2$. The integral over Σ consists of an integration between $\chi = 0$ and $\chi = \infty$ along the $\tau = 0$ surface and back along $\tau = \pi$, and of an integration between $\tau = 0$ and $\tau = \pi$ along the $\chi = 0$ surface, and back along the internal infinity surface $\chi = \infty$. The non-vanishing contribution to the Maxwell boundary term in (11.7) comes only from the integration along the internal infinity boundary $\Sigma_\infty^{\text{int}}$, and is given by

$$-\frac{1}{4\pi}\int_{\Sigma_\infty^{\text{int}}} d^{D-1}x\sqrt{h}\, F^{\chi\tau}n_\chi A_\tau = -\frac{1}{8\pi}\int_{\mathcal{M}} d^D x\sqrt{g}\, F^2. \tag{11.24}$$

Due to the fact that $\chi_0 \to \infty$ it might seem that the contribution from (11.21), (11.22) and (11.24) diverges. This is not however the case since these three terms cancel each other. The only contribution to the action (11.7) of the higher dimensional ultracold instanton (onwards the subscript "u" means ultracold) comes from (11.23) yielding

$$I_{\text{u}} = -\frac{\rho_{\text{u}}^{D-2}}{4}\frac{\pi^{(D-1)/2}}{\Gamma[(D-1)/2]}, \tag{11.25}$$

which, for $D = 4$, reduces to the result of [169]. The ultracold action coincides with the minimum value of the cold action range (11.13), and is equal to one half the maximum value of the Nariai action range (11.19).

The pair creation rate of extreme ultracold black holes is given by (11.6),

$$\Gamma_{\text{u}} = \eta\, e^{-2I_{\text{u}}+2I_{\text{dS}}}, \tag{11.26}$$

where I_{dS} is given by (11.8), and η is the one-loop contribution not computed here. The process studied in this subsection describes the nucleation of a higher dimensional Nariai$-$Bertotti-Robinson universe that is unstable, and decays through the pair creation of extreme ultracold black holes.

11.2.4 The higher dimensional lukewarm pair creation rate

The evaluation of the Euclidean action of the higher dimensional lukewarm instanton follows as in the cold case as long as we replace ρ by r_+. Therefore, the action (11.7) of the higher dimensional lukewarm instanton (onwards the subscript "ℓ" means lukewarm) is given by

$$I_\ell = \frac{\pi^{(D-3)/2}}{\Gamma[(D-1)/2]}\frac{\beta}{4}\left[-\frac{\Lambda\left(r_{\text{c}}^{D-1} - r_+^{D-1}\right)}{(D-2)(D-1)} + \frac{(D-3)Q^2}{2}\left(r_+^{-(D-3)} - r_{\text{c}}^{-(D-3)}\right)\right]. \tag{11.27}$$

and the pair creation rate of nonextreme lukewarm black holes is given by (11.6).

11.2.5 Pair creation rate of higher dimensional nonextreme sub-maximal black holes

The cold, Nariai, ultracold and lukewarm instantons are saddle point solutions free of conical singularities both in the r_+ and r_{c} horizons. The corresponding black holes may then nucleate in the dS background, and we have computed their pair creation rates in the last four subsections. However, these particular black holes are not the only ones that can be pair created. Indeed, it has been shown in [155, 156] that Euclidean solutions with conical singularities may also be used as saddle points for the pair creation process. In this way, pair creation of nonextreme sub-maximal black holes is allowed (by this nomenclature we mean all the nonextreme black holes other than the lukewarm ones that are in the region interior to the close line $ONUO$ in Fig. 10.1), and their pair creation rate may be computed. In order to calculate this rate, the action is given by (11.7) and, in addition, it has now an extra contribution from the conical singularity (c.s.) that is present in one of the horizons (r_+, say) given by [291, 97]

$$\frac{1}{16\pi}\int_{\mathcal{M}} d^D x\sqrt{g}\,(R - 2\lambda)\bigg|_{\text{c.s. at } r_+} = \frac{\mathcal{A}_+\,\delta}{4\,D\,\pi}, \tag{11.28}$$

where $\mathcal{A}_+ = \frac{2\pi^{(D-1)/2}}{\Gamma[(D-1)/2]} \, r_+^{D-2}$ is the area of the $(D-2)$-sphere spanned by the conical singularity, and

$$\delta = 2\pi \left(1 - \frac{\beta_c}{\beta_+}\right) \tag{11.29}$$

is the deficit angle associated to the conical singularity at the horizon r_+, with $\beta_c = 4\pi/|f'(r_c)|$ and $\beta_+ = 4\pi/|f'(r_+)|$ being the periods of τ that avoid a conical singularity in the horizons r_c and r_+, respectively. The contribution from (11.7) follows straightforwardly in a similar way as the one shown in subsection 11.2.4 with the period of τ, β_c, chosen in order to avoid the conical singularity at the cosmological horizon, $r = r_c$.

11.3   Discussion of the results

We have studied in detail the quantum process in which a pair of black holes is created in a higher dimensional de Sitter (dS) background, a process that in $D = 4$ was previously discussed in [169]. The energy to materialize and accelerate the pair comes from the positive cosmological constant. The dS space is the only background in which we can discuss analytically the pair creation process of higher dimensional black holes, since the C-metric and the Ernst solutions, that describe respectively a pair accelerated by a string and by an electromagnetic field, are not know yet in a higher dimensional spacetime.

   In previous works on black hole pair creation in general background fields it has been well established that the pair creation rate is proportional to the exponential of the gravitational entropy S of the system, $\Gamma \propto e^S$, with the entropy being given by one quarter of the the total area $\mathcal{A}$ of all the horizons present in the instanton, $S = \mathcal{A}/4$. It is straightforward to verify that these relations also hold for the higher dimensional dS instantons. Indeed, in the cold case, the instanton has a single horizon, the cosmological horizon at $r = r_c$, in its Euclidean section, since $r = r_+$ is an internal infinity. So, the total area of the cold instanton is $\mathcal{A}_c = \Omega_{D-2} \, r_c^{D-2}$. Thus, $S_c = -2I_c = \mathcal{A}_c/4$, where I_c is given by (11.12). In the Nariai case, the instanton has two horizons in its Euclidean section, namely the cosmological horizon $r = r_c$ and the black hole horizon r_+, both at $r = \rho = B^{-1/2}$, and thus they have the same area. So, the total area of the Nariai instanton is $\mathcal{A}_N = 2\Omega_{D-2} \, B^{-(D-2)/2}$. Again, one has $S_N = -2I_N = \mathcal{A}_N/4$, where I_N is given by (11.18). In the ultracold case, the instanton has a single horizon, the Rindler horizon at $\chi = 0$, in its Euclidean section, since $\chi = \infty$ is an internal infinity. The total area of the ultracold instanton is then $\mathcal{A}_c = \Omega_{D-2} \, \rho_u^{D-2}$. Thus, $S_u = -2I_u = \mathcal{A}_u/4$, where I_u is given by (11.25).

   The ultracold instanton is a limiting case of both the charged Nariai instanton and the cold instanton (see Fig. 10.1). Then, as expected, the action of the cold instanton gives, in this limit, the action of the ultracold instanton (see 11.13). However, the ultracold frontier of the Nariai action is given by two times the ultracold action (see 11.19). The reason for this behavior is clear. Indeed, in the ultracold case and in the cold case, the respective instantons have a single horizon (the other possible horizon turns out to be an internal infinity). This horizon gives the only contribution to the total area, $\mathcal{A}$, and therefore to the pair creation rate. In the Nariai case, the instanton has two horizons with the same area, and thus the ultracold limit of the Nariai action is doubled with respect to the true ultracold action.

   A property of the higher dimensional lukewarm instanton is worth of mention. In $D = 4$ it is known that the lukewarm instanton has an ADM mass equal to its ADM charge. This relation is valid in several background fields, e.g., in a dS background, in an electromagnetic background and in a cosmic string background. For $D \geq 5$ we have shown that the dS lukewarm instanton no longer has an ADM mass equal to its ADM charge.

   In order to clarify the physical interpretation of the results, in this Appendix we heuristically derive the nucleation rates for the processes discussed in the main body of the paper. An estimate for the nucleation probability is given by the Boltzmann factor, $\Gamma \sim e^{-E_0/W_{\text{ext}}}$, where E_0 is the energy of the system that nucleates and $W_{\text{ext}} = F\ell$ is the work done by the external force F, that provides the

energy for the nucleation, through the typical distance ℓ separating the created pair. We can then show that the creation probability for a black hole pair in a dS background is given by $\Gamma \sim e^{-M/\sqrt{\Lambda}}$, in agreement with the exact results. Indeed, one has $E_0 \sim 2M$, where M is the rest energy of the black hole, and $W_{\text{ext}} \sim \sqrt{\Lambda}$ is the work provided by the cosmological background. To derive $W_{\text{ext}} \sim \sqrt{\Lambda}$ one can argue as follows. In the dS case, the Newtonian potential is $\Phi = \Lambda r^2/3$ and its derivative yields the force per unit mass or acceleration, Λr, where r is the characteristic dS radius, $\Lambda^{-1/2}$. The force can then be written as $F = \text{mass} \times \text{acceleration} \sim \sqrt{\Lambda}\sqrt{\Lambda}$, where the characteristic mass of the system is $\sqrt{\Lambda}$. Thus, the characteristic work is $W_{\text{ext}} = \text{force} \times \text{distance} \sim \Lambda\Lambda^{-1/2} \sim \sqrt{\Lambda}$, where the characteristic distance that separates the pair at the creation moment is $\Lambda^{-1/2}$. So, from the Boltzmann factor we indeed expect that the creation rate of a black hole pair in a dS background is given by $\Gamma \sim e^{-M/\sqrt{\Lambda}}$. This expression is in agreement with our results since from (10.24), one has $M \sim \rho^{D-3} \sim \Lambda^{-(D-3)/2}$, and thus $\Gamma \sim e^{-M/\sqrt{\Lambda}} \sim e^{\Lambda^{-(D-2)/2}}$.

Chapter 12

Gravitational radiation in higher dimensional spacetimes and energy released during black hole creation

Contents

One expects to finally detect gravitational waves in the forthcoming years. If this happens, and if the observed waveforms match the predicted templates, General Relativity will have pass a crucial test. Moreover, if one manages to cleanly separate gravitational waveforms, we will open a new and exciting window to the Universe, a window from which one can look directly into the heart of matter, as gravitational waves are weakly scattered by matter. A big effort has been spent in the last years trying to build gravitational wave detectors, and a new era will begin with gravitational wave astronomy [213, 214]. What makes gravitational wave astronomy attractive, the weakness with which gravitational waves are scattered by matter, is also the major source of technical difficulties when trying to develop an apparatus which interacts with them. Nevertheless, some of these highly non-trivial technical difficulties have been surmounted, and we have detectors already operating [215, 216, 217]. Another effort is being dedicated by theoreticians trying to obtain accurate templates for the various physical processes that may give rise to the waves impinging on the detector. We now have a well established theory of wave generation and propagation, which started with Einstein and his quadrupole formula. The quadrupole formula expresses the energy lost to gravitational waves by a system moving at low velocities, in terms of its energy content. The quadrupole formalism is the most famous example of slow motion techniques to compute wave generation. All these techniques break Einstein's equations non-linearity by imposing a power series in some small quantity and keeping only the lowest or the lowest few order terms. The quadrupole formalism starts from a flat background and expands the relevant quantities in R/λ, where R is the size of source and λ the wavelength of waves. Perturbation formalisms on the other hand, start from some non-radiative background, whose metric is known exactly, for example the Schwarzschild metric, and expand in deviations from that background metric. For a catalog of the various methods and their description we refer the reader to the review works by Thorne [218] and Damour [219]. The necessity to develop all such methods was driven of course by the lack of exact radiative solutions to Einstein's equations (although there are some worthy exceptions, like the C-metric [84]), and by the fact that even nowadays solving the full set of Einstein's equations numerically is a monumental task, and has been done only for the more tractable physical situations. All the existing methods seem to agree with each other when it comes down to the computation of waveforms and energies radiated during physical situations, and also agree with the few available results from a fully numerical evolution of Einstein's equations.

In this chapter we extend some of these results to higher dimensional spacetimes. There are several reasons why one should now try to do it. It seems impossible to formulate in four dimensions a consistent theory which unifies gravity with the other forces in nature. Thus, most efforts in this direction have considered a higher dimensional arena for our universe, one example being string theories which have recently made some remarkable achievements. Moreover, recent investigations [193] propose the existence of extra dimensions in our Universe in order to solve the hierarchy problem, i.e., the huge difference between the electroweak and the Planck scale, $m_{\mathrm{EW}}/M_{\mathrm{Pl}} \sim 10^{-17}$. The fields of standard model would inhabit a 4-dimensional sub-manifold, the brane, whereas the gravitational degrees of freedom would propagate throughout all dimensions. One of the most spectacular consequences of this scenario would be the production of black holes at the Large Hadron Collider at CERN [194, 198, 197, 297] (for recent relevant work related to this topic we refer the reader to [226, 225, 224, 220, 222]). Now, one of the experimental signatures of black hole production will be a missing energy, perhaps a large fraction of the center of mass energy [220]. This will happen because when the partons collide to form a black hole, some of the initial energy will be converted to gravitational waves, and due to the small amplitudes involved, there is no gravitational wave detector capable of detecting them, so they will appear as missing. Thus, the collider could in fact indirectly serve as a gravitational wave detector. This calls for the calculation of the energy given away as gravitational waves when two high energy particles collide to form a black hole, which lives in all the dimensions. The work done so far on this subject [201, 200] in higher dimensions, is mostly geometric, and generalizes a construction by Penrose to find trapped surfaces on the union of two shock waves, describing boosted Schwarzschild black holes. On the other hand, there are clues [220, 222] indicating that a formalism described by Weinberg [184] to compute the gravitational energy radiated in the collision of two point particles, gives results correct to a order of magnitude when applied to the collision of two black holes. This formalism assumes a hard collision, i.e., a collision lasting zero seconds. It would be important to apply this formalism in higher dimensions, trying to see if there is agreement between both results. This will be one of the topics discussed in this chapter. The other topic we study in this chapter is the quadrupole formula in higher dimensions. Due to the difficulties in handling the wave tails in odd dimensions we concentrate our study in even dimensions.

In this chapter we follow [185] and it is organized as follows. In section 12.1 we linearize Einstein's equations in a flat D-dimensional background and arrive at an inhomogeneous wave equation for the metric perturbations. The source free equations are analyzed in terms of plane waves, and then the general solution to the homogeneous equation is deduced in terms of the D-dimensional retarded Green's function. In section 12.2 we compute the D-dimensional quadrupole formula (assuming slowly moving sources), expressing the metric and the radiated energy in terms of the time-time component of the energy-momentum tensor. We then apply the quadrupole formula to two cases: a particle in circular motion in a generic background, and a particle falling into a D-dimensional Schwarzschild black hole. In section 12.3 we consider the hard collision between two particles, i.e., the collision takes zero seconds, and introduce a cutoff frequency necessary to have meaningful results. We then apply to the case where one of the colliding particles is a black hole. We propose that this cutoff should be related to the gravitational quasinormal frequency of the black hole, and compute some values of the scalar quasinormal frequencies for higher dimensional Schwarzschild black holes, expecting that the gravitational quasinormal frequencies will behave in the same manner. Finally, we apply this formalism to compute the generation of gravitational radiation during black hole pair creation in four and higher dimensions, a result that has never been worked out, even for $D = 4$. In our presentation we shall mostly follow Weinberg's [184] exposition.

12.1 Linearized D-dimensional Einstein's equations

Due to the non-linearity of Einstein's equations, the treatment of the gravitational radiation problem is not an easy one since the energy-momentum tensor of the gravitational wave contributes to its own gravitational field. To overcome this difficulty it is a standard procedure to work only with the

weak radiative solution, in the sense that the energy-momentum content of the gravitational wave is small enough in order to allow us to neglect its contribution to its own propagation. This approach is justified in practice since we expect the detected gravitational radiation to be of low intensity.

12.1.1 The inhomogeneous wave equation

We begin this subsection by introducing the general background formalism (whose details can be found, e.g., in [184]) that will be needed in later sections. Then we obtain the linearized inhomogeneous wave equation.

Greek indices vary as $0, 1, \cdots, D-1$ and latin indices as $1, \cdots, D-1$ and our units are such that $c \equiv 1$. We work on a D-dimensional spacetime described by a metric $g_{\mu\nu}$ that approaches asymptotically the D-dimensional Minkowski metric $\eta_{\mu\nu} = \mathrm{diag}(-1, +1, \cdots, +1)$, and thus we can write

$$g_{\mu\nu} = \eta_{\mu\nu} + h_{\mu\nu} \qquad \mu, \nu = 0, 1, \cdots, D-1, \tag{12.1}$$

where $h_{\mu\nu}$ is small, i.e., $|h_{\mu\nu}| << 1$, so that it represents small corrections to the flat background. The exact Einstein field equations, $G_{\mu\nu} = 8\pi \mathcal{G} T_{\mu\nu}$ (with $\mathcal{G}$ being the usual Newton constant), can then be written as

$$R^{(1)}{}_{\mu\nu} - \frac{1}{2}\eta_{\mu\nu} R^{(1)\,\alpha}{}_{\alpha} = 8\pi \mathcal{G}\ \tau_{\mu\nu}, \tag{12.2}$$

with

$$\tau^{\mu\nu} \equiv \eta^{\mu\alpha} \eta^{\nu\beta} \left(T_{\alpha\beta} + t_{\alpha\beta}\right). \tag{12.3}$$

Here $R^{(1)}{}_{\mu\nu}$ is the part of the Ricci tensor linear in $h_{\mu\nu}$, $R^{(1)\,\alpha}{}_{\alpha} = \eta^{\alpha\beta} R^{(1)}{}_{\beta\alpha}$, and $\tau_{\mu\nu}$ is the effective energy-momentum tensor, containing contributions from $T_{\mu\nu}$, the energy-momentum tensor of the matter source, and $t_{\mu\nu}$ which represents the gravitational contribution. The pseudo-tensor $t_{\mu\nu}$ contains the difference between the exact Ricci terms and the Ricci terms linear in $h_{\mu\nu}$,

$$t_{\mu\nu} = \frac{1}{8\pi\mathcal{G}} \left[R_{\mu\nu} - \frac{1}{2} g_{\mu\nu} R^{\alpha}{}_{\alpha} - R^{(1)}{}_{\mu\nu} + \frac{1}{2}\eta_{\mu\nu} R^{(1)\,\alpha}{}_{\alpha} \right]. \tag{12.4}$$

The Bianchi identities imply that $\tau_{\mu\nu}$ is locally conserved,

$$\partial_\mu \tau^{\mu\nu} = 0. \tag{12.5}$$

Introducing the cartesian coordinates $x^\alpha = (t, \mathbf{x})$ with $\mathbf{x} = x^i$, and considering a $D-1$ volume V with a boundary spacelike surface S with dimension $D-2$ whose unit exterior normal is $\mathbf{n}$, eq. (12.5) yields

$$\frac{d}{dt} \int_V d^{D-1}\mathbf{x}\ \tau^{0\nu} = -\int_S d^{D-2}\mathbf{x}\ n_i \tau^{i\nu}. \tag{12.6}$$

This means that one may interpret

$$p^\nu \equiv \int_V d^{D-1}\mathbf{x}\ \tau^{0\nu} \tag{12.7}$$

as the total energy-momentum (pseudo)vector of the system, including matter and gravitation, and $\tau^{i\nu}$ as the corresponding flux. Since the matter contribution is contained in $t^{\mu\nu}$, the flux of gravitational radiation is

$$\mathrm{Flux} = \int_S d^{D-2}\mathbf{x}\ n_i t^{i\nu}. \tag{12.8}$$

In this context of linearized general relativity, we neglect terms of order higher than the first in $h_{\mu\nu}$ and all the indices are raised and lowered using $\eta^{\mu\nu}$. We also neglect the contribution of the gravitational energy-momentum tensor $t_{\mu\nu}$ (i.e., $|t_{\mu\nu}| << |T_{\mu\nu}|$) since from (12.4) we see that $t_{\mu\nu}$ is of higher order in $h_{\mu\nu}$. Then, the conservation equations (12.5) yield

$$\partial_\mu T^{\mu\nu} = 0. \tag{12.9}$$

In this setting and choosing the convenient coordinate system that obeys the harmonic (also called Lorentz) gauge conditions,

$$2\partial_\mu h^\mu{}_\nu = \partial_\nu h^\alpha{}_\alpha \tag{12.10}$$

(where $\partial_\mu = \partial/\partial x^\mu$), the first order Einstein field equations (12.2) yield

$$\Box h_{\mu\nu} = -16\pi\mathcal{G}S_{\mu\nu}\,, \tag{12.11}$$

$$S_{\mu\nu} = T_{\mu\nu} - \frac{1}{D-2}\,\eta_{\mu\nu}\,T^\alpha{}_\alpha\,, \tag{12.12}$$

where $\Box = \eta^{\mu\nu}\partial_\mu\partial_\nu$ is the D-dimensional Laplacian, and $S_{\mu\nu}$ will be called the modified energy-momentum tensor of the matter source. Eqs. (12.11) and (12.12) subject to (12.10) allow us to find the gravitational radiation produced by a matter source $S_{\mu\nu}$.

12.1.2   The plane wave solutions

In vacuum, the linearized equations for the gravitational field are $R^{(1)}{}_{\mu\nu} = 0$ or, equivalently, the homogeneous equations $\Box h_{\mu\nu} = 0$, subjected to the harmonic gauge conditions (12.10). The solutions of these equations, the plane wave solutions, are important since the general solutions of the inhomogeneous equations (12.10) and (12.11) approach the plane wave solutions at large distances from the source. Setting $k_\alpha = (-\omega, \mathbf{k})$ with ω and $\mathbf{k}$ being respectively the frequency and wave vector, the plane wave solutions can be written as a linear superposition of solutions of the kind

$$h_{\mu\nu}(t, \mathbf{x}) = e_{\mu\nu}\,e^{ik_\alpha x^\alpha} + e^*_{\mu\nu}\,e^{-ik_\alpha x^\alpha}\,, \tag{12.13}$$

where $e_{\mu\nu} = e_{\nu\mu}$ is called the polarization tensor and * means the complex conjugate. These solutions satisfy eq. (12.11) with $S_{\mu\nu} = 0$ if $k_\alpha k^\alpha = 0$, and obey the harmonic gauge conditions (12.10) if $2\,k_\mu e^\mu{}_\nu = k_\nu e^\mu{}_\mu$.

An important issue that must be addressed is the number of different polarizations that a gravitational wave in D dimensions can have. The polarization tensor $e_{\mu\nu}$, being symmetric, has in general $D(D+1)/2$ independent components. However, these components are subjected to the D harmonic gauge conditions that reduce by D the number of independent components. In addition, under the infinitesimal change of coordinates $x'^\mu = x^\mu + \xi^\mu(x)$, the polarization tensor transforms into $e'_{\mu\nu} = e_{\mu\nu} - \partial_\nu\xi_\mu - \partial_\mu\xi_\nu$. Now, $e'_{\mu\nu}$ and $e_{\mu\nu}$ describe the same physical system for arbitrary values of the D parameters $\xi^\mu(x)$. Therefore, the number of independent components of $e_{\mu\nu}$, i.e., the number of polarization states of a gravitational wave in D dimensions is $D(D+1)/2 - D - D = D(D-3)/2$. From this computation we can also see that gravitational waves are present only when $D > 3$. Therefore, from now on we assume D > 3 whenever we refer to D. In what concerns the helicity of the gravitational waves, for arbitrary D the gravitons are always spin 2 particles.

To end this subsection on gravitational plane wave solutions, we present the average gravitational energy-momentum tensor of a plane wave, a quantity that will be needed later. Notice that in vacuum, since the matter contribution is zero ($T_{\mu\nu} = 0$), we cannot neglect the contribution of the gravitational energy-momentum tensor $t_{\mu\nu}$. From eq. (12.4), and neglecting terms of order higher than h^2, the gravitational energy-momentum tensor of a plane wave is given by

$$t_{\mu\nu} \simeq \frac{1}{8\pi\mathcal{G}}\left[R^{(2)}{}_{\mu\nu} - \frac{1}{2}\eta_{\mu\nu}R^{(2)\,\alpha}{}_\alpha\right]\,, \tag{12.14}$$

and through a straightforward calculation (see e.g. [184] for details) we get the average gravitational energy-momentum tensor of a plane wave,

$$\langle t_{\mu\nu}\rangle = \frac{k_\mu k_\nu}{16\pi\mathcal{G}}\left[e^{\alpha\beta}e^*_{\alpha\beta} - \frac{1}{2}|e^\alpha{}_\alpha|^2\right]\,. \tag{12.15}$$

Chapter 12. Gravitational radiation in higher dimensional spacetimes and energy released during black hole creation

12.1.3 The D-dimensional retarded Green's function

The general solution to the inhomogeneous differential equation (12.11) may be found in the usual way in terms of a Green's function as

$$h_{\mu\nu}(t,\mathbf{x}) = -16\pi\mathcal{G}\int dt'\int d^{D-1}\mathbf{x}'S_{\mu\nu}(t',\mathbf{x}')G(t-t',\mathbf{x}-\mathbf{x}') + \text{homogeneous solutions}, \quad (12.16)$$

where the Green's function $G(t-t',\mathbf{x}-\mathbf{x}')$ satisfies

$$\eta^{\mu\nu}\partial_\mu\partial_\nu G(t-t',\mathbf{x}-\mathbf{x}') = \delta(t-t')\delta(\mathbf{x}-\mathbf{x}'), \quad (12.17)$$

where $\delta(z)$ is the Dirac delta function. In the momentum representation this reads

$$G(t,\mathbf{x}) = -\frac{1}{(2\pi)^D}\int d^{D-1}\mathbf{k}e^{i\mathbf{k}\cdot\mathbf{x}}\int d\omega\frac{e^{-i\omega t}}{\omega^2 - k^2}, \quad (12.18)$$

where $k^2 = k_1^2 + k_2^2 + ... + k_{D-1}^2$. To evaluate this, it is convenient to perform the k-integral by using spherical coordinates in the $(D-1)$-dimensional k-space. The required transformation is given by

$$x_1 = r\prod_{i=1}^{D-2}\sin\theta_i$$

$$\cdots$$

$$x_j = r\left(\prod_{i=1}^{D-j}\sin\theta_i\right)\cos\theta_{D+1-j}, \quad \text{for } 3 \le j < D$$

$$\cdots$$

$$x_{D-1} = r\cos\theta_1. \quad (12.19)$$

The result for the retarded Green's function in these spherical coordinates is

$$G^{\text{ret}}(t,\mathbf{x}) = -\frac{\Theta(t)}{(2\pi)^{(D-1)/2}}\times\frac{1}{r^{(D-3)/2}}\int k^{(D-3)/2}J_{(D-3)/2}(kr)\sin(kt)dk, \quad (12.20)$$

where $r^2 = x_1^2 + x_2^2 + ... + x_{D-1}^2$, and $\Theta(t)$ is the Heaviside function defined as

$$\Theta(t) = \begin{cases} 1 & \text{if } t > 0 \\ 0 & \text{if } t < 0. \end{cases} \quad (12.21)$$

The function $J_{(D-3)/2}(kr)$ is a Bessel function [298, 292]. The structure of the retarded Green's function will depend on the parity of D, as we shall see. This dependence on the parity, which implies major differences between even and odd spacetime dimensions, is connected to the structure of the Bessel function. For even D, the index of the Bessel function is semi-integer and then the Bessel function is expressible in terms of elementary functions, while for odd D this does not happen. A concise explanation of the difference between retarded Green's function in even and odd D, and the physical consequences that entails is presented in [299] (see also [300, 301, 302]). A complete derivation of the Green's function in higher dimensional spaces may be found in Hassani [303]. The result is

$$G^{\text{ret}}(t,\mathbf{x}) = \frac{1}{4\pi}\left[-\frac{\partial}{2\pi r\partial r}\right]^{(D-4)/2}\left[\frac{\delta(t-r)}{r}\right], \quad D \text{ even}. \quad (12.22)$$

$$G^{\text{ret}}(t,\mathbf{x}) = \frac{\Theta(t)}{2\pi}\left[-\frac{\partial}{2\pi r\partial r}\right]^{(D-3)/2}\left[\frac{1}{\sqrt{t^2 - r^2}}\right], \quad D \text{ odd}. \quad (12.23)$$

It is sometimes convenient to work with the Fourier transform (in the time coordinate) of the Green's function. One finds [303] an analytical result independent of the parity of D

$$G^{\text{ret}}(\omega,\mathbf{x}) = \frac{i^D\pi}{2(2\pi)^{(D-1)/2}}\left(\frac{\omega}{r}\right)^{(D-3)/2}H_{(D-3)/2}^1(\omega r), \quad (12.24)$$

where $H^1_\nu(z)$ is a modified Bessel function [292, 298]. Of course, the different structure of the Green's function for different D is again embodied in these Bessel functions. Equations (12.22) and (12.24), are one of the most important results we shall use in this chapter. For $D = 4$ (12.22) obviously reproduce well known results [303]. Now, one sees from eq. (12.22) that although there are delta function derivatives on the even-D Green's function, the localization of the Green's function on the light cone is preserved. However, eq. (12.23) tells us that the retarded Green's function for odd dimensions is non-zero inside the light cone. The consequence, as has been emphasized by different authors [299, 302, 304], is that for odd D the Huygens principle does not hold: the fact that the retarded Green's function support extends to the interior of the light cone implies the appearance of radiative tails in (12.16). In other words, we still have a propagation phenomenum for the wave equation in odd dimensional spacetimes, in so far as a localized initial state requires a certain time to reach a point in space. Huygens principle no longer holds, because the effect of the initial state is not sharply limited in time: once the signal has reached a point in space, it persists there indefinitely as a reverberation.

This fact coupled to the analytic structure of the Green's function in odd dimensions make it hard to get a grip on radiation generation in odd dimensional spacetimes. Therefore, from now on we shall focus on even dimensions, for which the retarded Green's function is given by eq. (12.22).

12.1.4 The even D-dimensional retarded solution in the wave zone

The retarded solution for the metric perturbation $h_{\mu\nu}$, obtained by using the retarded Green's function (12.22) and discarding the homogeneous solution in (12.16) will be given by

$$h_{\mu\nu}(t, \mathbf{x}) = 16\pi\mathcal{G} \int dt' \int d^{D-1}\mathbf{x}' S_{\mu\nu}(t', \mathbf{x}') G^{\text{ret}}(t - t', \mathbf{x} - \mathbf{x}'), \tag{12.25}$$

with $G^{\text{ret}}(t - t', \mathbf{x} - \mathbf{x}')$ as in eq. (12.22). For $D = 4$ for example one has

$$G^{\text{ret}}(t, \mathbf{x}) = \frac{1}{4\pi} \frac{\delta(t - r)}{r}, \quad D = 4, \tag{12.26}$$

which is the well known result. For $D = 6$, we have

$$G^{\text{ret}}(t, \mathbf{x}) = \frac{1}{8\pi^2} \left(\frac{\delta'(t - r)}{r^2} + \frac{\delta(t - r)}{r^3} \right), \quad D = 6, \tag{12.27}$$

where the $\delta'(t - r)$ means derivative of the Dirac delta function with respect to its argument. For $D = 8$, we have

$$G^{\text{ret}}(t, \mathbf{x}) = \frac{1}{16\pi^3} \left(\frac{\delta''(t - r)}{r^3} + 3\frac{\delta'(t - r)}{r^4} + 3\frac{\delta(t - r)}{r^5} \right), \quad D = 8. \tag{12.28}$$

We see that in general even-D dimensions the Green's function consists of inverse integer powers in r, spanning all values between $\frac{1}{r^{(D-2)/2}}$ and $\frac{1}{r^{D-3}}$, including these ones. Now, the retarded solution is given by eq. (12.25) as a product of the Green's function times the modified energy-momentum tensor $S_{\mu\nu}$. The net result of having derivatives on the delta functions is to transfer these derivatives to the energy-momentum tensor as time derivatives (this can be seen by integrating (12.25) by parts in the t-integral).

A close inspection then shows that the retarded field possesses a kind of peeling property in that it consists of terms with different fall off at infinity. Explicitly, this means that the retarded field will consist of a sum of terms possessing all integer inverse powers in r between $\frac{D-2}{2}$ and $D - 3$. The term that dies off more quickly at infinity is the $\frac{1}{r^{D-3}}$, typically a static term, since it comes from the Laplacian. As a matter of fact this term was already observed in the higher dimensional black hole by Tangherlini [202] (see also Myers and Perry [203]). We will see that the term falling more slowly, the one that goes like $\frac{1}{r^{(D-2)/2}}$, gives rise to gravitational radiation. It is well defined,

in the sense that the power crossing sufficiently large hyperspheres with different radius is the same, because the volume element goes as r^{D-2} and the energy as $|h|^2 \sim \frac{1}{r^{D-2}}$.

In radiation problems, one is interested in finding out the field at large distances from the source, $r >> \lambda$, where λ is the wavelength of the waves, and also much larger than the source's dimensions R. This is defined as the wave zone. In the wave zone, one may neglect all terms in the Green's function that decay faster than $\frac{1}{r^{(D-2)/2}}$. So, in the wave zone, we find

$$h_{\mu\nu}(t, \mathbf{x}) = -8\pi\mathcal{G} \frac{1}{(2\pi r)^{(D-2)/2}} \partial_t^{(\frac{D-4}{2})} \left[\int d^{D-1}\mathbf{x}' S_{\mu\nu}(t - |\mathbf{x} - \mathbf{x}'|, \mathbf{x}') \right], \qquad (12.29)$$

where $\partial_t^{(\frac{D-4}{2})}$ stands for the $\frac{D-4}{2}$th derivative with respect to time. For $D = 4$ eq. (12.29) yields the standard result [184]:

$$h_{\mu\nu}(t, \mathbf{x}) = -\frac{4\mathcal{G}}{r} \int d^{D-1}\mathbf{x}' S_{\mu\nu}(t - |\mathbf{x} - \mathbf{x}'|, \mathbf{x}'), \quad D = 4. \qquad (12.30)$$

To find the Fourier transform of the metric, one uses the representation (12.24) for the Green's function. Now, in the wave zone, the Green's function may be simplified using the asymptotic expansion for the Bessel function [292]

$$H^1_{(D-3)/2}(\omega r) \sim \sqrt{\frac{2}{\pi(\omega r)}} e^{i\left[\omega r - \frac{\pi}{4}(D-2)\right]}, \quad \omega r \to \infty. \qquad (12.31)$$

This yields

$$h_{\mu\nu}(\omega, \mathbf{x}) = -\frac{8\pi\mathcal{G}}{(2\pi r)^{(D-2)/2}} \omega^{(D-4)/2} e^{i\omega r} \int d^{D-1}\mathbf{x}' S_{\mu\nu}(\omega, \mathbf{x}'). \qquad (12.32)$$

This could also have been arrived at directly from (12.29), using the rule time derivative $\to -i\omega$ for Fourier transforms. Equations (12.29) and (12.32) are one of the most important results derived in this chapter, and will be the basis for all the subsequent section. Similar equations, but not as general as the ones presented here, were given by Chen, Li and Lin [305] in the context of gravitational radiation by a rolling tachyon.

To get the energy spectrum, we use (12.12) yielding

$$\frac{d^2E}{d\omega d\Omega} = 2\mathcal{G} \frac{\omega^{D-2}}{(2\pi)^{D-4}} \left(T^{\mu\nu}(\omega, \mathbf{k}) T^*_{\mu\nu}(\omega, \mathbf{k}) - \frac{1}{D-2} |T^\lambda_{\ \lambda}(\omega, \mathbf{k})|^2 \right). \qquad (12.33)$$

12.2 The even D-dimensional quadrupole formula

12.2.1 Derivation of the even D-dimensional quadrupole formula

When the velocities of the sources that generate the gravitational waves are small, it is sufficient to know the T^{00} component of the gravitational energy-momentum tensor in order to have a good estimate of the energy they radiate. In this subsection, we will deduce the D-dimensional quadrupole formula and in the next subsection we will apply it to (1) a particle in circular orbit and (2) a particle in free fall into a D-dimensional Schwarzschild black hole.

We start by recalling that the Fourier transform of the energy-momentum tensor is

$$T_{\mu\nu}(\omega, \mathbf{k}) = \int d^{D-1}\mathbf{x}' e^{-i\mathbf{k}\cdot\mathbf{x}'} \int dt \, e^{i\omega t} \, T^{\mu\nu}(t, \mathbf{x}) + \text{c.c.}, \qquad (12.34)$$

where c.c. means the complex conjugate of the preceding term. Then, the conservation equations (12.9) for $T^{\mu\nu}(t, \mathbf{x})$ applied to eq. (12.34) yield $k^\mu T_{\mu\nu}(\omega, \mathbf{k}) = 0$. Using this last result we obtain $T_{00}(\omega, \mathbf{k}) = \hat{k}^j \hat{k}^i T_{ji}(\omega, \mathbf{k})$ and $T_{0i}(\omega, \mathbf{k}) = -\hat{k}^j T_{ji}(\omega, \mathbf{k})$, where $\hat{k} = \mathbf{k}/\omega$. We can then write the energy spectrum, eq. (12.33), as a function only of the spacelike components of $T^{\mu\nu}(\omega, \mathbf{k})$,

$$\frac{d^2E}{d\omega d\Omega} = 2\mathcal{G} \frac{\omega^{D-2}}{(2\pi)^{D-4}} \Lambda_{ij,lm}(\hat{k}) T^{*ij}(\omega, \mathbf{k}) T^{ij}(\omega, \mathbf{k}), \qquad (12.35)$$

where

$$\Lambda_{ij,\,lm}(\hat{k}) = \delta_{il}\delta_{jm} - 2\hat{k}_j\hat{k}_m\delta_{il} + \frac{1}{D-2}\left(-\delta_{ij}\delta_{lm} + \hat{k}_l\hat{k}_m\delta_{ij} + \hat{k}_i\hat{k}_j\delta_{lm}\right) + \frac{D-3}{D-2}\hat{k}_i\hat{k}_j\hat{k}_l\hat{k}_m\,. \quad (12.36)$$

At this point, we make a new approximation (in addition to the wave zone approximation) and assume that $\omega R << 1$, where R is the source's radius. In other words, we assume that the internal velocities of the sources are small and thus the source's radius is much smaller than the characteristic wavelength $\sim 1/\omega$ of the emitted gravitational waves. Within this approximation, one can set $e^{-i\mathbf{k}\cdot\mathbf{x}'} \sim 1$ in eq. (12.34) (since $R = |\mathbf{x}'|_{\max}$). Moreover, after a straightforward calculation, one can also set in eq. (12.35) the approximation $T^{ij}(\omega,\mathbf{k}) \simeq -(\omega^2/2)D_{ij}(\omega)$, where

$$D_{ij}(\omega) = \int d^{D-1}\mathbf{x}\, x^i\, x^j\, T^{00}(\omega,\mathbf{x})\,. \quad (12.37)$$

Finally, using

$$\int d\Omega_{D-2}\hat{k}_i\hat{k}_j = \frac{\Omega_{D-2}}{D-1}\delta_{ij}\,,$$

$$\int d\Omega_{D-2}\hat{k}_i\hat{k}_j\hat{k}_l\hat{k}_m = \frac{3\Omega_{D-2}}{D^2-1}(\delta_{ij}\delta_{lm} + \delta_{il}\delta_{jm} + \delta_{im}\delta_{jl})\,, \quad (12.38)$$

where Ω_{D-2} is the $(D-2)$-dimensional solid angle defined in (10.12), we obtain the D-dimensional quadrupole formula

$$\frac{dE}{d\omega} = \frac{2^{2-D}\pi^{-(D-5)/2}\mathcal{G}\,(D-3)D}{\Gamma[(D-1)/2](D^2-1)(D-2)}\,\omega^{D+2}\left[(D-1)D_{ij}^*(\omega)D_{ij}(\omega) - |D_{ii}(\omega)|^2\right]\,, \quad (12.39)$$

where the Gamma function $\Gamma[z]$ is defined in (10.13). As the dimension D grows it is seen that the rate of gravitational energy radiated increases as ω^{D+2}. Sometimes it will be more useful to have the time rate of emitted energy

$$\frac{dE}{dt} = \frac{2^{2-D}\pi^{-(D-5)/2}\mathcal{G}\,(D-3)D}{\Gamma[(D-1)/2](D^2-1)(D-2)}\left[(D-1)\partial_t^{(D+2)/2}D_{ij}^*(t)\partial_t^{(D+2)/2}D_{ij}(t) - |\partial_t^{(D+2)/2}D_{ii}(t)|^2\right]\,. \quad (12.40)$$

For $D = 4$, eq. (12.40) yields the well known result [184]

$$\frac{dE}{dt} = \frac{\mathcal{G}}{5}\left[\partial_t^3 D_{ij}^*(t)\partial_t^3 D_{ij}(t) - \frac{1}{3}|\partial_t^3 D_{ii}(t)|^2\right]\,. \quad (12.41)$$

12.2.2 Applications of the quadrupole formula: test particles in a background geometry

The quadrupole formula has been used successfully in almost all kind of problems involving gravitational wave generation. By successful we mean that it agrees with other more accurate methods. Its simplicity and the fact that it gives results correct to within a few percent, makes it an invaluable tool in estimating gravitational radiation emission. We shall in the following present two important examples of the application of the quadrupole formula.

12.2.2.a A particle in circular orbit

The radiation generated by particles in circular motion was perhaps the first situation to be considered in the analysis of gravitational wave generation. For orbits with low frequency, the quadrupole formula yields excellent results. As expected it is difficult to find in nature a system with perfect circular orbits, they will in general be elliptic. In this case the agreement is also remarkable, and one finds that the quadrupole formalism can account with precision for the increase in period of the pulsar PSR 1913+16, due to gravitational wave emission [306]. In four dimensions the full treatment

of elliptic orbital motion is discussed by Peters [307]. In dimensions higher than four, it has been shown [202] that there are no stable geodesic circular orbits, and so geodesic circular motion is not as interesting for higher D. For this reason, and also because we only want to put in evidence the differences that arise in gravitational wave emission as one varies the spacetime dimension D, we will just analyze the simple circular, not necessarily geodesic motion, to see whether the results are non-trivially changed as one increases D. Consider then two bodies of equal mass m in circular orbits a distance l apart. Suppose they revolve around the center of mass, which is at $l/2$ from both masses, and that they orbit with frequency ω in the $x - y$ plane. A simple calculation [307, 308] yields

$$D_{xx} = \frac{ml^2}{4} \cos(2\omega t) + \text{const} , \tag{12.42}$$

$$D_{yy} = -D_{xx} , \tag{12.43}$$

$$D_{xy} = \frac{ml^2}{4} \sin(2\omega t) + \text{const} , \tag{12.44}$$

independently of the dimension in which they are imbedded and with all other components being zero. We therefore get from eq. (12.40)

$$\frac{dE}{dt} = \frac{2\mathcal{G}D(D - 3)}{\pi^{(D-5)/2}\Gamma[(D - 1)/2](D + 1)(D - 2)} m^2 l^4 \omega^{D+2}. \tag{12.45}$$

For $D = 4$ one gets

$$\frac{dE}{dt} = \frac{8\mathcal{G}}{5} m^2 l^4 \omega^6 , \tag{12.46}$$

which agrees with known results [307, 308]. Eq. (12.45) is telling us that as one climbs up in dimension number D, the frequency effects gets more pronounced.

12.2.2.b   A particle falling radially into a higher dimensional Schwarzschild black hole

As yet another example of the use of the quadrupole formula eq. (12.40) we now calculate the energy given away as gravitational waves when a point particle, with mass m falls into a D-dimensional Schwarzschild black hole, a metric first given in [202]. Historically, the case of a particle falling into a $D = 4$ Schwarzschild black hole was one of the first to be studied [309, 310] in connection with gravitational wave generation, and later served as a model calculation when one wanted to evolve Einstein's equations fully numerically [311, 312]. This process was first studied [310] by solving numerically Zerilli's [309] wave equation for a particle at rest at infinity and then falling into a Schwarzschild black hole. Davis et al [310] found numerically that the amount of energy radiated to infinity as gravitational waves was $\Delta E_{\text{num}} = 0.01\frac{m^2}{M}$, where m is the mass of the particle falling in and M is the mass of the black hole. It is found that the $D = 4$ quadrupole formula yields [313] $\Delta E_{\text{quad}} = 0.019\frac{m^2}{M}$, so it is of the order of magnitude as that given by fully relativistic numerical results. Despite the fact that the quadrupole formula fails somewhere near the black hole (the motion is not slow, and the background is certainly not flat), it looks like one can get an idea of how much radiation will be released with the help of this formula. Based on this good agreement, we shall now consider this process but for higher dimensional spacetimes. The metric for the D-dimensional Schwarzschild black hole in $(t, r, \theta_1, \theta_2, .., \theta_{D-2})$ coordinates is (see section 10.1)

$$ds^2 = -\left(1 - \frac{16\pi\mathcal{G}M}{(D - 2)\Omega_{D-2}}\frac{1}{r^{D-3}}\right) dt^2 + \left(1 - \frac{16\pi\mathcal{G}M}{(D - 2)\Omega_{D-2}}\frac{1}{r^{D-3}}\right)^{-1} dr^2 + r^2 d\Omega_{D-2}^2. \tag{12.47}$$

Consider a particle falling along a radial geodesic, and at rest at infinity. Then, the geodesic equations give

$$\frac{dr}{dt} \sim \frac{16\pi\mathcal{G}M}{(D - 2)\Omega_{D-2}}\frac{1}{r^{D-3}} , \tag{12.48}$$

Table 12.1: The energy radiated by a particle falling from rest into a higher dimensional Schwarzschild black hole, as a function of dimension. The integration is stopped at $b \times r_+$ where r_+ is the horizon radius.

$\Delta E \times \frac{M}{m^2}$		
D	$b = 1$:	$b = 1.2$:	$b = 1.3$:
4	0.019	0.01	0.0076
6	0.576	0.05	0.0167
8	180	1.19	0.13
10	24567	6.13	0.16
12	3.3×10^6	14.77	0.0665

where we make the flat space approximation $t = \tau$. We then have, in these coordinates, $D_{11} = r^2$, and all other components vanish. From (12.40) we get the energy radiated per second, which yields

$$\frac{dE}{dt} = \frac{2^{2-D}\pi^{-(D-5)/2}\mathcal{G}\,(D-3)}{\Gamma[(D-1)/2](D^2-1)}D|\partial_t^{(\frac{D+2}{2})}D_{11}|^2\,, \tag{12.49}$$

We can perform the derivatives and integrate to get the total energy radiated. There is a slight problem though, where do we stop the integration? The expression for the energy diverges at $r = 0$ but this is no problem, as we know that as the particle approaches the horizon, the radiation will be infinitely red-shifted. Moreover, the standard picture [313] is that of a particle falling in, and in the last stages being frozen near the horizon. With this in mind we integrate from $r = \infty$ to some point near the horizon, say $r = b \times r_+$, where r_+ is the horizon radius and b is some number larger than unit, and we get

$$\Delta E = A\frac{D(D-2)\pi}{2^{2D-4}} \times b^{(9-D^2)/2} \times \frac{m^2}{M}\,, \tag{12.50}$$

where

$$A = \frac{(3-D)^2(5-D)^2(7-3D)^2(8-4D)^2(9-5D)^2...(D/2+4-D^2/2)^2}{\Gamma[(D-1)/2]^2(D-1)(D+1)(D+3)} \tag{12.51}$$

To understand the effect of both the dimension number D and the parameter b on the total energy radiated according to the quadrupole formula, we list in Table 1 some values ΔE for different dimensions, and b between 1 and 1.3.

The parameter b is in fact a measure of our ignorance of what goes on near the black hole horizon, so if the energy radiated doesn't vary much with b it means that our lack of knowledge doesn't affect the results very much. For $D = 4$ that happens indeed. Putting $b = 1$ gives only an energy 2.6 times larger than with $b = 1.3$, and still very close to the fully relativistic numerical result of $0.01\frac{m^2}{M}$. However as we increase D, the effect of b increases dramatically. For $D = 12$ for example, we can see that a change in b from 1 to 1.3 gives a corresponding change in ΔE of 3×10^6 to 0.0665. This is 8 orders of magnitude lower! Since there is as yet no Regge-Wheeler-Zerilli [309, 314] wavefunction for higher dimensional Schwarzschild black holes, there are no fully relativistic numerical results to compare our results with. Thus $D = 4$ is just the perfect dimension to predict, through the quadrupole formula, the gravitational energy coming from collisions between particles and black holes, or between small and massive black holes. It is not a problem related to the quadrupole formalism, but rather one related to D. A small change in parameters translates itself, for high D, in a large variation in the final result. Thus, as the dimension D grows, the knowledge of the cutoff radius $b \times r_+$ becomes essential to compute accurately the energy released.

12.3 Instantaneous collisions in even D-dimensions. Energy released during black hole pair creation

In general, whenever two bodies collide or scatter there will be gravitational energy released due to the changes in momentum involved in the process. If the collision is hard meaning that the incoming and outgoing trajectories have constant velocities, there is a method first envisaged by Weinberg [184, 315], later explored in [316] by Smarr to compute exactly the metric perturbation and energy released. The method is valid for arbitrary velocities (one will still be working in the linear approximation, so energies have to be low). Basically, it assumes a collision lasting for zero seconds. It was found that in this case the resulting spectra were flat, precisely what one would expect based on one's experience with electromagnetism [187], and so to give a meaning to the total energy, a cutoff frequency is needed. This cutoff frequency depends upon some physical cutoff in the particular problem. We shall now generalize this construction for arbitrary dimensions.

12.3.1 Derivation of the Radiation Formula in terms of a cutoff for a head-on collision. Energy released during formation of black hole at LHC

Consider therefore a system of freely moving particles with D-momenta P_i^μ, energies E_i and $(D-1)$-velocities $\mathbf{v}$, which due to the collision change abruptly at $t = 0$, to corresponding primed quantities. For such a system, the energy-momentum tensor is

$$T^{\mu\nu}(t, \mathbf{v}) = \sum \frac{P_i^\mu P_i^\nu}{E_i} \delta^{D-1}(\mathbf{x} - \mathbf{v}t)\Theta(-t) + \frac{P_i'^\mu P_i'^\nu}{E_i'} \delta^{D-1}(\mathbf{x}' - \mathbf{v}'t)\Theta(t) , \qquad (12.52)$$

from which, using eqs. (12.32) and (12.33) one can get the quantities $h_{\mu\nu}$ and also the radiation emitted. Let us consider the particular case in which one has a head-on collision of two particles, particle 1 with mass m_1 and Lorentz factor γ_1, and particle 2 with mass $m = m_2$ with Lorentz factor γ_2, colliding to form a particle at rest. Without loss of generality, one may orient the axis so that the motion is in the (x_{D-1}, x_D) plane, and the x_D axis is the radiation direction [see (12.19)]. We then have

$$P_1 = \gamma_1 m_1 (1, 0, 0, ..., v_1 \sin\theta_1, v_1 \cos\theta_1) ; \quad P_1' = (E_1', 0, 0, ..., 0, 0) \qquad (12.53)$$
$$P_2 = \gamma_2 m_2 (1, 0, 0, ..., -v_2 \sin\theta_1, -v_2 \cos\theta_1) ; \quad P_2' = (E_2', 0, 0, ..., 0, 0). \qquad (12.54)$$

Momentum conservation leads to the additional relation $\gamma_1 m_1 v_1 = \gamma_2 m_2 v_2$. Replacing (12.53) and (12.54) in the energy-momentum tensor (12.52) and using (12.33) we find

$$\frac{d^2 E}{d\omega d\Omega} = \frac{2\mathcal{G}}{(2\pi)^{D-2}} \frac{D-3}{D-2} \frac{\gamma_1^2 m_1^2 v_1^2 (v_1 + v_2)^2 \sin\theta_1{}^4}{(1 - v_1 \cos\theta_1)^2 (1 + v_2 \cos\theta_1)^2} \times \omega^{D-4} . \qquad (12.55)$$

We see that the for arbitrary (even) D the spectrum is not flat. Flatness happens only for $D = 4$. For any D the total energy, integrated over all frequencies would diverge so one needs a cutoff frequency which shall depend on the particular problem under consideration. Integrating (12.55) from $\omega = 0$ to the cutoff frequency ω_c we have

$$\frac{dE}{d\Omega} = \frac{2\mathcal{G}}{(2\pi)^{D-2}} \frac{1}{D-2} \frac{\gamma_1^2 m_1^2 v_1^2 (v_1 + v_2)^2 \sin\theta_1{}^4}{(1 - v_1 \cos\theta_1)^2 (1 + v_2 \cos\theta_1)^2} \times \omega_c^{D-3} . \qquad (12.56)$$

Two limiting cases are of interest here, namely (i) the collision between identical particles and (ii) the collision between a light particle and a very massive one. In case (i) replacing $m_1 = m_2 = m$, $v_1 = v_2 = v$, eq. (12.56) gives

$$\frac{dE}{d\Omega} = \frac{8\mathcal{G}}{(2\pi)^{D-2}} \frac{1}{D-2} \frac{\gamma^2 m^2 v^4 \sin\theta_1{}^4}{(1 - v^2 \cos^2\theta_1)^2} \times \omega_c^{D-3} . \qquad (12.57)$$

In case (ii) considering $m_1\gamma_1 \equiv m\gamma << m_2\gamma_2$, $v_1 \equiv v >> v_2$, eq. (12.56) yields

$$\frac{dE}{d\Omega} = \frac{2\mathcal{G}}{(2\pi)^{D-2}} \frac{1}{D-2} \frac{\gamma^2 m^2 v^4 \sin\theta_1{}^4}{(1-v\cos\theta_1)^2} \times \omega_c^{D-3}. \tag{12.58}$$

Notice that the technique just described is expected to break down if the velocities involved are very low, since then the collision would not be instantaneous. In fact a condition for this method to work would can be stated

Indeed, one can see from eq. (12.56) that if $v \to 0$, $\frac{dE}{d\omega} \to 0$, even though we know (see Subsection (12.3.1)) that $\Delta E \neq 0$. In any case, if the velocities are small one can use the quadrupole formula instead.

12.3.2 Applications: The cutoff frequency when one of the particles is a black hole and radiation from black hole pair creation

12.3.2.a The cutoff frequency when one of the head-on colliding particles is a black hole

We shall now restrict ourselves to the case (ii) of last subsection, in which at least one of the particles participating in the collision is a massive black hole, with mass $M >> m$ (where we have put $m_1 = m$ and $m_2 = M$). Formulas (12.56)- (12.58) are useless unless one is able to determine the cutoff frequency ω_c present in the particular problem under consideration. In the situation where one has a small particle colliding at high velocities with a black hole, it has been suggested by Smarr [316] that the cutoff frequency should be $\omega_c \sim 1/2M$, presumably because the characteristic collision time is dictated by the large black hole whose radius is $2M$. Using this cutoff he finds

$$\Delta E_{\text{Smarr}} \sim 0.2\gamma^2 \frac{m^2}{M}. \tag{12.59}$$

The exact result, using a relativistic perturbation approach which reduces to the numerical integration of a second order differential equation (the Zerilli wavefunction), has been given by Cardoso and Lemos [222], as

$$\Delta E_{\text{exact}} = 0.26\gamma^2 \frac{m^2}{M}. \tag{12.60}$$

This is equivalent to saying that $\omega_c = \frac{0.613}{M} \sim \frac{1}{1.63M}$, and so it looks like the cutoff is indeed the inverse of the horizon radius. However, in the numerical work by Cardoso and Lemos, it was found that it was not the presence of an horizon that contributed to this cutoff, but the presence of a potential barrier V outside the horizon. By decomposing the field in tensorial spherical harmonics with index l standing for the angular quantum number, we found that for each l, the spectrum is indeed flat (as predicted by eq. (12.56) for $D = 4$), until a cutoff frequency ω_{c_l} which was numerically equal to the lowest gravitational quasinormal frequency ω_{QN}. For $\omega > \omega_{c_l}$ the spectrum decays exponentially. This behavior is illustrated in Fig. 1. The quasinormal frequencies [317] are those frequencies that correspond to only outgoing waves at infinity and only ingoing waves near the horizon. As such the gravitational quasinormal frequencies will in general have a real and an imaginary part, the latter denoting gravitational wave emission and therefore a decay in the perturbation. There have been a wealth of works dwelling on quasinormal modes on asymptotically flat spacetimes [317], due to its close connection with gravitational wave emission, and also on non-asymptotically flat spacetimes, like asymptotically anti-de Sitter [318] or asymptotically de Sitter [319] spacetimes, mainly due to the AdS/CFT and dS/CFT [320] correspondence conjecture. We argue here that it is indeed the quasinormal frequency that dictates the cutoff, and not the horizon radius. For $D = 4$ it so happens that the weighted average of ω_{c_l} is $\frac{0.613}{M}$, which, as we said, is quite similar to $r_+ = \frac{1}{2M}$. The reason for the cutoff being dictated by the quasinormal frequency can be understood using some WKB intuition. The presence of a potential barrier outside the horizon means that waves with some frequencies get reflected back on the barrier while others can cross.
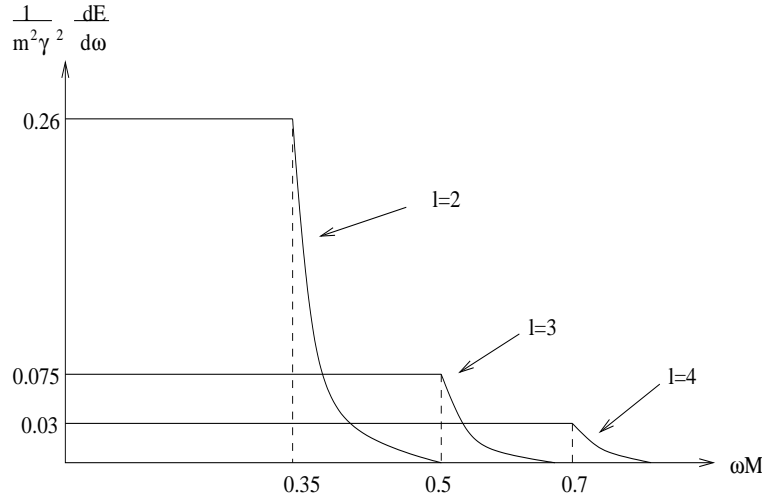
Figure 12.1: The energy spectra as a function of the angular number l, for a highly relativistic particle falling into a $D = 4$ Schwarzschild black hole [222]. The particle begins to fall with a Lorentz factor γ. Notice that for each l there is a cutoff frequency ω_{c_l} which is equal to the quasinormal frequency ω_{QN} after which the spectrum decays exponentially. So it is clearly seen that ω_{QN} works as a cutoff frequency. The total energy radiated is a given by a sum over l, which is the same as saying that the effective cutoff frequency is given by a weighted average of the various ω_{c_l}.

Frequencies such that ω^2 is lower than the maximum barrier height V_{max} will be reflected back to infinity where they will be detected. However, frequencies ω^2 larger than the maximum barrier height cross the barrier and enter the black hole, thereby being absorbed and not contributing to the energy detected at infinity. So only frequencies ω^2 lower than this maximum barrier height are detected at infinity. It has been shown [321] that the gravitational quasinormal frequencies are to first order equal to the square root of the maximum barrier height. In view of this picture, and considering the physical meaning of the cutoff frequency, it seems quite natural to say that the cutoff frequency is equal to the quasinormal frequency. If the frequencies are higher than the barrier height, they don't get reflected back to infinity. This discussion is very important to understand how the total energy varies with the number D of dimensions. In fact, if we set $\omega_c \sim \frac{1}{r_+}$, we find that the total energy radiated decreases rapidly with the dimension number, because r_+ increases rapidly with the dimension. This conflicts with recent results [201, 200], which using shock waves that describe boosted Schwarzschild black holes, and searching for apparent horizons, indicate an increase with D. So, we need the gravitational quasinormal frequencies for higher dimensional Schwarzschild black holes. To arrive at an wave equation for gravitational perturbations of higher dimensional Schwarzschild black holes, and therefore to compute its gravitational quasinormal frequencies, one needs to decompose Einstein's equations in D-dimensional tensorial harmonics, which would lead to some quite complex expressions. It is not necessary to go that far though, because one can get an idea of how the gravitational quasinormal frequencies vary by searching for the quasinormal frequencies of scalar perturbations, and scalar quasinormal frequencies are a lot easier to find. One hopes that the scalar frequencies will behave with D in the same manner as do the gravitational ones. Scalar perturbations in D-dimensional Schwarzschild spacetimes obey the wave equation (consult [322] for details)

$$\frac{\partial^2 \phi(\omega, r)}{\partial r_*^2} + \left[\omega^2 - V(r)\right] \phi(\omega, r) = 0. \tag{12.61}$$

The potential $V(r)$ appearing in equation (12.61) is given by

$$V(r) = f(r) \left[\frac{a}{r^2} + \frac{(D-2)(D-4)f(r)}{4r^2} + \frac{(D-2)f'(r)}{2r}\right], \tag{12.62}$$

12.3 Instantaneous collisions in even D-dimensions. Energy released during black hole pair creation

Table 12.2: The lowest scalar quasinormal frequencies for spherically symmetric ($l = 0$) scalar perturbations of higher dimensional Schwarzschild black holes, obtained using a WKB method [321]. Notice that the real part of the quasinormal frequency is always the same order of magnitude as the square root of the maximum barrier height. We show also the maximum barrier height as well as the horizon radius as a function of dimension D. The mass M of the black hole has been set to 1.

D	$\mathrm{Re}[\omega_{QN}]$:	$\mathrm{Im}[\omega_{QN}]$:	$\sqrt{V_{\max}}$:	$1/r_+$:
4	0.10	-0.12	0.16	0.5
6	1.033	-0.713	1.441	1.28
8	1.969	-1.023	2.637	1.32
10	2.779	-1.158	3.64	1.25
12	3.49	-1.202	4.503	1.17

where $a = l(l + D - 3)$ is the eigenvalue of the Laplacian on the hypersphere S^{D-2}, the tortoise coordinate r_* is defined as $\frac{\partial r}{\partial r_*} = f(r) = \left(1 - \frac{16\pi\mathcal{G}M}{(D-2)\Omega_{D-2}} \frac{1}{r^{D-3}}\right)$, and $f'(r) = \frac{df(r)}{dr}$. We have found the quasinormal frequencies of spherically symmetric ($l = 0$) scalar perturbations, by using a WKB approach developed by Schutz, Will and collaborators [321]. The results are presented in Table 2, where we also show the maximum barrier height of the potential in eq. (12.62), as well as the horizon radius.

The first thing worth noticing is that the real part of the scalar quasinormal frequency is to first order reasonably close to the square root of the maximum barrier height $\sqrt{V_{\max}}$, supporting the previous discussion. Furthermore, the scalar quasinormal frequency grows more rapidly than the inverse of the horizon radius $\frac{1}{r_+}$ as one increases D. In fact, the scalar quasinormal frequency grows with D while the horizon radius r_+ gets smaller. Note that from pure dimensional arguments, for fixed D, $\omega \propto \frac{1}{r_+}$. The statement here is that the constant of proportionality depends on the dimension D, more explicitly it grows with D, and can be found from Table 2. Assuming that the gravitational quasinormal frequencies will have the same behavior (and some very recent studies [323] relating black hole entropy and damped quasinormal frequencies seem to point that way), the total energy radiated will during high-energy collisions does indeed increase with D, as some studies [201, 200] seem to indicate.

12.3.2.b   The gravitational energy radiated during black hole pair creation

As a new application of this instantaneous collision formalism, we will now consider the gravitational energy released during the quantum creation of pairs of black holes, a process which as far as we know has not been analyzed in the context of gravitational wave emission, even for $D = 4$. It is well known that vacuum quantum fluctuations produce virtual electron-positron pairs. These pairs can become real [130] if they are pulled apart by an external electric field, in which case the energy for the pair materialization and acceleration comes from the external electric field energy. Likewise, a black hole pair can be created in the presence of an external field whenever the energy pumped into the system is enough in order to make the pair of virtual black holes real (see chapter 9). If one tries to predict the spectrum of radiation coming from pair creation, one expects of course a spectrum characteristic of accelerated masses but one also expects that this follows some kind of signal indicating pair creation. In other words, the process of pair creation itself, which involves the sudden creation of particles, must imply emission of radiation. It is this phase we shall focus on, forgetting the subsequent emission of radiation caused by the acceleration.

Pair creation is a pure quantum-mechanical process in nature, with no classical explanation. But given that the process does occur, one may ask about the spectrum and intensity of the radiation accompanying it. The sudden creation of pairs can be viewed for our purposes as an instantaneous creation of particles (i.e., the time reverse process of instantaneous collisions), the violent acceleration of particles initially at rest to some final velocity in a very short time, and the technique described

at the beginning of this section applies. This is quite similar to another pure quantum-mechanical process, the beta decay. The electromagnetic radiation emitted during beta decay has been computed classically by Chang and Falkoff [186] and is also presented in Jackson [187]. The classical calculation is similar in all aspects to the one described in this section (the instantaneous collision formalism) assuming the sudden acceleration to energies E of a charge initially at rest, and requires also a cutoff in the frequency, which has been assumed to be given by the uncertainty principle $\omega_c \sim \frac{E}{\hbar}$. Assuming this cutoff one finds that the agreement between the classical calculation and the quantum calculation [186] is extremely good (specially in the low frequency regime), and more important, was verified experimentally. Summarizing, formula (12.57) also describes the gravitational energy radiated when two black holes, each with mass m and energy E form through quantum pair creation. The typical pair creation time can be estimated by the uncertainty principle $\tau_{\text{creation}} \sim \hbar/E \sim \frac{\hbar}{m\gamma}$, and thus we find the cutoff frequency as

$$\omega_c \sim \frac{1}{\tau_{\text{creation}}} \sim \frac{m\gamma}{\hbar} \,. \tag{12.63}$$

Here we would like to draw the reader's attention to the fact that the units of Planck's constant $\hbar$ change with dimension number D: according to our convention of setting $c = 1$ the units of $\hbar$ are $[M]^{\frac{D-2}{D-3}}$. With this cutoff, we find the spectrum of the gravitational radiation emitted during pair creation to be given by (12.55) with $m_1 = m_2$ and $v_1 = v_2$ (we are considering the pair creation of two identical black holes):

$$\frac{d^2 E}{d\omega d\Omega} = \frac{8\mathcal{G}}{(2\pi)^{D-2}} \frac{D-3}{D-2} \frac{\gamma^2 m^2 v^4 \sin\theta_1{}^4}{(1 - v^2 \cos^2\theta_1)^2} \times \omega^{D-4} \,, \tag{12.64}$$

and the total frequency integrated energy per solid angle is

$$\frac{dE}{d\Omega} = \frac{8\mathcal{G}}{(2\pi)^{D-2}(D-2)} \frac{v^4 \sin\theta_1{}^4}{(1 - v^2 \cos^2\theta_1)^2} \times \frac{(m\gamma)^{D-1}}{\hbar^{D-3}} \,. \tag{12.65}$$

For example, in four dimensions and for pairs with $v \sim 1$ one obtains

$$\frac{dE}{d\omega} = \frac{4\mathcal{G}}{\pi} \gamma^2 m^2 \,, \tag{12.66}$$

and will have for the total energy radiated during production itself, using the cutoff frequency (12.63)

$$\Delta E = \frac{4\mathcal{G}}{\pi} \frac{\gamma^3 m^3}{\hbar} \,. \tag{12.67}$$

This could lead, under appropriate numbers of m and γ to huge quantities. Although one cannot be sure as to the cutoff frequency, and therefore the total energy (12.67), it is extremely likely that, as was verified experimentally in beta decay, the zero frequency limit (12.66) is exact.

12.4 Summary and discussion

We have developed the formalism to compute gravitational wave generation in higher D dimensional spacetimes, with D even. Several examples have been worked out, and one cannot help the feeling that our apparently four dimensional world is the best one to make predictions about the intensity of gravitational waves in concrete situations, in the sense that a small variation of parameters leads in high D to a huge variation of the energy radiated. A lot more work is still needed if one wants to make precise predictions about gravitational wave generation in D dimensional spacetimes. For example, it would be important to find a way to treat gravitational perturbations of higher dimensional Schwarzschild black holes. One of the examples worked out, the gravitational radiation emitted during black hole pair creation, had not been previously considered in the literature, and it seems to be a good candidate, even in $D = 4$, to radiate intensely through gravitational waves.

Bibliography

[1] V. P. Frolov, I. D. Novikov, *Black Hole Physics: Basic concepts and new developments*, Kluwer Academic, Dordrecht, Netherlands (1998).

[2] S. Chandrasekhar, *The Mathematical Theory of Black Holes*, Oxford University Press, New York (1992).

[3] B. K. Harrison, K. S. Thorne, M. Wakano, J. A. Wheeler, *Gravitation Theory and Gravitational Collapse*, University of Chicago Press, Chicago (1965).

[4] J. Maldacena, *The large N limit of superconformal field theories and supergravity*, Adv. Theor. Math. Phys. **2**, 231 (1998).; O. Aharony, S. Gubser, J. Maldacena, H. Ooguri, Y. Oz, *Large N field theories, string theory and gravity*, Phys. Rep. **323**, 183 (2000).

[5] S. W. Hawking, Commun. Math. Phys. **25**, 152 (1972); S. W. Hawking, G. F. R. Ellis, *The large scale structure of space-time* (Cambridge University Press, England, 1973); G. J. Galloway, K. Scheich, D. M. Witt, E. Woolgar, Phys. Rev. D**60**, 3840 (1996).

[6] J. P. S. Lemos, Class. Quant. Grav. **12**, 1081 (1995);*Cylindrical black hole in general relativity*, Phys. Lett. B**353**, 46 (1995).

[7] J. P. S. Lemos and V. T. Zanchin, *Rotating charged black strings in general relativity*, Phys. Rev. D**54**, 3840 (1996).

[8] O. J. C. Dias, J. P. S. Lemos, *Magnetic strings in anti-de Sitter general relativity*, Class. Quantum Grav. **19**, 2265 (2002).

[9] D. Klemm, V. Moretti, L. Vanzo, Phys. Rev. D**57**, 6127 (1998).

[10] C. G. Huang, C-B. Liang, Phys. Lett. A**201**, 27 (1995).

[11] S. Åminnenborg, I. Bengtsson, S. Holst, P. Peldán, *Making anti-de Sitter black holes*, Class. Quant. Grav. **13**, 2707 (1996); D. R. Brill, *Multi-black holes in 3D and 4D anti-de Sitter spaces*, Helv. Phys. Acta **69**, 249 (1996); S. L. Vanzo, *Black holes with unusual topology*, Phys. Rev. D **56**, 6475 (1997); D. R. Brill, J. Louko, P. Peldán, *Thermodynamics of (3+1)-dimensional black holes with toroidal or higher genus horizons*, Phys. Rev. D **56**, 3600 (1997); R. B. Mann, *Black holes of negative mass*, Class. Quant. Grav. **14**, 2927 (1997); S. Holst, P. Peldan, *Black holes and causal structure in anti-de Sitter isometric spacetimes*, Class. Quant. Grav. **14**, 3433 (1997).

[12] J. P. S. Lemos, Phys. Rev. D**57**, 4600 (1998); Phys. Rev. D**59**, 044020 (1999).

[13] J. P. S. Lemos, Class. Quantum Grav. **12**, 1081 (1995); Phys. Lett. B**353**, 46 (1995).

[14] J. R. Gott, M. Alpert, Gen. Rel. Grav. **16**, 243 (1984).

[15] S. Giddings, J. Abbot, K. Kuchař, Gen. Rel. Grav. **16**, 751 (1984).

[16] S. Deser, R. Jackiw, G. t' Hooft, *Three-dimensional einstein gravity: Dynamics of flat space-time*, Ann. Phys. (N.Y.) **152**, 220 (1984).

[17] J. D. Barrow, A. B. Burd, D. Lancaster, Class. Quant. Grav. **3**, 551 (1986).

[18] R. Jackiw, Nucl. Phys. B**252**, 343 (1985).

[19] R. Jackiw, *Diverse topics in theoretical and mathematical physics* (World Scientific, 1988).

[20] J. D. Brown, *Lower dimensional gravity* (World Scientific, 1988).

[21] A. Staruszkiewicz, Acta. Phys. Polon. **24**, 734 (1963).

[22] G. Clément, Int. J. Theor. Phys. **24**, 267 (1985).

[23] S. Deser, P. O. Mazur, Class. Quant. Grav. **2**, L51 (1985).

[24] J. R. Gott, J. Z. Simon, M. Alpert, Gen. Rel. Grav. **18**, 1019 (1986).

[25] M. A. Melvin, Class. Quant. Grav. **3**, 117 (1986).

[26] S. Deser, R. Jackiw, Ann. Phys. (N.Y.) **192**, 352 (1989).

[27] G. Grignani, C. Lee, Ann. Phys. (N.Y.) **196**, 386 (1989).

[28] G. Clément, Ann. Phys. (N.Y.) **152**, 241 (1990).

[29] P. Menotti, D. Seminara, Ann. Phys. (N.Y.) **208**, 449 (1991); Nucl. Phys. B**376**, 411 (1992).

[30] S. Deser, R. Jackiw, Ann. Phys. (N.Y.) **153**, 405 (1984).

[31] J. D. Brown, M. Henneaux, Commun. Math. Phys. **104**, 207 (1986).

[32] J. R. Gott, *Closed timelike curves produced by pairs of moving cosmic strings: Exact solutions*, Phys. Rev. Lett. **66**, 1126 (1991).

[33] C. Cutler, *Global structure of Gott's two string spacetime*, Phys. Rev. D**45**, 487 (1992).

[34] S. M. Carrol, E. Fahri, A. H. Guth, *An obstacle to building a time machine*, Phys. Rev. Lett. **68**, 263 (1992).

[35] Carrol, Fahri, Guth, Olum, *Energy-momentum restrictions on the creation of Gott-time machine*, Phys. Rev. D**50**, 6190 (1994).

[36] P. Menotti, D. Seminara, *Energy theorem for 2+1 dimensional gravity*, gr-qc/9406016 (1994).

[37] S. Holst, *Gott time machines in the Anti-de Sitter space*, Gen. Relativ. Gravit. **28**, 387 (1996).

[38] G. t'Hooft, *Causuality in (2+1)-dimensional gravity*, Class. Quant. Grav. **9**, 1335 (1992); *Classical N-particle cosmology in 2+1 dimensions*, Class. Quant. Grav. **10**, S79 (1993).

[39] M. Bañados, C. Teitelboim, J. Zanelli, Phys. Rev. Lett. **69**, 1849 (1992).

[40] M. Bañados, M. Henneaux, C. Teitelboim, J. Zanelli, Phys. Rev. D**48**, 1506 (1993).

[41] R. B. Mann, S. F. Ross, *Gravitationally collapsing dust in (2+1)-dimensions*, Phys. Rev. D**47**, 3319 (1993).

[42] H.-J. Matschull, *Black hole creation in 2+1 dimensions*, Class. Quant. Grav. **16**, 1069 (1999).

[43] S. Holst, H.-J. Matschull, *The anti-de Sitter Gott universe: a rotating BTZ wormhole*, Class. Quant. Grav. **16**, 3095 (1999).

Bibliography

[44] D. Birmingham, S. Sen, *Gott time machines, BTZ black hole formation, and Choptuik scaling*, Phys. Rev. Lett. **84**, 1074 (2000).

[45] S. Carlip, C. Teiltelboim, *Aspects of black hole quantum mechanics and thermodynamics in 2+1 dimensions*, Phys. Rev. D**51**, 622 (1995).

[46] N. Cruz, J. Zanelli, *Stellar equilibrium in (2+1)-dimensions*, Class. Quant. Grav. **12**, 975 (1995).

[47] M. Lubo, M. Rooman, Ph. Spindel, *(2+1) dimensional stars*, Phys. Rev. D**59**, 044012 (1999).

[48] G. Clément, Class. Quant. Grav. **10**, L49 (1993).

[49] C. Martínez, C. Teitelboim and J. Zanelli, *Charged rotating black hole in three spacetime dimensions*, Phys. Rev. **D61**, 104013 (2000).

[50] M. Cataldo, *Azimuthal electric field in a static rotationally symmetric (2+1)-dimensional spacetime*, Phys. Lett. B**529**, 143 (2002).

[51] E. W. Hirschmann, D. L. Welch, Phys. Rev. D**53**, 5579 (1996).

[52] M. Cataldo, P. Salgado, Phys. Rev. D**54**, 2971 (1996).

[53] O. J. C. Dias, J. P. S. Lemos, JHEP **0201:006** (2002).

[54] M. Kamata, T. Koikawa, Phys. Lett. B**353**, 196 (1995).

[55] M. Kamata, T. Koikawa, Phys. Lett. B**391**, 87 (1997).

[56] M. Cataldo, P. Salgado, Phys. Lett. B**448**, 20 (1999).

[57] K. C. K. Chan, Phys. Lett. B**373**, 296 (1996).

[58] S. Deser, R. Jackiw, S. Templeton, Ann. Phys. (N.Y.) **140**, 372 (1982); (E) **185** , 406 (1988); Phys. Rev. Lett. **48**, 975 (1982).

[59] I. Vuori, *Parity violation and the effective gravitational action in three dimensions* Phys. Lett. B**175**, 176 (1986); J. van der Bij, R. Pisarski, S. Rao, *Topological mass term for gravity induced by matter*, Phys. Lett. B**179**, 87 (1986); M. Gonni, M. Valle, *Massless fermions and (2+1)-dimensional gravitational massive action* Phys. Rev. D**34**, 648 (1986).

[60] S. Deser, Yang Z., *Is topologically massive gravity renormalizable?* Class. Quant. Grav. **7**, 1603 (1990); B. Keszthelyi, G. Kleppe, *Renormalizibity of $D = 3$ topologically massive gravity*, Phys. Lett. B**281**, 33 (1992).

[61] S. Carlip, Nucl. Phys. B**324**, 106 (1989).

[62] P. Gerbert, Nucl. Phys. B**346**, 440 (1990).

[63] S. Deser, A. R. Steif, *Gravity theories with light sources in $D = 3$*, hep-th/9208018.

[64] G. Clément, Phys. Lett. B**367**, 70 (1996).

[65] S. Fernando and F. Mansouri, Indian J. Commun. Math. and Theor. Phys. **1**, 14 (1998); gr-qc/9705015.

[66] T. Dereli and Yu. N. Obukhov, Phys. Rev. D**62**, 024013 (2000).

[67] R. V. Wagoner, *Scalar-tensor theory and gravitational waves*, Phys. Rev. D**1**, 3209 (1970).

[68] C. Callan, D. Friedan, E. Martinec and M. Perry, Nucl. Phys. **262**, 593 (1985).

[69] P. M. Sá, A. Kleber, J. P. S. Lemos, Class. Quant. Grav. **13**, 125 (1996).

[70] P. M. Sá, J. P. S. Lemos, Phys. Lett. B**423**, 49 (1998).

[71] O. J. C. Dias, J. P. S. Lemos, *Static and rotating electrically charged in three-dimensional Brans-dicke gravity theories*, Phys. Rev. D**64**, 064001 (2001).

[72] O. J. C. Dias, J. P. S. Lemos, *Magnetic point sources in three dimensional Brans-dicke gravity theories*, Phys. Rev. D**66**, 024034 (2002).

[73] K. C. K. Chan and R. B. Mann, Phys. Rev. **D50**, 6385 (1994);(E) Phys. Rev. D**52**, 2600 (1995).

[74] S. Fernando, Phys. Lett. B**468**, 201 (1999).

[75] Y. Kiem, D. Park, Phys. Rev. D**55**, 6112 (1997).

[76] D. Park, J. K. Kim, J. Math. Phys. **38**, 2616 (1997).

[77] T. Koikawa, T. Maki, A. Nakamula, Phys. Lett. B**414**, 45 (1997).

[78] C. -M. Chen, Nucl. Phys. **B544**, 775 (1999).

[79] S. Carlip, *Quantum gravity in 2+1 dimensions*, (Cambridge Univ. Press: Cambridge, 1998).

[80] S. Carlip, *The (2+1)-dimensional black hole*, Class. Quant. Grav. **12**, 2853 (1995); *Lectures on (2+1)-dimensional gravity*, `gr-qc/9503024`; Mann, R. B. *Lower dimensional black holes: inside and out*, `gr-qc/9501038`.

[81] D. Kramer, H. Stephani, M. MacCallum, E. Herlt, *Exact solutions of Einstein's Field Equations* (Cambridge University Press, 1980).

[82] T. Levi-Civita, *ds^2 einsteiniani in campi newtoniani*, Rend. Acc. Lincei **27**, 343 (1918).

[83] H. Weyl, *Bemerkung über die axissymmetrischen lösungen der Einsteinschen gravitations-gleinchungen*, Ann. Phys. (Germany) **59**, 185 (1919).

[84] W. Kinnersley, M. Walker, *Uniformly accelerating charged mass in General Relativity*, Phys. Rev. D**2**, 1359 (1970).

[85] F. J. Ernst, *Removal of the nodal singularity of the C-metric*, J. Math. Phys. **17**, 515 (1976).

[86] J. F. Plebański, M. Demiański, *Rotating, charged and uniformly accelerating mass in general relativity*, Annals of Phys. (N.Y.) **98**, 98 (1976).

[87] O. J. C. Dias, J. P. S. Lemos, *Pair of accelerated black holes in a anti-de Sitter background: the AdS C-metric*, Phys. Rev. D **67**, 064001 (2003).

[88] O. J. C. Dias, J. P. S. Lemos, *Pair of accelerated black holes in de Sitter background: the dS C-metric*, Phys. Rev. D **67**, 084018 (2003).

[89] O. J. C. Dias, J. P. S. Lemos, *The extremal limits of the C-metric: Nariai, Bertotti-Robinson and anti-Nariai C-metrics*, Phys. Rev. D**68** (2003) 104010; `hep-th/0306194`.

[90] W. Israel, K. A. Khan, *Collinear particles and dipoles in general relativity*, Nuovo Cimento **33**, 331 (1964).

[91] R. Bach, H. Weyl, *Nene Lösungen der Einsteinschen Gravitationsgleichungen*, Math. Z. **13**, 134 (1922).

[92] M. Aryal, L. H. Ford, A. Vilenkin, *Cosmic strings and black holes*, Phys. Rev. D**34**, 2263 (1986).

Bibliography

[93] M. S. Costa, M. J. Perry, *Interacting Black Holes*, Nucl. Phys. B**591** (2000) 469.

[94] A. Tomimatsu, *Condition for equilibrium of two Reissner-Nordtröm black holes*, Prog. Theor. Phys. **71**, 409 (1984).

[95] W. B. Bonnor, Phys. Lett. A**83**, 414 (1981).

[96] T. Ohta, T. Kimura, Prog. Theor. Phys. **68**, 1175 (1982).

[97] P. Ginsparg, M. J. Perry, *Semiclassical perdurance of de Sitter space*, Nucl. Phys. B **222**, 245 (1983).

[98] A. Vilenkin, *Gravitational field of vacuum domain walls*, Phys. Lett. B**133**, 177 (1983); *Cosmic strings and domain walls*, Phys. Rep. **121**, 263 (1985); A. Vilenkin, E. P. S. Shellard, *Cosmic strings and other topological defects*, (Cambridge University Press, 2000).

[99] J. Ipser, P. Sikivie, *Gravitationally repulsive domain wall*, Phys. Rev. D**30**, 712 (1984).

[100] J. Ehlers, W. Kundt, *Exact solutions of the gravitational field equations*, in *Gravitation: an introduction to current research*, edited by L. Witten (Wiley, New York, London, 1962).

[101] J. D. Brown, *Black hole pair creation and the entropy factor*, Phys. Rev. D **51**, 5725 (1995).

[102] M. A. Melvin, Phys. Lett. **8**, 65 (1964).

[103] H. Farhoosh, R. L. Zimmerman, *Stationary charged C-metric*, J. Math. Phys. **20**, 2272 (1979); *Killing horizons and dragging of the inertial frame about a uniformly accelerating particle*, Phys. Rev. D **21**, 317 (1980); *Interior C-metric*, Phys. Rev. D **23**, 299 (1981).

[104] A. Ashtekar, T. Dray, *On the existence of solutions to Einstein's equation with non-zero Bondi-news*, Comm. Phys. **79**, 581 (1981).

[105] W. B. Bonnor, *The sources of the vacuum C-metric*, Gen. Rel. Grav. **15**, 535 (1983); *The C-metric with $m = 0$, $e \neq 0$*, Gen. Rel. Grav. **16**, 269 (1984).

[106] F. H. J. Cornish, W. J. Uttley, *The interpretation of the C metric. The vacuum case*, Gen. Rel. Grav. **27**, 439 (1995); *The interpretation of the C metric. The charged case when $e^2 \leq m^2$*, Gen. Rel. Grav. **27**, 735 (1995).

[107] W. Yongcheng, *Vacuum C-metric and the metric of two superposed Schwarzschild black holes*, Phys. Rev. D **55**, 7977 (1997).

[108] C. G. Wells, *Extending the black hole uniqueness theorems I. Accelerating black holes: The Ernst solution and C-metric*, `gr-qc/9808044`.

[109] V. Pravda, A. Pravdova, *Co-accelerated particles in the C-metric*, Class. Quant. Grav. **18**, 1205 (2001).

[110] J. Podolský, J. B. Griffiths, *Null limits of the C-metric*, Gen. Rel. Grav. **33**, 59 (2001).

[111] J. Bičák, B. G. Schmidt, *Asymptotically flat radiative space-times with boost-rotation symmetry: The general structure*, Phys. Rev. D **40**, 1827 (1989).

[112] J. Bičák, *Gravitational radiation from uniformly accelerated particles in general relativity*, Proc. Roy. Soc. A **302**, 201 (1968).

[113] V. Pravda, A. Pravdova, *Boost-rotation symmetric spacetimes - review*, Czech. J. Phys. **50**, 333 (2000); *On the spinning C-metric*, in *Gravitation: Following the Prague Inspiration*, edited by O. Semerák, J. Podolský, M. Zofka (World Scientific, Singapore, 2002), `gr-qc/0201025`.

[114] H. F. Dowker, J. P. Gauntlett, D. A. Kastor, J. Traschen, *Pair creation of dilaton black holes*, Phys. Rev. D **49**, 2909 (1994).

[115] H. Farhoosh, R. L. Zimmerman, *Surfaces of infinite red-shift around a uniformly accelerating and rotating particle*, Phys. Rev. D **21**, 2064 (1980).

[116] P. S. Letelier, S. R. Oliveira, *On uniformly accelerated black holes*, Phys. Rev. D **64**, 064005 (2001).

[117] J. Bičák, V. Pravda, *Spinning C-metric as a boost-rotation symmetric radiative spacetime*, Phys. Rev. D **60**, 044004 (1999).

[118] H. F. Dowker and S. Thambyahpillai, Class. Quantum Grav. **20**, 127 (2003).

[119] K. Hong and E. Teo, Class. Quantum Grav. **20**, 3269 (2003); gr-qc/0410002.

[120] J. Podolský, J.B. Griffiths, *Uniformly accelerating black holes in a de Sitter universe*, Phys. Rev. D **63**, 024006 (2001).

[121] R. Emparan, G. T. Horowitz, R. C. Myers, *Exact description of black holes on branes*, JHEP **0001** 007 (2000); *Exact description of black Holes on branes II: Comparison with BTZ black holes and black strings*, JHEP **0001** 021 (2000).

[122] J. Podolský, *Accelerating black holes in anti-de Sitter universe*, Czech. J. Phys. **52**, 1 (2002).

[123] A. Chamblin, *Capture of bulk geodesics by brane-world black holes*, Class. Quant. Grav. **18**, L17 (2001).

[124] R. Emparan, (private communication).

[125] H. Nariai, *On some static solutions of Einstein's gravitational field equations in a spherically symmetric case*, Sci. Rep. Tohoku Univ. **34**, 160 (1950); *On a new cosmological solution of Einstein's field equations of gravitation*, Sci. Rep. Tohoku Univ. **35**, 62 (1951).

[126] H. Nariai, H. Ishihara, *On the de Sitter and Nariai solutions in General Relativity and their extension in higher dimensional spacetime*, in *A Random Walk in Relativity and Cosmology*, edited by P. N. Dadhich, J. K. Rao, J. V. Narlikar, C. V. Vishveshwara (John Wiley & Sons, New York).

[127] B. Bertotti, *Uniform electromagnetic field in the theory of general relativity*, Phys. Rev. **116**, 1331 (1959); I. Robinson, Bull. Acad. Polon. **7**, 351 (1959).

[128] M. Caldarelli, L. Vanzo, Z. Zerbini, *The extremal limit of D-dimensional black holes*, in *Geometrical Aspects of Quantum Fields*, edited by A. A. Bytsenko, A. E. Gonçalves, B. M. Pimentel (World Scientific, Singapore, 2001); `hep-th/0008136`; N. Dadhich, *On product spacetime with 2-sphere of constant curvature*, `gr-qc/0003026`.

[129] R. Bousso, *Proliferation of de Sitter space*, Phys. Rev. D **58**, 083511 (1998); *Adventures in de Sitter space*, `hep-th/0205177`.

[130] J. Schwinger, Phys. Rev. **82**, 664 (1951).

[131] O. J. C. Dias, J. P. S. Lemos, *Pair creation of de Sitter black holes on a cosmic string background*, Phys. Rev. D**69** (2004) 084006; [`hep-ph/0310068`].

[132] O. J. C. Dias, *Pair creation of anti-de Sitter black holes on a cosmic string background*, Phys. Rev. D**70** (2004) 024007.

Bibliography

[133] S. W. Hawking, S. F. Ross, *Pair production of black holes on cosmic strings*, Phys. Rev. Lett. **75**, 3382 (1995).

[134] D. M. Eardley G. T. Horowitz, D. A. Kastor, J. Traschen, *Breaking cosmic strings without black holes*, Phys. Rev. Lett. **75**, 3390 (1995).

[135] A. Achúcarro, R. Gregory, K. Kuijken, *Abelian Higgs hair for black holes*, Phys. Rev. D **52**, 5729 (1995).

[136] R. Gregory, M. Hindmarsh, *Smooth metrics for snapping strings*, Phys. Rev. D **52**, 5598 (1995).

[137] J. Preskill, A. Vilenkin, Phys. Rev. D **47**, 2324 (1993).

[138] D. J. Gross, M. J. Perry, L. G. Yaffe, *Instability of flat space at finite temperature*, Phys. Rev. D **25**, 330 (1982).

[139] J.S. Langer, Ann. Phys. **41**, 108 (1967).

[140] S. Coleman, Phys. Rev. D **15**, 2629 (1977); Phys. Rev. D **16**, 1248 (1977)(E).

[141] C.G. Callan, S. Coleman, Phys. Rev. D **16**, 1762 (1977).

[142] S. Coleman, F. De Luccia, Phys. Rev. D **21**, 3305 (1980).

[143] M.B. Voloshin, I.Yu. Kobzarev, L.B. Okun Yad. Fiz. **20**, 1229 (1974) [Sov. J. Nucl. Phys. **20**, 644 (1975)].

[144] M. Stone, Phys. Lett. B **67**, 186 (1977).

[145] V.G. Kiselev, K.G. Selivanov, Pisma Zh. Eksp. Teor. Fiz. **39**, 72 (1984) [JETP Lett. **39**, 85 (1984)].

[146] V.G. Kiselev, K.G. Selivanov, Yad. Fiz. **43**, 239 (1986) [Sov. J. Nucl. Phys. **43**, 153 (1986)].

[147] V.G. Kiselev, Phys. Rev. D **45**, 2929 (1992).

[148] M.B. Voloshin, Sov. J. Nucl. Phys. **42**, 644 (1985).

[149] M.B. Voloshin, in *International School of Subnuclear Physics*, (Ettore Majorana Centre for Scientific Culture, Italy, 1995).

[150] O. J. C. Dias, J. P. S. Lemos, *False vacuum decay: effective one-loop action for pair creation of domain walls*, J. Math. Phys. **42**, 3292 (2001); O. J. C. Dias, *Pair creation of particles and black holes in external fields* in: Proceedings of Xth Portuguese Meeting on Astronomy and Astrophysics, edited by J. P. S. Lemos, A. Mourão, et al (World Scientific, Singapore, 2001), gr-qc/0106081.

[151] J. H. Miller Jr, G. Cardenas, A. Garcia-Perez, W. More, A. W. Beckwith, J. P. McCarten, *Quantum pair creation of soliton domain walls*, J. Phys. A **36**, 9209 (2003); *Soliton tunneling transistor*, cond-mat/0105409.

[152] I.K. Affleck, N.S. Manton, Nucl. Phys. B **194**, 38 (1982).

[153] I.K. Affleck, O. Alvarez, N.S. Manton, Nucl. Phys. B **197**, 509 (1982).

[154] S. W. Hawking , in *Black holes: an Einstein Centenary Survey*, edited by S. W. Hawking, W. Israel (Cambridge University Press, 1979); *Euclidean Quantum Gravity*, edited by G. W. Gibbons, S. W. Hawking (Cambridge University Press, 1993).

[155] Z. C. Wu, *Quantum creation of a black hole*, Int. J. Mod. Phys. D **6**, 199 (1997); *Real tunneling and black hole creation*, Int. J. Mod. Phys. D **7**, 111 (1998).

[156] R. Bousso, S. W. Hawking, *Lorentzian condition in quantum gravity*, Phys. Rev. D **59**, 103501 (1999); **60**, 109903 (1999) (E).

[157] G. W. Gibbons, in *Fields and Geometry*, Proceedings of the 22nd Karpacz Winter School of Theoretical Physics, edited by A. Jadczyk (World Scientific, Singapore, 1986).

[158] D. Garfinkle, S. B. Giddings, *Semiclassical Wheeler wormhole production*, Phys. Lett. B**256**, 146 (1991).

[159] D. Garfinkle, S. B. Giddings, A. Strominger, *Entropy in black hole pair production*, Phys. Rev. D **49**, 958 (1994)

[160] H. F. Dowker, J. P. Gauntlett, S. B. Giddings, G. T. Horowitz, *Pair creation of extremal black holes and Kaluza-Klein monopoles*, Phys. Rev. D **50**, 2662 (1994).

[161] S. Ross, *Pair creation rate for $U(1)^2$ black holes*, Phys. Rev. D **52**, 7089 (1995).

[162] P. Yi, *Toward one-loop tunneling rates of near-extremal magnetic black hole pair creation*, Phys. Rev. D **52**, 7089 (1995).

[163] J. D. Brown, *Duality invariance of black hole pair creation rates*, Phys. Rev. D **51**, 5725 (1995).

[164] S. W. Hawking, G. T. Horowitz, S. F. Ross, *Entropy, area, and black hole pairs*, Phys. Rev. D **51**, 4302 (1995).

[165] S. W. Hawking, G. T. Horowitz, *The gravitational hamiltonian, action, entropy and surface terms*, Class. Quant. Grav. **13**, 1487 (1996).

[166] R. Emparan, *Correlations between black holes formed in cosmic string breaking*, Phys. Rev. D **52**, 6976 (1995).

[167] F. Mellor, I. Moss, *Black holes and quantum wormholes*, Phys. Lett. B **222**, 361 (1989); *Black holes and gravitational instantons*, Class. Quant. Grav. **6**, 1379 (1989).

[168] L. J. Romans, *Supersymmetric, cold and lukewarm black holes in cosmological Einstein-Maxwell theory*, Nucl. Phys. B **383**, 395 (1992).

[169] R. B. Mann, S. F. Ross, *Cosmological production of charged black hole pairs*, Phys. Rev. D **52**, 2254 (1995).

[170] R. Bousso, S. W. Hawking, *The probability for primordial black holes*, Phys. Rev. D **52**, 5659 (1995); *Pair production of black holes during inflation*, Phys. Rev. D **54**, 6312 (1996); S. W. Hawking, *Virtual black holes*, Phys. Rev. D **53**, 3099 (1996).

[171] R. Garattini, Nucl. Phys. B (Proc. Suppl.) **57**, 316 (1997); Nuovo Cimento B**113**, 963 (1998); Mod. Phys. Lett. A **13**, 159 (1998); Class. Quant. Grav. **18**, 571 (2001).

[172] M. Volkov, A. Wipf, *Black hole pair creation in de Sitter space: a complete one-loop analysis*, Nucl. Phys. B**582**, 313 (2000).

[173] I. S. Booth, R. B. Mann, *Complex instantons and charged rotating black hole pair creation*, Phys. Rev. Lett. **81**, 5052 (1998); *Cosmological pair production of charged and rotating black holes*, Nucl. Phys. B **539**, 267 (1999).

[174] R. Bousso, *Charged Nariai black holes with a dilaton*, Phys. Rev. D **55**, 3614 (1997).

Bibliography

[175] R. Emparan, *Pair production of black holes joined by cosmic strings*, Phys. Rev. Lett. **75**, 3386 (1995).

[176] R. R. Caldwell, A. Chamblin, G. W. Gibbons, *Pair creation of black holes by domain walls*, Phys. Rev. D **53**, 7103 (1996).

[177] R. Bousso, A. Chamblin, *Patching up the no-boundary proposal with virtual Euclidean wormholes*, Phys. Rev. D **59**, 084004 (1999).

[178] R. Mann, *Pair production of topological anti-de Sitter black holes*, Class. Quantum Grav. **14**, L109 (1997); *Charged topological black hole pair creation*, Nucl. Phys. B **516**, 357 (1998).

[179] R. Parentani, S. Massar, *The Schwinger mechanism, the Unruh effect and the production of accelerated black holes*, Phys. Rev. D **55**, 3603 (1997); J. Garriga, M. Sasaki, *Brane-world creation and black holes*, Phys. Rev. D **62**, 043523 (2000); R. Emparan, R Gregory, C. Santos, *Black holes on thick branes*, Phys. Rev. D **63**, 104022 (2001).

[180] Z. C. Wu, *Pair creation of black holes in anti-de Sitter space background (I)*, Gen. Rel. Grav. **31**, 223 (1999); *Pair creation of black hole in anti-de Sitter space background*, Phys. Lett. B **445**, 274 (1999); *Quantum creation of topological black hole*, Mod. Phys. Lett. A **15**, 1589 (2000).

[181] S. W. Hawking, S. F. Ross, *Duality between electric and magnetic black holes*, Phys. Rev. D **52**, 5865 (1995).

[182] S. W. Hawking, *Breakdown of predictability in gravitational collapse*, Phys. Rev. D**14**, 2460 (1976).

[183] D. N. Page, *Black hole information*, Int. J. Mod. Phys. D**3**, 93 (1994); T. Banks, *Lectures on black holes and information loss*, `hep-th/9412131`; L. Thorlacius, *Black hole evolution*, `hep-th/9411020`; S. B. Giddings, *Quantum mechanics of black holes*, `hep-th/9412138`; P. C. Argyres, A. O. Barvinski, V. Frolov, S. B. Giddings, D. A. Lowe, A. Strominger, L. Thorlacius, *Quantum aspects of gravity*, `astrp-ph/9412046`; Y. Kazama, *On quantum black holes*, `hep-th/941224`; S. B. Giddings, *The black hole information paradox*, `hep-th/9508151`; *Why aren't black holes infinitely produced?*, Phys. Rev. D **51**, 6860 (1995); L. Susskind, *Trouble for remnants*, `hep-th/9501106`.

[184] S. Weinberg, *Gravitation and Cosmology* (Wiley, New York, 1972).

[185] V. Cardoso, O. J. C. Dias, J. P. S. Lemos, *Gravitational radiation in D-dimensional spacetimes*, Phys. Rev. D **67**, 064026 (2003).

[186] C. S. Wang Chang and D. L. Falkoff, Phys. Rev. **76**, 365 (1949).

[187] J. D. Jackson, *Classical Electrodynamics*, (J. Wiley, New York 1975).

[188] J. Bičák, P. Krtouš, *Accelerated sources in de Sitter spacetime and the insuffiency of retarded fields*, Phys. Rev. D **64**, 124020 (2001); *The fields of uniformly accelerated charges in de Sitter spacetime*, Phys. Rev. Lett. **88**, 211101 (2002).

[189] P. Krtouš, J. Podolský, *Radiation from accelerated black holes in de Sitter universe*, `gr-qc/0301110`.

[190] J. Podolský, M. Ortaggio, P. Krtouš, *Radiation from accelerated black holes in an anti-de Sitter universe*, `gr-qc/0307108`.

[191] J. M. Overduin, P. S. Wesson, *Kaluza-Klein gravity*, `gr-qc/9805018`.

[192] S. B. Giddings, *Black holes at accelerators*, `hep-th/0205027`; G. Landsberg, *Black holes at future colliders and beyond: a review*, `hep-th/0211043`.

[193] N. Arkani-Hamed, S. Dimopoulos and G. Dvali, Phys. Lett. **B429**, 263 (1998); Phys. Rev. D**59**, 086004 (1999); I. Antoniadis, N. Arkani-Hamed, S. Dimopoulos and G. Dvali, Phys. Lett. **B436**, 257 (1998).

[194] P. C. Argyres, S. Dimopoulos, J. March-Russell, , Phys. Lett. B**441**, 96 (1998).

[195] Banks, Fischler, , JHEP **9906**, 014 (1999).

[196] Emparan, Horowitz, Myers, , Phys. Rev. Lett. **85**, 499 (2000).

[197] S. B. Giddings, S. Thomas, *High energy colliders as black hole factories: The end of short distance physics*, Phys. Rev. D**65**, 056010 (2002).

[198] S. Dimopoulos, G. Landsberg, *Black holes at the LHC*, Phys. Rev. Lett. **87**, 161602 (2001).

[199] P. D. D'Eath, P. N. Payne, *Gravitational radiation in high speed black hole collisions. 1. Perturbation treatment of the axisymmetric speed of light collision*, Phys. Rev. D**46**, 658 (1992); *Gravitational radiation in high speed black hole collisions. 2. Reduction to two independent variables and calculation of the second order news function Perturbation treatment of the axisymmetric speed of light collision*, Phys. Rev. D**46**, 675 (1992); *Gravitational radiation in high speed black hole collisions. 3. Results and conclusions*, Phys. Rev. D**46**, 694 (1992).

[200] H. Yoshino and Y. Nambu, *High-energy head-on collisions of particles and hoop conjecture*, Phys. Rev. **D67**, 024009 (2003).

[201] D. M. Eardley and S. B. Giddings, *Classical black hole production in high energy collisions*, Phys. Rev. **D66**, 044011 (2002).

[202] F. R. Tangherlini, Nuovo Cim. **27**, 636 (1963).

[203] R. C. Myers and M. J. Perry, *Black holes in higher dimensional space-times* Annals Phys. **172**, 304 (1986).

[204] Boulware, S. Deser, Phys. Rev. Lett. **55**, 2656 (1985).

[205] M. Cvetic, D. Youm, Nucl. Phys. **B476**, 118 (1996).

[206] M. Cvetic, F. Larsen, Phys. Rev. D**56**, 4994 (1997).

[207] G. W. Gibbons, C. A. R. Herdeiro, Class. Quant. Grav. **16**, 3619 (1999).

[208] C. A. R. Herdeiro, Nucl. Phys. **B582**, 363 (2000).

[209] R. Emparan, H. S. Reall, Phys. Rev. Lett. **88** 101101 (2002); Phys. Rev. D**65** 084025 (2002).

[210] N. L. Santos, O. J. C. Dias and J. P. S. Lemos, *Global embedding Minkowskian spacetime procedure in higher dimensional black holes:*
Matching between Hawking temperature and Unruh temperature, Phys. Rev. D, submitted (2004).

[211] V. Cardoso, O. J. C. Dias, J. P. S. Lemos, *Nariai, Bertotti-Robinson and anti-Nariai solutions in higher dimensions*, Phys. Rev. D**70** (2004) 024002.

[212] O. J. C. Dias, J. P. S. Lemos, *Pair creation of higher dimensional de Sitter black holes*, Phys. Rev. D, submitted (2004); hep-th/0410279.

Bibliography

[213] B. F. Schutz, Class. Quant. Grav. **16**, A131 (1999); B. F. Schutz and F. Ricci, in *Gravitational Waves*, eds I. Ciufolini et al, (Institute of Physics Publishing, Bristol, 2001).

[214] S. A. Hughes, astro-ph/0210481.

[215] K. Danzmann et al., in *Gravitational Wave Experiments*, eds. E. Coccia, G. Pizzella and F. Ronga (World Scientific, Singapore, 1995).

[216] A. Abramovici et al., Science **256**, 325 (1992).

[217] C. Bradaschia et al., in *Gravitation* 1990, Proceedings of the Banff Summer Institute, Banff, Alberta, 1990, edited by R. Mann and P. Wesson (World Scientific, Singapore, 1991).

[218] K. S. Thorne, Rev. Mod. Phys, **52**, 299 (1980); K. S. Thorne, in *General Relativity: An Einstein Centenary Survey*, eds. S. W. Hawking and W. Israel (Cambridge University Press, 1989).

[219] T. Damour, in *Gravitational Radiation*, eds Nathalie Deruelle and Tsvi Piran (North Holland Publishing Company, New York, 1983).

[220] V. Cardoso and J. P. S. Lemos, "Gravitational Radiation from the radial infall of highly relativistic point particles into Kerr black holes" gr-qc/0211094.

[221] E. Berti, M. Cavaglià, L. Gualtieri, *Gravitational energy loss in high energy particle collisions: ultrarelativistic plunge into a multidimensional black hole*, `hep-th/0309203`.

[222] V. Cardoso and J. P. S. Lemos, Phys. Lett. **B 538**, 1 (2002); Gen. Rel. Gravitation (in press), gr-qc/0207009.

[223] D. N. Page, *Particle emissions rates from a black hole: massless particles from an uncharged, nonrotating hole*, Phys. Rev. D**13**, 198 (1976); *Particle emissions rates from a black hole. II. Massless particles from a rotating hole*, Phys. Rev. D**14**, 3260 (1976).

[224] V. Frolov and D. Stojkovic, *Quantum radiation from a 5-dimensional rotating black hole*, Phys. Rev. Lett. **89**, 151302 (2002).

[225] D. Ida, Kin-ya Oda, S. C. Park, *Rotating black holes at future colliders: Greybody factors for brane fields*, Phys. Rev. D**67**, 064025 (2003).

[226] P. Kanti, J. March-Russell, *Calculable corrections to brane black hole decay. I: The scalar case*, Phys. Rev. D**66**, 024023 (2002); *Calculable corrections to brane black Hole decay II: Greybody factors for spin 1/2 and 1* , Phys. Rev. D**67**, 104019 (2003).

[227] A. R. Steif, *Supergeometry of three dimensional black holes*, Phys. Rev. D**53**, 5521 (1996).

[228] H. Soodak, M. S. Tiersten, Am. J. Phys. **61**, 3955 (1993).

[229] V. Cardoso, S. Yoshida, O. J. C. Dias, J. P. S. Lemos, *Late-time tails of wave propagation in higher dimensional spacetimes*, Phys. Rev. D **68**, 061503 (2003) [Rapid Communications].

[230] C. A. R. Herdeiro, O. J. C. Dias, unpublished work.

[231] J. H. Horne, G. T. Horowitz, Nucl. Phys. B**368**, 444 (1992).

[232] G. T. Horowitz, D. L. Welch, Phys. Rev. Lett. **71**, 328 (1993).

[233] J. Stachel, Phys. Rev. D**26**, 1281 (1982).

[234] T. Regge, C. Teitelboim, Ann. Phys. (NY) **88**, 286 (1974).

[235] W. A. Moura-Melo, J. A. Helayel-Neto, Phys. Rev. D**63**, 065013 (2001).

[236] A. García, `hep-th/9909111`.

[237] Y. Kiem and D. Park, Phys. Rev. **D55**, 6112 (1997).

[238] R. H. Boyer, R. W. Lindquist, J. Math. Phys. **8**, 265 (1967).

[239] B. Carter, Phys. Rev. **174**, 1559 (1968).

[240] E. Witten, Phys. Rev. D **44**, 314 (1991).

[241] G. Mandal, A. M. Sengupta and S. R. Wadia, Mod. Phys. Lett. A **6**, 1685 (1991).

[242] D. Park and S. Yang, Gen. Rel. Grav. **31**, 1343 (1999).

[243] J. D. Brown, C. Teitelboim, Nucl. Phys. B**297**, 297 (1988).

[244] S. G. Ghosh, Phys. Rev. D**62**, 127505 (2000).

[245] J. L. Friedman, K. Schleich, D. W. Witt, Phys. Rev. D**71**, 1486 (1993); (E) **75**, 1872 (1995); T. Jacobson, S. Venkatararamani, Class. Quantum Grav. **12**, 1055 (1995); G. J. Galloway, K. Schleich, D. W. Witt, E. Woolgar, Phys. Rev. D**60**, 104039 (1999).

[246] A. Ghosh, P. Mitra, Phys. Rev. Lett. **78**, 1858 (1997); D. R. Brill, J. Louko, P. Peldán in [11]; A. Chamblin, R. Emparan, C. V. Johnson, R. C. Myers, Phys. Rev. D**60**, 104026 (1999); C. Peça, J. P. S. Lemos, Phys. Rev. D**59**, 124007 (1999); C. Peça, J. P. S. Lemos, J. Math. Physics **41**, 4783 (2000).

[247] A. DeBenedictis, Class. Quantum Grav. **16**, 1955 (1999); Gen. Rel. Grav. **31**, 1549 (1999).

[248] M. M. Caldarelli, D. Klemm, Nucl. Phys. B**545**, 434 (1999); J. P. S. Lemos, Nucl. Phys. B**600**, 272 (2001).

[249] V. Cardoso, J. P. S. Lemos, Class. Quant. Grav. **18**, 5257 (2001).

[250] J. P. S. Lemos, in: *Astronomy and Astrophysics: Recent Developments* (World Scientific, 2001) , `gr-qc/0011092`.

[251] L. Witten, in: *Gravitation: an introduction to current research* (Wiley, 1962).

[252] J. P. S. Lemos, *Thermodynamics of the two-dimensional black hole in the Teitelboim-Jackiw theory*, Phys. Rev. D **54**, 6206 (1996).

[253] S. Deser, O. Levin, *Accelerated detectors and temperature in (anti-) de Sitter spaces*, Class. Quant. Grav. **14**, L163 (1997).

[254] G. Gibbons, S. Hawking, *Cosmological event horizons, thermodynamics, and particle creation*, Phys. Rev. D **15**, 2738 (1977); K. Lake, R. Roeder, *Effects of a nonvanishing cosmological constant on the spherically symmetric vacuum manifold*, Phys. Rev. D **15**, 3513 (1977).

[255] F. Mellor, I. G. Moss, Phys. Rev. D **41**, 403 (1990); Class. Quant. Grav. **9**, L43 (1992); P. R. Brady, E. Poisson, Class. Quant. Grav. **9**, 121 (1992); P. R. Brady, D. Nunez, S. Sinha, Phys. Rev. D **47**, 4239 (1993).

[256] L. M. Burko, A. Ori, in *Internal structure of black holes and spacetime singularities*, edited by L. M. Burko and A. Ori (IOP, Bristol, 1997).

[257] G. T. Horowitz, H. J. Sheinblatt, Phys. Rev. D **55**, 650 (1997).

Bibliography

[258] S. F. Hawking, G. F. R. Ellis, *The Large Scale Structure of Space-Time*, (Cambridge University Press, 1976).

[259] B. Carter, *General theory of statinary black holes*, in *Black holes* edited by B. DeWitt and C. DeWitt (Gordon and Breach, New York, 1973).

[260] M. Ortaggio, *Impulsive waves in the Nariai universe*, Phys. Rev. D **65**, 084046 (2002).

[261] R. Bousso, S. W. Hawking, *(Anti-)evaporation of Schwarzschild-de Sitter black holes*, Phys. Rev. D **57**, 2436 (1998); R. Bousso, *Proliferation of de Sitter space*, Phys. Rev. D **58**, 083511 (1998).

[262] S. Nojiri, S. D. Odintsov, *Quantum evolution of Schwarzschild-de Sitter (Nariai) black holes*, Phys. Rev. D **59**, 044026 (1999); *De Sitter space versus Nariai black hole: stability in d5 higher derivative gravity*, Phys. Lett. B **523**, 165 (2001).

[263] L. A. Kofman, V. Sahni, A. A. Starobinski, *Anisotropic cosmological model created by quantum polarization of vacuum*, Sov. Phys. JETP **58**, 1090 (1983).

[264] A. J. M. Medved, *Nearly degenerated dS horizons from a 2-D perpective*, `hep-th/0302058`.

[265] A. S. Lapedes, *Euclidean quantum field theory and the Hawking effect*, Phys. Rev. D **17**, 2556 (1978).

[266] O. B. Zaslavsky, *Geometry of nonextreme black holes near the extreme state*, Phys. Rev. D **56**, 2188 (1997); *Entropy of quantum fields for nonextreme black holes in the extreme limit*, Phys. Rev. D **57**, 6265 (1998).

[267] R. B. Mann, S. N. Solodukhin, *Universality of quantum entropy for extreme black holes*, Nucl. Phys. B **523**, 293 (1998).

[268] D. J. Navarro, J. Navarro-Salas, P. Navarro, *Holography, degenerated horizons and entropy*, Nucl. Phys. B **580**, 311 (2000); A. J. M. Medved, *Reissner-Nordström Near extremality from a Jackiw-Teiltelboim perpective*, `hep-th/0111091`. A. Barvinsky, S. Das, G. Kunstatter, *Quantum mechanics of charged black holes*, Phys. Lett. B **517**, 415 (2001).

[269] M. Ortaggio, J. Podolský, *Impulsive waves in electrovac direct product spacetimes with Lambda*, Class. Quant. Grav. **19**, 5221 (2002).

[270] J. Maldacena, J. Michelson, A. Strominger, *Anti-de Sitter fragmentation*, JHEP **9902:11**, (1999); *Vacuum states for AdS_2 black holes*, M. Spradlin, A. Strominger, JHEP **9911:021**, (1999).

[271] G. T. Horowitz, H. J. Sheinblatt, *Tests of cosmic censorship in the Ernst spacetime*, Phys. Rev. D **55**, 650 (1997).

[272] K. Hong, E. Teo, *A new form of the C-metric*, `gr-qc/0305089`.

[273] S. Coleman, Phys. Rev. D **11**, 2088 (1975).

[274] S.P. Gavrilov, D.M. Gitman, Phys. Rev. D **53**, 7162 (1996).

[275] R. Soldati, L. Sorbo, Phys. Lett. B **426**, 82 (1998).

[276] Q.-G. Lin, J. Phys. G **25**, 17 (1999); J. Phys. G **25**, 1793 (1999); J. Phys. G **26**, L17 (2000).

[277] B. Körs, M.G. Schmidt, Eur. Phys. J. C **6**, 175 (1999).

[278] C. Montonen, D.I. Olive, Phys. Lett. B **72**, 117 (1977).

[279] N.S. Manton, Nucl. Phys. B **150**, 397 (1978).

[280] R. Rajamaran, "Solitons and Instantons", (Holland, Amsterdam, 1989).

[281] J. Garriga, Phys. Rev. D **49**, 6327 (1994).

[282] G. Lavrelashvili, Nucl. Phys. Proc. Suppl. **88**, 75 (2000).

[283] J.B. Hartle, S.W. Hawking, *Wave function of the Universe*, Phys. Rev. D **28**, 2960 (1983).

[284] G. W. Gibbons, S. W. Hawking, M. J. Perry, *Path integral and the indifiniteness of the gravitational action*, Nucl. Phys. B **138**, 141 (1978).

[285] G. W. Gibbons, M. J. Perry, *Quantizing gravitational instantons*, Nucl. Phys. B **146**, 90 (1978).

[286] S. M. Christensen, M. J. Duff, *Quantizing gravity with cosmological constant*, Nucl. Phys. B **146**, 90 (1978).

[287] R. E. Young, *Semiclassical stability of asymptotically locally flat spaces*, Phys. Rev. D **28**, 2420 (1983).

[288] R. E. Young, *Semiclassical instability of gravity with positive cosmological constant*, Phys. Rev. D **28**, 2436 (1983).

[289] J. D. Brown, J. W. York, *Quasilocal energy and conserved charges derived from the gravitational action*, Phys. Rev. D **47**, 1407 (1993); , *Microcanonical functional integral for the gravitational field*, Phys. Rev. D **47**, 1420 (1993).

[290] G. W. Gibbons, S. W. Hawking, *Action integrals and partition functions in quantum gravity*, Phys. Rev. D **15**, 2752 (1977).

[291] T. Regge, Nuovo Cimento **19**, 558 (1961); G. W. Gibbons, M. J. Perry, Phys. Rev. D **22**, 313 (1980).

[292] M. Abramowitz, I. A. Stegun, *Handbook of Mathematical Functions*, (Dover, New York, 1970).

[293] H. F. Goenner, *General Relativity and Gravitation*, edited by A. Held (Plenum, New York, 1980), p. 441.

[294] S. Deser, Orit Levin, *Mapping Hawking into Unruh thermal properties*, Phys. Rev. D **59**, 064004 (1999).

[295] D. Birmingham, *Topological black holes in anti-de Sitter space*, Class. Quant. Grav. **16**, 1197 (1999).

[296] A. M. Awad, *Higher dimensional charged rotating solutions in (A)dS space-times*, hep-th/0209238 (2002).

[297] S. D. H. Hsu, hep-ph/0203154; H. Tu, hep-ph/0205024; A. Jevicki and J. Thaler, Phys. Rev. **D66**, 024041 (2002); Y. Uehara, hep-ph/0205199.

[298] G. N. Watson, *A Treatise on the Theory of Bessel Functions* (Cambridge University Press, 1995)

[299] R. Courant and D. Hilbert, *Methods of Mathematical Physics*, Chapter VI (Interscience, New York, 1962).

[300] J. Hadamard, *Lectures on Cauchy's Problem in Linear Partial Differential Equations* (Yale University Press, New Haven, 1923).

Bibliography

[301] J. D. Barrow and F. J. Tipler, *The Anthropic Cosmological Principle* (Oxford University Press, Oxford, 1986).

[302] D. V. Gal'tsov, Phys. Rev. **D66**, 025016 (2002).

[303] S. Hassani, *Mathematical Physics*, (Springer-Verlag, New York, 1998).

[304] P. O. Kazinski, S. L. Lyakhovich and A. A. Sharapov, Phys. Rev. **D66**, 025017 (2002); B. P. Kosyakov, Theor. Math. Phys. **119**, 493 (1999).

[305] B. Chen, M. Li and Feng-Li Lin, JHEP **0211**, 050 (2002).

[306] J. M. Weisberg and J. H. Taylor, astro-ph/0211217.

[307] P. C. Peters, Phys. Rev. **136**, B1224 (1964); P. C. Peters and J. Mathews, Phys. Rev. **131**, 435 (1963).

[308] B. F. Schutz, *A First Course in General Relativity*, (Cambridge University Press, 1985).

[309] F. Zerilli, Phys. Rev. Lett. **24**, 737(1970); F. Zerilli, Phys. Rev. **D2**, 2141 (1970).

[310] M. Davis, R. Ruffini, W. H. Press, and R. H. Price, Phys. Rev. Lett. **27**, 1466 (1971).

[311] S. L. Smarr (ed.), *Sources of Gravitational Radiation*, (Cambridge University Press, 1979).

[312] P. Anninos, D. Hobill, E. Seidel, L. Smarr, and W. M. Suen, Phys. Rev. Lett. **71**, 2851 (1993); R. J. Gleiser, C. O. Nicasio, R. H. Price, and J. Pullin, Phys. Rev. Lett. **77**, 4483 (1996).

[313] R. Ruffini, Phys. Rev. **D7**, 972 (1973); M. J. Fitchett, *The Gravitational Recoil Effect and its Astrophysical Consequences*, (PhD Thesis, University of Cambridge, 1984).

[314] T. Regge, J. A. Wheeler, Phys. Rev. **108**, 1063 (1957).

[315] S. Weinberg, Phys. Lett. **9**, 357 (1964); Phys. Rev. **135**, B1049 (1964).

[316] L. Smarr, Phys. Rev. **D15**, 2069 (1977); R. J. Adler and B. Zeks, Phys. Rev. **D12**, 3007 (1975).

[317] K. D. Kokkotas and B. G. Schmidt, Living Rev. Rel. **2**, 2(1999).

[318] G. T. Horowitz and V. E. Hubeny Phys. Rev. **D62**, 024027 (2000); V. Cardoso and J. P. S. Lemos, Phys. Rev. **D63**, 124015 (2001); Phys. Rev. **D64**, 084017 (2001); Class. Quantum Grav. **18**, 5257 (2001); D. Birmingham, I. Sachs and S. N. Solodukhin, Phys. Rev. Lett. **88**, 151301 (2002); R. A. Konoplya, hep-th/0205142; S. F. J. Chan and R. B. Mann, Phys. Rev. **D55**, 7546 (1997); I. G. Moss and J. P. Norman, Class. Quant. Grav. **19**, 2323 (2002); R. Aros, C. Martinez, R. Troncoso and J. Zanelli, hep-th/0211024; D. T. Son, A. O. Starinets, JHEP **0209**:042, (2002).

[319] F. Mellor and I. Moss, Phys. Rev. **D41**, 403(1990); E. Abdalla, B. Wang, A. Lima-Santos and W. G. Qiu, Phys. Lett. **B538**, 435 (2002).

[320] J. M. Maldacena, Adv. Theor. Math. Phys. **2**, 253 (1998).

[321] B. F. Schutz and C. M. Will, Astrophys. Journal **291**, L33 (1985); C. M. Will and S. Iyer, Phys. Rev. **D35**, 3621 (1987); S. Iyer, Phys. Rev. **D35**, 3632 (1987).

[322] V. Cardoso and J. P. S. Lemos, Phys. Rev. **D66**, 064006 (2002).

[323] O. Dreyer, gr-qc/0211076; G. Kunstatter, gr-qc/0211076.

[324] I. S. Gradshteyn and I. M. Ryzhik, *Table of Integrals, Series and Products*, (Academic Press, New York, 1965).